PB84-145580

Proceedings of Workshop on Catalytic Combustion (5th) Held at San Antonio, Texas on September 1981

Acurex Corp., Mountain View, CA

Prepared for

Industrial Environmental Research Lab.
Research Triangle Park, NC

Jan 84

U.S. Department of Commerce
National Technical Information Service
NTIS

PB84-145580

EPA-600/9-84-002
January 1984

PROCEEDINGS: FIFTH WORKSHOP ON CATALYTIC COMBUSTION
(San Antonio, Texas, September 1981)

John P. Kesselring, Compiler

Acurex Corporation
Energy & Environmental Division
485 Clyde Avenue
Mountain View, California 94042

Contract No. 68-02-3122

Project Officer:
W. Steven Lanier

Office of Environmental Engineering and Technology
Industrial Environmental Research Laboratory
Research Triangle Park, North Carolina 27711

Prepared for

U.S. ENVIRONMENTAL PROTECTION AGENCY
Office of Research and Development
Washington, D.C. 20460

REPRODUCED BY
NATIONAL TECHNICAL
INFORMATION SERVICE
U.S. DEPARTMENT OF COMMERCE
SPRINGFIELD, VA. 22161

TECHNICAL REPORT DATA

(Please read Instructions on the reverse before completing)

1. REPORT NO. EPA-600/9-84-002

2.

3. RECIPIENT'S ACCESSION NO. PB84 145580

4. TITLE AND SUBTITLE Proceedings: Fifth Workshop on Catalytic Combustion (San Antonio, Texas, September 1981)

5. REPORT DATE January 1984

6. PERFORMING ORGANIZATION CODE

7. AUTHOR(S) John P. Kesselring, Compiler

8. PERFORMING ORGANIZATION REPORT NO.

9. PERFORMING ORGANIZATION NAME AND ADDRESS
Acurex Corporation
485 Clyde Avenue
Mountain View, California 94033

10. PROGRAM ELEMENT NO.

11. CONTRACT/GRANT NO. 68-02-3122

12. SPONSORING AGENCY NAME AND ADDRESS
EPA, Office of Research and Development
Industrial Environmental Research Laboratory
Research Triangle Park, NC 27711

13. TYPE OF REPORT AND PERIOD COVERED Proceedings: 1/81-9/81

14. SPONSORING AGENCY CODE EPA/600/13

15. SUPPLEMENTARY NOTES IERL-RTP project officer is W. Steven Lanier, Mail Drop 65, 919/541-2432. EPA-600/9-80-035 and EPA-600/7-79-038 describe the four previous workshops.

16. ABSTRACT

The proceedings document the major presentations at the Fifth Workshop on Catalytic Combustion, in San Antonio, Texas, September 15-16, 1981. Sponsored by the Combustion Research Branch of EPA's Indistrial Environmental Research Laboratory--Research Triangle Park, the workshop served as a forum for the presentation of results of recent research in the areas of catalyst performance, use of heavy fuels in catalytic combustion, and applications of catalytic combustion. The workshop provided industrial, university, and government representatives with the current state-of-the-art in the application of catalytic combustion systems for pollution control and performance improvement. Applications include firetube and watertube boilers, stationary and mobile gas turbines, and diesel engine exhaust systems.

17. KEY WORDS AND DOCUMENT ANALYSIS

a. DESCRIPTORS	b. IDENTIFIERS/OPEN ENDED TERMS	c. COSATI Field/Group
Pollution	Pollution Control	13B
Combustion	Stationary Sources	21B
Catalysis		07D
Boilers		13A
Gas Turbines		13G
Diesel Engines		21G

18. DISTRIBUTION STATEMENT Release to Public

19. SECURITY CLASS *(This Report)* Unclassified

20. SECURITY CLASS *(This page)* Unclassified

21. NO. OF PAGES 432

22. PRICE

EPA Form 2220-1 (9-73)

NOTICE

This document has been reviewed in accordance with U.S. Environmental Protection Agency policy and approved for publication. Mention of trade names or commercial products does not constitute endorsement or recommendation for use.

PREFACE

This proceedings document covers the presentations of the Fifth Workshop on Catalytic Combustion, held September 15-16, 1981, in San Antonio, Texas. Sponsored by the Combustion Research Branch of the EPA's Industrial Environmental Research Laboratory—Research Triangle Park, the workshop served as a forum for the presentation of results of recent research in the areas of catalyst performance, the use of heavy fuels in catalytic combustors, and applications of catalytic combustion. The First and Second Workshops on Catalytic Combustion were held in Raleigh, North Carolina, on May 25-26, 1976 and June 21-22, 1977, respectively. The Third Workshop on Catalytic Combustion was held in Asheville, North Carolina, on October 3-4, 1978, and the Fourth Workshop on Catalytic Combustion was held in Cincinnati, Ohio, on May 14-15, 1980. Summaries of the First and Second Workshops and the Proceedings of the Third Workshop appear in EPA-600/7-79-038, "Proceedings: Third Workshop on Catalytic Combustion." The Proceedings of the Fourth Workshop appear in EPA-600/9-80-035, "Proceedings: Fourth Workshop on Catalytic Combustion."

John P. Kesselring, Acurex Corporation, acted as Workshop Coordinator, and W. Steven Lanier, Combustion Research Branch, U.S. Environmental Protection Agency, was the Project Officer.

ABSTRACT

The proceedings document the major presentations at the Fifth Workshop on Catalytic Combustion, held in San Antonio, Texas, September 15-16, 1981. Sponsored by the Combustion Research Branch of EPA's Industrial Environmental Research Laboratory—Research Triangle Park, the workshop served as a forum for the presentation of results of recent research in the areas of catalyst performance, use of heavy fuels in catalytic combustion, and applications of catalytic combustion. The workshop provided industrial, university, and government representatives with the current state of the art in the application of catalytic combustion systems for pollution control and performance improvement. Applications include firetube and watertube boilers, stationary and mobile gas turbines, and diesel engine exhaust systems.

TABLE OF CONTENTS

Page

Session I — Catalyst Performance 1

"Minimizing Fuel NO_x Using a Transitional Metal Oxide Catalytic Combustor," Lawrence A. Kennedy, Ravi Prasad, Eli Ruckenstein 2

"High Temperature Durable Catalyst Development," G. C. Snow and Henry Tong 32

"High Temperature Catalytic Reactions of $CO/O_2/H_2$, A, He, CO_2/H_2O Mixtures on Platinum," C. Bruno, P. M. Walsh, D. Santavicca, F. V. Bracco 70

"Mechanisms and Kinetics in Catalytic Combustion," G. C. Snow, W. V. Krill, R. M. Kendall 105

"Ignition Instabilities in Catalytic Combustion," E. G. Seebauer, J. H. Foster, W. F. Banholzer, R. I. Masel 134

"Catalytic Combustion in a Shear Flow," C. K. Law 153

"Minimum Pressure Drop for Cleaning Up Large Gas Flows," William B. Retallick 177

Session II — Heavy Fuels Use in Catalytic Combustion 187

"Investigation of Partially-Vaporized Residual Oil Catalytic Combustion," T. J. Rosfjord. 188

"Demonstration of Catalytic Combustion with Residual Fuel," Willard J. Dodds 221

"Catalytic Combustion of Residual Fuels," Daniel L. Bulzan and Robert R. Tacina 257

Session III — Applications of Catalytic Combustion 295

"Development of a System to Utilize Flue Gas from Enhanced Recovery Underground Combustion Projects," Stephen E. Kaye 296

Page

"Assessment of Infrared and Catalytic Burner Gas Appliances," W. V. Krill, R. J. Schreiber, and J. P. Kesselring 297

"Catalytic Combustion for Gas Turbines," H. Fukuzawa, Y. Ishihara, Y. Hasegawa 320

"Development of a Catalytic/Radiative Watertube Boiler," M. A. Friedman, W. V. Krill, J. P. Kesselring 333

"Development of a Low NO_x Combustor for Gas-Fired Firetube Boilers," E. B. Merrick, W. V. Krill, J. P. Kesselring, M. A. Friedman 353

"Full-Scale, Full-Pressure Tests of Catalytic Burners for Combustion Turbines," P. W. Pillsbury, P. E. Scheihing, J. L. Toof, K. R. Burns . 368

"CATATHERMAL® Combustion of Diesel Exhaust to Produce an Inert Gas," M. Durilla and K. R. Burns 403

SESSION I

CATALYST PERFORMANCE

MINIMIZING FUEL NO_x USING A TRANSITIONAL METAL OXIDE CATALYTIC COMBUSTOR

By:
Lawrence A. Kennedy
Ravi Prasad
Eli Ruckenstein
Department of Mechanical & Aerospace Engineering
State University of New York at Buffalo
Amherst, New York 14260

ABSTRACT

The results of an experimental study are reported concerning the oxidation of a nitrogen containing fuel in a catalytic combustor for both fuel lean and fuel rich conditions.

The catalytic combustor employs a binary mixture of chromium and cobalt oxides deposited on high surface area alumina pellets. (5.6% Cr_2O_3, 1.87% Co_3O_4, balance alumina). Propane doped with 1% by weight ammonia was burned with a O_2/Ar mixture to eliminate the contribution of thermal NO_x to the measured species. For a wide range of inlet conditions, the exit concentrations of the dominant fixed nitrogen species (NO_x, NH_3 and HCN) as well as the other major species (O_2, CO_2, H_2O, C_3H_8) were measured.

Under fuel lean operation the sole product of fuel -N conversion was NO_x, while in fuel rich operation HCN and unconverted NH_3 were also detected. The conversion to HCN and NH_3 increases and to NO_x decreases as the operation becomes more fuel rich. The concentration of HCN increases, while those of NH_3 and NO_x decreases as the inlet temperature (T_{in}) increases. The sum of the fixed nitrogen species shows a minimum at an equivalence ratio (Φ_{in}) of about 1.43.

The most significant result was that at sufficiently high T_{in} (600-640°C) the total emission levels of fixed nitrogen compounds (NO_x, NH_3 and HCN combined) can be reduced to very low levels (5-20% of the fuel -N present at the combustor inlet) in both fuel lean as well as fuel rich regions. Most of the fuel -N is converted to molecular nitrogen. By comparison, fuel lean operation with noble metal catalysts, typically yields 50-90% fuel -N conversion to NO_x.

ACKNOWLEDGEMENTS

The work described in this paper was partially supported by DOE grant DE-FG22-80PC30220 and by an unrestricted Ford Motor Co. grant to the Combustion Laboratory.

SECTION 1

INTRODUCTION

Studies directed towards the reduction of nitrogen oxides emissions from combustion processes in the past have been directed towards minimizing thermal NO_x. More recently with the potential large scale use of fuels containing significant quantities of nitrogen species, considerable effort has been directed towards reducing the formation of NO_x from these fuel-bound species.

Catalytic combustion has been shown to be an effective technique for reducing thermal NO_x emissions. It also has the potential to reduce NO_x emissions resulting from nitrogen bound fuels. In this technique a catalyst is used to promote the combustion process.

For nitrogen free fuels, NO_x forms due to the fixation of atmospheric nitrogen primarily via the Zeldovich mechanism which is strongly temperature dependent. If the combustor is operated under sufficiently fuel lean conditions, then the temperatures that result would be low enough to minimize the formation of thermal NO_x. These temperatures are adequate for many practical applications but in conventional combustors the flame is not stable at such fuel lean conditions. However, they are feasible in catalytic combustors, where the heterogeneous reactions combined with the thermal inertia of the bed stabilizes the combustion process. The type of catalyst used does not significantly affect the formation of thermal NO_x and a reduction of one to two orders of magnitude in thermal NO_x emission has been achieved using catalytic combustion. (Pfefferle et al. 1975, Blazowski et al. 1975, DeCorso et al. 1975, Anderson et al. 1975, Prasad et al. 1980).

In the case of nitrogen bound fuels, the fuel -N compounds are more readily oxidized to NO_x than is the atmospheric nitrogen (Appleton and Heywood, 1973). As a result, conventional combustors, in fuel lean operation, tend to preferentially oxidize the fuel -N to NO_x, yielding high emission levels of NO_x. In principle, the use of a catalytic combustor can alleviate this problem, if the catalyst could selectively oxidize the fuel, while converting the fuel -N to N_2. However, the catalytic combustion results reported in literature (Chu et al. 1979, Pogson et al. 1979, Folsom et al. 1979, Folsom et al. 1980, Matthews et al. 1977) show a high degree of conversion of fuel -N to NO_x in fuel lean operations, implying that the catalysts used in those experiments did not possess this type of selectivity. Only by operating in the fuel rich region, where the amount of oxygen is insufficient for complete combustion, was it possible to significantly reduce the emission level of the total fixed nitrogen (TFN) compounds (such as NO_x, NH_3, HCN) (Chu et al. 1979, Folsom et al. 1979, Folsom et al. 1980, Matthews and Sawyer 1977).

Almost all the studies on fuel -N oxidation in catalytic combustors have been done with noble metal catalysts. Since Pt is the commercially used catalyst for ammonia oxidation to NO and since NH_3 is representative of fuel bound nitrogen compounds, in fuel lean combustion it is to be expected that a high degree of fuel -N conversion to NO_x would occur using this catalyst. This agrees with the results reported in literature (Chu et al. 1979, Matthews et al. 1977, Folsom et al. 1980) and indicates additionally that, in catalytic combustion, the fuel -N conversion mechanism is dominated by the surface reactions. Consequently, the nature of the catalyst used would be expected to have a strong effect on the conversion of fuel -N. This is substantiated by the results of Folsom et al. 1980, who showed that significant reduction in fuel -N conversion, in the fuel rich region, could be achieved by using a NiO-Pt catalyst as opposed to a Pt catalyst alone.

The objective of the present experiments was to study the oxidation of a nitrogen bound fuel over a binary transition metal oxide catalyst. The catalyst used was one that had been found in an earlier study (Prasad et al. 1980) to be suitable for lean fuel propane oxidation. The nitrogen bound fuel was simulated using propane doped with 1% by wt. ammonia. The oxidizer used was a mixture of O_2/Ar which eliminated the formation of thermal NO_x from air.

The equivalence ratio (Φ_{in}), inlet temperature (T_{in}) and inlet velocity (V_{in}) have been varied systematically over a wide range and their affects on the emission levels of NO_x, NH_3 and HCN have been studied. The results indicate that, using this catalyst, remarkably low fuel -N conversions (10-20%) are attainable under fuel lean operations if T_{in} is sufficiently high.

SECTION 2

EXPERIMENTAL DETAILS

A schematic sketch of the experimental facility is shown in Fig. 1. The test section consists of a stainless steel tube, 7.6 cm long and 1.65 cm is diameter (i.d.), in which the catalyst bed is mounted and the oxidation of the fuel takes place. Pieces of monolith without catalyst, 1.5 cm long each, were placed before and after the catalyst bed to make the flow more uniform and to reduce heat losses from the combustor in the axial direction. The test section was heavily insulated and heated from the outside using electrical guard heaters to minimize radial heat losses. The power supply to these guard heaters could be regulated to vary the heating rate.

The catalyst used consisted of binary transition metal oxides mixture deposited on high surface area alumina pellets (5.6% wt. Cr_2O_3, 1.87% CO_3O_4, balance alumina). The fuel used was propane doped with 1% by weight ammonia. This simulated other nitrogen bound fuels as well, because the fuel -N conversion is only weakly dependent on the type of fuel -N species (Chu et al. 1979, Matthews et al. 1977). The oxidizer used was a mixture of 2.4% O_2 and 97.6% Ar, to eliminate the formation of thermal NO_x. The oxygen concentration was chosen so that the adiabatic flame temperature, for all inlet conditions, would remain below approximately 1225°K. This ensured that catalyst deactivation would be negligible during the experiment.

The O_2/Ar mixture entering the test section was heated in two stages. In the first stage, consisting of a stainless steel heat exchanger, the above mixture is heated to approximately 300°C, using a hot air stream. The second stage consisted of a three zone Lindberg electric furnace whose temperature could be accurately controlled. Using this furnace the temperature of the O_2/Ar mixture could be further increased to approximately 700°C. The ammonia doped fuel was injected into the gas stream using a multi-port opposed jet injector. The injector could be located either upstream or downstream of the Lindberg furnace and the propane could be preheated, if necessary, up to 800°C. Flow rates of O_2/Ar and C_3H_8/NH_3 were monitored and controlled using pre-caliberated Linde flow meters.

Temperature measurements were made using Alumel-Chromel thermocouples located at the inlet, exit and at six points along the centerline within the bed. Five stainless steel gas sampling probes were present in the bed to measure the axial gas concentrations therein. In addition, there was another gas sampling probe located before the bed to measure the gas composition at the inlet of the combustor. Due to spatial limitations, these probes could be water cooled only outside the combustor. The exit gas analysis was carried out using a water jacketed stainless steel probe which could be moved axially.

Measurements of oxygen, nitrogen, carbon monoxide, ammonia and carbon dioxide concentrations were carried out using a Varian 3700 dual column gas chromatograph. Low concentrations of ammonia were detected by passing known volumes of gas samples through 0.05N H_2SO_4 solution which was subsequently analyzed. The concentrations of unburnt hydrocarbons and HCN were determined using a Varian 3700 flame ionization chromatograph. The NO_x concentration was measured with a Thermal Electron Model 44 Chemiluminescent Analyzer. No attempt has been made to determine the precise fate of the total fuel -N introduced. Instead, following other researchers (Chu et al. 1979, Folsom et al, 1980), only the dominant fixed nitrogen species (such as NH_3, HCN and NO_x) have been measured.

The range of inlet conditions studied were $0.5 < \Phi_{in} < 1.9$, $410 < T_{in} < 650°C$, $1.96 < V_{in} < 4.07$ m/sec.

Two types of experiments have been carried out. In the first type, T_{in} and V_{in} were fixed, while Φ_{in} was varied in steps from fuel lean to fuel rich conditions. Therefore T_{in} or V_{in} have been changed and the experiments repeated. In the second type, Φ_{in} and V_{in} were fixed, while T_{in} was varied from a low (410-430°C) to a high (620-650°C) value. Subsequently Φ_{in} or V_{in} have been altered and the experiments were repeated. Note that due to the possible existence of multiple steady states (Prasad et al. 1981), all these experiments were conducted in a heating up mode.

For every set of inlet conditions selected, the axial temperature profile was measured and gas samples from the inlet and exit of the combustor were analyzed to determine the concentrations of N_2, O_2, CO, CO_2, NH_3, NO_x, HCN and unburnt hydrocarbons. Attempts were also made to monitor the axial gas concentration profiles in the bed. In most cases, however, these measurements could not be carried out because the open ends of the gas sampling probes, inside the bed, became blocked by catalyst pellets drawn to them by the suction. Consequently, the results reported herein are based on exit measurements of gas composition.

SECTION 3

RESULTS AND DISCUSSION

EFFECTS OF INJECTOR LOCATION AND FUEL PREHEATING

Four different combinations of injector location and fuel preheating were tried. These were: (1) Injector upstream of furnace and no preheating of fuel (2) Injector upstream of the furnace and fuel preheating (3) Injector downstream of the furnace and fuel preheating (4) Injector downstream of the furnace and no preheating of fuel.

Placing the injector upstream of the furnace resulted in significant oxidation of both fuel and fuel-N inside the furnace. Preheating the fuel to the same temperature as the exit gas temperature from the furnace, yielded very uniform temperature profiles at the inlet of the combustor, but introduced two difficulties. First, the preheating of fuel increased the probability of flashback and consequently, in many cases where preheating was used, a flame was found at the injector ports. The second difficulty was that at high degree of preheating, the propane was found to partially dissociate on the stainless steel walls of the fuel line. This led to carbon deposits on the walls that grew with time and finally choked the fuel line.

In view of these results the configuration used in most of the experiments was the one with no preheating of fuel and the injector downstream of the furnace. This was also found, in general, to yield the lowest emission levels of Total Fixed Nitrogen (TFN), while the configuration with the injector upstream of the furnace and preheating of fuel had the highest emission levels of TFN. It should be mentioned that the configuration chosen has very significant effects on both the NO_x emission levels as well as the dependence of the NO_x emission level on inlet parameters. Thus in Figure 2 it is seen the for V_{in} = 2.93 m/sec, and Φ_{in} = 0.72 the fuel-N conversion is very different with the injector upstream and preheating of fuel, as opposed to the injector downstream and no preheating of fuel. In particular, at high T_{in} the former configuration shows increasing fuel-N conversion to NO_x, while the latter configuration shows decreasing fuel-N conversion to NO_x.

EFFECTS OF Φ_{in} ON FUEL-N CONVERSION

Figures 3-5 show the conversion, at the combustor exit, or fuel-N to various fixed nitrogen species as a function of % Theoretical Oxidizer (TO) (which is in the present case the equivalent of the Theoretical Air) for three different T_{in}. Since % Theoretical Oxidizer = $100/\Phi_{in}$, value to TO greater than 100 denote fuel lean operations, while values less than 100 correspond to fuel-rich operations. All three figures show that under fuel lean operations, the sole product of fuel-N oxidation is NO_x. Only in the fuel rich region do HCN and unconverted NH_3 appear. This is consistent with the results reported for noble metal based catalytic combustors. (Chu et al. 1979, Folsom et al. 1980).

Under fuel lean operations, the conversion of fuel-N to NO_x depends strongly on the inlet temperature and tends to decrease with increasing T_{in}. Thus for TO = 170%, percent fuel-N conversion to NO_x is 68% at T_{in} = 507°C, 40% at T_{in} = 560°C and only 12% at T_{in} = 603°C. In addition, the fuel-N conversion to NO_x exhibts a maximum with respect to TO. As T_{in} decreases the maximum displaces to larger values to TO, being at TO = 100 for T_{in} = 603°C and TO = 120 for T_{in} = 560°C. For T_{in} = 507°C the maximum occurs at more lean conditions than those plotted in Figure 3. The peak of fuel-N conversion to NO_x decreases as T_{in} increases, being 51% at T_{in} = 560°C, but only 28% at T_{in} = 603°C.

It should be noted that using mixed oxide catalyst, even in lean fuel operations and sufficiently high values of T_{in} (e.g. 603°C, Figure 5), the fuel-N conversion to NO_x is very low (12%-28%). The major nitrogenous species produced is N_2. This represents a significant improvement over the results reported for the noble metal catalysts. On these catalysts, typically, 50-90% fuel-N conversion to NO_x is obtained under lean fuel conditions.

For $TO < 100$ (fuel-rich), the fuel-N conversion to NO_x decreases monotonically with decreasing TO (increasing Φ_{in}). Close to stoichiometric conditions (80-100% TO), NO_x is the dominant fixed nitrogen species and the conversion to HCN and NH_3 are small. However, as the operation becomes increasingly fuel rich (TO < 70%), the concentration of NH_3 and HCN rise sharply and they soon become major fixed nitrogen species. This is to be expected because under fuel rich conditions, the formation of NO_x is inhibited by the lack of available oxygen. Similar results have also been found for noble metal based catalytic combustors as well as in conventional combustors. (Chu et al. 1979, Song et al. 1980). In those combustors, however, somewhat lower levels of NO_x emission were observed in the fuel rich region. This is believed to be because, the adiabatic flame temperature used in them were significantly higher, leading to more effective reduction of the NO_x by the hydrocarbon species or CO present. Indeed it may be seen from Figure 2, that at high T_{in} the NO_x production is very low with this catalyst in the fuel rich region.

The total of the three fixed nitrogen species measured (NO_x, HCN, NH_3), denoted by Total Fixed Nitrogen (TFN), exhibits a local minimum under fuel rich conditions. This occurs because, in the fuel rich region, there is a tradeoff between decreasing fuel-N conversion to NO_x and increasing fuel-N conversion to HCN and NH_3. The minimum occurs at about TO = 70 and its magnitude diminished at higher T_{in}. At T_{in} = 603°C the minimum is barely evident.

EFFECT OF T_{in} ON FUEL-N CONVERSION:

O_2/Ar Mixture as Oxidizer:

Figures 6 and 7 show the fuel-N conversion to various fixed nitrogen species as a function of T_{in} for $\Phi_{in} = 1.67$ and two different values of V_{in}. It is seen that the conversion to NO_x first increases slightly and then drops sharply with increasing T_{in}. The decrease in fuel-N conversion to NO_x begins at about 580°C and the decline is more rapid at lower V_{in}. The concentration of NH_3 decreases monotonically, while that of HCN increases monotonically with increasing T_{in}. In the range of T_{in} used, the TFN decreases continuously with increasing T_{in}. However, it appears likely that if T_{in} is increased beyond come critical value, the conversion of fuel-N to TFN will start either to increase or to level off, due to the rising conversion to HCN. This should represent the value of T_{in} to be used for the catalytic combustor operation, in the fuel rich region, to minimize the emission levels of TFN.

The effect of T_{in} on the fuel-N conversion to NO_x is shown in Figures 2, 8, 9 and 10 for various Φ_{in} and V_{in}. It is seen that, at low T_{in} (below 500°C), the fuel-N conversion to NO_x increases with increasing T_{in}, reaching a maximum in the range of 500-560°C. The maximum fuel-N conversion depends strongly on Φ_{in}, being higher in the fuel lean region and decreasing to much lower values in the fuel rich region (Figure 2). Thus the peak fuel-N conversion is 60-70% for $\Phi_{in} = 0.72$, but only 30-38% for $\Phi_{in} = 1.67$ (Figures 8,10). Further increases in T_{in} causes the fuel-N conversion to drop sharply and reach very low values (5-20%) if T_{in} is in the range of 600-640°C. At such high T_{in} most of the fuel-N is converted to N_2. The decline in fuel-N conversion is very rapid under fuel lean conditions and slightly less rapid as the operation becomes fuel rich. Decreasing V_{in} also causes the fuel-N conversion to decline more rapidly at higher T_{in}.

The above observations on the variation of fuel-N conversion to NO_x with temperature in the fuel lean and fuel rich regions may be explained in the following manner:

Fuel Rich Region:

At low T_{in} the NO_x formation reactions are inhibited due to the lack of sufficient oxygen. This results in relatively low levels of fuel-N conversion to NO_x, but significant emission of unconverted fuel-N might occur (Figure 6 and 7). Hence at low T_{in}, the reactions leading to the formation of molecular nitrogen do not appear to be dominant. As T_{in} increases two things happen (1) the reaction leading to the formation of N_2 and HCN from fuel-N become more significant leading to a decrease in the emission of unconverted fuel-N (Figures 6 and 7). (2) The NO_x formed is more effectively reduced by CO and hydrocarbon species. Due to both these mechanisms, fuel-N conversion to NO_x and TFN drop with increasing T_{in}. This explanation is consistent with the fact that a low T_{in} the fuel-N conversion to NO_x is higher than that reported for noble metal based catalytic combustors where much higher combustor temperatures were used.

Fuel Lean Region:

At low T_{in} the NO_x formation reactions are the dominant reactions in fuel-N conversion and the reactions leading to N_2 formation do not play a major role. Increasing T_{in} shifts the concentration and temperature profiles towards the entrance of the bed. Consequently, the reactions that at lower T_{in} were significant only towards the end of the bed, now become significant further upstream in the bed. Thus, the reactions leading to the oxidation of fuel-N now occur earlier in the bed. If this is true, then one would expect to see high conversions of fuel-N to NO_x early in the bed for those cases where the exit conversion to NO_x is small. This indeed was found in the few cases where concentration measurements could be made at a few points inside the bed. The sharp decline in fuel-N conversion at high T_{in} implies, however, that the NO_x formed in the initial part of the bed is reduced in the latter part of the bed, possibly by CO or hydrocarbon species. These reduction reactions become more rapid at higher temperatures and also occur over a greater portion of the bed length. In addition it is possible that, at high T_{in}, the reaction leading to N_2 formation become more significant. The combined effects cause a sharp decrease in fuel-N conversion at high T_{in}.

It is important to note that, for this catalyst, at sufficiently high temperatures (T_{in} = 600-640°C) the fuel-N conversion to TFN is very low (5-20%). By contrast, with Pt catalysts, typically 50-90% fuel-N conversion to NO_x may be expected under fuel lean operation. This observation represents the most significant contribution of this paper. The fact that the results obtained using this catalyst are significantly different from those obtained using noble metal catalysts, or with conventional combustors indicates that the fuel-N conversion reactions are primarily taking place on the catalyst surface.

Air as Oxidizer:

All the experiments reported in this paper hitherto have used an O_2/Ar mixture for the oxidizer. The question arises as to whether the trends observed would be valid if air is used as the oxidizer. To check this further, the combustor was operated under fuel lean conditions using air as the oxidizer and the ammonia doped propane as fuel.

Figure 11 shows the fuel-N conversion to NO_x as a function of T_{in} for Φ_{in} = 0.155, using air as the oxidizer. The conversion of fuel-N to NO_x is seen to first increase with T_{in} reaching a maximum of about 73% at

T_{in} = 550°C. For T_{in} higher than this value, the conversion to NO_x falls rapidly being only 30% at T_{in} = 650°C. Hence the behavior is similar to that obtained using O_2/Ar mixture as the oxidizer. Note that the fuel-N conversion to NO_x shown in the figure includes the NO_x formed due to thermal fixation. However, for such fuel lean conditions, this catalyst had, in an earlier study (Prasad et al. 1980), produced only $<$ 5ppm of thermal NO_x. Therefore the error introduced is not expected to be large.

In the fuel rich region, since little thermal NO_x forms from the atmospheric nitrogen, one would not expect to see significant differences if air is used instead of O_2/Ar as the oxidizer.

EFFECT OF V_{in} ON FUEL-N CONVERSION:

The effect of V_{in} on the conversion of fuel-N to NO_x is plotted in Figures 8 to 10. They show that for low T_{in}, in fuel rich as well as fuel lean operations, the conversion to NO_x increases as V_{in} decreases. This is consistent with the earlier explanation that the NO_x formation reactions are dominant at low T_{in}. Consequently, increasing V_{in} (decreasing the residence time) should lead to lower NO_x emissions, but also to increasing amounts of NH_3. This was indeed observed experimentally, since at V_{in} = 4.07 m/sec, for low T_{in}, NH_3 was detected at the combustor exit, even for fuel lean operations.

At higher T_{in}, the fuel-N conversion to NO_x increases as V_{in} increases. This again is consistent with the earlier explanation because, at high T_{in}, the reaction leading to the formation of N_2 and reduction of NO_x become more significant. Therefore with increasing residence time (decreasing V_{in}), one would expect to obtain lower fuel-N conversion to NO_x.

The foregoing arguments suggest that the effect of V_{in} is primarily through its effects on the residence time. Therefore at low T_{in}, as V_{in} increases, one would expect to see increased NH_3 and decreased HCN emissions, while at high T_{in}, as V_{in} decreases, one would expect to see decreased NH_3 and increased HCN emissions. These have again been observed experimentally.

SECTION 4

CONCLUSION

In this paper we have studied the effect of inlet parameters (Φ_{in}, V_{in} and T_{in}) on the oxidation of fuel bound nitrogen in a mixed transition metal oxides based catalytic combustor. The nitrogen bound fuel was simulated by propane doped with 1% by weight ammonia. The oxidizer was a mixture of O_2/Ar which eliminated the formation of thermal NO_x from N_2 contained in air.

The most significant result found was that by operating the combustor at sufficiently high T_{in}, the fuel-N conversion to NO_x could be reduced to very low values (5-20%), even under lean fuel conditions. By comparison, noble metal catalysts typically produce 50-90% conversion of fuel-N to NO_x under lean fuel conditions.

At low values of T_{in}, significant fuel-N conversion ($\sim$70%) to NO_x can occur under lean fuel operation. This suggested that at high T_{in}, the NO_x formed in the initial part of the bed is subsequently destroyed, by secondary reactions, later in the bed. The measurements appear to support this explanation.

Under lean fuel operation the sole product of fuel-N conversion is NO_x, while under fuel rich conditions, the concentrations of NH_3 and HCN become significant. The conversion to NH_3 and NH_3 increases and to NO_x decreases as the operation becomes increasingly fuel rich. Increasing T_{in} causes the conversion to HCN to increase, while decreasing the concentration of NH_3.

The effect of V_{in} occurs primarily through the residence time. At low T_{in}, increasing V_{in} decreases the conversion to NO_x and HCN and increases that to NH_3. At high T_{in}, decreasing V_{in} decreases NH_3 and NO_x and increases HCN.

Lastly it should be mentioned that the results presented here indicate that the type of catalyst used has a significant effect on the oxidation of fuel-bound nitrogen. It appears possible to selectively oxidize the fuel while converting the fuel-N primarily to N_2. Further research however has to be done in the development of catalysts that may have better thermal stability and possess this type of selectivity.

REFERENCES

1. Appleton, J.P. and Heywood J.B. (1973), The Effect of Imperfect Fuel-Air Mixing in a Burner on NO Formation from Nitrogen in the Air and Fuel, Fourteenth Symposium (International) on Combustion, The Combustion Institute. Pittsburg, Pa., pp. 777-786.

2. Anderson, D.N., Tacina, R.R., and Mroz, T.S. (1975). Performance of a catalytic reactor at simulated gas turbine operating conditions, NASA TM X-71747, NASA Lewis Research Center.

3. Blazowski, W.S., and Walsh, D.E. (1975). Catalytic combustion: An important consideration for future applications. Combustion Science and Technology 10,233-244.

4. Chu, E.K., and Kesselring, J.P. (1979). Fuel-NO_x Control in Catalytic Combustion. Environmental Protection Agency Publication EPA-600/7-79-038, pp. 281-330.

5. DeCorso, S.M., Mumford, S., Carrubba, R., and Heck, R. (1976). Catalysts for gas turbine combustors-Experimental test results. ASME Paper No. 76-GT-4.

6. Folsom, B.A., Courtney, C.W., and Heap, M.P. (1979). Environmental aspects of low Btu gas-fired catalytic combustion. Environmental Protection Agency Publication. EPA-600/7/79-038, pp. 345-384.

7. Folsom, B.A., Clark, W.D., Courtney, C.W., Heap, M.P., and Seeker, W.R. (1980). Fuel nitrogen conversion-The impact of catalyst type. Environmental Protection Agency Publication EPA-600/9-80-035, pp. 432-455.

8. Matthews, R.D., and Sawyer, R.F. (1977). Fuel nitrogen conversion and catalytic combustion. Paper No. 77-40, Fall Meeting, Western States Section/Combustion Institute.

9. Pfefferle, W.C., Carrubba, R.V., Heck, R.M., and Roberts, G.W. (1975). Catathermal combustion: A new process for low-emission fuel conversion. ASME Paper No. 75-WA/FU-1.

10. Pogson, J., and Monsour, M.N. (1979). Catalytic combustion of No. 6 fuel oil. Environmental Protection Agency Publication EPA-600/7-79-038, pp. 111-138.

11. Prasad, R., Catalytic Combustion of Propane using Transitional Metal Oxides. M.S. Thesis. Dept. of Mechanical Engineering, State University of New York at Buffalo, (1979).

12. Prasad, R., Kennedy, L.A., and Ruckenstein, E. (1980). Catalytic combustion of propane using transitional metal oxides. Combustion Science and Technology, 22, 271-280.

13. Prasad, R., Tsai, H.L., Kennedy, L.A., and Ruckenstein, E. (1981). Occurrence of multiple steady states in the catalytic combustion of propane. Combustion Science and Technology. 26, 1 and 2, 51-64 (1981).

14. Song, Y.H., Blair, D.W., Siminski, V.J., and Bartok, W. (1980). Conversion of fixed nitrogen to N_2 in rich combustion. 18th International Symposium on Combustion, August 17-22.

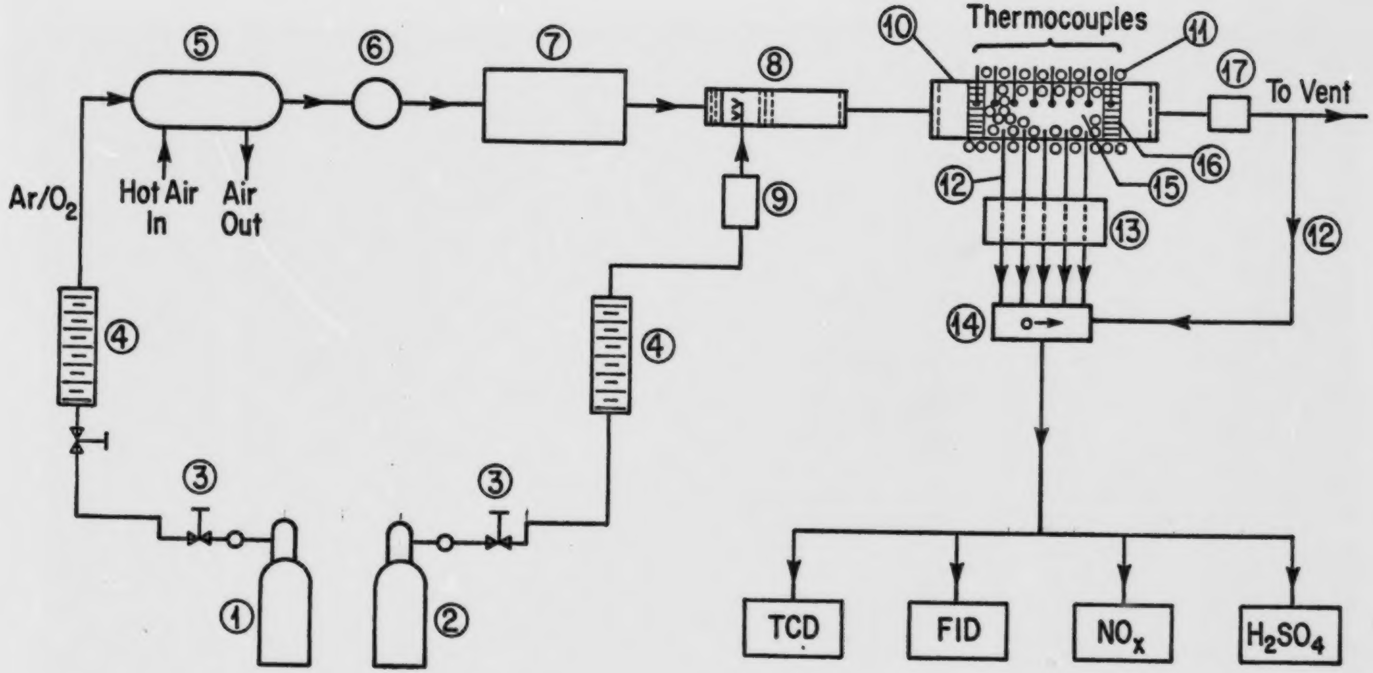
Ar/O$_2$
⑤
Hot Air In
Air Out
⑥
⑦
⑧
⑨
④
④
③
③
①
②
⑩
Thermocouples
⑪
⑰
To Vent
⑯
⑮
⑫
⑬
⑫
⑭
TCD
FID
NO$_x$
H$_2$SO$_4$

Figure 1: Schematic sketch of experimental facility.

(1) Ar/O_2 gas cylinder; (2) C_3H_8/NH_3 gas cylinder; (3) Pressure regulators; (4) Flow meters; (5) Heat exchanger; (6) Upstream location of fuel injector; (7) Furnace; (8) Fuel Injector - downstream location; (9) Fuel preheater; (10) Combustor; (11) Heating elements; (12) Gas sampling lines; (13) Water bath; (14) Gas sample line selector; (15) Pellet Bed; (16) Blank Monolith; (17) Water Jacketed Probe; TCD - Thermal Conductivity Detector; FID - Flame Ionization Detector; NO_x - Chemiluminescent NO_x Analyzer; H_2SO_4 - Wet Chemistry for NH_3.

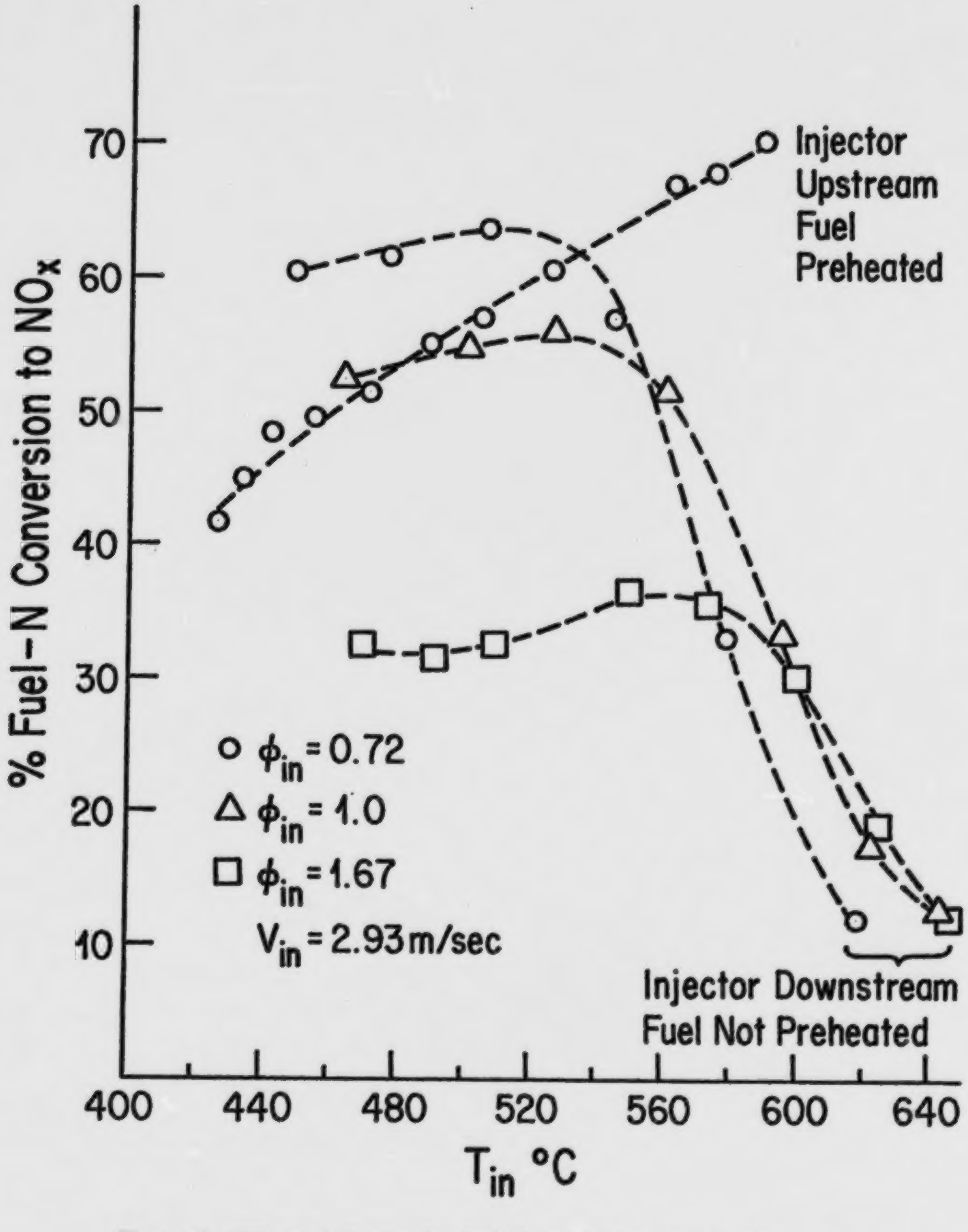

Figure 2: Effect of T_{in} on the fuel-N conversion to NO_x for various equivalence ratios. $V_{in} = 2.93$ m/sec.

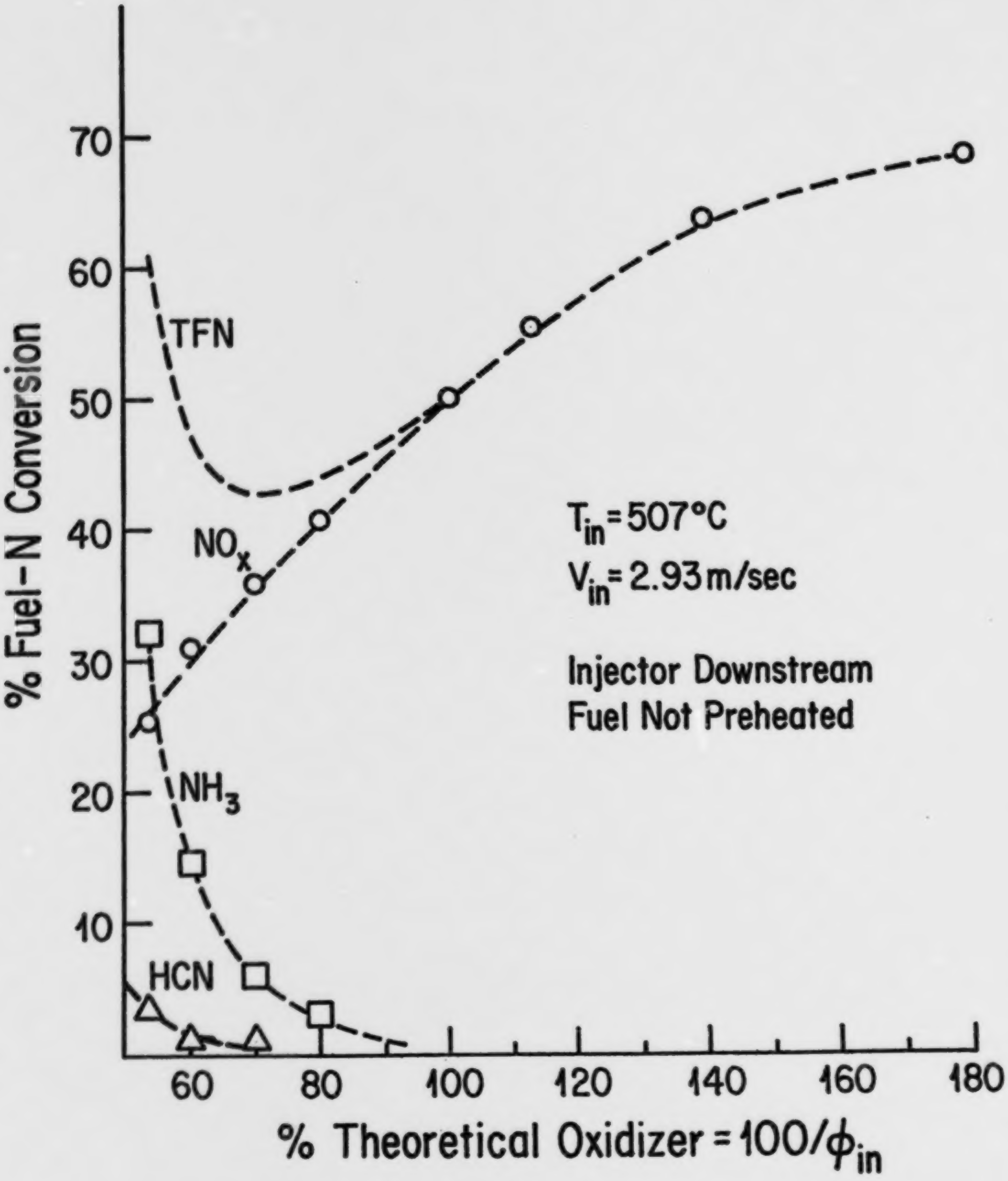

Figure 3: Effect of % theoretical oxidizer on the fuel-N conversion to various fixed nitrogen species. T_{in} = 507°C, V_{in} = 2.93 m/sec.

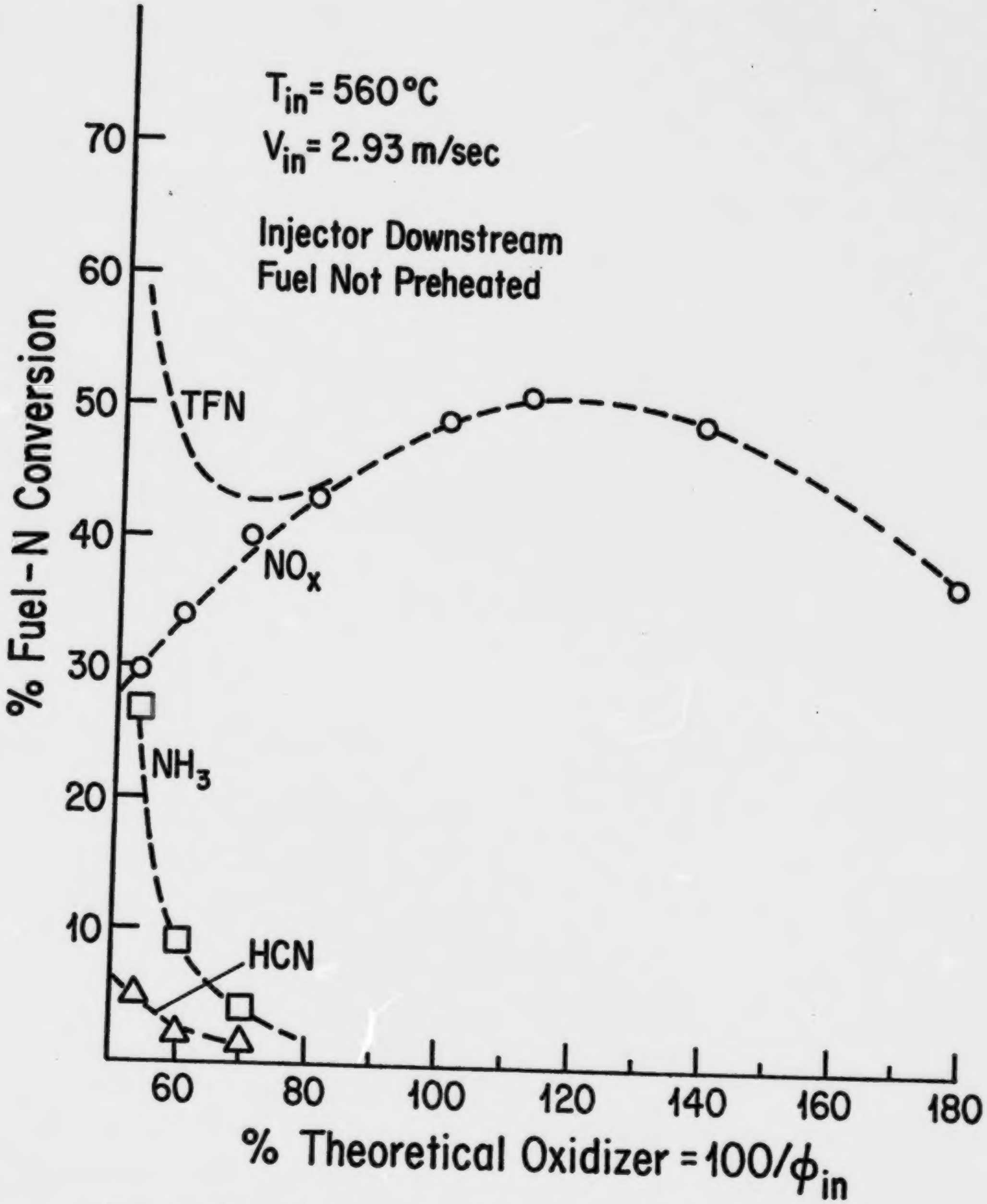

Figure 4: Effect of % theoretical oxidizer on the fuel-N conversion to various fixed nitrogen species. T_{in} = 560°C, V_{in} = 2.93 m/sec.

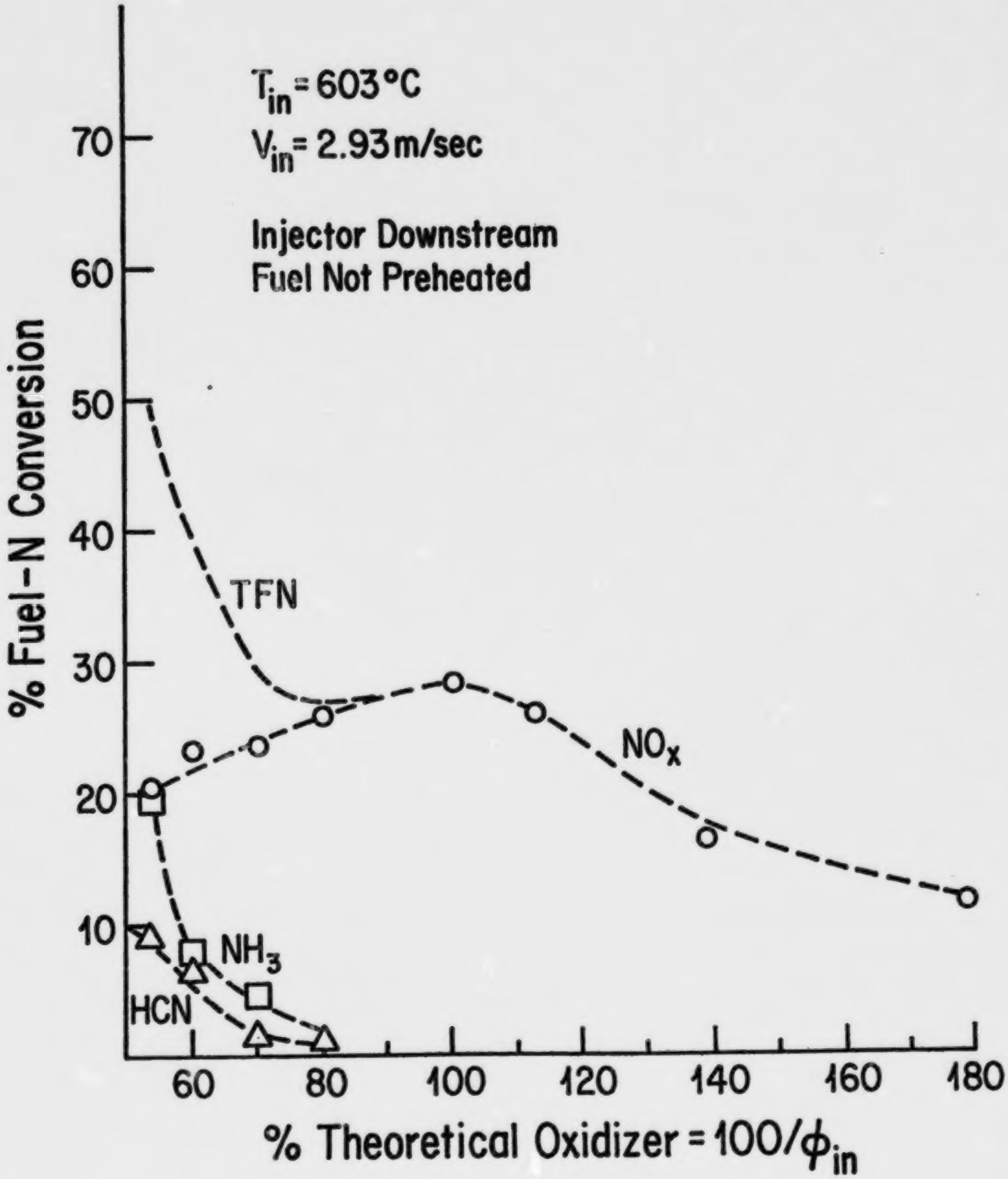

Figure 5: Effect of % theoretical oxidizer on the fuel-N conversion to various fixed nitrogen species. T_{in} = 603°C, V_{in} = 2.93 m/sec.

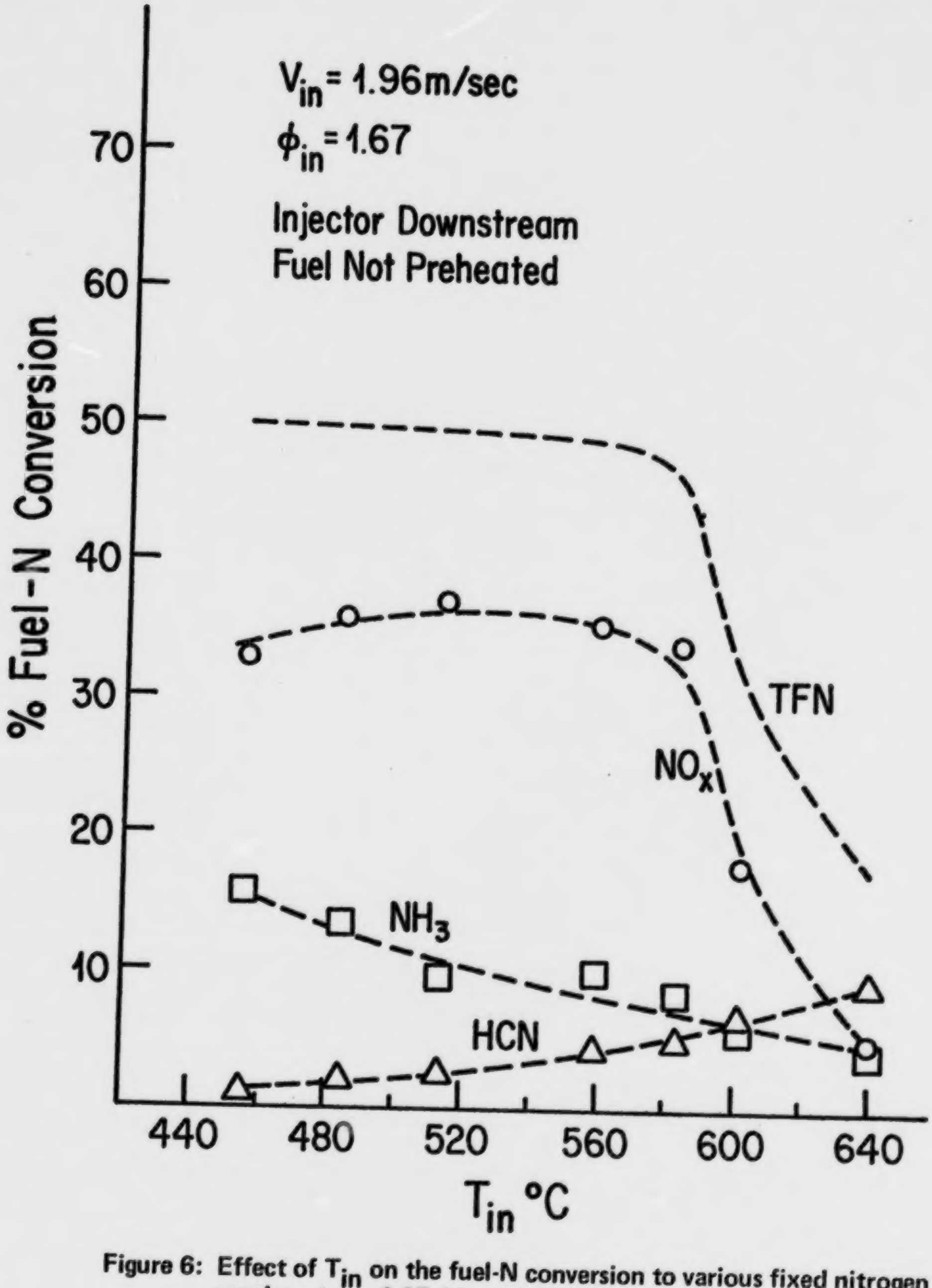

Figure 6: Effect of T_{in} on the fuel-N conversion to various fixed nitrogen species. ϕ_{in} = 1.67, V_{in} = 1.96 m/sec.

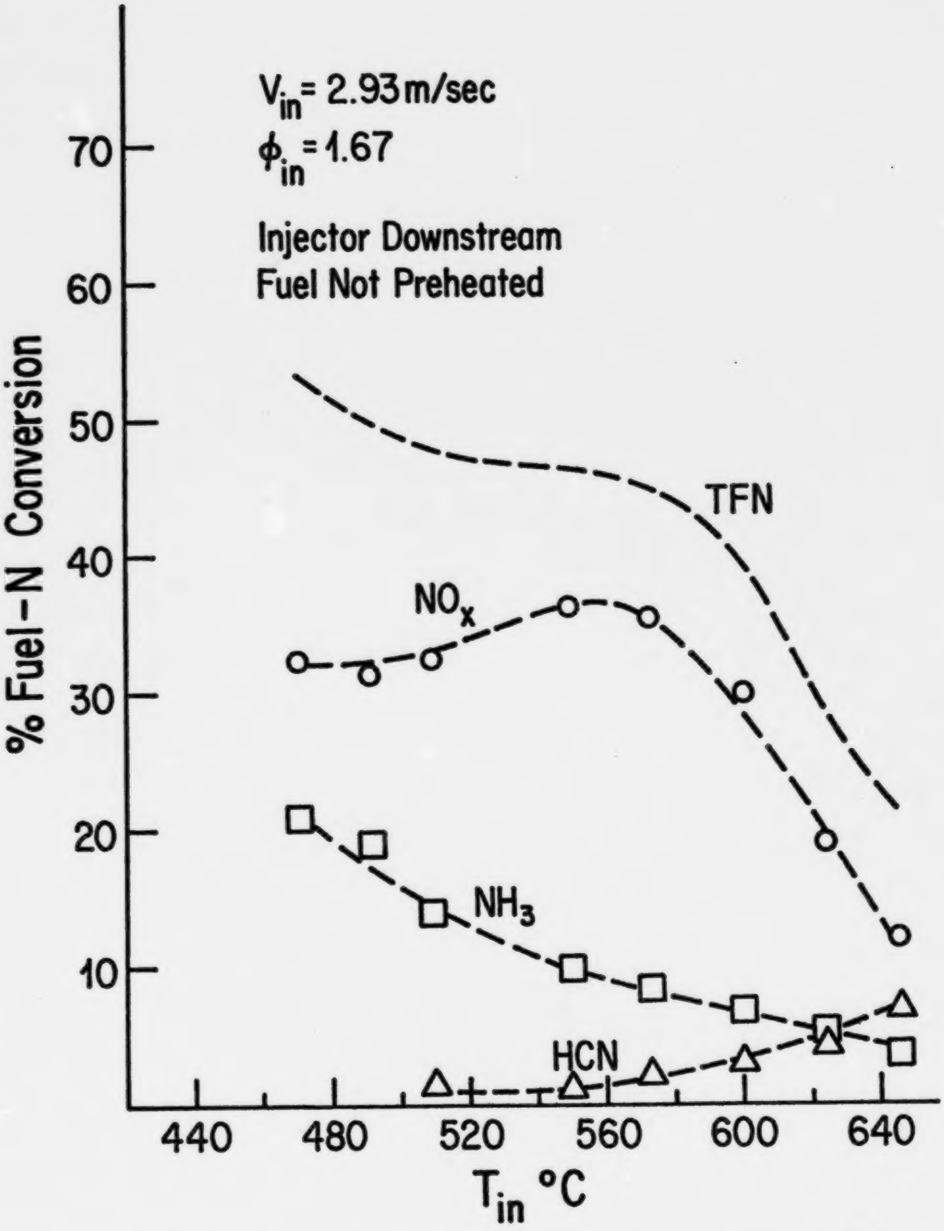

Figure 7: Effect of T_{in} on the fuel-N conversion to various fixed nitrogen species. ϕ_{in} = 1.67, V_{in} = 2.93 m/sec.

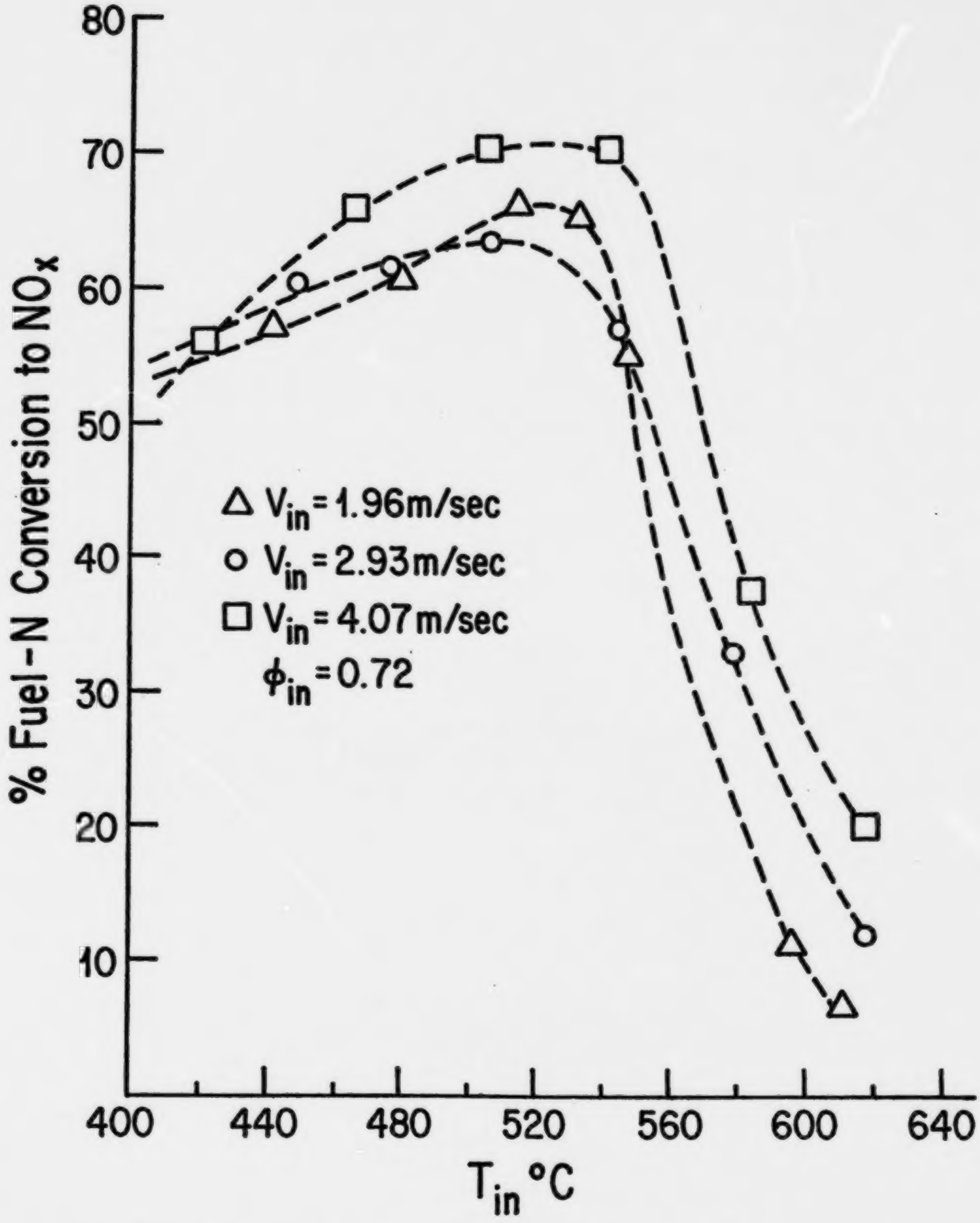

Figure 8: Effect of T_{in} on the fuel-N conversion to NO_x for various V_{in}. $\phi_{in} = 0.72$.

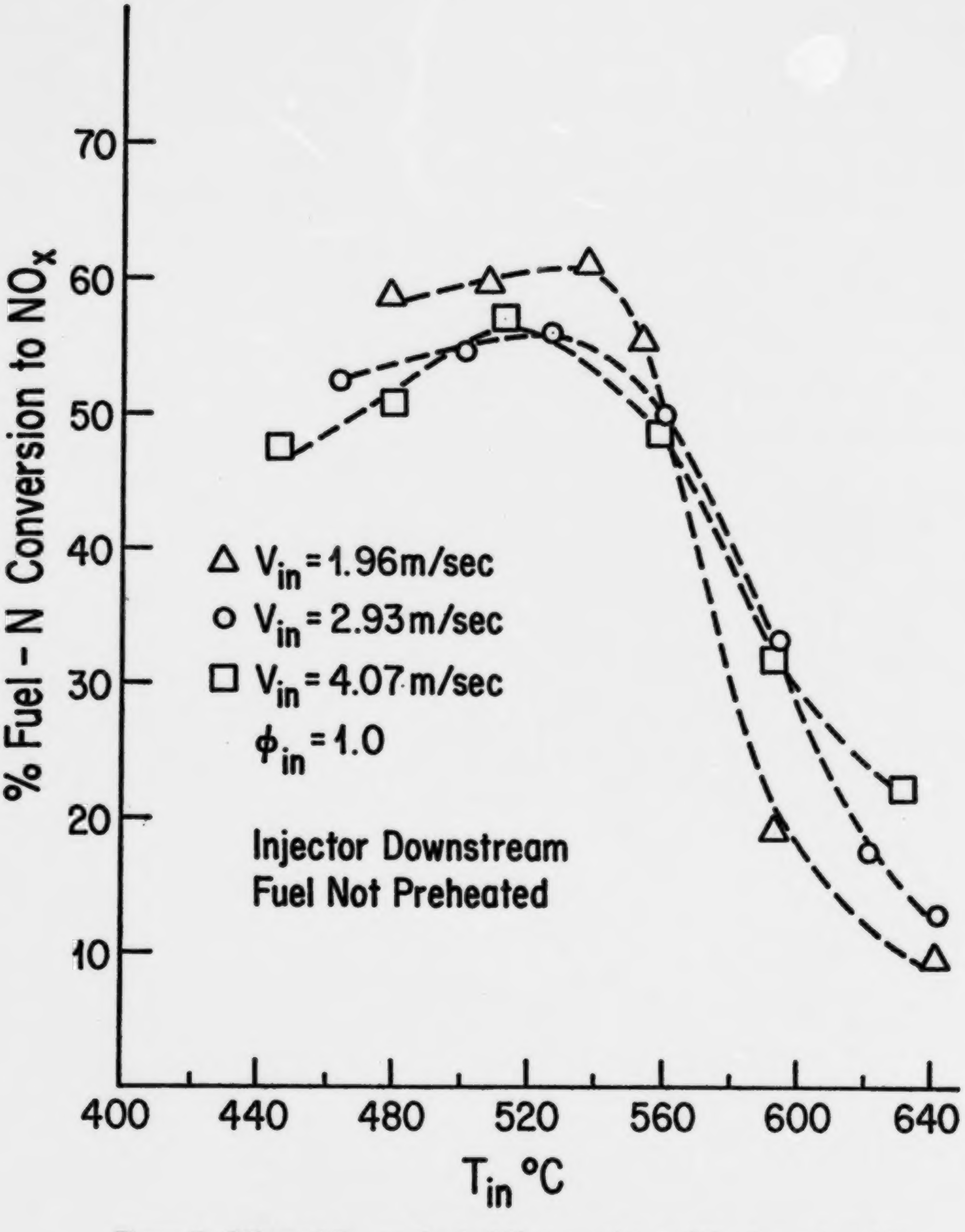

Figure 9: Effect of T_{in} on the fuel-N conversion to NO_x for various V_{in}. ϕ_{in} = 1.0.

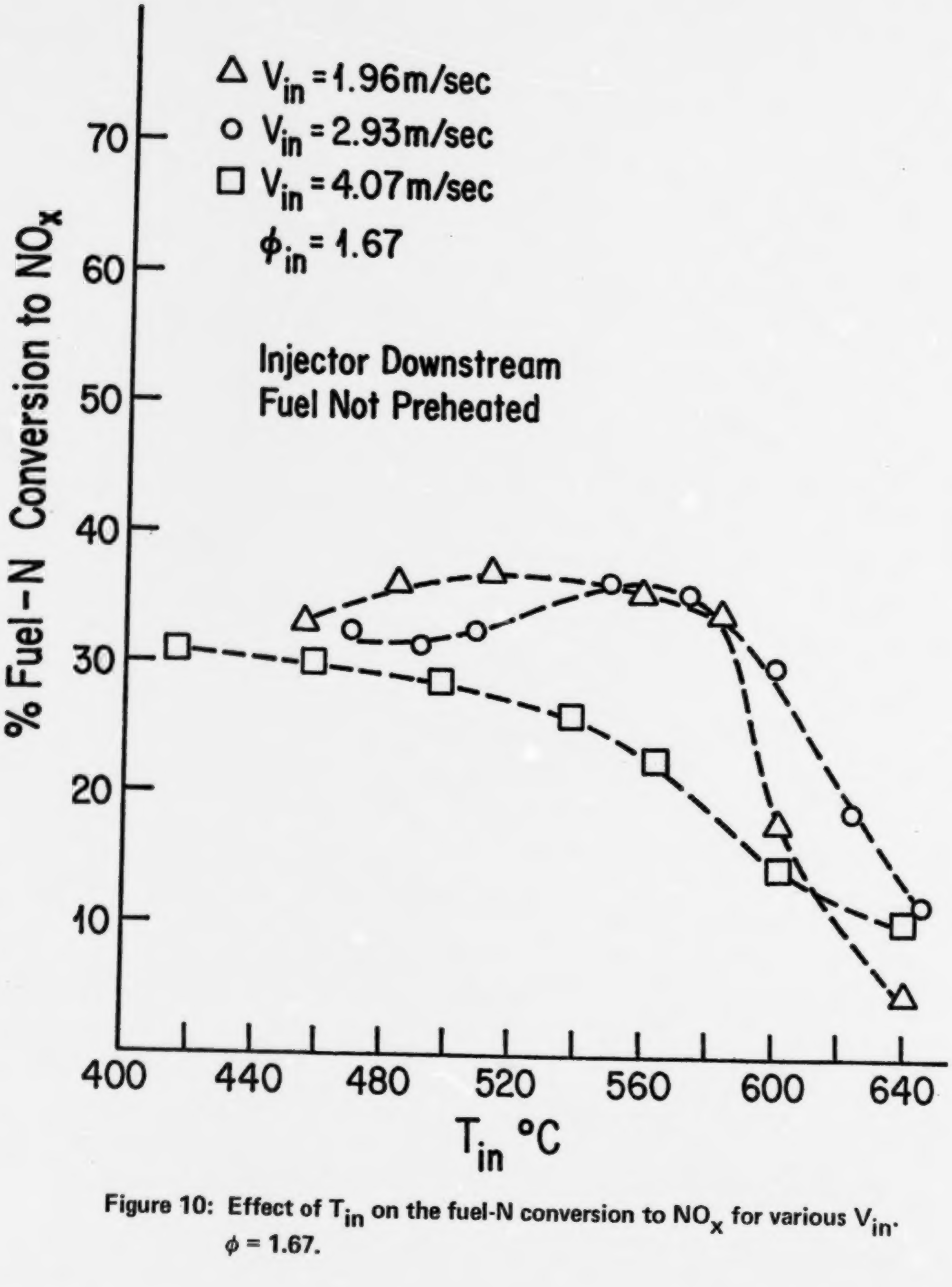

Figure 10: Effect of T_{in} on the fuel-N conversion to NO_x for various V_{in}. ϕ = 1.67.

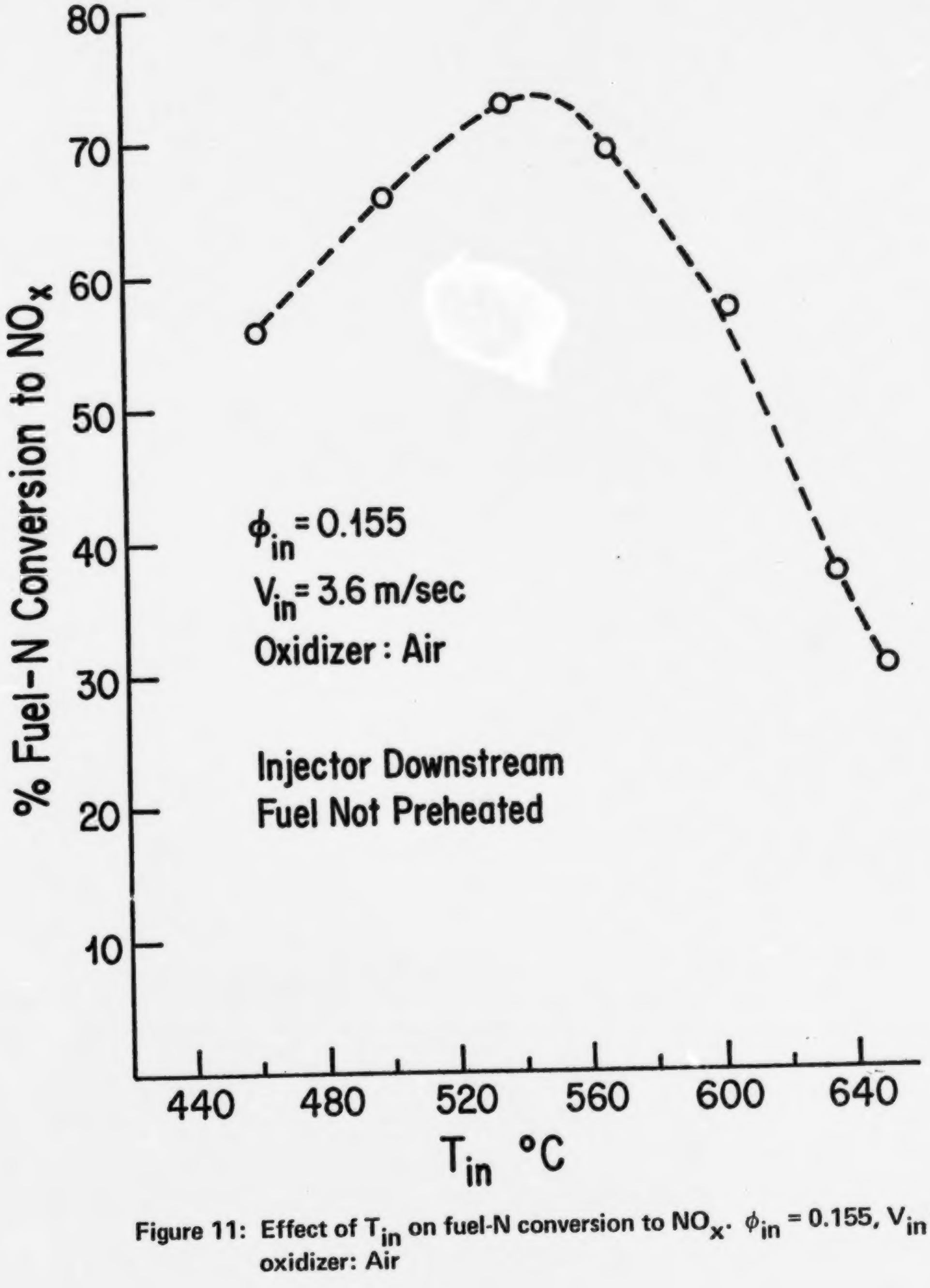

Figure 11: Effect of T_{in} on fuel-N conversion to NO_x. ϕ_{in} = 0.155, V_{in} = 3.6 m/sec., oxidizer: Air

HIGH TEMPERATURE DURABLE CATALYST DEVELOPMENT

by

G. C. Snow and H. Tong
Acurex Corporation, Energy & Environmental Division
485 Clyde Avenue
Mountain View, California 94042

ABSTRACT

An experimental program was performed to develop durable catalytic reactors for advanced gas turbine engines. Under the DOE-sponsored Gas Turbine Highway Vehicle Systems Project, administered by the NASA-Lewis Research Center, such engines are being proposed to achieve high operating efficiencies through regenerative preheat and high combustor temperatures. The objectives of the program included definition of a catalytic reactor system having a high probability of successful integration into an advanced automotive gas turbine engine, a 1000-hour demonstration of catalyst combustion durability at representative conditions, and the evaluation of laboratory furnace thermal aging as a cost effective catalytic reactor screening test. Following an extensive survey combined with furnace aging and combustion testing, a catalytic reactor was identified and (under joint NASA-Lewis EPA, and Acurex sponsorship) successfully operated for 1000 hours. This durability reactor consisted of a graded cell honeycomb support with a combination of noble metal and metal oxide catalyst coatings. At a 740 K air preheat temperature and a propane fuel/air ratio of 0.028 by mass ($\phi_{FA} = 0.44$), the adiabatic flame temperature was held at about 1700 K. The graded cell monolithic reactor measured 5 cm in diameter by 10.2 cm in length and was operated at a reference velocity of 14.0 m/s at 1 atmosphere pressure. Measured NO_x levels remained below 5 ppm while unburned hydrocarbon concentrations registered near zero and carbon monoxide levels were nominally below 20 ppm. The durability test included several parametric turndown studies and ended with a series of on/off cycling tests to further characterize reactor performance. At the completion of testing, the reactor remained catalytically active and structurally sound.

ACKNOWLEDGEMENT

The authors express their gratitude for the support provided by NASA-Lewis Research Center, Contract No. DEN3-83 and to the contract Officer, D. N. Anderson. In addition, the support provided by the U.S. Environmental Protection Agency, Contract No. 68-02-3122, and Acurex Corporation is gratefully acknowledged. Also recognized are the many individuals of the Acurex staff who were of assistance during this program.

INTRODUCTION

A compact, high efficiency gas turbine is one of the candidates for fuel efficient automobiles to be developed for the late eighties and early nineties. To achieve high operating efficiences, the gas turbine engine must operate at high turbine inlet temperature and correspondingly high average combustor temperatures. In addition, efficiency increases will be obtained through the use of regenerative heat exchangers to provide a high combustor inlet temperature. Two favored methods for low emissions gas turbine combustors are the catalytic and lean premixed combustors (Reference 1). Catalytic combustion offers wider flame stability limits and lower NO_x emissions but requires the development of catalyst and substrates which are durable at high combustion temperature.

The principal objective of this program was to develop catalytic reactors capable of operation in environments representative of those anticipated for advanced automotive gas turbine engines. Research activities prior to and during the course of this program (References 1 through 10) have demonstrated the benefits of catalytic combustion. Durability testing for up to 1000 combustion hours were reported in References 3 and 4 for adiabatic flame temperatures up to about 1530 K with No. 2 diesel fuel on 0.025 m diameter honeycomb catalysts. In this program, the combustion temperature was increased to 1700 K and the reactor diameter was increased to 0.051 m.

Nominal design combustion conditions for catalytic reactor evaluation were:

• Pressure	1×10^5 Pa
• Reference velocity	15 m/s
• Reactor inlet temperature	800 K
• Adiabatic flame temperature	1700 K
• Fuel	No. 2 diesel

Specifically, program goals were:

1. Evaluation of furnace aging as a cost-effective catalytic reactor screening test
2. Definition of a catalytic reactor system with a high probability of successful integration into an automotive gas turbine engine
3. Development of a catalytic reactor to demonstrate 1000 hours durability in the combustion of No. 2 diesel fuel with a reactor temperature of about 1700 K

To evaluate catalyst performance, four different kinds of tests were conducted. These were catalyst characterization, furnace aging, combustion at 1700 K, and parametric combustion tests. The results of these tests led to the selection of a reactor for long life durability testing. The durability test program was modified after the original candidate failed to complete the planned 1000 hours of combustion time. A new and different reactor was prepared and tested with propane (rather than diesel) at 1700 K for the planned 1000 hours. At an air preheat of 740 K and 1 atmosphere combustor pressure, the reference velocity was 14.0 m/s. Measured NO_x levels remained below 5 ppm while unburned hydrocarbon concentrations registered near zero and carbon monoxide levels were nominally below 20 ppm. The durability test included several parametric turndown studies and ended with a series of on/off cycling tests to further characterize reactor performance.

The program results show that materials are not yet available for high temperature catalytic combustion applications such as the advanced automotive gas turbines. However, the 1000 hours of combustion at 1700 K show that there is a high probability that materials and systems could be developed in the next 5 years to meet the durability requirements of the advanced automotive as well as stationary power plant gas turbines.

EXPERIMENTAL FACILITIES

Preliminary catalyst evaluation as well as the investigation of long term high temperature effects on substrates and coatings was conducted in a laboratory furnace. The low cost and ease of furnace testing makes it a potentially valuable tool for initial screening of catalyst material durability for systems known to have significant catalytic activity. However, it does not provide a direct evaluation of combustion performance since catalyst surface reactions and fluid transport are not simulated. The furnace aging facility, installed at Catalysis Research Corporation in Palisades Park, New Jersey, is a "Unique Kiln" gas-fired model, Model U.S.-A-6, rated to 1756 K, with a 0.170 cubic meter load space (constant temperature zone). The chamber size is 61.0 cm by 53.3 cm with an overall size of 168 cm by 117 cm by 112 cm. The oven temperature is automatically regulated with a Baker Coleman Model 202C controller. Excellent temperature control was shown by a close temperature-time agreement between and within furnace runs.

For aging tests the catalysts are placed in the center of the furnace, supported by a plate of silicon carbide raised off the floor of the furnace. The catalyst test area is surrounded by six plates of silicon carbide, which shield the catalysts from the radiation of the furnace walls. Each catalyst is supported (within its sheath) by a small piece of alumina, so catalysts do not rest on the silicon carbide base plate.

Due to the large refractory mass of the furnace, it was not possible to obtain information on thermal shock effects on the substrates, only time-at-temperature effects could be deduced. Typical kiln heat-up times were programmed to attain 1700 K in about 5 hours. Following a prescribed number of hours at 1700 K, the furnace gas and air flow was terminated and the furnace allowed to cool for about 24 hours or until the sample temperatures were less than 500 K before the kiln was opened to the atmosphere.

All combustion testing for screening, parametric studies, and durability evaluation were performed in the Acurex catalytic combustion test faciliites which are described in detail elsewhere (References 6, 11). A schematic of the test rig is shown in Figure 1. The catalytic reactors were mounted within a test section using a compliant wrap of ceramic fiber insulation felt and castable refractory. The test section was oriented vertically with the combustion mixture flowing from top to bottom. Combustion air was preheated through electrical resistance elements before mixing with gaseous or atomized liquid fuels. In operation, propane was used as a lightoff and preheating fuel except in the final durability test in which it was the test fuel. The flow rates of the propane and air were measured by glass tube rotameters as was the No. 2 diesel liquid fuel. Emissions measurements of carbon species and oxygen was used as a final check on fuel/air ratio and corresponding fuel flow rate.

Gas samples were collected about 20 cm downstream of the reactor with a water-cooled stainless steel sample probe. The measurement of major product spcies, CO_2, CO, unburned hydrocarbons, O_2, and NO_x, was accomplished by continuous flow analyzers (Reference 11).

Temperature measurements were taken upstream and downstream of the reactor bed as well as within the bed itself. Chromel versus alumel (K-type) thermocouples were used upstream to measure the preheat temperature entering the reactor. Exit gas temperature was monitored by a K-type thermocouple located near the entrance to the sample probe. Bed temperature measurements were taken with up to six in-depth thermocouples, platinum versus platinum with 13 percent rhodium (R-type).

CATALYST SELECTION AND SCREENING

The ultimate selection of a catalytic reactor was based on a series of extensive screening and aging evaluations. Measurements of BET surface area and noble metal dispersion (Reference 11) (when allowed by catalyst manufacturers) were utilized to characterize the catalyst surfaces throughout the selection process. The overall approach is represented in Figure 2. The preliminary furnace aging evaluation provided an initial screening of catalyst candidates and their response to a 24 hour exposure to a 1700 K environment. From these, six catalysts were subjected to combustion screening, longer term furnace aging and parametric combustion tests. Finally, a reactor was selected for a 1000 hour combustion durability test at the aforementioned conditions.

Early in the program, catalyst manufacturers and suppliers were surveyed to obtain recommendations for catalysts to meet the program goals. These recommendations along with prior combustion experience were combined with a similar selection process for substrate materials to identify 14 reactor concepts for preliminary furnace screening. A list of the catalytic reactors, their suppliers, and general descriptions are given in Table I. The ATT-B and ATT-C reactors consisted of a bundle of active substrate tubes supplied by Trans-Tech, Inc. The bundle, measuring 7.62 cm in length and 5.08 cm in overall diameter, was oriented so that the tube axes were parallel to the reactant flow stream during combustion testing. The remaining reactors in Table I were 6.35 cm in diameter and consisted of three segments to give an overall length of 7.62 cm.

The results of the preliminary furnace aging tests were not as conclusive as desired. In general, all of the materials survived the test with only minor observable damage. Since combustion testing was not performed, conclusions about the potential combustion performance of each reactor could only be implied from the post-test characterization measurements and previous combustion experience with similar reactor concepts. Table II summarizes these observations. The post-test characterization measurements showed a significant decrease in BET surface area and catalyst dispersion (for noble metal reactors). Within the accuracy of the measuring apparatus, the BET surface area of all reactors was reduced to essentially zero due to the 24 hour exposure at 1700 K. For noble metal group, UOP-A, UOP-B, UOP-C, MBI-B and HAP-A, the three that had Torvex substrates (UOP-A, UOP-C and MIB-B) appeared to have washcoat-to-substrate bonding problems. This was evidenced by blistering, flaking or delamination of the washcoat and catalyst coating. The two reactors with MCB-12 substrates were visually good after the aging test. The WRG-A and ATT-D reactors appeared to have suffered significant volatilization of their catalyst coatings. Except for a slight darkening of OC-B, the remaining candidates showed little, if any, visual degradation from the 24 hour test.

The above results led to the selection of five reactors: UOP-B, OC-B, ATT-A, ATT-C, and ATT-E for further evaluation. Based on the delamination problems of washcoats on Torvex alumina substrates, the proprietary MBI coating was applied to an MCB-12 substrate and included with the others for further testing. This reactor was designated MBI-D. Samples of each of the six reactors were prepared for furnace aging and combustion screening tests. Separate samples were aged for periods of 24, 180, 430, 680, and 1000 hours at 1700 K in the furnace. Also, a sample of each reactor was aged for 24 hours, combustion tested, aged for an additional 1000 hours, and combustion tested again. Combustion screening was conducted at the nominal design conditions of pressure, reference velocity, and temperature with No. 2 diesel fuel. Combustion tests included parametric sequences in which the fuel/air ratio was progressively decreased until an increase in carbon monoxide or unburned hydrocarbons was detected. The point at which combustion degradation occurs is representative of the level of catalyst activity. With all other parameters constant, a comparison of minimum fuel/air ratio or minimum stable catalyst temperature achieved from test to test indicates changes in catalyst activity. At various times, samples were characterized by measuring their BET area and, where applicable, the noble metal dispersion.

From the furnace aging part of the screening tests, it is apparent that chemical and physical changes could be induced by long exposure to elevated temperatures. However, the inability to cause rapid temperature cycling did not subject the reactors to thermal stresses which would be representative of combustion conditions. Further, from previous combustion experience with some of the reactor materials, the catalyst depletion rate appears to be very slow in the furnace when compared to combustion results. This is apparently due to the very low convection rates in the catalyst during furnace aging.

All substrates tested in the furnace exhibited significant degradation in mechanical strength after 1000 hours at temperature. On some materials, similar degradation has been observed after about 10 to 20 hours of combustion testing. The furnace is therefore a very conservative measure of the effects of temperature on mechanical properties.

After 24 hours of aging, combustion could be achieved on all samples although not necessarily at the prescribed baseline conditions. Of the six reactors parametrically tested, the most active was UOP-B. For this reactor, combustion was stable and uniform throughout the parametric test matrix. Qualitatively the remaining reactors are ranked in the following order of decreasing combustion performance. ATT-A, MBI-D, ATT-E, OC-B, and ATT-C. For the last two reactors, it was very difficult to achieve stable combustion conditions even at very low reference velocities.

After 1000 hours of furnace aging none of the reactors would sustain stable combustion. All samples examined with SEM/KEVEX showed silicon on the surface and this may be part of the reason for the inability to achieve stable combustion conditions for these samples. The silicon, in the form of silica, apparently had a poisoning or shielding effect on the catalyst. This condition undoubtedly was an artifact of the aging procedure within the silicon carbide lined furnace.

Since the combustion ability of the reactors after 1000 hours of aging may have been masked by silica coatings, the selection of a reactor for durability testing was based on the parametric test results following 24 hours of aging. Of the six reactors, UOP-B was clearly the most active and stable. A sample of this reactor which had been subjected to 24 hour furnace aging was used in the following combustion durability test.

DURABILITY TESTING

The durability test plan was to combustion test at steady conditions for 24 hours, then shut down and perform characterization measurements on the sample. The sample would then be reinstalled in the catalytic test facility and combustion tested continuously for 1000 hours or until such time that the catalyst became inactive. At various intervals, a parametric test series would be run to determine any change in the lowest temperature at which high combustion efficiency could be maintained. Following lightoff and ignition with propane fuel, operation on No. 2 diesel fuel was established at the nominal design conditions. A chronological event chart is shown in Figure 3 which indicates a test termination far short of the planned 1000 hours. Initially, CO and NO_x emissions both remained below 15 ppm and unburned hydrocarbons measured zero. Initial parametric tests also indicated good catalytic activity. However, the condition of the catalyst and the substrate degraded giving eventually poor performance. After 80 hours of operation, a dark area covering 10 to 20 percent of the cross section was observed on the back face of the reactor. At about 110 hours, the center of the exit catalyst element fractured and a number of small pieces fell away. Fracturing continued and at 200 hours into the test, essentially all of this element had fallen away leaving only two remaining elements. At this point, CO emissions climbed to about 30 ppm and NO_x levels reached 20 ppm indicating decreased catalytic combustion but continued homogeneous gas phase reactions. After 226 hours, the reactor was functioning primarily as a flameholder becoming unstable and oscillatory at 250 hours. At 283 hours, a fuse for the air preheaters failed causing a facility shutdown and test termination.

The remaining catalyst segments were removed from the facility for examination. These segments also exhibited fracture damage and the substrate was much weaker than untested material, but otherwise these two segments were intact. The physical appearance of the surface suggested that there was very little active noble metal left on the reactor. A subsequent dispersion measurement indicated essentially zero dispersion.

The durability test showed that available catalysts and substrates were not adequate to meet the advanced automotive gas turbine combustion conditions.

PHASE II SELECTION AND DURABILITY TEST

The objective of the Phase II effort was to evaluate newly available catalyst and substrate materials which had the potential for meeting program goals. It was clear that concentration should be on materials that have low vapor pressures at elevated temperatures and good high temperature stability. Thus, current technology noble metal catalyst would not be acceptable, at least in the catalyst sections where high temperatures are to be sustained. New developments here were directed towards metal oxides that could be applied to a honeycomb substrate by slurry coating or solution impregnation. Two new materials were selected based on a limited amount of available data that suggested good structural behavior under combustion conditions. Table III gives a summary description of each of the newly selected candidates.

Three different honeycomb materials were used in Phase II. Two of these, JNM and JNX, were proprietary materials from a ceramics manufacturer and one was a magnesium-aluminum-titanate (Corning MCB-1). In contrast to the uniform cell density used in the previous reactors, approximately 15.5 cells/cm^2 (100 cells/in^2), the honeycombs used here were of various densities. The large cell entrance segments contained 1.40 cells/cm^2 (9 cells/in^2) and the finest cell exit segments had 31.0 cells/cm^2 (200 cells/in^2). The graded cell configuration (Reference 12) enhances stable ignition of the incoming reactants on the lower activity metal oxide catalysts while still providing sufficient surface area to promote complete combustibles conversion. All substrate elements were 5.0 cm in diameter by 2.5 cm in length.

Catalyst coating selections were based on a combination of previous experience, estimated or known vapor pressures, anticipated high temperature stability, and an estimate of potential catalytic activity at high temperatures. Catalyst materials included lanthanum/chromium oxide, yttria/chromium oxide and magnesium aluminate iron ferrite (MAFF) which were slipcoated on the substrates and a terbium/cerium/thorium oxide which was coated by solution impregnation and calcination. The slipcoating method puts a distinct surface layer of the oxide catalyst onto the substrate. The solution impregnation method allows the formation of catalyst throughout the depth of the substrate webs. Slipcoated reactors were sintered at 1700 K and solution impregnated reactors were calcined at about 1200 K.

Graded cell catalytic reactors were assembled using four elements for the JNM and JNX substrate materials and three elements for the MCB-1 material. These reactors were not subjected to furnace screening and aging but underwent combustion screening and parametric testing as previously described.

Five of the eight candidate catalysts were not active at the combustion conditions tested. These were the MAFF and LaCr formulations on both MCB-1 and JNM substrates and the YCr catalyst on the JNM substrate. Three reactors, however, did demonstrate limited catalytic activity and allowed the collection of combustion data. In order of increasing apparent performance, these were the YCr/MCB, TCT/JNX, and TCT/JNM reactors. Each reactor required very high surface temperatures before activity was sustained, indicating low catalytic activity. In addition, measured catalyst temperatures were often up to 25 percent below the corresponding adiabatic flame temperature. Of the three reactors which were able to sustain combustion, the TCT/JNM formulation gave the best performance. This judgement was based on reactor temperature and emission measurements as well as physical appearance. The structural performance of the substrate was at least as good as that of any of the eight reactors tested.

Based on the accumulated test experience in this program, it appeared that, individually, neither the noble metal nor the metal oxide catalyst approach would be appropriate for meeting the autmotive gas turbine goals. Noble metals do not have the required durability at high temperatures and metal oxides do not have sufficient catalyst activity to achieve stable combustion conditions over anything other than a very small temperature range. A combination reactor was therefore designed using the graded cell concept described in Reference 12.

The reactor design for the Phase II durability tests is a first attempt at applying the graded cell concept to incorporate the strength and weaknesses of current noble metal and metal oxide catalyst technology. The basic premises are:

1. With consideration for kinetic rates and heat and mass balances, the graded cell approach can be used to attain specific reactor temperature distributions.
2. Noble metal catalysts have excellent activity, especially at low temperatures, but cannot be used for sustained high temperature application.

3. Metal oxide catalysts are believed to have good high temperature durability but do not have sufficient activity for low temperature operation except possibly with high inlet gas preheat.

The noble metal leading element was designed to operate at a temperature of 1400-1500 K at which good durability has been shown in previous programs (References 2 and 6). This element would essentially be a preheater for the metal oxide elements which would achieve the 1700 K nominal operating temperature. Figure 4 represents the reactor configuration and gives descriptions of the substrate and catalyst.

Because of some difficulties encountered in achieving a uniform, premixed, prevaporized diesel fuel mixture, the Phase II durability tests were conducted using propane fuel at the following nominal conditions:

•	Pressure	1×10^5 Pa
•	Reference velocity	14 m/s
•	Reactor inlet temperature	730 K
•	Adiabatic flame temperature	1700 K
•	Stoichiometry	$\phi_{FA} = 0.43$

Representative combustion data are shown in Table IV. At the above conditions, there were no measurable unburned hydrodarbons, carbon monoxide levels on a dry basis were consistently below 20 ppm, NO_x levels were below 5 ppm, and calculated combustion efficiencies were above 99.9 percent. A chronology of events for this durability test is shown in Figure 5. During the testing period, seven parametric tests were conducted and the catalyst was shut down and restarted six times. After 1002 hours, the testing was continued with five on/off cycles, a final parametric test and a short period of operation on diesel fuel.

The emissions performance of the reactor during the durability test is given in Figures 6 and 7. The plots show only a fraction of the total amount of data, as measurements were recorded approximately every 2 hours. Figure 6 shows that the O_2 and CO_2 levels remained fairly level throughout the test, indicating the steady state operation. The parametric tests appear as points of reduced CO_2 and increased O_2 as the fuel/air ratio was decreased. The drift in oxygen level was probably due to a malfunctioning O_2 analyzer which ultimately failed at about 890 hours. A comparison of CO_2, CO, and UHC levels with input fuel flow results in a carbon balance fuel/air ratio within 5 to 8 percent of the metered fuel/air ratio.

The average carbon monoxide concentration in the exhaust sample apparently increased slighly throughout the test, as indicated in Figure 7 and is probably due to slow catalyst deactivation. UHC concentrations remained essentially zero during steady state operation. The measurements shown in Figure 7 appear to be primarily instrument noise. Parametric testing data was omitted from Figure 7. Figure 8 shows that the calculated combustion efficiency remained high throughout the tests. The only major influence on combustion efficiency was the parametric tests.

NO_x emissions levels are not shown since a malfunctioning chemiluminescent analyzer did not allow successive measurements. The instrument was operating at the beginning of the test and concentrations of from 1 to 3 ppm were recorded. A temporary repair at 740 hours gave a measurement of 4 ppm. The analyzer was fully operational prior to the on/off cycling tests and measured levels ranged from 2 to 5 ppm. The sample probe positioning 20 cm downstream of the catalyst exit undoubtedly allowed continued gas phase oxidation to potentially reduce levels of combustibles. Indeed, this region downstream of the catalytic reactor is an important design parameter, and significant performance and emissions benefits can be realized if it is incorporated into an application (Reference 13). However, downstream combustion is no substitute for efficient catalytic combustion and flameholding will not mask a poorly performing catalyst. To achieve low levels of CO and NO_x in combustors with reasonable residence times, catalytic surface reactions must dominate the process. It has been shown (Reference 14) that, during fuel-lean catalytic combustion, most hydrocarbons, including propane, convert to CO_2 and H_2O at the surface without forming CO. A poorly performing catalyst operating primarily as a flameholder will generate high levels of CO through gas phase fuel reactions. At the present reference velocity (14 m/s) insufficient residence time is available for complete conversion of CO to CO_2 before the sample probe is encountered or the flow enters the turbine section in an actual application. In addition, significant amounts of gas phase combustion will produce high levels of thermal NO_x (Reference 2).

A total of eight parametric tests were included in which the fuel/air ratio was progressively decreased until an increase in carbon monoxide or unburned hydrocarbons was detected. Plots of combustion efficiency versus catalyst temperature are shown in Figures 9 and 10. Curiously, the parametric tests indicated improving catalytic activity with increasing time.

Following the life test, the reactor was removed for inspection. The surface appeared much lighter in color, indicating a probable loss of catalyst coating. Structurally, the monolith had distorted slightly and fused to the refractory holder, but major cracks, loss of substrate, or other damage had not occurred. Photographs of the noble metal lead element and the metal oxide exit segment in the refractory holder are shown in Figures 11 and 12, respectively.

The catalyst was reinstalled for the on/off cyclic tests which resulted in the performance plot of Figure 13. Prior to each lightoff of the catalyst, the bed temperature was brought to about 750 K by passing preheated air over the reactor for about 1 hour. The first lightoff was performed with the opposed jet igniter while the subsequent four lightoffs were catalytic. Following each lightoff, temperature and emission data were collected over a 1- to 2-hour period before shutdown. The reactor was allowed to cool to room temperature following shutdown before the next lightoff. During the last cycle, a final parametric test was conducted to note any further changes in activity. A final inspection of the disassembled reactor revealed no further damage or change due to the cycling tests.

Although the Phase II durability test was conducted with propane rather than diesel fuel, it demonstrated that a catalytic reactor could be designed to operate at 1700 K for extended periods. After more than 1000 hours of sustained combustion, the reactor was still active and structurally complete. However, some loss of catalyst and distortion of the substrate was apparent. Loss of the metal oxide catalyst was surprising since the oxides of terbium, cerium and thorium have very high vaporization temperatures. Apparently even with very low vapor pressures, significant amounts of oxide may be removed by the high mass transfer and combustion conditions in the reactor. The distortion of the JNM substrate is believed to be a result of continued sintering of the honeycomb material. Surprisingly, the uneven sintering did not cause structural failures.

CONCLUSIONS AND RECOMMENDATIONS

The combustion results of this program demonstrate that efficient stable combustion can be achieved at advanced automotive gas turbine conditions. It was shown that reactors can be fabricated for at least 1000 hours of service at combustion temperatures of 1700 K and 14 m/s reference velocity. At the conclusion of 1000 hours, the reactor was still active so that its ultimate life was not determined. However, some catalytic material was lost and the substrate was distorted by the sustained high temperatures. Thus some degradation of the reactor was occurring and further development activities should be directed at:

- The design of graded cell-graded catalyst reactors to obtain optimum operating temperatures for various catalytic materials including noble metal entrance segments and subsequent metal oxide elements
- The development of metal oxide catalysts with lower depletion rates, better application methods, and active substrate potential
- Improved long-term high-temperature sustrate life
- An evaluation of the durability of a graded cell-graded catalyst reactor concept with No. 2 diesel fuel at gas turbine operating pressures.

It was also concluded that hour-for-hour, furnace aging was not representative of combustion operation on honeycomb catalytic reactors. Depletion rates of catalyst materials during furnace aging were significantly below that for combustion operation at the same temperature. This may be due to a combination of chemical effects, more vigorous convective forces, and dilute free stream conditions during combustion. Silicon from the furnace refractory was found to have deposited on the surface of the aged reactors which probably contributed to their poor combustion performance. Furnace aging is still considered an attractive and cost effective substitute but these problems must be remedied before this is successful.

REFERENCES

1. Mumford, S. E., Hung, W. S. Y., Singh, P. P. A Potential Low-NO_x Emission Combustor for Gas Turbine Using the Concept of Hybrid Combustion. Journal of Engineering for Power, p. 361, October 1977.

2. Kesselring, J. P., et al. Catalytic Combustion Component and System Prototype Development. Second Annual Report, EPA Contract No. 68-02-3122, Acurex Corporation, Mountain View, California, November 1980.

3. Heck, R. M., et al. Durability Testing at One Atmosphere of Advanced Catalysts and Catalyst Supports for Automotive Gas Turbine Engine Combustors, Part 1. Final Report, NASA CR-135132, Engelhard Minerals and Chemicals Corporation, June 1977.

4. Olson, B. A., et al. Durability Testing at 5 Atmospheres of Advanced Catalysts and Catalyst Supports for Gas Turbine Engine Combustors. Final Report, DOE/NASA/9416-802, NASA CR-159839, Engelhard Minerals and Chemicals Corporation, April 1980.

5. DeCorso, S. M., et al. Catalysts for Gas Turbine Combustors -- Experimental Test Results. Journal of Engineering for Power, p. 159, April 1977.

6. Chu, E. K., Snow, G. C., and Tong, H. Catalytic Combustion of Coal-Derived Liquid Fuels. Final Report, AP-1666, Research Project 989-3 for EPRI, Acurex Corporation, Mountain View, California, January 1981.

7. Krill, W. V., Kesselring, J. P., Chu, E. K. and Kendall, R. M. Catalytic Combustion for System Applications. ASME publication 79-HT-54, Joint ASME/AIChE 18th National Heat Transfer Conference, San Diesgo, California, August 8, 1979.

8. Bulzan, D. L. and Tacina, R. R. Catalytic Combustion of Coal-Derived Liquids. DOE/NASA/10350-21, NASA TM-81594, Twenty-Sixth Annual Gas Turbine Conference, Houston, Texas, March 8-12, 1981.

9. Kaye, S. E., et al. Development of A System to Utilize Flue Gas from Enhanced Recovery Underground Combustion Projects. SPE-8360, 54th Annual Fall Technical Conference and Exhibition of the Society of Petroleum Engineers of AIME, Las Vegas, Nevada, September 23-26, 1979.

10. Development of a Catalytic Combustor for Aircraft Gas Turbine Engines. Technical Report AFAPL-TR-76-80, Government Research Laboratories, Exxon Research and Engineering Company, Linden, New Jersey, September 1976.

11. Tong, H., Snow, G. C., Chu, E. K., Chang, R. L. S., Angwin, M. J. and Pessagno, S. L. Development of High Temperature Durable Catalyst for Use in Catalytic Combustors for Advanced Automotive Gas Turbine Engines. Final Report, NASA CR-165396, Acurex Corporation, Mountain View, California, June 1981.

12. Kesselring, J. P., Krill, W. V., Atkins, H. L., Kendall, R. M., and Kelly, J. T. Design Criteria for Stationary Source Cataytic Combustion Systems. EPA-600/7-79-181, 1979.

13. T'ien, J. S. and Anderson, D. N. Gas Phase Oxidation Downstream of a Catalytic Combustor. DOE/NASA/1040-16, NASA TM-8155, Thirteenth Middle Atlantic Regional Meeting of the American Chemical Society, West Long Branch, New Jersey, March 19-23, 1979.

14. Schwartz, A., Holbrook, L. L., and Wise, H. Catalytic Studies with Platinum and Palladium. Journal of Catalysis, Vol. 21, pp. 199-207, 1971.

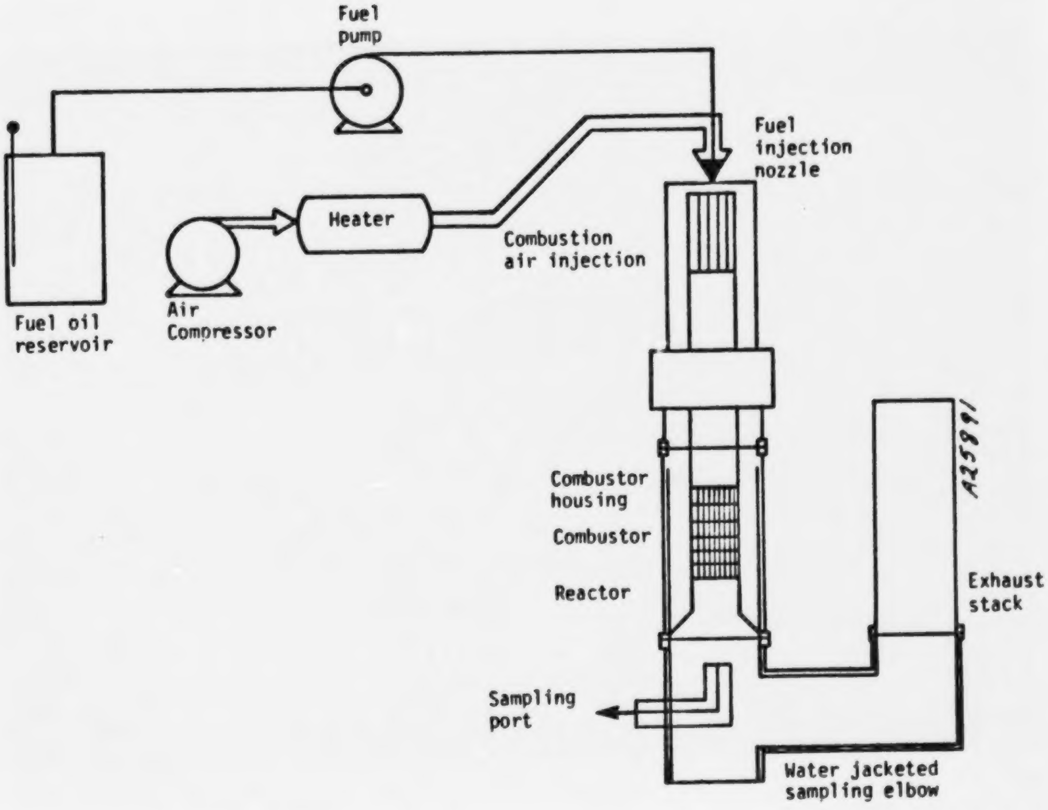
Fuel pump
Fuel injection nozzle
Heater
Combustion air injection
Fuel oil reservoir
Air Compressor
A25891
Combustor housing
Combustor
Reactor
Exhaust stack
Sampling port
Water jacketed sampling elbow

Figure 1. Catalytic combustion test rig.

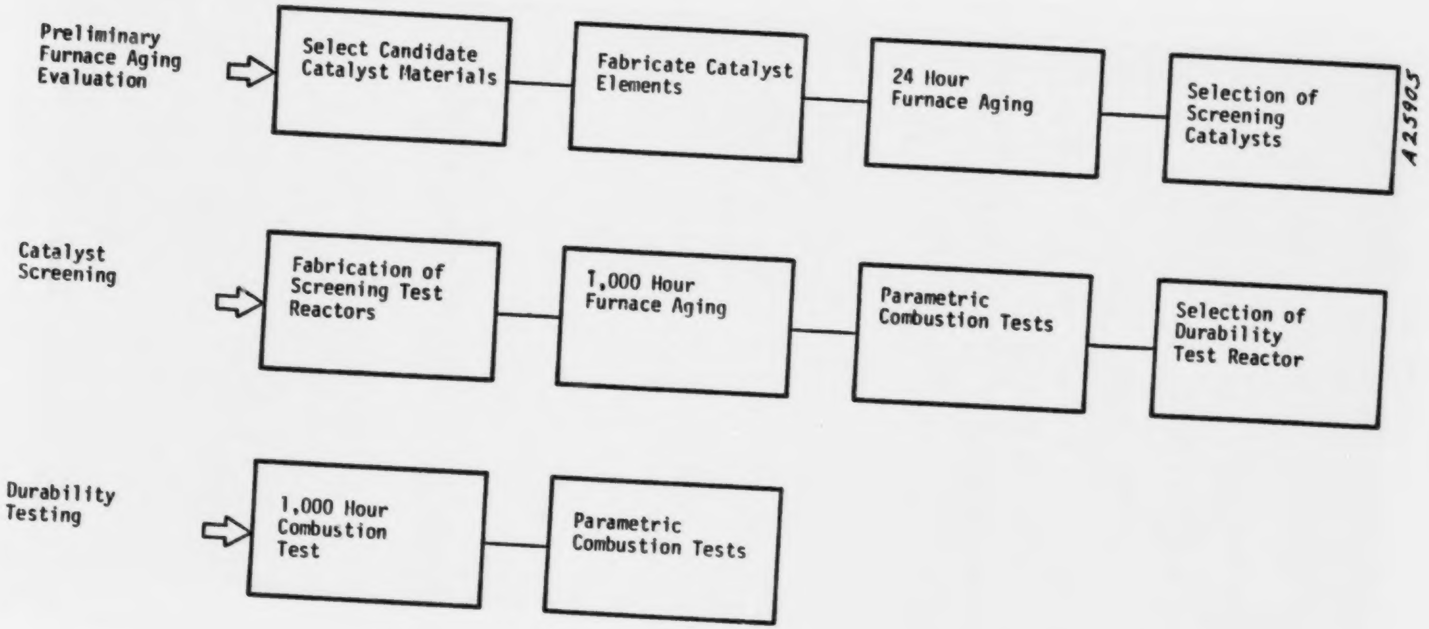
Preliminary Furnace Aging Evaluation
Select Candidate Catalyst Materials
Fabricate Catalyst Elements
24 Hour Furnace Aging
Selection of Screening Catalysts
A25905
Catalyst Screening
Fabrication of Screening Test Reactors
1,000 Hour Furnace Aging
Parametric Combustion Tests
Selection of Durability Test Reactor
Durability Testing
1,000 Hour Combustion Test
Parametric Combustion Tests

Figure 2. Program approach.

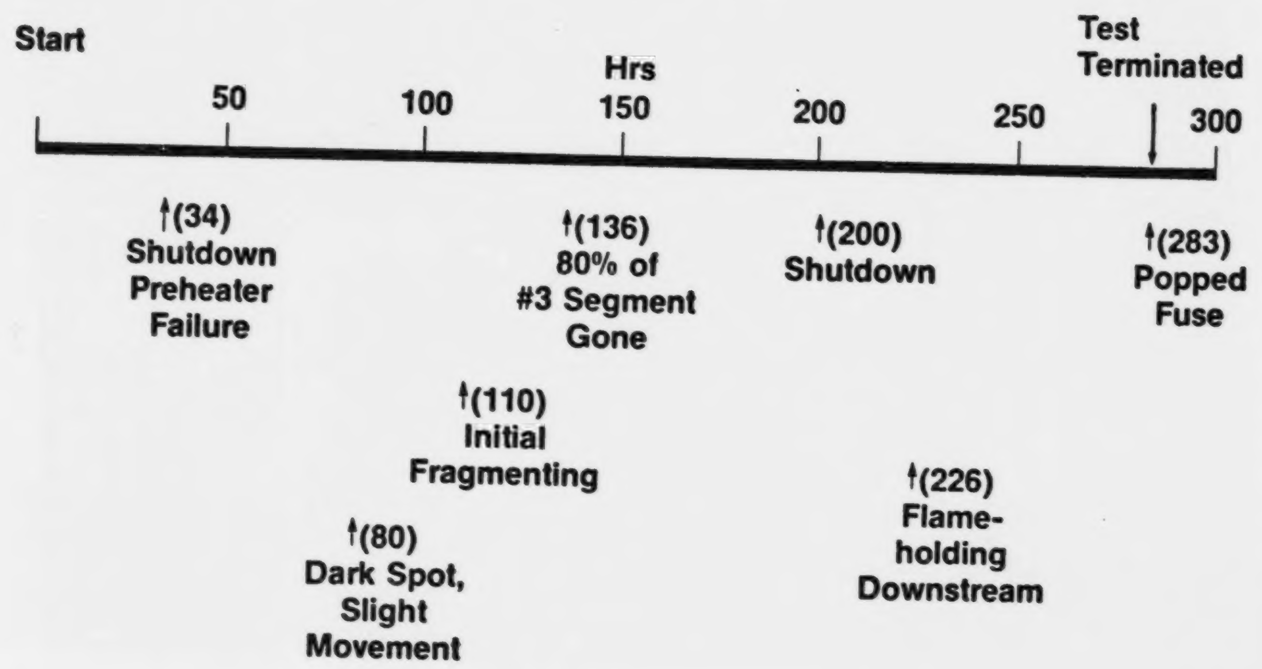

Figure 3. Combustion durability test.

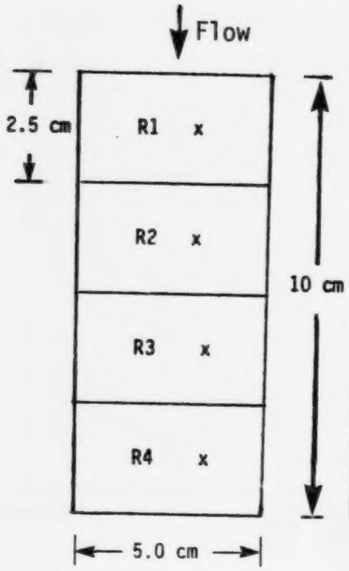

Element No.	Substrate	Catalyst
1	Corning MCB-12 16 Cells/in^2, square	UOP-B
2	JNM 9 Cells/in^2, square	Terbium, Cerium/ Thorium oxides 12 percent weight
3	JNM 16 Cells/in^2, square	Terbium, Cerium/ Thorium oxides 12 percent weight
4	JNM 6 Cells/in^2, square	Terbium, Cerium/ Thorium oxides 12 percent weight

Figure 4. Phase II durability reactor.

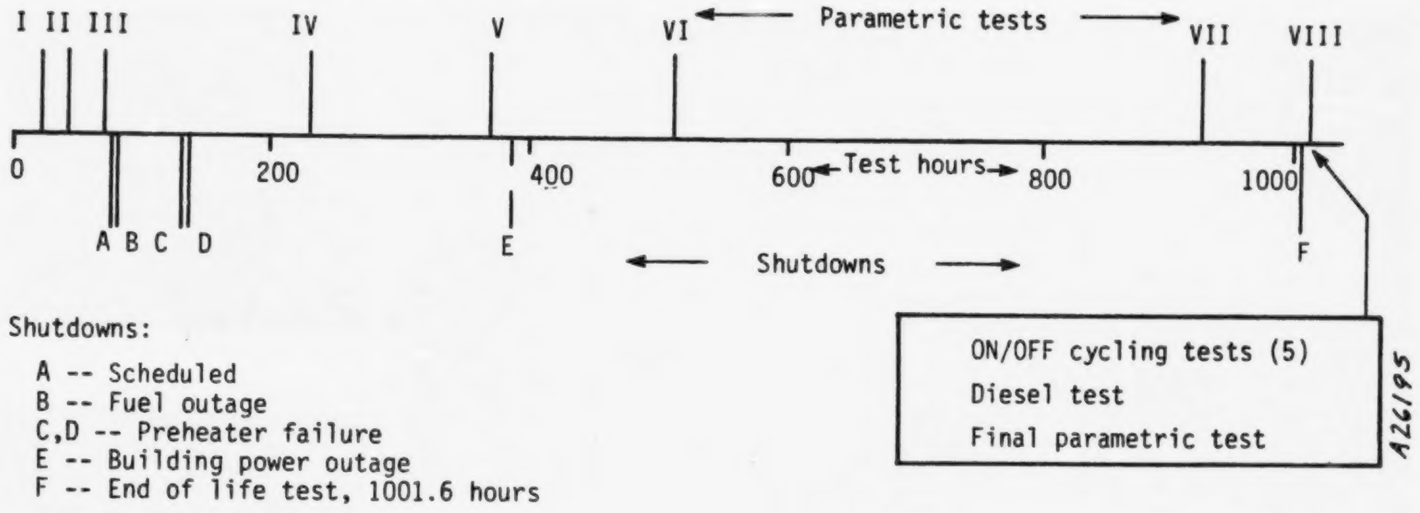

Figure 5. Durability test event chart.

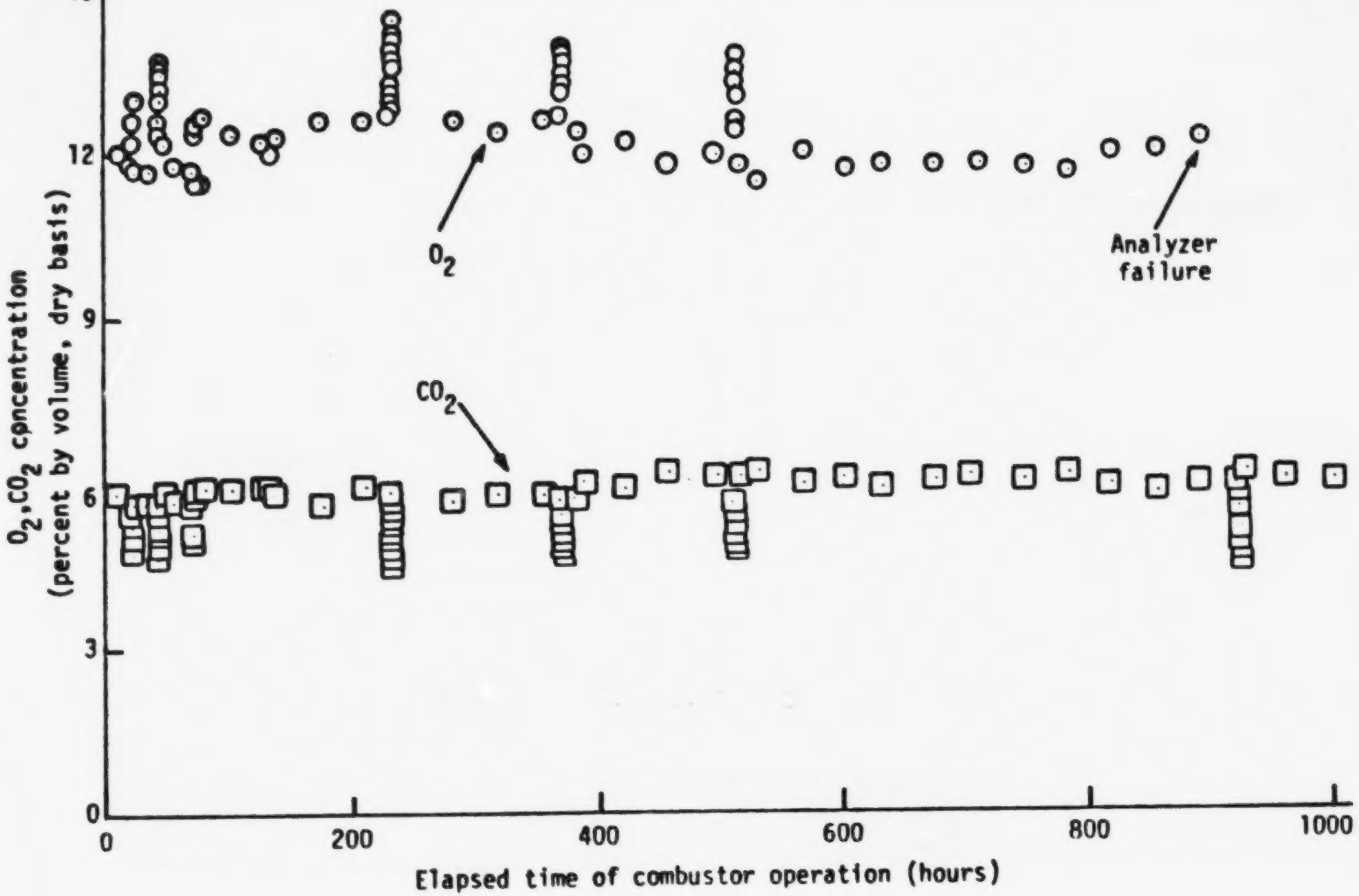

Figure 6. Durability test O_2 and CO_2 emission levels.

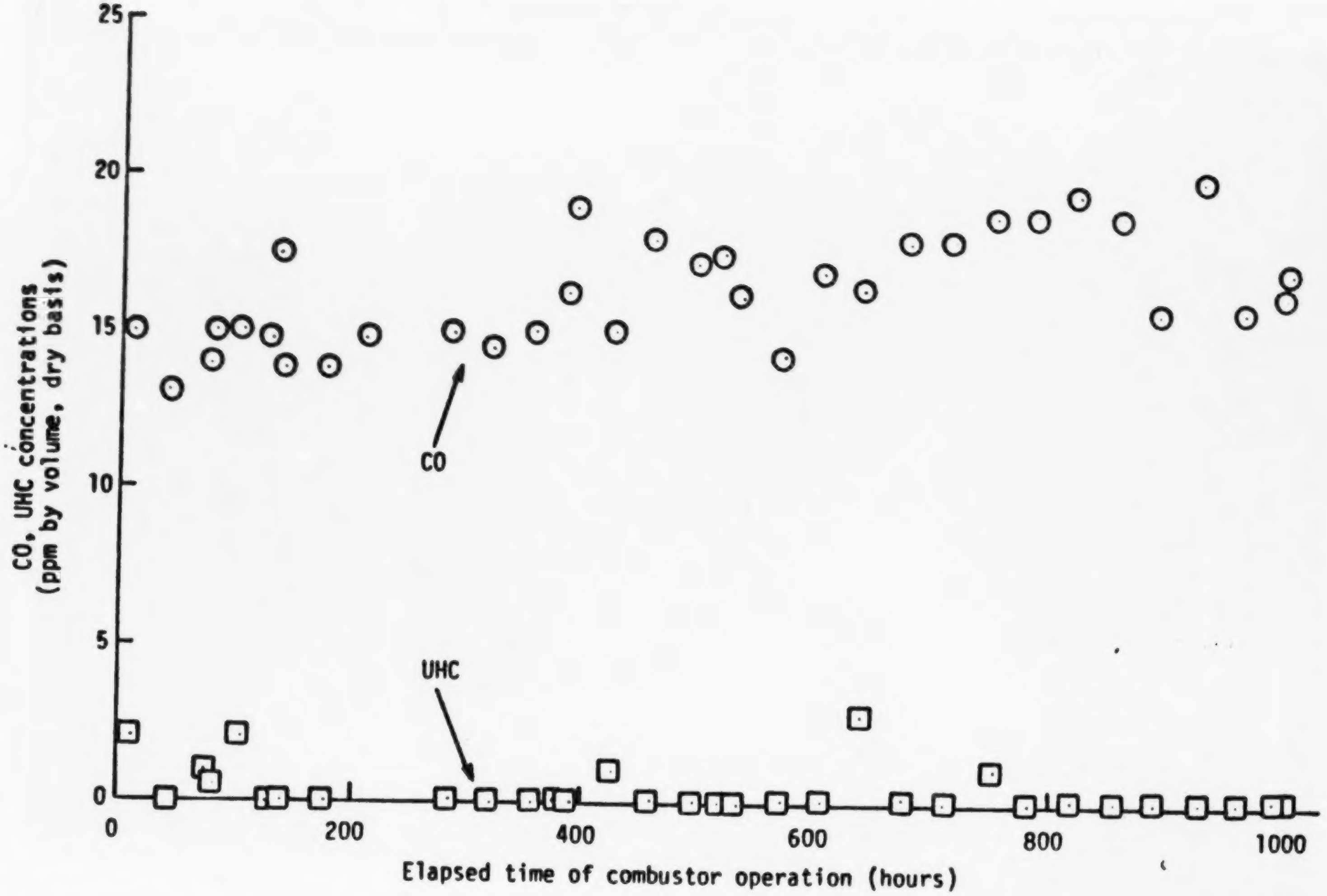

Figure 7. Durability test CO and UHC emissions levels.

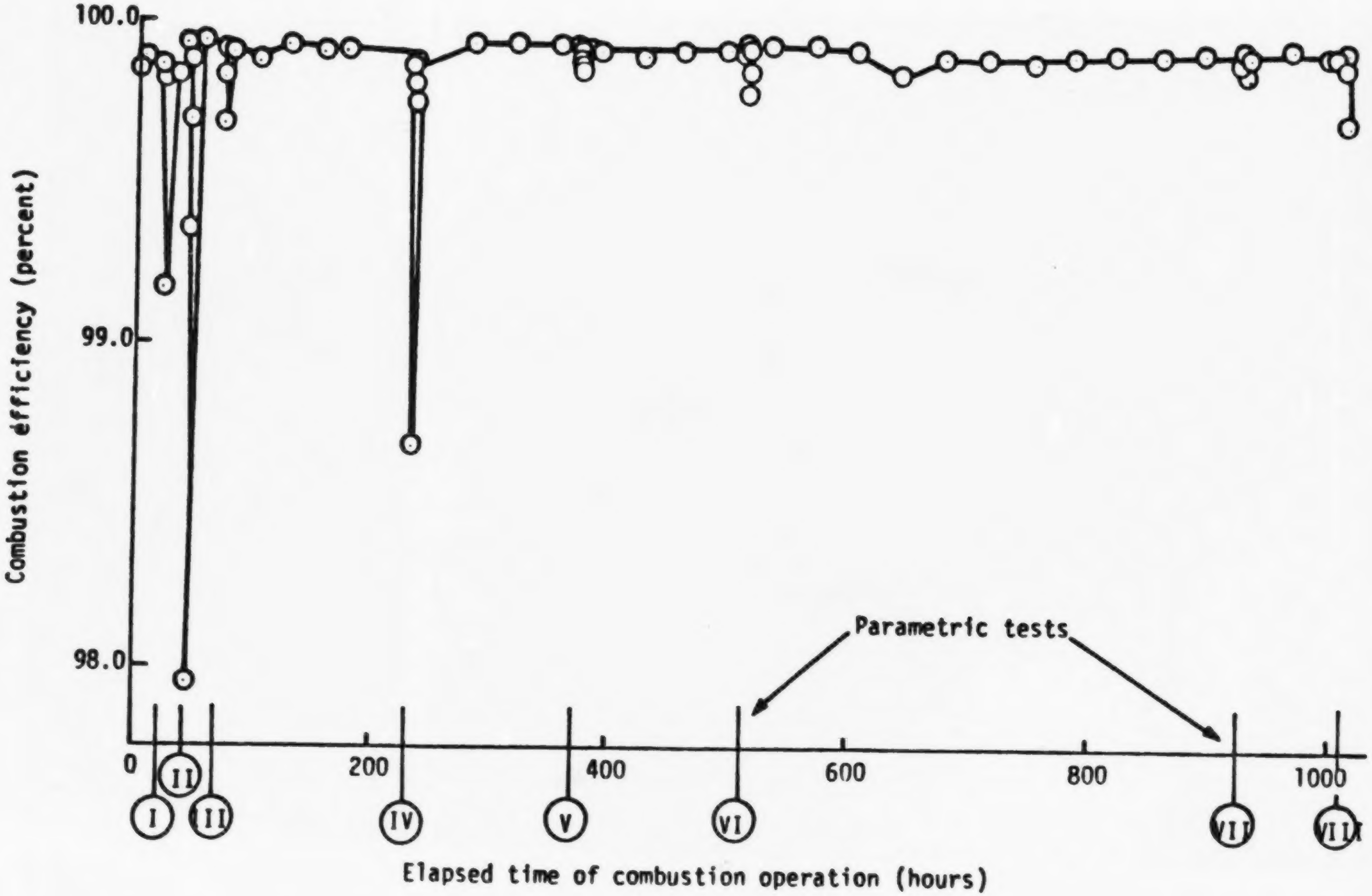

Figure 8. Durability test combustion efficiency performance.

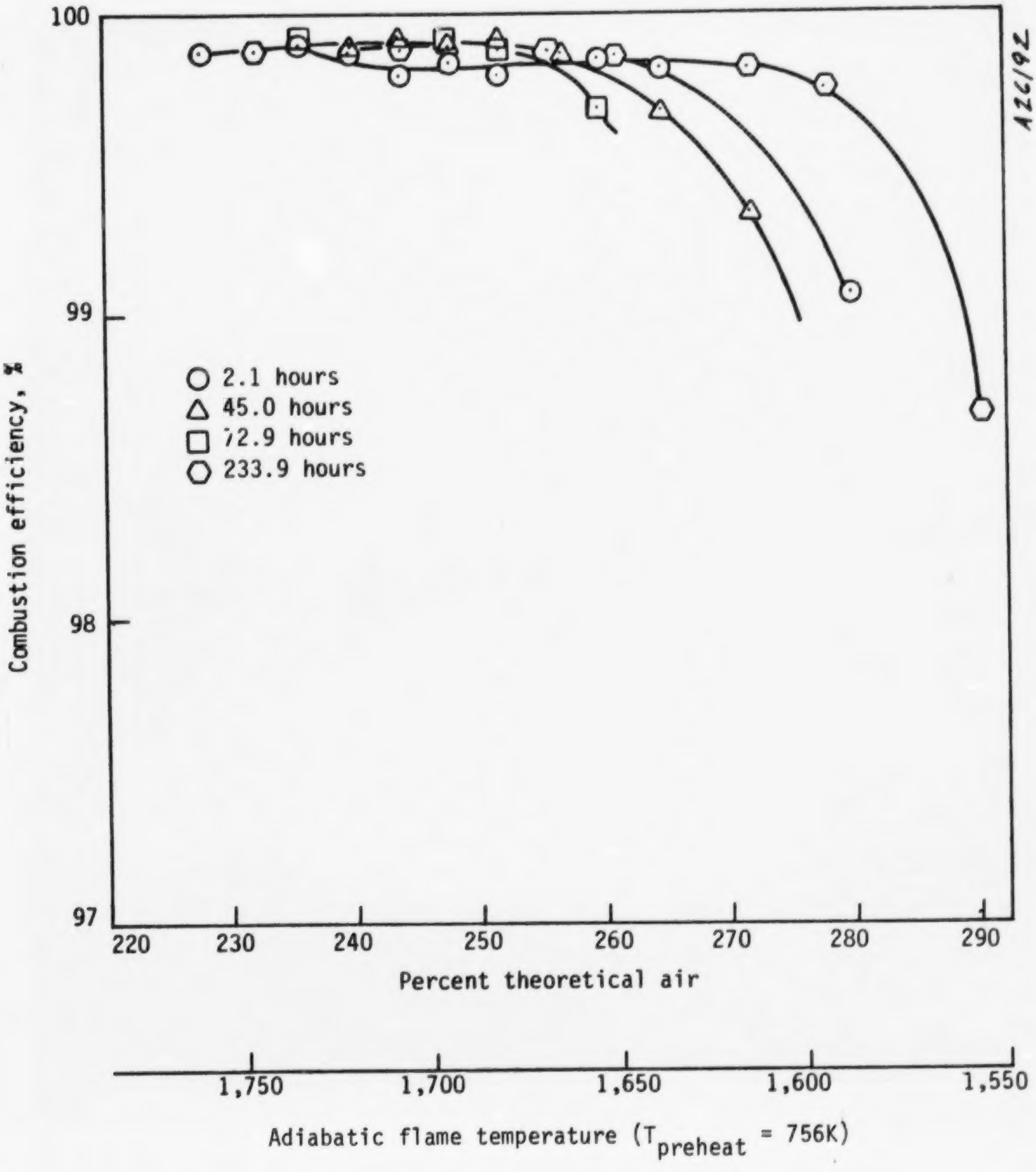

Figure 9. Parametric tests -- effects of turndown on combustion efficiency.

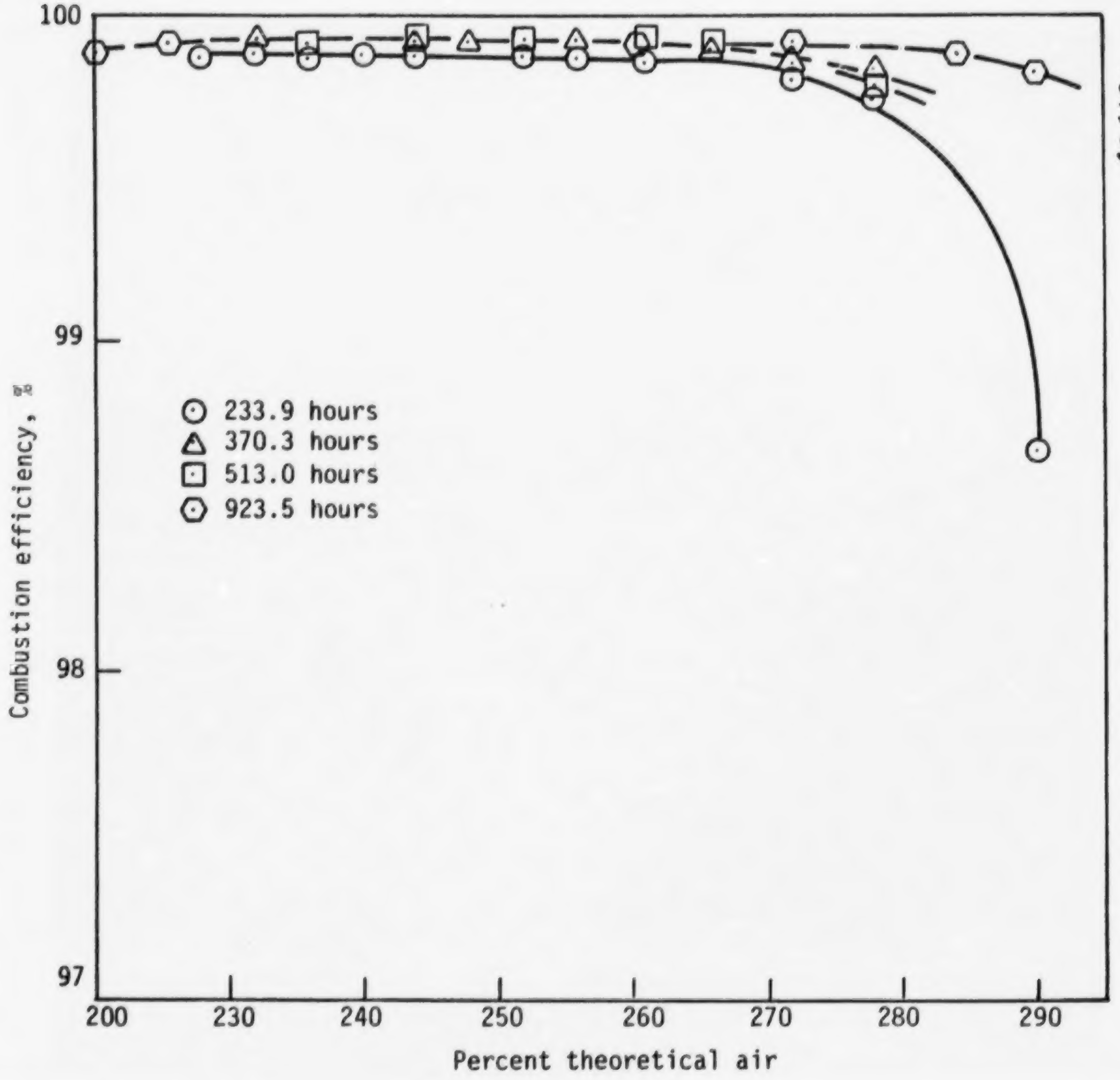

A26191

Figure 10. Parametric tests -- effects of turndown on combustion efficiency.

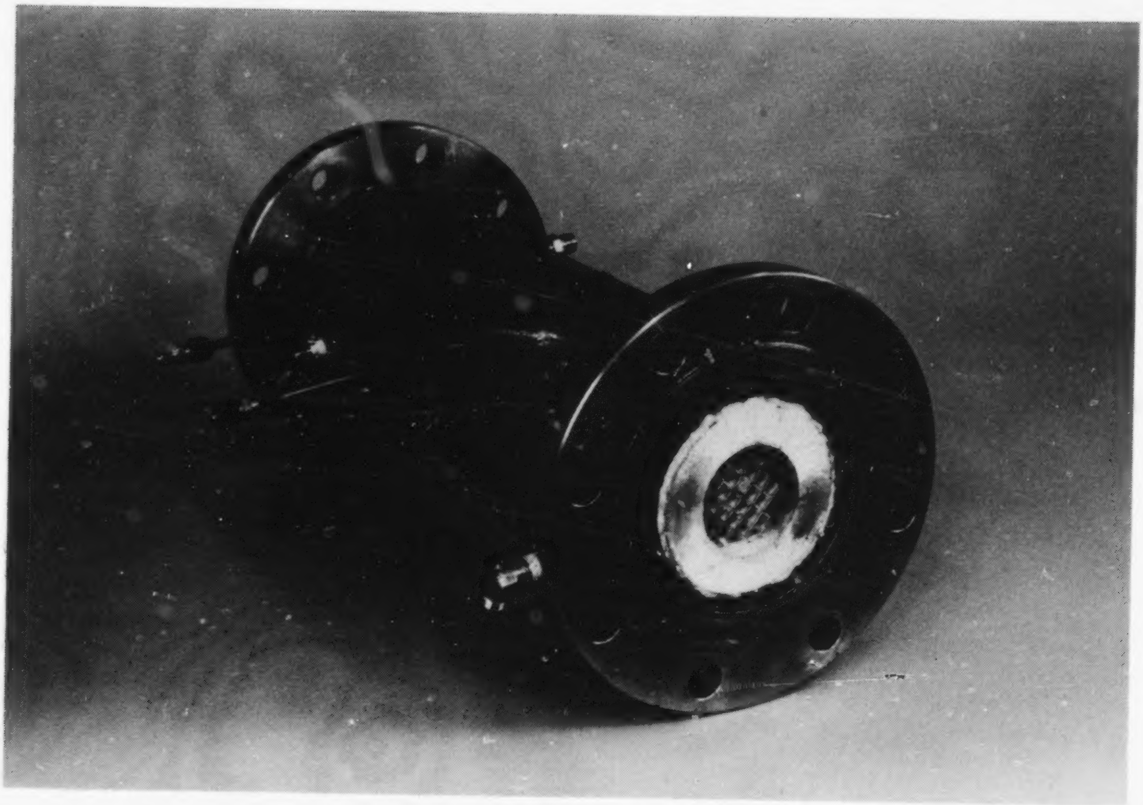

Figure 11. Catalyst mounting configuration entrance segment (post test).

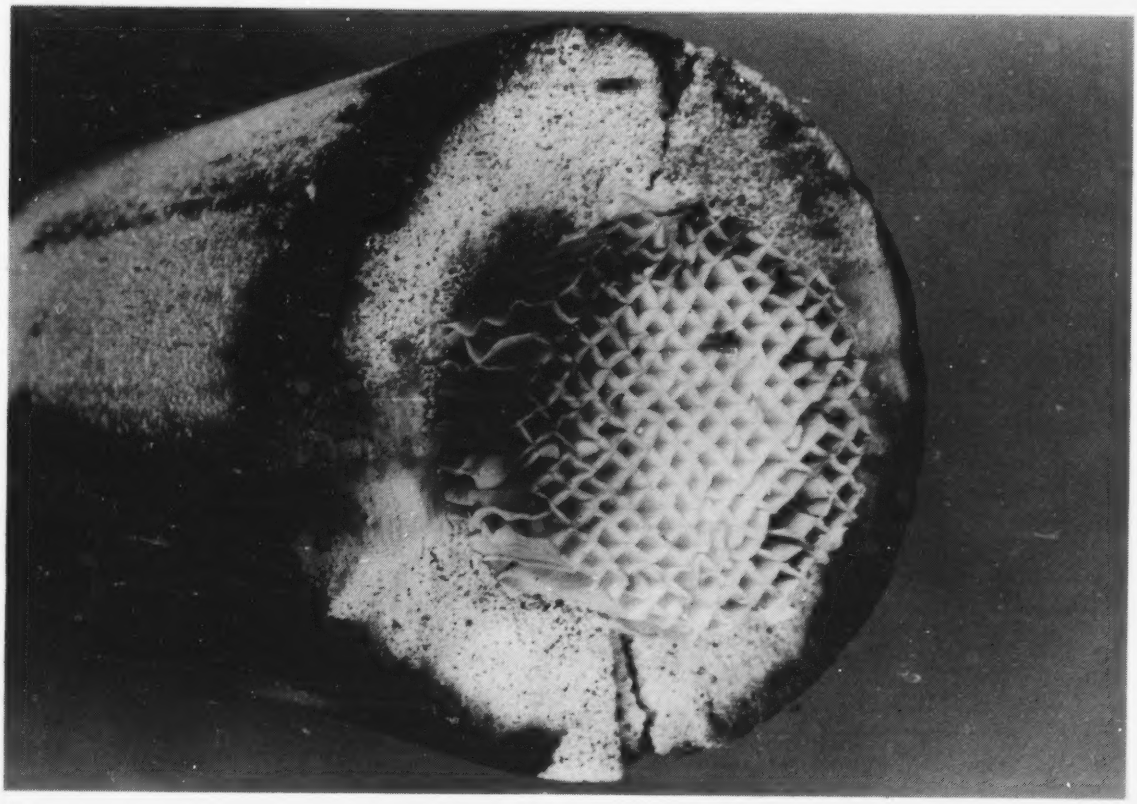

Figure 12. Durability reactor post test condition (exit view).

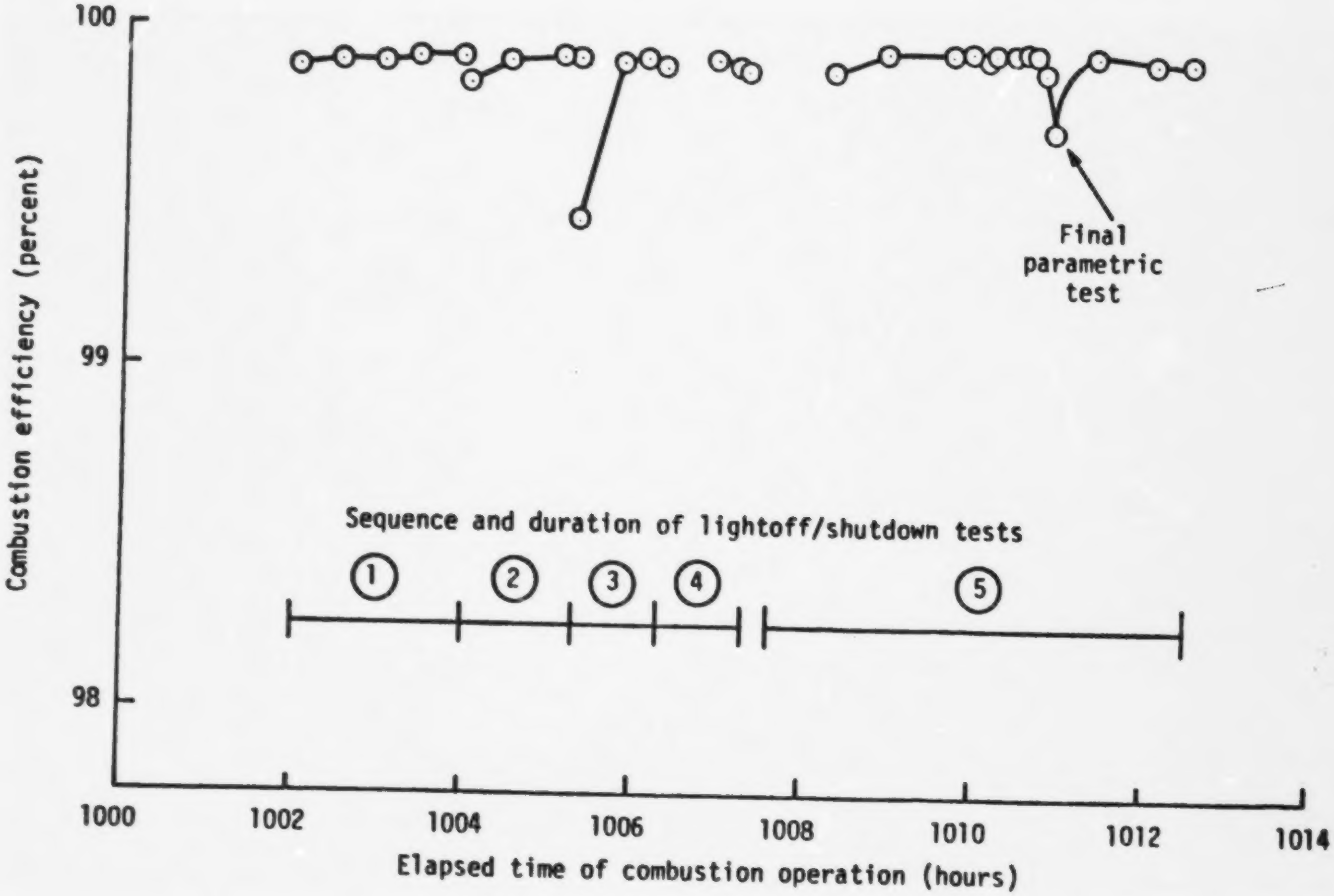

Figure 13. Thermal cycling performance.

TABLE 1. CATALYST DESCRIPTIONS

Designation	Supplier	Substrate	Catalyst/Washcoat	Element No.
UOP-A	UOP, Inc.	DuPont Torvex alumina, 100 cells/in^2, hexagonal	Proprietary washcoat, noble metal "A"	All
UOP-B	UOP, Inc.	Corning MCB-12 100 cells/in^2, "Flexcell"	Proprietary washcoat, noble metal "B"	All
UOP-C	UOP, Inc.	DuPont Torvex alumina, 100 cells/in^2, hexagonal	Proprietary washcoat, stabilizer and catalyst	All
MBI-B	Matthey Bishop, Inc.	DuPont Torvex alumina, 100 cells/in^2, hexagonal	Proprietary washcoat, stabilizer and catalyst	All
OC-~~A~~B	Oxy-Catalyst	Corning MCB-12, 100 Cells/in^2, "Flexcell"	Metal oxide coating	All
WRG-A	W. R. Grace, Inc.	Corning MCB-12, 100 cells/in^2, "Flexcell"	Slip coat of base and noble metals stabilized with metal oxide anchoring	All
HAP-A	Houdry Air Products	Corning MCB-12 100 cells/in^2, "Flexcell"	Proprietary alumina washcoat, noble metal	All
HAP-C	Houdry Air Products	Corning MCB-12, 100 cells/in^2, "Flexcell"	Chromium "activated" substrate	All
ATT-A	Acurex	Corning MCB-12, 100 cells/in^2, "Flexcell"	5-10% wt NiO, 1.5% wt Pt 5-10% wt NiO	1 2, 3

TABLE I. Continued

Designation	Supplier	Substrate	Catalyst/Washcoat	Element No.
ATT-B	**Trans-Tech**	**$NiAl_2O_4$ (25% mole) $MgAl_2O_4$ (75% mole) ~60 cells/in^2, circular**	**NA**	**NA**
ATT-C	Trans-Tech	$LaCrO_3$ (25% mole) $LaAlO_3$ (75% mole) ~60 cells/in^2 circular	NA	NA
ATT-D	Acurex	Corning Proprietary Honeycomb 100 cells/in^2, "Flexcell"	None	All
ATT-E	Acurex	DuPont Torvex alumina, 100 cells/in^2, hexagonal	La_2O_3-Cr_2O_3(5-10% wt), Pt (1.5% wt) La_2O_3-Cr_2O_3 (5-10% wt)	1 2, 3
ATT-F	Trans-Tech	MgAl O : Fe O (9/1 mole ratio) ~60 cells/in^2, circular	NA	NA

TABLE II. PRELIMINARY FURNACE AGING RESULTS SUMMARY

Material	Pretest BET and Dispersion		Posttest BET and Dispersion		Previous Combustion Test Results	Posttest Condition
	m^2/g	mole H_2/g	m^2/G	mole H_2/g		
UOP-A	5.66	45.5	0	14.66	Not available	Blistered coating
UOP-B	3.49	9.3	0	0.39	Good with all fuels	No visual degradation
UOP-C	4.84	40.0	0	11.14	Not available	Flaking coating
MBI-B	3.27	0.79	0	0.33	Not available	Fractured
HAP-A	0.25	0.95	0	0.16	Poor	No visual degradation
HAP-C	0.79		0		Poor	No visual degradation
WRG-A	1.06	1.42	0	0.16	Moderate/poor	Material volatilized
OC-B	1.83		0		Good	Slight darkened
ATT-A	0.26	1.16	0	0.26	Good	Some material depletion
ATT-D					Good with clean fuels,poor with others	Material volatilized
ATT-E	0.09	1.36	0	0.31	Good	No degradation
ATT-B					Not available	No degradation
ATT-C					Good with applied material	No visual degradation
ATT-F					Not available	No degradation

TABLE III. PHASE II REACTOR DESCRIPTIONS

Designation	Substrate	Catalyst	Cell Densities	Application Method
LaCr/MCB	Corning MCB-1	Lanthanum/chromium oxide 5 percent weight	9, 16, 100	Slip coating
YCr/MCB	Corning MCB-1	Yttria/chrominum oxide 5 percent weight	9, 16, 100	Slip coating
MAFF/MCB	Corning MCB-1	Magnesium aluminate iron ferrite 5 percent weight	9, 16, 100	Slip coating
LaCr/JNM	Proprietary	Lanthanum/chrominum oxide 12 percent weight	9, 16, 100, 200	Slip coating
YCr/JNM	Proprietary	Yttria/chromium oxide 12 percent weight	9, 16, 100, 200	Slip coating
MAFF/JNM	Proprietary	Magnesium aluminate iron ferrite 12 percent weight	9, 16, 100, 200	Slip coating
TCT/JNM	Proprietary	Terbium/cerium/thorium oxide	9, 16, 100, 200	Solution impregnation
TCT/JNX	Proprietary	Terbium/cerium/thorium	9, 16, 100, 200	Solution impregnation

TABLE IV. REDUCED DATA TABLE, PHASE II DURABILITY TEST

Data Point	Air Flow (SCFM)	C_3H_8 SCFM	Vref (ft/s)	% T/A from Flow Measurement	% T/A From Emissions	T Preheat (°F)	T Adiabatic From Emissions (°F)	T In Depth Element 3 (°F)	From Emissions (%)	Based on T (%)	NO_x (ppm)	CO (ppm)	UHC (ppm)	O_2 (%)	CO_2 (%)	NO_x Correct to 15% O_2 (ppm)	Elapsed Time (Hr)
1	23.5	0.437	45	226	228	837	2,650	2,611	99.85	97.9	2	21	2	11.4	5.8	1	.4
2	23.5	0.433	45	228	228	839	2,650	2,565	99.90	95.3	3	20	0	11.2	5.8	2	1.0
6	23.5	0.421	45	235	236	846	2,600	2,534	99.90	96.2	3	15	1	11.9	5.6	2	4.6
12	23.5	0.422	45	234	236	848	2,600	2,548	99.87	97.0	2	15	2	12.0	5.6	1	10.7
22	23.5	0.416	45	237	236	828	2,600	2,537	99.9	96.4	2	14	1	11.8	5.6	1	20.7
38	23.5	0.420	45	235	232	829	2,630	2,551	99.9	95.6	1	13	0	11.7	5.7	1	30.8
47	23.5	0.420	45	235	232	832	2,630	2,561	99.9	96.2	1	13	2	11.6	5.7	1	40.8
65	23.5	0.418	45	236	224	824	2,680	2,531	99.9	92.0		14	0	12.0	5.9		50.8
75	23.5	0.420	44	235	228	833	2,650	2,556	99.9	94.8		13	0	11.6	5.8		60.1
85	23.5	0.420	44	235	228	830	2,650	2,596	99.9	97.0		14	2	11.5	5.8		70.8
96	23.5	0.421	44	235	228	835	2,650	2,587	99.91	96.5		14	1	11.5	5.8		77.5
116	23.3	0.423	44	233	224	836	2,690	2,581	99.88	94.1		15	2	12.4	5.9		102.0
185	23.1	0.418	45	232	224	899	2,720	2,609	99.81	93.9		14.8	5	12.6	5.9		212.0
256	23.1	0.420	45	231	228	882	2,690	2,601	99.93	45.1		14.5	0	12.5	5.8		320.0
378	23.1	0.432	45	225	216	884	2,780		99.92			17.3	0	12.0	6.1		495.6
492	23.1	0.438	45	222	216	873	2,760		99.90			18	1	11.8	6.1		711.6
564	23.0	0.440	45	220	228	878	2,680		99.91			18.8	0	12.0	5.8		855.6
647	23.1	0.450	45	216	224	881	2,730		99.92			17	0		5.9		1,001.6

HIGH TEMPERATURE CATALYTIC REACTIONS OF $CO/O_2/N_2$, A, He, CO_2/H_2O MIXTURES ON PLATINUM

By
C. Bruno*, P.M. Walsh+, D. Santavicca*, and F.V. Bracco*
*Mechanical and Aerospace Engineering Dept.
Princeton University, Princeton, NJ 08544

+Energy Laboratory, Massachusetts Institute of Technology,
Cambridge, Mass.

ABSTRACT

Platinum (4.2 kg/m^3 loading) deposited by means of a γ-alumina washcoat over a honeycomb cordierite substrate of 0.0254x0.0254 m cross section, 0.076 m length and with a characteristic channel diameter of 0.0014 m was used as a catalyst in a steady flow reactor.

Measurements of substrate temperature at ten axial locations, CO, CO_2, and O_2 exhaust concentrations, and of pressure drop across the monolith were taken with CO/air mixtures at 600 K inlet temperature, 110 and 200 kPa pressures, 10 to 70 m/s inlet velocities, 0.013 to 0.32 equivalence ratios, and 0.54 mol% water content. Also employed were CO/CO_2, N_2, A, He/O_2 mixtures at 600 and 700 k inlet temperatures, 110 kPa pressure, 11 and 13 m/s inlet velocities and 0.031 to 0.56 equivalence ratios. The measured quantities were also computed with a two-dimensional steady-state model including axial and radial convection and diffusion of mass, momentum and energy, and homogeneous and heterogeneous, single step irreversible reactions. The model equations were the complete, two-dimensional laminar-flow conservation equations for the flow in the monolith channels and were solved by a numerical technique based on the TEACH code. The model required the measured substrate wall temperature as input.

Comparisons of computed and measured quantities were adequate to satisfactory over the entire range of parameters investigated.

It is concluded that, under the conditions tested, oxidation of CO proceeds mostly in a diffusion-controlled regime and that homogeneous reactions are important only for the lowest velocities and highest equivalence ratios. Indications were found that the presence of water increases significantly the rate of high temperature catalytic oxidation of CO.

LIST OF SYMBOLS

C_p = gas specific heat

$D = D_h$ = hydraulic diameter

D_{ik} = binary diffusion coefficient for species i, k

E = activation energy

k = thermal conductivity

p = pressure

r = channel radial coordinate

R = channel radius; universal gas constant

Re = Reynolds number

S_ϕ = source term in generalized conservation equation

t = time

T = gas temperature

u = axial gas velocity component

v = radial gas velocity component

x = channel axial coordinate

X_k = molar fraction of species k

Y_k = mass fraction of species k

W_k = molecular weight of species k

Greek Symbols:

Γ = gas transport property in generalized conservation equation
λ = gas thermal conductivity
μ = gas viscosity

ρ = gas density

ϕ = equivalence ratio = $(Y_{CO}/Y_{O_2})/(Y_{CO}/Y_{O_2})_{\text{STOICHIOMETRIC OXIDATION}}$

Subscripts

$(\ )_{in} = (\ )_2 =$ at the channel inlet

$(\ )_w$ = at the wall

ACKNOWLEGEMENTS

This research was supported by the Air Force Office of Scientific Research under Grant No. AFOSR-76-3052, Dr. B.T. Wolfson, Grant Monitor; by the Department of Energy under Contract No. DE-AC21-80MC14036, Mr. V. Kothari, Technical Project Officer, and by NASA-Lewis Research Center, Dr. Andrew Szaniszlo, Grant Monitor.

The authors are indebted to Dr. W.C. Pfefferle for his many valuable suggestions.

I. INTRODUCTION

The technology and data base needed to incorporate catalytic reactors in practical heat and power systems are expanding rapidly. The work in progress includes development of catalytic combustors for aircraft gas turbines *(1)(2)(3)(4)(5)(6)*, stationary gas turbines *(7)(8)(9)(10)(11)(12)*, highway vehicle gas turbines *(13)(14)(15)(16)(17)*, and boilers *(10)*. Other studies have focused on catalyst design for particular fuels such as low-Btu gases *(18)*, No. 6 oil *(19)*, heavy fuels *(20)*, and coal-derived liquids *(21)*. Still other work has been concerned with catalyst durability *(22)*. Demonstrated advantages of catalytic, when compared with conventional, combustion are lower emissions of HC, CO, NO_x, and smoke, higher efficiency, stable operation at lower equivalence ratio, improved pattern factor (for gas turbines) and use of fuels of wider specification. Potential for low conversion of fuel-bound nitrogen to NO_x has also been demonstrated *(23)(19)(24)(25)*. Further development and optimization could be facilitated by better knowledge of the processes which control fuel conversion in the channels of a monolithic catalyst.

A number of physical and chemical processes have been suggested as important determinants of steady catalytic combustor performance *(27)(28)(29)*, namely axial and radial convection of species, heat, and momentum, axial and radial diffusion of species, heat, and momentum, axial heat transfer in substrate by conduction and radiation, gas and wall chemical reactions, but only some of them have been considered in published work. In particular, only two studies account for the following subprocesses in one-dimensional steady models: axial convection with variable gas velocity, radial heat and mass transport, variable wall temperature, gas and wall reactions.

Cerkanowicz, Cole, and Stevens *(30)* modeled the steady state operation of a catalyst including one-step homogeneous and heterogeneous reactions, radial heat and mass transport, axial heat conduction in the solid, and axial variation in pressure and flow velocity. They assumed plug flow and constant transfer coefficients. The results were compared with the experimental data of Pfefferle, et al *(5)*, on catalytic combustion of propene. The model successfully predicted the transition from surface reaction to diffusion control, and the ignition of homogeneous reactions, as inlet temperature increases. It also correctly predicted the equivalence ratio at which homogeneous reaction is ignited with fixed inlet temperature. The model exhibited ignition-extinction hysteresis, which has also been observed experimentally.

Kelly, Kendall, Chu, and Kesselring *(28)* modeled steady state operation using multiple homogeneous reactions, one-step wall reaction, axial heat and species diffusion, and axial substrate heat transfer by conduction and radiation. Flow velocity was variable, but pressure was fixed. Radial transport was treated using variable transfer coefficients. Studies with this model showed that a distinct light-off transition for homogeneous reactions depends on the inclusion of axial diffusion of both heat and species. The model predicted that blowout mass throughput and emissions both increase with increasing channel diameter. These observations led to the development of graded cell catalysts with improved performance *(31)*.

T'ien *(32)* modeled one-dimensional steady state operation in a fashion similar to Kelly et al., but neglecting axial conduction and radiative heat transfer in the substrate. He concentrated on the effects of catalyst length on fuel conversion.

A major unresolved question concerns the effects of radial convection and diffusion on the rates of the homogeneous and wall reactions. These interactions are not properly accounted for in a one-dimensional description

In this paper results are reported of two-dimensional computations of the homogeneous and heterogeneous oxidation of CO in air over a platinum catalyst and comparisons with measured CO emissions versus inlet pressure, temperature, equivalence ratio, and velocity.

From the point of view of applications, the oxidation of CO has long been known to be important in the homogeneous combustion of hydrocarbons *(33)*, while the choice of platinum is due to its low light-off temperature, ease of fabrication, and a substantial body of knowledge already existing on its performance in the oxidation of CO, albeit at lower temperatures. Its high cost and short high temperature life, however, make it an unlikely candidate for most high temperature applications, for which cheaper and stabler catalysts are being designed and evaluated.

II. EXPERIMENTAL APPARATUS

a. Test rig

A sketch of the experimental apparatus is shown in Figure 1. Preheated air at a measured flowrate is supplied to a 690 mm long test section with a 25.4 mm square cross section channel. The catalyst is placed with its downstream end 90 mm from the test section outlet, and insulated from the wall by Fiberfrax paper. Details of the catalyst section are shown in Figure 2. A fuel injector consisting of five 1.6 mm diameter tubes, each containing five 0.3 mm diameter holes, is located 440 mm from the catalyst inlet. A combination pitot tube and thermocouple is mounted 200 mm from the catalyst inlet. In addition to measuring gas velocity and temperature, the pitot tube is used to extract gas samples which are analyzed to determine equivalence ratio. Pressure is regulated by a valve in the exhaust pipe, and taps placed up and downstream of the catalyst are used to measure inlet pressure and pressure drop. A mass flowmeter (Hastings Model AHL-100P with H-3M/L-100 Transducer) measured the air flowrate. The water content of the inlet air was measured using a semiconductor sensor (Thunder Model 2000 with BR-101B probe) mounted in the airstream between the receiving tank and the heaters.

Efforts were made to minimize crosswise gradients in temperature, velocity, and fuel concentration of the inlet stream. The entire test section is insulated so that uniform temperature across the width of the test section is obtained when sufficient time (~1 hr) has elapsed after startup of the air preheat system. The uniformity is found to be independent of air flowrate over the range of velocities used. Sufficient fuel/air mixing was obtained by placing baffles downstream of the fuel injector, which affect the velocity profile. By trying various configurations, the velocity uniformity was improved while maintaining a uniform fuel/oxidizer composition. The final arrangement used consisted of two screens, each containing four 8 mm diameter holes, placed 30 and 110 mm downstream of the fuel injector. Another screen perforated with 1.6 mm diameter holes was 190 mm from the injector and 50 mm upstream of the pitot tube. The resulting fuel distribution showed good uniformity (±3%) over the measured range. Velocity profiles were less satisfactory (range ±6% over 50% of the channel width). Average reference velocities were determined using the CO and air flowrates, inlet temperature and pressure, and the cross section area of the catalyst. The catalyst inlet velocity, taking into account the fraction of open monolith area, is $u_{in} = (1.67 \pm .06)\ u_{ref}$.

b. Substrate and exhaust measurements

Substrate temperatures were measured by a method similar to that described by Kesselring, Krill, and Kendall *(31)*. Ni-Cr/Ni-Al thermocouples were fed through the test section wall and into the ends of catalyst channels. The lengths of wire inside the catalyst were covered by mullite insulator and both ends of the channel sealed with ceramic adhesive. The lifetime of these thermocouples under test conditions was short (5-20 hr). Exhaust gas samples were taken through an expansion quenched, water cooled, stainless steel probe mounted in an elbow downstream of the test section. Exhaust gas temperature was measured with a thermocouple mounted on the probe. CO and CO_2 were determined by infrared absorption (Horiba Model AIA-21), and O_2 by magnetic susceptibility (Scott Model 250).

c. Catalyst and fuel

The catalyst was platinum supported on split cell corrugated Cordierite with γ-alumina washcoat. The overall dimensions of the monolith were 24 x 24 x 76 mm, the open area was 64%, the channel cross-section area was 1.9 mm^2, and the platinum loading was 4.2 kg/m^3. The physical properties of the catalyst are listed in Table 1. The sample was pretreated by burning propane for two hours with the maximum substrate temperature at 1480 K. The fuel was carbon monoxide, C.P. 99.5 mole%min.

III. MATHEMATICAL MODEL

Only an individual channel of the catalytic monolith was modeled, assuming negligible heat transfer between adjacent channels. Insulation of the monolith and of the test section limited crosswise gradients to ~ 6 k/mm, or ~10 k/channel. Since the embedded thermocouples and the combination thermocouple/sample probe measure quantities related to the central channels, errors due to nonuniform channel performance were minimized.

Axial symmetry was also assumed in modeling the individual channel, whose cross section is roughly trapezoidal. The diameter of the model channel was chosen as the hydraulic diameter $D_h = \frac{2 \times \text{Area}}{\text{perimeter}}$. For the monolith used in the present work $D_h = 1.4$ mm.

a. Gas equations

The equations for the gas inside each channel are the complete, steady, two-dimensional conservation equations for reactive, laminar (Re<1900) flows *(34)*. They were solved numerically by a method based on the TEACH code documented by Gosman and Ideriah *(47)*. The code used in the present work differs by the original TEACH by the introduction of variable density, species and energy conservation equation, and equation of state, linking pressure, density and species mass fractions.

In this code the general conservation equation is written as

$$\frac{\partial \rho\phi}{\partial t} + \frac{1}{r}\left[\frac{\partial}{\partial x}(\rho r u \phi) + \frac{\partial}{\partial r}(\rho r v \phi) - \frac{\partial}{\partial x}\left(r\,\Gamma\,\frac{\partial \phi}{x}\right) - \frac{\partial}{\partial r}\left(r\,\Gamma\,\frac{\partial \phi}{\partial r}\right)\right] = S_\phi$$

where $\phi \equiv u, v, T, Y_k$, etc; Γ is the appropriate transport property, such as μ, k, ρD_{ik}, and S_ϕ is the appropriate source term, such as $-\frac{\partial p}{\partial x}$, or the rate of formation for the species equations.

The general equation is integrated over the elemental cell volume, so that only convective and diffusive fluxes, and sources appear inside the computer code. The resulting finite difference equations are linear and are solved iteratively. To this purpose the integration domain is divided into mesh subdomains (cells) and the code solver computes for each variable a new line of values at each longitudinal location x. After the entire mesh has been "swept", the code computes the total amount of the quantities to be conserved, compares them to the fluxes entering the inlet of the monolith channel and keeps iterating if the percentage difference is above a specified value, typically 0.5%. Further details may be found in *(47)*.

The model chosen for the homogeneous kinetics of CO with O_2 is a simple, one-step overall reaction $CO + \frac{1}{2} O_2 \rightarrow CO_2$. The rate was taken from *(35)*:

$$\frac{d[CO]}{dt} = - k_o [CO][O_2]^{0.5}[H_2O]^{0.5} \exp(-E/RT)$$

with $k_o = 1.3 \times 10^{14}$ cm^3/mole · s

$E = 126$ KJ/mole = 30 Kcal/mole

Justification for this crude model lies mainly in its simplicity.

b. Gas boundary conditions

At the inlet (x=0) all physical variables ϕ are assumed to be known. At the outlet (x=L) their gradients are set to zero: $\frac{\partial \phi}{\partial x} = 0$. This linear condition simplifies the solution, and is also observed in practice, provided the L/D ratio of the channel is sufficiently large. Tests with imposed, arbitrary, large $(\frac{\partial \phi}{\partial x})_{x=L}$ did not show any detectable effect on the results except of course very near the outlet itself.

The other boundary conditions express radial symmetry, i.e. $\frac{\partial \phi}{\partial r} = 0$ at $r = 0$, and appropriate physical behavior at the channel wall, $r = R$. At $r = R$ no-slip conditions apply to u, v. The temperature, obtained from the wall thermocouple measurements, is specified as a function of x over the entire length of the channel. This procedure tests the validity of the gas-phase model more strictly by separating gas-phase from substrate effects, and has as an additional advantage the implicit inclusion of radiative effects (provided the gas is optically thin), since the experimental wall temperature does include the effects of radiation *(36)*. As for the chemical species, N_2 and H_2O are assumed inert, and thus their radial gradient zero at r = R, while heterogeneous kinetics rates were imposed to CO at the wall, i.e.

$$\rho D_{CO,N_2} \frac{\partial Y_{CO}}{\partial r} = - A_w \rho Y_{CO} \exp(-E_w/R\ T_w)$$

expressing the balance of diffusion and reaction rate at the wall. Further assuming that also at the wall CO is oxidized via the reaction

$$CO + \frac{1}{2} O_2 \rightarrow CO_2$$

the boundary conditions for O_2 and CO_2 at r = R are written as

$$\frac{\partial Y_{O_2}}{\partial r} = \frac{1}{2} \frac{\partial Y_{CO}}{\partial r} \frac{W_{O_2}}{W_{CO}} \frac{D_{CO,N_2}}{D_{O_2,N_2}}$$

$$\frac{\partial Y_{CO_2}}{\partial r} = - \frac{\partial Y_{CO}}{\partial r} \frac{W_{CO_2}}{W_{CO}} \frac{D_{CO,N_2}}{D_{CO_2,N_2}}$$

From *(37)* $A_w = 3.82 \times 10^3$ m/s and E_w = 104.25 KJ/mole = 24.9 Kcal/mole.

However, no good matching between computed and measured data could be obtained using this heterogeneous rate. Much better agreement was achieved by increasing A_w by $O(10^3)$ and refining the computational mesh by a factor 2 in both directions. Finer mesh is necessary when some terms, such as kinetic rates, are increased, to compensate for the inevitable averaging associated with finite differencing. This averaging tends to predict higher than real rates for the larger cells. Further reduction of the mesh size changed the results only slightly.

Clearly, the rate developed in *(37)* for automotive exhaust catalytic converters, applies in a temperature regime much lower than the one of interest in this study. Unfortunately, the finer mesh producing good data was also very expensive in execution time. To overcome this very practical problem, the heterogeneous CO rate was assumed infinitely fast and the boundary condition for CO changed to

$$(Y_{CO})_{r=R} = 0$$

while the two other conditions for O_2 and CO_2 were unchanged.

VI. RESULTS

a. CO/Air mixtures

A total of 78 runs were performed.

The inlet conditions are summarized below:

Inlet temperature (T_{in}) = 600 ± 10 K

Inlet pressure (P_{in}) = 110 ± 5 KPa and 200 ± 7 KPa

Inlet velocity (u_{in}) = 10 ± 4 to 70 ± 9 m/s

CO/air equivalence ratio (ϕ) = 0.03 ± 0.006 to 0.32 ± 0.07

H_2O = 0.54 ± 0.07 mol%

Analysis of the computed $\Delta p/p$ across the monolith indicates that the hydraulic diameter choice 2R = 1.4 mm reproduces the experimental data at both p = 110 and p = 200 KPa. Trends are as expected, with $\Delta p/p$ increasing with velocity and ϕ,due to increases of the velocity gradient at the wall and of the viscosity (see Fig. 3 and 4.)

A sample of measured wall temperature profiles is shown in Fig. 5. At the same equivalence ratio there is hardly any effect of velocity or pressure, meaning that the wall temperature is very close to the adiabatic flame temperature. If the Lewis-Semenov number $Le \equiv C_p \rho \, D_{CO,N_2}/\lambda$ is also close to unity, then the implication is that the process is diffusion-controlled. Emissions, in terms of $X_{CO}/(X_{CO} + X_{CO_2})$ at the outlet, i.e. in terms of unburnt carbon, are plotted versus ϕ in Fig. 6 and 7. The model predicts emissions well in the middle-to-high velocity range, while is less satisfactory when the velocity is low.

Figure 6 shows the main features of CO oxidation. At constant velocity (or mass flow) and $\phi = 0$ there are no emissions and the emission parameter $(X_{CO}/(X_{CO} + X_{CO_2})$ is unity. As ϕ is slightly increased, catalytic reactions begin, and emissions decrease rapidly. This regime, where the fuel diffusing to the wall is oxidized at a finite rate (of the type suggested by Voltz et al in *(37)*) is the heterogeneous-kinetics controlled regime.

Increasing ϕ further accelerates the wall reaction(s), until they become as fast, or faster, than the rate of diffusional transport to the wall. At this point the regime becomes diffusion-controlled, which is shown by an invariance of the emission parameter with ϕ. This flat part of the emission curves is broader at higher flow velocities (short residence time) and becomes very narrow, in fact barely noticeable, for long residence times.

Eventually, as ϕ is further increased, more and more CO is oxidized in the gas phase, and emissions decrease rapidly controlled by homogeneous-kinetics rates.

Increasing or reducing the flow velocity alters events quantitatively but not qualitatively. In particular, the emission plateau corresponding to the pure diffusion-controlled regime broadens as the velocity is increased, until when the velocity is infinitely large, occupies the entire ϕ range, i.e. $X_{CO}/(X_{CO} + X_{CO_2}) = 1$.

The effect of pressure can be observed in Fig. 7. Since the diffusion coefficients are inversely proportional to pressure, increasing p from 110 to 200 KPa raises emissions and widens the diffusion-controlled region. For $\phi \gtrsim .3$ the experimental data show a steeper slope for $p = 200$ KPa. This is again the effect of gas-phase kinetics, which is roughly proportional to p^2, thus favoring emission reductions when the pressure is raised.

The model underpredicts emissions slightly at larger ϕ and for longer residence times, i.e. where gas-phase kinetics contributes substantially to CO conversion. It is possible that the overall, one-step CO oxidation rate of Howard et al. *(35)* proposed for CO/air lean mixtures at p = 1 atm., may not be applicable to higher pressures and larger ϕ.

Given the reasonable matching between data and predictions, it is useful to look at the importance of radial gradients by comparing the predicted ratio between CO oxidized in the gas phase to CO oxidized at the catalytic wall in Figs. 8 through 11.

Figs. 8 and 9 show that gas phase becomes important for CO conversion toward the outlet of the channel, where temperature is highest. They also indicate that for either large ϕ or large residence times the rapid depletion of fuel in the gas phase results in declining gas phase importance toward the outlet. When the contributions of gas phase and surface to the CO conversion are integrated over the entire channel the model predictions indicate that most of CO is oxidized at the surface. However, Fig. 10 and 11 point out to the large effects of residence time and pressure at the larger ϕ, and therefore to the importance of gas phase reactions in this region. For small ϕ and at shorter residence times the results of the model become insensitive to the presence of gas phase kinetics, in accordance with the experiments.

The apparent contradiction between the observation of higher unburnt CO and same substrate temperature for the high pressures and high velocity cases is due to the fact that mass and heat transfer rates are comparable for the gas mixture tested (Lewis number = unity). Thus the wall temperature in a diffusion-dominated regime depends on ϕ only. While higher pressure reduces the diffusional mass transfer and would tend to reduce the substrate temperature, it also reduces the thermodiffusivity of the gas, which tends to increase the wall temperature. In contradistinction, CO emissions depend on pressure, since a reduction in the CO mass transfer rate to the catalytic wall due to pressure results automatically in more CO in the exhaust. This explanation was also supplied by Hegedus *(38)*.

b. CO/Inert/O_2 mixtures

To verify the effect of diffusion on CO conversion a total of 51 runs were performed with fuel/oxidizer combinations in which air was replaced by mixtures of an inert (N_2, CO_2, He, A) and O_2. The experimental procedure consisted in bringing the temperature of the test section and connected hardware to the desired steady-state conditions with air and then injecting the CO/Inert/O_2 mixtures.

With reference to the locations in Fig. 2, the parameters and conditions kept fixed are summarized below:

Inert Gas:	A	He	N_2	CO_2
Pressure p_o:	110 ± 4	110 ± 4	110 ± 4	110 ± 4 KPa
Inlet Temperature T_o:	600 + 10	700 ± 20	700 ± 10	690 ± 14 K
Inlet Velocity u_2:	11 ± 6	13 ± 7	13 ± 5	13 ± 4 m/s
Equivalence Ratio:	0.013-0.29	0.022-0.25	0.024-0.38	0.03-0.56

A change of the inert gas affects diffusion, heat transfer and final combustion temperature through the change in the specific heat of the mixture.

The influence of diffusion can be estimated in terms of the binary diffusion coefficient, which for a mixture of gases depend on the molecular weights of the individual components in a rather complex way. For simplicity, since the mass fraction of the inert dominates, and since the molecular weights of CO and O_2 are similar, the effect of replacing N_2 by A, He or CO_2 may be studied by looking only at the change in the binary diffusion coefficient of CO and the inert gas. The combined effect of diffusion and heat transfer is shown by the Lewis number of the mixture, defined as $Le = \lambda/C_p\rho D_{1,2}$ where $1 \equiv CO$ and $2 = O_2 + \text{inert}$. Finally, the effect of CO on the measured wall temperature (Fig. 14), may be estimated by calculating the adiabatic flame temperature for the different inert gases. The results are summaried below:

Inert Gas	$D_{1,2}/D_{1N_2}$	Le	$T^{(*)}_{wall,max}$	$T^{(*)}_{adiabatic\ flame}$
CO_2	0.86	0.7	1000.	1025.
N_2	1.00	1.0	1200.	1200.
A	1.03	1.6	1280.	1280.
He	2.84	1.3	1410.	1380.

(*) at $\phi = 0.20$.

From the comparison of these three effects is clear that while pure diffusion is faster for, say, He, than for N_2, the larger heat transfer from the wall to the gas more than balances the faster mass transfer of CO to the wall, and the observed temperatures do not correlate with the Lewis number. They do, instead, with the adiabatic flame temperature corresponding to each inert gas, indicating that the dominant effect in determining the wall temperature is the effect of the mixture specific heat.

CO conversion is illustrated in Figs. 12 and 13. Figure 12 shows the dependence on equivalence ratio for the case of CO_2 and N_2 as inert. Comparing the results with the ones for A and He in Fig. 13, it is clear that unburned CO increases with the average molecular weight of the gas mixture.

Three features of these experimental runs are immediately apparent when comparing runs with N_2 as inert (Fig. 12 and 14) to the runs with air under the same conditions (Fig. 5 and 6): 1) with N_2 CO emissions are about one to two orders of magnitude higher; 2) they increase with ϕ; and 3) the substrate temperature is approximately the same.

While the last observation reflects the diffusion-controlled nature of the process and the fact that the Lewis number is close to unity, the first two are puzzling. In particular, the emissions of the $CO/N_2/O_2$ runs are higher even though the inlet temperature is 100 K higher than in the CO/air runs.

Degradation of the catalyst was at first suspected and then eliminated, since the runs with $CO/N_2/O_2$ were performed immediately after the runs with CO/air. The only difference between the two series is the water content of the inlet gas. In the CO/air series the H_2O molar fraction was 0.0054. In the $CO/Inert/O_2$ series the water content was determined by the H_2O present in the gas bottles, typically a few ppm., and by the residual water left in the test rig by the preheating with air. No reliable measurements of H_2O were taken (due to the hygrometer characteristics) except for $CO/N_2/O_2$, where the H_2O molar fraction at the hygrometer station decreased from 0.002 to 0.0004 during consecutive runs, i.e. while ϕ also was increased. It is conceivable that H_2O may have been even lower at locations further downstream of the hygrometer and close to the hotter test section. The gradual flushing out of

H_2O while taking the data with dry mixtures parallels the abnormal emission trend with ϕ.

That CO oxidation depends on H_2O content would not be surprising at all if it took place in the gas phase. However, both experiments and predictions indicate that almost all CO is converted to CO_2 at the catalyst surface and not in the gas, except for low velocity and high ϕ, where the gas phase contributes for at most 30% of the total CO converted. This, however, cannot explain the order(s) of magnitude increase in the emissions. The only explanation left seems to be that H_2O affects markedly the high temperature oxidation of CO on platinum.

This conclusion opens the door to some interesting speculations: it is known that gas phase oxidation of CO requires OH radicals *(39)*. It is conceivable that at high temperature the conventional CO oxidation mechanism on Pt, proceeding via chemisorption of either or both CO and O_2 *(40)(41)(42)*,gives way to a different mechanism in which OH radicals produced at the platinum surface by the H_2O present in the incoming stream,attack the CO molecules in a thin gas layer adjacent to the catalyst, thus actually simulating an heterogeneous oxidation. It is also interesting that high temperature OH desorption from Pt has been proposed as a "clean" source of OH for chemical kinetics studies *(43)(44)*. Low pressure studies indicate that OH escapes the platinum surface only above a temperature ~800 K *(45)*.

Even though catalytic processes generating radicals have been observed before and the term heterohomogeneous catalysis has been coined to describe them *(46)*, they do not seem to have been previously reported as possibly being important in a practical combustion device. Further work is in progress to check quantitatively the oxidation mechanism postulated above.

V. CONCLUSIONS

Catalytic oxidation of CO in air and in inert/O_2 mixtures over a platinum monolithic catalyst has been investigated over a wide range of flow velocities and equivalence ratios and at different pressure. Under the tested conditions, oxidation proceeds in a diffusion-controlled regime and gas-phase chemical reactions become important only for the lowest velocities and highest equivalence ratios.

The model predicts reasonably well emissions and pressure drops through the catalyst; discrepancies for the CO/Air case are likely to depend on the simplifying assumption of one-step overall kinetics for the oxidation of CO in the gas phase.

It appears that the presence of water is necessary for the catalytic oxidation of CO even in regimes where gas-phase kinetics is slow. A mechanism has been postulated that explains this result as the effect of OH radicals, generated at high temperature at the platinum surface by the presence of water.

TABLE I. CATALYST PROPERTIES

SUBSTRATE: Cordierite, American Lava Corp., AlSiMag 795, split cell

length 0.0760 ± 0.0003 m

wall thickness 0.25×10^{-3}

open area 64%

channels per unit area 0.35×10^{6} m^{-2}

open area per channel 1.9×10^{-6} m^{2}

ratio surface area to total volume 2100 m^2/m^3

ratio surface area to gas volume 3260 m^2/m^3

channel hydraulic diameter (4/3260) 0.00123 m

bulk density 610 kg/m^3

solid density 1700 kg/m^3

safe operating temperature 1473 K

specific heat 800 J/kg·K

coefficient of thermal expansion (linear, 294 - 1033 K) 3.8×10^{-6} K^{-1}

thermal conductivity of solid (572 K) 1.4 J/m·s·k

approximate channel cross-section is a trapezoid with base lengths .0011 m and .0023 m, and height .0012 m

WASHCOAT: γ-alumina

loading 115-125 kg/m^3

surface area (BET)(29.2 - 33.0) $\times 10^{6}$ m^2/m^3

CATALYST: platinum

loading 4.2 kg/m^3

surface area (CO chemisorption) 6×10^{4} m^2/m^3

The γ-alumina and platinum were applied by Matthey Bishop, Inc., Malvern, PA.

REFERENCES

1. Blazowski, W.S. and Bresowar, G.E., Air Force Appl. Prop. Lab. Tech. Rep. TR-74-32,(1974).
2. Rosfjord, T.J., AIAA Pap. 76-46, (1976).
3. Siminski, V.J. and Shaw, H.,J. Eng. Power, Vol. 100, p. 267, (1978).
4. Szaniszlo, A.J., Environ. Prot. Agency, Off. Res. Dev. Rep. 600/7-79-038, p. 385, (1979).
5. Angello, L.C. and Rosfjord, R.J., Environ. Prot. Agency, Off. Res. Dev. Rep. 600/7-79-038, p. 61, (1979).
6. Osgerby, I.T., Heck, R.M., Carrubba, R.V., Gleason, C.C., and Mularz, E.J., Environ. Prot. Agency, Off. Res. Dev. Rep. 600/9-80-035, p. 398, (1980).
7. Pfefferle, W.C., Carrubba, R.V., Heck, R.M., and Roberts, G.W., Am. Soc. Mech. Eng. Pap. 75-WA/Fu-1, (1975).
8. Carrubba, R.V., Chang, M., Pfefferle, W.C., and Polinski, L.M., Spec. Rep.-Electr. Power Res. Inst. (Palo Alto, Calif) SR-39, p. 316, (1976).
9. DeCorso, S.M., Mumford, S., Carrubba, R., and Heck, R.M., Am. Soc. Mech. Eng. Pap. 76-GT-4, (1976).
10. Krill, W.V. and Kesselring, J.P., Environ. Prot. Agency, Off. Res. Dev. Rep. 600/7-79-038, p. 259, (1979).
11. DeCorso, S.M. and Carl, D.C., Environ. Prot. Agency, Off. Res. Dev. Rep. 600/7-79-038, p. 139, (1979).
12. Fukuzawa, H. and Ishihara, Y., Environ. Prot. Agency, Off. Res. Dev. Rep. 600/9-80-035, p. 349, (1980).
13. Anderson, D.N., NASA Tech. Mem. TM-73796, (1977).

14. Anderson, D.N., "Effect of Catalytic Reactor Length and Cell Density on Performance," presented at the U.S. Environ. Prot. Agency, Off. Res. Dev., Second Workshop on Catalytic Combustion, Raleigh, NC, June 21-22, 1977.

15. Anderson, D.N., NASA Tech. Mem. TM-78977, (1978).

16. Anderson, D.N., Environ. Prot. Agency, Off. Res. Dev. Rep. 600/7-79-038, p. 403, (1979).

17. Anderson, D.N., Tacina, R.R., and Mroz, T.S., NASA Tech. Mem. TM X-73589, (1977).

18. Carrubba, R. and Osgerby, I.T., Environ. Prot. Agency, Off. Res. Dev. Rep. 600-7-79-038, p. 435, (1979).

19. Pogson, J.T. and Mansour, M.N., Environ. Prot. Agency, Off. Res. Dev. Rep. 600/7-79-038, p. 111, (1979).

20. Rosfjord, T.J., Environ. Prot. Agency, Off. Res. Dev. Rep. 600/9-80-035, p. 527, (1980).

21. Tong, H., Chu, E.K., and Snow, G.C., Environ. Prot. Agency, Off. Res. Dev. Rep. 600/9-80-035, p. 490, (1980).

22. Heck, R.M., Chang, M., Hess, H., and Carrubba, R., NASA Contract.Rep. CR 135132, (1977).

23. Matthews, R.D. and Sawyer, R.F., West. Sect. Combust. Inst., Prepr. Pap. 77-40, (1977).

24. Chu, E.K. and Kesselring, J.P., Environ. Prot. Agency, Off. Res. Dev. Rep. 600/7-79-038, p. 291, (1979).

25. Folsom, B.A., Courtney, C.W., and Heap, M.P., Environ. Prot. Agency, Off. Res. Dev. Rep. 600/7-79-038, p. 345, (1979).

26. Chu, E.K., Environ. Prot. Agency, Off. Res. Dev. Rep. 600/7-79-038, p. 538, (1980).

27. Lavid, M. and Bracco, F.V., Report No. 1282, Dept. of Mech. and Aerosp. Eng., Princeton University, Princeton, (1976).

28. Kelly, J.T., Kendall, R.M., Ch[illegible], and Kesselring, J.P., West. Sect. Combust. Inst. Prepr. Pap. 77-33, (1977).

29. Pfefferle, W.C., J. Energy, Vol. 2, p. 142, (1978).

30. Cerkanowicz, A.E., Cole, R.B., and Stevens, J.G. J. Eng. Power, Vol. 99, Series A, No. 4, p. 593, (1977).

31. Kesselring, J.P., Krill, W.V., and Kendall, R.M., West. Sect. Combust. Inst., Prepr. Pap. 77-32, (1977).

32. T'ien, J.S., AIAA Pap. 80-1289, (1980).

33. Fristrom, R.M., Avery, W.H., and Greenfelder, C., in VII Symposium (International) on Combustion, Butterworths Scientific Publications, London, p. 304, 1959.

34. Williams, F.A., "Combustion Theory". Addison-Wesley Pub. Co., Reading, 1965.

35. Howard, J.B., Williams, G.C., and Fine, D.H., in XIV Symposium (International) on Combustion, The Combustion Institute, Pittsburgh, p.975,(1973).

36. Bracco, F.V., AIAA J., Vol. 13, No. 11, p. 1421, (1975).

37. Voltz, S.E., Morgan, C.R., Liederman, D., and Jacob, S.M., Ind. Eng. Chem. Prod. Res. Dev., Vol. 12, No. 4, p. 294, (1973).

38. Hegedus, L.L., AIChE J., Vol. 21, No. 5, p. 849, (1975).

39. Gardiner, W.C. and Olson, D.B., in "Annual Review of Physical Chemistry," (B.S. Rabinovitch, J.M. Schurr and H.L. Strauss. Eds.), Annual Reviews, Inc., Palo Alto, p. 377, (1980).

40. Engel, T. and Ertl, G., in "Advances in Catalysis," (D.D. Elay, H. Pines and P.B. Weisz. Eds.), Vol. 28, p. 2, Academic Press, New York, 1979.

41. Campbell, C.T., Ertl, G., Kuipers, H., and Segner, J., J. Chem. Phys., Vol. 73, No. 11, p. 5862, (1980).

42. Strozier, J.A., Brookhaven Nat. Lab. Rep. BNL-25406, (1980).

43. Talley, L.D., Tevault, D.E., and Lin, M.D., J. Chem. Phys., Vol. 72(5), p. 3314, (1979).

44. Talley, L.D., Sanders, W.A., Bogan, D.J., and Lin, M.C., Chem. Phys. Lett., Vol. 78, No. 3, p. 500, (1981).

45. Tevault, D.E., Talley, L.D., and Lin, M.C., Chem. Phys. Lett., Vol. 66, No. 3, p. 584, (1979).

46. Satterfield, C.N., "Heterogeneous Catalysis in Practice," McGraw Hill Book Co., NY, p. 10, (1980).

47. Gosman, A.D. and Ideriah, F.J.K., 1976, "TEACH-T: A general Computer Program for Two-Dimensional, Turbulent, Recirculating Flow," Dept. of Mechanical Engineering, Imperial College, London.

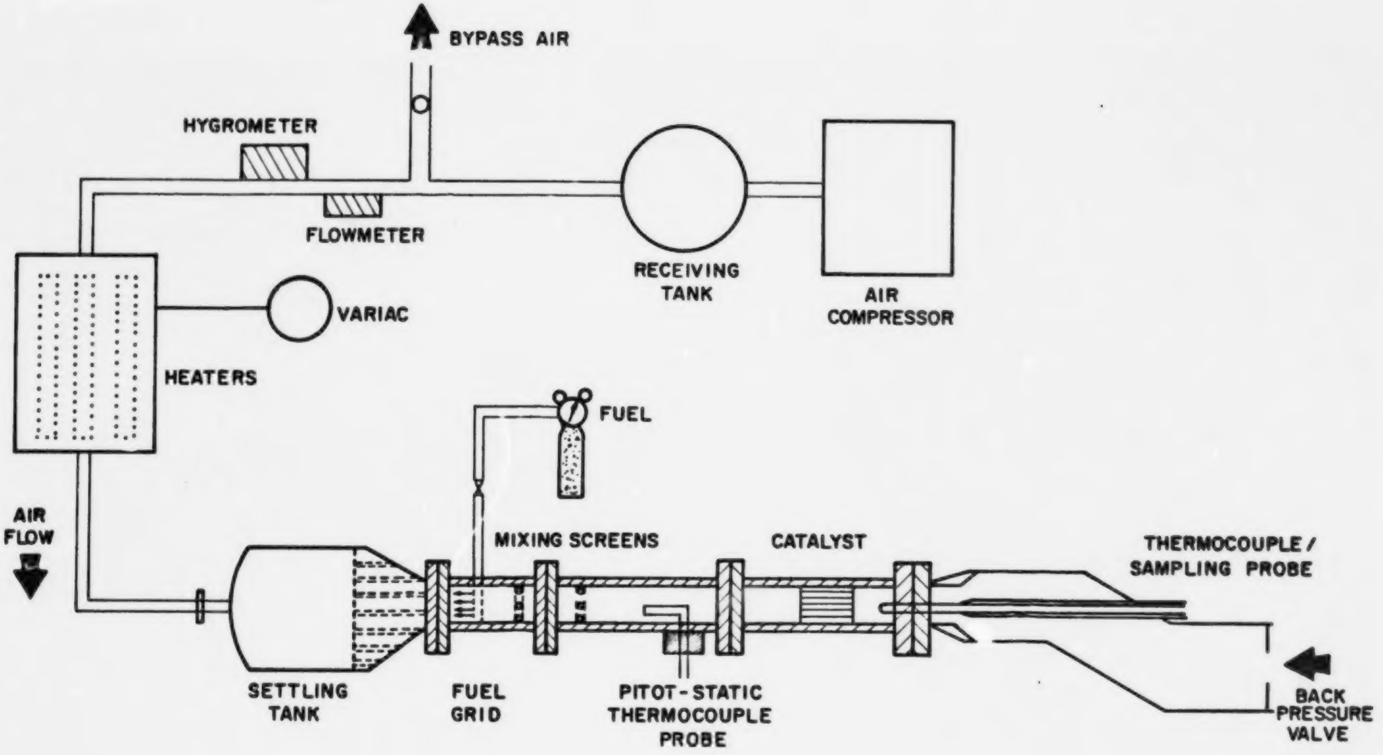
BYPASS AIR
HYGROMETER
FLOWMETER
RECEIVING TANK
AIR COMPRESSOR
VARIAC
HEATERS
FUEL
AIR FLOW
MIXING SCREENS
CATALYST
THERMOCOUPLE / SAMPLING PROBE
SETTLING TANK
FUEL GRID
PITOT-STATIC THERMOCOUPLE PROBE
BACK PRESSURE VALVE

Figure 1. Schematic diagram of the flow reactor with catalytic combustion test section.

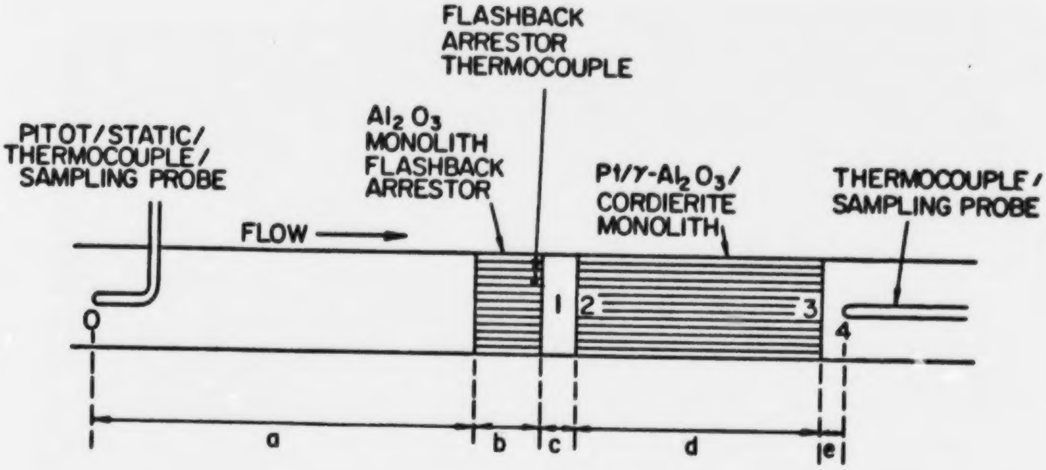
FLASHBACK ARRESTOR THERMOCOUPLE
Al_2O_3 MONOLITH FLASHBACK ARRESTOR
PITOT/STATIC/ THERMOCOUPLE/ SAMPLING PROBE
Pt/γ-Al_2O_3/ CORDIERITE MONOLITH
THERMOCOUPLE/ SAMPLING PROBE
FLOW
0
1
2
3
4
a
b
c
d
e

a	0.217 ± 0.001 m
b	0.0132 OR 0.0262 ± 0.0003 OR 0
c	0.001 TO 0.003
d	0.0760 ± 0.0003
e	0.0010 ± 0.0005

Figure 2. Details of the catalyst test section.

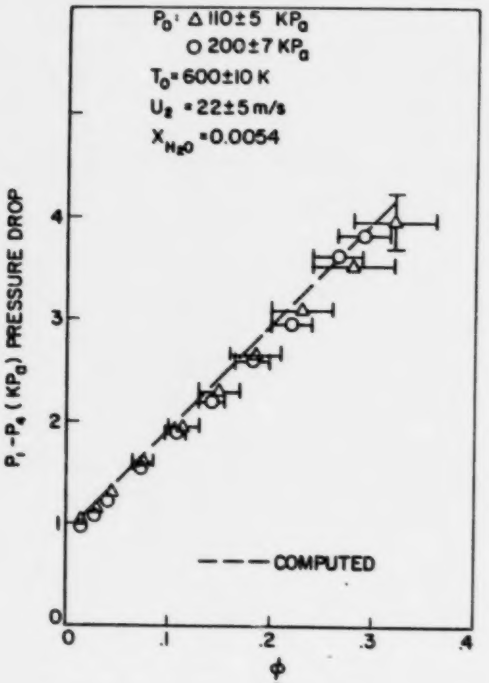

Fig. 4

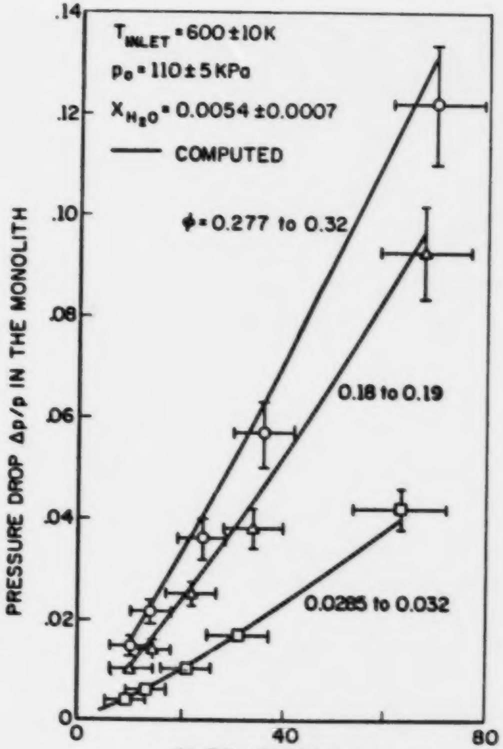

Fig. 3

Figures 3 and 4. Measured and computed pressure drop vs. equivalence ratio and inlet velocity at specified inlet temperature, pressure and water content.

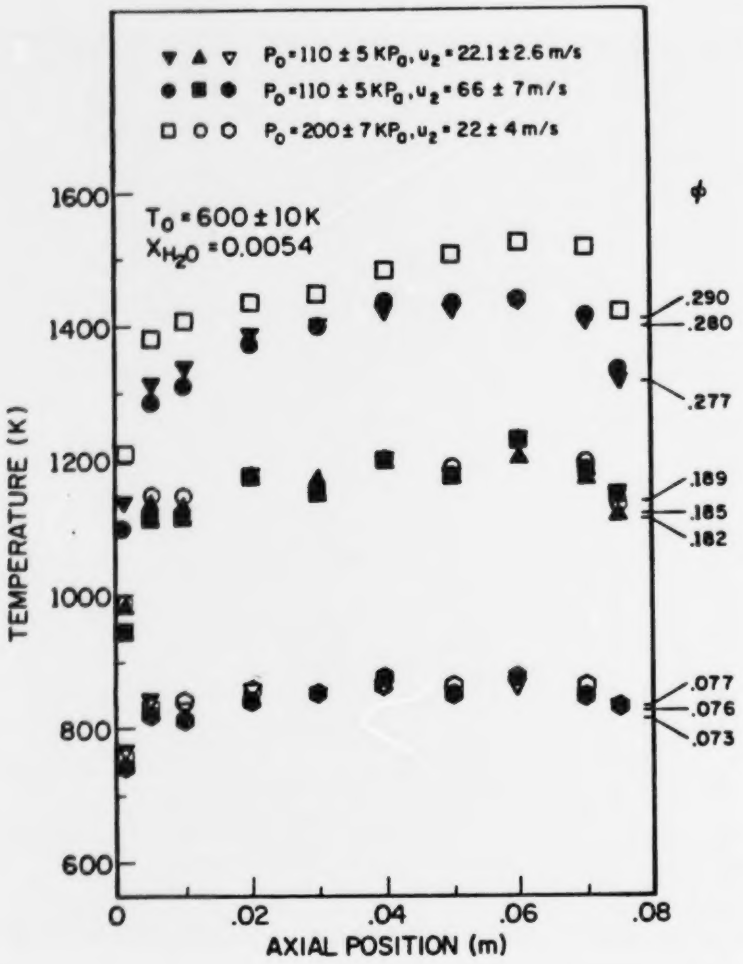

Figure 5. Measured substrate temperature as a function of axial position equivalence ratio, pressure and velocity.

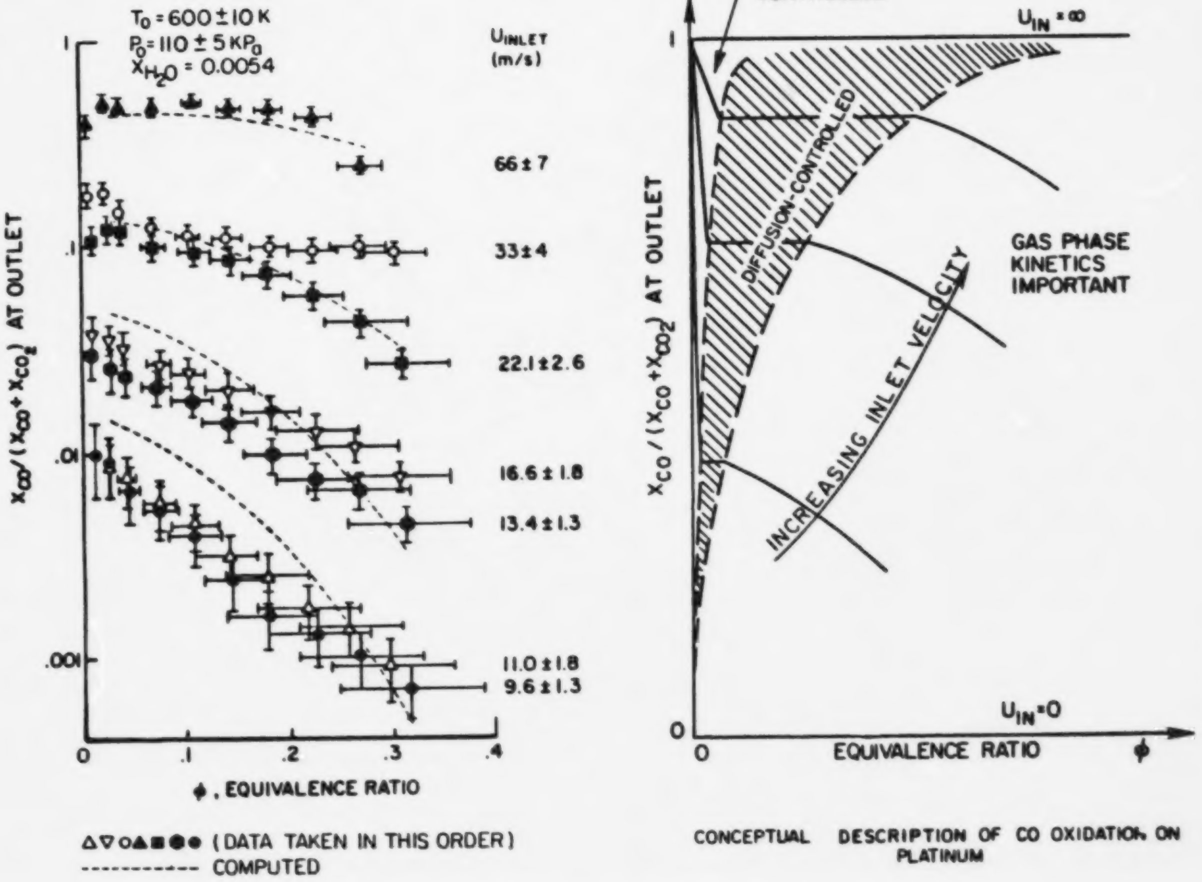

Figure 6. Measured and computed CO emissions vs. equivalence ratio and inlet velocity at specified pressure, inlet temperature and water content.

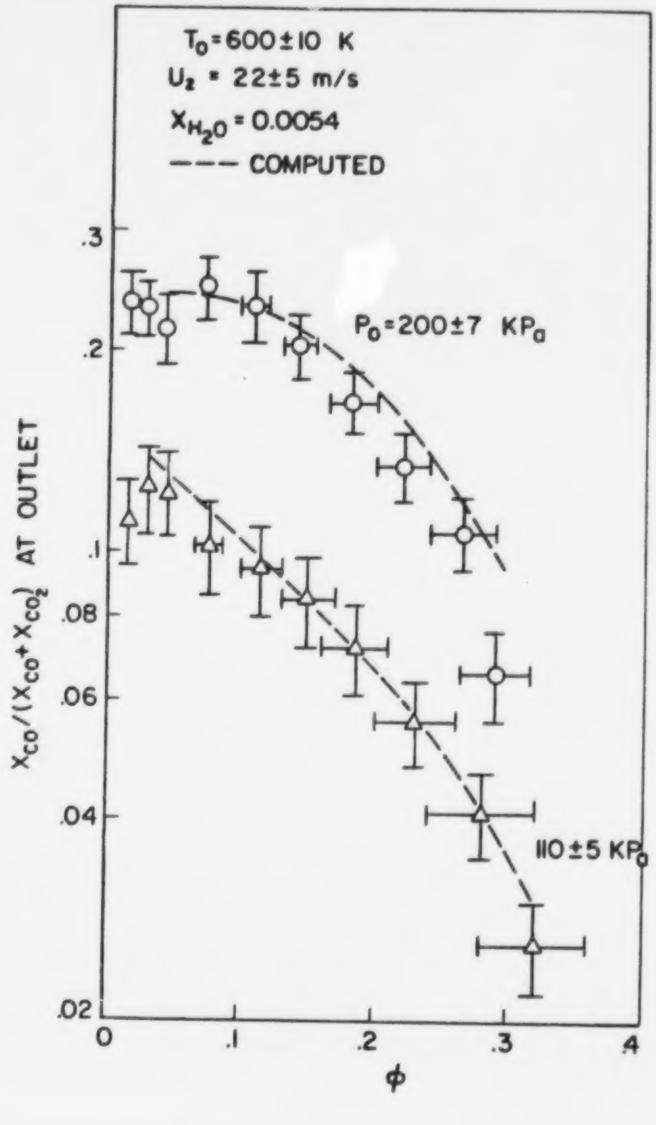

Figure 7. Fraction of CO unburned vs. equivalence ratio and pressure at specified inlet temperature, velocity and water content.

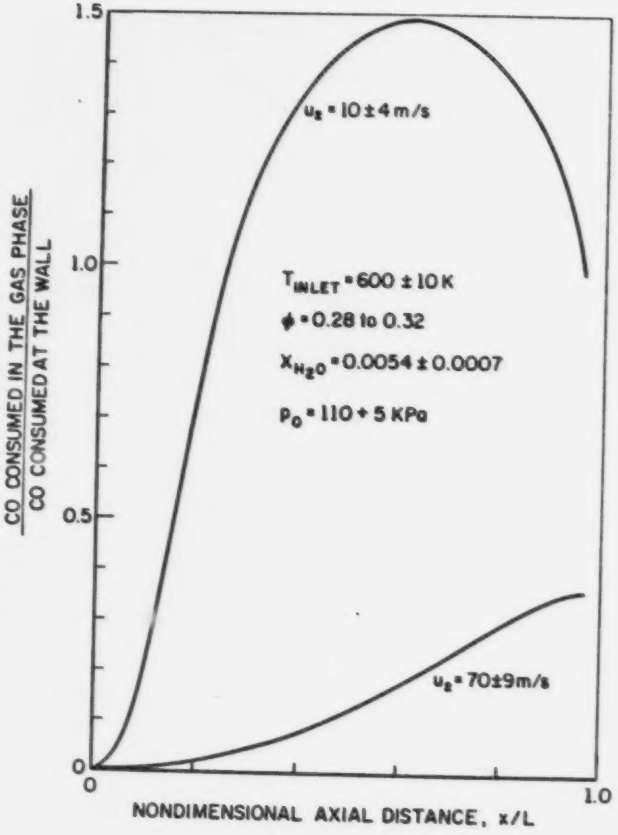

Fig. 9

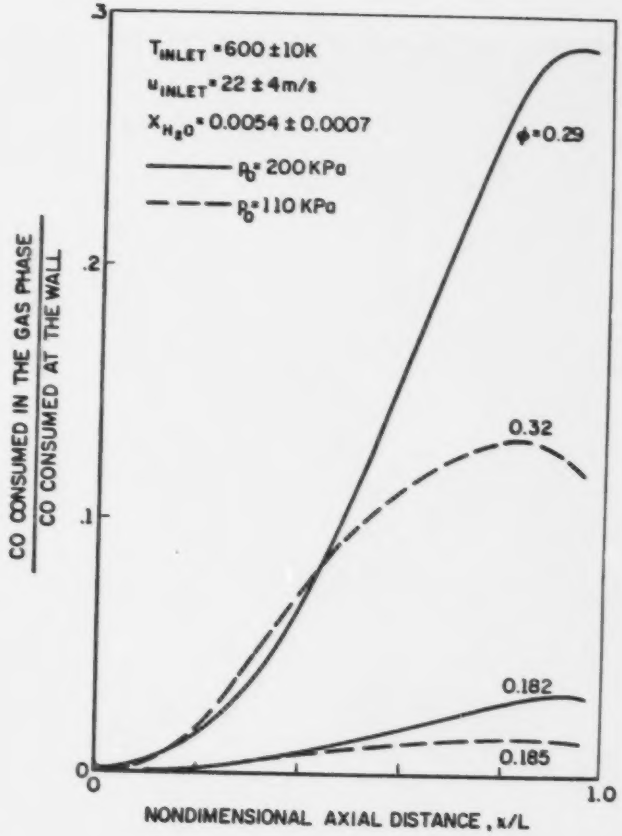

Fig. 8

Figures 8 and 9. CO/air oxidation on platinum — computed local gas phase vs. surface contribution: effect of velocity, equivalence ratio and pressure.

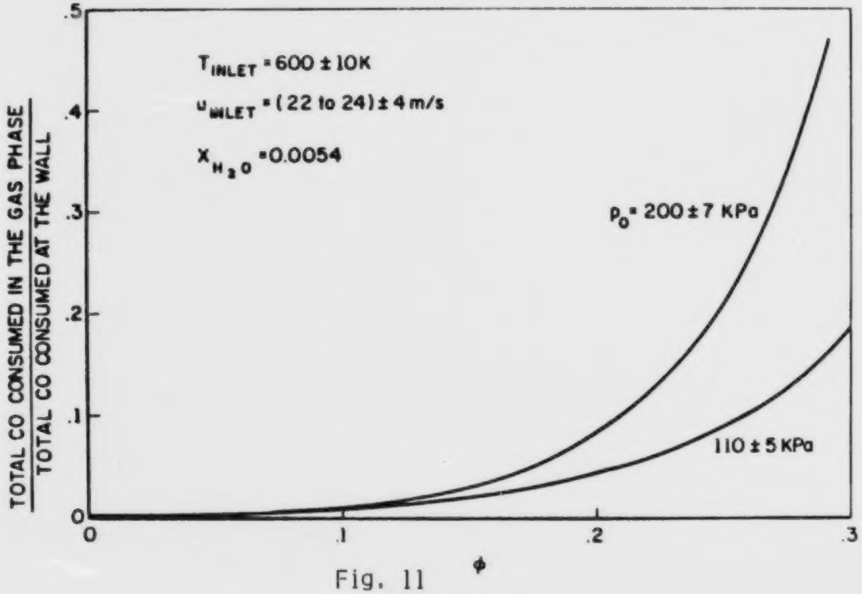

Fig. 11

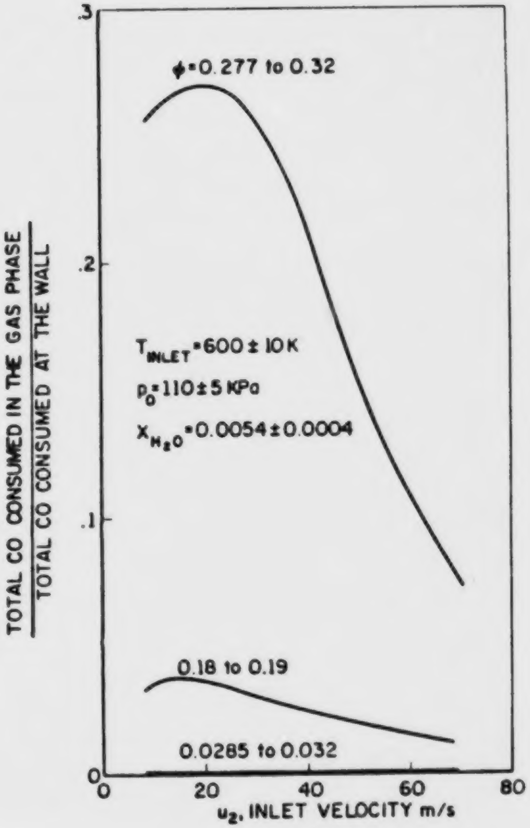

Fig. 10

Figures 10 and 11. CO/air oxidation on platinum — computed effect of equivalence ratio, pressure and velocity.

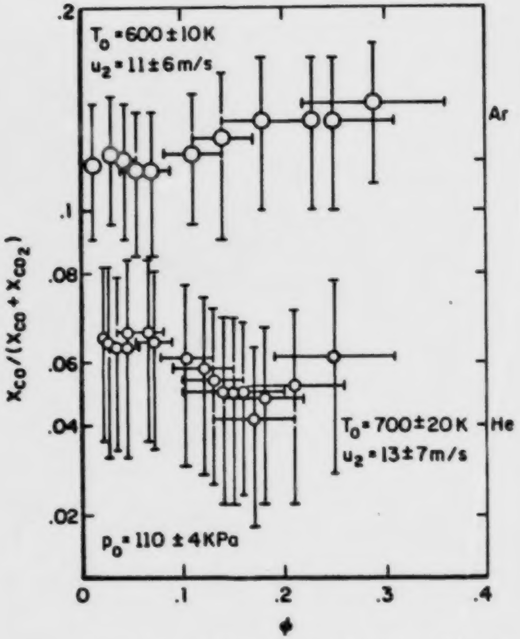

Fig. 13. $CO/O_2/Ar$ and $CO/O_2/He$ mixtures: measured fraction of unburned CO vs. equivalence ratio at specified inlet temperatures, pressures, and velocities

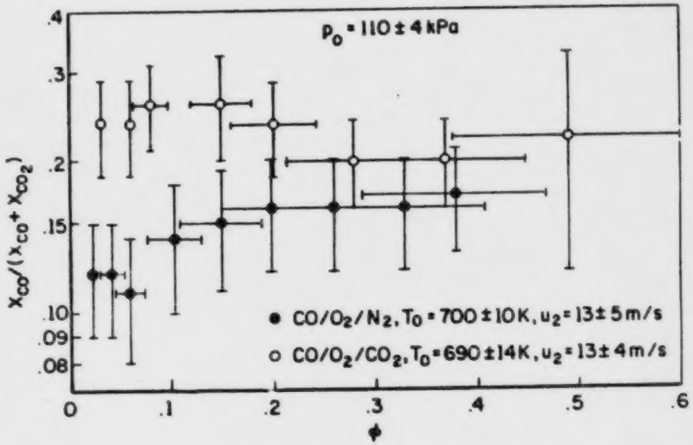

Fig. 12. $CO/O_2/N_2$ and $CO/O_2/CO_2$ mixtures: measured fraction of unburned CO vs. equivalence ratio at specified inlet temperatures, pressures and velocities.

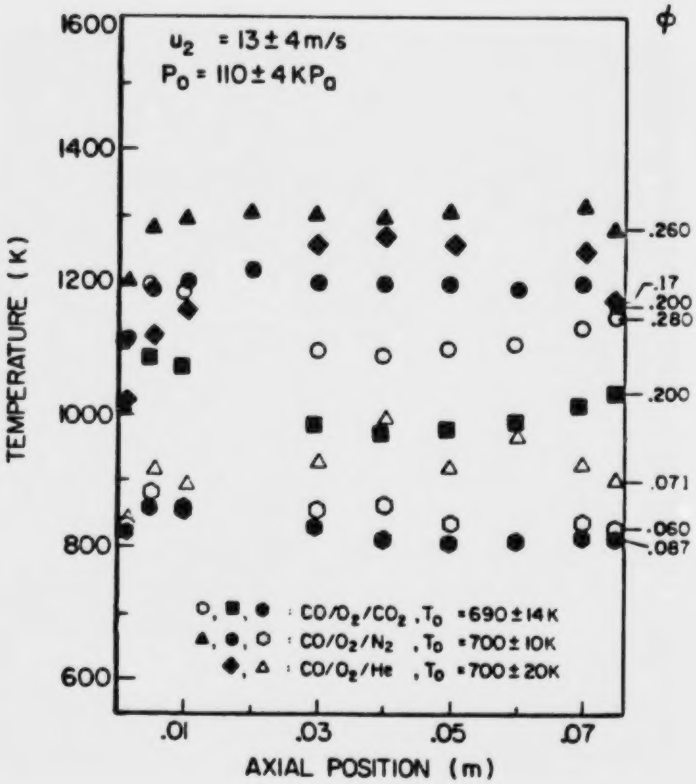

Figure 14. Substrate temperature vs. axial distance for $CO/O_2/CO_2$, $CO/O_2/N_2$ and $CO/O_2/He$ at specified inlet temperatures, velocities, pressure and equivalence ratios.

MECHANISMS AND KINETICS IN CATALYTIC COMBUSTION

by

G. C. Snow, W. V. Krill, E. K. Chu, and R. M. Kendall
Acurex Corporation, Energy & Environmental Division
485 Clyde Avenue
Mountain View, California 94042

ABSTRACT

Experiments show that platinum-coated alumina cylinders held in a cross-flow configuration are successful in isolating the heterogeneous portion of catalytic combustion. Under oxygen-rich conditions, carbon dioxide is shown to be the dominant product of methane surface combustion. Adding small percentages of hydrogen in the reactant mixture provided precise control of the catalyst surface temperature over ranges in which methane and propane heterogeneous kinetics could be quantified. By eliminating the effects of reactant diffusion, activation energies were experimentally determined to be 7.70×10^7 J/kg-mole for methane and 6.95×10^7 J/kg-mole for propane.

NOTATION

A	pre-exponential factor	m^3/m^2-s
C	molar concentration of reactant species	kg-mole/m^3
CL	flow duct centerline	
D_{cyl}	diameter of catalyst cylinder	m
E	activation energy	J/kg-mole
k	first order reaction rate constant	m^3/m^2-s
Nu	Nusselt number	
R	gas constant,	8.314×10^3 J/kg-mole-K
RR	species reaction rate	kg-mole/m^2-s
Re	Reynolds number	
T_p	reactant flow preheat temperature	K
T_s	catalyst surface temperature	K
V_∞	freestream reactant flow velocity	m/s
X	mole fraction	
η	reactant conversion	%
ν	kinematic viscosity	m^2/s
ρ	density	kg/m^3
ϕ_{FA}	fuel-air equivalence ratio, $(F/A)_{actual}/(F/A)_{stoichiometric}$	

Subscripts

f	film temperature conditions
i	species
∞	freestream conditions

ACKNOWLEDGEMENT

The authors express their gratitude for the support provided by the U.S. Environmental Protection Agency, contract no. 68-02-3122, and to the contract officer, G. B. Martin. Also, the significant contributions of J. P. Kesselring are appreciated.

INTRODUCTION

Existing catalytic combustor design information has been obtained through analytical and experimental studies. This information has led to catalytic reactors with improved lightoff, maximum throughput, and lifetime characteristics. For example, the graded cell monolithic reactor developed by Kesselring, et al., (Ref. 1), is able to sustain very high throughputs (space velocities to 4.9×10^5 hr^{-1}) with correspondingly high combustion efficiencies and low pollutant emissions.

Further optimization requires a more fundamental understanding of fuel oxidation and pollutant formation processes. In particular, it is important to know the mechanisms describing heterogeneous reactions in catalytic combustion and whether carbon monoxide or carbon dioxide is the product of fuel oxidation at catalyst active sites. This will lead to a more complete definition of the role of surfaces in promoting efficient fuel conversion. Knowledge of the compositional as well as temperature state existing at the surface facilitates the description of enthalpy gradients driving heat and species transfer processes.

EXPERIMENTAL

Experimental data were collected utilizing platinum coated cylinders held in a crossflow configuation relative to the flowing reactants. The alumina cylinders were obtained from Coors Porcelain Company in two diameters, 3.18×10^{-3}m and 6.35×10^{-3}m, and measured 5.08×10^{-2}m in length. Nominal cylinder weights were 1.876×10^{-3} kg and 4.340×10^{-3} kg. Oxy-Catalyst, Inc. applied the γ-alumina washcoat, and platinum catalyst coatings of nominally 0.45 percent of cylinder weight were done at Acurex. The platinum loading was obtained by brushing an aqueous solution of chloroplatinic acid (H_2PtCl_6), fixing with hydrogen sulfide, and calcining at approximately 673K for 3 hours. The resulting catalytic surface was considered to be more representative of a prototype catalytic combustor than investigations utilizing pure platinum filaments (e.g., Rader and Weller, Ref. 2 and Hiam, et al., Ref. 3). To allow for washcoat sintering prior to experimental data collection, the cylinders were held at approximately 1310K for 1 hour by fuel-lean surface combustion.

The details of catalytic cylinder mounting and experimental facility are described elsewhere (Snow, et al., Ref. 4). Briefly, Combinations of one, two, or three cylinders of a given diameter were mounted in parallel within flow ducts of various cross sections. The cylinders were oriented in a plane normal to the flow duct axis. The degree of flow blockage was designed to yield about 5 percent fuel conversion through sub-stoichiometric heterogeneous combustion. Mixing of the surface combustion products with the remaining unreacted flow occurred downstream of the cylinder surfaces. The objective was not to achieve complete combustion of the fuel, but rather to study the process by reacting a small portion of the flow. At this condition, gas phase ignition and homogeneous combustion were not present, yet sufficient product concentrations were available for accurate measurement.

Sampling of major product species was done with a water cooled, low pressure (ca. 37.3 kPa), traversing probe downstream of the cylinders. Flow temperatures were made with upstream and downstream thermocouples while surface temperatures were obtained by locating thermocouples within the hollow cylinders.

RESULTS AND DISCUSSION

Data were collected on methane (CH_4) and propane (C_3H_8) fuels with air as the oxidizer. Methane alone was used in screening and reaction characterization studies while kinetics data were obtained on both fuels.

REACTION CHARACTERIZATION

An early objective in the experimentation was to confirm the operational characteristics of the cylinder in crossflow catalyst configuration. Another goal was to identify whether the dominant product from heterogeneous combustion of methane was carbon monoxide or carbon dioxide. This would identify the global oxidation mechanism for methane at a catalyst active site as either $CH_4 \rightarrow CO$ or $CH_4 \rightarrow CO_2$. Under fuel-lean steady state operation, reactants diffuse to the catalyst and react at active sites on and within the surface. The reaction rate increases with surface temperature until it is faster than the maximum inward diffusion rate of the lean reactant. Thus, mass transfer limitations begin to control the conversion rate of methane at about 1000K and of propane at about 625K. Under this diffusionally controlled heterogeneous process, only the reactants reaching the surface were converted to products, providing the free stream mixture remains below ignition temperatures.

Figures 1 through 4 show the results of sample probe traverses downstream of three parallel cylinders in the crossflow configuration. The cylinders were 3.18×10^{-3}m in diameter and were located in a duct of diameter 5.08×10^{-2}m. The nominal test conditions for the data shown are a methane-air equivalence ratio of $\phi_{FA} = 0.86$, reactant preheat temperature of 644K, and an approach velocity of 6 m/s. These results combined with visual observations indicate that downstream flameholding or gas phase reaction was not present. All gas phase concentration measures are presented on a dry volume basis.

These figures show a considerable variation of gas phase concentration measurements with sample probe position. Figure 1 gives CO and CO_2 measurements as the sample probe was traversed across the test section, 5.08×10^{-4}m downstream of the cylinders. The profiles are very cyclical and indicate a clear definition between surface combustion products and the unreacted freestream. Additional results taken further downstream are shown in Figures 2 through 4. At each location, CO and CO_2 concentrations are both maximum directly behind the cylinder, with CO_2 as the dominant product. The sharp division between concentrations directly behind a cylinder and the freestream (midway between cylinders) becomes less pronounced at increasing downstream positions as a result of cross-stream mixing.

At the furthest downstream point, shown in Figure 4, the profiles are essentially flat, indicating a well mixed condition. The broken horizontal line at the CO_2 concentration of 0.5 percent shows the results of an approximate integration over the test duct cross section of the CO_2 profile in Figure 7. If significant homogeneous combustion was occurring downstream of the cylinders, the measured CO_2 level at 2.84×10^{-2}m (Figure 4) would be somewhat higher than the broken line prediction. Scatter in the data is due primarily to uncertainty in positioning of the sample probe. This is of little concern, however, as the traversing was done mainly to verify the nonexistence of gas phase combustion reactions. Measurements used for computational purposes are taken with the probe fixed in the well mixed downstream region.

Measurements of CO_2, CO, unburned hydrocarbons (UHC), and gas temperature were also made in the streamwise direction for the 3.18×10^{-3}m diameter cylinders. Figure 5 shows the variation in gas species concentrations in the streamwise direction behind one cylinder. Carbon dioxide and carbon monoxide decrease while UHC concentrations increase with axial distance due to mixing of the combustion products with the unreacted freestream. Figure 6 shows the same measurements taken midway between two cylinders. Here the trends are reversed, as expected, and the product concentrations reach the same level as in Figure 5 at a downstream distance of 4.0×10^{-2}m. A typical axial temperature profile behind a cylinder is shown in Figure 7. These results indicate that downstream combustion does not exist under the test conditions, and changes in measured species are due solely to cross-stream mixing.

The above data can be replotted as the ratio of CO to CO_2 concentrations, shown as a function of stoichiometry in Figure 8. The ratio is small throughout the range of fuel-lean mixtures, indicating CO_2 to be the major product. This agrees with the investigations of Schwartz, et al. (Ref. 5) and Anderson (Ref. 6) which showed that in oxygen-rich systems most hydrocarbons, including propane, convert into CO_2 and H_2O at the surface without forming CO.

The ratio increases as the stoichiometric condition is approached from the fuel-lean side, reflecting an increased production of CO. Figure 8 also indicates that the reactant preheat temperature has a small effect on the relative amounts of CO and CO_2 as compared to the fuel/air equivalence ratio. It appears that the thermal environment in which the reaction occurs is influenced more by the reactant stoichiometry at the surface than by the reactant gas temperature.

Under the diffusionally controlled reaction, low levels of input fuel conversion to CO_2 (and CO) can be represented by:

$$\eta = \frac{\left(X_{CO_2} + X_{CO}\right)_{\text{products}}}{\left(X_{\text{fuel}}\right)_{\text{reactants}}} \times 100$$

$$= \frac{\text{rate of fuel diffusion to surface}}{\text{total fuel flowrate}} \times 100 \qquad (1)$$

The diffusional process may be predicted through a heat transfer analogy (Kays, (Ref. 7). The applicable heat transfer model is Hilpert's (Ref. 8) cylinder in crossflow correlation as modified by Morgan (Ref. 9) for closed duct blockages and revised thermophysical property data. The correlation is given by:

$$Nu_f = 0.583(Re_f)^{0.471} \qquad (2)$$

Combining Equations (1) and (2) we find:

$$\eta \propto \frac{(Re_f)^{0.471}}{Re_f} = (Re_f)^{-0.529} \qquad (3)$$

Figure 9 shows measured methane conversion as a function of cylinder Reynolds number (total flowrate). The data are well described by the functional behavior of Equation (3) confirming the overall transfer process. The measured conversion is also plotted as a function of reactant stoichiometry in

Figure 10. Only a weak dependence with stoichiometry (or surface temperature) is indicated. This again suggests the dominant role of mass transfer, especially in the near-stoichiometric higher surface temperature regime. Shown as the horizontal solid line in Figure 10 is the predicted level based on Equation (1) with properties evaluated at the average of surface and freestream temperatures. As can be seen, the measured reaction rates are significantly increased over the model. However, since the freestream turbulence levels and velocity profiles are not well defined in the present data, their effects are not included in the correlations. Comings, et al. (Ref. 10) found Nusselt number increases over baseline calculations of 26 to 45 percent at turbulence intensities of 2.7 to 8 percent, respectively. The high temperature difference between the cylinder surface and the freestream also enhances the Nusselt number over that based on correlations of data under more modest temperatures. Recorrelations for large temperature differences have been presented by Douglas and Churchill (Ref. 11) which result in about a 3 percent increase in the diffusional limit at the present experimental conditions. Morgan (Ref. 9) reviewed the work of Churchill and Brier, Gosse, and others for loading factors to be used under high temperature differences. The recommended corrections give an increase of up to 6 percent in the mass transfer coefficient at the present conditions. Morgan cautioned, however, that more work was essential before the effects could be better quantified.

HETEROGENEOUS KINETICS

To obtain global heterogeneous kinetic rate information on the platinum catalyst, the methane and propane reactions were studied at surface temperatures below 1000K and 625K, respectively. In these temperature ranges, the overall reaction rates were limited by chemical processes and kinetic rates were directly observable. Control of the surface temperature was made possible by combusting a small amount of hydrogen on the catalyst. By adding concentrations of 1.4 to 4.9 percent by volume to the reactant flow, the surface temperature could be varied between 465K and 1333K. Within this range, the hydrogen reaction remained diffusionally limited. Without the stability and control furnished by the hydrogen augmentation, the kinetically limited heat release rate, being insufficient to overcome losses, would lead to rapid extinguishment of the methane or propane reaction.

Experimental data were correlated with the first order Arrhenius rate equation:

$$\frac{RR}{C_\infty} = k = Ae^{-E/RT_s}$$

The rate of fuel consumption, RR, was measured by product levels of CO_2 and CO which were corrected for background concentrations contained in the fuel and combustion air. To assess possible reaction mechanism effects due to the presence of hydrogen, the relative reactant concentrations were fixed while the test duct flow velocity was varied. The resulting variation in hydrogen diffusion rates and corresponding surface temperature behavior gave identical methane and propane kinetic data. In addition, no apparent effect on reaction mechanisms or kinetic information was seen as reactant volume concentrations were changed from 2.8 percent to 4.5 percent for methane and from 0.5 percent to 1.2 percent for propane. Figures 11 and 12 show semi-logarithmic plots of the rate constant, k, versus inverse surface temperature, T_s. The slope of the plotted data gives the apparent activation energy, E. Since the free-stream fuel concentration, C_∞, was used in the correlation, the apparent activation energy depends on the rate of lean reactant diffusion to the catalyst surface. The effects of mass transport limitations become more significant in the higher temperature ranges as the reaction rate increases. For the methane reaction shown in Figure 10, the effects of diffusional limitations are apparent above 1000K. The transition occurs at about 625K for propane, shown in Figure 12. Because of variations in the local Nusselt number around the cylinder circumference, transition to diffusional control is not as abrupt as expected, nor is it apparently complete in the temperature range studied. The horizontal lines on Figures 11 and 12 predict the high temperature rate constant behavior based on full diffusional control. Again, these are somewhat below the measured performance due to complexities in the diffusional process not fully accounted for in the calculated mass transfer coefficient.

In the low temperature kinetically controlled regime, the slope of the plot represents the true activation energy. A least squares linear fit was used to quantify the kinetic parameters which are summarized in Table 1 along with those reported by other workers. The values for activation energy obtained in the present study show good agreement with the other entries. This term is most useful since it is widely applicable to various configurations and operational characteristics of a given catalyst providing the reaction mechanism remains unchanged. Table I indicates a wider range in the values of the pre-exponential factor, however. Unlike the activation energy, this parameter is dependent on individual catalyst characteristics such as geometry, active sites dispersion, and flow properties. The pre-exponential factor in this work is based on total catalyst geometric surface area presented to the reactant flow. Anderson, et al. (Ref. 12) reported a pre-exponential factor based on bulk catalyst volume as 2.24 x 10^7 m^3/m^3-s. Trimm and Lam (Ref. 13) studied methane combustion on a fiber pad burner and found pre-exponential factors of 1.03 x 10^{-5} kg-mole/m^2-s and 3.20 x 10^{-6} kg-mole/m^2-s, respectively, for porous and nonporous alumina pad fibers. Their results were based on platinum metal surface area determined by CO adsorption. Table II gives a comparison of rate constant temperature dependence for methane and propane derived from the present work.

CONCLUSIONS

The experimental technique has proven useful for studying the heterogeneous portion of catalytic combustion. In the higher temperature ranges of operation (near stocihiometric), the surface reaction rate on the cylinder in crossflow configuration is limited by lean reactant diffusion. In this regime, the combustion of methane was promoted essentially to completion by the catalyst with carbon dioxide as the major product. This data is most useful for understanding normal, steady state operation encountered in honeycomb monolith type catalysts. It will allow further optimization in the amount of surface area required for a specific energy release rate.

Small amounts of hydrogen in the reactant flow gave precise catalyst surface temperature control over ranges in which methane and propane heterogeneous kinetics could be quantified. The experimentally measured activation energies were 7.70×10^7 J/kg-mole for methane and 6.95×10^7 J/kg-mole for propane. These values compare favorably with those reported by other workers. Also, the relative magnitudes agree with experience in which propane ignition occurs earlier and at a lower temperature and is more difficult to blow out than methane on a given catalyst. This surface reaction rate information is required for efficient design of catalyst entry regions. The Nusselt number (Sherwood number for mass transfer) is large in these or other zones where flow stagnation may occur giving high mass transfer rates. Additionally, kinetic information is necessary to predict lightoff characteristics and maximum throughput capabilities before catalyst blowout.

Further studies are recommended to understand and quantify the combustion process for other fuels on both noble metal and oxide catalyst formulations. Also recommended are investigations into the overall effect of catalyst configuration (such as a fiber pad burner) on operating regime.

REFERENCES

1. Kesselring, J. P., Krill, W. V., Atkins, H. L., Kendall, R. M., and Kelly, J. T. Design Criteria for Stationary Source Catalytic Combustion Systems. EPA-600/7-79-181, 1979.

2. Rader, C. G. and Weller, S. W. Ignition on Catalytic Wires: Kinetic Parameter Determination by the Heated-Wire Technique. AIChE. j., Vol. 20, p. 515, 1974.

3. Hiam, L., Wise, H., and Chaikin, S. Catalytic Oxidation of Hydrocarbons on Platinum. J. Catal., Vol. 10, pp. 272-276, 1978.

4. Snow, G. C., Chu, E. K., Krill, W. V., Kesselring, J. P., and Kendall, R. M. Fundamental Studies in Catalytic Combustion. Paper No. WSS/CI 81-27, Western States Section, The Combustion Institute, 1981 Spring Meeting, Pullman, WA, 1981.

5. Schwartz, A., Holbrook, L. L., and Wise, H. Catalytic Oxidation Studies with Platinum and Palladium. J. Cata., Vol. 21, pp. 199-207, 1971.

6. Anderson, D. M. Preliminary Results from Screening Tests of Commerical Catalysts with Potential Use in Gas Turbine Combustors, Part I. Furnace Studies of Catalyst Activity. NASA TMX-73410, 1976.

7. Kays, W. M. Convective Heat and Mass Transfer. McGraw-Hill, New York, 1966.

8. Hilpert, R. Warmeabgabe von geheizten Drahten und Rohren im Lufstrom. Forsch. Geb. Ingenieurw., Vol. 4, pp. 215-224, 1933.

9. Morgan, V. T. The Overall Convective Heat Transfer from Smooth Circular Cylinders. Advances in Heat Transfer, Vol. 2, pp. 199-264, Academic Press, New York, 1975.

10. Comings, E. W., Clapp, J. T., and Taylor, J. F. Air Turbulence and Transfer Processes. Flow Normal to Cylinders. Industrial and Engineering Chemistry, Vol. 4, pp. 1076-1082, 1948.

11. Douglas, W. J. M. and Churchill, S. W. Recorrelation of Data for Convective Heat Transfer Between Gases and Single Cylinders with Large Temperature Differences. Chem. Eng. Progr., Symposium Series, Vol. 52 (18), pp. 23-28, 1956.

12. Anderson, R. B., Stein, K. C., Feenan, J. J., and Hofner, L. J. E. Catalytic Oxidation of Methane. Ind. & Eng. Chem., Vol. 53 (10), pp. 809-812, 1971.

13. Trimm, D. L. and Lam, C. W. The Combustion of Methane on Platinum-Alumina Fibre Catalysts -- I Kinetics and Mechanism. Chem. Eng. Sci., Vol. 35, pp. 1405-1413, 1980.

14. Bracco, F. V., Bruno, C., Yaw, Y., and Walsh, P. M. Computed and Measured Emissions from the Catalytic Combustion of Propane/Air Mixtures. Presented at the Fourth Workshop on Catalytic Combustion, sponsored by EPA/IERL, May 14-15, 1980.

15. Marteney, P. J. Determination of the Rate of Heterogeneous Reaction on Catalytic Surfaces. Proceedings: Third Workshop on Catalytic Combustion. EPA-600/7-79-038, 1978.

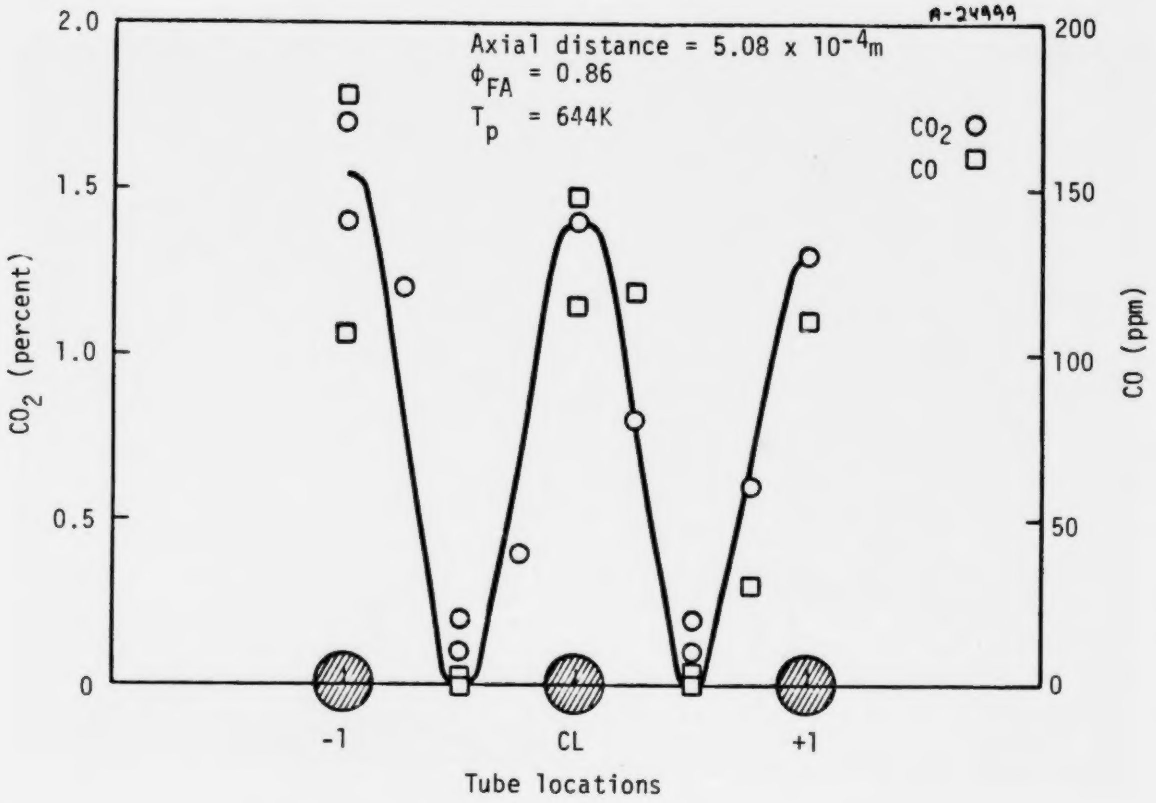

Figure 1. Radial distribution of CO_2 and CO concentrations at 5.08×10^{-4}m for 3.18×10^{-3}m cylinders.

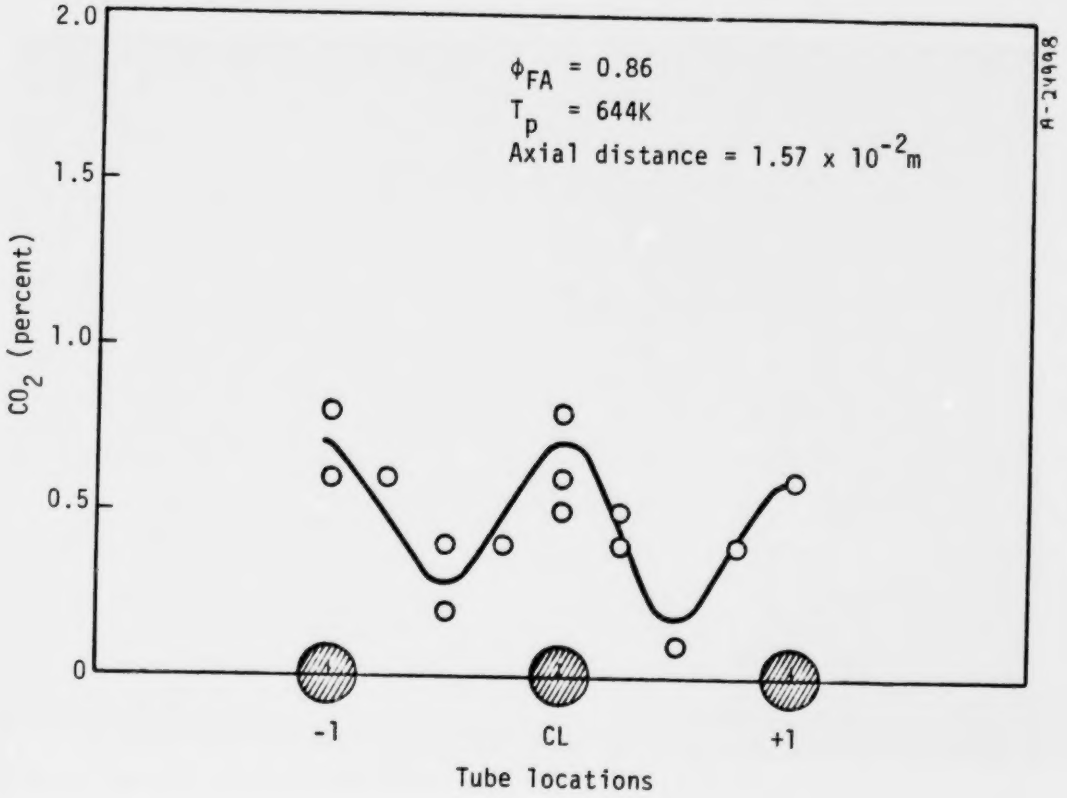

Figure 2. Radial distribution of CO_2 concentration at 1.57 x 10^{-2}m for 3.18 x 10^{-3}m cylinders.

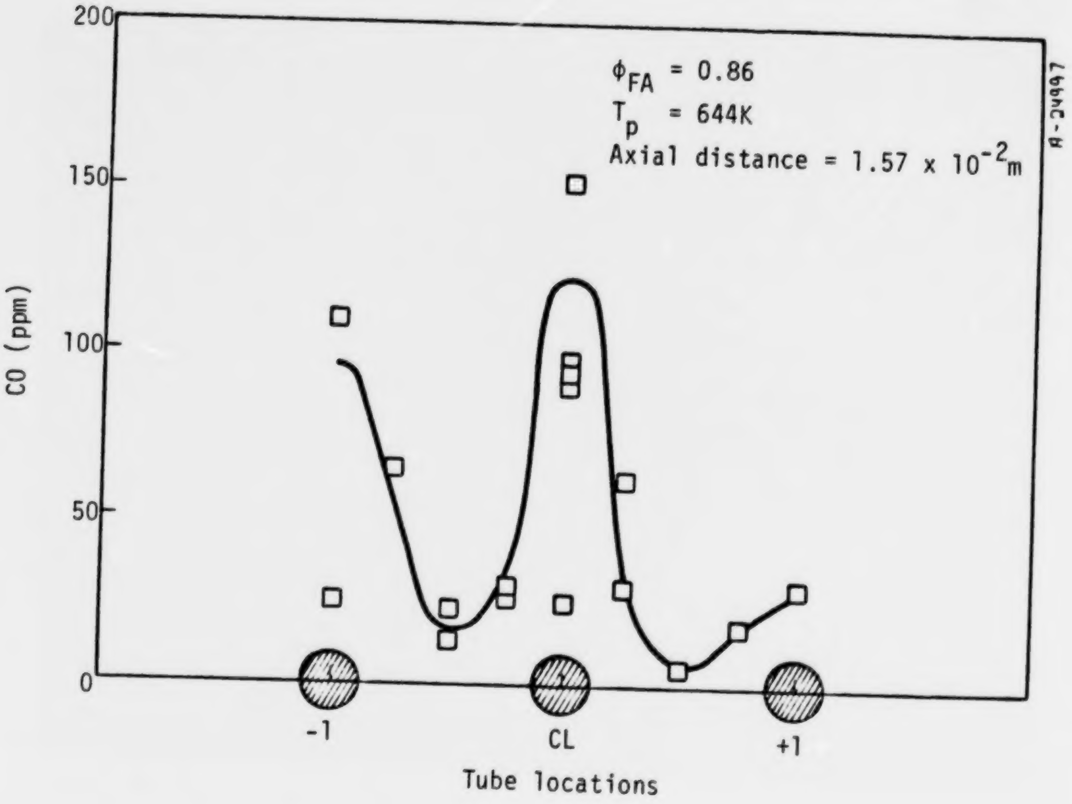

Figure 3. Radial distribution of CO concentration at 1.57 x 10^{-2}m for 3.18 x 10^{-3}m cylinders.

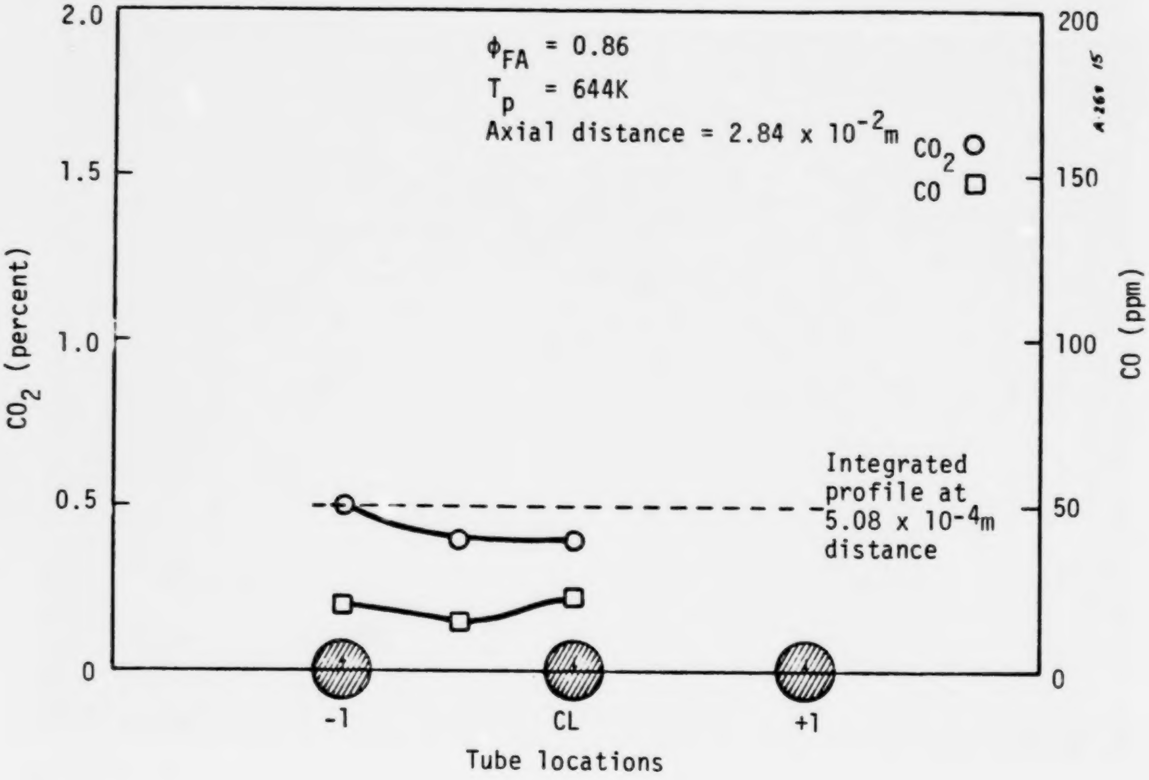

Figure 4. Radial distribution of CO_2 and CO concentration at 2.84×10^{-2}m and 3.18×10^{-3}m cylinders.

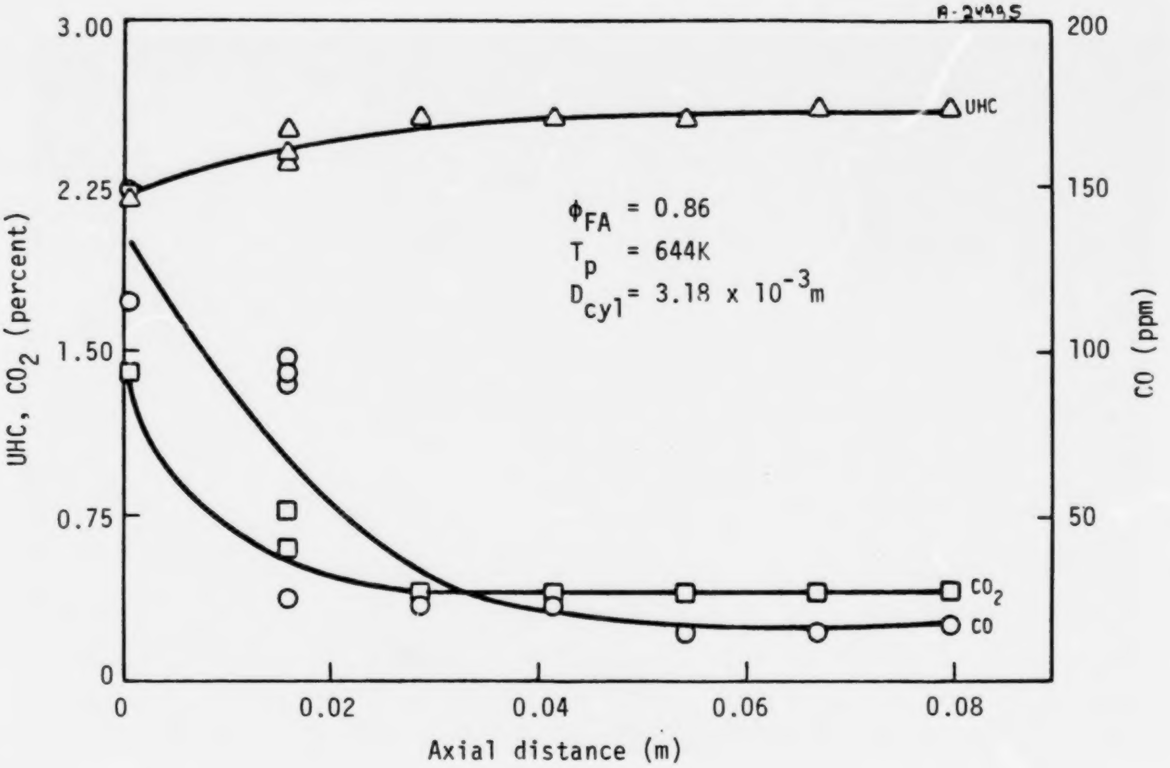

Figure 5. Species concentration measurements in the axial direction in line with catalyst cylinder.

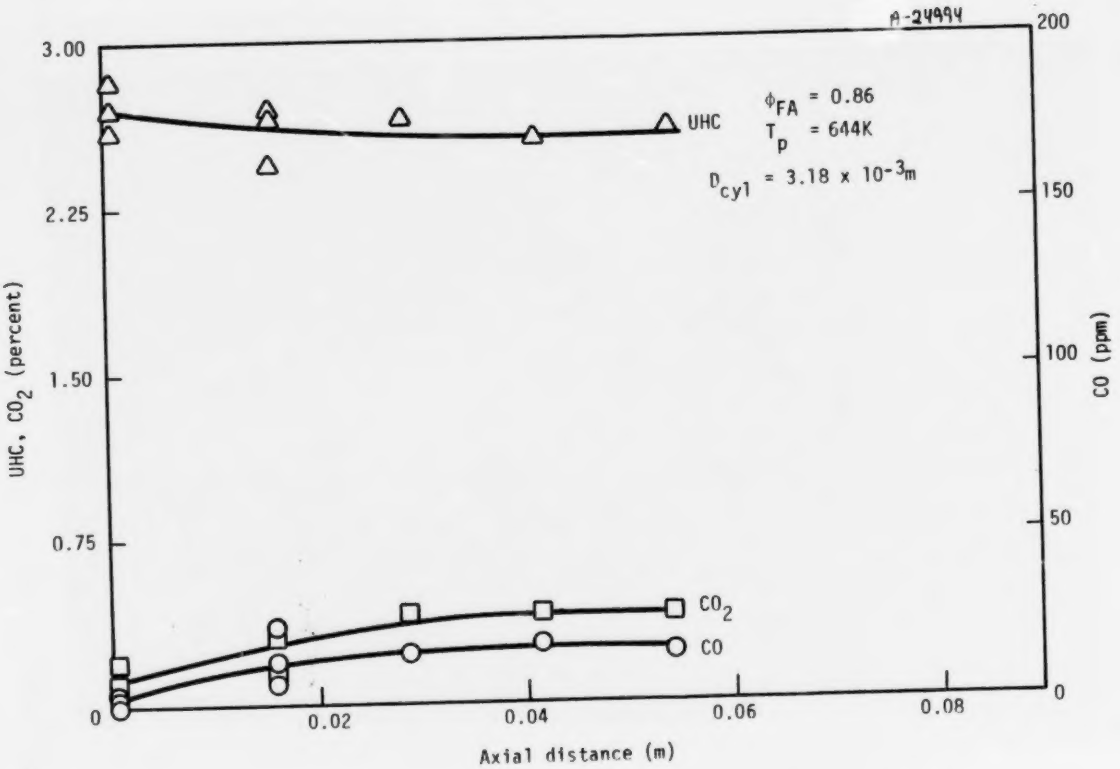

Figure 6. Species concentration measurements in the axial direction midway between catalyst cylinders.

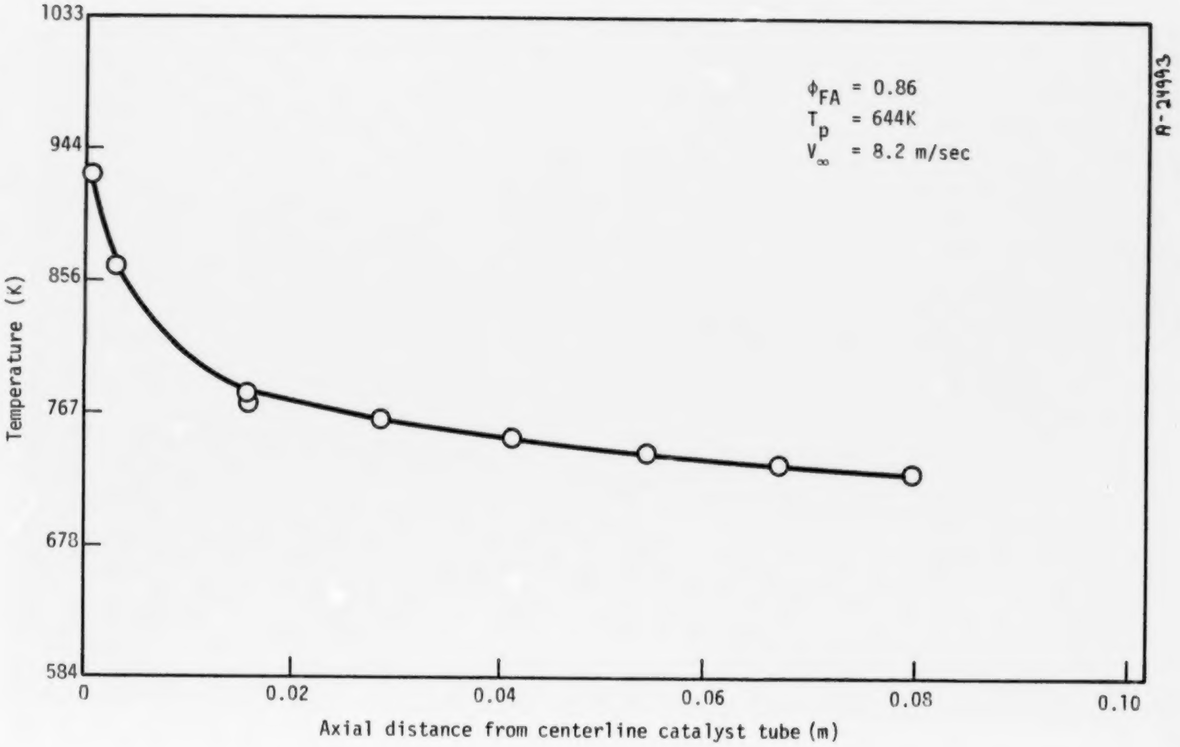

Figure 7. Temperature downstream of centerline catalyst cylinder.

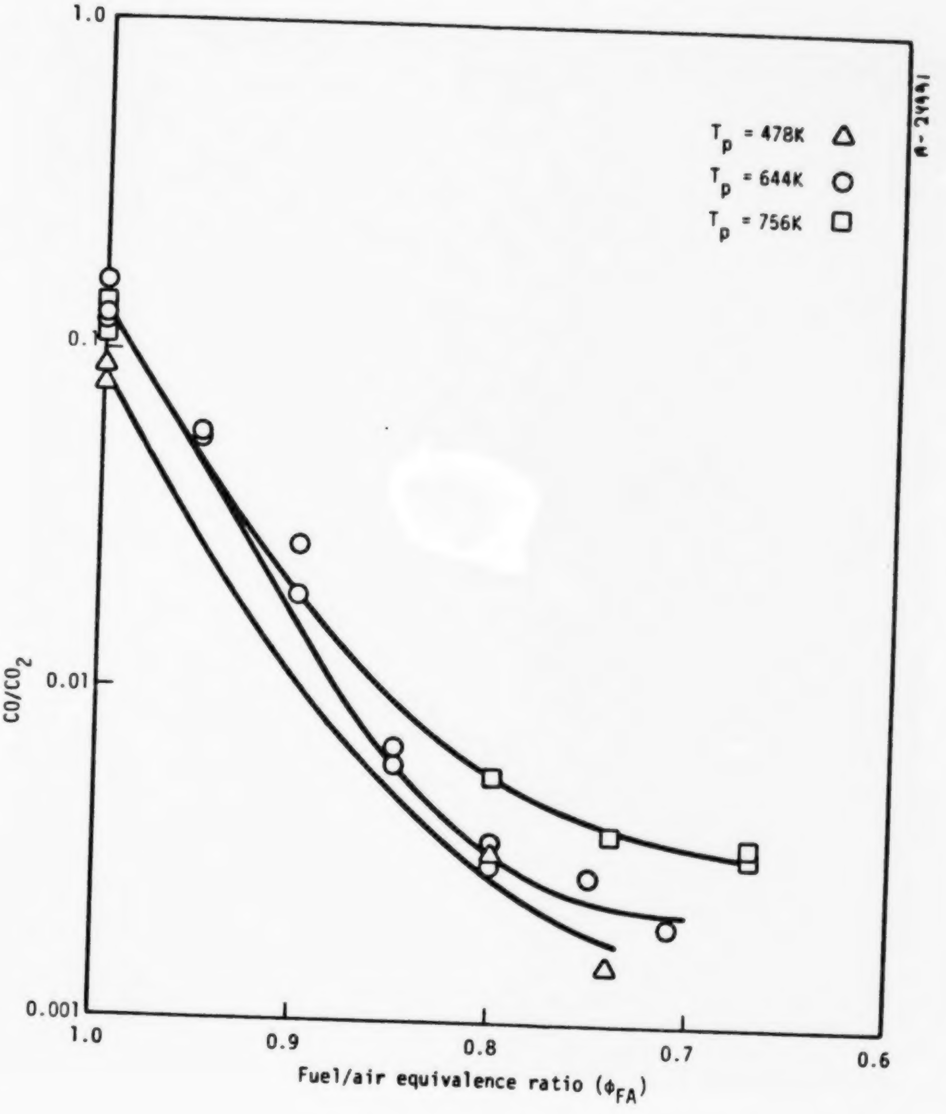

Figure 8. CO/CO$_2$ ratio for 6.35×10^{-3}m platinum coated cylinders.

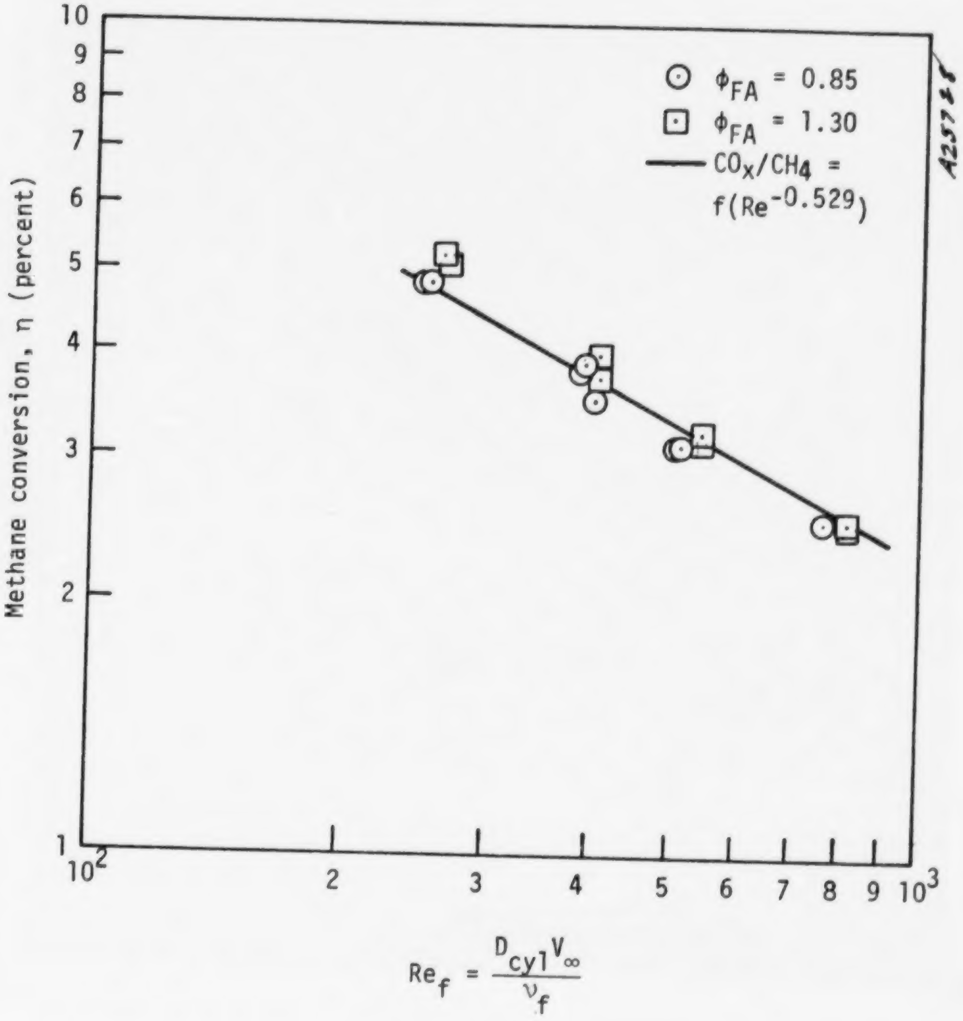

Figure 9. CH_4 conversion to CO_2 + CO at variable throughput.

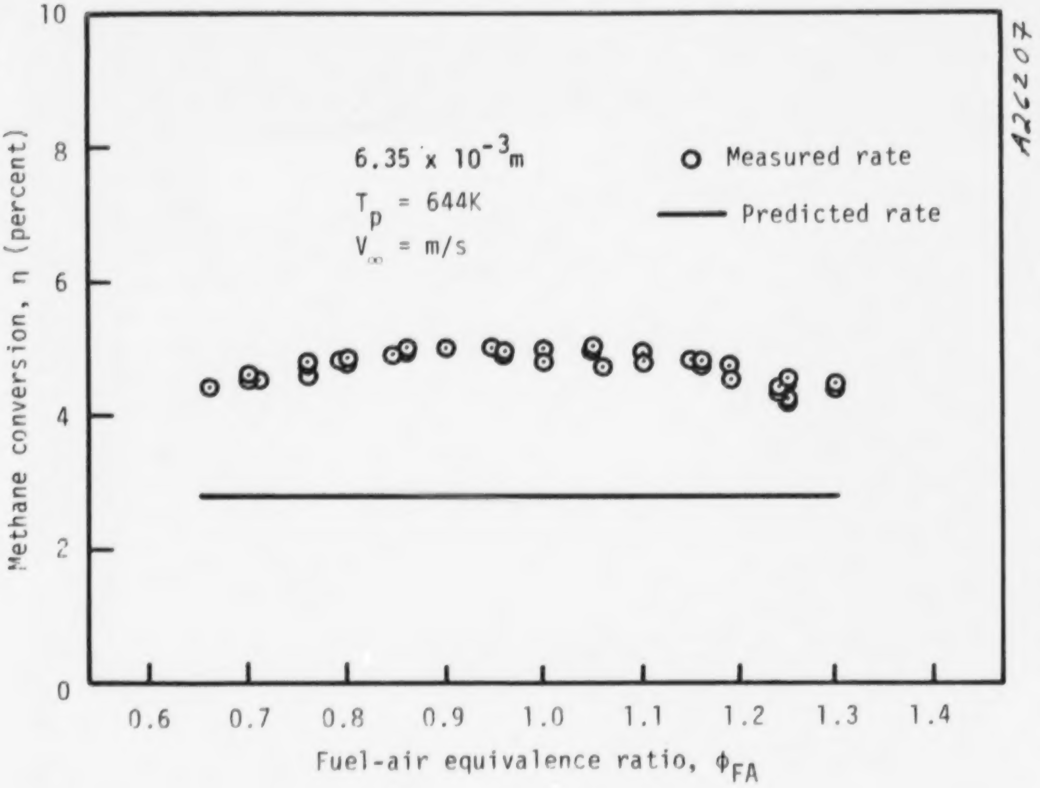

Figure 10. CH_4 conversion to CO, CO_2 as a function of stoichiometry.

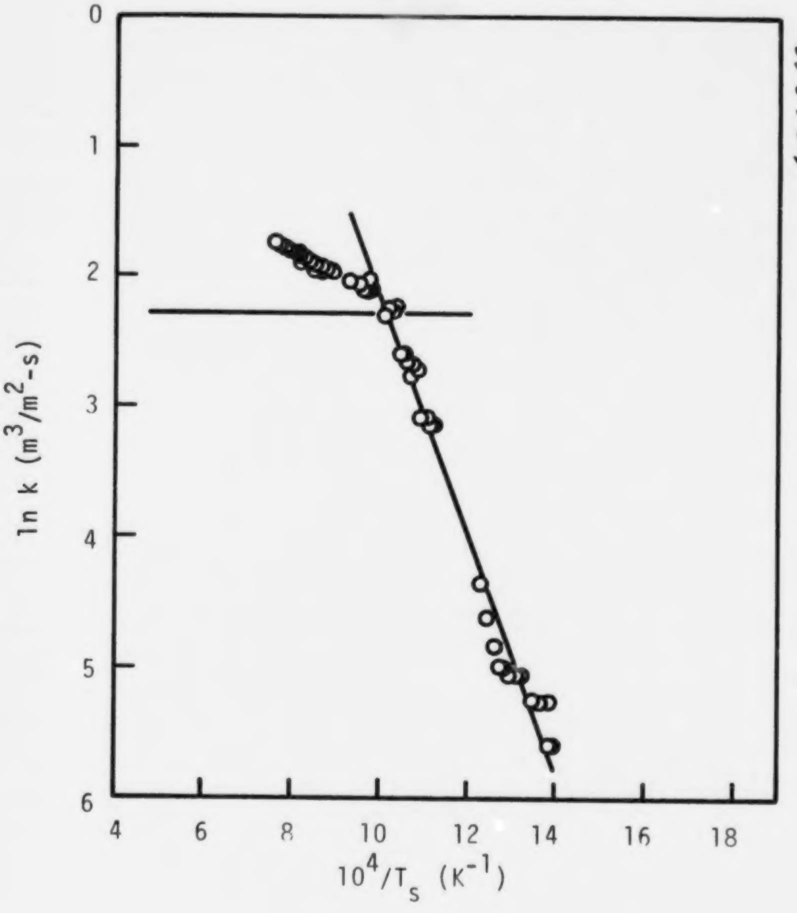

A2C209

Figure 11. Heterogeneous kinetics, methane on platinum.

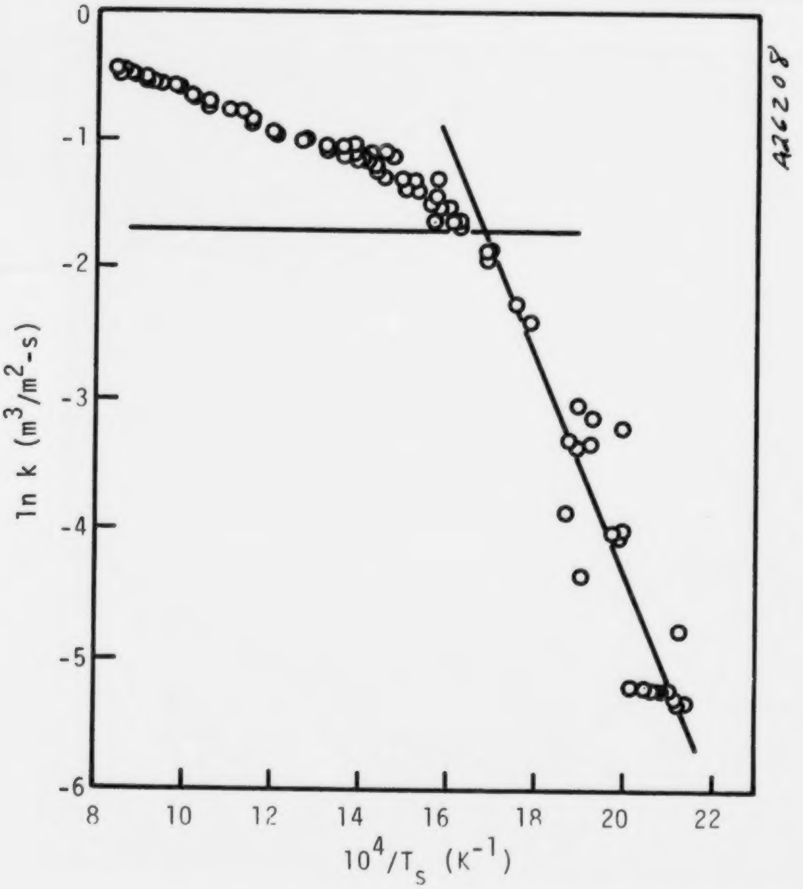

Figure 12. Heterogeneous kinetics, propane on platinum.

TABLE I. HETEROGENEOUS KINETIC PARAMETERS

Reference	Fuel/Catalyst	Pre-exponential Factor, A $\left(\frac{m^3}{m^2\text{-s}}\right)$	Activation Energy, E $\left(\frac{J}{kg\text{-mole}}\right)$	$\left(\frac{kcal}{mole}\right)$
This work	CH_4/Pt on alumina γ-alumina washcoat	1.27×10^3	7.70×10^7	18.4
Anderson, et al. (Ref.12)	CH_4/Pt on γ-alumina	*	9.84×10^7	23.5
Trimm & Lam (Ref.13)	CH_4/Pt on porous alumina fiber	*	8.58×10^7	20.5
Trimm & Lam (Ref.13)	CH_4/Pt on nonporous alumina fiber	*	7.58×10^7	18.1
This work	C_3H_8/Pt on alumina, γ-alumina washcoat	2.32×10^5	6.95×10^7	16.6
Bracco, et al. (Ref.14)	C_3H_8/Pt on cordierite, γ-alumina washcoat	1.09×10^7	7.37×10^7	17.6
Marteney (Ref.15)	C_3H_8/Pt on ceramic honeycomb	8.00×10^8**	4.19×10^7	10
Hiam, et al. (Ref.3)	C_3H_8/Pt wire filament, 99.99% purity	1.1×10^7	7.12×10^7	17.0

*See text

**Reported as 960 kg/m^2-s

TABLE II. HETEROGENEOUS RATE CONSTANTS
(this work)

T_s (°K)	k_{CH_4} $\left(\frac{m^3}{m^2\text{-}s}\right)$	$k_{C_3H_8}$ $\left(\frac{m^3}{m^2\text{-}s}\right)$
500	1.15×10^{-5}	1.27×10^{-2}
1000	1.21×10^{-1}	5.43×10^{1}
1500	2.64×10	8.81×10^{2}

IGNITION INSTABILITIES IN CATALYTIC COMBUSTION

By:

E. G. Seebauer
J. J. Foster
W. F. Banholzer
R. I. Masel

Department of Chemical Engineering
University of Illinois
Urbana, IL 61801

This work was supported by
The Army Research Office
under Contract
DAAG 29-80-C-0111

ABSTRACT

In a previous paper we showed that ignition instabilities in catalytic combustion could be induced by protrusions on the surface of the catalyst. Here, a mathematical model of the process is developed. Oscillations are predicted which agree qualitatively with the experiments.

INTRODUCTION

At this conference there are several papers that have considered what happens when a catalytic combustion system is started up. In most cases, rather simple initial behavior is observed. Either the system ignites and quickly goes to steady state; or nothing happens, and the conversion is negligible. However, there are many catalytic systems in which the ignition and extinction phenomena are more complicated. For example, Sault, et al. (1) considered the case of hydrogen oxidation on a nickel foil, they measured the temperature of the catalyst as a function of time at fixed inlet flowrates and compositions. A typical plot of the data is given in Figure 1. The graph shows that the catalyst's temperature continuously oscillates with an amplitude of approximately 200 Kelvin. This oscillatory behavior persists for several hours. The shape of the oscillations changes as a function of time, but thus far there has been no evidence that the system ever reaches steady state.

Similar oscillations have been observed during the catalytic oxidation of hydrogen, carbon monoxide, butane, butene, cyclohexane, cyclohexene, methanol, and ammonia. The catalysts employed were supported and unsupported platinum, nickel, copper oxide, and zeolite catalysts (see References 2-4 for Reviews). All of the work so far has been done under very rich conditions, although it is not clear whether this is a fundamental limitation.

Over the years several models have been proposed to explain these oscillations. Numerical simulations have shown that processes such as periodic oxidation/reduction of the catalyst, reversible adsorption of an inhibitor, coverage-dependent activation energies, changes in the mechanism of the reaction with coverage, hot spots due to protrusions on the surface, or amplification of concentration fluctuations in the gas phase could cause the reaction rate to oscillate. Changes in the form of the oscillations are thought to occur because of slow changes in the composition or structure of the catalyst.

In a previous paper (1) we considered the effects of catalyst pretreatment on the presence and form of self-sustained thermal oscillations during hydrogen ocidation on a nickel foil. We found that the pretreatment procedures used had a profound effect on the results. Rapid ignition to a high temperature state was observed with catalysts produced by some of the pretreatment procedures, whereas catalysts produced by other procedures showed oscillations under the same conditions. Examination of the catalysts with a scanning auger microprobe revealed that in all of the cases where oscillations were seen, there were 5-20 micron protrusions on the surface of the catalyst. The form of the oscillations could be correlated with the distribution of sizes and shapes of the protrusions. The samples that did not have protrusions did not show oscillatory behavior. The surface composition of the various catalysts were also measured. It was found that there was no significant difference between the surface compositions of the catalysts which catalyze oscillations and those that do not.

These experiments did not demonstrate how the protrusions induced the oscillations. However, Jensen and Ray (2) have done some previous theoretical work on the subject. They showed that if transport resistances are large, there can be a significant difference between the temperature and fuel concentration on a protrusion and that on the rest of the wire. They then derived a model based on several simplifying assumptions. The major ones were that transport resistances in the gas phase are negligible, that the reaction rate on the bulk wire is much less than that on the protrusions, and that the temperature did not carry over the surface of the protrusion. The result was a set of ordinary differential equations in the temperature and surface composition. A stability analysis showed that the system should oscillate; numerical simulations verified that oscillations occur.

Many of the predictions of the Jensen and Ray model agreed with our data. The model predicted oscillations whose shape varied with the distribution of protrusion sizes, in the way that was observed experimentally. However, the Jensen and Ray model predicted an oscillation period that was too small, and the predicted amplitude of the oscillations did not correlate with those measured in the experiments. Furthermore, Jensen and Ray predicted that the flat catalysts would be much less active than those that were covered by protrusions, but experimentally the flat catalysts are more active than the protrusion-covered ones.

This paper attempts to develop a model that more closely conforms to the experimental findings. We will consider as Jensen and Ray did, the protrusions to be separate entities from the bulk wire with their own temperatures and surface compositions. However unlike Jensen and Ray, we will allow for the possibility of a finite resistance to mass transfer in the gas phase and oxygen dissolution into the bulk. The reactivity of the parts of the foil between the protrusions will be presumed to be the same as that on the protrusions, however, we will allow a difference in the mass transfer rates to the two regions. We will then derive a set of differential equations, which will be solved numerically. Results of the calculations will be presented which show oscillations that more closely agree with the experiment.

THE MODEL

In the model, we will view the system as given in Figure 2. It will be assumed that there are a series of isolated protrusions of uniform size, with a uniform surface temperature, T_p, and fractional coverage of oxygen θ_p. The bulk wire will also be assumed to have a uniform temperature, and fractional coverage θ_B. All of the transport processes will be modeled using a quasisteady approximation and specifically it will be assumed that the temperature varies linearly from the top to the bottom of the protrusion. If one then assumes that the reaction follows the mechanism.

$$H_2 + 2s \underset{-1}{\overset{1}{\rightleftharpoons}} 2\,H_{ad}$$

$$O_2 + 2s \xrightarrow{2} 2\,O_{ad}$$

$$2H_{ad} + O_{ad} \xrightarrow{3} H_2O$$

With Step 2 in equilibrium and a low fractional coverage of hydrogen, then one can derive the following equations for the changes in temperature and composition of the protrusion and wire with time.

$$\frac{d\theta p}{dt} = k_2 C_{O_2 P} (1 - \theta p)^2 - \frac{k_3 k_1}{k-1} \theta p (1 - \theta p)^2 C_{H_2} + k_s (\theta_{BP} - \theta p) \qquad (1)$$

$$\frac{2\rho V_p c_p}{A_p} \frac{dT_p}{dt} = Q\,(-\Delta H_A)\, S k_2 C_{o_2 p}\,(1 - \theta p)^2 + (-\Delta H_R)\,\frac{k_3 k_1}{k_{-1}}\, S\, \theta p\, (1-\theta p)^2 C_{H_2} Q$$

$$+ Q\,(-\Delta H_s)\, S\, k_s\, (\theta_{BP} - \theta_p) + \left(\frac{Ac}{Ap}\right) h(T_w - T_p) + h_g\,(T_g - T_p) \qquad (2)$$

$$L_A \frac{d\theta_{BP}}{dt} = k_s\,(\theta_p - \theta_{BP}) \qquad (3)$$

$$\frac{d\theta w}{dt} = k_2 C_{o_2 w}(1-\theta w)^2 - \frac{k_3 k_1}{k-1}\,\theta w\,(1-\theta w)^2\, D_{H_2} \qquad (4)$$

$$+ k_s\,(\theta_{Bw} - \theta w)$$

$$\frac{\rho V_w c_w}{A_w} \frac{dT_w}{dt} = (1 - \varepsilon)\,(-\Delta H_A)\, S k_2 C_{o_2 w}\,(1 - \theta w)^2\, Q + (-\Delta H_R)\,\frac{k_3 k_1}{k_{-1}}\, S$$

$$\theta w\,(1-\theta w)^2 C_{H_2}(1 - \varepsilon)\, Q \qquad (5)$$

$$+ Q\,(1 - \varepsilon)\,(-\Delta H_s)\, S\, k_s\,(\theta_{Bw} - \theta_w) + \left(\frac{Ac}{Aw}\right) h\,(T_p - T_w) + H_g\,(T_g - T_w)$$

$$(1 - \varepsilon)\, L_A \frac{d\theta_{Bw}}{dt} = k_s\,(\theta_w - \theta_{Bw}) \qquad (6)$$

The notation is defined in the Appendix.

The experiments were performed under conditions where the time constants for the reaction steps are much larger than the corresponding time constants for the gas phase mass transfer steps. As a result it is reasonable to assume a pseudo-steady state approximation for the mass transfer to and from the surface. In the pseudo-steady state approximation the net mass transfer rate of the reactants to the surface is equal to the rate of gas adsorption by the catalyst.

$$F_{mt} = F_r \tag{7}$$

It was not evident from the experimental results if the gas is being mixed along the surface, so two different limiting cases were tried. The first is that there is little mixing between the gas immediately above a protrusion and the gas directly above the rest of the surface.

$$C_{o_2 p} = \frac{C_{o_2}}{1 + \frac{k_2 S(1 - \theta_p)^2}{K_p} Q} \tag{8a}$$

$$C_{o_2 w} = \frac{C_{o_2}}{1 + \frac{k_2 S(1 - \theta_w)^2}{K_p} Q} \tag{8b}$$

And a second approximation where complete mixing is assumed

$$C_{o_2 p} = \frac{C_{o_2}}{1 + \frac{S\varepsilon \; k_2(1 - \theta_p)^2}{K_p} + \frac{S(1 - \varepsilon)\, k_2(1 - \theta_w)^2 Q}{K_p \left[1 + \frac{SK_2 \, (1 - \theta_w)^2 Q}{K'_w} \right]}} \tag{9a}$$

$$C_{o_{2w}} = \frac{C^P_{o_2}}{1 + \frac{K_2 \, (1 - \theta_w)^2 Q}{K'_w}} \tag{9b}$$

with $$\frac{1}{K'_w} = \frac{1}{K_w} - \frac{1}{K_p} \tag{9c}$$

Substituting arhenius expressions in for each of the rate constants, and converting to dimensionless variables yields

$$\frac{d\theta_p}{dt'} = Da_A\, \alpha_p\, (1 - \theta_p)^2 \exp\left[\frac{\gamma_A}{\gamma_R} \frac{X_p}{1 + X_p/\gamma_R}\right]$$

$$-Da_R\, \theta_p\, (1 - \theta_p)^2 \exp\left[\frac{X_p}{1 + X_p/\gamma_R}\right] \qquad (10)$$

$$+Da_S\, (\theta_{\beta P} - \theta_p) \exp\left[\frac{\gamma_S}{\gamma_R} \frac{X_p}{1 + X_p/\gamma_R}\right]$$

$$Le_p \frac{dX_p}{dt'} = -(1 + \beta_p)X_p + B_A\, Da_A\, \alpha_p\, (1 - \theta_p)^2 \exp\left[\frac{\gamma_A}{\gamma_R} \frac{X_p}{1 + X_p/\gamma_R}\right]$$

$$+ B_R\, Da_R\, \theta_p\, (1 - \theta_p)^2 \exp\left[\frac{X_p}{1 + X_p/\gamma_R}\right] \qquad (11)$$

$$+ B_S\, Da_S\, (\theta_{BP} - \theta_p) \exp\left[\frac{\gamma_S}{\gamma_R} \frac{X_p}{1 + X_p/\gamma_R}\right]$$

$$+ \beta_p\, X_W$$

$$\frac{d\theta_W}{dt'} = Da_A \, \alpha_W \, (1 - \theta_W)^2 \, \exp\left[\frac{\gamma_A}{\gamma_R} \frac{X_W}{1 + X_W/\gamma_R}\right] \qquad (12)$$

$$- Da_R \, \theta_W \, (1 - \theta_W)^2 \, \exp\left[\frac{X_W}{1 + X_W/\gamma_R}\right]$$

$$+ Da_S \, (\theta_{BW} - \theta_W) \, \exp\left[\frac{\gamma_S}{\gamma_R} \frac{X_W}{1 + X_W/\gamma_R}\right]$$

$$Le_W \frac{dX_W}{dt'} = -(1 - \varepsilon - \beta_W) \, X_W + B_W \, X_p$$

$$+(1 - \varepsilon) \, B_A \, Da_A \, \alpha_W \, (1 - \theta_p)^2 \, \exp\left[\frac{\gamma_A}{\gamma_R} \frac{X_W}{1 + X_R/\gamma_R}\right] \qquad (13)$$

$$+(1 - \varepsilon) \, B_R \, Da_R \, \theta_W (1 - \theta_W)^2 \, \exp\left[\frac{X_W}{1 + X_W/\gamma_R}\right]$$

$$+(1 - \varepsilon)\ B_S\ Da_S\ (\theta_{BW} - \theta_W)\ \exp\left[\frac{\gamma_S}{\gamma_R}\ \frac{X_W}{1 + X_W/\gamma_R}\right]$$

$$L_A \frac{d\theta_{BW}}{dt'} = Da_S\ (\theta_W - \theta_{BW}) \tag{14}$$

$$L_A \frac{d\theta_{BP}}{dt'} = Da_S\ (\theta_p - \theta_{BP}) \tag{15}$$

Where the two limiting cases for the mass transfer become,

$$\alpha_{p,1} = \frac{1}{1 + \dfrac{Da_A\ (1 - \theta_p)^2}{Da_p}} \tag{16a}$$

$$\alpha_{W,1} = \frac{1}{1 + \dfrac{Da_A\ (1 - \theta_W)^2}{Da_W}} \tag{16b}$$

and

$$\alpha_{p,2} = \frac{1}{1 + \dfrac{\varepsilon Da_A\ (1 - \theta_p)^2}{Da_W} + \dfrac{(1 - \varepsilon)\ Da_A\ (1 - \theta_W)^2}{1 + \dfrac{Da_A\ (1 - \theta_W)^2}{Da_W}}} \tag{17a}$$

$$\alpha_{W,2} = \frac{\alpha_{p,2}}{1 + \frac{Da_A (1 - \theta_W)^2}{Da_W}} \qquad (17b)$$

The dimensionless equations were integrated numerically using the ISML Gear routine. For each of the two transport resistance limiting cases, thermal oscillations were predicted. Figure 3 is a plot of the dimensionless wire temperature as a function of the dimensionless time obtained using the first approximation to the mass transfer coefficient. In this calculation, we have assumed that all of the protrusions have the same size. On the basis of the results obtained, we predict regular oscillations in the catalyst temperature when the protrusion sizes are all the same.

The mechanism of the oscillations can be described as follows. At the start of an experiment, the surface of the catalyst is clean. Oxygen is adsorbed rapidly, but the surface temperature is low, resulting in a small reaction rate. Nevertheless, the system gradually heats up and the reaction rate increases. In fact, the small thermal mass of the protrusions permits their temperature to rise very quickly as the reaction rate becomes significant. Up until this temperature change, however, the protrusions have accumulated oxygen on their surfaces. This oxygen remains on the catalyst as the reaction rate rises; therefore, there is excess oxygen on the surface of the protrusions when the expected steady state temperature is reached. Bolstered by the extra oxygen, the reaction rate continues to increase, pushing the temperature beyond its anticipated steady state value. This high rate of oxidation soon consumes the extra oxygen on the protrusions, however, thereby causing the rate to fall. In fact, the oxygen supply is so depleted that there is no longer enough left to maintain the predicted steady state reaction rate. Consequently, the reaction is quenched, and the temperature falls to its original low value. At this point, oxygen accumulation resumes, and the reaction rate begins to increase again. The process described above then repeats, giving rise to the observed oscillatory behavior. It is important to note that this mechanism predicts that the bulk of the catalyst is heated significantly only by conduction from the protrusions, and not by combustion on the areas between the protrusions.

Using this model, we have tried to fit our data employing the first limiting case for the mass transfer terms, i.e., no mixing along the surface. Generally, the fit is somewhat better than that obtained using the model of Jensen and Ray. Their model predicts oscillation periods and amplitudes that are too small. However, our model dictates that oxygen accumulate in the bulk during the low temperature part of the cycle; therefore, it takes longer for the protrusions to ignite. However, once ignition occurs, the bulk of the catalyst provides a steady source of oxygen, resulting in a larger amplitude of oscillation. Thus, we were able to obtain better results by adjusting the oxygen storage step.

Unfortunately, in order to correctly fit our data, we had to assume an unreasonably small value for the mass transfer coefficient to the bulk of the catalyst. If the mass transfer coefficients to the protrusions and to the bulk surface are roughly equivalent, then the model predicts a simple ignition to the high steady-state temperature under our experimental conditions. We found it necessary to reduce the mass transfer coefficient to the flat areas between the protrusions by an order of magnitude in order to properly fit the data. One might expect the mass transfer to be reduced to these areas, but an order of magnitude is difficult to justify.

We have just started to use the second limiting mass transfer term (i.e., complete mixing) to fit the experimental data. In general, the results approximate those obtained by assuming no mixing. However, there is one important difference arising from the possibility that combustion on the protrusions can deplete the boundary layer, and so reduce the mass transfer to the rest of the foil. During the initial phase of an oscillation, the reaction rate on the protrusions and on the bulk surface rises. Thus, the foil bulk is heated both by conduction from the protrusions and by the combustion between them. However, because of the small thermal mass of the protrusions, they heat up quickly; the reaction rate on the protrusions increases far more rapidly than on the rest of the catalyst. Good mixing then requires that the entire boundary layer above the catalyst surface be depleted of oxygen. Consequently, the reaction is quenched both on the protrusions and on the bulk surface.

Such a mechanism can be expected to alter the nature of an oscillation from that expected with poor mixing. In fact, if the conditions are such that reaction quenching occurs before the bulk foil can heat significantly, it is possible that the catalyst's temperature will remain low even though it would be expected to rise to the high temperature state in the absence of protrusions. This suggests a paradox: protrusions, which are normally associated with rapid reaction rate, may actually lower the overall rate of reaction on the catalyst's surface.

REFERENCES

1. Sault, A. G., and R. I. Masel. J. Cat. Submitted.

2. Jensen, K., and W. H. Ray. Chem. Eng. Sci., 35: 2439, 1980.

3. Steintuch, M., and R. A. Schmitz. Cat. Rev., 15: 107, 1977.

4. Slinko, M. G., and Slinko, M. M. Cat. Rev., 17: 114, 1978.

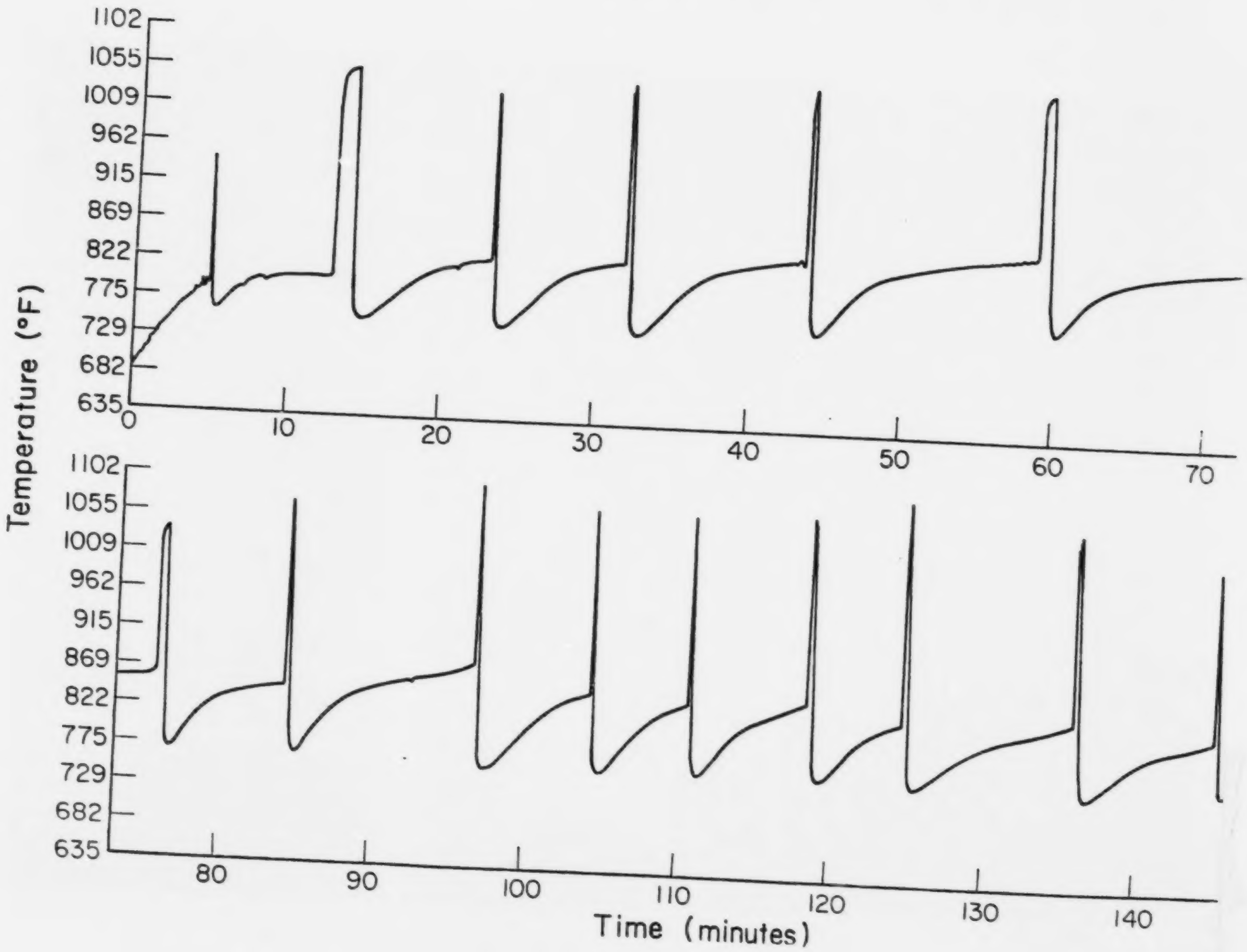

Figure 1. The catalyst temperature as a function of time during hydrogen oxidation and nickel foil from Sault, et al. (1).

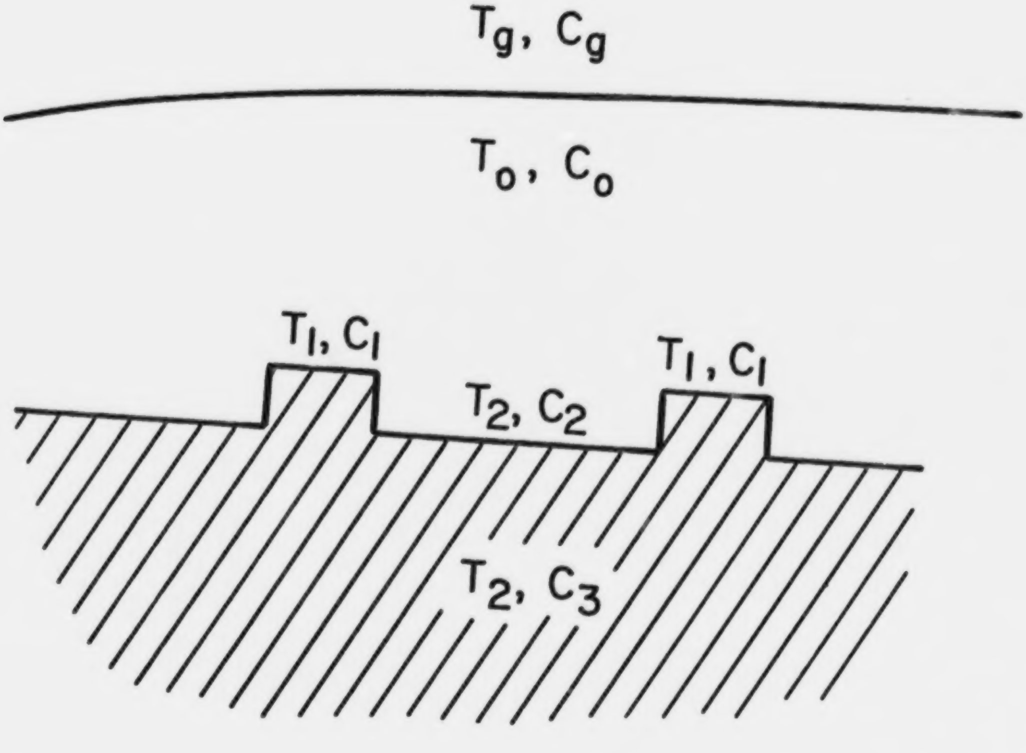
T_g, C_g
T_o, C_o
T_1, C_1
T_1, C_1
T_2, C_2
T_2, C_3

Figure 2. Schematic of the model system.

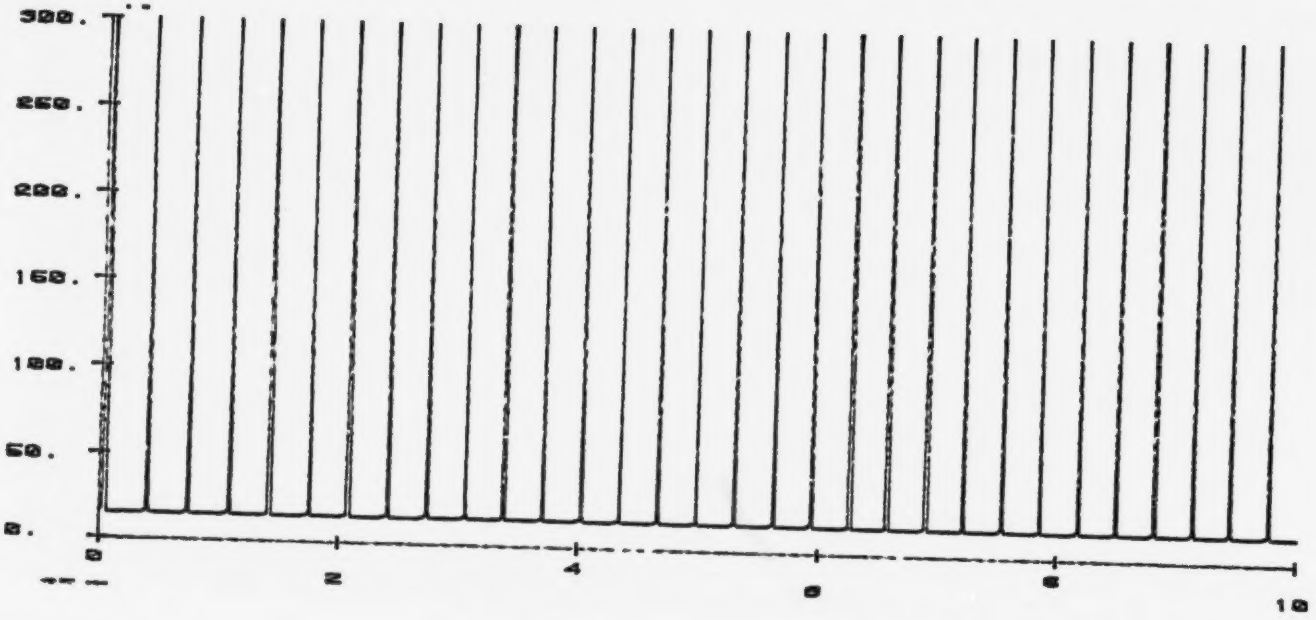

Figure 3. Changes in the wire temperature, degrees, as a function of time (mins) predicted by the model.

CATALYTIC COMBUSTION IN A SHEAR FLOW*

by

C. K. Law
Department of Mechanical and Nuclear Engineering
Northwestern University
Evanston, Illinois 60201

---

[*] Prepared for the Fifth Workshop on Catalytic Combustion, Environmental Protection Agency, San Antonio, Texas, Sept. 15-16, 1981.

Preceding page blank

ABSTRACT

The gas-phase ignition, steady burning, extinction, and heat-transfer characteristics of a combustible premixture in the stagnation-point flow of a catalytic surface have been studied both theoretically and experimentally. An explicit ignition criterion as function of all system parameters has been derived for an isothermal surface, showing that gas-phase ignition is hindered in the presence of surface catalytic reactions. It is further discussed that the surface catalyst has no effect on the steady burning characteristics of a flow with Lewis number $Le > 1$, but may extend the extinction limit when $Le < 1$. Existing experimental results substantiate these theoretical concepts.

I. INTRODUCTION

Recently there exist much interest in the potential of using heterogeneous catalyst to improve the performance of gas turbine engines in terms of efficiency, stability, and pollutant formation. The interest arises from the recognition that gas turbines can only operate with very lean fuel-air mixtures from thermal stress considerations. However, such lean mixtures are outside the flammability limit and cannot be ignited. Hence conventional gas turbine operation involves first igniting and burning a mixture which is close to stoichiometric. The hot combustion products are then diluted with air to about 2500°F before being passed through the turbine for power generation.

Therefore except for stability, combustion in the gas turbine need not take place at such high temperatures. The penalties for doing so are the high rate of local heat transfer to the engine hardware and the excessively high levels of pollutants formed, particularly soot and NO_x. Due to finite rates of chemical reactions, these pollutants once formed frequently do not have time to be chemically destroyed in the colder dilution zone.

In order to remove these constraints, the catalytic ignition and combustion concept has been advanced. It involves either coating the surface of the conventional flame-holder with catalysts or simply using a coated monolithic structure as the flame-holder. Then as a fuel-lean mixture passes over the catalyzed surface, gas-phase ignition is promoted through the surface reactions. With this design exceedingly lean mixtures have been ignited and burned, resulting in a colder combustion product which can be directly utilized by the gas turbine. Hence with catalytic combustion the overall combustion efficiency is increased whereas the amount of pollutants formed is drastically reduced. Since the combustion efficiency of gas turbines is generally high, an alternate way to view the benefits of catalytic combustion is that by reducing the ignition/combustion time the combustor can be made more compact.

Research methodology on catalytic combustion falls into three categories, namely (1) Actual combustor testings; (2) Small-scale laboratory experiments involving simple flow systems; and (3) Detailed studies of the surface kinetics. The present project belongs to the second category.

The flow systems for laboratory experiments can be further divided into two types, that is (2a) Evolutionary as typified by flows over a flat plate (Schefer et al., 1980), or through tubes (Bracco et al., 1980; Prasad et al., 1981; and Tien, 1981); (2b) Steady-state as typified by the stagnation-point flow (Ablow et al., 1980). The evolutionary flow types have the advantage of exhibiting the progressive intensification of the catalytic action as the combustible premixture flows downstream, and simulate the situation within practical combustors. However, analysis and data interpretation of these flow systems are necessarily quite involved because the flow is basically two-dimensional.

On the other hand the stagnation-point flow is truly steady state in that flow variations occur mainly in the direction normal to the stagnation surface, and therefore offers simplicity in analysis and data interpretation. We have therefore adopted the stagnation-point flow as our model system.

Thus the methodology of the present investigation is the following. The ignition, steady-burning, extinction, and heat generation and transfer characteristics of a premixed combustible flow impinging onto a catalytic stagnation surface are systematically mapped. Parallel to the experimental effort, theoretical modeling are conducted allowing for different gas-phase and catalytic reaction mechanisms. Thus by comparing the theoretical and experimental results the dominant kinetic mechanisms, and the associated kinetic constants, can be identified.

We shall present in the following some preliminary theoretical and experimental results. In the next section the general governing equations are stated, which is followed by a detailed analysis for the weakly-reactive gas flows leading to gas-phase ignition. The surface catalytic reaction can assume any intensity. In Section IV gas-phase extinction will be discussed. Experimental set-up and some preliminary experimental results will be presented in Section V.

II. GOVERNING EQUATIONS

The problem of interest is schematically shown in Fig. 1. Here a combustible mixture with temperature T_∞, reactant mass fractions $Y_{i\infty}$, and velocity u_∞ impinges onto a catalytic surface which is either adiabatic or is held at a constant temperature T_s. Reactions take place both in the gas phase as well as on the surface.

The steady-state two-dimensional and axisymmetric boundary layer flow for a chemically-reacting mixture is governed by (Williams, 1965)

Continuity: $$\frac{\partial(\rho u R^j)}{\partial x} + \frac{\partial(\rho v R^j)}{\partial y} = 0 \qquad (1)$$

Momentum: $$\rho u \frac{\partial u}{\partial x} + \rho v \frac{\partial u}{\partial y} - \frac{\partial}{\partial y}\left(\mu \frac{\partial u}{\partial y}\right) = \rho_\infty u_\infty \frac{du_\infty}{dx} \qquad (2)$$

Species: $$\rho u \frac{\partial \tilde{Y}_i}{\partial x} + \rho v \frac{\partial \tilde{Y}_i}{\partial y} - \frac{\partial}{\partial y}\left(\rho D \frac{\partial \tilde{Y}_i}{\partial y}\right) = -\omega_g, \quad i = 0, F \qquad (3)$$

Energy: $$\rho u \frac{\partial \tilde{T}}{\partial x} + \rho v \frac{\partial \tilde{T}}{\partial y} - \frac{\partial}{\partial y}\left(\frac{\lambda}{C_p} \frac{\partial \tilde{T}}{\partial y}\right) = \omega_g \qquad (4)$$

in which it has been assumed that the pressure and viscous heating terms are negligible in Eq. (4), that a single binary diffusion coefficient D exists for all species pairs, and that the specific heat C_p is a constant.

The gas and surface reactions between the fuel F and oxidizer O leading to the formation of the product P can be represented by a one-step overall irreversible reaction

$$\nu_O[O] + \nu_F[F] \rightarrow \nu_P[P] \tag{5}$$

which has a gas-phase reaction rate

$$\left(\frac{\omega_g}{\nu_F W_F}\right) = B_g T^{n_g} \left(\frac{X_O p}{R^o T}\right)^{a_{Og}} \left(\frac{X_F p}{R^o T}\right)^{a_{Fg}} e^{-E_g/R^o T} \tag{6}$$

and a surface reaction rate

$$\frac{\omega_s}{\nu_F W_F} = B_s T_s^{n_s} \left(\frac{X_{Os} p}{R^o T_s}\right)^{a_{Os}} \left(\frac{X_{Fs} p}{R^o T_s}\right)^{a_{Fs}} e^{-E_s/R^o T_s} \tag{7}$$

By further assuming an ideal gas equation of state

$$p = \rho R^o T/\overline{W} \tag{8}$$

where $\overline{W}$ is the average molecular weight $\overline{W}^{-1} = \Sigma Y_i/W_i$, Eqs. (6) and (7) can be respectively written as

$$\omega_g = \left(\frac{B_g \nu_F W_F}{W_O^{a_{Og}} W_F^{a_{Fg}}}\right) \left(\frac{p\overline{W}}{R^o}\right)^{(a_{Og}+a_{Fg})} T^{(n_g - a_{Og} - a_{Fg})} Y_O^{a_{Og}} Y_F^{a_{Fg}} e^{-E_g/R^o T} \tag{9}$$

$$\omega_s = \left(\frac{B_s \nu_F W_F}{W_O^{a_{Os}} W_F^{a_{Fs}}}\right) \left(\frac{p\overline{W}}{R^o}\right)^{(a_{Os}+a_{Fs})} T_s^{(n_s - a_{Os} - a_{Fs})} Y_{Os}^{a_{Os}} Y_{Fs}^{a_{Fs}} e^{-E_s/R^o T_s} \tag{10}$$

It is significant to note that we have used quite a generalized representation of the reaction rate, which has arbitrary reaction orders with respect to the fuel and the oxidizer, and which depends on the temperature through both the Arrhenius factor and a power variation T^n. It will be shown subsequently that explicit solutions are obtainable even with this generalized kinetic expression. Finally, we note that $R^j(x)$ describes the curvature of the surface such that j = 0 for two-dimensional flow and j = 1 for axisymmetric flow.

Equations (1) to (4) are to be solved subject to the boundary conditions

$$u(x,0) = v(x,0) = 0 \quad ; \quad u(x,\infty) = u_\infty \tag{11}$$

$$\tilde{Y}_i(x,\infty) = \tilde{Y}_{i\infty} \tag{12}$$

$$\left(\rho D \frac{\partial \tilde{Y}_i}{\partial y}\right)_{y=0} = \omega_s \tag{13}$$

$$\tilde{T}(x,\infty) = \tilde{T}_\infty \tag{14}$$

and

$$\tilde{T}(x,0) = \tilde{T}_s \qquad \text{(Isothermal surface)} \tag{15a}$$

or

$$\left(\frac{\lambda}{C_p} \frac{\partial \tilde{T}}{\partial y}\right)_{y=0} = -\,\omega_s \qquad \text{(Adiabatic surface)} \tag{15b}$$

Using the conventional boundary layer variables

$$s = \int_0^x \rho_\infty(x')\mu_\infty(x')u_\infty(x')R^{2j}(x')dx' \tag{16}$$

$$\eta = u_\infty R^j (2s)^{-1/2} \int_0^y \rho(x,y')dy' \tag{17}$$

and

$$f(s,\eta) = \psi(x,y)/(2s)^{1/2} \quad , \tag{18}$$

where the stream function $\psi(x,y)$ is defined by

$$\rho u R^j = \frac{\partial\psi}{\partial y} \quad , \quad \rho v R^j = -\frac{\partial\psi}{\partial x} \tag{19}$$

such that the continuity equation is automatically satisfied, it can be shown that at the stagnation point Eqs. (2) to (4) are respectively transformed to

$$\frac{d^3 f}{d\eta^3} + f\frac{d^2 f}{d\eta^2} + \frac{1}{2^j}\left[\left(\frac{\rho_\infty}{\rho}\right) - \left(\frac{df}{d\eta}\right)^2\right] = 0 \tag{20}$$

$$\frac{d^2\tilde{Y}_i}{d\eta^2} + f\frac{d\tilde{Y}_i}{d\eta} = \frac{\omega_g}{2^j\alpha\rho} \tag{21}$$

$$\frac{d^2\tilde{T}}{d\eta^2} + f\frac{d\tilde{T}}{d\eta} = -\frac{\omega_g}{2^j\alpha\rho} \tag{22}$$

while the boundary conditions Eqs. (11) to (15) become

$$f(0) = f'(0) = 0 \quad , \quad f'(\infty) = 1 \tag{23}$$

$$\tilde{Y}_i(\infty) = \tilde{Y}_{i\infty} \tag{24}$$

$$\left(\frac{d\tilde{Y}_i}{d\eta}\right)_0 = \frac{\omega_s}{(2^j\alpha\rho_\infty\mu_\infty)^{1/2}} \tag{25}$$

$$\tilde{T}(\infty) = \tilde{T}_\infty \tag{26}$$

and

$$\tilde{T}(0) = \tilde{T}_s \qquad \text{(Isothermal surface)} \tag{27a}$$

or

$$\left(\frac{d\tilde{T}}{d\eta}\right)_0 = -\frac{\omega_s}{(2^j\alpha\rho_\infty\mu_\infty)^{1/2}} \qquad \text{(Adiabatic surface)} \tag{27b}$$

In deriving the above equations it has also been assumed that the product $\rho\mu$ is a constant, and that the Prandtl number $\mu C_p/\lambda$ and the Schmidt number $\mu/\rho D$ are both unity. The constant α characterizes the external flow through $u_\infty = \alpha x$.

By further defining a new independent variable

$$\xi = H(\eta)/H(\infty) \tag{28}$$

where

$$H(\eta) = \int_0^\eta \exp\{-\int_0^{\eta'} f(\eta'')d\eta''\}\, d\eta' \quad , \tag{29}$$

Eqs. (21) and (22) can be equivalently represented as

$$\frac{d^2(\tilde{Y}_i + \tilde{T})}{d\xi^2} = 0 \tag{30}$$

and

$$\frac{d^2\tilde{T}}{d\xi^2} = -\left[\frac{H(\infty)}{(dH/d\eta)}\right]^2 \frac{\omega_g}{2^j\alpha\rho} \tag{31}$$

where we have used the Shvab-Zeldovich formulation to eliminate the production term from one of the equations.

In ξ-space the boundary conditions become

$$\tilde{Y}_i(1) = \tilde{Y}_{i\infty} \tag{32}$$

$$\left(\frac{d\tilde{Y}_i}{d\xi}\right)_0 = \left[\frac{H(\infty)}{(dH/d\eta)_0}\right] \frac{\omega_s}{(2^j\alpha\rho_\infty\mu_\infty)^{1/2}}$$

$$= S \tag{33}$$

$$\tilde{T}(1) = \tilde{T}_\infty \tag{34}$$

and

$$\tilde{T}(0) = \tilde{T}_s \qquad \text{(Isothermal surface)} \tag{35a}$$

$$\left(\frac{d\tilde{T}}{d\xi}\right)_0 = -\left[\frac{H(\infty)}{(dH/d\eta)_0}\right] \frac{\omega_s}{(2^j \alpha \rho_\infty \mu_\infty)^{1/2}} \quad \text{(Adiabatic surface)}$$

$$= -S \tag{35b}$$

The advantages of working in the ξ-space are that it is bounded by [0,1] and that for a chemically-frozen flow $\tilde{T}(\xi)$ and $\tilde{Y}_i(\xi)$ are linear functions of ξ. Therefore the presence of chemical reactions can be easily "detected" by observing deviations from linearity of these functions.

Equation (30) can be readily integrated, yielding an explicit relation between $\tilde{Y}_i$ and $\tilde{T}$ as

$$(\tilde{Y}_i+\tilde{T}) = (\tilde{Y}_{i\infty}+\tilde{T}_\infty) - \left[S + \left(\frac{d\tilde{T}}{d\xi}\right)_0\right](1-\xi) \tag{36}$$

which also implies that

$$\tilde{Y}_{O\infty} - \tilde{Y}_O = \tilde{Y}_{F\infty} - \tilde{Y}_F \tag{37}$$

Therefore using Eq. (36) for $\tilde{Y}_i = \tilde{Y}_i(T;\xi)$, the final equations we need to solve are the coupled Eqs. (20) and (31), subject to the boundary conditions Eqs. (23) and (35).

Equation (31) can also be written in expanded form as

$$\frac{d^2\tilde{T}}{d\xi^2} = -\delta_g\left[\frac{H(\infty)}{(dH/d\eta)}\right]^2 \tilde{Y}_O^{a_{Og}} \tilde{Y}_F^{a_{Fg}} \tilde{T}^{a_{Tg}} e^{-\tilde{T}_{ag}/\tilde{T}} \tag{38}$$

where

$$\delta_g = \frac{B_g}{2^j\alpha} \frac{\nu_F W_F}{W_O^{a_{Og}} W_F^{a_{Fg}}} \left(\frac{p\bar{W}}{R^O}\right)^{a_{Og}+a_{Fg}-1} \left(\frac{Q}{C_p}\right)^{a_{Tg}} \sigma^{a_{Og}}, \tag{39}$$

$T_{ag} = E_g/R^O$, $\sigma = \nu_O W_O/\nu_F W_F$, $a_{Tg} = n_g+1-a_{Og}-a_{Fg}$, and $\tilde{Y}_i(\tilde{T})$ is given by Eq. (36). Similarly S can be expressed as

$$S = \delta_s \left[\frac{H(\infty)}{(dH/d\eta)_0}\right] \tilde{Y}_{Os}^{a_{Os}} \tilde{Y}_{Fs}^{a_{Fs}} \tilde{T}_s^{a_{Ts}} \; e^{-\tilde{T}_{as}/\tilde{T}_s} \tag{40}$$

where

$$\delta_s = \frac{B_s}{(2^j \alpha \rho_\infty \mu_\infty)^{1/2}} \; \frac{\nu_F W_F}{W_O^{a_{Os}} W_F^{a_{Fs}}} \left(\frac{p\bar{W}}{R^0}\right)^{a_{Os}+a_{Fs}} \left(\frac{Q}{C_p}\right)^{a_{Ts}} \sigma^{a_{Os}} \tag{41}$$

$T_{as} = E_s/R^0$, and $a_{Ts} = n_s - a_{Os} - a_{Fs}$.

III. IGNITION AT ISOTHERMAL SURFACE

We restrict our ignition analysis to the case of isothermal surface because it conforms with our experimental set-up to be discussed later.

(1) Solution with Frozen Gas-Phase Reaction

When the gas-phase reaction is completely frozen, that is for $\tilde{T}_{ag} \to \infty$, Eq. (38) becomes

$$\frac{d^2\tilde{T}_o}{d\xi^2} = 0 \tag{42}$$

subject to

$$\tilde{T}_o(0) = \tilde{T}_s \quad , \quad \tilde{T}_o(1) = \tilde{T}_\infty \tag{43}$$

The solution is simply

$$\tilde{T}_o(\xi) = \tilde{T}_s - \beta\xi \tag{44}$$

where

$$\beta = \tilde{T}_s - \tilde{T}_\infty \tag{45}$$

is the heat transfer parameter.

Substituting Eq. (44) into Eq. (36), we obtain the concentration distributions:

$$\tilde{Y}_{io} = \tilde{Y}_{i\infty} - S(1-\xi) \tag{46}$$

The species concentrations $\tilde{Y}_{iso}$ at the surface can be solved by evaluating Eq. (46) at the surface for fuel and oxidizer. Thus, for example, $\tilde{Y}_{Fso}$ can be iteratively determined from

$$\tilde{Y}_{Fso} = \tilde{Y}_{F\infty} - \delta_s \left[\frac{H(\infty)}{(dH/d\eta)_0}\right] (\tilde{Y}_{O\infty} - \tilde{Y}_{F\infty} + \tilde{Y}_{Fso})^{a_{Os}} \tilde{Y}_{Fso}^{\;a_{Fs}} \tilde{T}_s^{\;a_{Ts}} e^{-\tilde{T}_{as}/\tilde{T}_s} \tag{47}$$

while

$$\tilde{Y}_{Oso} = \tilde{Y}_{O\infty} - \tilde{Y}_{F\infty} + \tilde{Y}_{Fso}$$

For large but finite values of $\tilde{T}_a$, gas-phase reactions are expected to initiate first near the hot wall since it has the highest temperature in the flow field. However, at a short distance away from the wall the slight decrease in temperature is sufficient to freeze the reactions due to the temperature-sensitive Arrhenius factor. Therefore the flow field is expected to consist of an inner, diffusive-reactive region next to the wall, and an outer, diffusive-convective region away from it. The characteristics of these two regions will be analyzed in the following.

2. Outer Solution

In the outer region chemical reactions will be assumed to be frozen to all orders. Hence using the boundary condition at $\xi = 1$, Eq. (38) shows that the perturbed temperature profile is still linear, given by

$$\tilde{T}_{out} = \tilde{T}_\infty + A_0(1-\xi) + \varepsilon A_1(1-\xi) + O(\varepsilon^2) \tag{48}$$

where $\varepsilon = \tilde{T}_s^2/\tilde{T}_{ag}$ is the small parameter of expansion for the present problem.

(3) Inner Solution

In the inner region weak chemical reactions take place and are responsible for the onset of the ignition event. Let the inner variable be $\chi = \beta\xi/\varepsilon$ and the inner temperature distribution $\tilde{T}_{in}$ be slightly perturbed from its frozen value by an amount $\varepsilon\theta(\chi)$ such that

$$\tilde{T}_{in} = \tilde{T}_s + \varepsilon[\theta(\chi)-\chi] + O(\varepsilon^2) \tag{49}$$

Equation (36) then shows that the species distribution in the inner region is given by

$$\tilde{Y}_{i,in} = \tilde{Y}_{i\infty} - \left[S+\beta\left(\frac{d\theta}{d\chi}\right)_0\right] + O(\varepsilon) \tag{50}$$

Hence putting Eqs. (49), (50), and the relation (Law, 1978)

$$\frac{dH}{d\eta} = 1 + O(\varepsilon^3) \qquad \text{as } \eta \to 0$$

into Eq. (38), we get

$$\frac{d^2\theta}{d\chi^2} = -\frac{\Delta}{2}e^{(\theta-\chi)} \tag{51}$$

where

$$\Delta = \frac{2\delta_g\varepsilon}{\beta^2}H_o^2(\infty)\left\{\tilde{Y}_{O\infty}-\left[S+\beta\left(\frac{d\theta}{d\chi}\right)_0\right]\right\}^{a_{Og}}\left\{\tilde{Y}_{F\infty}-\left[S+\beta\left(\frac{d\theta}{d\chi}\right)_0\right]\right\}^{a_{Fg}}$$

$$\tilde{T}^{a_{Tg}}e^{-\tilde{T}_{ag}/\tilde{T}_s} \tag{52}$$

and $H_o(\infty)$ has been extensively tabulated (Cohen and Reshotko, 1954; Law, 1978).

Equation (51) is to be solved subject to

$$\theta(0) = 0 \tag{53}$$

and a second boundary condition obtained through matching with the outer solution.

4. Matching and Final Solutions

Matching the outer and inner solutions in the limit of $\chi \to \infty$, we have

$$\lim_{\chi\to\infty} \left\{\tilde{T}_\infty + (A_o+\varepsilon A_1)(1-\varepsilon\chi/\beta)\right\}$$

$$= \lim_{\chi\to\infty} \left\{\tilde{T}_s + \varepsilon[\theta(\chi)-\chi]\right\}$$

Hence to zeroth order we have

$$A_o = \beta$$

as should be. To the first order we have

$$\theta(\infty) = A_1 \tag{54}$$

and

$$\left(\frac{d\theta}{d\chi}\right)_\infty = 0 \tag{55}$$

The solution of Eq. (51) subject to Eqs. (53) and (55) are

$$\theta(\chi) = \chi + \ln \left\{\frac{1}{\Delta}\left[1 - \left(\frac{\Lambda e^{\pm\chi}-1}{\Lambda e^{\mp\chi}+1}\right)^2\right]\right\} \tag{56}$$

where

$$\Lambda = \frac{1 + (1-\Delta)^{1/2}}{1 - (1-\Delta)^{1/2}}$$

Using Eq. (56), we also find

$$\left(\frac{d\theta}{d\chi}\right)_0 = 1 \mp (1-\Delta)^{1/2} \tag{57}$$

which is to be used in Eq. (50) for $\tilde{Y}_{is} = \tilde{Y}_{i,in}$ and in Eq. (52) for Δ. This results in two transcendental equations for the two unknown Δ and, say, $\tilde{Y}_{Fs}$ because $\tilde{Y}_{Os}$ is given by Eq. (37).

The heat transfer rate at the wall is proportional to

$$\left(\frac{d\tilde{T}_{in}}{d\chi}\right)_0 = \mp (1-\Delta)^{1/2} \tag{58}$$

In physical quantities we have

$$\begin{aligned}
\left(\lambda \frac{\partial T_{in}}{\partial y}\right)_0 &= \left(\frac{\lambda_s Q}{C_{ps}}\right)\left(\frac{\partial \tilde{T}_{in}}{\partial y}\right)_0 \\
&= \left(\frac{\lambda_s Q}{C_{ps}}\right)\left\{\left(\frac{\partial \eta}{\partial y}\right)\left(\frac{d\xi}{d\eta}\right)\left(\frac{d\chi}{d\xi}\right)\left(\frac{d\tilde{T}_{in}}{d\chi}\right)\right\}_s \\
&= \mp\left(\frac{\lambda_s Q}{C_{ps}}\right)\left(\frac{\beta}{\varepsilon}\right)H_o(\infty)\left(\frac{2^j\alpha}{\rho_\infty \mu_\infty}\right)^{1/2} \rho_s (1-\Delta)^{1/2} \\
&= \mp \left\{\frac{\beta Q H_o(\infty)}{\varepsilon}\right\}\left\{2^j \alpha \rho_\infty \mu_\infty (1-\Delta)\right\}^{1/2}
\end{aligned} \tag{59}$$

Figure 2 shows some typical curves of Eq. (56). It is seen that for $\Delta < 1$ two solutions exist whereas for $\Delta > 1$ no solution exists. This behavior indicates the occurrence of some critical phenomena, viz. ignition for the present case, when $\Delta = 1$, as will be further elaborated in the following.

(5) Response Curve and Ignition Criteria

From Eq. (56) it can be easily shown that

$$\theta(\infty) = \ell n \left\{\frac{4}{\Delta}\left[\frac{1 \mp (1-\Delta)^{1/2}}{1 \pm (1-\Delta)^{1/2}}\right]\right\} \tag{60}$$

which is plotted in Fig. 3. It is obvious that we have obtained the lower half of the S-shaped ignition/extinction response curve (Fendell, 1965). Hence the lower branch in Fig. 3, given by the positive root of Eq. (56), represents states with weak gas-phase chemical activities. At $\Delta = 1$, the slope of the response cuve becomes infinite and ignition is expected to occur. The system then instantaneously assumes an active burning mode represented by the upper branch of the S-curve which is not obtained here. Threfore ignition for a system is expected to be possible for

$$\Delta \geqslant 1 \tag{61}$$

The middle branch of the S-curve, given by the negative roots of Eq. (56), represents unstable states.

Using Eq. (52) for Δ, it can therefore be stated that ignition should occur for

$$\left(\frac{2\delta_g \varepsilon}{\beta^2}\right) H_o^2(\infty)\{\tilde{Y}_{O\infty}-(S+\beta)\}^{a_{Og}}\{\tilde{Y}_{F\infty}-(S+\beta)\}^{a_{Fg}}\tilde{T}^{a_{Tg}}\, e^{-\tilde{T}_{ag}/\tilde{T}_s} \geqslant 1 \tag{62}$$

The criterion (62) shows two interesting results. First there exists an absolute ignitability limit given by either

$$\tilde{Y}_{O\infty} = (S+\beta) \tag{63a}$$

or

$$\tilde{Y}_{F\infty} = (S+\beta) \tag{63b}$$

depending on whether the mixture is oxidizer or fuel lean. Ignition is not possible for leaner concentrations. Physically it implies that even all the leaner reactant is consumed in the surface region, there is still not enough heat generated to induce thermal runaway. It may also be noted that this limit is independent of the gas-phase kinetics.

The second point to note is that, for a given $\tilde{T}_s$, Eq. (62) is more easily satisfied for a noncatalytic surface, with $S \equiv 0$, than for a catalytic surface. In other words the presence of catalyst hinders the initiation of gas-phase reactions. This phenomenon has been experimentally observed before (Lewis and von Elbe, 1961). The reason being that for the present isothermal surface, the catalytic heat generated is not used to heat the gas because the surface temperature is fixed. Thus the presence of the catalyst only implies less external heating is needed to maintain this temperature. At the same time, however, the catalytic reaction depletes the reactant concentrations near the surface. Therefore the gas-phase reaction is retarded. The above result is illustrated in Fig. 4.

Finally, Eqs. (58) or (59) also show that during the weakly burning case there is always heat transfer from the wall to the gas. At the ignition point $\Delta = 1$ the heat transfer from the wall ceases. This result demonstrates that to first order of accuracy the adiabaticity criterion for ignition is exactly the S-curve ignition criterion.

IV. EXTINCTION PHENOMENA

After ignition, a flat flame is established in the stagnation-point flow. Subsequently, extinction of this flame can be brought about through a variety of means, for example by increasing the flow velocity (i.e. the extent of blowing) or by steadily leaning the concentration of the deficient component. We are interested in understandig the effect of the surface catalyst on the extinction state. Rather than detailing the mathematical analysis, we shall instead discuss the dominant physical processes involved which may lead to extinction.

First we note that for a flame to be stabilized in the divergent flow field of a stagnation point (Fig. 1), the flame propagation velocity S_L must be equal to the normal component of the upstream gas velocity, u_n. Therefore if we attempt to extinguish the flame by, say, increasing the upstream velocity, the flame will be pushed toward the stagnation surface such that the balance $S_L = u_n$ is again established.

The change in the flame temperature as a result of the change in the flame location depends on the thermal diffusivity α_t of the mixture, and the mass diffusivity α_m of the deficient, and therefore, controlling species. To illustrate this point let us take the control volume as shown in Fig. 1. Since heat and mass diffusion occur in the direction normal to the flame while convective transpot is along the divergent streamlines, it is obvious that the flame segment in the control volume loses thermal energy to the indicated streamline which leaves the control volume, while it gains chemical energy carried by the reactants from this streamline. Therefore these two effects tend to reduce and increase the flame temperature respectively. In particular if the thermal and mass diffusivities are the same, that is $\alpha_t = \alpha_m$ or $Le = \alpha_t/\alpha_m = 1$, then the flame temperature is the adiabatic temperature, T_{ad}, which is invariant with changes in the blowing intensity. On the other hand we expect the flame temperature to decrease with increasing blowing for $Le > 1$ and increase for $Le < 1$. Therefore with increasing blowing extinction is possible for $Le > 1$ and not possible for $Le < 1$. For the latter case the flame will eventually be pushed to the wall. Only with further blowing can extinction occur because chemical reaction cannot be completed due to the reduced residence time. The above concepts are illustrated in Fig. 5 for the reaction rate profiles and Fig. 6 for the response curve.

Finally we consider the effect of surface catalyticity. When the flame is situated away from the wall, almost complete consumption of the reactants occur when crossing the flame. Therefore the presence of the suface catalyst downstream of the flame will have no effect on the flame behavior. Since for Le > 1 the flame is away from the wall even at extinction, we expect that surface catalyticity will have no effect on the extinction limit. However, for Le < 1 the flame will collapse onto the surface before extinction. In this case surface catalyticity can extend the extinction limit.

V. EXPERIMENTAL

A schematic of the experiment is shown in Fig. 7. The experiment involves passing gaseous fuel and air through flowmeters, a mixing chamber, an electric preheater, a diffuser packed with glass beads, a settling chamber with damping screens, and a water-cooled nozzle with a contraction ratio of eight. The mixture then impinges onto a flat stagnation surface which may or may not be catalyzed. The surface temperature can be controlled by water-cooling, or resistive heating, or torch heating at the back. The chamber is enclosed such that pressure variations between 0.1 atm to 5 atm can be achieved.

From our preliminary experiments we did find that extinction of lean propane/air mixtures (Le > 1) occurs away from the surface and is also at a constant velocity gradient α. The extinction limit is practically independent of the surface conditions including the temperature and catalyticity. For rich propane/air mixtures the flame is located much closer to the surface when extinction occurs, and is more sensitive to the surface conditions.

More detailed experiments are currently underway.

Acknowledgements

This work is supported by the Office of Naval Research under Contract No. N00014-80-C-0586.

References

Ablow, C. M., Schechter, S., and Wise, H. (1980), "Catalytic Combustion in a Stagnation Point Boundary Layer," Combust. Sci. Tech. 22, pp. 107-117.

Bracco, F. V., Bruno, C., Yaw, Y., and Walsh, P. M. (1980), "Computed and Measured Emissions from the Catalytic Combustion of Propane/Air Mixtures," Proceedings of the Fourth Workshop on Catalytic Combustion, May, 1980.

Cohen, C. B. and Reshotko, E. (1954), "Similar Solutions for the Compressible Boundary Layer with Heat Transfer and Pressure Gradient," NACA TN 3325.

Fendell, F.E. (1965), "Ignition and Combustion in Initially Unmixed Reactants," J. Fluid Mech. 21, pp. 281-303.

Law, C. K. (1978), "On the Stagnation Point Ignition of a Premixed Combustible," Int. J. Heat Mass Transfer 21, pp. 1363-1368.

Prasad, R., Tsai, H. L., Kennedy, L. A., and Ruckenstein, E. (1981), "Ocurrence of Multiple Steady States in the Catalytic Combustion of Propane," Combust. Sci. Tech. 26, pp. 51-64.

Schefer, R. W., Robben, F., and Cheng, R. K. (1980), "Catalyzed Combustion of H_2/Air Mixtures in a Flat-Plate Boundary Layer: I. Experimental Results," Combust. Flame 38, pp. 51-63.

Tien, J. S. (1981), "Transient Catalytic Combustor Model," Combust. Sci. Tech. 26, pp. 65-75.

Williams, F. A. (1965), Combustion Theory, Addison-Wesley, Reading, Mass.

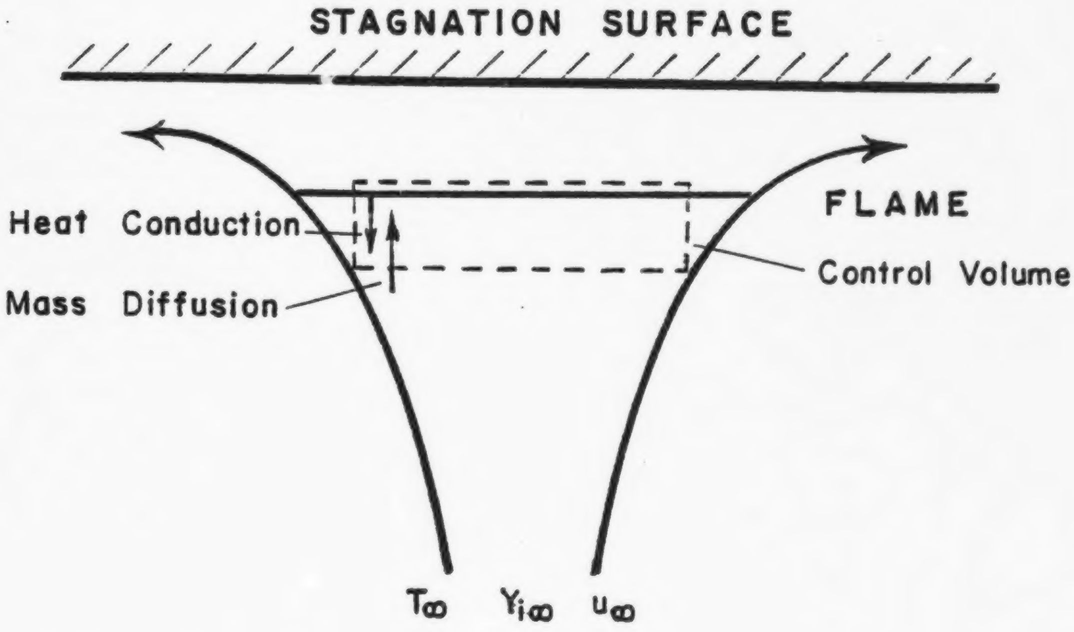
STAGNATION SURFACE
FLAME
Heat Conduction
Mass Diffusion
Control Volume
T_∞
$Y_{i\infty}$
u_∞

Figure 1. Schematic of Stagnation-Point Flow Illustrating the Directions of Heat and Mass Diffusion.

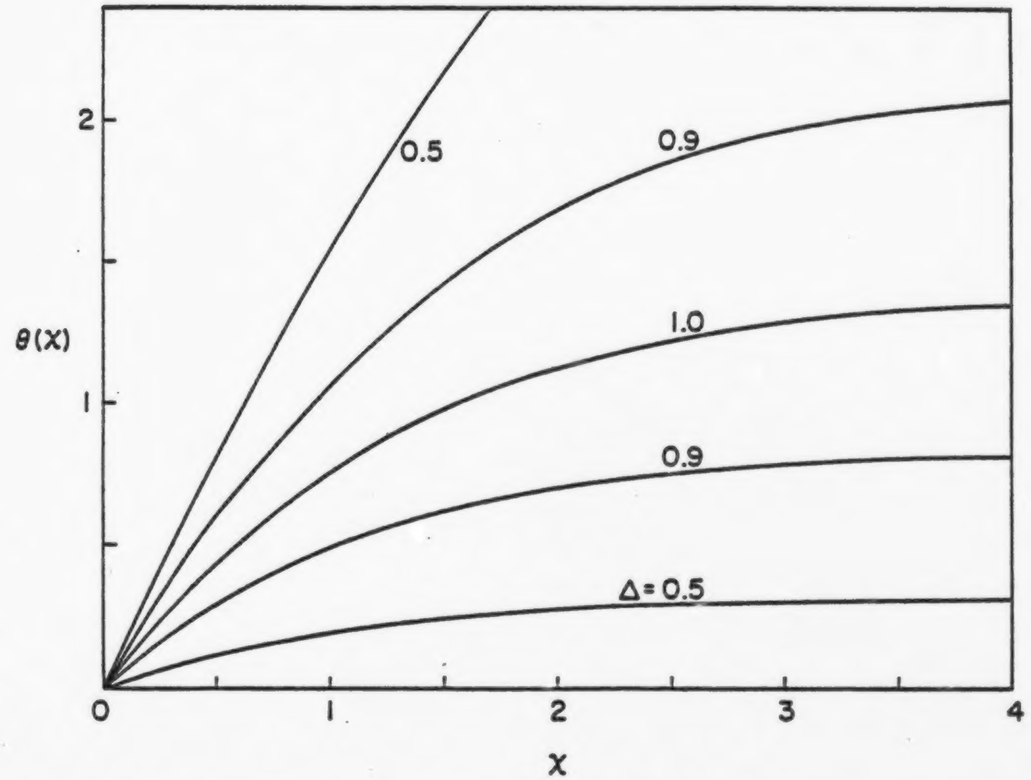

Figure 2. Profile of Temperature Increase due to Chemical Reaction.

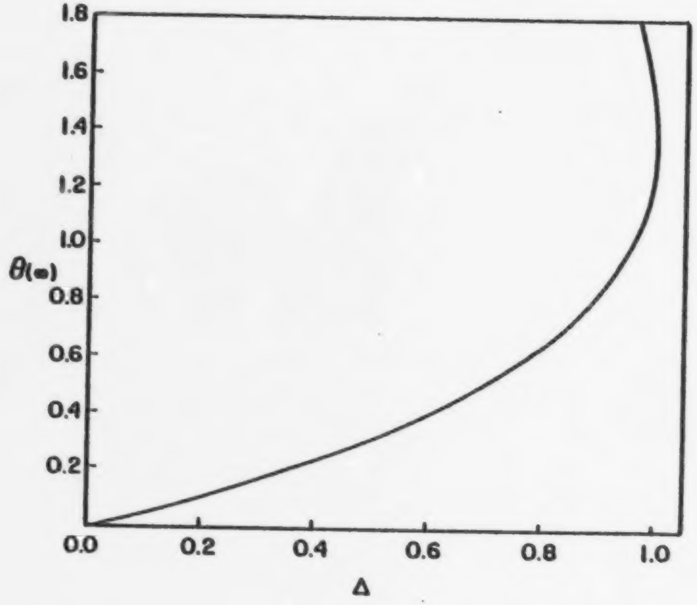

Figure 3. Maximum Temperature Increase as Function of the Damkohler Number, Showing Ignition Occurs at $\Delta = 1$.

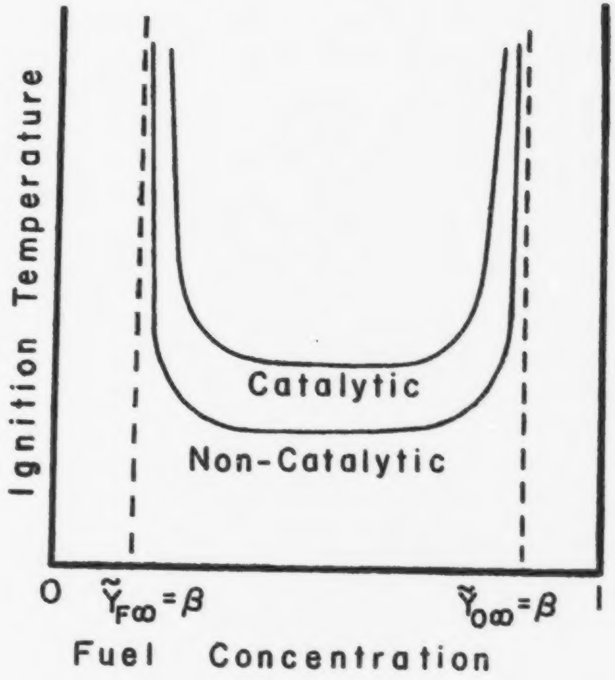

Figure 4. Plot Showing the Ignition Limits for Catalytic and Non-Catalytic Surfaces.

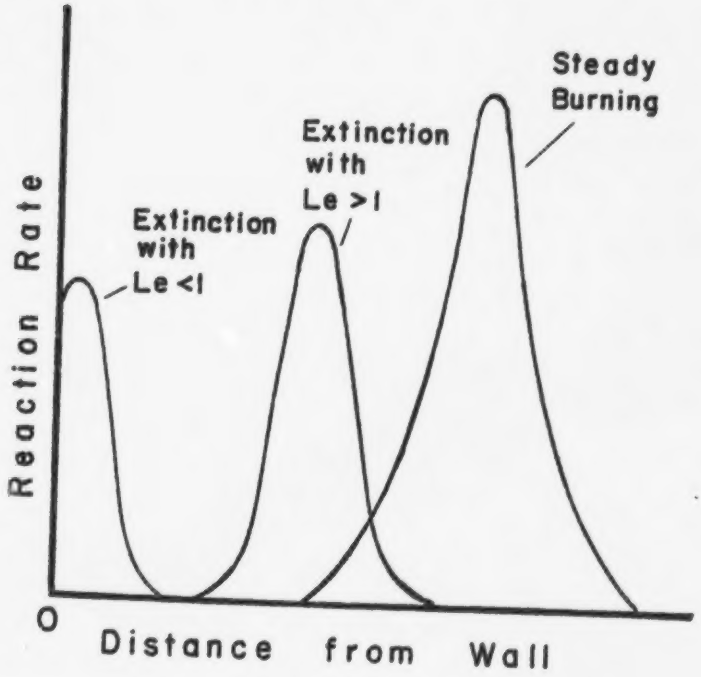

Figure 5. Reaction Rate Profile at Extinction for Le ⪌1.

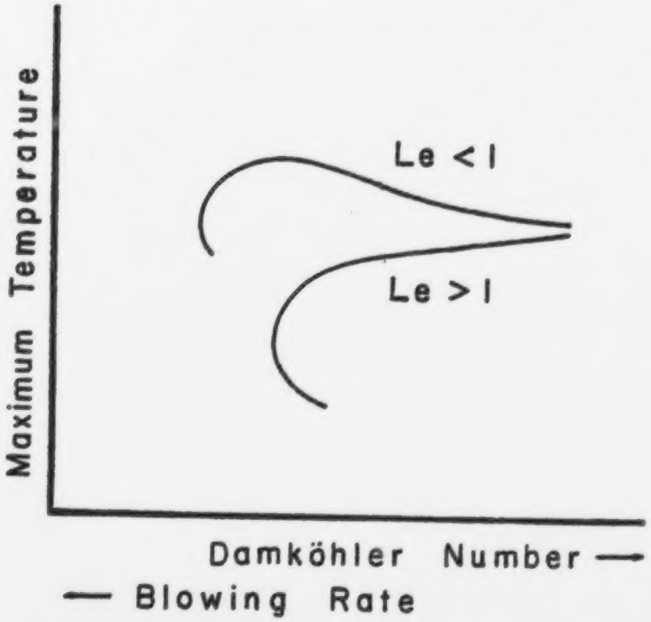

Figure 6. Response Curve for Le ⪌ 1.

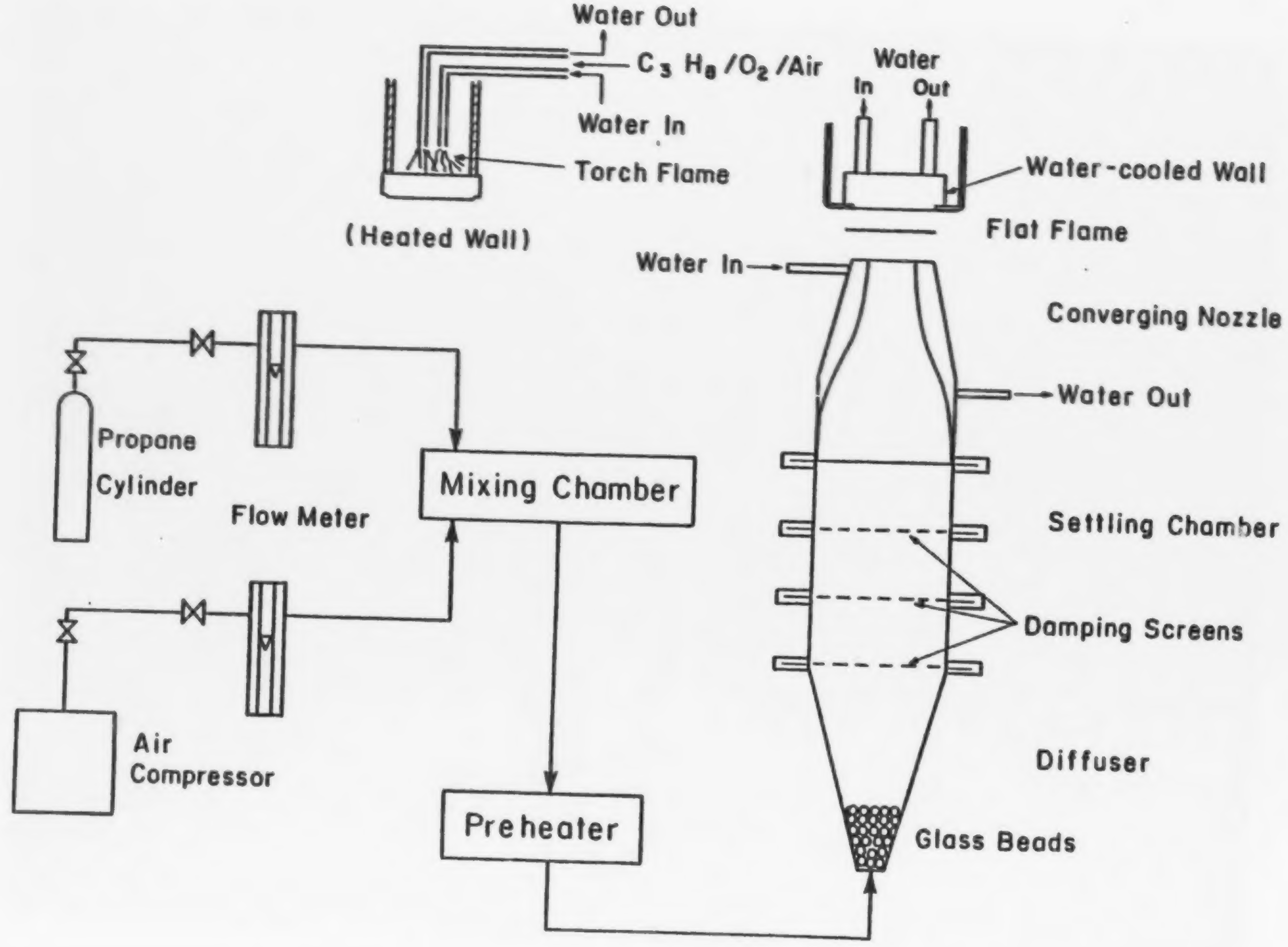
Water Out
$C_3H_8/O_2/Air$
Water In
Torch Flame
(Heated Wall)
Water
In
Out
Water-cooled Wall
Flat Flame
Water In
Converging Nozzle
Water Out
Propane
Cylinder
Flow Meter
Mixing Chamber
Settling Chamber
Damping Screens
Air
Compressor
Diffuser
Preheater
Glass Beads

Figure 7. Schematic of the experimental apparatus.

MINIMUM PRESSURE DROP FOR CLEANING UP LARGE GAS FLOWS

by:

William B. Retallick
Consultant
West Chester, PA 19380

ABSTRACT

In cleaning up a large flow of waste gas, the energy consumed in pressure drop is expensive. When mass transfer of the pollutant is the rate limiting step, there is a theoretical minimum pressure drop for any fractional cleanup and any inlet volocity. We will calculate this minimun pressure drop for a ceramic honeycomb, a metal honeycomb, and a packed bed. It is lowest for the metal honeycomb and is prohibitively high for the packed bed.

SYMBOLS

Re	Reynolds number
Sc	Schmidt number
f	Friction factor
K	Mass transfer coefficient, $\frac{\text{Length}}{\text{Time}}$
ρ	Density, $\frac{\text{Mass}}{\text{Volume}}$
d	Effective diameter of a channel, $\frac{4\ (\text{Sectional Area})}{\text{Wetted Perimeter}} = \frac{4}{a}$
v	Velocity, $\frac{\text{Length}}{\text{Time}}$
ΔP_f	Pressure drop from fluid friction, $\frac{\text{Force}}{\text{Area}}$
g_c	Gravitational constant, $\frac{(\text{Mass})(\text{Length})}{(\text{Force})(\text{Time})^2}$
D	Diffusion coefficient $\frac{(\text{Length})^2}{\text{Time}}$
N	Number of mass transfer units, dimensionless
H	Number of velocity heads in one mass transfer unit, dimensionless

IN GENERAL

In a previous paper we showed that when mass transfer is the rate limiting step, there is a minimum length of reactor for any fractional cleanup (Reference 1). Here we will calculate the pressure drop that goes with this minimum length.

When mass transfer is rate limiting, the rate is

$$\frac{dC}{dL} = \frac{-aKC}{v}$$

and the length of a mass transfer unit was defined as

$$L_m = \frac{v}{Ka}$$

If the length of the reactor is L, the number of transfer units is

$$N = \frac{L}{L_m} ,$$

and the concentration at the outlet is

$$\frac{C_L}{C_{inlet}} = e^{-N}$$

For any desired cleanup we can calculate N. The pressure drop that goes with this value of N is the minimum pressure drop for the cleanup.

The velocity head is defined as $\frac{v^2}{2g_c}$ and it has the dimensions of energy per unit mass of the fluid. This can be converted into pressure drop as a percent of the total pressure, or into inches of water when the total pressure is nearly constant at one atmosphere. We calculate the number of velocity heads by rearranging the equation for the Fanning friction factor:

$$\frac{-\Delta P_f}{\rho}\frac{2g_c}{v^2} = \frac{4fL}{d} = afL$$

This is the number of velocity heads lost in any length L. When $L = L_m = \frac{v}{aK}$, the number of velocity heads H is simply $\frac{fv}{K}$. All of this applies to both turbulent and laminar flow.

TURBULENT FLOW

In turbulent flow, the friction factor and the mass transfer coefficient are related by the Reynolds analogy, in this way:

$$\frac{v}{Ka} = \frac{2}{fa},$$

so that $H = \frac{fv}{K} = 2$.

The Reynolds analogy assumes that there is no diffusional resistance to transfer. In the usual case, when diffusional resistance is not completely negligible, Colburn's analogy corrects for the diffusional resistance, so that

$$H = 2\ (Sc)^{2/3}$$

LAMINAR FLOW

The number of velocity heads H is still $\frac{fv}{K}$, and K is eliminated by the relationship $\frac{Kd}{D} = C_1$ a constant that depends on the shape of the duct. This leads to

$$H = \frac{1}{C_1}\frac{fvd}{D} = \frac{1}{C_1} f(Re)(Sc)$$

This can be simplified further because $f(Re) = C_2$, another constant that depends on the shape of the duct. Finally we have

$$H = \frac{C_2}{C_1} Sc$$

and from Reference 1:

$$L_m = \frac{1}{4C_1}\frac{vd^2}{D}$$

Shape of the Duct	The Constants for Laminar Flow	
	C_1	C_2
Circular	4.4	16
Square	~ 4.4	14
Parallel Plates	4.1	21

CALCULATIONS

In Table I we calculate the minimum pressure drop for burning out 98% of the CO in an air stream at 800°F. The rate of oxidation at 800°F is so high that mass transfer is practically controlling. Four mass transfer units are needed since $e^{-4} \sim 0.02$. The number of velocity heads per mass transfer unit is

$$\frac{C_2}{C_1} Sc = \frac{(14)}{4.4}(0.66) = 2.1.$$

The bottom line in Table I is the pressure drop in the four mass transfer units. This is the minimum for the 98% cleanup and the gas velocities chosen. The two honeycombs have the same approach velocity, 30 ft./sec. The metal honeycomb has thinner walls, lower velocity in the holes, and lower pressure drop. The approach velocity for the packed bed is only 8 ft./sec. Without this drastic reduction in velocity, the pressure drop in the packed bed would have been prohibitive. Packed beds waste pressure drop by forming vortices that contribute nothing to mass transfer.

The minimum thickness of honeycomb is only 4 X .65 = 2.6 inches. We would probably install twice this thickness and suffer twice the pressure drop. The pressure drop for the metal honeycomb will be lower for the same thickness and the same approach velocity.

REFERENCES

1. Retallick, W. B.,"Preliminary Design of Catalytic Combustors, in: Proceedings of Fourth Workshop on Catalytic Combustion, Cincinnati, Ohio, 1980, EPA - 600/9-80-035.

2. Sherwood, T. K., R. L. Pigford, and C. R. Wilke, Mass Transfer, McGraw-Hill, New York, 1975.

TABLE I

THE MINIMUM PRESSURE DROP FOR BURNING OUT 98% OF CO POLLUTANT AT 800°F, WHEN MASS TRANSFER IS CONTROLLING

	CERAMIC HONEYCOMB	METAL HONEYCOMB	PACKED BED OF SPHERES 0.18 INCH IN DIAMETER
Square holes per square inch	200	200	
Wall thickness, inch	.012	.004	
Hole diameter, inch	.059	.067	
% open frontal area or % void volume	72	90	40
Approach velocity, ft. per sec.	30	30	8
Velocity in holes, ft. per sec.	42	33	20
Reynolds number in holes	290	260	
Schmidt number	0.66	0.66	0.66
Velocity heads per mass transfer unit	2.1	2.1	
Number of mass transfer units	4	4	4
Length of one mass transfer unit, inch	0.65	0.65	0.27 (1)
Number of velocity heads	8.4	8.4	
Inches of water per velocity head	0.17	0.10	
Inches of water lost in 4 mass transfer units	1.4	0.8	1.2 (1)

(1) In the packed bed the length of a mass transfer unit is $\frac{1}{1.17a}\left(\frac{d_p v \rho}{\mu}\right)^{0.415} Sc^{2/3} = 0.27$ inch (Ref. 2). At 8 ft./sec. approach velocity, the measured pressure drop for 1.1 inches of bed, corrected from room temperature to 800°F, is 1.2 inches of water

SESSION II

HEAVY FUELS USE IN CATALYTIC COMBUSTION

Investigation of Partially-Vaporized Residual Oil Catalytic Combustion

T. J. Rosfjord
United Technologies Research Center
United Technologies Corporation

ABSTRACT

An experimental program to investigate catalytic combustion of fuel-lean mixtures of incompletely-vaporized residual fuel and air has been conducted. The 7.6-cm diameter, graded-cell reactor tested was constructed from zirconia-spinel substrate and catalyzed with a noble metal catalyst. Tests were performed with No. 6 oil and blends of residual fuel (no. 6 oil or shale residual oil) and No. 2 oil over a range of conditions including: inlet pressure = 0.3 to 0.6 MPa, inlet temperature = 600 to 895K, and reference velocity = 10 to 40 m/s. Tests with incompletely-vaporized No. 6 oil did not result in stable combustor operation. Streams of luminous particles were observed exiting the reactor, presumably the result of fuel deposition and carbonization on the substrate. A similar phenomenon was observed in tests performed with blends of No. 6 and No. 2 oil. Blends of shale residual oil and No. 2 oil were identified which resulted in stable operation. Tests performed with shale oil blends indicated that the combustor performance degraded with reduced degree of fuel vaporization. A similar effect was observed in tests performed with No. 2 oil.

INTRODUCTION

The current concerns regarding pollutant emissions are occurring at a time when continued development of the gas turbine engine as an industrial prime mover depends in part on its capability to use fuel with far less attractive physical and chemical properties than those of the fuels currently used. Increasingly stringent emission standards prompt even greater emission reductions, particularly of NO_x, than may be attainable with current combustor design technology. Therefore, to increase the options available for low emissions, fuel flexible engine designs, novel combustion concepts ought to be investigated. Catalytic combustion appears as an attractive candidate in this application. Considerable effort has been made in developing and demonstrating stable catalytic combustion systems which achieve high combustion efficiency at exceptionally lean fuel-air ratios (e.g., Refs. 1 and 2). The preponderence of combustion related work with catalysts has involved the use of either gaseous or relatively volatile fuels coupled with fuel-air preparation systems configured so that a high degree of fuel vaporization was achieved. Among candidate fuels for future gas turbine use are residual fuels, either petroleum or synthetically based, which will be difficult to vaporize. Therefore, it is necessary that investigations be undertaken to elucidate the behavior o. catalytic combustion systems using such fuels in lean fuel-air mixtures.

There are several mechanisms which occur in the catalytic reactor. The reactants must diffuse to the catalyst and be adsorbed. Surface chemical reactions occur followed by desorption and diffusion of the products into the bulk flow. Homogeneous gas phase reactions may also be present. The mechanism which controls the energy release process changes as the reactants flow along the tube. At the inlet, the gas temperature is too low for significant gas phase reactions; the lower activation energy surface reactions control. As the surface temperature increases, the heterogeneous reaction rates become greater than the reactant diffusion rates, resulting in a mass-transfer-limited rate of energy release. The gas temperature increases because of heat transfer from the hot surface. In a properly designed reactor, the gas temperature will increase sufficiently for gas phase reactions to dominate, with subsequent rapid consumption of the fuel and partially-oxidized (CO, UHC) species. Each of these mechanisms must exist; insufficient surface reactivity will fail to initiate the mechanism chain while the absence of gas-phase reactions will result in poor fuel conversion.

The foregoing description applies to reactors fueled with either fully- or mostly-vaporized fuel. The presence of incompletely-vaporized fuel can, however, influence the reactor performance in two ways. First, the presence of fuel in liquid form can reduce the wall temperatures at the inlet, and thus reduce the surface reaction rates, which would at best retard the gas temperature rise, reducing homogenious burnup, or may even destabilize the reactor. The droplets can depress the wall temperatures directly by impinging on the substrate, or indirectly by reducing the gas-phase fuel-air ratio, since it is the consumption of the gas-phase species which provides the energy release required to heat the walls. Second, incompletely-vaporized fuel can require an increased reactor length to allow sufficient residence time to achieve complete consumption of the fuel. In particular, additional length may be required to complete fuel vaporization prior to combustion within the reactor. A catalytic reactor properly designed for incompletely-vaporized fuel would allow for these effects.

United Technologies Research Center (UTRC) under contract with NASA/Lewis Research Center, with funding provided by U.S. Department of Energy, has conducted an experimental program directed toward demonstrating efficient catalytic combustion of fuel-lean mixtures of residual fuel and air, and assessing the influence of *incomplete* fuel vaporization on the performance of a catalytic reactor. The features of the residual fuel, particularly its low volatility and high viscosity, demanded that special considerations be given to the design of a fuel preparation system and catalytic reactor. A fuel injection system was designed to produce highly-atomized sprays of residual fuel by shearing the fuel stream with a high velocity airstream. Control of the fuel atomization was achieved by control of the fuel temperature, and therefore of its viscosity. A 7.6-cm diameter catalytic reactor was designed to combust the incompletely-vaporized residual fuel and air mixture. Design analyses extended techniques applicable to fully-vaporized systems to include considerations of the droplet vaporization and ignition within the catalytic reactor. Acurex Corporation, as a subcontractor to United Technologies, supported UTRC in the design and fabrication of the catalytic reactors. Tests were performed over a matrix of conditions to evaluate the influence of changes in inlet air temperature, reference velocity, and combustor fuel-air ratio. The design of the injector and reactor and the results of the test program are presented. A more complete description of the effort is contained in Reference 3.

TEST SECTION DESIGN

The test section consisted of two components--the fuel preparation section and the catalytic reactor section. A brief review of the designs and the specifications of the final configuration of each of these components is given in the subsections below. The designs depended, of course, on the characteristics of the fuel to be used. The primary test fuel for the program and the fuel for which the test section was designed was a No. 6 residual fuel supplied by NASA. A sample of the fuel was analyzed by Southern Petroleum Laboratories to determine its physical and chemical properties. These data, presented in Table 1, were used to develop correlations for the variation of density, viscosity, and surface tension with fuel temperature required to predict the extent of fuel atomization (see below). The distillation characteristics were used to predict the degree of vaporization of the oil in the mixer/vaporizer duct. As a result of analysis of data obtained in tests using No. 6 oil alone, some tests were performed with blends of either No. 6 and No. 2 fuel oil, or residual shale oil and No. 2 fuel oil. The former blends were investigated to determine whether a threshold No. 6 content suitable for acceptable operation could be identified. In the latter blends, another heavy oil (shale) was used to produce mixtures not only less volatile than No. 2, but also without the very high molecular weight species contained in the No. 6/No. 2 blends. Analyses of the shale oil and the No. 2 oil are also presented in Table 1.

Fuel Preparation System

A fuel preparation system consisting of a fuel injector and a mixer/vaporizer duct was designed to inject No. 6 fuel oil and satisfy three operational requirements at the following conditions: inlet air temperature = 600 K; pressure = 0.6 MPa; reference velocity = 20 m/s; and fuel-air ratio = 0.020. The first requirement, which was derived from the operational characteristics of a catalytic combustor, was that the system must provide distributions of fuel-air ratio, temperature and velocity which were uniform to within ± 10 percent of the mean value at the catalytic reactor inlet. The second and third requirements for the fuel preparation system related to producing an incompletely-vaporized fuel-air mixture. In particular, the fuel injection system was required to produce sprays characterized by a Sauter Mean Diameter (SMD) of either less than 30 microns or in the range of 70-150 microns. In addition, it was required that less than 50 percent of the fuel be vaporized at the catalytic reactor inlet.

The requirements were satisfied by designing a system which employed a multiple-venturi fuel injector followed by a straight mixer/vaporizer duct. As a result of the atomization analyses, the injector contained 19 venturi tubes distributed over a 7.6 cm-diameter circular area (Fig. 1). The injector was fabricated by an electrical-discharge machining technique to permit the 7-deg conical half angle diffusers to terminate along the natural cone intersections. This geometry eliminated regions of recirculating base flow which would have promoted autoignition within the fuel preparation system. The test fuel tubes had an internal diameter of 0.76 mm, were 28 cm long and penetrated 30 percent across each venturi throat. A test fuel tube was located at the throat of each venturi; a Jet A fuel tube (0.58 mm ID, 152 cm long), used to inject fuel during reactor start-up, was located 0.5 cm directly upstream from each test fuel tube. A 0.4-cm diameter well was milled into the injector body for each fuel tube to provide an air gap between the tube and the body, diminishing the potential to overheat the fuel. Each set of fuel tubes was calibrated to assure that it consisted of fluid mechanically equivalent tubes.

A review of correlations developed for the atomization of heavy fuels concluded that an expression developed for an air spray injector by Jasuja (Ref. 4) was applicable for the multiple-venturi injector. The correlation developed was:

$$SMD = 0.19 \frac{(\sigma_\ell/\rho_\ell)^{0.35}}{u_a \rho_a{}^{0.35}} \left(1 + \frac{1}{AFR}\right)^{0.25} + 0.127\,\mu_\ell \left(\frac{D}{\rho_\ell \sigma_\ell}\right)^{0.50} \left(1 + \frac{1}{AFR}\right)$$

where: SMD - droplet diameter, m
σ_ℓ - liquid surface tension, N/m
ρ_ℓ - liquid density kg/m^3
μ_ℓ - liquid viscosity, Ns/m^2
ρ_a - air density, kg/m^3
μ_a - air velocity, m/s
D - orifice diameter, m
AFR - air to fuel ratio in injector by weight

The correlation is the sum of two terms; the first is dominated by the air velocity while the second is responsive to the liquid (i.e., fuel) viscosity. Proper design of injector blockage and selection of fuel temperature would produce the air velocity and fuel viscosity, respectively, which would result in calculated droplet sizes which satisfied the requirements of the program. In order to produce small droplets both terms were minimized by having a high air velocity and low viscosity. Calculations using the properties of the test fuel led to the specification of a venturi throat diameter of 0.54 cm to produce a velocity of 245 m/s at the fuel injection site, insuring that the first term of the atomization correlation would always have a small value. Larger diameter droplets were to be obtained by allowing a higher viscosity (lower fuel temperature) which overrode the atomizing tendency of the high air flow. Analyses based on a 0.76-mm inside diameter fuel tube and the fuel properties indicated that for a fuel temperature of 373 K, a spray characterized by an SMD of 25 microns would have been obtained, while at a temperature of 329 K a spray having an SMD of 100 microns would be formed. The tradeoff in the droplet diameter with fuel temperature for the range of reference velocities investigated in this program is shown in Figure 2.

The mixer/vaporizer design was based upon representing the fuel as a pure substance with a vapor pressure which corresponded to the 25 percent point of the No. 6 distillation characteristic--half of the maximum desired extent of evaporation. Design calculations were performed for cases in which fuel droplets with diameters of 30 and 35 microns at initial temperatures of 373 K and of 100 microns at 329 K were injected into an airstream. The initial air velocity was assumed to be 245 m/s as would exist at the throat of any one of the 19 fuel injector venturi throats; the air velocity then decreased in accordance with the area change associated with the 7-deg half-angle diffuser prior to assuming a constant value corresponding to the mixer/vaporizer air velocity. The maximum allowable spray SMD at the injector was approximately 35 microns in order to simultaneously limit the vaporization to the 50 percent maximum limit and achieve a mean droplet diameter of less than 30 microns at the reactor inlet. Therefore, as shown by the calculation results (Fig. 3) the mixer/vaporizer had to be shorter than 19 cm. During the course of the test program, as a result of an internally-sponsored UTRC program, the spray vaporization code was modified to treat multicomponent fuels using a technique based upon the work of Cox (Ref. 5). Cox assumed that at any instant during the vaporization process the behavior of the distillate fuel could be represented by that of a pure substance; however, different pure substances characterized the fuel as the droplet vaporized. This technique simulated a droplet in which the lighter components were preferentially-vaporized while the relatively non-volatile species were retained. The full distillation curve (which was obtained at one atmosphere) was used to determine the representative pure substance at any instant. The expected level of fuel vaporization was recalculated after acquiring the capability to track the complete fuel distillation signature. The results, also shown in Figure 3, were significantly different from those obtained in the design activity. Initially, the vaporization gradient (change of vaporization with distance traveled) was higher, reflecting the vaporization of the low molecular weight components ("light ends"), while further along the duct the gradient fell to a relatively low level. This character indicated that the droplet was approaching a steady state temperature at which the vapor pressure of the remaining components, and hence the droplet vaporization rate, was low. Whereas the design calculations indicated that 50 percent vaporization would be achieved at a distance 18 cm from the fuel tube for a 35-micron diameter droplet, the improved calculation procedure predicted only a 30 percent level. Higher degrees of vaporization were predicted for smaller droplets which heated more rapidly (higher surface-to-volume ratio), providing relatively high vapor pressures and vaporization rates in the initial portion of the mixer/vaporizer. This higher vapor pressure decreased further down the duct because only the relatively non-volatile components remained. As indicated above, the ability to perform these calculations was attained subsequent to the design of the mixer/vaporizer; the device used in the test program was based on the single component representation of the fuel. As a consequence of the improved calculation results, tests were performed with smaller initial droplet diameters and elevated air temperatures to achieve the level of vaporizaton sought in the original design.

Catalytic Reactor

Acurex Corporation, as a subcontractor to UTRC, designed the catalytic reactor used in the tests with No. 6 oil. A detailed account of their design procedure is contained in Ref. 6; the following summarizes their effort.

A 7.6-cm diameter reactor was designed to achieve a 99.5 percent combustion efficiency of No. 6 oil at the following condition: inlet air temperature = 600 K; pressure = 0.6 MPa; reference velocity = 20 m/s; and adiabatic combustion temperature = 1400 K. A 50 percent level of fuel vaporization was assumed. A three-phase design analysis was performed. In the initial phase, it was assumed that the reactor was adiabatic and the fuel droplets did not ignite. The second analysis phase superimposed the droplet combustion phenomena on the initial results by considering the ignition and combustion times for the droplets within the reactor. The third phase of the analysis considered the non-adiabatic characteristics of the reactor, particularly the destabilizing influence of radiation from the upstream face of the bed.

In the initial adiabatic analysis, governing differential equations for the bulk gas energy and mass balances, droplet energy and mass balances, and surface energy balance were solved using a finite difference procedure. Surface catalytic rates would control the energy release at the inlet of the reactor. However, because of the lack of quantitative data on kinetic rates for residual fuel and air catalytic reaction, it was assumed that the fuel consumption rate was diffusion limited. An initial catalytic reactor configuration was selected based upon past experience with the combustion of highly-vaporized No. 6 fuel oil (Ref. 7). This device was patterned after a graded-cell concept which had been investigated by Acurex (Ref. 8). This graded-cell catalytic reactor was a device in which the cell diameters become progressively smaller along the streamwise direction; larger cell honeycomb substrates were used at the catalytic reactor inlet, while smaller cell diameter elements were used near the reactor exit. Most of the reactor length consisted of small cell diameter elements which were required to achieve complete burn-up of the partially-oxidized species. The larger cells at the reactor entrance promoted stable operation. That is, since the fuel consumption rate was controlled by the surface catalytic rates at the entrance, it was desirable to obtain high substrate temperature to maximize these rates. Heat loss to the convecting airstream was minimized by using large cell diameters thereby reducing the heat transfer coefficients. The rate of fuel conversion would not be affected since surface reaction rates, and not transport processes, were controlling.

The initial reactor investigated was configured to include 5-cm, 2.5-cm, and 15-cm lengths of 0.63-cm, 0.32-cm, and 0.16-cm diameter cell monolithic substrates, respectively. A typical result from the adiabatic analysis is shown in Fig. 4 which depicts the variation in the substrate temperature, bulk gas temperature, droplet radius, local gaseous fuel-air ratio, and fuel conversion efficiency with distance along the reactor length at the design condition. As indicated, the events were guided by the droplet evaporation. As the droplet vanished the wall temperature increased to the adiabatic temperature and the bulk gas temperature and the fuel conversion efficiency increased more rapidly. These results indicated that in the absence of homogeneous combustion or droplet ignition the goal of 99.5 percent combustion efficiency would require a reactor length significantly in excess of 25 cm. These results were for a mass-transfer-limited system, and therefore were conservative. That is, at the temperature levels experienced in the latter parts of the reactor, homogeneous gas phase reactions would dominate and rapidly consume the partially-oxidized species. With these reactions it was estimated that the fuel would be consumed a few centimeters after complete evaporation of the fuel droplet, for a total reactor length of approximately 24 cm. Note that these calculated reactor lengths were considerably in excess of reactors designed for operation on light-distillate fuels (e.g., Jet A). In essence, the device designed for residual fuel provided the additional length (residence time) required to achieve complete evaporation of the relatively non-volatile components. This was not identical to providing a similarly longer mixer/vaporizer as the droplet evaporation rate within the reactor would be higher than experienced within the mixer/vaporizer because of the intense temperature field within the cells. In addition to projecting reactor lengths for adiabatic operation, the analysis provided the gas and droplet temperature histories required to calculate the distance traveled by the droplet prior to ignition. Using these results, the calculated ignition length was approximately 21 cm, with complete combustion of the droplet occurring within two additional centimeters.

The reactor performance calculations indicated that an approximately 24-cm long device would be sufficient to completely consume the fuel. An implicit assumption was that the reactor would operate stabily; that is, the substrate at the reactor inlet would remain hot enough to adequately promote the surface catalytic reactions. One influence on the substrate temperature was the upstream radiation loss from the reactor inlet. An analysis of this effect indicated that approximately a 100 K depression in the substrate temperature would be experienced on the face; the radiation loss would affect the temperature of the initial 2-cm length of the catalytic reactor. Therefore the length of the large cell elements was chosen to be greater than the penetration of the temperature depression.

It was also recognized that the presence of non-vaporized fuel could destabilize the reactor by either impinging on the reactor surface or by reducing the gas-phase fuel-air ratio. The former affect was minimized with the graded-cell concept by providing large flow channels at the inlet of the reactor. In an attempt to minimize the second effect, a catalyst preparation available from UOP was selected. Previous Acurex experience indicated it to be an active catalyst, offering the possiblity of acceptable activity even at the temperature associated with the reduced gas-phase fuel-air ratio. (Note that with the 50 percent vaporization limit, this fuel-air ratio would be half the overall value, being as low as 0.010 for simulated gas turbine operation.)

Based upon analyses of several reactor geometries at the design condition and near-design conditions, the reactor was specified to be a 7.6-cm diameter, graded-cell device made with Corning MCB-12 zirconia-spinel substrate (Fig. 5). Catalytic elements, each 2.5-cm thick, were assembled into 5-cm, 2.5-cm, and 17.5-cm lengths of 0.63-cm, 0.32-cm, and 0.16-cm square cell segments, respectively. The elements were catalyzed with a UOP noble metal, proprietary catalyst. The reactor was assembled by Acurex and instrumented with high temperature thermocouples embedded in a dedicated substrate channel. The assembled segments were cemented into a Carborundum Fiberfrax T30R sleeve for insertion into the test rig. The Fiber frax sleeve had a nominal 1.2-cm wall thickness which reduced heat loss from the reactor to less than one percent of the energy released.

TESTS RESULTS

Tests were performed to evaluate catalytic combustion of mixtures of residual fuel and air, and to determine the influences of incomplete fuel vaporization and the presence of droplets on the performance of the reactor. The ranges of the test parameters are indicated in Table 2. As will be discussed more fully below, it was necessary to expand the ranges of these parameters; the expanded limits are also shown on the Table. This section of the report presents test results under both the original and the expanded test conditions. The test results are divided into two sections: tests performed with No. 6 residual fuel, and tests performed with blends of residual fuel and No. 2 fuel oil.

Performance With No. 6 Fuel Oil

In the tests performed with No. 6 fuel oil, the residual fuel was not injected into a cold (i.e., non-operating) reactor. Rather, Jet A fuel was first injected from the multiple-venturi injector into the heated airflow required for the test condition. The startup fuel flow was increased until the combustor exit temperature was approximately 1400 K. Simultaneously, the residual fuel was heated using the startup recirculation leg of the fuel system [illegible] establish the desired fuel flow rate and fuel temperature. Once the reactor [illegible] abilized on the startup fuel, the residual fuel was routed to the multiple venturi injector. The temperatures exiting the reactor were monitored; the residual fuel flow rate was increased and the [illegible] A fuel flow decreased to maintain the exit temperature in the range of 1400 K to 1550 K. Several schemes for this transition process were tried, attempting either to achieve a rapid, but unsteady, transistion or a slow multiple steady state transistion. None of these schemes was found to be totally satisfactory. While slow transitions were desirable to assess the ability of the reactor to combust a combination of Jet A and residual fuels, they often placed unsatisfiable fuel control system demands for small changes; rapid transistions could potentially result in undesirably high fuel-air ratio excursions. (Note: The quasi-steady approach was not identical to blending the fuels since the injection characteristics of the blend would differ from the characteristics of the individual fuels.)

Stable catalytic combustion of the No. 6 oil was not achieved. Fifteen combinations of the test parameters (pressure, temperature, reference velocity, fuel temperature) were investigated as indicated in Table 3. Also included in the table are the calculated spray SMD and degree of vaporization at the reactor inlet. (Degree of vaporization was calculated using the multiple-component representation of the fuel.) Initially, the tests were performed at 0.6 MPa and an air temperature of 600 K, as this was the design condition for the test section. High fuel temperatures were used (up to 400 K) to increase the atomization and subsequent vaporization of the fuel. The reactor was brought into a steady operating condition on Jet A fuel as evidenced both by a uniformly bright exit plane as seen in the closed-circuit television system and by reactor exit temperature levels within three percent of the mean. As the No. 6 fuel was introduced, the exit plane of the reactor darkened, occasionally being high-lighted with intermittent bright zones; the thermocouples at the exit plane of the reactor showed significant spatial and temporal variations. These phenomena were accompanied by bursts of luminous particles exiting the reactor. The reactor exit plane became totally dark and an insignificant temperature rise existed across the reactor when half of the total fuel flow consisted of residual fuel. Similar phenomena were observed for tests performed with inlet temperatures up to 700 K at either 0.45 MPa or 0.6 MPa. Half of the eight conditions with temperatures up to 700 K had calculated degrees of fuel vaporization of 50 percent or higher. Apparently this level of fuel vaporization was insufficient to sustain stable, catalytic combustion. In general, whenever the No. 6 oil was flowing condensed phase particles were observed exiting the reactor. These particles could have been either fuel droplets passing through the device or carbonaceous solids produced from droplet impingement on the reactor walls. The former explanation was not likely however as the droplets had a torturous path through the 25-cm long reactor. Rather, it was felt that heavy, non-volatile components of the fuel were being deposited on the reactor walls where they carbonized and subsequently flaked-off into the gas path. Such a deposition would reduce the temperature of the large cell elements, reducing the surface reaction rates and thus destabilizing the reactor.

The activity of the reactor was diminished after each test with the residual oil as evidenced by the inability to satisfactorily react a subsequent flow of Jet A fuel. Either of two rejuvenation processes were followed to restore catalytic activity. Initially, rejuvenation was attained by flowing air at a temperature of 800 K through the reactor for approximately one hour. When successful, this period of exposure to hot air satisfactorily oxidized the remaining fuel deposits and restored the catalytic activity. It was discovered that this process could be accelerated to require only fifteen minutes if a flow of Jet A fuel was introduced to produce an exit temperature of 1400 K. Three copies of the reactor described earlier were assembled. A new reactor would have been substituted for the test reactor if the emission levels for Jet A operation after rejuvenation did not duplicate the initial levels. Substitution was not required and a single reactor was used for the tests at 600 K and 700 K; it was rejuvenated approximately ten times. The reactor did not experience any major physical damage. Cracks were observed in the walls of the large cell elements presumably because of excessive thermal stress, however the substrate did not crumble while it was in the test section. The reactor was removed subsequent to these tests; the large cell elements collapsed when handled.

The inability to sustain stable catalytic combustion was attributed to an insufficient level of fuel vaporization. Tests were performed with a fresh (i.e. unused) reactor at higher inlet air temperatures (750 K to 840 K) and with smaller initial droplet diameters to achieve nearly 100 percent fuel vaporization. The conditions for these tests and the calculated degree of fuel vaporization are also included in Table 3.

Pre-ignition was encountered in the mixer/vaporizer for all tests performed at inlet temperatures up to 840 K once the No. 6 oil was introduced; pre-ignition did not occur during startup on Jet A fuel at these conditions. The phenomenon was detected by two thermocouples which were installed with the sensor flush with the inner wall of the mixer/vaporizer duct. Prior to ignition, the thermocouple outputs indicated a temperature slightly less than the air preheat temperature. At the onset of ignition both outputs increased at a moderate rate (approximately 200 K/sec), not the rapid rate expected if a homogenous autoignition had occurred. The output from the thermocouples measuring the reactor substrate temperature rose to the complete combustion temperature subsequent to the pre-ignition. Changes in test conditions to a reduced pressure and a high reference velocity (low residence time) were unsuccessful in preventing this phenomenon.

A review of both these ignition events and the experiences gained in other programs at UTRC led to the supposition that excessive fuel deposits on the mixer-vaporizer duct wall contributed to the ignition. That is, while complete vaporization of fuel was predicted at the reactor inlet, this level would not have been achieved until passing through approximately 70 percent of the mixer/vaporizer duct. Hence, wall deposition would be possible. The deposits would produce a fuel-air ratio gradient ranging from very fuel-rich on the wall to fuel-lean in the bulk airstream. The presence of near stoichiometric mixtures in the boundary layer would be condusive to flashback, particularly if combustor pressure perturbations momentarily stagnated the flow. Additionally, since the residence time of fuel traveling in the boundary layer would be longer than the residence time of the fuel in the bulk airstream, reactions leading to an autoignition could be initiated; this situation would also be aggravated for stoichiometric mixtures.

Discussions with engineers at NASA (Ref. 9) revealed observations similar to those experienced in this program and which were diagnosed to be caused by fuel deposition. In particular, tests with a residual fuel were successfully conducted at NASA for air preheat levels of 1000 K while frequent pre-ignitions were experienced at a 750 K preheat. These results suggest that at high temperatures the fuel was vaporized sufficiently to preclude significant deposition. At lower temperatures, liquid fuel impingement on the mixer-vaporizer duct was probably experienced, resulting in boundary layer mixture ratios which supported a pre-ignition mechanism.

Tests were conducted in an attempt to minimize the deposition. The several tests performed followed either of two approaches--avoiding deposition by restricting the fuel injection near the walls or avoiding deposition by accelerating the rate of fuel vaporization.

In tests following the former approach, fuel was injected at only six of the nineteen injection sites; no fuel was injected through the central or outer ring of venturi tubes. While the post test inspection did indicate a decrease in fuel deposition on the wall, a reduced tendency for a pre-ignition was not realized. Instead, an increased sensitivity was apparent as pre-ignition was regularly experienced during operation with Jet A fuel. Apparently the near stoichiometric mixture at the six injection sites (compared to an equivalence ratio of 0.3 if fuel was injected equally in all venturi tubes) was responsible for the worsened pre-ignition characteristics.

The second approach to minimizing fuel deposition relied upon achieving greater rates of fuel vaporization by further increasing the inlet air temperature. A change in test procedures and a re-evaluation of the air heater operational limit peritted achieving an inlet temperature of 895 K. Initial tests were performed at a reference velocity of 40 m/s to maximize fuel atomization. As before, complete vaporization was predicted, but with the highest air temperature this level was predicted to occur in the shortest distance in the mixer/vaporizer. Stable, but very inefficient, combustion of the No. 6 oil was attained. The combustion efficiency improved with increasing fuel-air ratio but was only approximately 75 percent for a fuel-air ratio of 0.028. Tests were also performed at reference velocities down to 20 m/s to increase the reactant residence time within the combustor. the lower velocities degraded the injector atomization (i.e., produced larger droplets), which apparently led to fuel deposition as pre-ignition was again experienced.

This observation pointed out a trade-off imposed by the fuel injector--namely, fine atomization required high air velocities which compromised the reactor by reducing the flow residence time. an independent control of atomizing air (i.e., air-assist) would have been desirable. This trade off became a significant factor only because it was necessary to operate outside the design conditions. That is, the fuel preparation system was designed to produce a partially-vaporized mixture of No. 6 fuel oil and air over the original range of conditions indicated in Table 2. Tests performed within these limits did not achieve stable combustion. In an attempt to achieve vaporization levels above the 50 percent limit, subsequent tests were performed at conditions which were more severe than originally anticipated. As a consequence, unexpected limitations were encountered--either pre-ignition, atomization or vaporization limitations. Because of these limitations, it was decided to perform tests with blends of residual fuel and No. 2 fuel oil.

Performance With Fuel Blends

As a consequence of the test results presented above, a series of tests was performed with blends of residual fuel and No. 2 fuel oil. The objective of these tests was to first determine a threshold concentration of the residual fuel blend which would result in acceptable performance (i.e., stable, highly efficient combustion without pre-iginition). Subsequently, tests were performed with No. 2 oil and the threshold blend in an attempt to assess the influence of incomplete fuel vaporization on the reactor performance. The fuel blends investigated were mixtures of either No. 6 oil and No. 2 oil, or shale residual oil and No. 2 oil. The shale residual oil was used as a blending component because its final boiling point was lower than the final point for the No. 6 (petroleum) oil. Therefore, shale oil blends did not have the very non-volatile species that were in a No. 6 blend. Blends were prepared according to weight fraction of the residual fuel in increments of 10 percent; samples of each blend were obtained and analyzed for specific gravity, viscosity and distillation characteristics. Tests to screen the fuel blends to determine the threshold level were performed at a condition defined by: pressure = 0.6 MPa; temperature = 670 K and reference velocity = 20 m/s. Once the threshold level was determined, performance characterization tests were performed at a pressure of 0.6 MPa; temperature = 600 K and 670 K, and reference velocity of 10 m/s and 20 m/s. In general, the tests were performed without use of a startup fuel as it was desirable to determine the blend composition which could be used directly. That is, it was desired to determine an acceptable fuel mixture such as might result from combining residual and distillate fuels in a large fuel tank. A startup fuel was used in some tests for blends above the threshold level to determine if alternative operating procedures could alter the level.

Tests were performed with blends of No. 6 oil and No. 2 oil using another fresh reactor. The screening tests began with performance characterization of No. 2 oil alone and proceeded with blends containing higher concentrations of the residual fuel. Acceptable performance was attained for the No. 2 oil and a 20-percent No. 6/No. 2 blend, but no significant reaction was observed with the use of a 40-percent No. 6/No. 2 blend. Subsequent tests with 30-percent and 20-percent blends also yielded unsatisfactory performance--a result in direct conflict with previous tests. A subsequent test with No. 2 oil alone produced a level of performance similar to that originally obtained. Additional tests with a 20-percent blend again produced unacceptable performance. Periods of rejuvenation with hot air and with Jet A did not affect these observations. It appeared that some component of the residual fuel was deposited on the catalytic surface which was not removed in the rejuvenation processes. The degraded reactor was apparently more sensitive to operation with residual oil blends than with Jet A or No. 2 fuel distillates. That is, the reactor was sufficiently overdesigned for light distillate fuels to preclude detection of the degradation. Similar screening tests were performed with a longer reactor (see below) with blends using the shale oil as the blending component. An initial test with No. 2 oil alone was followed by tests using blends with increasing weight concentration of the shale oil. Acceptable performance was attained with a 20-percent shale oil while unstable operation was observed with a 45-percent blend. The performance of the 20-percent blend was re-attained in a subsequent test, suggesting that it was the high molecular weight components in the No. 6 (and not in the shale oil) which previously affected the reactor performance. Additionally, bursts of luminous particles were not observed in tests using shale oil blends while they were still present in tests with No. 6 blends.

The apparent effect of fuel deposition experienced in tests with No. 6 oil or blends of No. 6 oil and No. 2 oil suggest that complete vaporization of No. 6 oil must be attained to achieve stable reactor operation. Long residence time vaporizers represent one approach to achieve complete vaporization at the relatively low combustor inlet temperatures associated with standard gas turbine operation. Such devices would be impractically long, however, unless extremely small fuel droplets were produced by the fuel injector. Alternative techniques which raise the inlet temperature (e.g., regenerative heat transfer) or otherwise augment the vaporization process may be necessary. One technique of the latter type is currently being evaluated--namely, the catalytic gasifier (Ref. 10). In limited tests, this device has shown the potential to gasify (i.e., vaporize and reform) extremely rich mixtures (equivalence ratio from 6 to 10) without the formation of carbon. Sufficient fuel reformation may occur such that even if complete vaporization was not attained, the remaining components would be acceptable for reactor operation.

A new, longer catalytic reactor was constructed from elements identical to those used to construct the device used in the tests with No. 6 oil alone. It was a graded cell reactor with lengths of large and medium cell segments equal to the original reactor; the length of the small cell segment was increased to 20 cm. The length of the gas phase reactor was 30 cm. The viscosity for fuel blends containing up to 50 percent residual fuel was 10 cs or less at a temperature of 300 K. Therefore, the calculated atomization was not sensitive to the available range of fuel viscosity (fuel temperature). Hence, for a given operating condition, the atomization and subsequent vaporization level was controlled by the reference velocity and the length of the mixer/vaporizer. Therefore to obtain differing levels of vaporization for equivalent operating conditions, tests were performed with the standard mixer/vaporizer length (18 cm) and a shortened mixer/vaporizer (9 cm).

Performance characterization tests were conducted with No. 2 oil and with 20-percent shale oil blends over the range of conditions indicated above, and with the two lengths of mixer/vaporizer. The essential results from the reactor performance characterization using No. 2 oil and a 20-percent shale oil/No. 2 oil blend are contained in Figs. 6 through 10. These figures show combustion efficiency (percent) versus fuel-air ratio for various test conditions. In general, they display a plateau of high performance which decreases rapidly below a certain fuel-air ratio. This rapid decrease is associated with extinguishing the gas phase chemical reactions which are required to complete the burnout of the partially oxidized species and to achieve high levels of combustion efficiency. Thus an important performance characteristic is the fuel-air ratio at which the rapid decline in performance begins--a breakpoint fuel-air ratio. The subsequent discussions will contrast the values of the breakpoint fuel-air ratio for comparative test conditions.

The reactor displayed the characteristic response to changing reference velocity (Fig. 6); that is, for higher reference velocities the breakpoint fuel-air ratio had a higher value. At higher reference velocities the residence time within the reactor was diminished, permitting insufficient time to achieve the gas temperature rise required to initiate the homogeneous reactions. As expected, the reactor performance improved with increased air preheat (Fig. 7). The breakpoint fuel-air ratio was reduced for higher inlet temperatures because of enhanced catalytic reactivity at the elevated temperature.

Results from tests to discern the influence of the degree of fuel vaporization on a reactor fired with No. 2 oil are contained in Fig. 8. The calculated degree of vaporization (DOV) depended on the air preheat level and the length of the mixer/vaporizer (L_{MV}). Calculations indicated that two of the data sets (circle and triangle symbols in Fig. 8) achieved equal levels of vaporization despite the differing mixer/vaporizer length. The performance for these two was essentially equivalent. The remaining two data sets in Fig. 8 represent different degrees of vaporization for the same operating condition because of differing mixer/vaporizer lengths. The standard performance signature was obtained for tests with the longer mixer/vaporizer, while for the shorter mixer/vaporizer, and associated lower degree of vaporization, a very poor performance characteristic was obtained (the temperature rise across the combustor indicated a combustion efficiency of approximately 80 percent). These results indicated an extreme sensitivity to the degree of fuel vaporization for the 600 K level of air preheat. This sensitivity could not be investigated at elevated air temperatures because complete vaporization was expected at the 670 K preheat level.

Not all tests performed to isolate the influence of the degree of vaporization were consistent, however. Figure 9 depicts the results for tests in which equivalent degrees of vaporization were expected to be obtained for the same test condition despite differing mixer/vaporizer lengths; equivalent performance was not obtained. These results suggested that the conditions at the reactor inlet were not equivalent for the two tests. The degree of vaporization prediction may have been optimistic, and less than complete vaporization may have been achieved in the shorter mixer/vaporizer. It is also possible that, for the shortened mixer/vaporizer test, the fuel and air were incompletely mixed to a degree that resulted in degraded reactor performance. This effect would be accentuated for the conditions shown in Fig. 9 as compared to those of Fig. 8 because of the higher reference velocity. Without a direct determination of the actual degree of vaporization it is not possible to fully explain the observed performances.

The reactor displayed the expected performance dependence on reference velocity when using the 20-percent shale oil blend. Again, lower values of the breakpoint fuel-air ratio were obtained for the low reference velocity which provided longer residence time within the reactor. The influence of degree of vaporization for the reactor using the shale oil blend is shown in Fig. 10. Two data sets (circle and diamond symbols) correspond to equivalent vaporization levels for the same operating condition; equivalent performance was obtained. Two of the data sets correspond to differing levels of fuel vaporization achieved by using differing mixer/vaporizer lengths. The higher breakpoint fuel-air ratio was obtained with decreased fuel vaporization because a reduced gas phase fuel-air ratio was unable to maintain a sufficiently hot catalytic surface.

A comparison of the reactor performance for the three fuels tested cannot be made because results from equivalent test conditions were not obtained. Test results did show that better performance was obtained with No. 2 oil than with No. 6/No. 2 blends. Qualitative impressions formed during tests performed with shale oil blends were that they were more reactive than No. 6 oil blends; the shale blends did not result in pre-ignition nor did they produce a stream of luminous particles exiting the reactor. It would be expected that a high performance level could be achieved (i.e., low breakpoint fuel-air ratio) for a reactor designed to operate with this fuel (e.g., improved catalyst formulation, longer reactor).

CONCLUSIONS

The objective of the experimental program was to demonstrate efficient catalytic combustion of fuel-lean mixtures of residual fuel and air and to assess the influence of incomplete fuel vaporization on the performance of a catalytic reactor. Tests were primarily conducted with a No. 6 residual fuel; some tests were performed with No. 2 oil or blends of residual fuel and No. 2 oil. Based upon test results in this program the following conclusions may be formed.

Stable catalytic reactor operation will not be achieved with incompletely-vaporized No. 6 oil. This characteristic was observed even for attempts to burn blends of No. 6 oil in No. 2 oil. In all cases, luminous particles, presumably the result of fuel deposition on the substrate, were observed exiting the reactor. System limitations precluded testing with fully vaporized No. 6 fuel because the conditions to achieve this level were significantly outside the original design envelope (efficient catalytic combustion of No. 6 oil has been obtained by other investigators (Ref. 9) if sufficient air preheat was used to assure complete vaporization). Therefore, fuel preparation devices which use techniques to achieve complete vaporization (e.g., regenerative heat transfer, catalytic gasifier) of the fuel need to be employed to sustain stable reactor operation.

Stable reactor operation can be achieved with fuel blends which contain incompletely-vaporized shale residual oil. Tests with shale oil blend did not lead to the catalytic reactor degradation experienced with No. 6 oil blends. It was concluded that the absence of the non-volatile, high-molecular weight components from the shale oil precluded lasting fuel contamination.

A significant performance degradation can exist for incomplete fuel vaporization. Significant performance degradation was obtained for 80 percent vaporized No. 2 oil or 90 percent vaporized shale oil blends.

REFERENCES

1. Kesselring, J. P. et. al: Design Criteria for Stationary Source Catalytic Combustion Systems. EPA-600/7-79-181, August 1979.

2. Anderson, D. N.: Performance and Emissions of a Catalytic Reactor with Propane, Diesel and Jet A Fuels. NASA TM-73786, September 1977.

3. Rosfjord, T. J.: Catalytic Combustion with Incompletely Vaporized Residual Fuel. NASA CR 165161, March 1981.

5. Cox, E. R.: Pressure-Temperature Chart for Hydrocarbon Vapors, Industrial and Engineering Chemistry, Vol. 15, No. 6, pp. 592-593, 1923.

6. Chu, E.: Catalytic Reactor Design for Combustion of Partially Vaporized No. 6 Fuel Oil. Acurex Project 7543 Report, 1979.

7. Pogson, J. T. and M. N. Mansour: No. 6 Fuel Oil Catalytic Combustion. Third Workshop on Catalytic Combustion, Asheville, NC, October 1978.

8. Kesselring, J. P. et. al: Recent Advances in Catalytic Combustion System Development. ASME Paper 79-WA/Fu-8, December 1979.

9. Anderson, D. N. and D. Bulzan: NASA Lewis Research Center, personal communication.

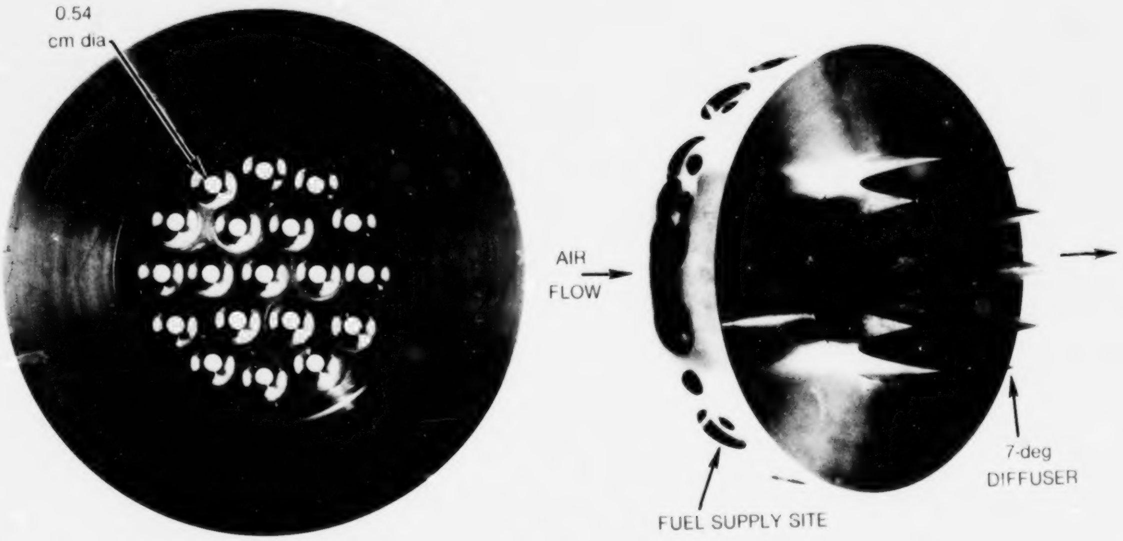
0.54
cm dia
AIR
FLOW
FUEL SUPPLY SITE
7-deg
DIFFUSER

a) VIEW FROM UPSTREAM

b) VIEW FROM DOWNSTREAM

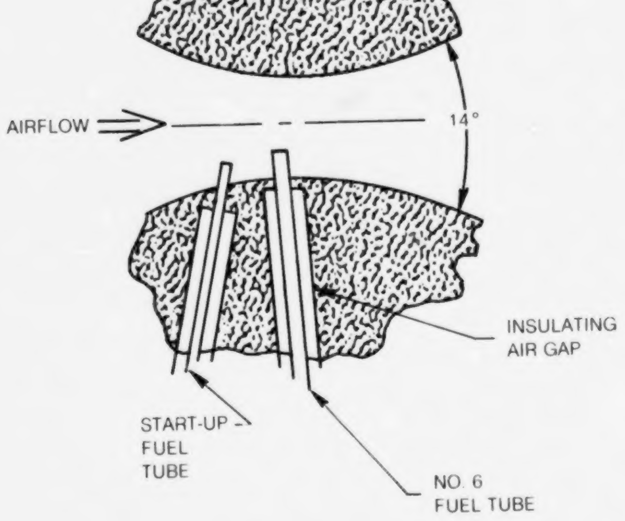
AIRFLOW
14°
INSULATING
AIR GAP
START-UP
FUEL
TUBE
NO. 6
FUEL TUBE

c) TYPICAL VENTURI THROAT

Figure 1 Multiple Venturi Fuel Injector

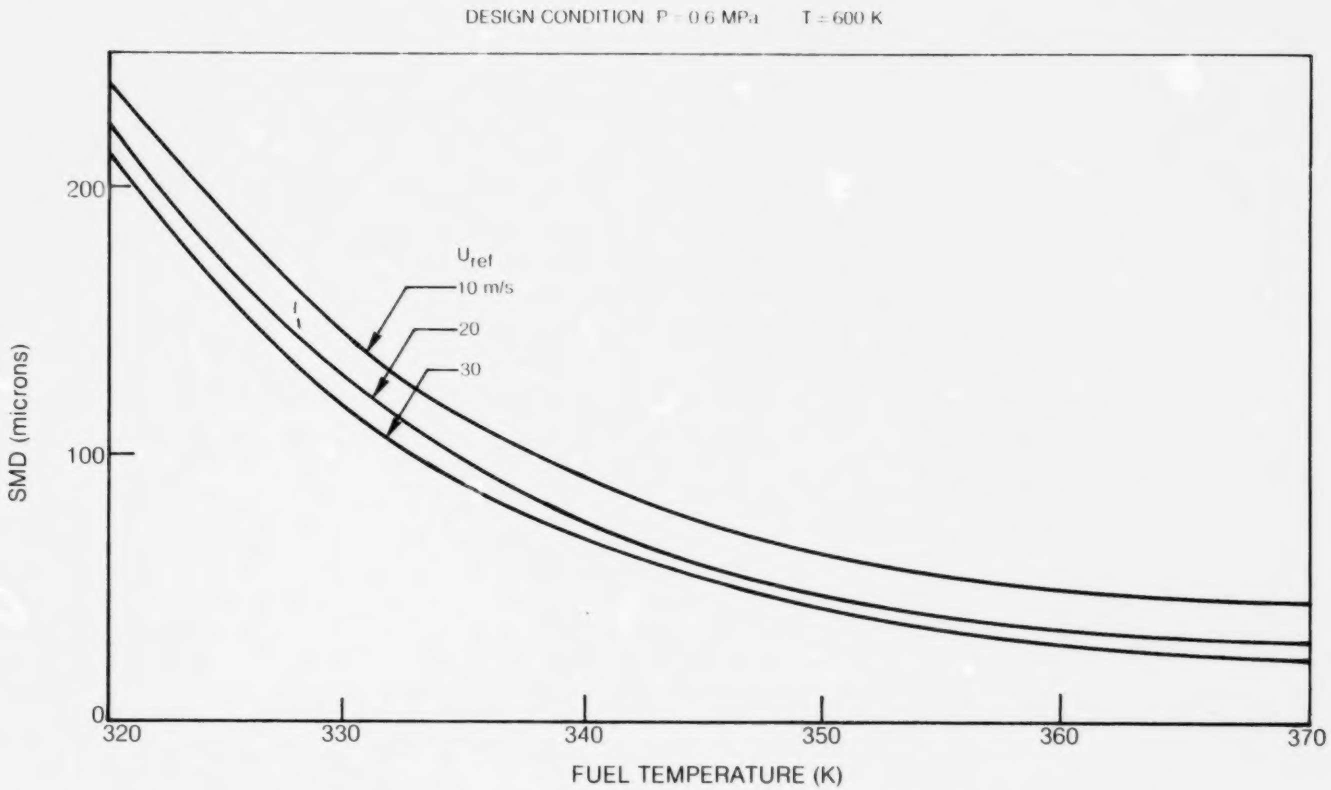

Figure 2 Calculated Atomization of No. 6 Fuel

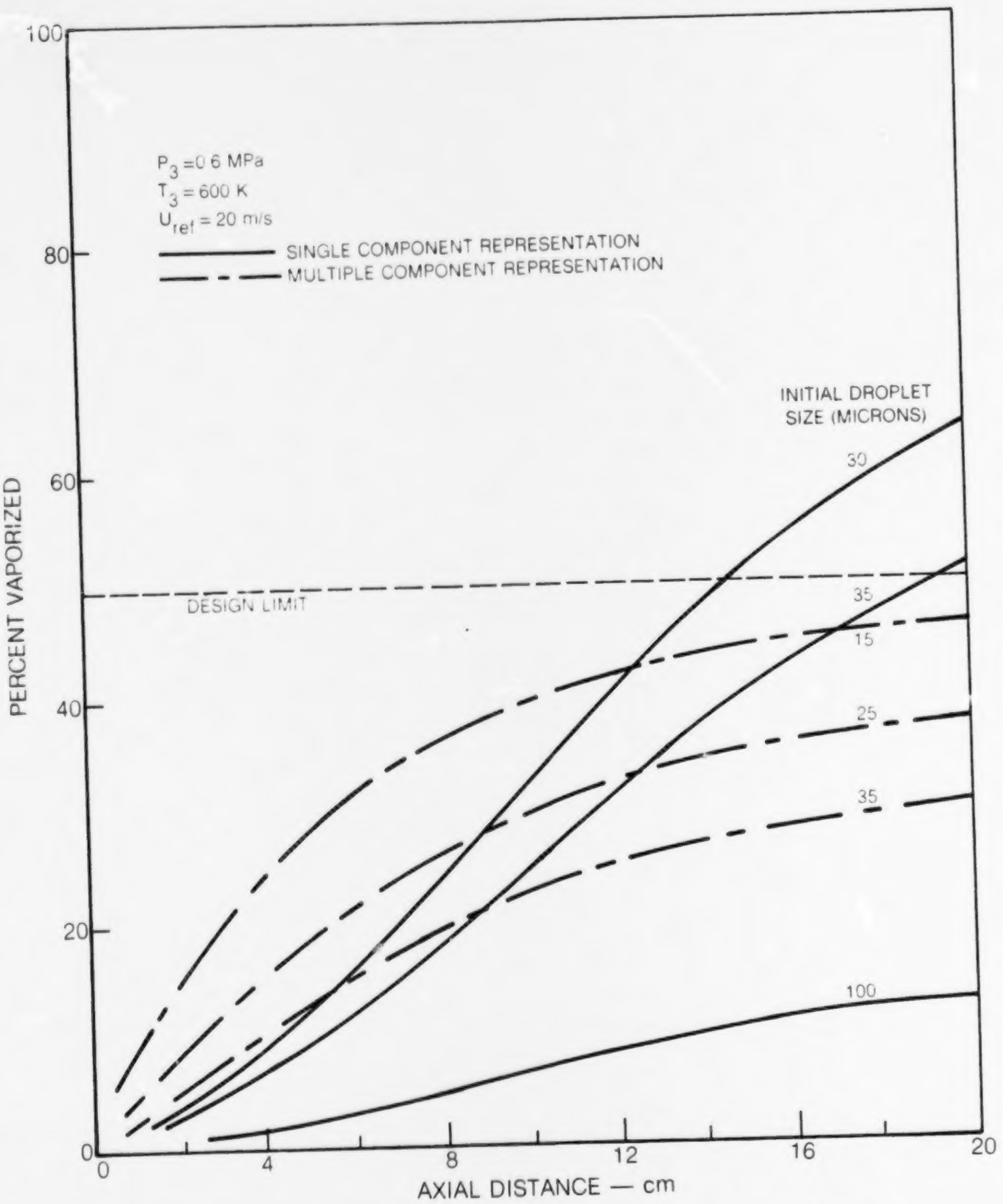

Figure 3 No. 6 Fuel Oil Droplet Evaporation Characteristics

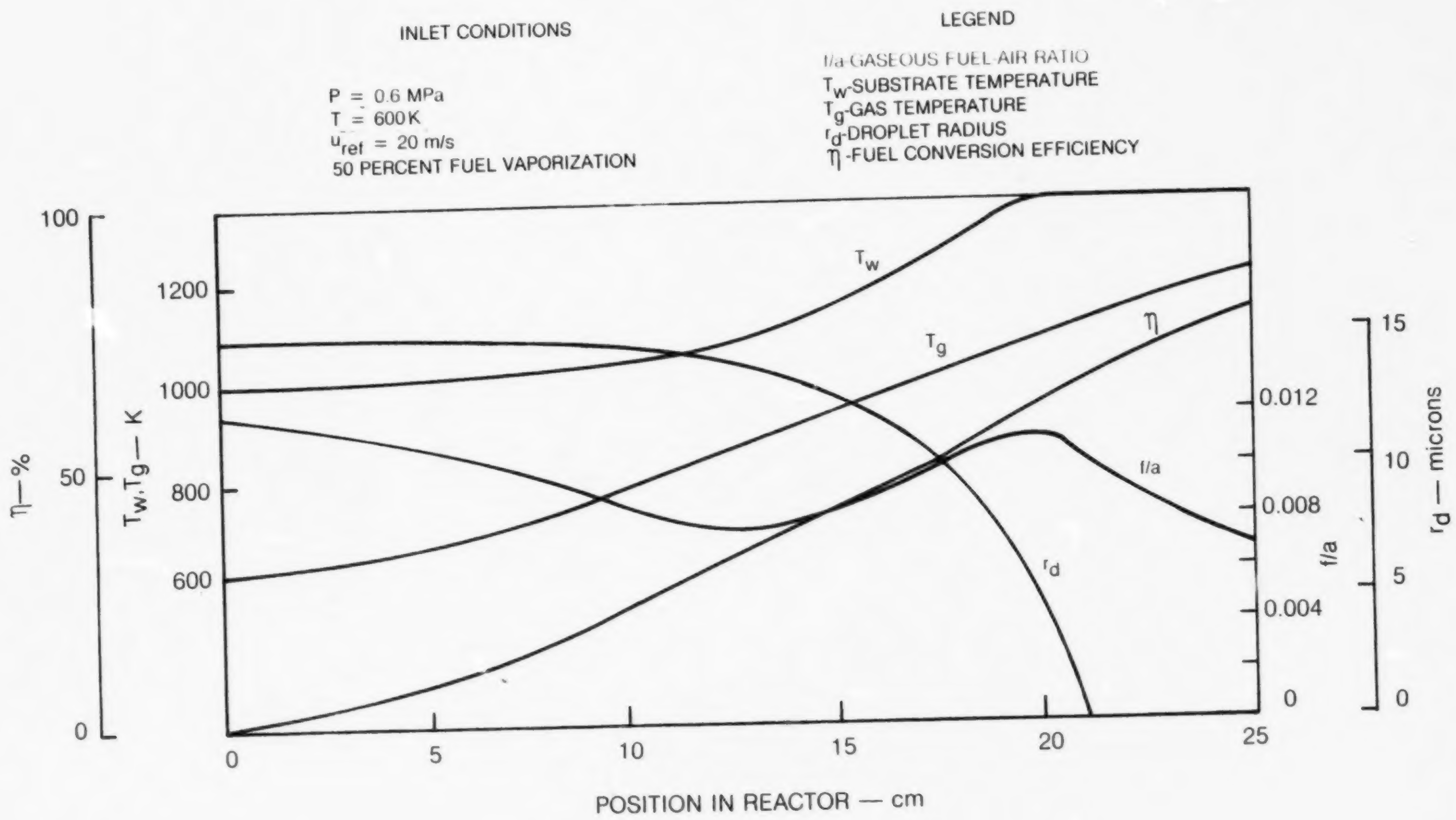

Figure 4 Fuel Vaporization and Consumption in Catalytic Reactor

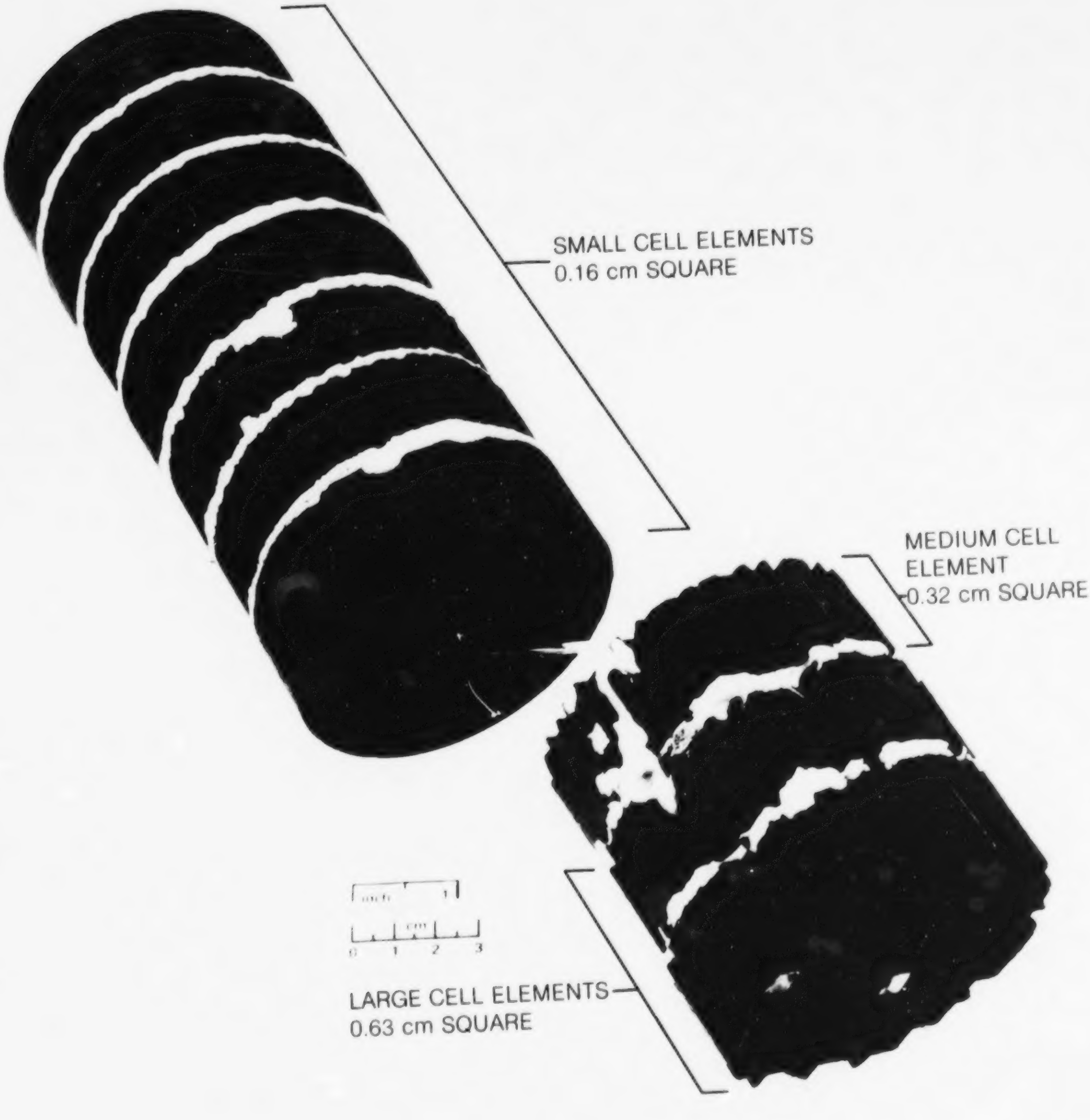
SMALL CELL ELEMENTS
0.16 cm SQUARE
MEDIUM CELL
ELEMENT
0.32 cm SQUARE
inch
1
cm
0
1
2
3
LARGE CELL ELEMENTS
0.63 cm SQUARE

Figure 5 Graded Cell Catalytic Reactor

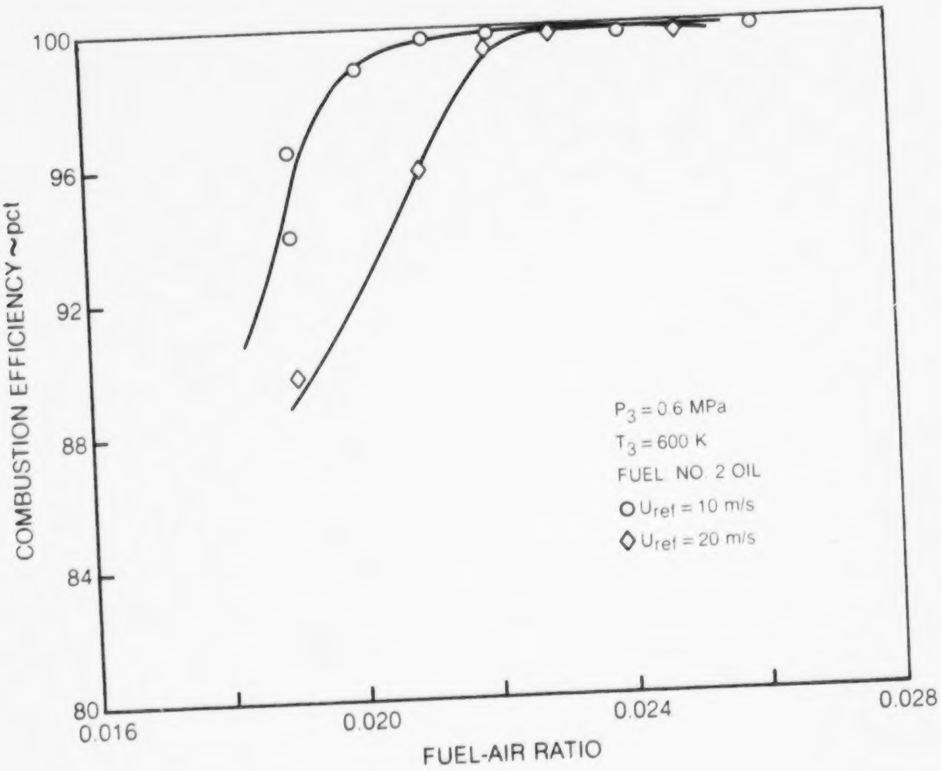

Figure 6 Reactor Performance With No. 2 Oil — Dependence on Reference Velocity

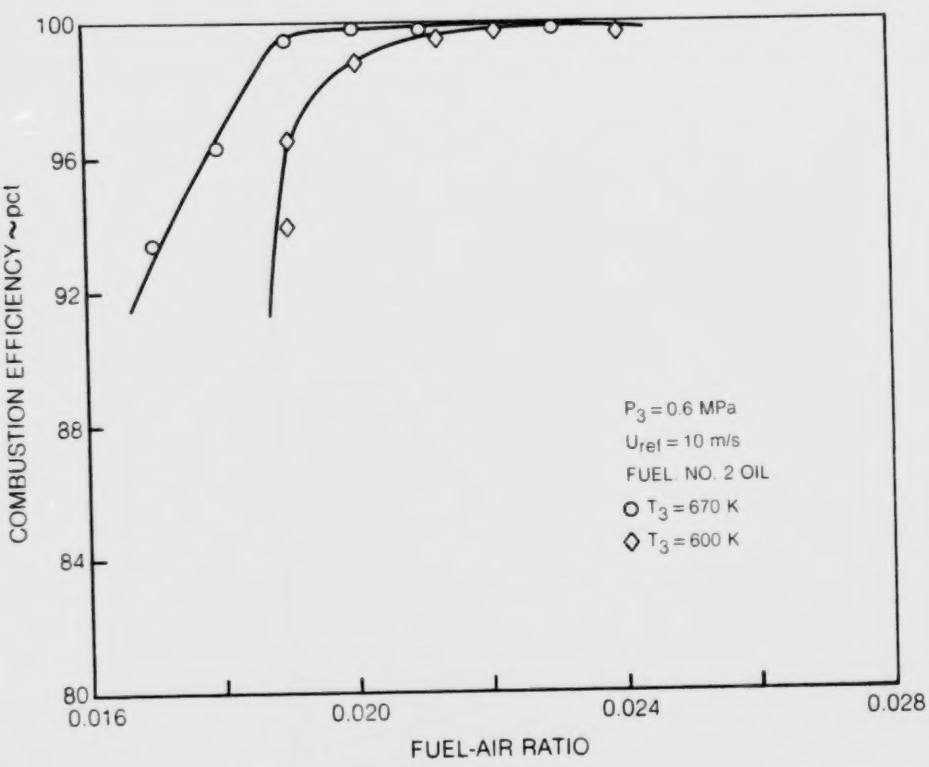

Figure 7 Reactor Performance With No. 2 Oil — Dependence on Air Preheat

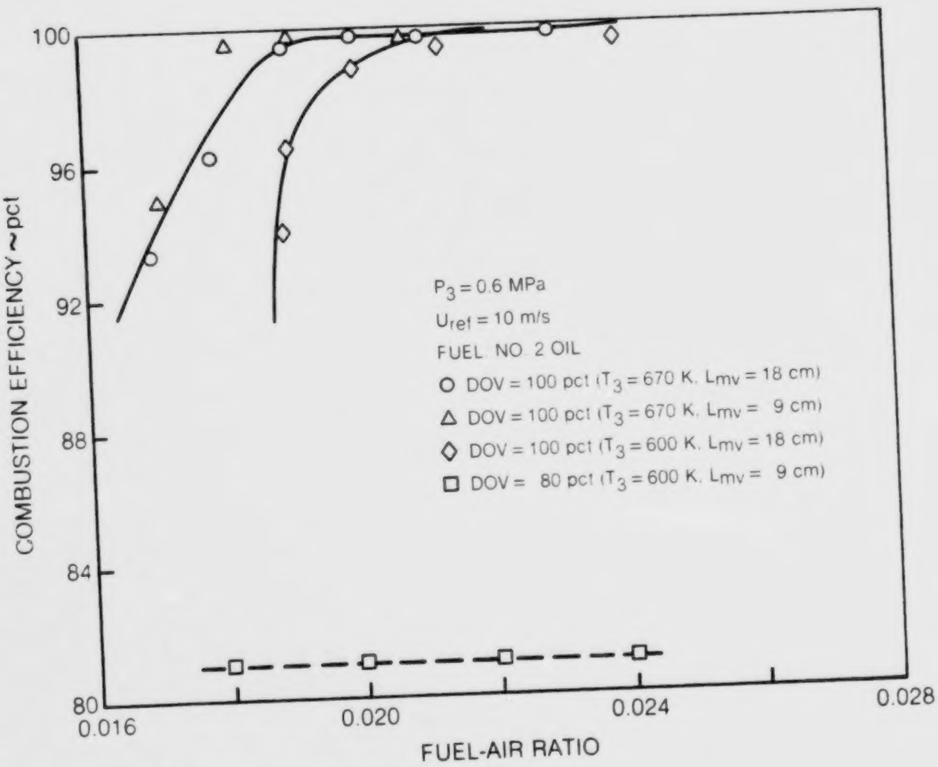

Figure 8 Influence of Degree of Vaporization on Reactor Performance Using No. 2 Oil

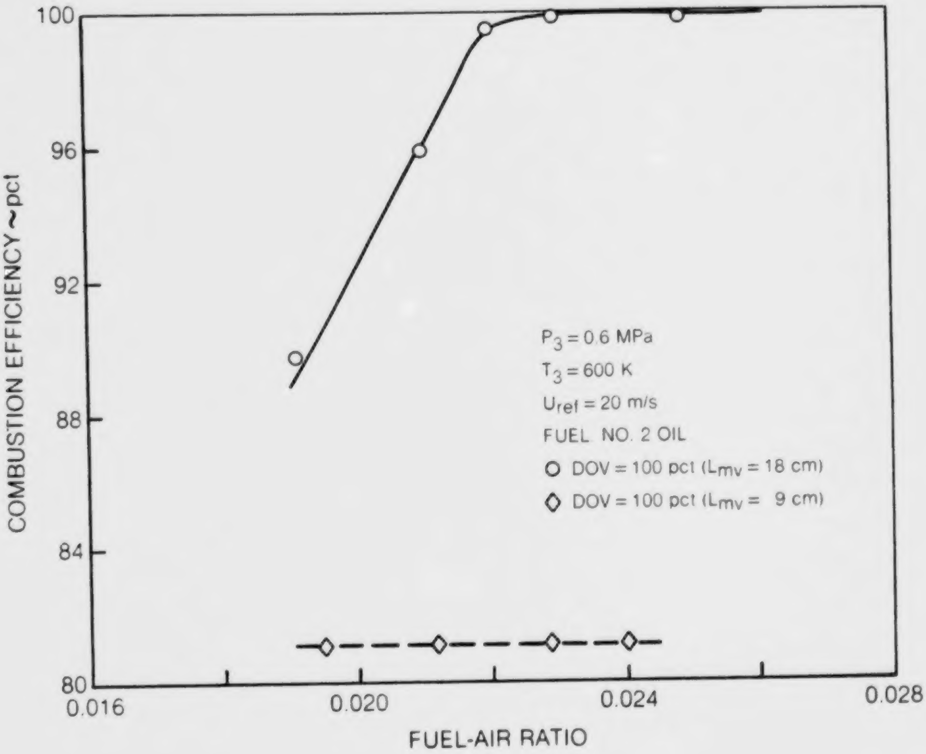

Figure 9 Inconsistent Reactor Performance Dependence on Degree of Vaporization

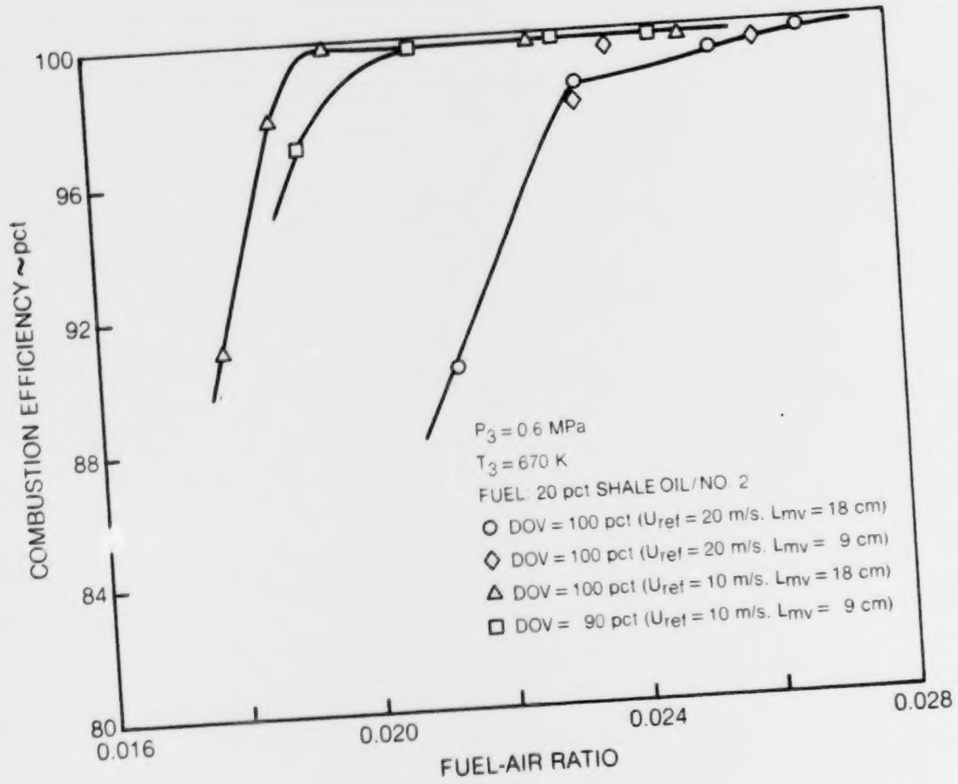

Figure 10 **Influence of Degree of Vaporization on Reactor Performance Using Shale Oil Blend**

TABLE 1

Fuel Properties

		No. 6	No. 2	Shale Oil
H content (wt. pct.)		11.0	12.95	12.69
N content (wt. pct.)		0.15		0.46
Heat of combustion (j/g)		42550	42570	42410
Aromatic content (vol. pct.)		62.4	34.5	
Density (g/cc)	289K		0.853	
	311K	0.933		0.863
	339K	0.899		
	367K	0.871		
Surface tension (dyne/cm)	311K	29.9		
	339K	27.2		
	367K	25.9		
Viscosity (cs)	311K	632	2.79	12.8
	339K	101.6		
	372K	25.5		3.77
Distillation (K)	IBP		455	5.22
	5	528		
	10	562	491	598
	20	658	503	618
	30	714	515	637
	40	758	527	655
	50	772	539	670
	60	797	549	683
	70		560	698
	80		573	714
	90		591	726
	EP		622	730
Residue (pct.)		40	1.5	6.0

TABLE 2

Test Parameter Ranges

Parameter	Original	Expanded
Reactor inlet pressure	0.6-0.9 MPa	0.3-0.6 MPa
Reactor inlet temperature	500-600K	600-900K
Reference velocity	10-30 m/s	13-40 m/s
Fuel-air ratio	0.016-0.026	0.016-0.028
Fuel	No. 6	No. 6, No. 2, Blends

TABLE 3

Conditions for No. 6 Oil Tests

	P_3 MPa	T_3 K	U_{ref} m/s	T_{fuel} K	SMD microns	Deg. of Vap. pct
1.	0.3	780	40	370	20	90
2.		840	20	405	20	100
3.		840	25	416	17	100
4.		895	38	405	13	100
5.	0.45	600	13	356	50	25
6.		700	14	353	55	35
7.		700	14	381	30	60
8.	0.6	600	22	378	23	35
9.		600	29	389	16	40
10.		670	20	369	28	55
11.		670	20	389	21	65
12.		670	31	400	14	50
13.		755	20	394	21	95
14.		755	30	367	25	75
15.		783	20	372	27	90

DEMONSTRATION OF
CATALYTIC COMBUSTION WITH RESIDUAL FUEL

By:

Willard J. Dodds
General Electric
Aircraft Engine Group
Evendale, Ohio 45215

ABSTRACT

An experimental program was conducted to demonstrate catalytic combustion of a residual fuel oil. Three catalytic reactors, including a baseline configuration and two backup configurations based on baseline test results, were operated on No. 6 fuel oil. All reactors were multi-element configurations consisting of ceramic honeycomb catalyzed with palladium on stabilized alumina. Stable operation on residual oil was demonstrated with the baseline configuration at a reactor inlet temperature of about 825 K (1025 °F). At lower inlet temperatures, operation was prevented by apparent plugging of the catalytic reactor with residual oil. Reduced plugging tendency was demonstrated in the backup reactors by increasing the size of the catalyst channels at the reactor inlet, but plugging still occurred at inlet temperatures below 725K (845 °F). Operation at the original design inlet temperature of 589K (600 °F) could not be demonstrated. Combustion efficiency above 99.5 percent was obtained with less than 5 percent reactor pressure drop. Thermally formed NO_x levels were very low (less than 0.5 g NO_2/kg fuel), but nearly 100 percent conversion of fuel-bound nitrogen to NO_x was observed.

SYMBOLS

Symbol	Reference	Units
$P_{1.9}$	Catalytic Reactor Inlet Pressure	MPa
SMD	Sauter Mean Diameter	μm
$T_{1.5}$	Catalytic Reactor Inlet Temperature	K
V_r	Catalytic Reactor Reference (Approach) Velocity	m/s
W_c	Catalytic Reactor Airflow	kg/s

ACKNOWLEDGMENTS

The work described herein was conducted by the General Electric Aircraft Engine Group under Contract DEN3-155. The work was sponsored by the U.S. Department of Energy and was performed under the direction of the NASA Lewis Research Center Project Manager, Dr. David N. Anderson.

Catalytic Reactors were designed and fabricated by Engelhard Industries under the direction of K. R. Burns, Venture Manager, and Drs. I.T. Osgerby and H. C. Lee.

A complete final report on this effort will be available as DOE/NASA/0155-1 (NASA CR-165369).

INTRODUCTION

This paper describes the results of an experimental program to demonstrate catalytic combustion of No. 6 residual oil. The use of catalytically supported combustion has been shown to be a promising means for reducing emissions of oxides of nitrogen (NO_x) from stationary gas turbine engines. By extending the lean stability limit, combustion catalysts allow operation at combustion temperatures below 1800 K, thereby reducing the amount of thermally-formed NO_x. The ability of catalytic reactors to operate under steady-state conditions simulating those encountered in industrial gas turbine engines has been well documented. However, a majority of data obtained to date describes catalyst operation with nearly homogeneous fuel-air mixtures containing gaseous or completely vaporized distillate fuel. In order to serve as a practical means for combustion in stationary gas turbine engines, the catalytic reactor should be able to utilize a wide range of fuels, including heavy residual oils.

The experimental program involved evaluation of three different catalytic reactors with No. 6 residual fuel oil. The three reactors consisted of one baseline reactor designed for operation at inlet conditions typical of those obtained in a large industrial gas turbine combustor, and two backup designs based on test results obtained with the baseline reactor. A fuel injection system designed to provide less than 50 percent fuel vaporization was used with each of the reactors. The use of an air assist nozzle in this injection system enabled the average droplet size to be varied from less than 30 μm to more than 100 μm at the design operating conditions.

Catalytic reactors for this program were noble metal on ceramic honeycomb substrate. Engelhard Industries Division of Engelhard Minerals and Chemicals Corporation designed and fabricated all of the catalytic reactors.

EXPERIMENTAL APPARATUS

The test rig assembly used in this experimental study is shown schematically in Figure 1. This rig was designed to accommodate a catalytic reactor having a nominal diameter of 11.4 cm (4.5 inches) at pressures up to 2.1 MPa (300 psia) with an inlet temperature of 811K (1000 °F). Specific design guidelines for the various test rig components are presented in Table I.

FUEL-AIR MIXTURE PREPARATION

The fuel-air mixture preparation system consisted of an air-assisted simplex fuel nozzle mounted at the throat of a converging/diverging premixing duct. The air assisted simplex injector design shown in Figure 2 was selected because of its proven ability to inject residual oil and the further ability to easily control drop size by varying the atomizing airflow rate. This injector is a variation of the design used in the Low NO_x Heavy Fuel Combustor Concept Program conducted for NASA by General Electric (Reference 1). The central core of this injector is essentially a simplex nozzle consisting of a fuel swirler, spin chamber, and orifice. When no atomizing air is supplied, this injector functions exactly as a simplex pressure atomizing nozzle. Improved atomization is obtained by using high velocity atomizing air. This air is ducted through an annular passage in the injector body to the air swirler.

Atomization with this air-assisted simplex injector design was predicted using a correlation reported in Reference 2. The predicted initial drop size as a function of fuel flow at two selected air velocities is shown in Figure 3. As indicated in this figure, over the planned range of fuel flows, drop sizes in the lower size range (less than 30 μm) are obtained with the atomizing air velocity set at 140 m/s, which corresponds to an atomizing air pressure ratio of 1.12 at the design conditions. When the nozzle is operated in the pressure atomizing mode (with no atomizing airflow), initial drop sizes are very close to the middle of the 70 to 150 μm range at the design point and are in this size range over most of the design fuel flow range.

Fuel vaporization for No. 6 oil was estimated using a computerized mathematical model based on work reported in Reference 3. This model consists of equations for heat transfer, mass transfer and drop velocity, which are solved using a triple iteration technique. Droplet radius, temperature, percent vaporization, distance from injection point, velocity and elapsed time are calculated at incremental drop temperatures until the droplet heatup period is complete (wet bulb temperature is reached), at which point a new time increment is used.

Droplet vaporization was calculated at the design point temperature and pressure for several different values of airstream velocity. Results of these calculations, shown in Figure 4, indicate that at the design inlet temperature and pressure, and over the range of airstream velocities considered, fuel vaporization is a function of residence time and drop size. For the diverging duct used in these tests, the design point residence time is about 25 ms, which corresponds to approximately 37 percent vaporization with 30 μm drops, and only about 5 percent vaporization with 100 μm drops.

CATALYTIC REACTOR

The catalytic reactor configurations for these tests were specified and supplied by Engelhard Industries Division of the Engelhard Minerals and Chemicals Corporation (Reference 4). A total of three different reactor configurations were built and tested. All of the reactors consisted of noble metal catalyst on ceramic honeycomb substrates.

The three reactor designs included a baseline and two backup configurations. The baseline and first backup configurations were specified prior to the start of testing. The second backup was specified after test results with the first two configurations had been reviewed. The three designs are described in Table II.

The baseline catalytic reactor was a three-element design, in which the first and second elements were sized to provide mass transfer area as required to meet the design combustion efficiency goal. The third element was sized primarily to provide adequate residence time for catalytically supported thermal reactions. Pressure drop was predicted using an empirical friction factor correlation. All of the elements were catalyzed with a proprietary (Engelhard) preparation of Palladium on stabilized alumina.

The first backup reactor configuration used an increased cell size in the first element, while the second and third elements were identical to those used in the baseline reactor. The objective of this configuration was to reduce the probability of reactor plugging due to the impingement of residual fuel droplets. The length of the first element was increased relative to the baseline design in order to provide approximately the same mass transfer conversion and pressure drop.

The second backup reactor configuration had larger cells than either the baseline or first backup reactors. Again, this increase in cell size of the inlet elements was to prevent reactor plugging. The cell size of the exit element was reduced, and overall length was increased, to provide the mass transfer surface area required to obtain the desired combustion efficiency.

All of the reactors were contained in thick wall spool pieces as shown in Figure 5. Each element was wrapped with an insulating compliant layer of ceramic fiber material and was constrained axially by stainless steel rings. These rings provided an open-face diameter of 11.4 cm (4.5 inches). Design point reactor heat loss with this housing was calculated to be less than one percent of the reaction heat release.

The catalytic reactors were mounted on an insulated exit instrumentation section which consists of a 50 cm (20 inch) length of stainless steel pipe having an inner diameter of 15.4 cm (6.1 inches), and a concentrically mounted 41 cm (16 inch) long replaceable metallic liner having an inner diameter of 11.4 cm (4.5 inches). The annular space between the casing and liner was packed with ceramic fiber insulation blanket to provide nearly adiabatic flow.

Bosses were provided for a water quench bar, as well as the sampling rake, thermocouple probes and pressure taps. The downstream end of this exit section was attached to the facility exit ducting, which contains a backpressure valve and filter/separator system.

INSTRUMENTATION

The test section was instrumented to measure temperatures and static pressures at the section inlet, in the premixing duct, and at three different axial stations downstream of the catalytic reactor. Temperatures at three axial locations and three radial locations within the reactor were measured with sheathed thermocouples embedded within the reactor channels.

Gas samples were withdrawn through a single point, water cooled probe mounted on the duct centerline, 15.2 cm (6 inches) downstream of the catalytic reactor exit. Samples were analyzed for CO, CO_2, Unburned Hydrocarbons (HC), and NO_x, using standard methods per SAE ARP 1256.

COMBUSTOR TEST FACILITY

All catalytic reactor testing in this program was conducted in the Advanced Combustion Laboratory located at Evendale, Ohio. This laboratory is designed and equipped to accommodate a variety of experimental investigations of moderately sized combustion systems. The laboratory is supplied with all services needed for combustion testing. Air at pressures up to 2.1 MPa (300 psia) is piped from a central air supply system at flow rates up to 4.5 kg/s (10 lb/s). Jet A and JP4 fuels are supplied by pipeline from large storage tanks located elsewhere in the plant.

A heated fuel system was used for the residual oil tests. With this system, the residual oil was maintained at about 350K (170°F) in a steam heated 25 m^3 (2000 gal) storage trailer. This trailer incorporates an air driven boost pump and an internal bypass line to continuously circulate the fuel. Either heated residual oil or distillate (Jet A) from the facility tanks, or a combination of the two can be supplied to the inlet of the main steam/fuel heat exchanger. Saturated steam to this heat exchanger was supplied at 1.2 MPa (175 psia), providing a maximum fuel preheat capability up to about 450K (350°F). Fuel leaving the heat exchanger was filtered, then input to the high pressure pump, which can provide fuel pressures up to 10.3 MPa (1500 psia). Total fuel flow was metered with a turbine flowmeter. When a mixture of residual and distillate fuel was used, the distillate flow was measured with a second turbine flowmeter.

An analysis of the No. 6 oil used in this program is presented in Table III. This table also shows a typical range of properties for No. 6 oil, as well as typical properties of the distillate fuel (Jet A), which was used for lightoff. As indicated in this table, the test fuel was quite thick, falling in the upper range of both viscosity and pour point. However, levels of sulfur and metals were relatively low.

RESULTS AND DISCUSSION

BASELINE CATALYTIC REACTOR TESTS

Initial checkout tests of the baseline catalytic reactor were conducted at an inlet temperature of 755 K (900 °F) and a pressure of 0.414 MPa (60 psia). The test plan called for ignition on Jet A, and subsequent transitions to mixtures containing 25, 50, 75, and 100% residual oil. A catalytic reactor inlet temperature well above the 589 K (600 °F) design point was selected for the initial tests to increase fuel vaporization and improve the chances of successful operation on residual oil.

Steady state operation was established at the above conditions, but, when transition to 50% residual fuel was attempted, the catalytic reactor pressure drop began to rise very rapidly before the transition could be completed, apparently due to plugging of the catalyst channels with a coating of the residual fuel.

When this increase in pressure drop occurred, fuel flow to the reactor was immediately terminated. It was found that the normal reactor pressure drop could be reestablished by purging the catalytic reactor with air at about 983K (950 °F) for 10 to 15 minutes.

After unsuccessful attempts to transition over a range of fuel-air ratios, rig inlet temperature was increased to 811K (1000°F). At this condition, steady state operation on fuel mixtures containing first 25%, then 50% residual oil was established. Transition to 75% residual oil was attempted but could not be completed due to reactor plugging.

Operation on 100% No. 6 oil was finally accomplished by increasing the rig inlet temperature to 867K (1100°F), while maintaining catalytic reactor inlet pressure at 0.414 MPa (60 psia) and reference velocity at 19.8 m/s (65 ft/s). Performance and emission data were then recorded over a range of fuel-air ratios at these inlet conditions.

Attempts to vary initial drop size above about 15 μm at the above conditions were unsuccessful because of burning upstream of the catalytic reactor. Upstream burning was indicated by two thermocouples mounted in the mixing duct a short distance downstream of the fuel injector. An automatic shutoff was used to terminate fuel flow when the thermocouple reading exceeded the rig inlet temperature by more than 140K (250°F).

Attempts to operate at a higher reference velocity were also unsuccessful due to catalytic reactor plugging. Operation at higher temperature, higher pressure and lower reference velocity were not attempted due to expected auto-ignition.

Based on the results of the baseline tests, the supplementary test point schedule shown in Table IV was defined for subsequent backup reactor tests. With this revised schedule, operation was initiated at the conditions demonstrated with the baseline reactor. Operation at successively higher reference velocities and lower inlet temperature was then attempted until steady state operation could no longer be obtained (either due to upstream burning or poor performance).

BACKUP CATALYTIC REACTOR TESTS

As discussed above, the first and second backup catalytic reactors had successively larger cells in the inlet catalyst element in order to reduce the probability of plugging with the residual oil.

The operating ranges of each of the backup catalytic reactors were significantly wider than that of the baseline reactor, as shown in Figure 6. The first backup reactor, with increased cell size in the inlet element, could be operated at reference velocities up to about 30 m/s (100 ft/s) at a reactor inlet temperature of 825 K (1025°F), or down to a 775 K (935°F) inlet temperature at the design point reference velocity. However, plugging still occurred when reference velocity was increased and inlet temperature was simultaneously reduced. The second backup reactor, which had increased cell size in both the inlet and center element, never actually plugged to the point where fuel flow had to be terminated. However, at inlet temperatures below about 750 K (890°F) with a nominal pressure of 0.414 MPa (60 psia), operation was unsteady. At these conditions, both catalytic reactor pressure drop and reactor substrate temperature cycled at about 10 to 15 second intervals. Pressure drop varied by about 50% of the nominal value, and the peak substrate temperature fluctuated by as much as ± 80 K (144°F).

The unsteady operation of the second backup catalytic reactor at the lower reactor temperature appeared to be due to coating and partial plugging of the catalyst channel with residual oil, followed by ignition and burning of the coating. This process was evidenced by a gradual increase in reactor pressure drop, accompanied by decreasing reactor substrate temperatures, followed by a more rapid reduction in pressure drop with increased substrate temperatures.

The upstream burning which had prevented dropsize variation in the baseline tests was studied further in tests of the backup catalytic reactors. Based on post-baseline test inspections, it was concluded that the automatic autoignition shutoff setting (140 K (250°F) above rig inlet temperature) was conservative. Therefore, during the first backup tests, the shutoff setting was increased to 278 K (500°F) above rig inlet temperature. With this setting, it was possible to operate over a wider range of drop sizes and inlet temperatures. Increased temperature was indicated occasionally on the two thermocouple probes located in the premixing section (Station 1.5), but this temperature rise appeared to be a very local phenomenon. Although the two premixing section thermocouple probes were only about 5 cm apart, an increase in temperature was often indicated on one thermocouple probe, while output from the other remained constant. It appeared either that small flames may have been stabilizing in the wake of the thermocouples, or that fuel droplets were impinging on these probes, then igniting and burning. For tests of the second backup reactor, the thermocouple probes were removed, and mixing section temperature was monitored using surface mounted thermocouples. With these surface mounted thermocouples, the indicated mixing section temperature was stable.

REACTOR EMISSIONS AND PERFORMANCE

Combustion Efficiency

Fuel-air ratio was varied at each set of inlet conditions to assess the effects of adiabatic flame temperature. Measured combustion efficiency for each of the three catalytic reactors operating on residual oil is shown as a function of calculated adiabatic flame temperature (based on inlet temperature and gas sample fuel-air ratio) in Figure 7. Combustion efficiency above 99.5% was obtained with all of the reactors at flame temperatures above about 1420 K (2100°F). At constant flame temperature, combustion efficiency was slightly improved with the first backup reactor, and significantly improved with the second. Efficiencies measured in limited tests with Jet A fuel were also very close to those obtained with the residual oil.

The effects of variation in catalytic reactor inlet temperature on combustion efficiencies measured with the second backup reactor are shown in Figure 8. The effect of inlet temperature was more pronounced at low adiabatic flame temperature, than at high flame temperature as would be anticipated.

Reference velocity had a strong effect on combustion efficiency, as shown in Figure 9 . At an adiabatic flame temperature of 1350 K, combustion efficiency was reduced from about 99.6% to about 97% when reference velocity was increased from 20 to 30 m/s.

NO_x Emissions

NO_x emissions were found to be almost entirely due to fuel bound nitrogen (FBN), with virtually 100% FBN conversion. This effect is shown in Figure 10, where NO_x levels are shown as a function of concentration of residual oil in the fuel mixture. The calculated NO_x emission index is shown for 100% conversion of the FBN in the residual fuel. The very low thermal NO_x production is indicated by the low NO_x emissions (< 0.5 g/kg) obtained during operation on Jet A, which has very little FBN.

The relationship between FBN conversion and combustion efficiency is shown in Figure 11. Between 80 and 100% combustion efficiency, FBN conversion increases linearly from about 55% to 100%.

Pressure Drop

Catalytic reactor pressure drop, corrected to the design point inlet conditions, is shown as a function of fuel/air ratio in Figure 12. The reactor pressure drop data are well ordered, and pressure drop increased approximately linearly when fuel/air ratio (and temperature rise) was increased. Pressure drop levels were generally less than four percent for both of the backup reactors. Baseline reactor pressure drop levels were higher and less consistent because of blockage due to internal damage incurred during the combustion tests.

Initial Drop Size Effects

The effect of initial drop size was studied during tests of the first backup reactor, where droplet SMD was varied from 12.8 to 72.5 μm. Combustion efficiency and CO emission index, corrected to the design point velocity and flame temperature, and measured NO_x emission index are shown as a function of drop size in Figure 13. Over the range of variation, drop size had very little effect on catalytic reactor emissions and performance. Combustion efficiency and CO levels were quite close to levels predicted for drop sizes less than 10 μm and showed no clear-cut trend with increasing drop size. NO_x levels appeared to increase very slightly as drop size was increased, but this effect was very weak.

The small magnitude of the initial drop size effect is not surprising if it is recalled that the fuel-air preparation system was designed to provide less than 50 percent evaporation at 589 K (600°F) and 0.621 MPa (90 psia), while the actual testing was conducted at 853K (1075°F) and 0.420 MPa (61 psia). Evaporation increases very rapidly as pressure is reduced and inlet temperature is increased, and at the actual high temperature, reduced pressure test conditions, virtually complete evaporation is predicted over the range of drop sizes tested.

Temperature Profiles

Measured temperature profiles with a 50 percent mixture of No. 6 oil and Jet A are shown in Figure 14. These profiles are typical of those obtained with all fuel mixtures. These profiles reflect the drop in temperature between the rig inlet (Station 1.0) and the mixing duct (Station 1.5) due to fuel vaporization and the addition of cold atomizing air. The rapid increase in temperature at the catalytic reactor inlet indicates good ignition capability, while the center peaked fuel distribution is evident from the higher temperatures on the reactor centerline. In the exit section, temperatures on the centerline and along the wall decrease gradually downstream of the reactor, probably due to heat losses to the sampling probe and the exit section wall, respectively. Midway between the centerline and wall (r = 2.5 cm), the measured temperature continues to increase downstream of the reactor, possibly due to continued reaction downstream of the reactor. Measured reactor exit temperatures on the duct centerline were generally within about 25 K (45°F) of the predicted flame temperature based on gas sample analysis.

Normalized catalytic reactor axial temperature profiles for high efficiency operation over a range of reactor inlet temperature and reference velocity are shown in Figure 15. The shape of these profiles was virtually unchanged by variation in these inlet conditions.

Catalytic Reactor Durability

Some degree of damage was apparent in post run inspection of all three of the catalytic reactors. For example, the second backup reactor, shown in Figure 16, had erosion damage on the inlet face of the first and second catalyst elements, and some melting in the second element. In several cases, the Torvex substrate material delaminated during disassembly, but, in all cases, the elements appeared to be intact before being removed from the catalyst holder.

It is thought that a majority of the damage to the reactor occurred during periods when partial or complete plugging occurred, probably when the coating of residual fuel was burned off.

CONCLUSIONS

The following conclusions have been drawn from the results of this program:

1. Residual oil can be successfully burned in a catalytic reactor with very high combustion efficiency and acceptable pressure drop.

2. The catalytic reactor operating range on residual oil is limited to inlet temperatures higher than those available in typical non-regenerative industrial gas turbines. At lower temperatures, operation is prevented by reactor plugging with the residual fuel.

3. The catalytic reactor operating range can be extended to slightly lower temperatures by increasing catalyst channel diameters, while also increasing reactor length to maintain performance.

4. The catalytic reactor operating range can be further extended by burning residual/distillate fuel blends.

5. Very high conversion of fuel bound nitrogen to NO_x is obtained in lean catalytic combustion of residual fuels.

6. Additional proof of long term catalytic reactor durability, resistance to erosion, and resistance to fuel poisoning would be required before catalytic combustion of residual fuel could be applied to a practical gas turbine system.

7. The single point, air assisted simplex injector fuel-air mixture preparation system provided good reliability and adequate mixture uniformity with virtually no system development. Additional development would be required to meet the mixture uniformity design guidelines.

REFERENCES

1. Cutrone, M.B., Hilt, M.B., Goyal, A., Ekstedt, E.E., and Notardonato, J., "Evaluation of Advanced Combustors for Dry NO_x Suppression with Nitrogen Bearing Fuels in Utility and Industrial Gas Turbine Engines", ASME Paper 81-GT-125, March 1981.

2. Simmons, H.C., "The Prediction of Sauter Mean Diameter for Gas Turbine Fuel Nozzles of Different Types", ASME Paper 79-WA/GT-51, December 1979.

3. El Wakil, M.M., Uyehara, D.A., and Myers, P.S., "A Theoretical Investigation of the Heating-Up Period of Injected Fuel Droplets Vaporizing in Air", Tech. Note 23179, NACA 1954.

4. Lee, H.C., "Technical Report on Catalytic Combustion of Incompletely Vaporized Fuels", Final Report prepared by Engelhard Industries under G.E. Subcontract P.O. 200-4-14R26753, June 1981.

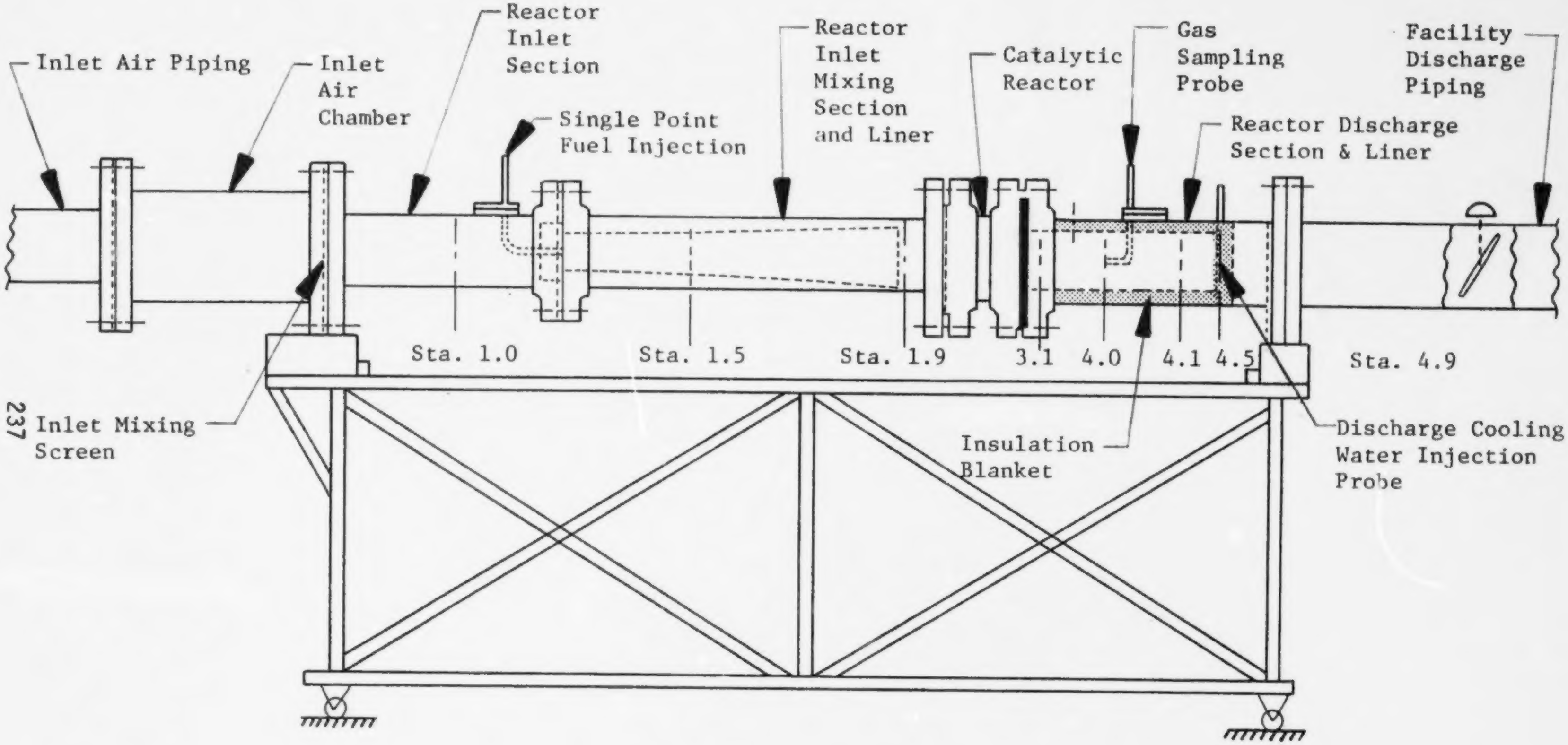
Inlet Air Piping
Inlet Air Chamber
Reactor Inlet Section
Single Point Fuel Injection
Reactor Inlet Mixing Section and Liner
Catalytic Reactor
Gas Sampling Probe
Reactor Discharge Section & Liner
Facility Discharge Piping
Sta. 1.0
Sta. 1.5
Sta. 1.9
3.1
4.0
4.1
4.5
Sta. 4.9
Inlet Mixing Screen
Insulation Blanket
Discharge Cooling Water Injection Probe

Figure 1. Catalytic Reactor Test Rig Assembly.

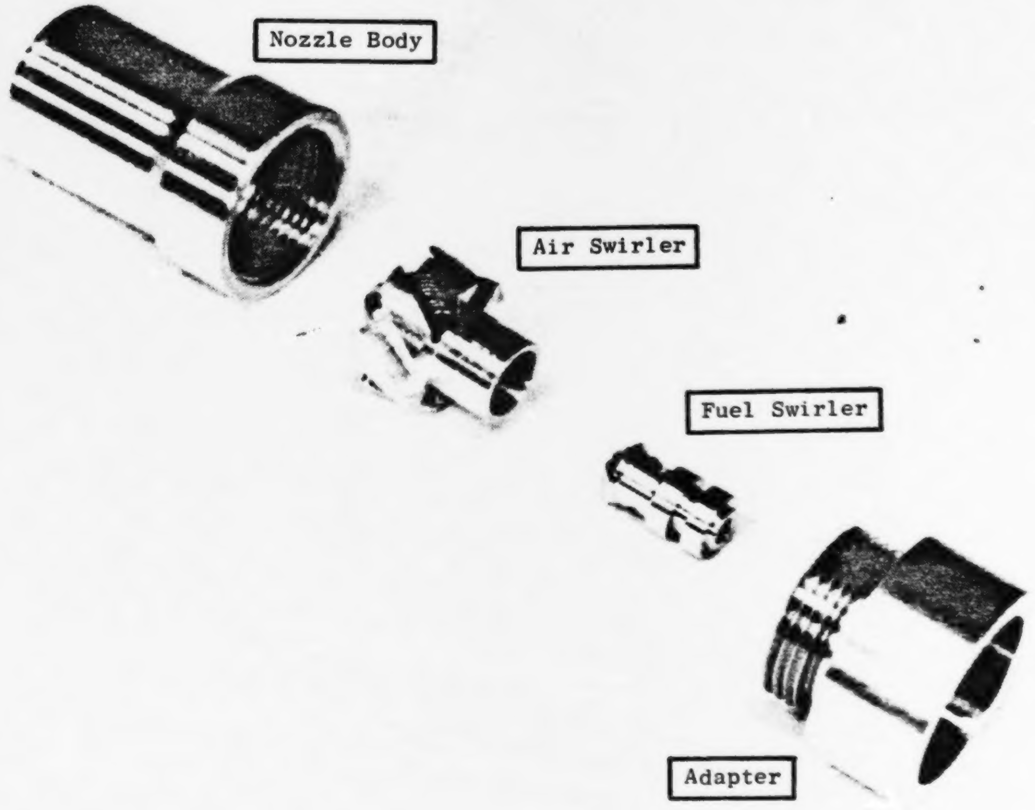
Nozzle Body
Air Swirler
Fuel Swirler
Adapter

Figure 2. Exploded View of Fuel Nozzle.

- Catalytic Reactor Inlet Pressure = 0.62 MPa (90 psia)
- Test Rig Inlet Temperature = 589 K (600° F)
- No. 6 Oil (Fuel) Temperature = 400 K (260° F)
- Atomizing-Air Temperature = 300 K (80° F)

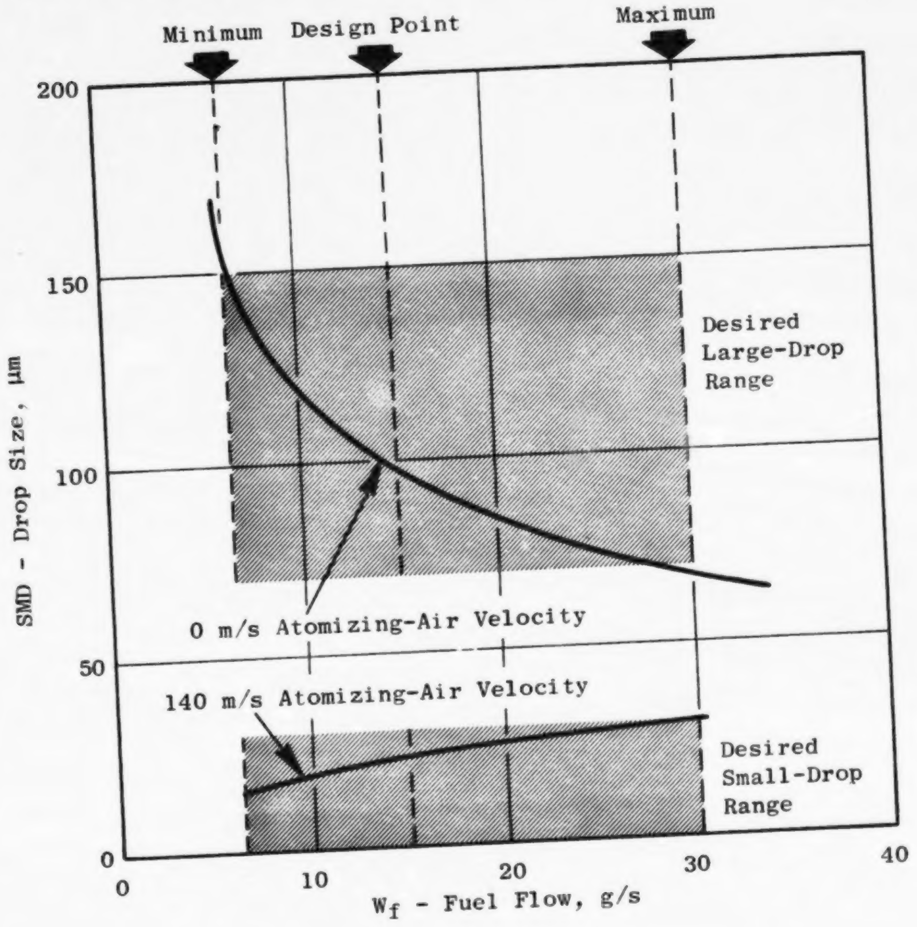

Figure 3. Predicted Design-Point Drop Size with No. 6 Oil.

- Air Temperature = 589 K (600° F)
- Pressure = 0.62 MPa (90 psia)
- No. 6 Oil (Fuel) Temperature = 394 K (250° F)

Airstream Velocity

○ 19.8 m/s (65 ft/s)
△ 30.5 m/s (100 ft/s)
□ 45.7 m/s (150 ft/s)

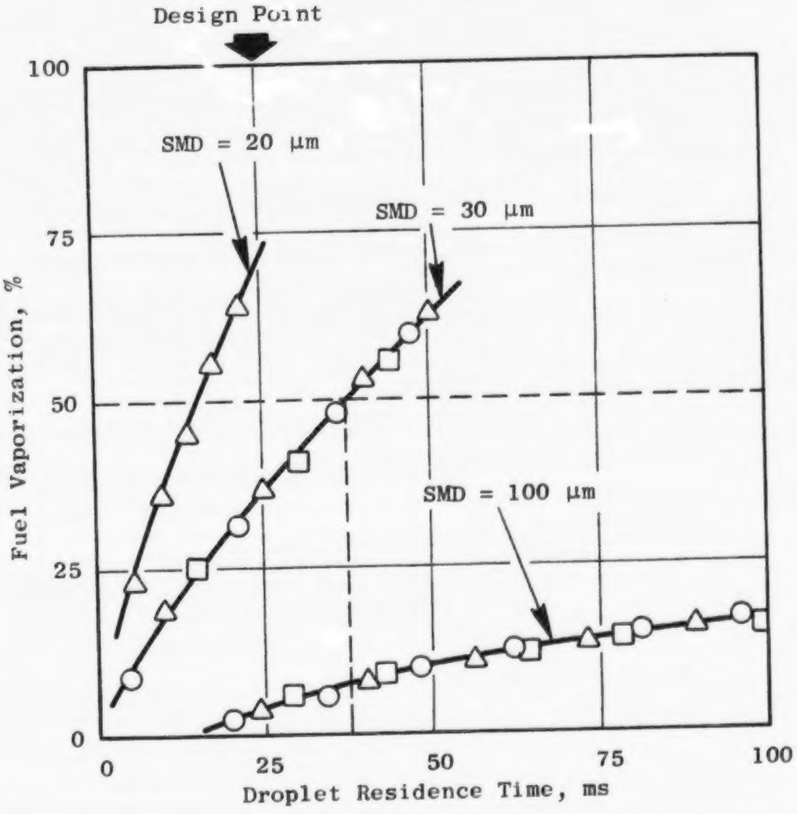

Figure 4. Effect of Drop Size on Predicted Fuel Vaporization (Design Point).

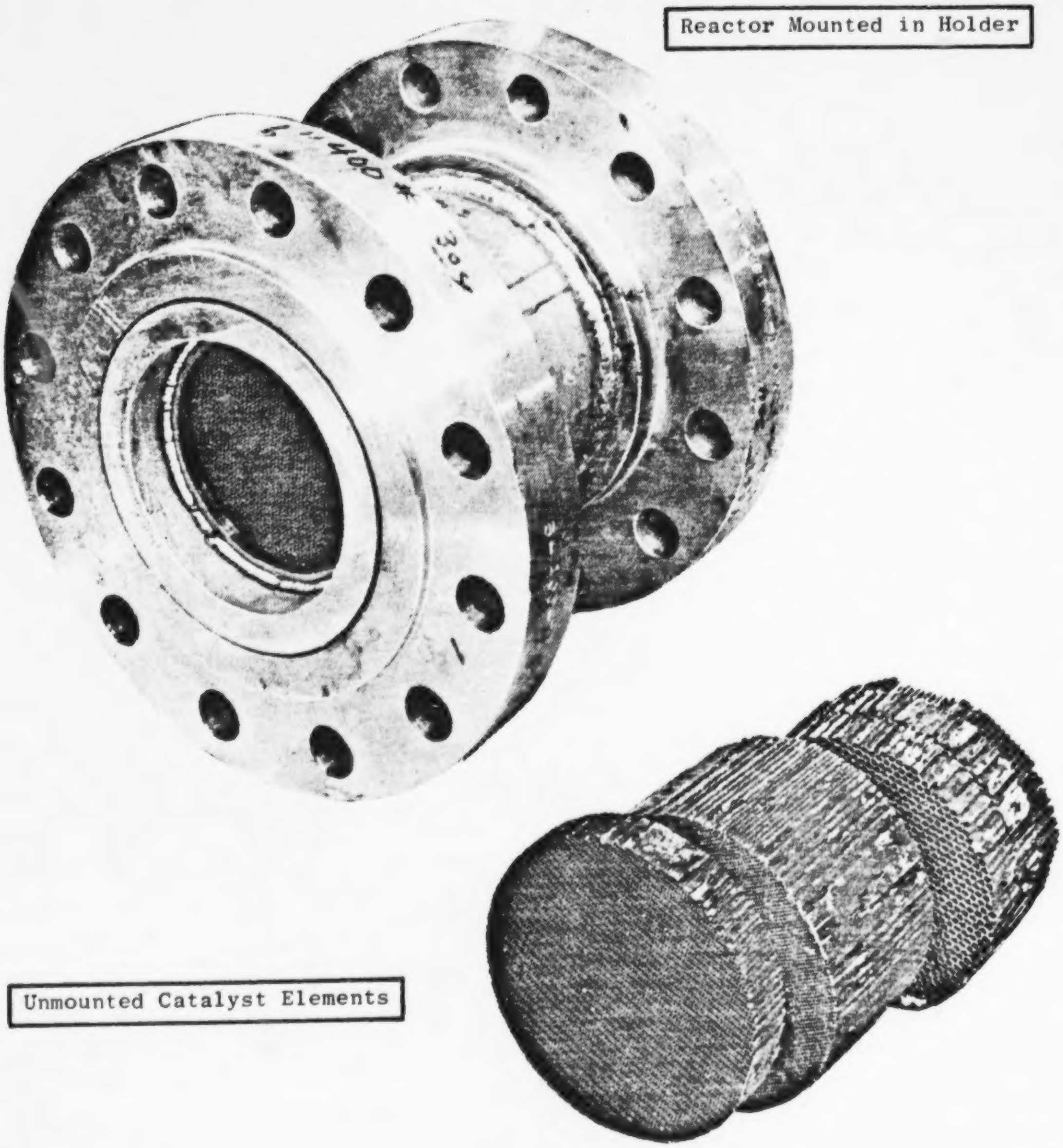
Reactor Mounted in Holder
Unmounted Catalyst Elements

Figure 5. Baseline Catalytic Reactor.

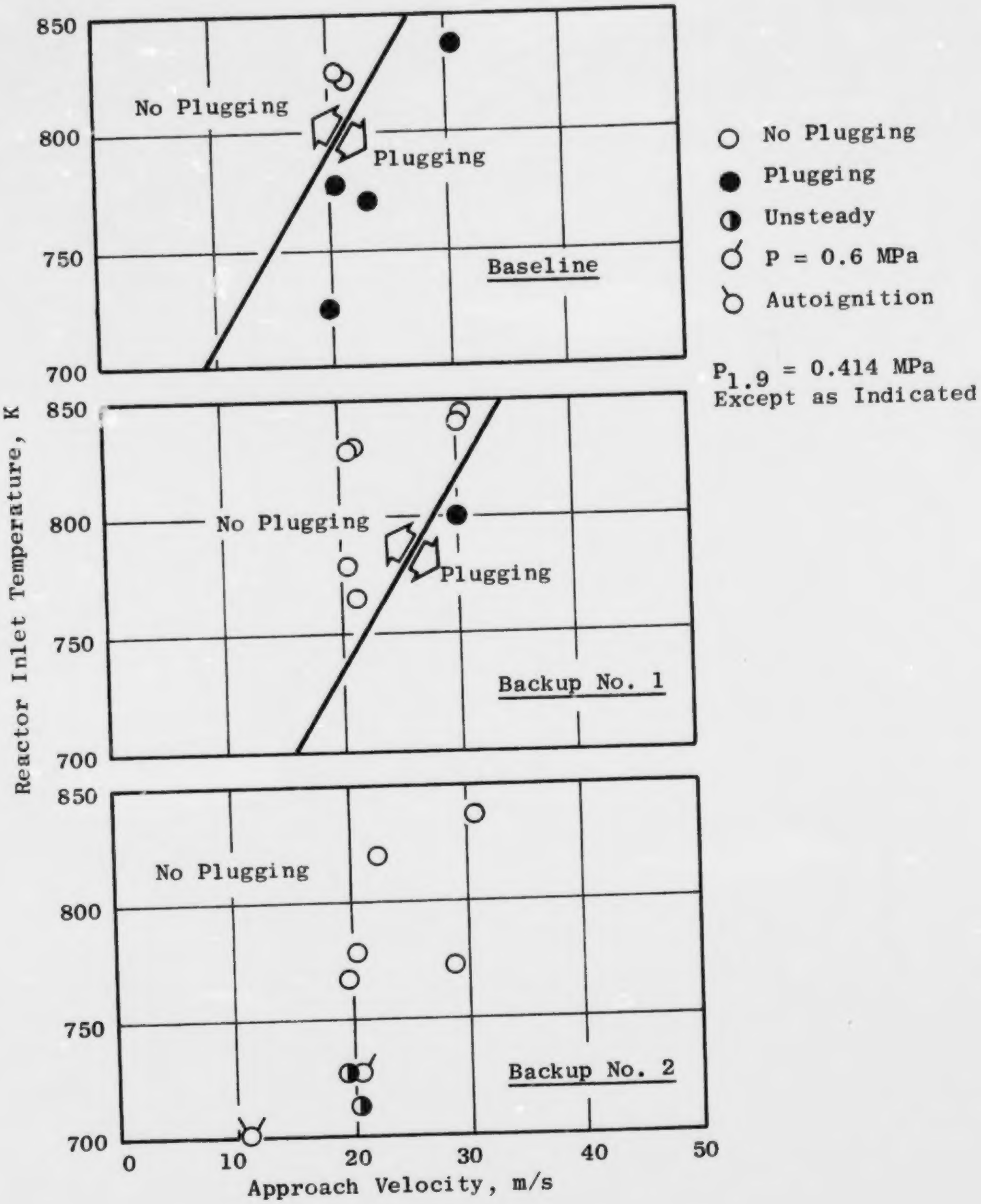

Figure 6. Catalytic Reactor Operating Range.

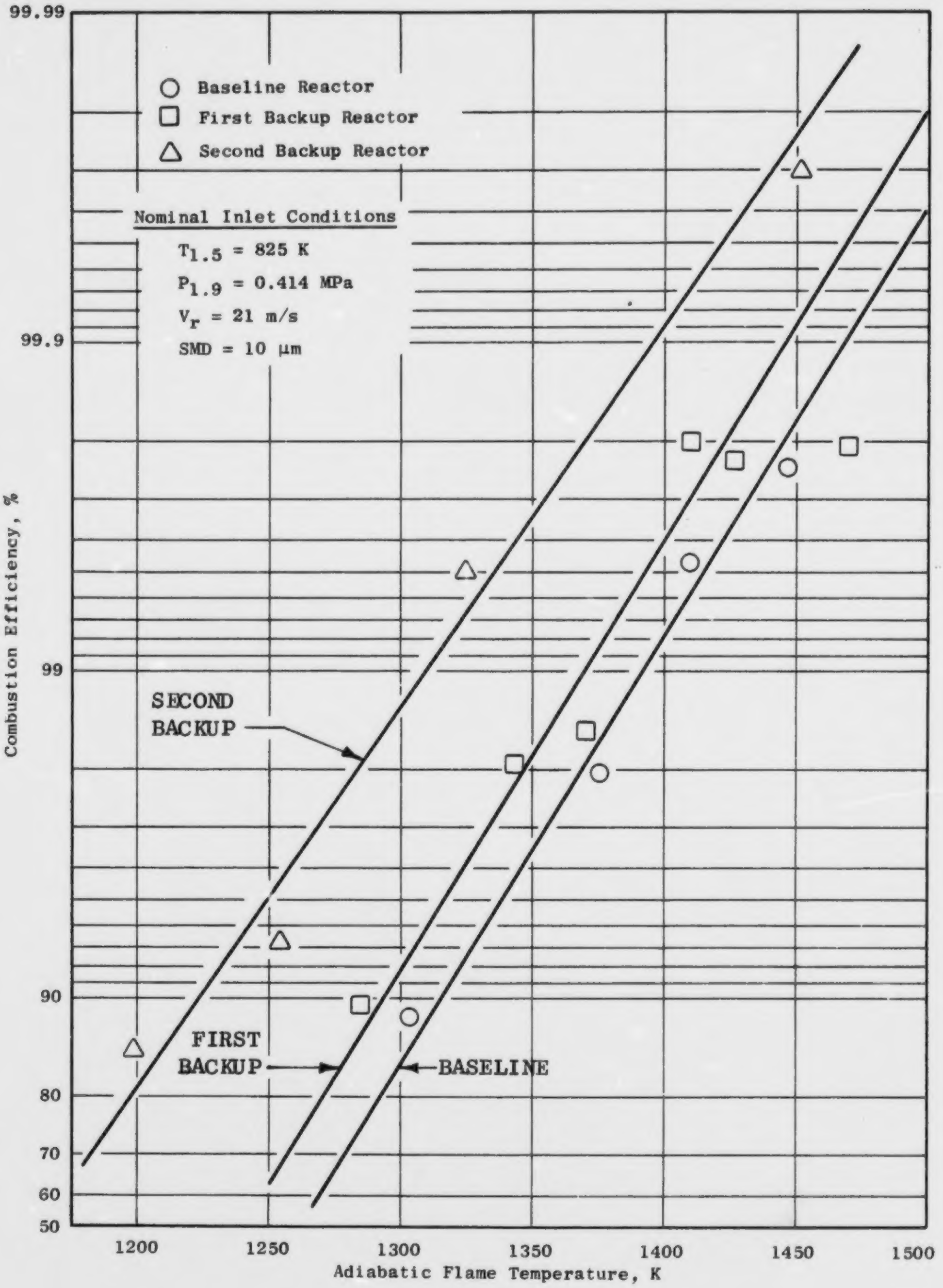

Figure 7 . No. 6 Oil Combustion Efficiency Comparison.

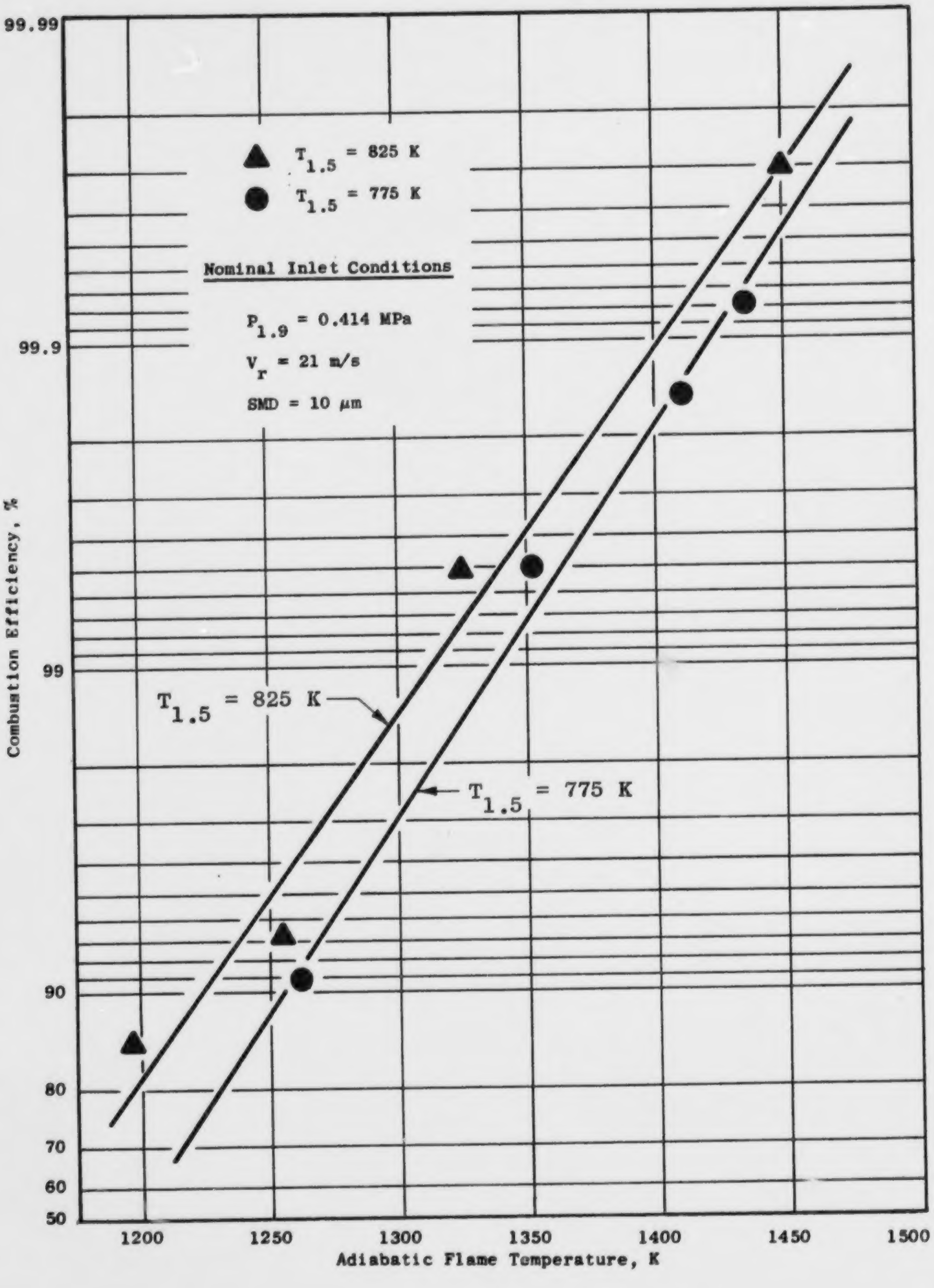

Figure 8. Effect of Reactor Inlet Temperature on Combustion Efficiency - Second Backup Reactor.

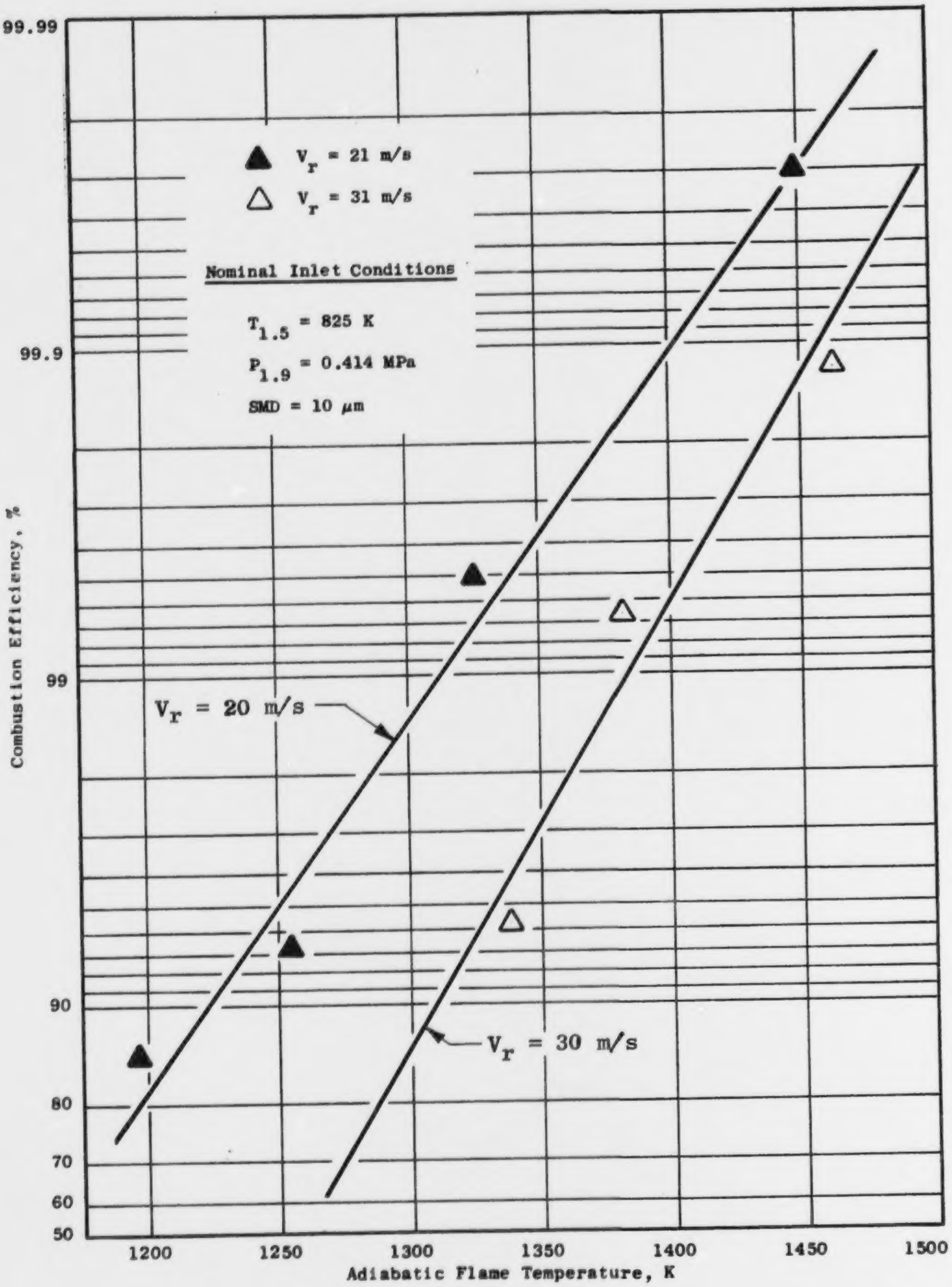

Figure 9. Effect of Reference Velocity on Combustion Efficiency - Second Backup Reactor

- Catalyst Inlet Temperature = 767 - 840 K (920 - 1050° F)
- Pressure = 0.41 MPa (60 psia)
- Fuel/Air Ratio = 10 - 15 g/kg
- Approach Velocity = 20 - 22 m/s (65 - 72 ft/s)

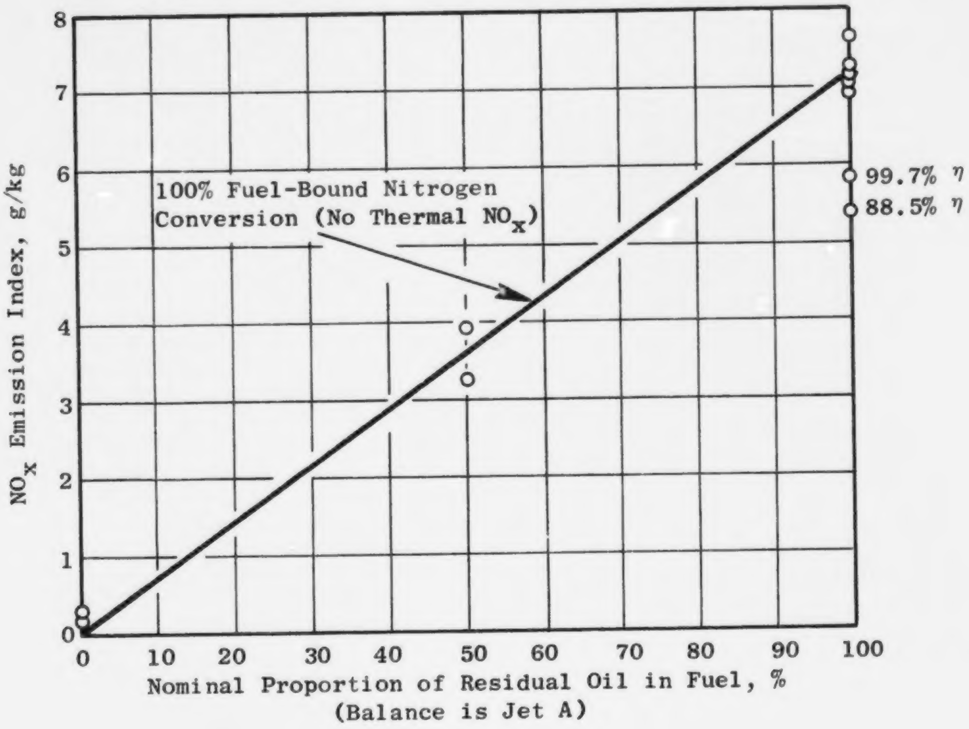

Figure 10. Fuel-Bound Nitrogen Conversion.

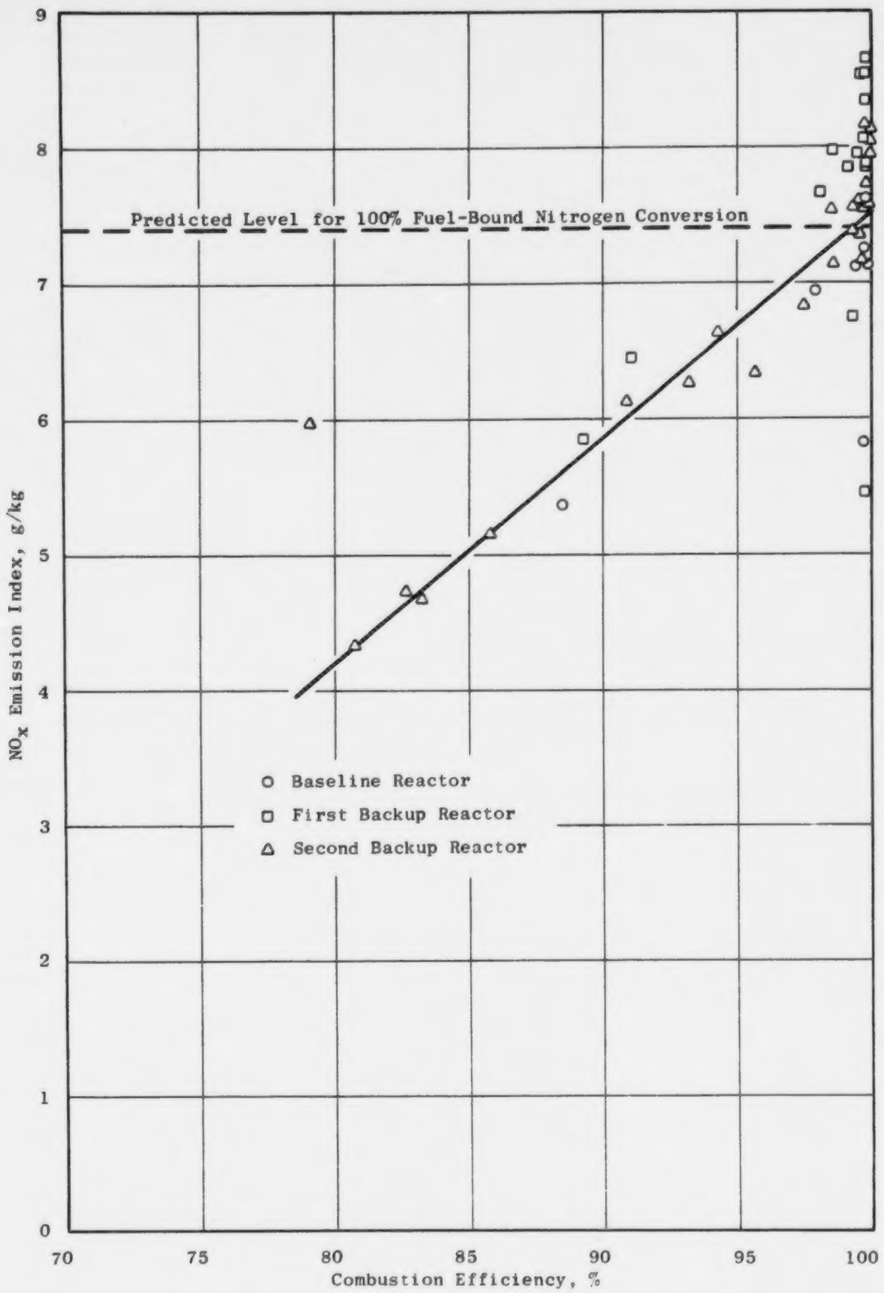

Figure 11. Relationship Between Combustion Efficiency and NO_x Emissions (No. 6 Oil).

$$\left|\Delta P/P\right|_{Corrected} = \left|\Delta P/P\right|_{Test} \left|W_c^2 T_{1.5}/P_{1.9}^2\right|_{Design} \left|W_c^2 T_{1.5}/P_{1.9}^2\right|_{Test}$$

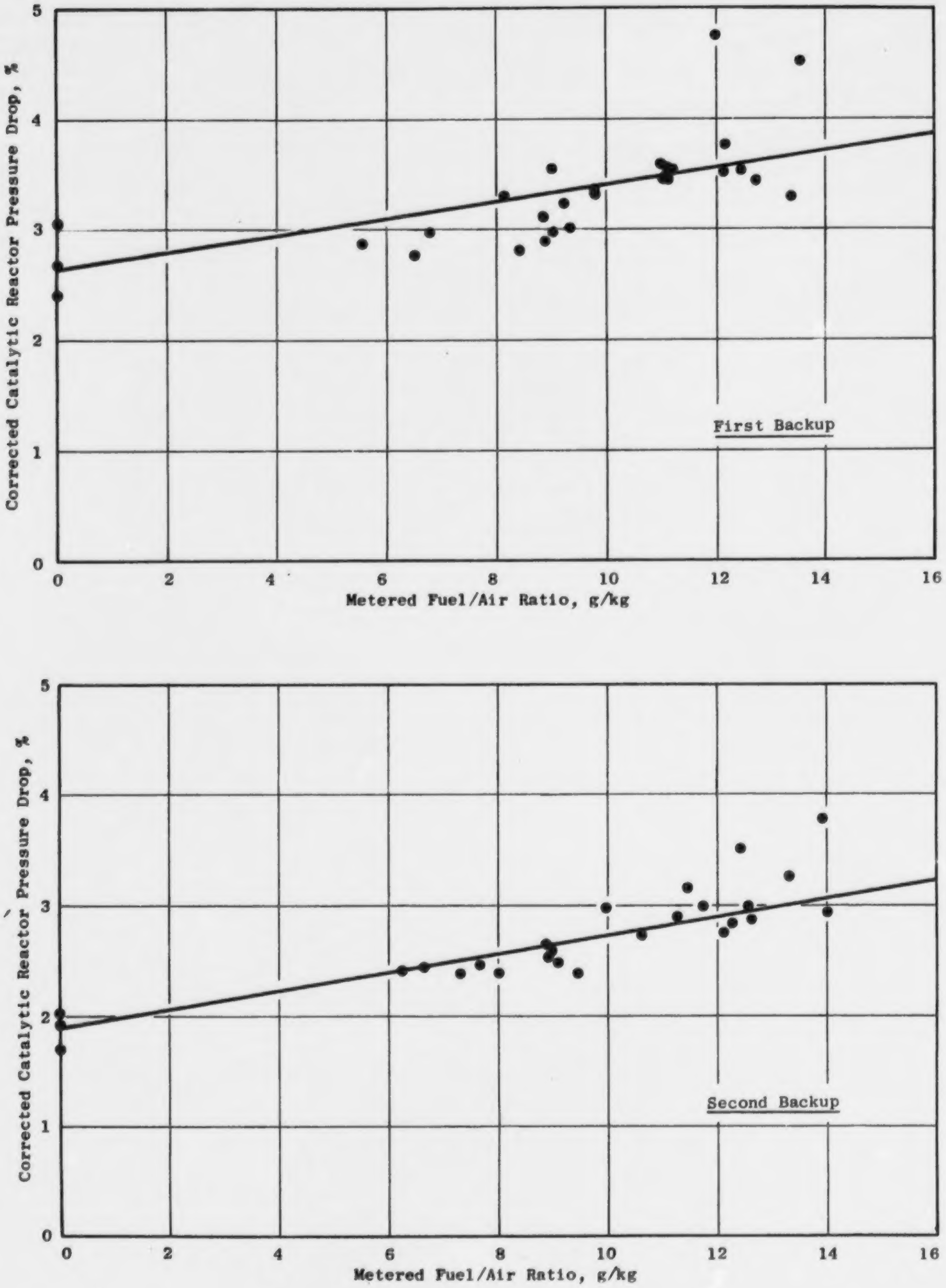

Figure 12. Backup Reactor Pressure Drop

Nominal Operating Conditions

Reactor Inlet Temperature = 853 K (1075° F)

Pressure = 0.420 MPa

Reference Velocity = 30.4 m/s (100 ft/s)

Fuel: No. 6 Residual Oil

Note: EICO and Combustion Efficiency are Corrected to Design-Point Velocity and Flame Temperature.

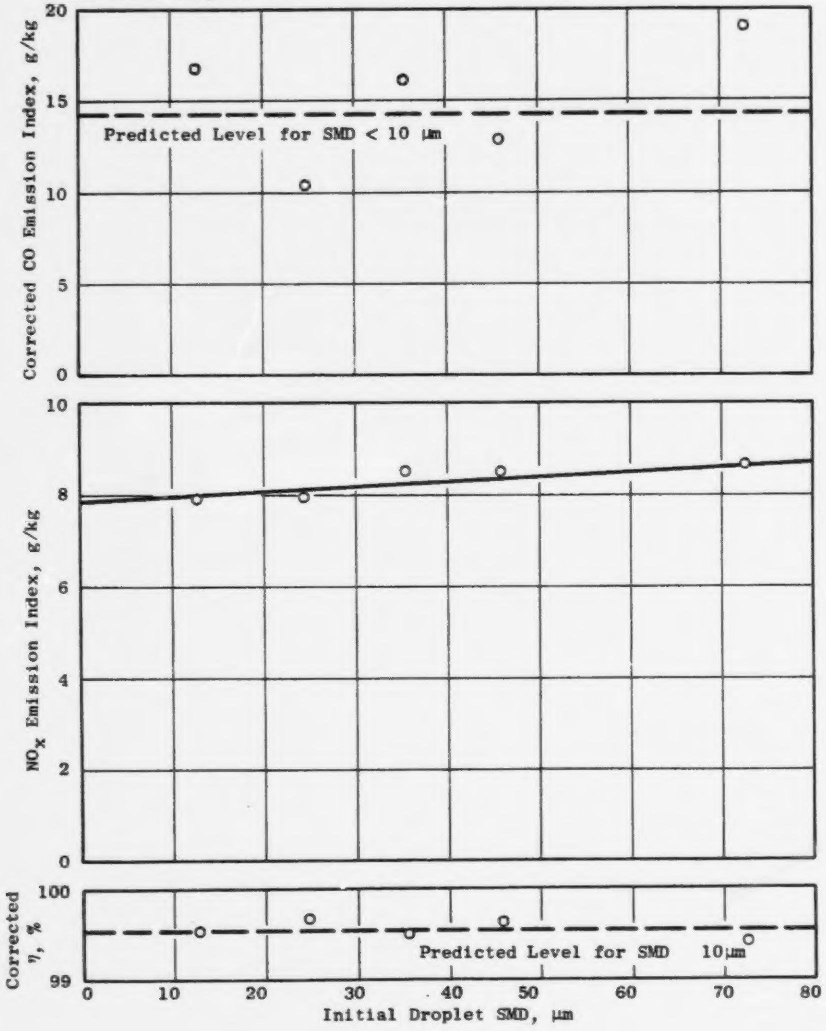

Figure 13. Effect of Initial Drop Size on First Backup Reactor Emissions and Performance

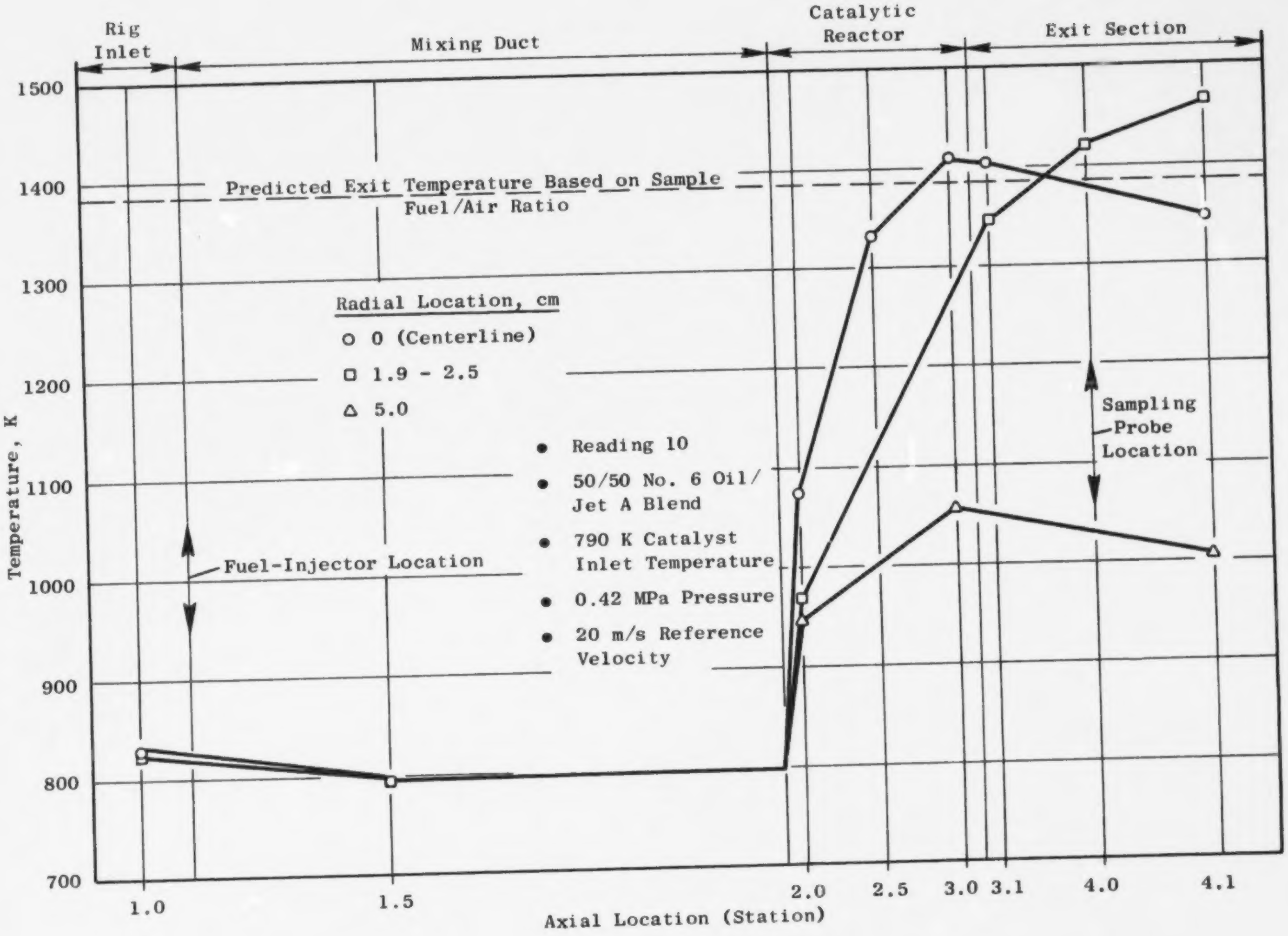

Figure 14. Typical Test Rig Temperature Profiles - Baseline Reactor.

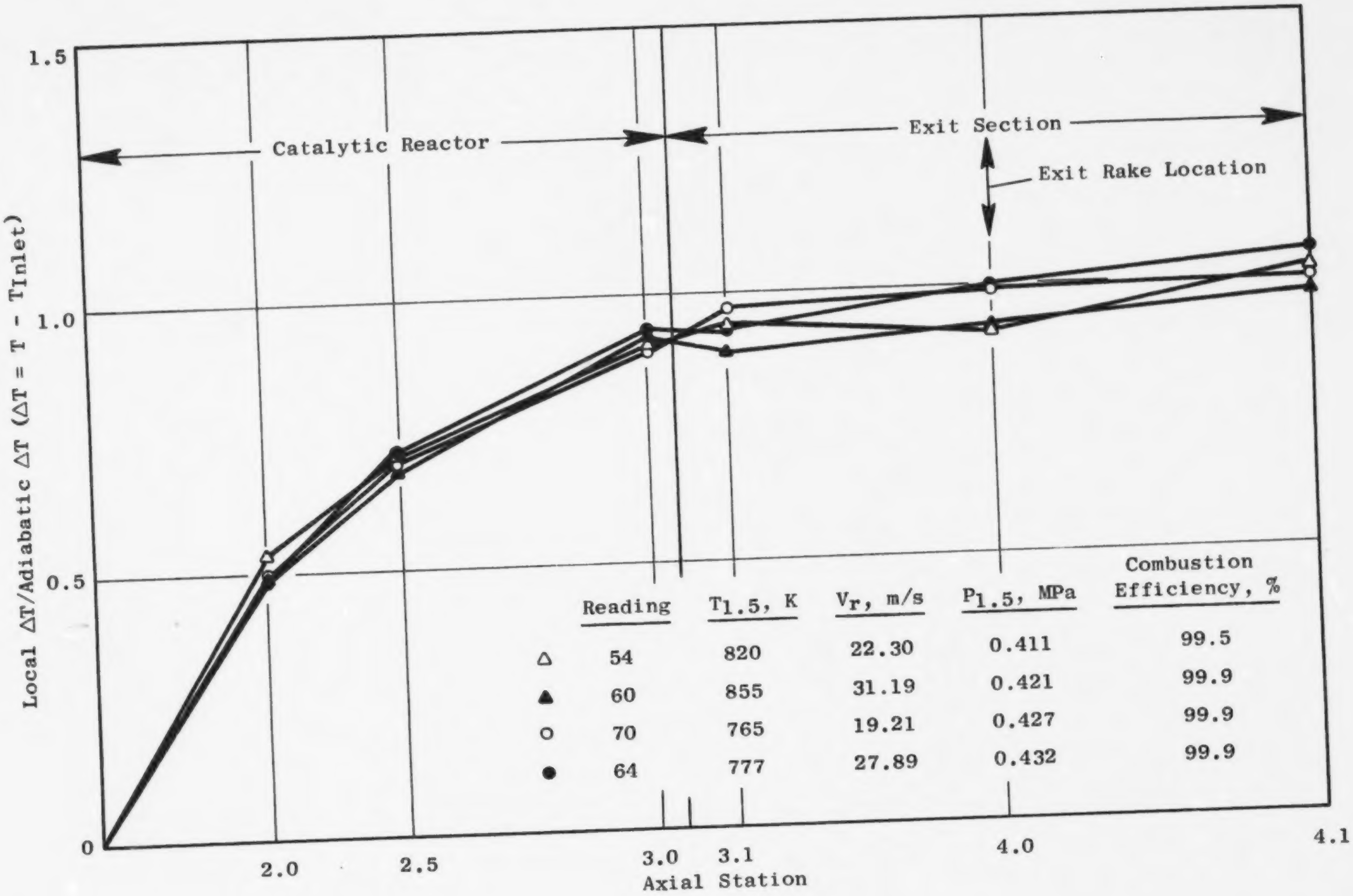

	Reading	$T_{1.5}$, K	V_r, m/s	$P_{1.5}$, MPa	Combustion Efficiency, %
△	54	820	22.30	0.411	99.5
▲	60	855	31.19	0.421	99.9
○	70	765	19.21	0.427	99.9
●	64	777	27.89	0.432	99.9

Figure 15. Second Backup Catalytic Reactor Axial Temperature Profiles.

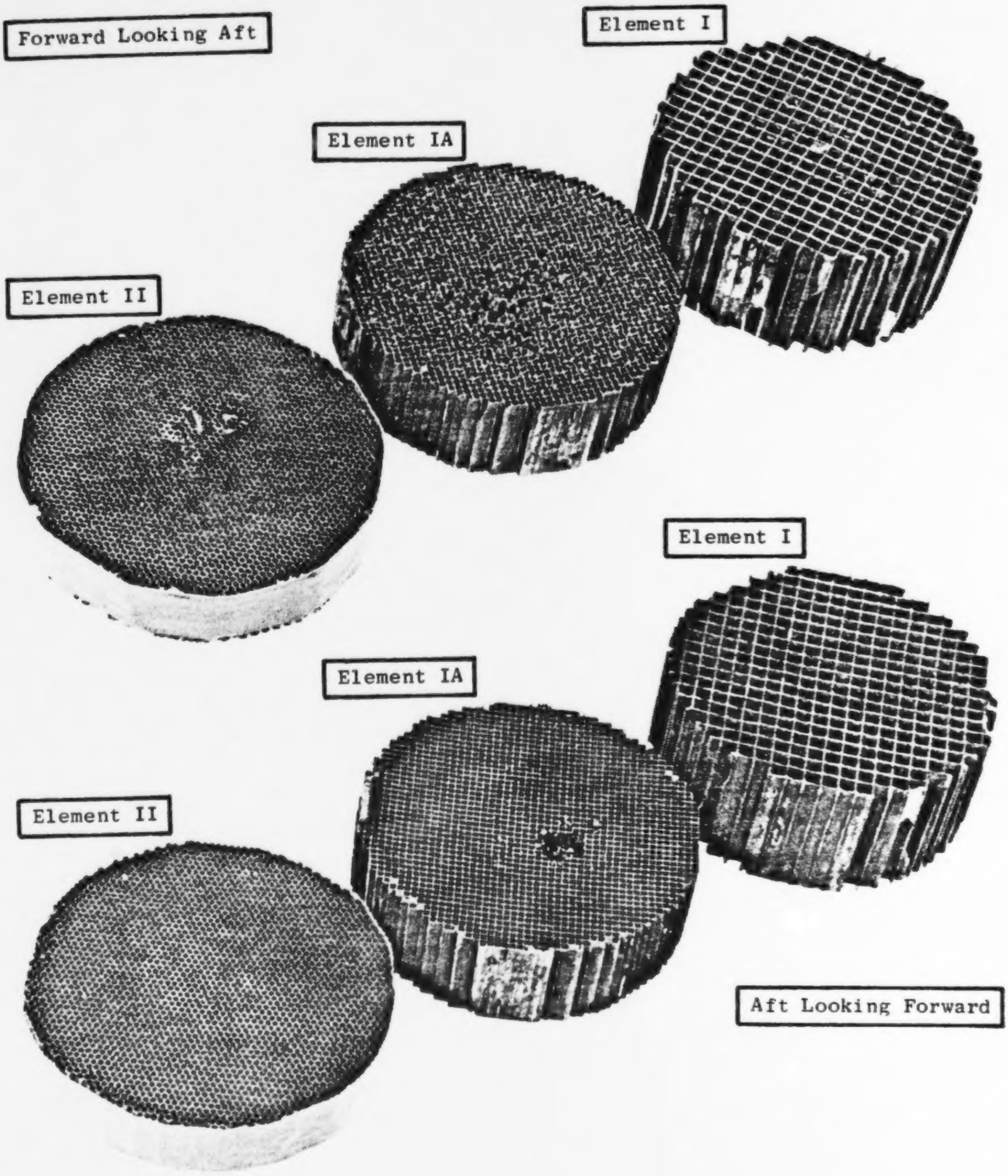
Forward Looking Aft
Element I
Element IA
Element II
Element I
Element IA
Element II
Aft Looking Forward

Figure 16. Postrun Photograph of Second Backup Reactor Elements.

Table I. Design Guidelines

o Design Conditions	Design Point	Range
- Inlet Air Temperature	589 K (600°F)	506 - 589 K
- Pressure	0.62 MPa (90 psia)	0.62 - 0.93 MPa
- Reference Velocity	19.8 m/s (65 ft/s)	10.7 - 30.5 m/s
- Fuel/Air Ratio	20 g/kg (.020 lb/lb)	16 - 26 g/kg
- Fuel	No. 6 Residual Oil	-

o Fuel Injector

- Less than 50% Evaporation
- Fuel/Air Ratio Uniformity Within ± 10%
- Velocity Uniformity Within ± 10%
- Average Drop Size at Catalytic Reactor Inlet:
  - Small Drop Mode $< 30\ \mu m$
  - Large Drop Mode $70 - 150\ \mu m$

o Catalytic Reactor

- 11.4 cm Diameter
- Pressure Drop Less Than 5%
- Combustion Efficiency At Least 99.5%
- Reactor Heat Loss Less Than 5% of Total Reaction Heat Release

o Exit Section

- Heat Loss Less Than 5% of Total Reaction Heat Release

Table II. Catalytic Reactor Configurations

ELEMENT DESCRIPTION *	CONFIGURATION		
	BASELINE	BACKUP #1	BACKUP #2
INLET			
LENGTH, cm	2.5	5	5
CELL DENSITY, CELLS/cm^2	47	4	3
SUPPORT MATERIAL	CORNING CORDIERITE	DUPONT TORVEX ALUMINA	CORNING CORDIERITE
CENTER			
LENGTH, cm	8.9	8.9	3.8
CELL DENSITY, CELLS/cm^2	47	47	16
SUPPORT MATERIAL	CORNING CORDIERITE	CORNING CORDIERITE	CORNING CORDIERITE
EXIT			
LENGTH, INCHES	7.6	7.6	17.8
CELL DENSITY, CELLS/cm^2	9	9	19
SUPPORT MATERIAL	DUPONT TORVEX ALUMINA	DUPONT TORVEX ALUMINA	DUPONT TORVEX MULLITE
TOTAL LENGTH **, cm	20.3	23.0	27.9
PREDICTED PRESSURE DROP, %	3.2	3.0	4.1

* ALL ELEMENTS CATALYZED WITH PALLADIUM ON STABILIZED ALUMINA

** INCLUDES 1/4" SPACE BETWEEN ELEMENTS

Table III. Test Fuel Properties

Property	No. 6 Oil		Jet A (Typical)
	Typical	Test	
Specific Gravity (289/289 K)	0.95	0.944	0.81
Hydrogen Content, wt %	-	11.52	14
Sulfur Content, wt %	< 0.8*	0.47	0.01
Nitrogen Content, wt %	-	0.22	-
Vanadium, ppm	0-150	26	-
Total Ash, %	-	0.022	-
Minor Constituents (Qualitative Analysis)	Fe, Ni	Ca, Ni	-
Net Heat of Combustion, MJ/kg	-	41.3	43
Viscosity, cs @ 311 K	180-1800	1345	1.65
Surface Tension, N/M @ 339 K	-	0.0329	0.020
Pour Point, K	< 289*	294	-
Distillation, K			
IBP	-	460	450
10%	560-617	541	470
40%	-	809**	-
50%	-	-	490
90%	-	-	510
FBP	-	-	630

* ASTM Specification D396

** Max Distillation Temperature

Table IV. Supplementary Test Point Schedule For Backup Reactors

Sequence*	Inlet Pressure, MPa(psia)	Rig Inlet Temperature, K (°F)	Reference Velocity, M/S(ft/s)
1	0.41(60)	867(1100)	19.8(65)
2	↓	↓	30.5(100)**
3	↓	811(1000)	19.8(65)
4	↓	↓	30.5(100)
5	↓	756(900)	19.8(65)**
6	0.62(90)	↓	10.7(35)**
7	↓	↓	30.5(100)**
8	↓	↓	19.8(65)
9	0.93(135)	↓	↓
10	0.62(90)	700(800)	↓
11	↓	644(700)	↓
12	↓	589(600)	19.8(65)**

* Three Fuel-Air Ratios At Each Condition

** Attempt Dropsize Variation

Prepared for the Fifth Workshop
on Catalytic Combustion, San Antonio,
Texas, September 15-16, 1981.

CATALYTIC COMBUSTION OF RESIDUAL FUELS

BY

Daniel L. Bulzan

and

Robert R. Tacina

ABSTRACT

A noble metal catalytic reactor was tested using two residual fuels at inlet air temperatures from 700 to 960K, pressures of 3×10^5 Pa and 6×10^5 Pa, and reference velocities of 10, 15, and 20 m/s. Combustion efficiencies greater than 99.5% were obtained for both residual fuels. Steady state operation of the catalytic reactor required inlet air temperatures of at least 800K for both residual fuels. At lower inlet air temperatures, upstream burning in the premixing zone occurred which was probably caused by fuel deposition and accumulation on the premixing zone walls. Increasing the inlet air temperature to 800K prevented this occurrence. Both residual fuels contained about .5% nitrogen by weight. NO_x emissions ranged from 50 to 110 PPM by volume at 15% excess O_2. Conversion of fuel-bound nitrogen to NO_x ranged from 25 to 50%.

INTRODUCTION

Lewis Research Center is currently evaluating catalytic combustion as part of the Critical Research and Advanced Technology Support project sponsored by the D.O.E. Office of Fossil Energy, Division of Coal Utilization. Catalytic combustion systems are able to complete the combustion reactions at relatively low flame temperatures compared to conventional combustors. This results in negligible thermal NO_x emission levels from fuels which do not contain significant amounts of nitrogen. Catalytic combustion has also been successfully demonstrated with coal-derived liquids (refences 3 and 4). These fuels typically contain reduced levels of hydrogen and increased levels of nitrogen when compared to petroleum-derived fuels.

The present study reports an experimental evaluation of catalytic combustion with two grades of petroleum-derived residual fuel. Residual fuels are typically very viscous, with high boiling points, and can also contain relatively high levels of fuel-bound nitrogen. Their use may become important for stationary gas turbine applications due to the unavailability of higher grade fuel or economic considerations. Due to the physical properties of the fuel, significant problems were anticipated in premixing and partially prevaporizing the fuel to achieve a uniform fuel-air distribution before entering a catalytic reactor. Tests at atmospheric pressure of a No. 6 fuel oil indicated problems with flashback into the premixing zone and unsteady operation of the catalytic reactor (reference 5). Catalytic combustion of residual fuel is also reported in references 6 and 7. Reference 6 reported upstream burning in the premixing zone which made steady operation of the reactor possible only with diesel No. 2 and residual fuel oil blends. Reference 7 reported stable operation with residual fuel at inlet temperatures above 725K.

In the present study, a noble metal catalytic reactor was tested at inlet air temperatures ranging from 700 to 960K, reference velocities from 10 to 20 m/s, and pressures of 3×10^5 and 6×10^5 Pa. Two residual fuels were used in the study. Temperatures, catalytic reactor pressure drops and emissions of CO_2, CO, NO_x, and unburned hydrocarbons were measured.

EXPERIMENTAL DETAILS

Test Rig

A schematic drawing of the test rig used for this study is shown in figure 1. It was fabricated from 15.2 cm. (6 in. nominal, schedule 40) diameter stainless steel pipe. Carborundum T30R fiberfrax tube insulation was inserted inside the pipe to minimize heat losses. A 0.16 cm. thick stainless steel liner was inserted inside the insulation upstream and downstream of the catalytic reactor to prevent erosion of the insulation.

The inlet air was indirectly preheated and its temperature was measured at a plane just upstream of the fuel injector with an array of 12 Chromel-Alumel thermocouples mounted in a flange. Test section inlet pressure was measured at a tap located in the flange containing the inlet thermocouples. Pressure was controlled by a back pressure valve. The airflow entering the test rig was measured with a standard ASME orifice.

The fuel injector used was of a design developed by Tacina (reference 8). It was the hexagonal tube airblast fuel injector previously used for testing coal-derived liquids (reference 3). It was constructed from 19 hexagonal tube modules welded together. Figure 2a is a schematic drawing of one of the modules which comprise the complete fuel injector. Fuel was injected through a .07 cm. inside diameter tube pointing downstream in the center of the smallest cross-sectional area of each module to provide good atomization and mixing. All fuel tubes were the same length, 25.4 cm., to provide equal flowrates to each module. As a precaution, to prevent plugging of the fuel tubes at the high inlet temperatures used for this study, cooling air was introduced into an outside tube which surrounded each fuel tube. All testing was performed with the cooling air, which comprised less than 5% of the total air flowrate. Figure 2b shows the inlet face of the fuel injector.

The premixing zone length of 30.6 cm. was held constant for all tests. A PT/PT-13% Rh thermocouple was used to detect upstream burning in the premixing zone.

The catalytic reactor used for this study consisted of 8 elements. Each element was 12 cm. in diameter and 2.54 cm. long. The elements were separated by a .31 cm. gap containing at least one thermocouple except for the last two elements which were not separated. This arrangement is shown in figure 1. The elements which comprise the reactor are described in Table I. The first two elements had the largest cells, the next two smaller, with the last two having the smallest cells. This graded cell arrangement was successful in preventing plugging of the first element passages when used in previous studies with coal-derived liquids. The static pressure drop across the catalytic reactor was measured with a differential pressure transducer connected between a tap at the premixing zone thermocouple station and one located in the flange at the first row of thermocouples downstream of the catalytic reactor.

At a distance 17.2 cm. downstream of the catalytic reactor, a fixed location single point water-cooled gas sampling probe, with a 0.6 cm. inside diameter sampling passage, was used to withdraw samples for emissions measurements. Temperatures were also measured downstream of the reactor at the locations shown in Figure 1. The gas sample line was electrically heated to prevent unburned hydrocarbons from condensing. Concentrations of CO and CO_2 were measured with monodispersive infrared analyses, unburned hydrocarbons with a flame ionization detector, and nitrogen oxides (total NO + NO_2) with a chemiluminescent analyzer.

The residual fuel tank and lines were electrically heated to 400K to reduce the fuel viscosity for pumping. Normal operating procedure for testing with residual fuel was to initially start the reactor with diesel no. 2 and then gradually introduce residual fuel flow while slowly decreasing the diesel fuel flow until the reactor was operating solely on residual fuel. The procedure generally required about 10 minutes to complete. This prevented residual fuel from impinging upon relatively cold catalytic reactor walls which would tend to plug the catalyst channels. Shutdown was accomplished by reversing the above procedure to purge the residual fuel from the small fuel injector tubes.

MEASUREMENTS AND COMPUTATIONS

Reference Velocity

The reference velocity was computed from the measured mass flow rate, the average inlet air temperature, the duct cross-sectional area, and the test-section inlet pressure.

Emission Index

Emissions were measured as concentrations in PPM by volume, corrected for water of combustion, and converted to emission indices using the expressions in reference 9.

Combustion Efficiency

Combustion efficiency was calculated from the following expression.

$$\mathrm{Eff} = 100 - 0.1\left(\mathrm{E.I.}_{HC} - \mathrm{E.I.}_{HC,EQ}\right) - 0.1\,\frac{HV_{CO}}{HV_{FUEL}}\left(\mathrm{E.I.}_{CO} - \mathrm{E.I.}_{CO,EQ}\right)$$

where

Eff	combustion efficiency, %
$\mathrm{E.I.}_x$	emission index of specie x, gx/kg fuel
$\mathrm{HV.}_x$	lower heating value of x, J/kg

Equilibrium concentrations ($\mathrm{E.I.}_x$, EQ) were obtained from the computer program of reference 10.

Fuel-Air Ratio

The fuel-air ratio was determined both from the metered fuel flow and airflow rates and by making a carbon balance from the measured concentrations of CO, CO_2, and unburned hydrocarbons. The two values agreed within ± 12%. The adiabatic reaction temperature was computed from the computer program of reference 10 using the carbon balance fuel-air ratio. The carbon balance fuel-air ratio was selected since it was the local fuel-air ratio at which the emissions data were obtained. It also included the small amount (less than 5% of the total airflow) of air used for cooling the fuel tubes.

NOx Emissions

Measured NO_x emissions were corrected to 15% O_2 from the following expression:

$$\left(NO_x\right)_{15\%\,O_2,\,PPMV} = \frac{\left(F/A\right)_{15\%\,O_2}}{\left(F/A\right)_{MEASURED}} \left(NO_x\right)_{MEASURED,\,PPMV}$$

where

$(F/A)_{15\%O_2}$ is the fuel-air ratio which will produce an exhaust of 15% O_2.

$(F/A)_{measured}$ is the carbon balance fuel-air ratio.

RESULTS AND DISCUSSION

Two residual fuels, batch 1 and batch 2, were used for this study. Fuel properties are listed in Table II. Both fuels contained about .5% by weight of fuel-bound nitrogen. Carbon and hydrogen contents of both fuels were also very similar. The viscosity of batch 2 residual fuel was considerably greater than batch 1. At 340 K, the viscosity of batch 2 was about 4 times greater than batch 1. The distillation curve for batch 1 fuel was taken from reference 6, it was the same fuel that was used for that study. At 797 K, 60% of the fuel was distilled with 40% remaining as residue. A complete distillation curve was not obtained for batch 2 residual fuel, however, no distillation was obtained for temperatures up to 589 K.

Combustion Efficiency

Combustion efficiency, as a function of adiabatic reaction temperature, is presented in figures 3a and 3b. Data are presented in figure 3a for both residual fuels at a reference velocity of 10 m/s for pressures of 3×10^5 and 6×10^5 Pa, and inlet air temperatures of 800, 900, and 960K. Combustion efficiencies greater than 99.5% were obtained for adiabatic reaction temperatures greater than 1350K. Batch 1 residual fuel had a greater combustion efficiency than batch 2 for a given adiabatic reaction temperature. This was probably caused by a lower percentage of batch 2 fuel being vaporized.

Reference 6 reported an effect of fuel vaporization on combustion efficiency. There are two reasons for batch 2 fuel having a lower percentage of fuel vaporized than batch 1. First, the greater viscosity of batch 2 would result in larger drop sizes (reference 11) and thus a lower vaporization rate. Second, less vaporization at a given temperature would occur for batch 2 residual fuel because of its increased distillation temperature.

Figure 3a also shows an effect of pressure on combustion efficiency. For batch 2 residual fuel, combustion efficiency was greater at a pressure of 6×10^5 Pa than at 3×10^5 Pa at adiabatic reaction temperatures less than 1400K. Increasing pressure and inlet temperature increase gas phase reactions (references 12 and 13). Increasing inlet temperature also initiates gas phase reactions sooner in the catalytic bed (ref. 13). For batch 2 residual fuel, preflame reactions in the premixing zone were increased at the higher pressure. At a reference velocity of 10 m/s, the premixing zone temperature was 1050 to 1100 K at a pressure of 6×10^5Pa and 950 to 1000K at a pressure of 3×10^5 Pa, independent of the inlet air temperature. Since this is the inlet gas temperature to the catalytic reactor, the increased inlet temperature would initiate gas phase reactions sooner in the catalytic bed which would then proceed at a faster rate because of the increased temperature and pressure.

At a constant pressure, little effect of inlet air temperature is shown. Reference 13 reported an increase in combustion efficiency for increased inlet air temperatures.

Preflame reactions in the premixing zone were observed with the residual fuel which resulted in a relatively constant fuel-air mixture temperature at the catalytic reactor inlet at a constant pressure. This could have eliminated the expected increase in performance with increased inlet air temperature.

Figure 3b presents combustion efficiency data at a reference velocity of 20 m/s and a pressure of 3×10^5 Pa for both residual fuels. Increasing reference velocity decreased combustion efficiency. At an inlet air temperature of 800K, an increase in fuel-air ratio corresponding to an adiabatic reaction temperature increase of about 50 K is required over that needed at 10 m/s to maintain the same combustion efficiency.

No data is presented for inlet air temepratures below 800K. Unstable operation of the system resulted for inlet air temperatures below 800K. For batch 1 residual fuel, at an inlet air temperature of 750K, the premixing zone thermocouple would rise from slightly less than 750 K to about 1400 K at intervals of approximately 8 minutes. A sharp increase in CO_2 and decrease in CO emissions would result from the temperature excursion. Between these perturbations, catalytic reactor performance was quite stable. At an inlet air temperature of 700 K, operation became more unstable with the premixing zone thermocouple rising from about 700 to 1500 - 1600 K at intervals of approximately 1 or 2 minutes. Emissions would also fluctuate at about the same rate. It seems likely that fuel was depositing on the premixing zone duct walls at the reduced inlet air temperature, accumulating, and then igniting. Inlet air temperatures of 800 K and above apparently vaporized enough of the fuel such that it did not accumulate sufficiently and steady state operation could be achieved. Batch 2 residual fuel showed similar results.

The catalytic reactor was operated for about 16 hours on the residual fuel. No degradation on poisoning of the reactor was observed during this period of testing.

CO EMISSION INDEX

The CO emission index in units of g CO/kg fuel is presented in figures 4a and 4b as a function of the adiabatic reaction temperature for reference velocities of 10 and 20 m/s. Figure 4a presents data for both residual fuels at a reference velocity of 10 m/s, pressures of 3×10^5 and 6×10^5 Pa, and inlet air temperatures from 800 to 960 K. Increasing the adiabatic reaction temperature decreased the CO emissions. Batch 2 residual fuel produced higher CO emissions than batch 1. This was probably caused by the increased dropsize and reduced vaporization of batch 2 as compared to batch 1 residual fuel.

An increase in pressure from 3×10^5 to 6×10^5 Pa decreased the CO emissions. This was probably due to the increased premixing zone temperature caused by preflame reactions and increased gas phase reactions at the higher pressure as previously discussed. As previously shown for combustion efficiency, little effect of inlet air temperature on CO emissions was shown. A comparison of figures 4a and 4b shows that increasing the reference velocity from 10 to 20 m/s increased the CO emission index for batch 1 fuel at an inlet air temperature of 800 K.

Unburned Hydrocarbons Emission Index

Figures 5a and 5b present the unburned hydrocarbons emission index in units of g HC/kg fuel as a function of the adiabatic reaction temperature for reference velocities of 10 and 20 m/s, pressures of 3×10^5 and 6×10^5 Pa, and inlet air temperatures from 800 to 960K. The results show the same trends as previously shown for the CO emission index. The measured unburned hydrocarbons were extremely low at these relatively high inlet air temperatures. Almost all of the combustion inefficiency, therefore, was caused by the CO emissions.

NOx Emissions

NO_x emissions, expressed as PPM by volume and corrected to 15% excess O_2 are presented in figures 6a and 6b for both residual fuels at reference velocities of 10 and 20 m/s. Figure 6a presents data taken at pressures of 3×10^5 and 6×10^5 Pa., and inlet air temperatures from 800 to 960 K at a reference velocity of 10 m/s. NO_x emissions were found to increase with adiabatic reaction temperature. The NO_x emission standard of 125 PPM by volume at 15% O_2 for new, modified, or reconstructed stationary gas turbines is shown for comparison (reference 14). It includes an allowance of 50 PPM for fuel-bound nitrogen and is based on a gas turbine thermal efficiency of 25%. NO_x emissions were less than the standard for all the test conditions. They ranged from 50 to 110 PPM at 15% O_2. No effect of inlet air temperature, pressure, or residual fuel batch is shown. NO_x emissions at a reference velocity of 20 m/s are presented in figure 6b. NO_x emissions at a given adiabatic reaction temperature were lower for the higher reference velocity, however, combustion efficiency was also reduced.

Figures 7a and 7b present the conversion of fuel-bound nitrogen to NO_x as a function of the adiabatic reaction temperature for both residual fuels at reference velocities of 10 and 20 m/s. The conversion was calculated assuming all measured NO_x emissions were due to fuel-bound nitrogen conversion. This was considered to be reasonable because of the relatively low flame temperatures of catalytic combustion. Conversion increased with increasing adiabatic reaction temperature. Conversion levels ranged from 25 to 50%. Reference 7 reported conversion levels approaching 100% with residual fuel. The fuel used for the study of reference 7, however, contained only .22% nitrogen. Reference 15 reported a strong dependence of fuel nitrogen content on the conversion of fuel-bound nitrogen to NO_x for lean catalytic combustion. Conversion decreased with increasing fuel nitrogen content. At .5% fuel-bound nitrogen, reference 15 reported a conversion to NO_x of 46%. Conversion levels for the petroleum - derived residual fuels were lower than those obtained previously for coal-derived fuel (reference 3). This was also reported in reference 15 for lean catalytic combustion of pyridine doped petroleum-derived ERBS and coal-derived SRCII.

A comparison of figures 7a and 7b shows the conversion at a reference velocity of 20 m/s was slightly lower at a given adiabatic reaction temperature than at 10 m/s but the combustion efficiency was also lower for the higher reference velocity.

Pressure Drop

Catalytic reactor pressure drop, as a percentage of inlet pressure is presented in figure 8 at an inlet temperature of 800K and a pressure of 3×10^5 Pa for batch 1 residual fuel at reference velocities of 10, 15, and 20 m/s. Pressure drop ranged from about 1.5% at a reference velocity of 10 m/s to 3.5% at 20 m/s for an adiabatic reaction temperature of 1350K. This is considered reasonable for an application.

SUMMARY OF RESULTS

A noble metal catalytic reactor was tested with two residual fuels at inlet air temperatures from 700 to 960K, pressures of 3×10^5 and 6×10^5 Pa, and reference velocities from 10 to 20 m/s. Combustion efficiencies greater than 99.5% were obtained from both residual fuels. A more viscous, higher boiling point residual fuel showed poorer performance than a less viscous, lower boiling point residual fuel. An increase of about 70K in adiabatic reaction temperature was required for the poorer fuel to maintain the same combustion efficiency.

The residual fuels which were used for this study contained from .53 to .55% by weight of fuel-bound nitrogen. For catalytic combustion under the fuel-lean conditions tested, NO_x emissions ranged from 50 to 110 PPM by volume, at 15% excess oxygen. Conversion of fuel-bound nitrogen ranged from 25 to 50%, a fairly low conversion level.

Successful catalytic combustion of the residual fuels used in this study required inlet air temperatures of at least 800 K to prevent significant upstream burning in the premixing zone. At inlet air temperatures below 800 K, upstream burning occurred which was probably caused by the accumulation of fuel on the walls of the premixing zone and subsequent ignition of that fuel-air mixture. The increased vaporization at inlet air temperatures of 800 K and above prevented significant deposition of fuel on the duct walls.

The catalytic reactor was operated for about 16 hours on the residual fuels. No degradation or poisoning was observed during this period of testing.

REFERENCES

1. Anderson, D. N., "Performance and Emissions of a Catalytic Reactor with Propane, Diesel, and Jet A", NASA TM-73786, 1977.

2. Pfefferle, W. C., et. al., "Catathermal Combustion: A New Process for Low-Emissions Fuel Conversion", ASME Paper 75-WA/FU-1, Dec. 1975.

3. Bulzan, D. L. and R. R. Tacina, "Catalytic Combustion of Coal-Derived Liquids", NASA TM-81594, 1981.

4. Chu, E. K., G. C. Snow, and H. J Tong, "Catalytic Combustion of Coal-Derived Liquid Fuels", EPRI AP-1666, 1981.

5. Pogson, J. T., and M. N. Mansour, "#6 Fuel Oil Catalytic Combustion", Proceedings: Third Workshop on Catalytic Combustion, Asheville, N.C., 1978.

6. Rosfjord, T. J., "Catalytic Combstion with Incompletely Vaporized Residual Fuel", NASA CR-165161, 1981.

7. Dodds, W. J. and E. E. Ekstedt, "Demonstration of Catalytic Combustion with Residual Fuel", NASA CR-165369, 1981.

8. Tacina, R. R., "Degree of Vaporization Using an Airblast Type Injector for a Premixed-Prevaporized Combustor", NASA TM-78836, 1978.

9. "Procedure for the Continuous Sampling and Measurement of Gaseous Emissions from Aircraft Turbine Engines", Aerospace Recommended Practice 1256, SAE, Oct. 1, 1971.

10. Gordon, S. and B. J. McBride, "Computer Program for Calculation of Complex Chemical Equilibrium Compositions, Rocket Performance, Incident and Reflected Shocks, and Chapman-Jouguet Detonations", NASA SP-273, Rev. 1976.

11. Jasuja, A. K., "Atomization of Crude and Residual Fuel Oils", ASME 78-GT-83, 1978.

12. Anderson, D. N., "Effect of Inlet Temperature on the Performance of a Catalytic Reactor", NASA TM-78977, 1978.

13. T'ien, J. S., "Catalytic Honeycomb Combustor: Steady State Model and Comparison with Experiment", AIAA-80-1289, 1980.

14. "Environmental Protection Agency, Standards of Performance for New Stationary Sources; Gas Turbines", Federal Register, Vol. 44, No. 176, Part II, September 10, 1979.

15. Lew, H. G., et al., "Low NO_x and Fuel Flexible Gas Turbine Combustors", ASME 81-GT-99, 1981.

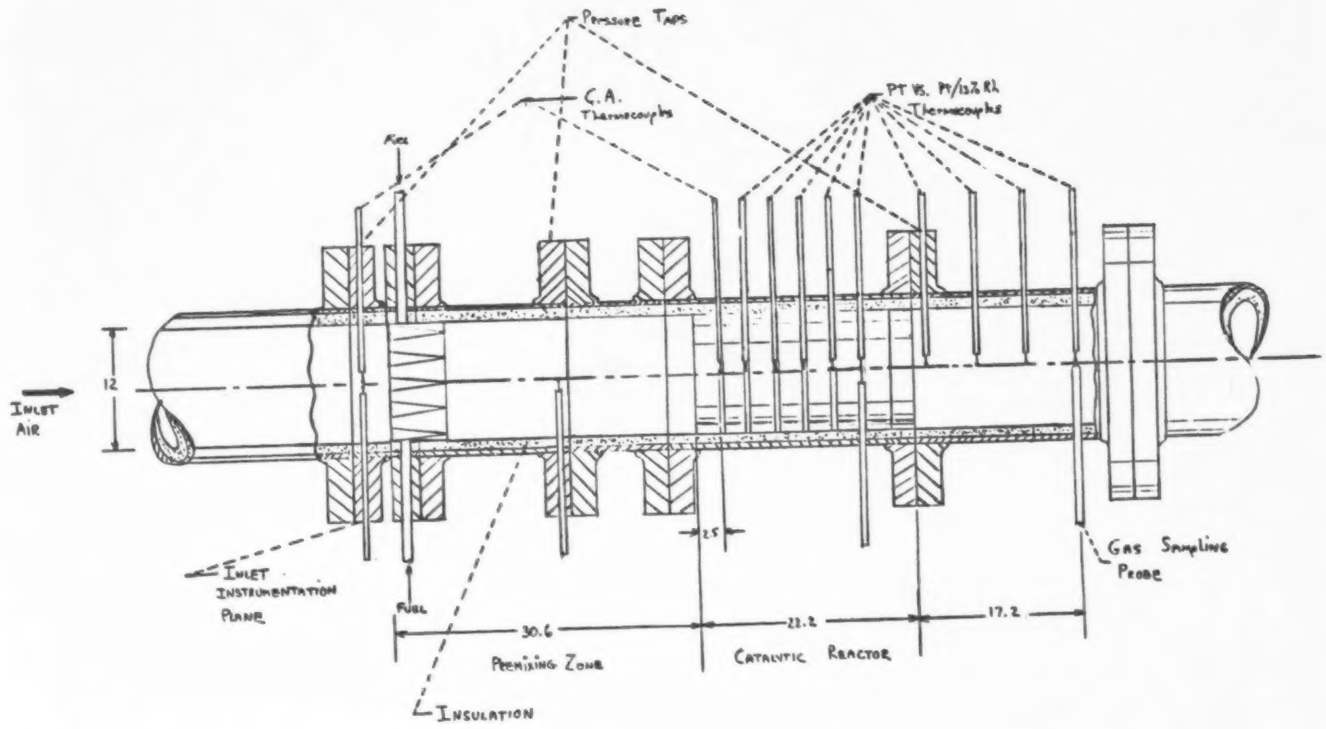
Pressure Taps
C.A. Thermocouples
PT vs. Pt/13% Rh Thermocouples
Air
Inlet Air
12
Inlet Instrumentation Plane
Fuel
2.5
Gas Sampling Probe
30.6
22.2
17.2
Premixing Zone
Catalytic Reactor
Insulation
Dimensions in CM

Figure 1. Test rig schematic.

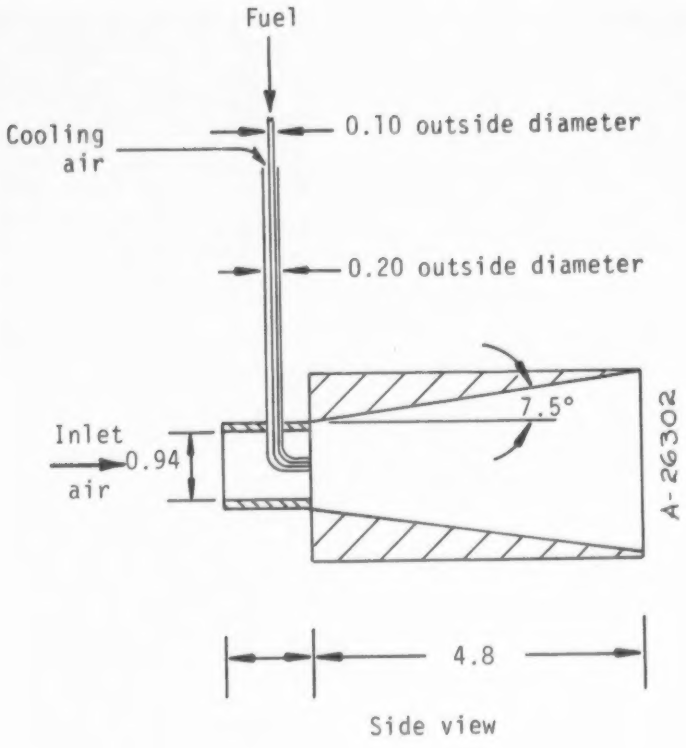
Fuel
Cooling air
0.10 outside diameter
0.20 outside diameter
7.5°
Inlet air
0.94
A-26302
4.8
Side view

a) Hex tube fuel injector module (one of 19)
(dimensions in cm)

Figure 2. Fuel injector.

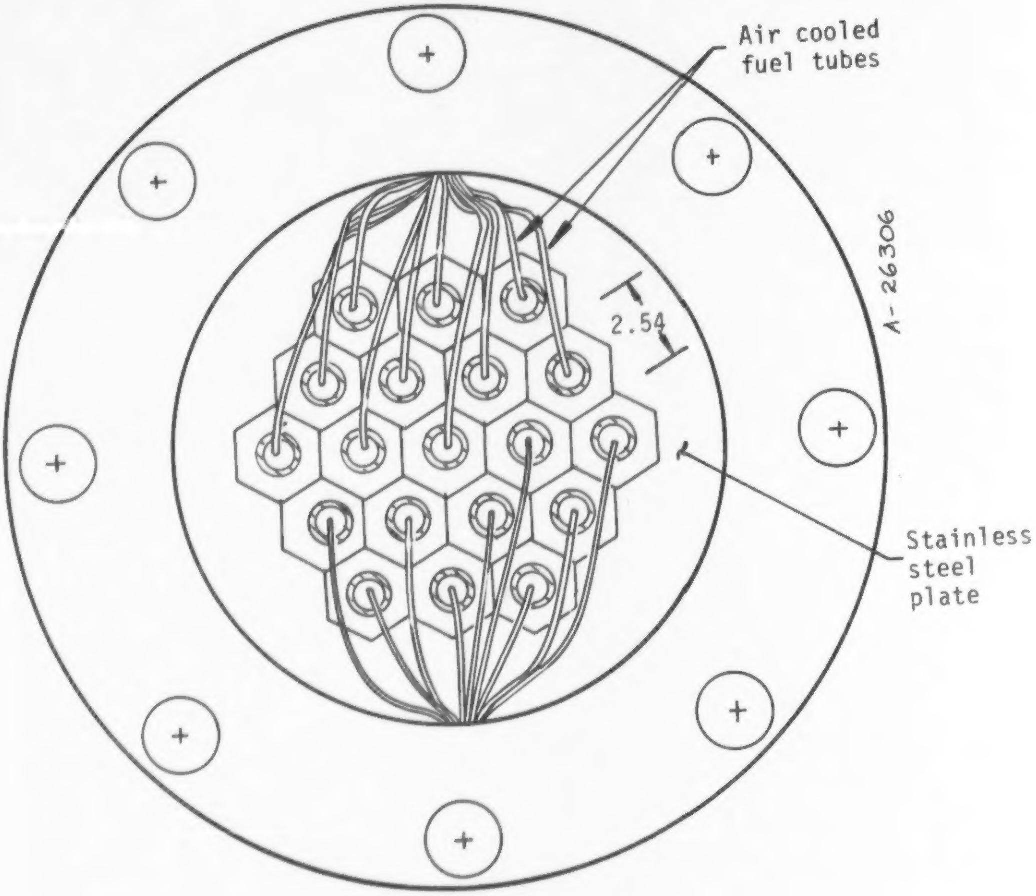
Air cooled fuel tubes
2.54
Stainless steel plate
A-26306

b) Inlet face view looking downstream (dimensions in cm)

Figure 2. Fuel injector.

A-26307

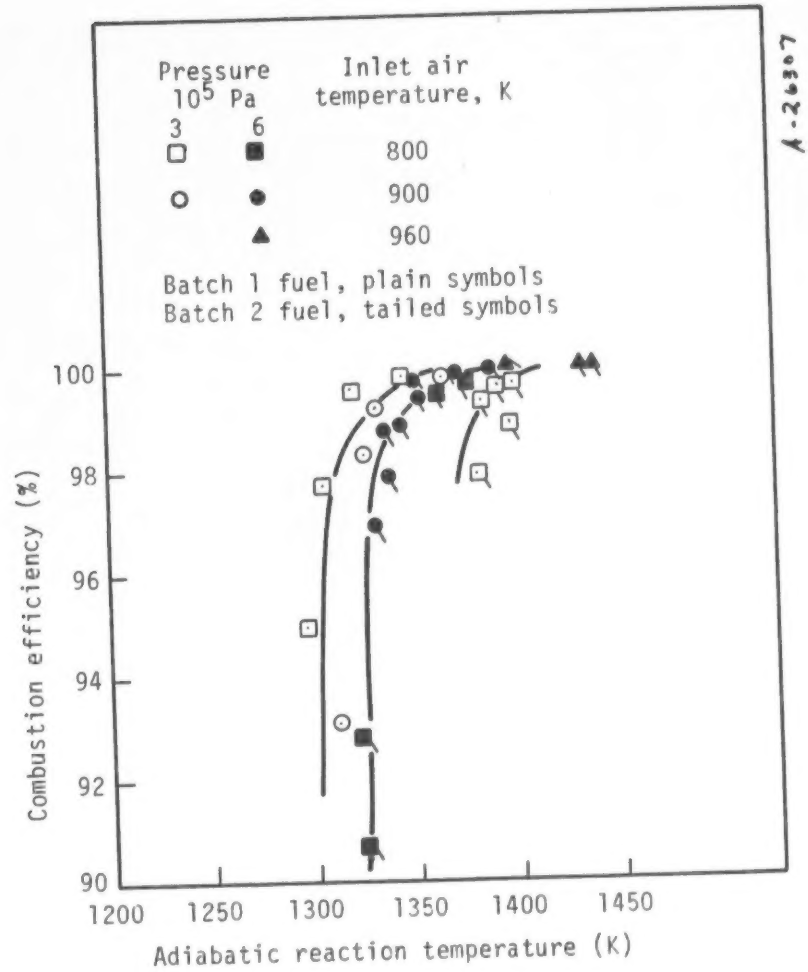

a) Reference velocity, 10 m/s

Figure 3. Combustion efficiency

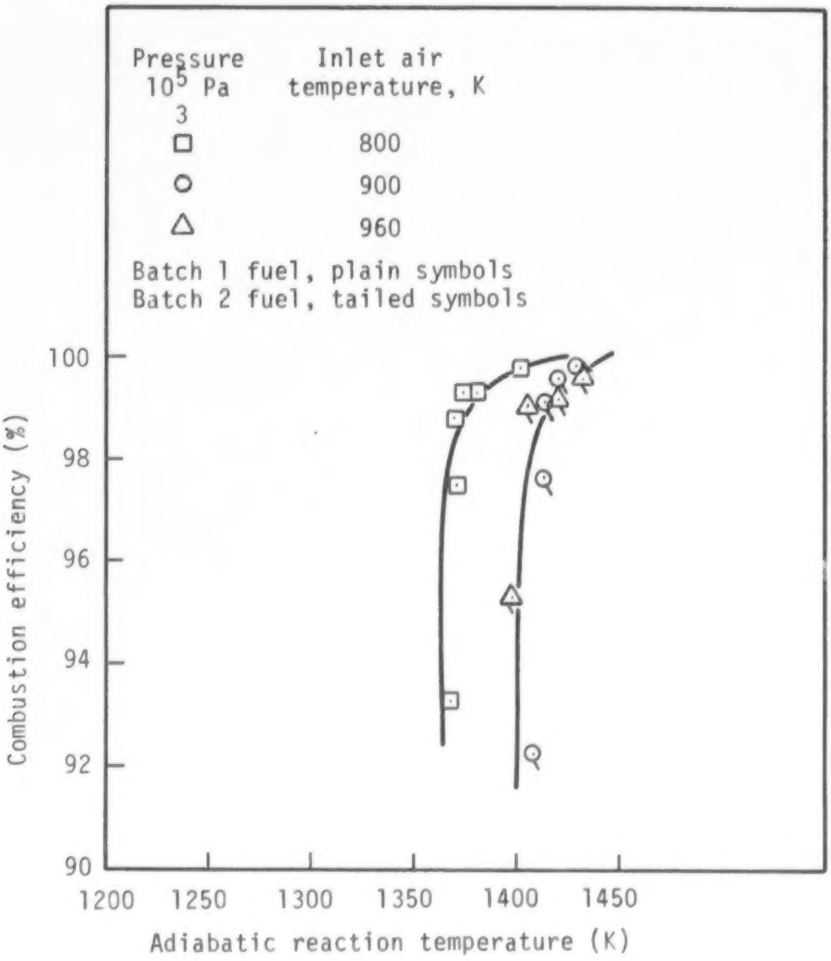

A-26308

b) Reference velocity, 20 m/s.

Figure 3. Combustion efficency.

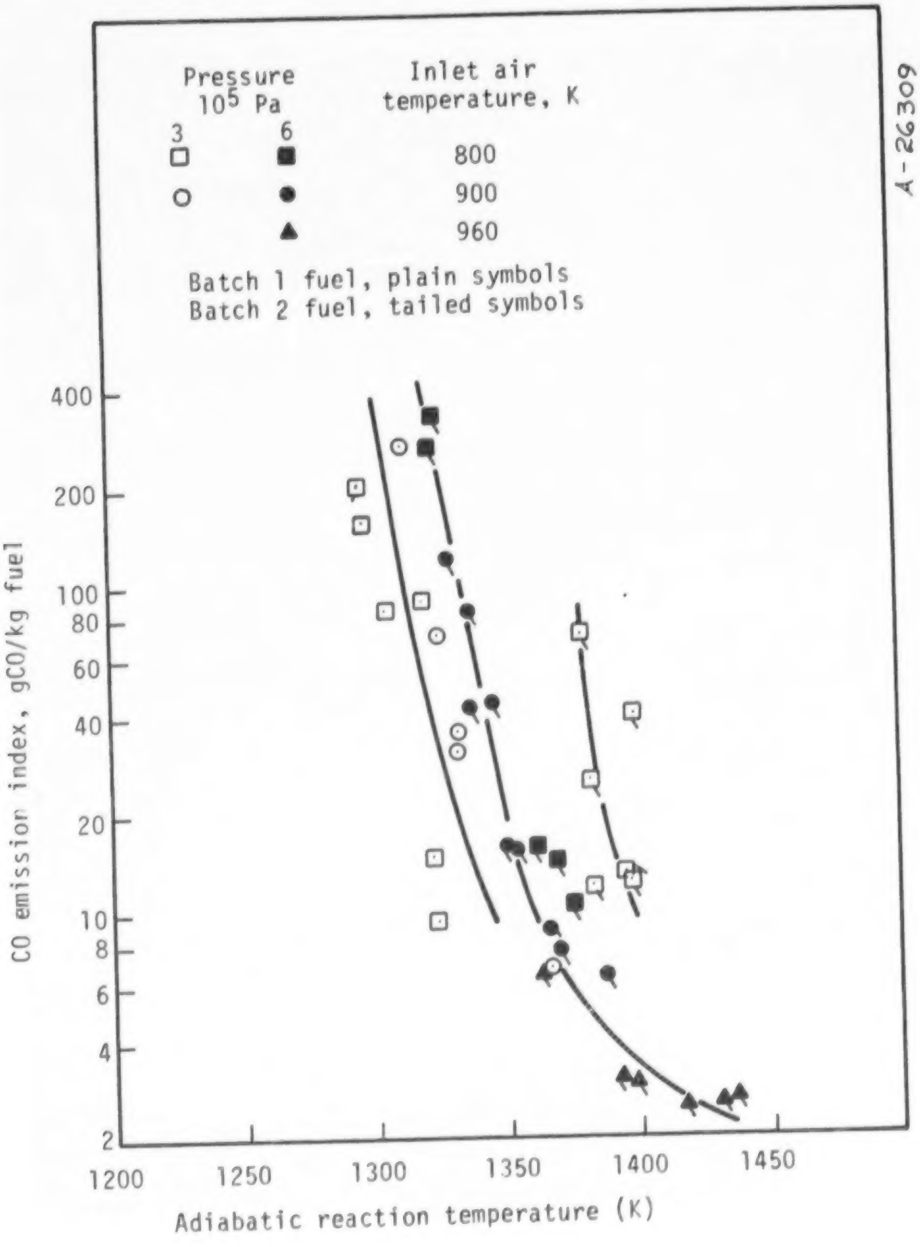

A-26309

a) Reference velocity, 10 m/s.
Figure 4. CO emissions.

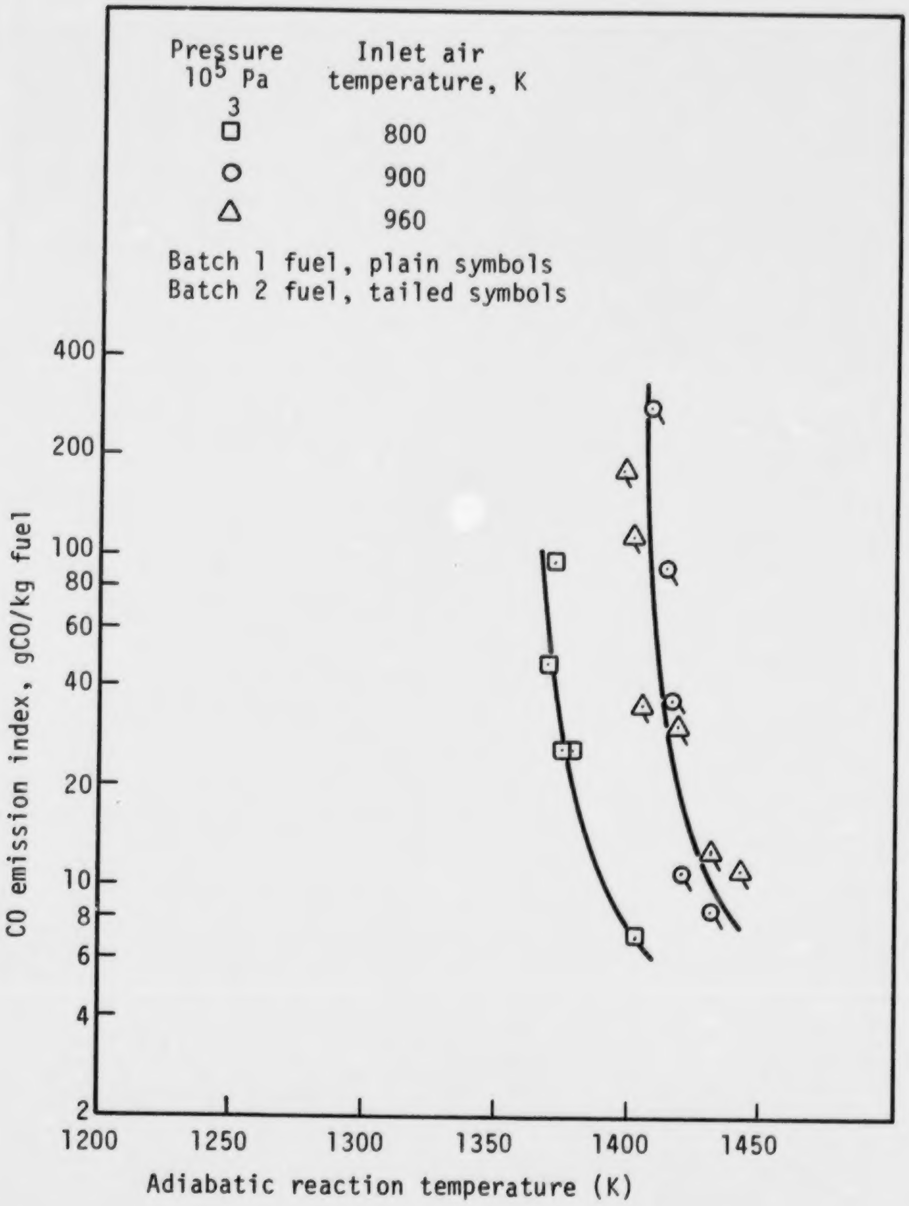

A-26310

b) Reference velocity, 20 m/s

Figure 4. CO emissions.

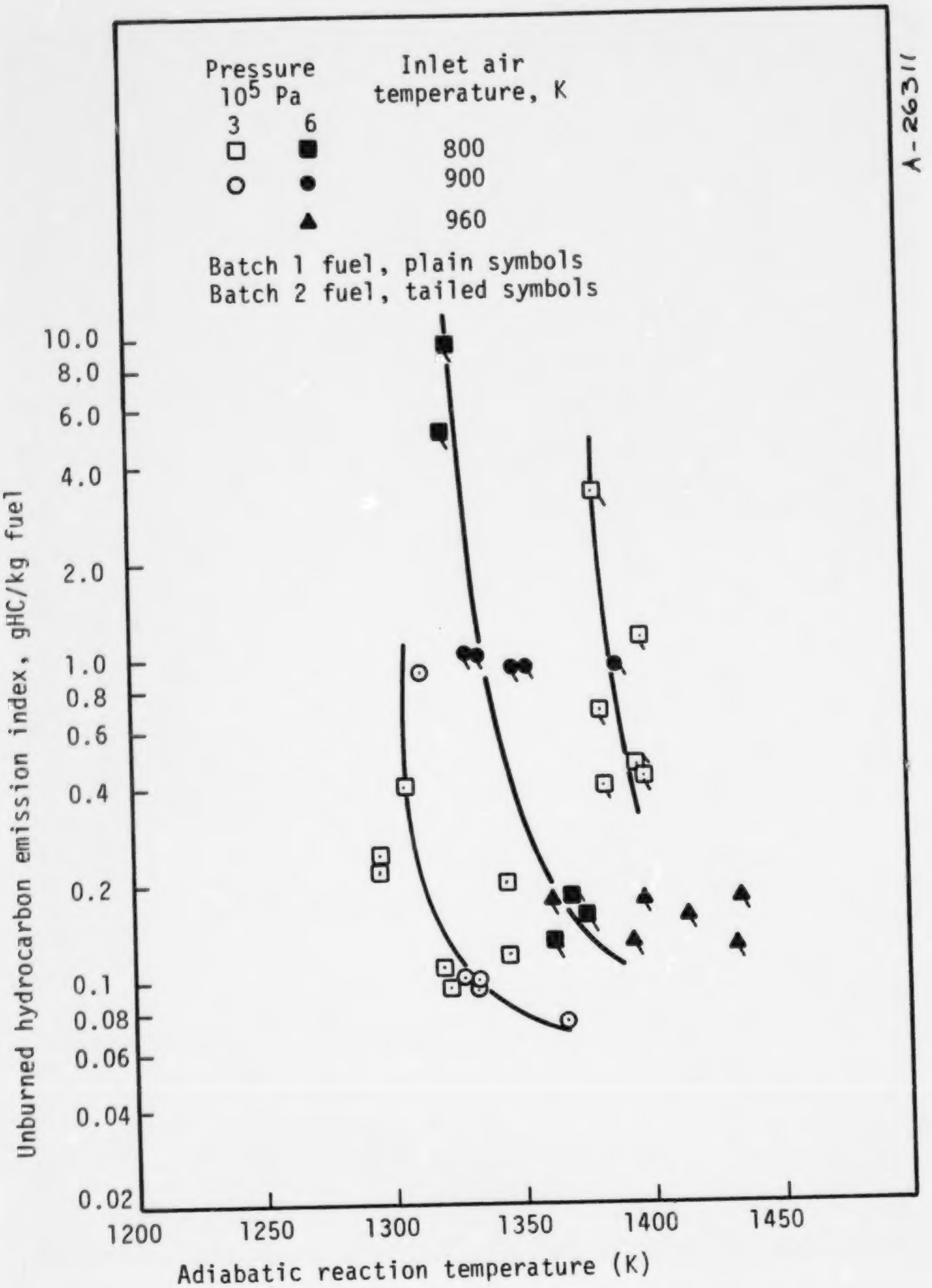

a) Reference velocity, 10 m/s

Figure 5. Unburned hydrocarbon emissions.

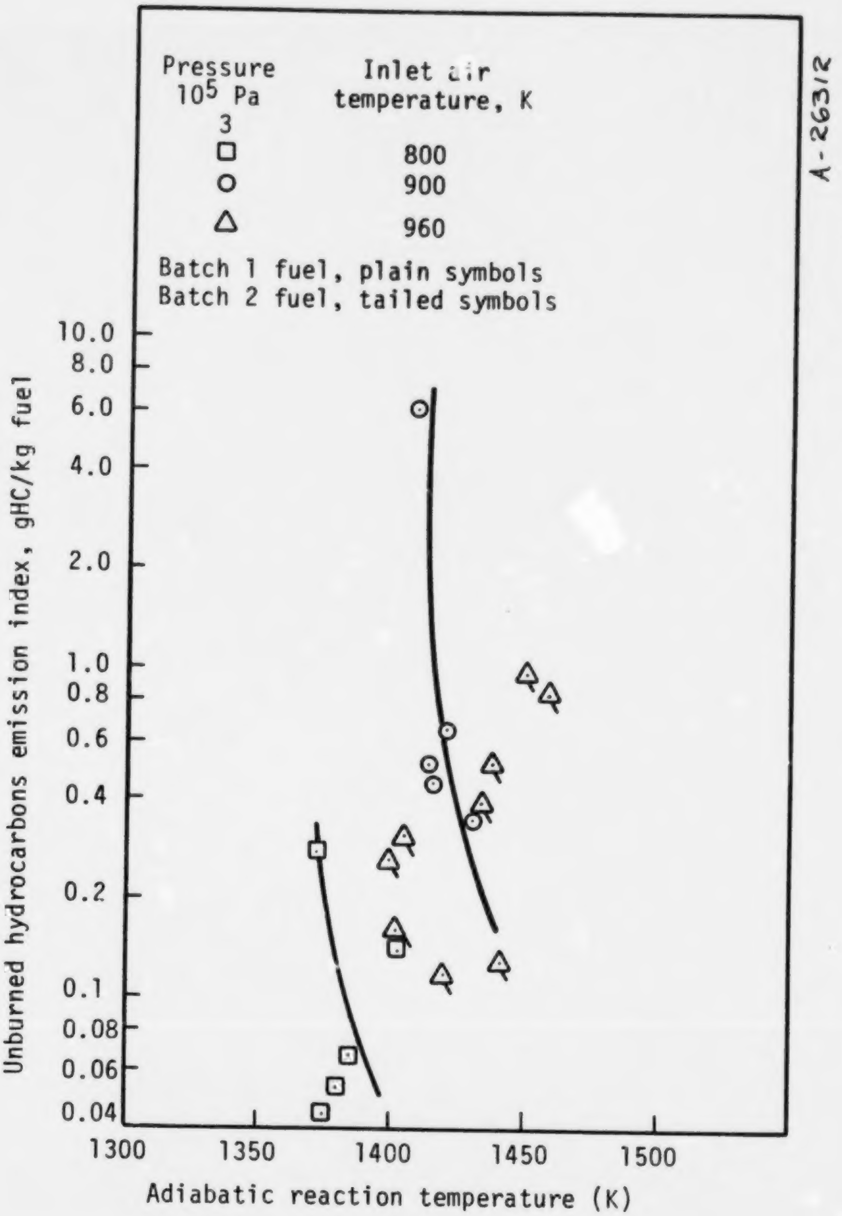

b) Reference velocity, 20 m/s

Figure 5. Unburned hydrocarbon emissions.

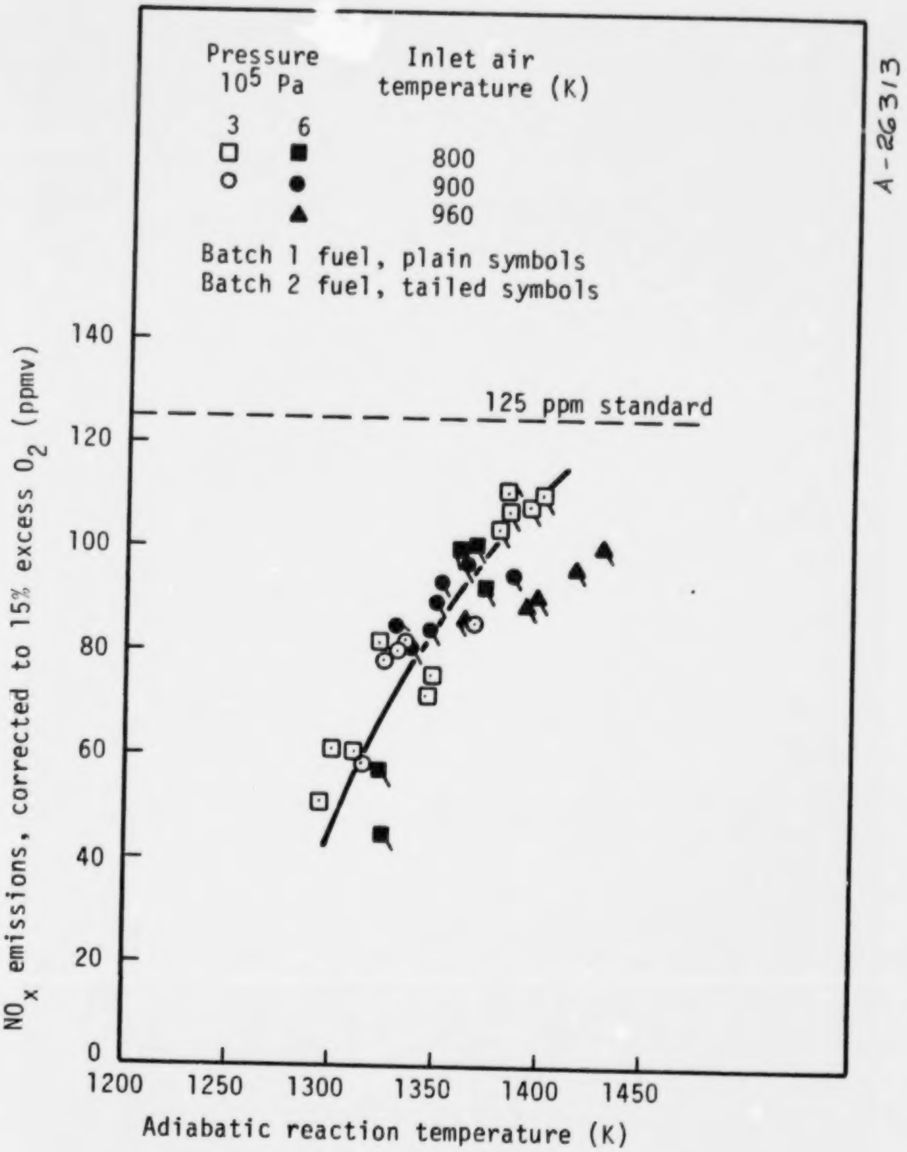

a) Reference velocity, 10 m/s

Figure 6. NO_x emissions.

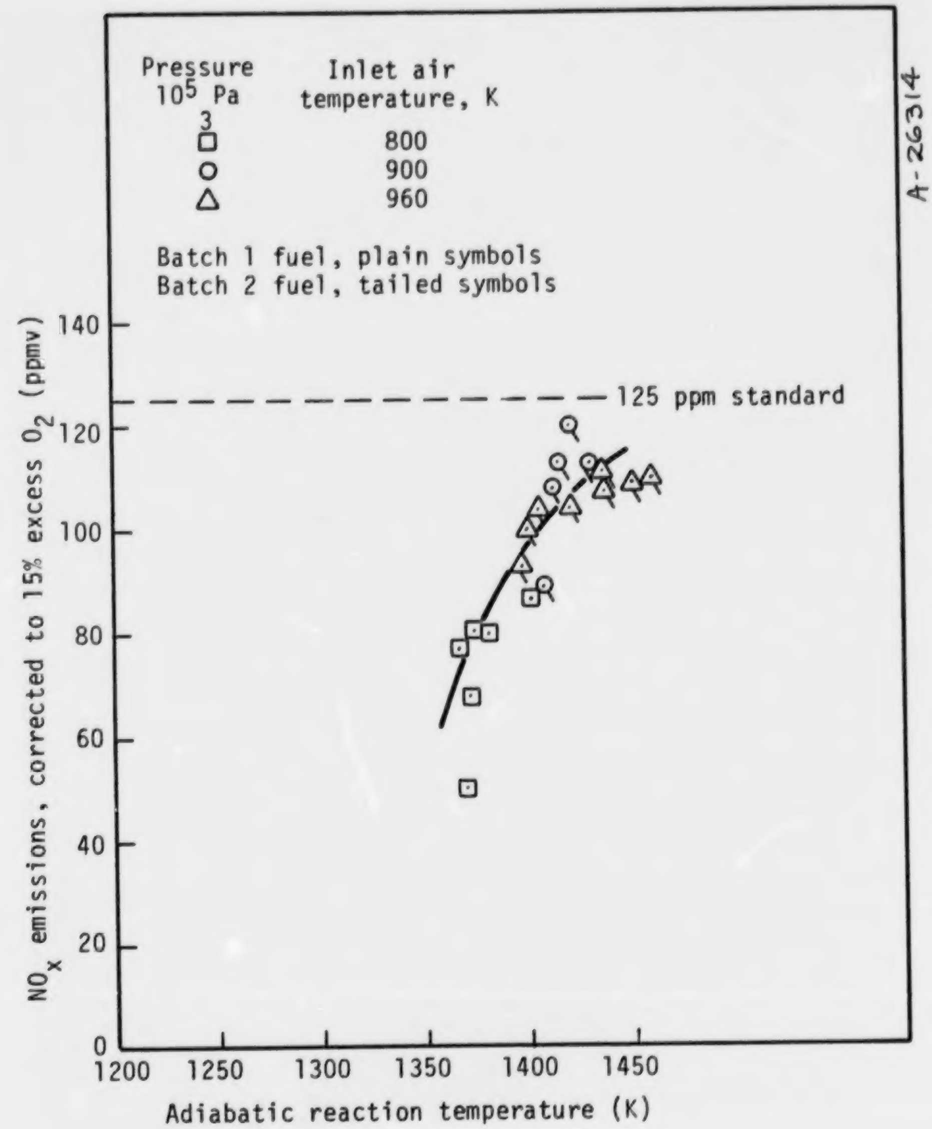

A-26314

b) Reference velocity, 20 m/s

Figure 6. NO_x emissions.

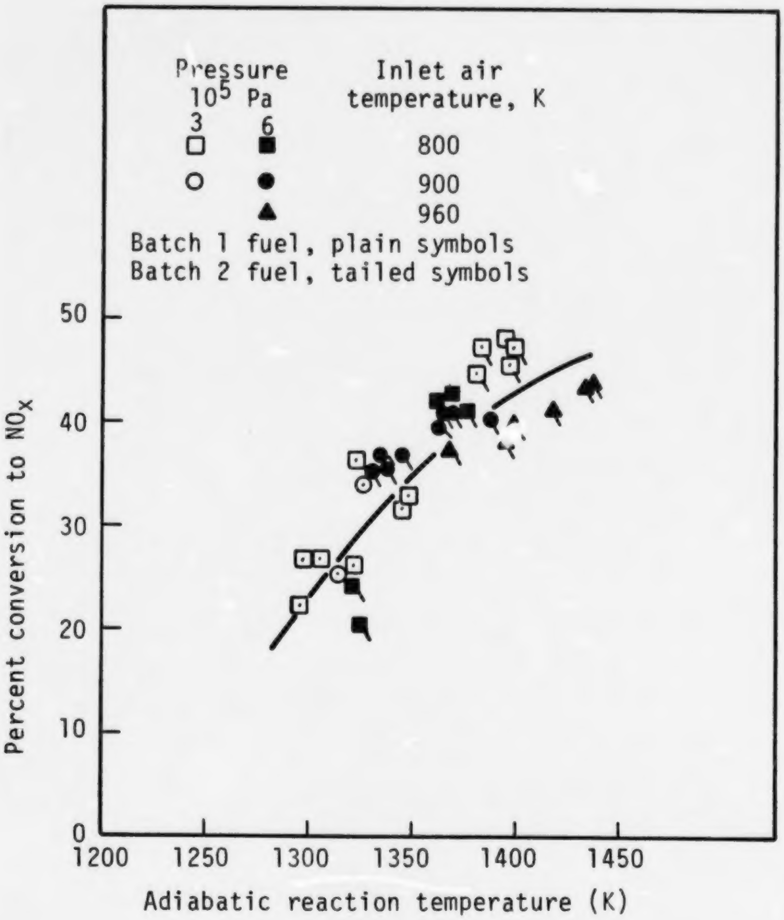

1-26315

a) Reference velocity, 10 m/s

Figure 7. Conversion of fuel-bound nitrogen to NO_x.

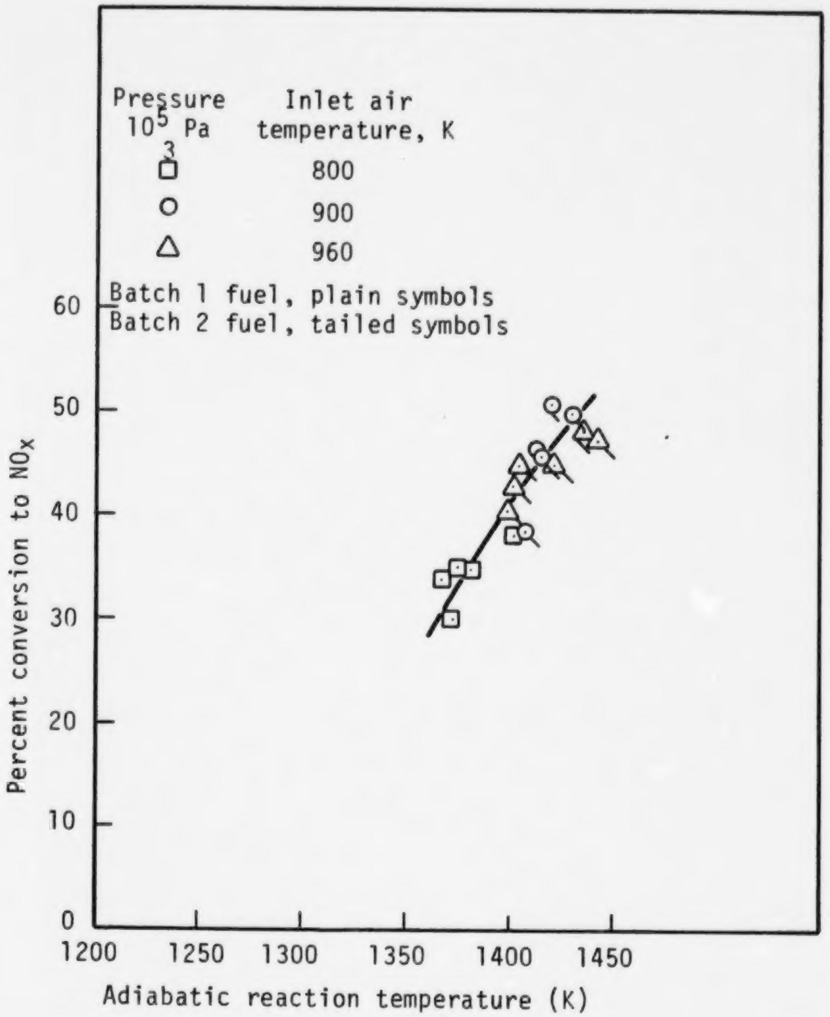

A-26316

b) Reference velocity, 20 m/s

Figure 7. Conversion of fuel-bound nitrogen to NO_x.

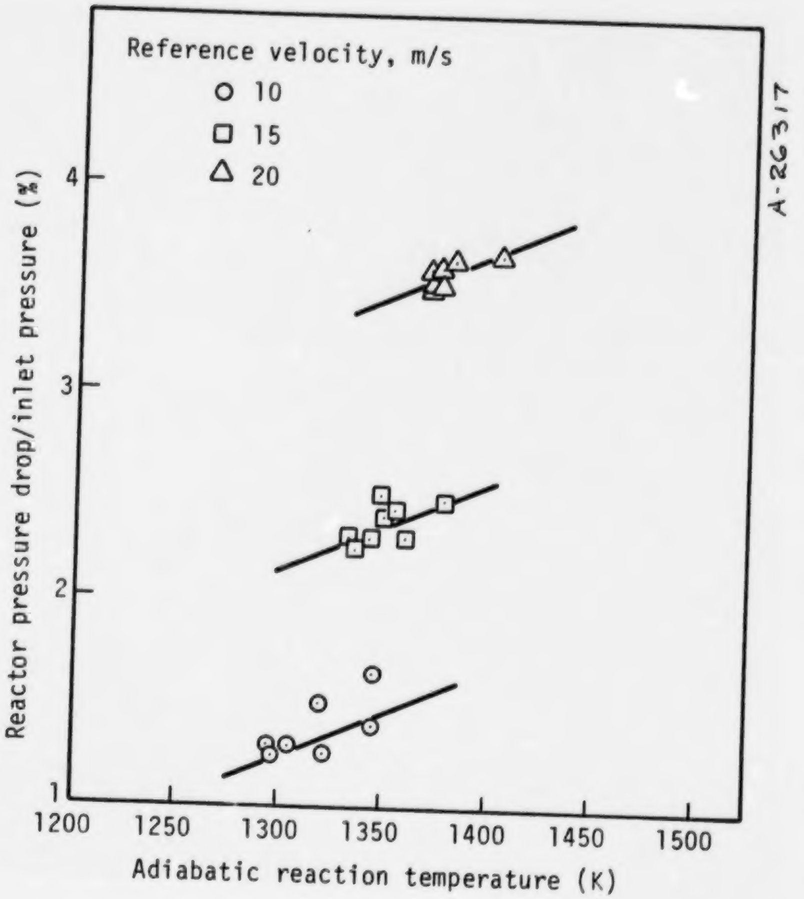

Figure 8. Effect of reference velocity on pressure drop, inlet air temperature 800 K, pressure 3 x 10^5 Pa, Batch 1 residual fuel.

TABLE I. DESCRIPTION OF CATALYTIC REACTOR ELEMENTS

ELEMENT	MATERIAL	CATALYST LOADING KG/M^3	SUBSTRATE MANUFACTURER	SUBSTRATE MATERIAL	CELL DENSITY CELLS/CM^2	OPEN AREA, %
1	Pt/Pd	3.6	Dupont	Mullite	2.6	75
2	Pt/Pd	3.6	Dupont	↓	2.6	75
3	2Pd/1Pt	1.8	Gen. Refractories	↓	10	78
4	↓	1.8	↓	↓	10	78
5	↓	3.6	↓	Cordierite	34	67
6	↓	↓	↓	Mullite	34	67
7	↓	↓	Corning	Cordierite	46.5	63
8	↓	↓	Corning	Cordierite	46.5	63

TABLE II. DESCRIPTION OF RESIDUAL FUELS

	BATCH 1	BATCH 2
Elementals, % by Weight		
Carbon	87.16	86.13
Hydrogen	10.65	11.02
Nitrogen	.53	.55
Sulfur	.16	.74
Ash	Not Determined	.01
Specific Gravity, at 339 K	.899	.864
Flash Point, K	434	434
Pour Point, K	285	280
Viscosity, CS	101 @ 339 K 25 @ 367 K	380.7 @ 344 K 78.5 @ 383 K 38.7 @ 433 K
Gross Heating Value of Combustion, J/kg	4.372 x 10^7	4.365 x 10^7
Distillation, K % by Volume		
5	528	No Distillation to 589 K
10	562	
20	658	
30	714	
50	772	
60	797	
Residue (pct)	40	

SESSION III

APPLICATIONS OF CATALYTIC COMBUSTION

DEVELOPMENT OF A SYSTEM TO UTILIZE FLUE GAS FROM ENHANCED RECOVERY UNDERGROUND COMBUSTION PROJECTS

Stephen E. Kaye
Gulf Research & Development Company
Pittsburgh, Pennsylvania 15230

This presentation was adopted from SPE Paper No. 8630, which was presented at the 54th Annual Fall Meeting of the Society of Petroleum Engineers.

ASSESSMENT OF INFRARED AND CATALYTIC BURNER GAS APPLIANCES

by

W. V. Krill, R. J. Schreiber, and J. P. Kesselring
Acurex Corporation/Energy & Environmental Division
485 Clyde Avenue
Mountain View, California 94042

ABSTRACT

A study has been conducted to identify the state of the art in infrared and catalytic burner development and application. It has also characterized the design features and operating conditions of major conventional gas appliances in the residential and commercial sectors. These two aspects of the program have shown the development of most major appliances with infrared burners to be technically feasible and, in many cases, desirable from the standpoints of economics, fuel efficiency, and emissions. The appliances considered for use with IR burners included four types of cooking appliances -- rangetops, ovens, broilers, and deep fat fryers -- as well as water heaters, room heaters, and central furnaces. Two infrared burner types -- the refractory tile and high temperature fiber matrix -- were found to have the appropriate characteristics to improve appliance efficiency and emissions. An increase in efficiency of 10 to 20 percent is anticipated for most appliance designs. NO_x and CO emission reductions of up to 90 percent appear to be possible. Four of the appliances -- the infrared rangetop, deep fat fryer, water heater, and warm air furnace -- also exhibit economic benefits on comparison of commercial size units, having computed payback periods of approximately 3 years or less.

INTRODUCTION

Of over 20 quads of energy produced from the combustion of natural gas each year in the United States, nearly 40 percent is consumed in the residential and commercial sectors. Most of this gas is consumed in appliances that were designed and developed when gas was inexpensive and readily available. These appliances have typical thermal efficiencies of 30 to 80 percent. With the projections of rapidly decreasing gas supplies and consequent increasing prices of the mid to late 1970's (consumer price tripling since 1970), a need for more efficient gas appliances has developed.

New gas appliances are currently being developed to meet this need. These appliances incorporate features such as condensing heat exchangers, forced convection, power burners, intermittent ignition devices, appliance integration, and radiant burners to increase the overall thermal efficiency. As a result, some future appliances are expected to operate with steady state efficiencies in excess of 90 percent. The potential for significant fuel savings and for extending the supply of natural gas is great.

The concern for improved air quality in this country is also increasing. Standards are currently being proposed for nearly all classes of combustion equipment. For gas appliances, the emissions of concern are nitrogen oxides (NO_x), carbon monoxide (CO), and hydrocarbons (HC). Atmospheric, Bunsen-type burners, used in most appliances, limit HC to very low levels -- generally less than 20 ppm. CO ranges from very low (20 ppm) to as much as 600 ppm. NO_x emissions are typically as high as 80 to 200 ppm. Reductions of the CO and NO_x pollutants are technically feasible by replacing the conventional burner with new burner designs. The radiant burner is a particularly attractive technique for simultaneously reducing CO and NO_x emissions.

Since the use of radiant infrared or catalytic burners is the one appliance modification that can benefit both efficiency and emissions, the Gas Research Institute has sponsored this study to update the current understanding of infrared burner technology and to assess the feasibility of implementation in commercial and residential appliances. Infrared burners had experienced widespread development in the 1950's and 1960's, leading to industrial process and space heating applications where the use of infrared heating was particularly advantageous. Early attempts to develop infrared appliances were technically successful but not economically competitive. The current economics of gas utilization suggest a stronger market position for these appliances than in past years.

Therefore, this study was designed to assess the current state of development of infrared and catalytic burners, conceptualize how these burners could be integrated into gas appliance systems, and identify the research and development efforts required to achieve their commercialization. Economic analysis is presented to evaluate the potential for commercialization.

EXISTING INFRARED AND CATALYTIC BURNER TECHNOLOGY

A survey of infrared (IR) and catalytic burners was made to define existing equipment, its application, and its potential for use in gas appliances. An infrared burner is generally defined as any device that consists of a self-contained infrared radiation source whose energy can be directed to an object to be heated. Catalytic burners can be considered as a subset of IR burners since they are usually similar in configuration and transfer their energy primarily by radiation. They differ in that the rate of fuel oxidation is enhanced by a catalyst material at the surface. The efficiency of a burner in converting input energy to radiant output is expressed as the ratio of input to output, or the radiation generating ratio. Burners which can operate at a ratio of 0.5 or higher are considered quite effective. Often, this ratio can be increased through improved heat transfer from the flame to the radiating surface (the original impetus for porous burner development). It is also important that the selected ceramic or metallic radiating surface has the appropriate spectral emissivity characteristics, emitting radiation primarily in the range of 1 to 10 μm.

Five major types of IR burners are currently in use:

1. Porous refractory monolith
2. Indirect fired
3. Direct fired
4. Porous fiber matrix
5. Metallic screen

All types can be fueled with either natural or LP gases. Each burner type is described briefly in the following paragraphs.

The porous refractory monolith burner allows a gas-air mixture to flow through the solid refractory to the exposed face where it is ignited by spark or pilot. A standing flame just off the burner surface heats both the radiating surface and the surrounding air. The monolith can be either a perforated or porous refractory tile. The perforated tile is the most popular form, having 40 or more perforations per square cm.

The indirect fired IR burner appears to be the next most popular type. This device consists of internally fired radiant metal or ceramic tubes. Its combustion and emission characteristics are the same as for a conventional powered or atmospheric gas burner since it utilizes a conventional Bunsen-type flame. Heat transfer is accomplished primarily by nonvisible IR radiation from the hot (up to 811K) radiating surface. It is a common configuration of space heater designs.

The direct fired IR burner consists of a flame, powered or atmospheric, impinging on a nonporous ceramic surface. The resulting incandescent ceramic surface is the source of the radiant energy. Again, this device uses a conventional burner, and its combustion and emissions performance are well known. The nonporous ceramic block has a higher temperature capability than the indirect fired device and may operate at surface temperatures to 1800K. This type of burner is commonly used for industrial process heating, commercial broilers, and in one commercial deep fat fryer design.

The porous fiber matrix burner features a layer of ceramic fibers through which reactants pass and ignite upon reaching the outer surface of the layer.

There is no attached flame front as in the case of the refractory tile. Rather, the combustion reaction takes place in a shallow zone just within the outer surface. The reaction heats the fibers to incandescence, which then radiate to the environment. Combustion is stabilized and flashback prevented by the balance between the convection associated with the incoming, cool reactants and back conduction from the combustion zone (which is retarded by the low conductivity fiber matrix). Operating temperature varies widely (480K to 1370K) among applications, mostly in comfort and process heating.

The last type of IR burner uses a metallic screen (usually Inconel) as a flameholder and radiator. The screen is mounted over a conventional flame or other IR burner surface. There are apparently few manufacturers of this burner type due to its reportedly poor durability.

The most common IR burner application is in industrial comfort heating by refractory monolith, indirect fired, and direct fired burners. These burners are also used in specific industrial process heating applications. The fiber matrix burner is gaining popularity for this application. Small numbers of gas appliances do employ IR burners, most notably food broilers, deep fat fryers, outdoor cookers, and camping heaters.

The eight appliances considered in this study, shown in Table I, have similar burner operating conditions due to their atmospheric blue flame,

TABLE I. CONVENTIONAL RESIDENTIAL AND COMMERCIAL GAS APPLIANCE CHARACTERIZATION

Appliance	T_{flame} (K)	Firing Rate (MJ/hr)	Ignition Source	Efficiency (unit/ combustion, %)	Emissions CO/NO_x (ppm, air-free)
Rangetop burner	1250-1800	16-21	Continuous pilot	40-50/100	130/90
Oven and broiler		42-84	Continuous pilot	40-50/100	90/95
Deep fat fryer		42-84	Continuous pilot	40-50/100	Not available
Residential water heater		42-84	IID	75-80/100	7/115
Commercial water heater		42-158	IID	75-80/100	7/180
Central warm air furnace		53-264	IID	75-80/100	14/95
Room heater		21	Continuous pilot	75-90/100	8/140

*All appliances operate at 7 to 13 cm W.C. fuel pressure, 80 percent primary theoretical air, and 50 to 80 percent excess air overall.

Bunsen-type burners. However, efficiency and emissions vary greatly due to differences in appliance heat transfer characteristics (Reference 1). As shown, the four cooking appliances are notably less efficient and may have appreciably higher CO emission levels. The application of IR burners appears feasible for all of these appliances which may significantly benefit their performance. The concepts for these appliances are discussed in the following section.

INFRARED APPLIANCE CONCEPTS

Related prior development and concepts for eight infrared appliances were considered in this study and are described here. The anticipated benefits of each of the appliance designs are discussed in the following section.

RANGETOP

Due to the generally fragile nature of IR burner radiating surfaces, it is necessary to protect them from utensil contact and food spills that occur in rangetop cooking. Therefore, the commercial solid top range was selected as an appropriate design. These appliances typically have multiple burners mounted below a cast steel top. The surface may be slanted as on griddles and frytops, or grooved for marking of meat products. Rangetops also have a fairly wide burner turndown (better than 4 to 1) compared to other appliances. Overall appliance efficiency is relatively low due to limitations in available heat transfer surface.

The infrared range concept is shown in Figure 1. Of the five types of IR burners described, the fiber matrix appears to have the greatest applicability due to its wide turndown capabilities. A combustion air blower would be required to operate these burners at the premixed, low excess air conditions desired. The burners are mounted flush with a plate that forms the lower surface of an exhaust chamber connected to a flue at the rear of the appliance. The group of burners radiates directly to the cooking surface. Although the infrared burners can be ignited by standing pilots, the concept shown includes an electronic ignition system to further reduce appliance gas consumption. A silicon carbide type igniter that ignites the gas-air mixture by resistance heating is appropriate. The control system for the IR rangetop is more complex than that of a conventional range due to the needs for powered combustion air, air and gas proportional valving, and flame proving. Two potential control systems have been envisioned under the program (see Reference 2).

Four prior IR rangetop development efforts are known. The first (by Tappan Co. in the late 1960's) is very similar to the concept presented above (Reference 3). The range was fully operational but did not obtain American Gas Association (AGA) approval due to the lack of flame proving capabilities. The addition of these components apparently prevented the concept from being economically viable. A similar unit was developed by Engelhard Industries for the Environmental Protection Agency's Clean Energy Van as a demonstration unit (Reference 4). The burners were hydrogen fueled, however, and only limited demonstration has occurred. Finally, separate developments of catalytic IR rangetop-type burners have been reported by AGA as early as 1960 and more recently by Comstock and Westcott, Incorporated (References 5,6).

OVEN

The residential gas-fired oven, usually combined with a broiler and/or rangetop, is a familiar appliance. Due to its simplicity and large population, the residential oven has been considered in this study for IR burner application. The physical and economic comparisons that follow, however, are for commercial size ovens which are more likely to have economic advantages when employing IR burners.

A typical commercial oven consists of an insulated enclosure heated from below by one or more burners. The enclosure is insulated on four sides and the top to control heat losses. The burner flame impinges on the bottom surface of the oven or on an intermediate surface to avoid high temperatures below the baking foods. Temperature control is by thermostat. The combustion products usually pass through slots in the oven bottom into the enclosure, travel up along the interior of the oven walls, and exhaust through a vent at the rear of the appliance. To aid circulation, avoid nonuniform temperatures, and decrease cooking time, room air is circulated into the enclosure with the burner products, drawn in by the natural draft of the system. This added room air is important to the quality of the baked food and is used to even greater advantage in convection ovens which induce large amounts of circulation by electric blowers.

The application of either perforated tile or fiber matrix porous refractory IR burners can be envisioned for the commercial oven. The burners would provide very uniform heating at the bottom of the compartment. It may be desirable, however, to include a double heat transfer wall between the burners and enclosure to prevent temperature nonuniformities resulting from the high heat transfer rate from the IR burners. This requirement would lessen any advantages that could be derived from the transfer of radiative energy. Some appliance efficiency increase is expected, however, from the IR burners' capability for operation at lower levels of excess air. The IR burner controls would operate analogous to those of conventional gas ovens with a thermostat controlling on/off cycling of the burners.

Although infrared burners have been applied to nearly all gas-fired cooking appliances, the oven appears to be a notable exception. Interest has been expressed, however, by manufacturers of commercial equipment contacted during the study.

BROILER

In commercial applications, the broiler may either be combined with an oven or rangetop or found as a stand-alone unit. It may be free standing or countertop supported and have one or more separate compartments. All broilers use one or two basic firing arrangements: over-fired or under-fired. Over-fired broilers are the most common and direct radiant energy to cook foods from above. The under-fired broiler was developed primarily for cooking meat, using an open flame from below to produce a seared cooking pattern. The under-fired broiler has not been considered in detail in this study due to its limited use.

Food in an over-fired broiler is placed on a grill (grid) several inches below the burners. This distance is adjustable to accommodate different heating rates. On commercial broilers, the grid usually rolls out for easy access to the entire cooking area. A pan at the bottom of the compartment catches drippings from the food and can be removed for cleaning. Blue flame burners direct a flame across the under-side of a ceramic or metallic surface. Heat transfer to the food is primarily from flame radiation. Infrared radiant burners are also in use on some marketed broilers.

An infrared over-fired commercial broiler has been conceptualized in this study. The concept uses two infrared rayheads, fed by a premixed gas-air mixture. Combustion air is supplied by a blower such that the burners can be totally premixed and operate at low excess air. The side by side IR burners would provide very uniform radiant heat to the food, with approximately 40 percent of their energy release as infrared radiation. Heatup rates and operating characteristics are expected to be comparable to units with blue flame burners. The porous ceramic contained in the burners could be either perforated tile or fiber matrix. A common problem with commercial broilers, however, occurs when cooking utensils come in contact with the burners. The perforated tile can stand some abuse, but the matrix material would almost certainly be damaged. Therefore, use of the fiber matrix burner would require a protective screen over the burner material.

The first report of a broiler incorporating infrared burners appeared in 1947 (Reference 7). AGA reported good operating characteristics for one demonstration unit, but troubles with the durability of the porous ceramic radiator and the higher initial cost of the unit apparently prevented commercialization. As the advantages of using radiant burners for broilers became better understood, the economics of owning an IR broiler began to change. Anetsberger Brothers Incorporated, The Montague Company, and South Bend Range Company all currently manufacture IR broilers. The success of these units demonstrates the effectiveness of infrared broiling. Currently, the thermal efficiency and emissions characteristics of these appliances are unknown, however, and there may be potential for significant improvements.

DEEP FAT FRYER

The deep fat fryer represents major sales in the commercial appliance market and therefore accounts for a significant quantity of natural gas consumption. A fryer consists of an oil tank in which the food is immersed and a burner system for bringing the frying oil to the proper temperature. Current fryer designs are of two possible arrangements:

1. Heated tank, with burners heating the exterior walls of the oil tank
2. Immersion tube, with burners firing through tubes that are immersed in the tank

The heated tank design enjoys the largest share of the current market, but immersion tube fryers are a significant percentage.

Most frying is performed at oil temperatures of 450K to 500K. The temperature in the tank is controlled by a thermostat set by the operator. There may also be a temperature limit control to avoid over-heating of the oil which can result in decomposition of the fat. Due to the relatively large firing rate, high oil temperature, and small amount of available heat transfer surface area, deep fat fryers have characteristically high flue gas temperatures, often exceeding 800K. The high flue temperature limits the appliance efficiency to 40 to 50 percent.

The infrared fryer can result in increased appliance efficiency by operation of the burners at lower excess air levels and by increasing heat transfer surface area downstream of the burners. In any fryer design, it is also important to consider durability, simplicity, ease of cleaning and servicing, gas consumption, ease of operation, product quality, heatup speed, capacity for heavy duty frying, life and turnover rate of oil, and space requirements. These factors have been considered for both the heated tank and immersion tube fryer designs. A typical infrared burner concept for the externally heated deep fat fryer has been developed by AGA Laboratories (Reference 2) and is not described here in detail.

A conceptual infrared immersion tube fryer is shown in Figure 2. Three tubes pass through the oil tank with a cylindrical fiber matrix burner held concentrically within each tube. The fiber matrix burners are expected to provide greater heating uniformity of the immersion tube, preventing hot spots which contribute to the breakdown of the frying oil. The concept of Figure 2 also includes increased heat transfer surface area. This is accomplished by passing the combustion products from the immersion tubes back toward the front of the appliance in a plenum below the tank and back along the tank walls to a rear vent opening. The greatly increased heat transfer area would reduce the exhaust temperature to near the oil temperature (450K) and significantly increase appliance efficiency.

The AGA-developed heated tank fryer is one of two known IR fryer applications. It utilizes perforated tile burners and a second pass of the exhaust products along fryer walls to increase efficiency. The unit is currently approaching commercialization. The second application is a heated tank fryer currently marketed by Frymaster Incorporated. Direct fired IR burners are employed. A slight efficiency increase may be inherent in the design due to the use of IR burners, but no emission benefits are expected. The appliance has seen wide application.

WATER HEATER

There are two basic designs of currently available water heaters: the storage-type and the instantaneous-type. The former design is by far the most popular in the U.S., storing heated water in an insulated tank until drawn off by the user. In contrast, the instantaneous water heater has essentially no storage capacity, using a compact coil heat exchanger and high capacity burner to provide the required water temperature rise during a single pass through the system. Both types of heaters use gravity-fired (naturally aspirated) gas burners, usually of the circular-body, multiport design. The steady state recovery efficiency of the instantaneous heater is greater than that of the storage-type, due mostly to smaller jacket losses. The instantaneous-type also usually has a considerably larger heat input rate than the storage type. The main cause of efficiency reduction in both types of heaters is flue loss (sensible and latent heat losses), usually about 25 to 30 percent of the heat input.

Infrared water heater designs were conceptualized for both heater types during the study. Since the storage heater is most popular, the storage heater concept is described in Figure 3. The concept includes a condensing, counterflow heat exchanger on the flue outlet to provide added appliance efficiency. The burner is a cylindrical fiber matrix burner with controls similar to existing designs. Its low excess air capabilities should increase system efficiency while simultaneously providing low emissions. The additional condensing heat exchanger can potentially bring total thermal efficiency to over 95 percent.

Very little past work has been done on developing an IR water heater. The Institute of Gas Technology (IGT) has developed units for natural gas and hydrogen combustion, but commercialization has not been achieved for these systems.

ROOM HEATERS

Room heaters are used to heat a single room or other small portions of a living or working space. This discussion centers on nonportable, permanently wall-mounted heaters.

Gas-fired room heaters are generally classified into vented and unvented types. In the vented type, a conventional atmospheric burner is enclosed in an air cooled (forced or natural draft) heat exchanger. This allows the flue products to be contained and eventually conducted outdoors. Combustion air comes from the outside, so the heater does not consume room oxygen. Because of the small amount of heat exchanger associated with this type of heater, its thermal efficiency is usually lower than a conventional central warm air furnace. However, in some circumstances this type of heater may save fuel compared to a central heater because it has fewer duct and cyclic losses. Since the device heats only one room rather than the entire house or commercial establishment, losses are further reduced. In contrast to the vented room heater, the unvented type releases all of its input energy into the space to be heated. This includes both the radiation from the flame and the hot flue products. Although the unvented heater is an efficient method of warming a room, its widespread use may be retarded due to current uncertainty in venting requirements.

Both vented and unvented IR room heaters have been conceptualized. The vented heater is designed to be mounted through the wall of an individual room with the combustion and circulating air inlets and the exhaust outlet on the outside of the building. The unit uses a low excess air, low emissions fiber matrix infrared burner for maximum efficiency and reduced air pollution and can be thermostatically controlled. The unvented heater concept also uses a cylindrical fiber matrix burner. In this case, however, the flue gas passes into the room rather than being vented outside, and the room occupants are directly exposed to the IR radiation from the burner. As a result, the thermal efficiency of this heater is essentially 100 percent.

Many infrared unvented room heaters are currently available. However, further R&D is required to achieve low CO and NO_x emissions from these appliances. In contrast, only minimal development has been performed on vented IR heaters. In the mid-1960's, AGA Laboratories tested several novel vented concepts (Reference 8) which apparently did not achieve commercialization. Another prototype vented room heater, using a high temperature fiber matrix burner, was developed in the early 1970's by W. D. Teaque for the Southern California Gas Company. Known as the Mini-Cal, this unit was not commercialized, although the inventor has apparently been successfully operating one of them for the past 10 years.

CENTRAL WARM AIR FURNACE

There are generally three types of residential and commercial forced air furnaces. Upflow, downflow, and horizontal. There is little variation among manufacturers in the overall layout. For an upflow unit, the house circulating air enters the bottom of the unit, flows through the main circulating fan, then to the heat exchanger and usually out the top to the distribution ducting. The gas burners are naturally aspirated, Bunsen-types consisting of three to four venturis, with distribution pipes consisting of rows of small orifices. The primary air is drawn into the venturi by the gas pressure and premixes with the gas prior to ignition. The primary air/fuel ratio can be controlled to some extent by small shutters at each venturi. Secondary air from the furnace room enters around the burners to quench the peak flame temperature and allow complete combustion. Secondary air flow cannot be controlled, which limits the ability to modify the furnace's emissions and efficiency. The flue products then proceed upward through a parallel flow sectional heat exchanger and exit into a common plenum. Units always include draft diverters which dilute the flue gas stream and prevent down drafts from blowing out the pilot.

An infrared warm air furnace concept with condensing heat exchanger and perforated tile burners has been developed. This concept, shown in Figure 4, uses a heat exchanger system similar to that used in some conventional oil-fired furnace designs. A drum-type heat exchanger encloses two powered infrared perforated tile burners which are mounted in standard rayheads. The drum acts as the radiative section, keeping the burners at their recommended operating temperature and accounting for over 50 percent of the total heat transferred in the system. The exhaust gas from the burners passes into the upper manifold. From there the gas is distributed to the six (three on each side of the drum) sectional heat exchangers. The gas passes down through these sections in counterflow to the circulating air coming from the fan below, thus providing sufficient surface area and temperature drop to cause condensation. The condensate is collected in the lower exhaust manifold and drained away. The combined IR burner and condensing heat exchanger can potentially raise appliance efficiency to above 95 percent.

Several R&D projects have focused on developing an IR warm air furnace. In the mid-1970's, an inventor named Bratko developed a prototype 84.4 MJ/hr residential furnace using a cylindrical fiber matrix burner made from Johns-Manville fibers. In performance tests by the U.S. Environmental Protection Agency (Reference 9), this furnace's efficiency was 80 percent and its NO_x emissions were less than 17 ppm (air-free) at a nominal operating point of 10 percent excess air. Although this furnace apparently operated successfully in the inventor's home for a number of heating seasons, it did not achieve final commercialization.

Another warm air furnace using an infrared burner is the Amana Corp. HTM ("Heat Transfer Module") unit. This device combines both heating and cooling functions. In its heating mode, the powered burner transfers its heat by radiation and convection to a finned tube heat exchanger containing an ethylene glycol/water mixture. The burner is a powered, metallic screen IR burner formed into a cylinder. Emissions testing of ths unit (Reference 10) under steady state conditions showed average NO_x emissions comparable to the Bratko furnace -- only 17 ppm, which corresponds to 9 ng of NO_x per Joule of useful heat. However, the unit's CO emissions were a factor of 10 higher than the

Bratko unit, but still well under the AGA limit (400 ppm at half load). The Amana furnace was on the market several years ago but was removed from sale due to reliability problems. It is apparently being modified by the manufacturer for re-release sometime in the future.

Another IR warm air furnace is currently being developed by Acurex Corporation for the Southern California Gas Company. This condensing furnace uses a fiber matrix burner and has achieved good emissions and efficiency performance.

INFRARED APPLIANCE BENEFITS

All eight IR appliance concepts formulated appear technically feasible. To evaluate their commercialization potential, comparisons of expected fuel consumption, emissions, and economics were performed.

Appliance thermal efficiencies vary with type, size, and design. In cases where data were not available, assumptions were made for efficiency based on knowledge of flue gas temperatures and other thermal losses. The greatest potential for efficiency gains with the use of IR burners is by operation at lower excess air. Additional increases may occur in some appliances due to the increased heat transfer intensity from the IR burners. A third efficiency benefit can be achieved independent of IR burner application. An increase in heat transfer surface area in those appliances that utilize convective heat transfer can further reduce the flue temperature. This latter effect has been considered in conjunction with IR burner implementation for the deep fat fryer, water heater, and warm air furnace concepts.

To determine potential emissions reductions due to IR burners, conventional appliance emissions were investigated first. Emissions of all conventional appliances are similar, due to the similar operating conditions of their Bunsen-type burners. The infrared burner emissions for various types of porous refractory materials have been quantified in other studies and were used to calculate the percentage reductions of CO and NO_x possible through IR burner implementation.

To compare costs of ownership of the dissimilar conventional burner and IR burner appliances, the Equivalent Uniform Annual Cost and Discounted Payback methods of economic analysis were used. The initial costs of the appliances were calculated from the difference in component cost between the two. A typical firing rate, yearly operating time, and a 10-year lifetime were assumed for all appliances. Additional assumptions were made regarding utility cost escalation factors, annual maintenance costs, and salvage value.

Table II summarizes the efficiency, emissions, and economic benefits foreseen for each of the appliances considered in the study. The four commercial cooking appliances have the greatest potential for efficiency increases due to the use of infrared burners alone because they are designed with very little convective surface area and consequently have relatively low thermal efficiencies. The rangetop and deep fat fryers appear most attractive for further development. For the higher efficiency appliances -- the water heater, room heater, and warm air furnace -- some efficiency gain can also result from the use of IR burners alone. The greatest benefit, however, can be realized from an increase in the convective heat transfer surface area. Up to 25 percent increases in steady state efficiency may occur for the water heater and warm air furnace if a condensing heat exchanger is used.

Since infrared burners are relatively low in both CO and NO_x emission levels, the percentage decrease of these pollutants for each appliance is proportional to the amount emitted by the conventional burner appliance. Because their conventional counterparts emit relatively high concentrations of CO, only the IR rangetop, oven, and broiler would have possible CO emissions reductions. The CO emissions of the other conventional appliances are already low, and IR burners would achieve no further reduction. In contrast, since the NO_x emissions for all residential and commercial appliances are near 100 ppm, a significant reduction of 80 to 90 percent should be achievable by using IR burners in all appliances. Of course, the CO and NO_x emission factors, calculated in terms of useful heat output, will be reduced as a result of the higher IR appliance efficiencies.

TABLE II. SUMMARY OF INFRARED APPLIANCE BENEFITS

Appliance	Thermal Efficiency		Emissions		Economics		
	Conventional[1] (%)	Infrared (%)	Conventional CO/NO_x (ppm)[2]	Infrared CO/NO_x Concentration Reduction (%)[3]	Conventional EUAC ($)	Infrared EUAC ($)	Infrared Payback (yrs)
Rangetop	40 - 50	50 - 60	130/100	88/80	1,750	1,655	3.1
Oven	40 - 50	50 - 60	90/95	83/79	482	483	10.0
Broiler	40 - 50	50 - 60	90/95	83/79	727	708	5.4
Deep fat fryer	40 - 50	50 - 70[4]	20/100[5]	0/80	1,236	1,081	1.4
Water heater	70 - 80	95[4]	10/100	0/90	1,347	1,150	3.2
Room heater							
• Vented	55	65 - 70	8/140	0/90	160	170	10.0
• Unvented	100	100	--[6]	--	--[7]	--	--
Warm air furnace	70 - 80	95[4]	14/95	0/90	1,370	1,140	2.9

[1] Assumes operation at 80 percent excess air
[2] Emissions on an air free basis
[3] Based on projected IR burner emissions of 15 ppm CO and 20 ppm NO_x
[4] Include additional convective heat exchange area -- condensing operation for water heater and furnace
[5] Assumed values, data not available
[6] Data not available
[7] No calculation performed due to lack of efficiency benefits

Appliances with the greatest efficiency increases are correspondingly the most economically advantageous. In future years, with gas prices increasing at an expected 15 to 20 percent per year, the higher appliance initial cost will be quickly paid back due to savings in gas consumption. The infrared rangetop, deep fat fryer, water heater, and warm air furnace concepts would all pay back in approximately three or fewer years of ownership.

CONCLUSIONS AND RECOMMENDATIONS

Based on the projected benefits of the eight infrared appliances studied, the rangetop, deep fat fryer, water heater, and warm air furnace are the most attractive for further development. Of the two cooking appliances, the deep fat fryer has the greater efficiency and economic advantages. Before a development program for any appliance is undertaken, however, consideration should be given to existing similar applications or R&D efforts. The heated tank deep fat fryer, for example, has been developed in two previous programs. The infrared immersion tube fryer has not been addressed, nor are there any currently known infrared rangetop development programs. R&D programs on the two heating appliances, the water heater and the warm air furnace, could both result in very high efficiency infrared units.

REFERENCES

1. Belles, F., et al. Measurement and Reduction of NO_x Emissions from Natural Gas-Fired Appliances. American Gas Association, presented at the 68th Annual APCA Meeting, June 1975.

2. Kesselring, et al. Infrared and Catalytic Burner Technology Assessment. GRI-80/0019, November 1980.

3. Guilfoyle, J. Roger. From the Ground Up, Industrial Design. November 1968.

4. Scholar, Niels E. EPA Van Operational Manual. EPA-600/9-76-020, August 1976.

5. Griffiths, J. C., et al. New or Unusual Burners and Combustion Processes. American Gas Association Laboratories Research Bulletin 96, August 1963.

6. Rice, Richard E. and Charles W. Peterson. Flameless Combustion and Method of Operation. U.S. Patent No. 4,189,294, February 1980.

7. Anon., Study of Possibilities of Heating Contemporary Gas Food Service Equipment with Power Burners. American Gas Association Testing Laboratories, Research Report 1090, September 1947.

8. DeWerth, D. W., et al. New and Improved Methods of Heating Localized Areas in and Around the Home. American Gas Association Research Bulletin 99, February 1964.

9. Martin, G. B. Evaluation of a Prototype Surface Combustion Furnace. EPA/600-7-79-038, February 1979.

10. Lange, H. B. Emissions Testing of an Amana EPCG Forced-Air Heating Unit. Prepared by KVB, Inc. for Southern California Gas Company, October 1979.

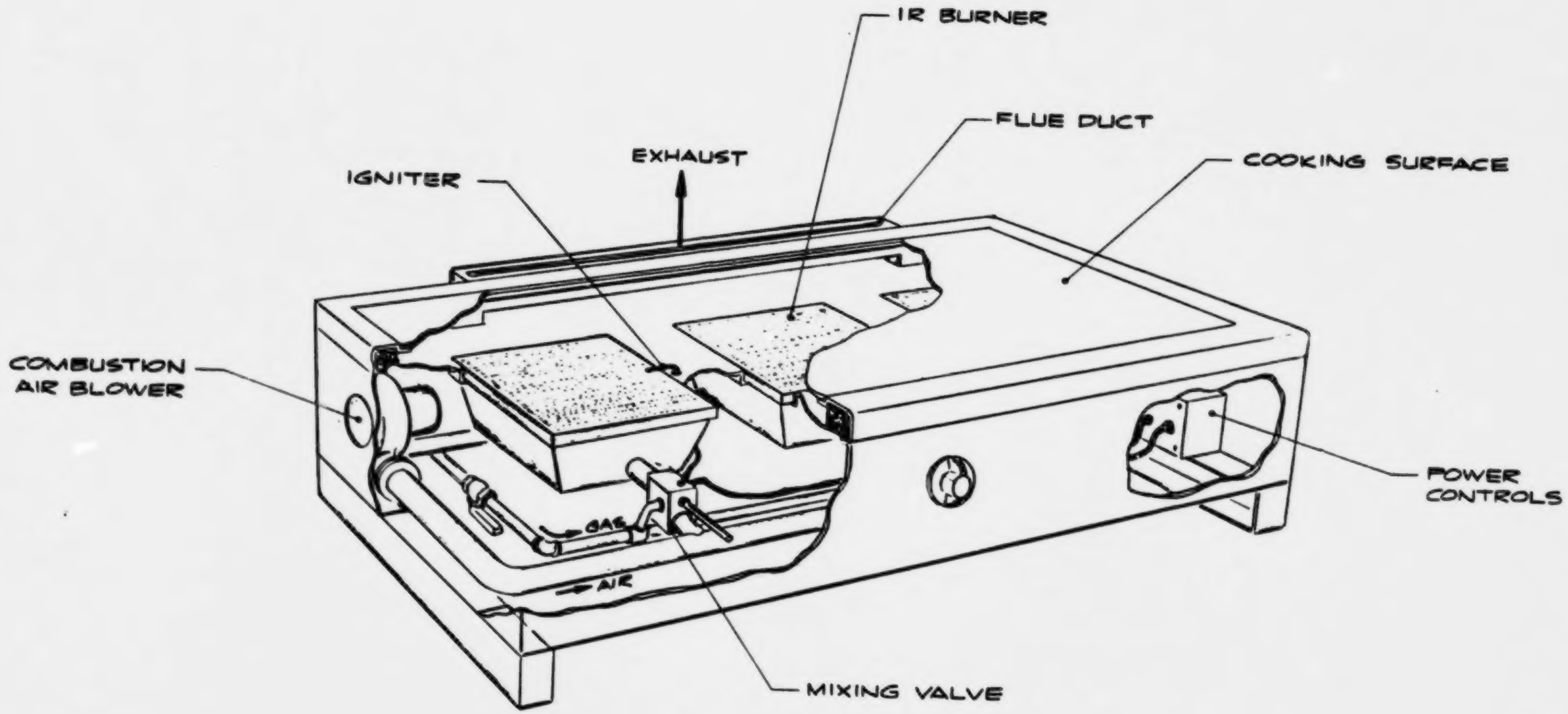
IR BURNER
FLUE DUCT
EXHAUST
IGNITER
COOKING SURFACE
COMBUSTION AIR BLOWER
GAS
AIR
POWER CONTROLS
MIXING VALVE

Figure 1. Infrared rangetop.

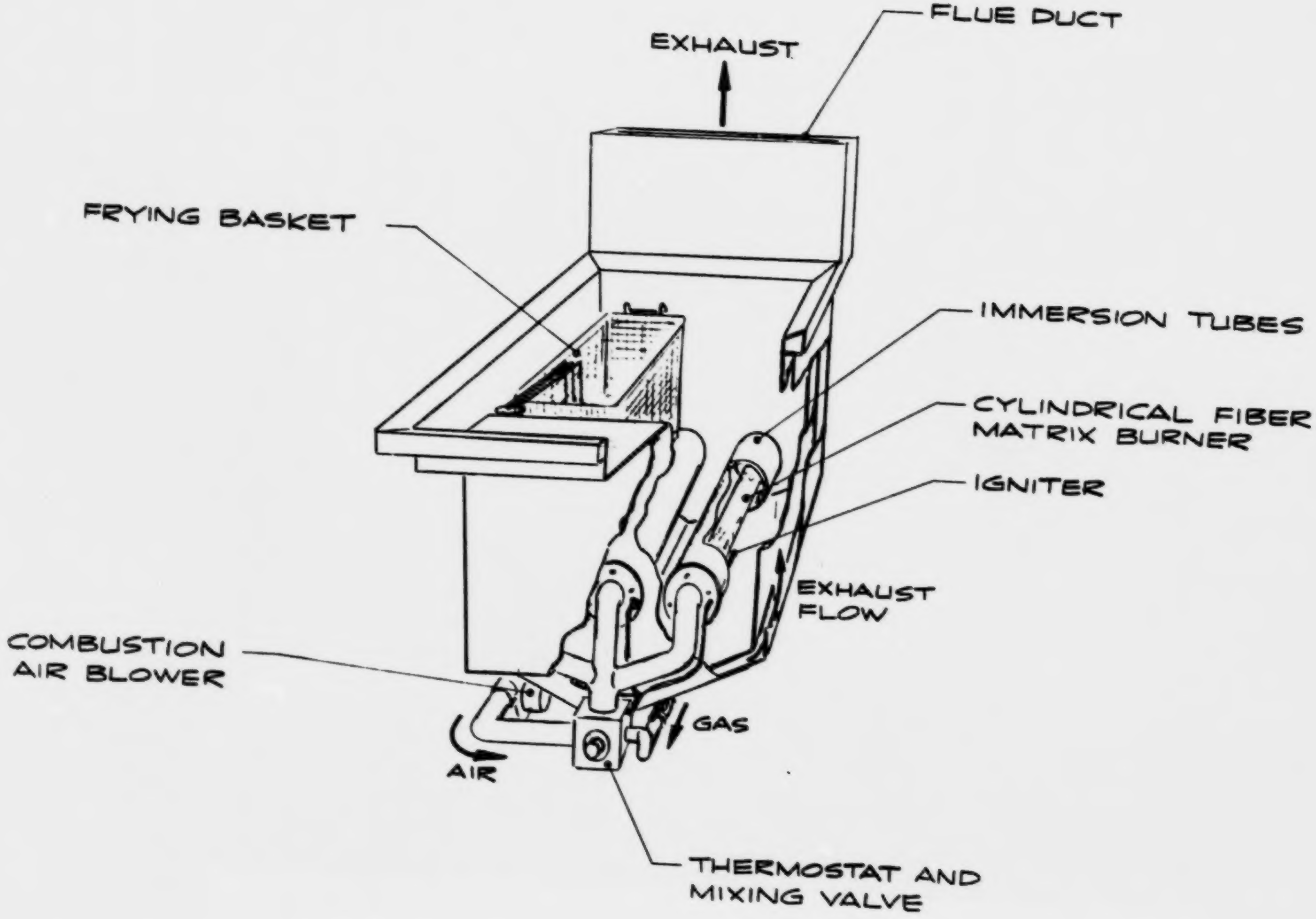
EXHAUST
FLUE DUCT
FRYING BASKET
IMMERSION TUBES
CYLINDRICAL FIBER MATRIX BURNER
IGNITER
EXHAUST FLOW
COMBUSTION AIR BLOWER
GAS
AIR
THERMOSTAT AND MIXING VALVE

Figure 2. Immersion tube infrared deep fat fryer.

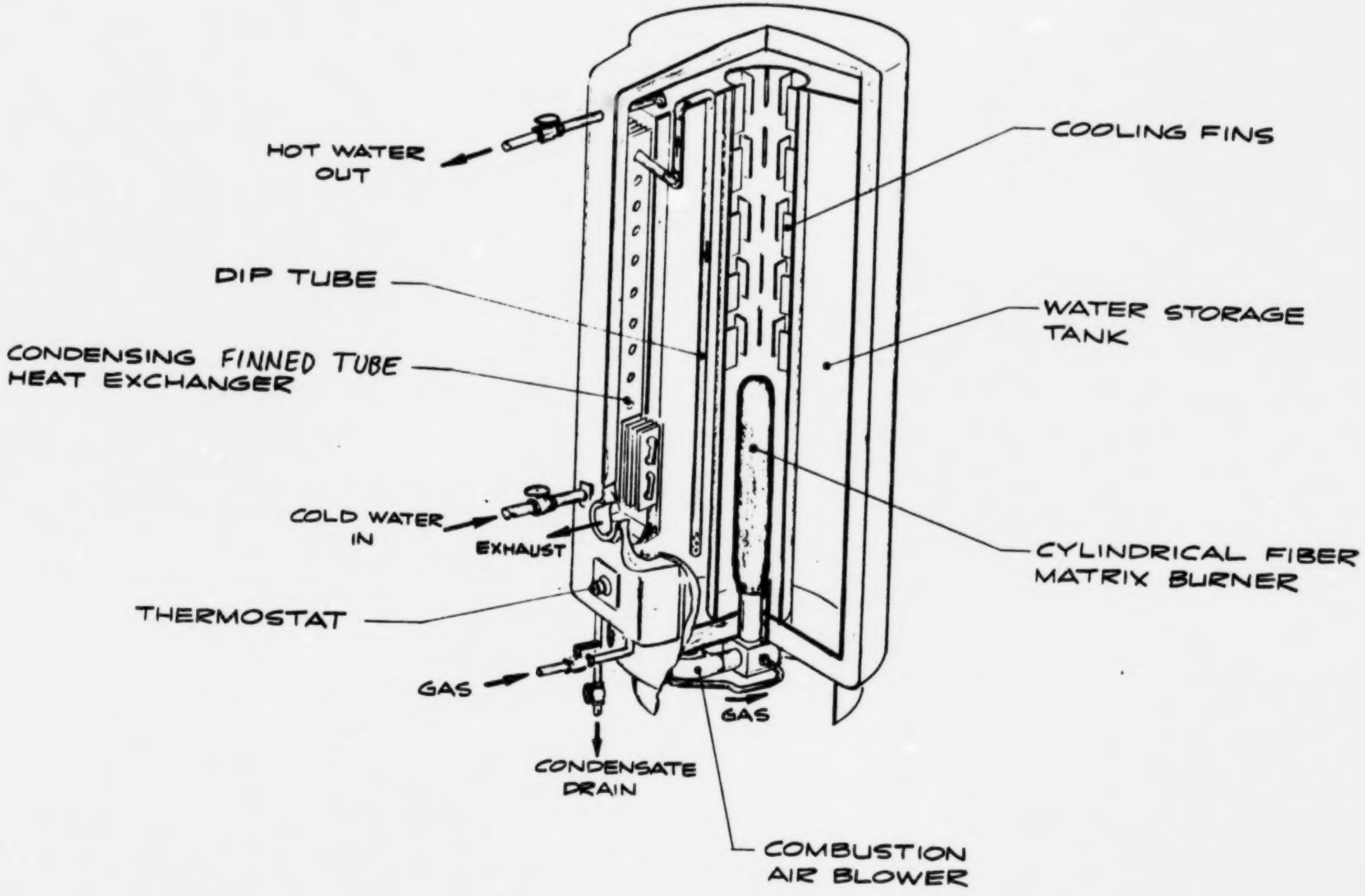
HOT WATER OUT
DIP TUBE
CONDENSING FINNED TUBE HEAT EXCHANGER
COLD WATER IN
EXHAUST
THERMOSTAT
GAS
CONDENSATE DRAIN
GAS
COMBUSTION AIR BLOWER
COOLING FINS
WATER STORAGE TANK
CYLINDRICAL FIBER MATRIX BURNER

Figure 3. Infrared water heater concept.

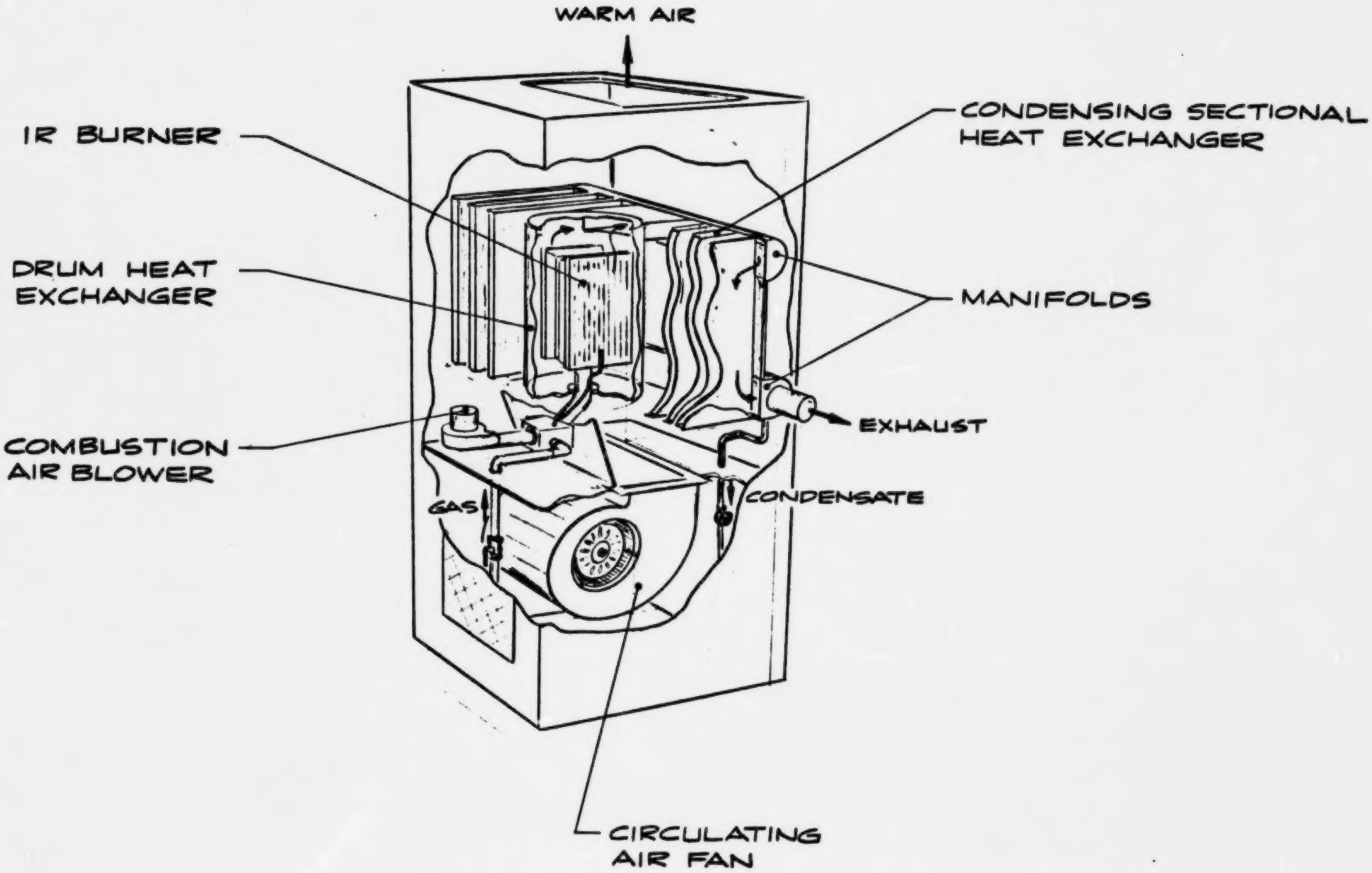
WARM AIR
IR BURNER
CONDENSING SECTIONAL HEAT EXCHANGER
DRUM HEAT EXCHANGER
MANIFOLDS
COMBUSTION AIR BLOWER
EXHAUST
GAS
CONDENSATE
CIRCULATING AIR FAN

Figure 4. Infrared warm air furnace.

CATALYTIC COMBUSTION FOR GAS TURBINES

by

H. Fukuzawa, Y. Ishihara and Y. Hasegawa
Energy and Environment Laboratory
Central Research Institute of Electric Power Industry
Komae-Shi, Tokyo 201, Japan

ABSTRACT

The CRIEPI R&D program on catalytic combustion for gas turbine combustors includes the development and evaluation of catalysts, determination of optimum operating conditions for combustibility and flue gas composition, and development of a model catalytic combustor. The last stage of the program is to develop a prototype low NO_x catalytic combustor for a high temperature gas turbine.

The advantages of catalytic combustion are as follows: i) complete combustion at low temperature, ii) extremely low emission of thermal NO_x, iii) stable combustion at wide range of fuel/air ratio.

The characteristics of catalytic combustion under atmospheric pressure and pressurized atmosphere were investigated using in-house manufactured catalysts. A part of the catalytic combustion tests under pressurized atmosphere was sponsored by the Agency of Industrial Science and Technology of the Ministry of International Trade and Industry.

The results are summarized as follows:

1. Thermal NO_x formation was reduced to as low as below 20 ppm at 1000 - 1500°C under 1 - 8 atm.
2. Complete catalytic combustion was achieved at 1100 - 1500°C under 1 - 8 atm.
3. The volumetric heat release rate increased as the combustion temperature, fuel flow rate and combustion pressure were raised, and more than 1300 x 10^6 kcal/hr-m^3-cat was obtained at 1500°C under 8 atm.

INTRODUCTION

The CRIEPI R&D program on catalytic combustion was intended to connect with the national project on the development of a high efficiency gas turbine for NO_x control. The program includes experiments on catalytic combustion under 1 - 8 atm in 1981 and the development of a model catalytic combustor in 1982. The objective of this program is the application of catalytic combustion technology to a high temperature gas turbine combustor to reduce NO_x formation. CRIEPI is conducting research in the following areas according to the R&D schedule shown in Table I.

1. Development and selection of catalysts
    (1) High operating capability
    (2) Combustion rate of fuels with each catalyst
    (3) Catalyst life at high temperatures
2. Operating conditions and flue gas compositions
    (1) Catalytic combustion under atmospheric pressure
    (2) Catalytic combustion under pressurized atmosphere
3. Model catalytic combustor tests for gas turbines
    (1) Development of a model catalytic combustor
    (2) Describing characteristics of a model catalytic combustor
    (3) Design of a full scale catalytic combustor

EXPERIMENTAL CATALYTIC COMBUSTION UNDER ATMOSPHERIC PRESSURE AND PRESSURIZED ATMOSPHERE

EXPERIMENTAL APPARATUS

The experimental apparatus for catalytic combustion under atmospheric pressure and pressurized atmosphere used in this investigation were constructed in 1979 and 1980, respectively. These apparatus consisted of a blower or a compressor, a catalytic reactor and a gas cooler. The specifications of these apparatus are shown in Table II.

LPG fuel was supplied from a cylinder, premixed with preheated air and sent into the reactor at a uniformly controlled velocity. The premixed fuel was oxidized completely on the catalyst surface, settled in the middle of the reactor, and expected temperatures were obtained by controlling fuel/air ratios. Gas temperatures were determined at positions upstream and downstream, and also the catalyst surface temperature was determined by PR thermocouples. Flue gas analyses of NO_x, UHC and CO were made separately by NDIR method analyzers, and the analysis of O_2 was made by paramagnetic method analyzer.

Most of the catalysts used in the tests under atmospheric pressure were monoliths 82 mm in diameter and 75 mm in length, including 25 mm long segments. Also most of the catalysts used in the tests under pressurized atmosphere were monoliths 25 mm in diameter and 150 mm in length, and 50 mm in diameter and 50 mm in length, including 25 mm long segments. These monoliths consisted of a 2.8 mm square cell mullite substrate washcoated with γ-alumina. Platinum catalysts were loaded on them.

THERMAL NO_x FORMATION

The maximum inlet temperature of the gas turbine is expected to be increased to 1300 - 1500°C by the national project on high efficiency gas turbines. Therefore, catalytic NO_x reduction FGT equipment will be installed for reducing NO_x, assumed to be formed at several hundred ppm.

With the objective of eliminating the FGT equipment, CRIEPI has started an R&D program on catalytic combustion technology. In experiments under 1 - 8 atm, we have confirmed the low thermal NO_x emission.

NO_x concentration which corrected to 0% excess air increased as the combustion temperature raised under 1 - 8 atm, as shown in Figures 1, 2, and 3. As these figures also show, NO_x concentrations, which were not significantly affected by various factors such as premixed gas velocity, space velocity and combustion pressure, were as low as 20 ppm at below 1500°C.

UNBURNED HYDROCARBONS AND CARBON MONOXIDE EMISSION

Small amounts of unburned hydrocarbons, which were analyzed as total hydrocarbons, were emitted in the combustion temperature range from 900 - 1100°C under 1 - 8 atm, but not above 1100°C. Carbon monoxide was also emitted at 20 ppm or less in the range from 900 - 1100°C under 1 - 8 atm, not at above 1100°C under 1 - 8 atm. But both concentrations of unburned hydrocarbons and carbon monoxide increased greatly at temperatures below 900°C.

As a result, a combustion temperature of approximately 1000°C or more was required to keep stable catalytic combustion using LPG fuel under 1 - 8 atm.

COMBUSTION TEMPERATURE

In the catalytic combustor, the premixed LPG fuel is oxidized on the preheated catalyst surface without an igniter. The preheated temperature required for platinum catalysts was above 300°C for the ignition.

Combustion temperature was controlled by controlling the preheated air temperature and the fuel/air ratio. The catalyst surface temperature obtained was approximately 10 - 160°C higher than the combustion gas temperature at above 1200°C under 1 - 8 atm. In the experiments under 1 - 8 atm, the preheated air temperatures were decreased up to 200°C after the ignition at 480°C. But the stable catalytic combustion was continued at 1500°C.

PRESSURE DROP IN CATALYTIC REACTORS

In a catalytic reactor, the pressure drop, which is affected by various factors such as catalyst shape, premixed gas flow rate, and space velocity, was increased as the combustion temperature raised.

In this investigation at 1300 - 1500°C, the pressure drop was obtained 100 - 140 mm H_2O using 82 mm diameter monoliths under atmospheric pressure, and also the pressure drop was obtained 500 - 600 mm H_2O using 25 mm diameter monoliths under 8 atm.

VOLUMETRIC HEAT RELEASE RATE

The volumetric heat release rate was increased as the premixed gas flow rate, the premixed gas velocity and the combustion temperature increased.

In catalytic combustion it is possible to burn a large quantity of fuel because the combustion rate is extremely fast. That is, the maximum volumetric heat release rate obtained under atmospheric pressure was 137×10^6 kcal/hr-m^3-cat at 1500°C of combustion temperature, 2.07 of air/theoretical air ratio, 83×10^4 m^3/m^3.h of space velocity. Further the maximum volumetric heat release rate obtained under 8 atm was 1700×10^6 kcal/hr-m^3-cat at 1500°C of combustion temperature, 2.10 of air/theoretical air ratio, 137×10^4 m^3/m^3-hr of space velocity.

Figure 4 and Figure 5 show that the volumetric heat release rates were raised extensively as both the premixed gas flow rate and the combustion pressure increased. The above value of the volumetric heat release rate indicates the catalyst volume is small enough to settle in the combustor designed for high efficiency gas turbines.

ACKNOWLEDGEMENTS

The authors wish to thank the Agency of Industrial Science and Technology of the Ministry of International Trade and Industry in Japan for the admission of publication of this paper.

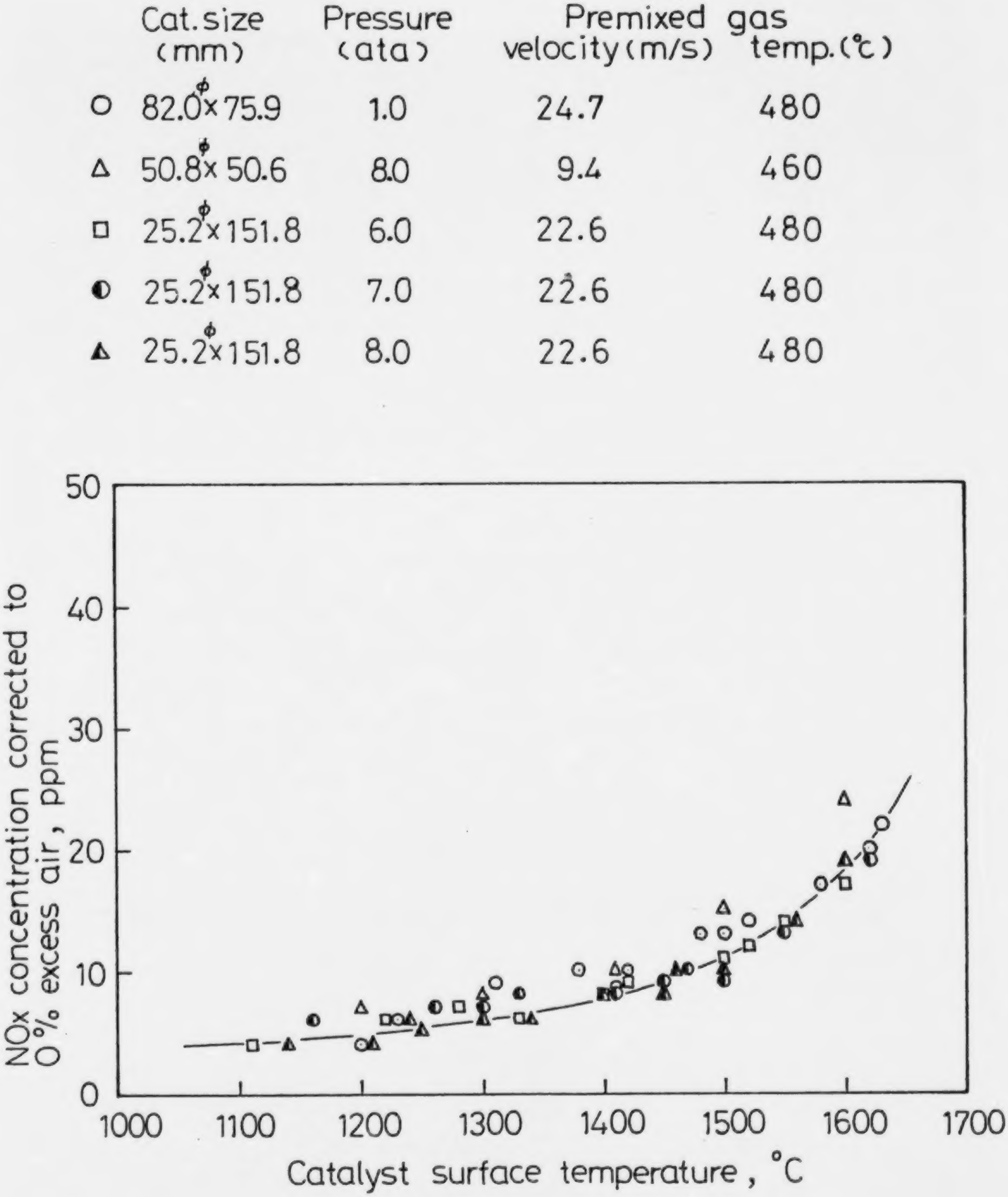

	Cat. size (mm)	Pressure (ata)	Premixed gas velocity (m/s)	Premixed gas temp. (°C)
○	82.0$^{\phi}$× 75.9	1.0	24.7	480
△	50.8$^{\phi}$× 50.6	8.0	9.4	460
□	25.2$^{\phi}$× 151.8	6.0	22.6	480
◐	25.2$^{\phi}$× 151.8	7.0	22.6	480
▲	25.2$^{\phi}$× 151.8	8.0	22.6	480

Figure 1. Thermal NO_x formation (1).

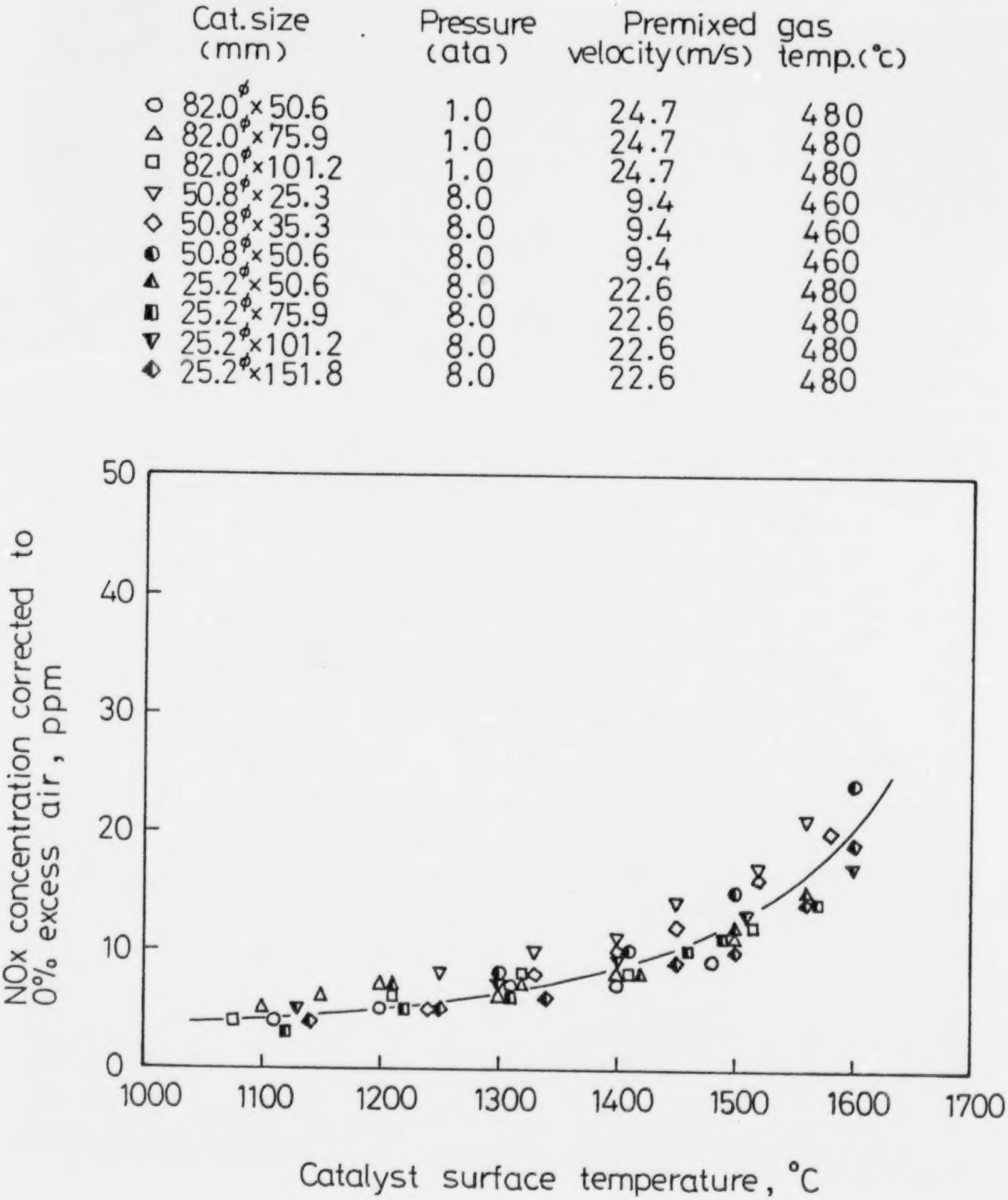

	Cat. size (mm)	Pressure (ata)	Premixed velocity (m/s)	gas temp. (°C)
○	$82.0^{\phi} \times 50.6$	1.0	24.7	480
△	$82.0^{\phi} \times 75.9$	1.0	24.7	480
□	$82.0^{\phi} \times 101.2$	1.0	24.7	480
▽	$50.8^{\phi} \times 25.3$	8.0	9.4	460
◇	$50.8^{\phi} \times 35.3$	8.0	9.4	460
◐	$50.8^{\phi} \times 50.6$	8.0	9.4	460
▲	$25.2^{\phi} \times 50.6$	8.0	22.6	480
◧	$25.2^{\phi} \times 75.9$	8.0	22.6	480
▼	$25.2^{\phi} \times 101.2$	8.0	22.6	480
◈	$25.2^{\phi} \times 151.8$	8.0	22.6	480

Figure 2. Thermal NO_x formation (2).

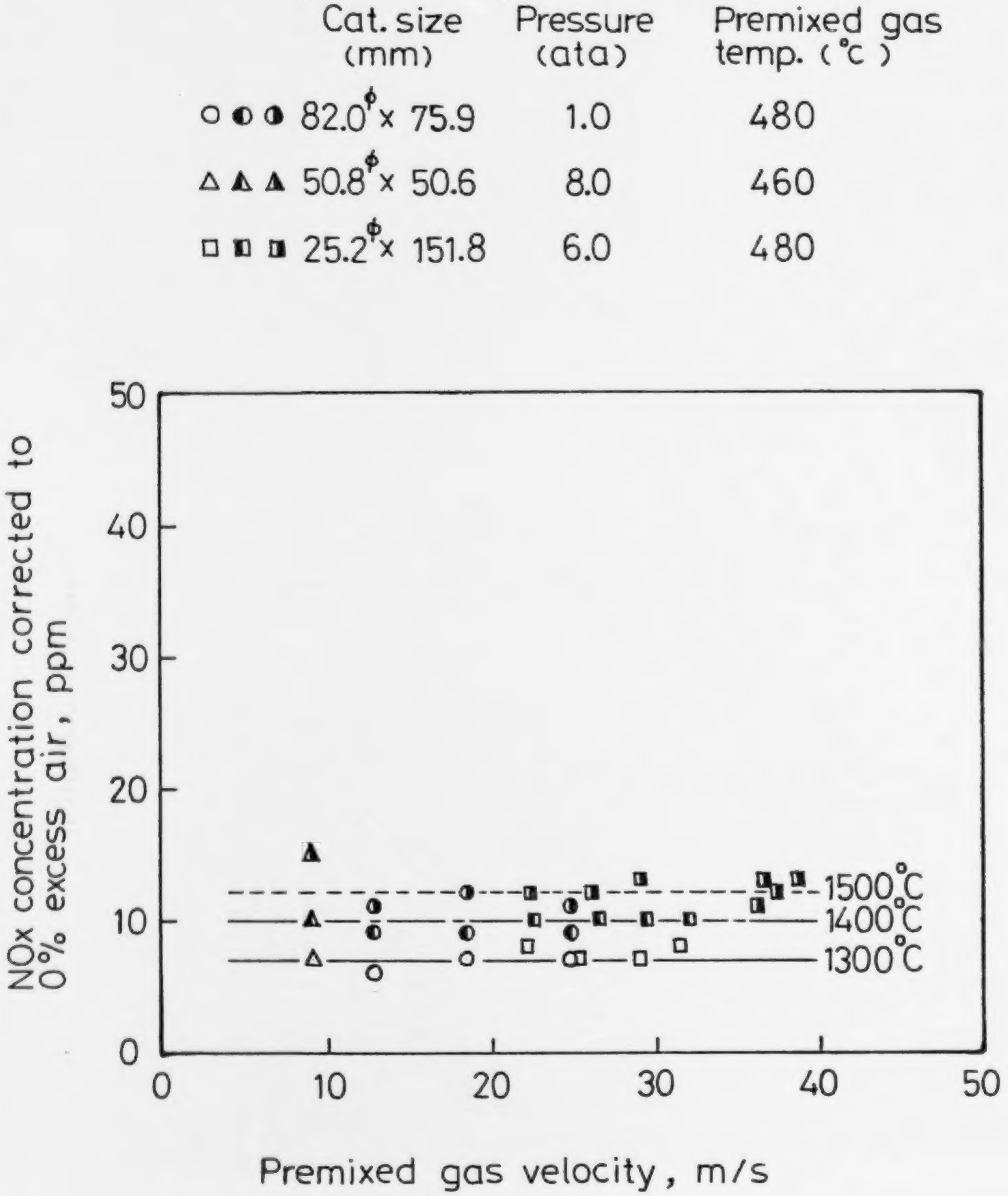

Figure 3. Thermal NO_x formation (3).

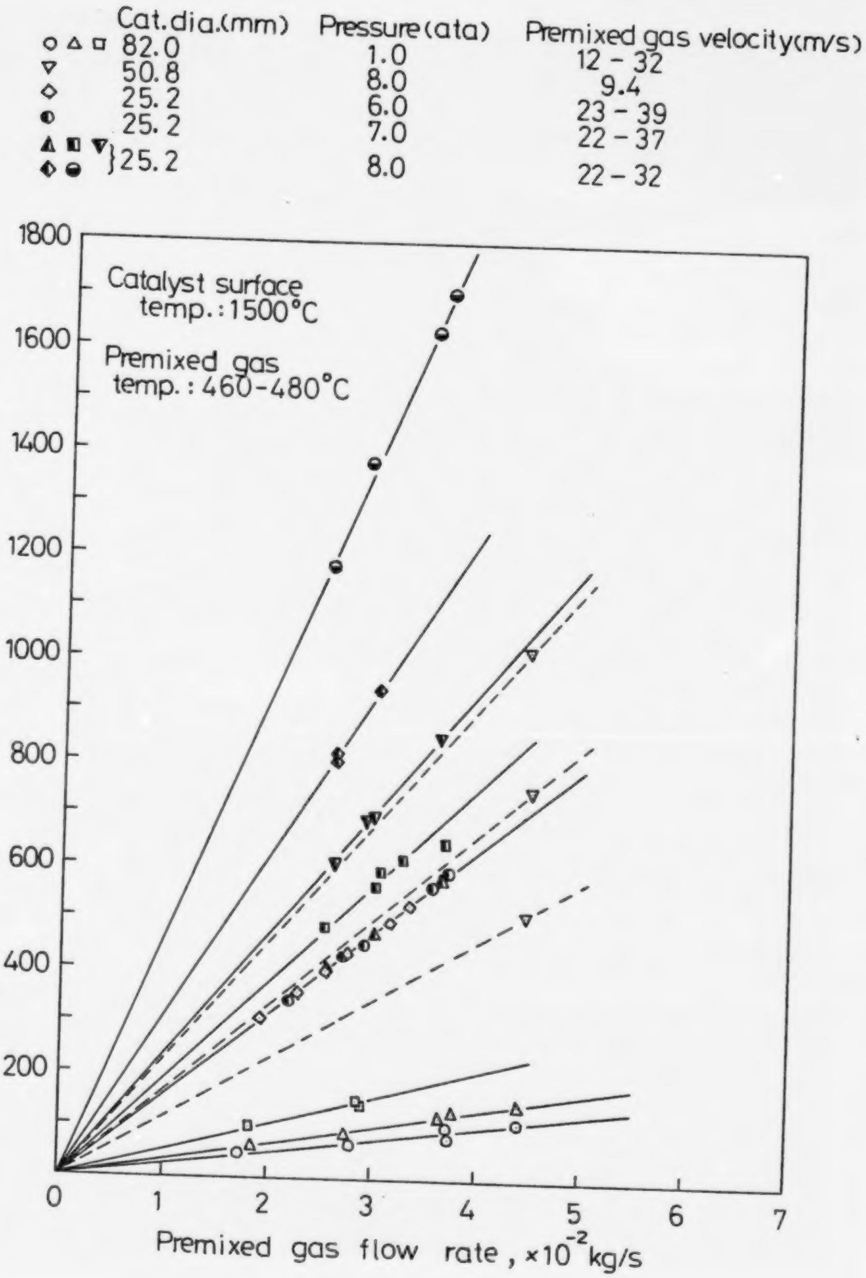

Figure 4. Relation between volumetric heat release rate and premixed gas flow rate.

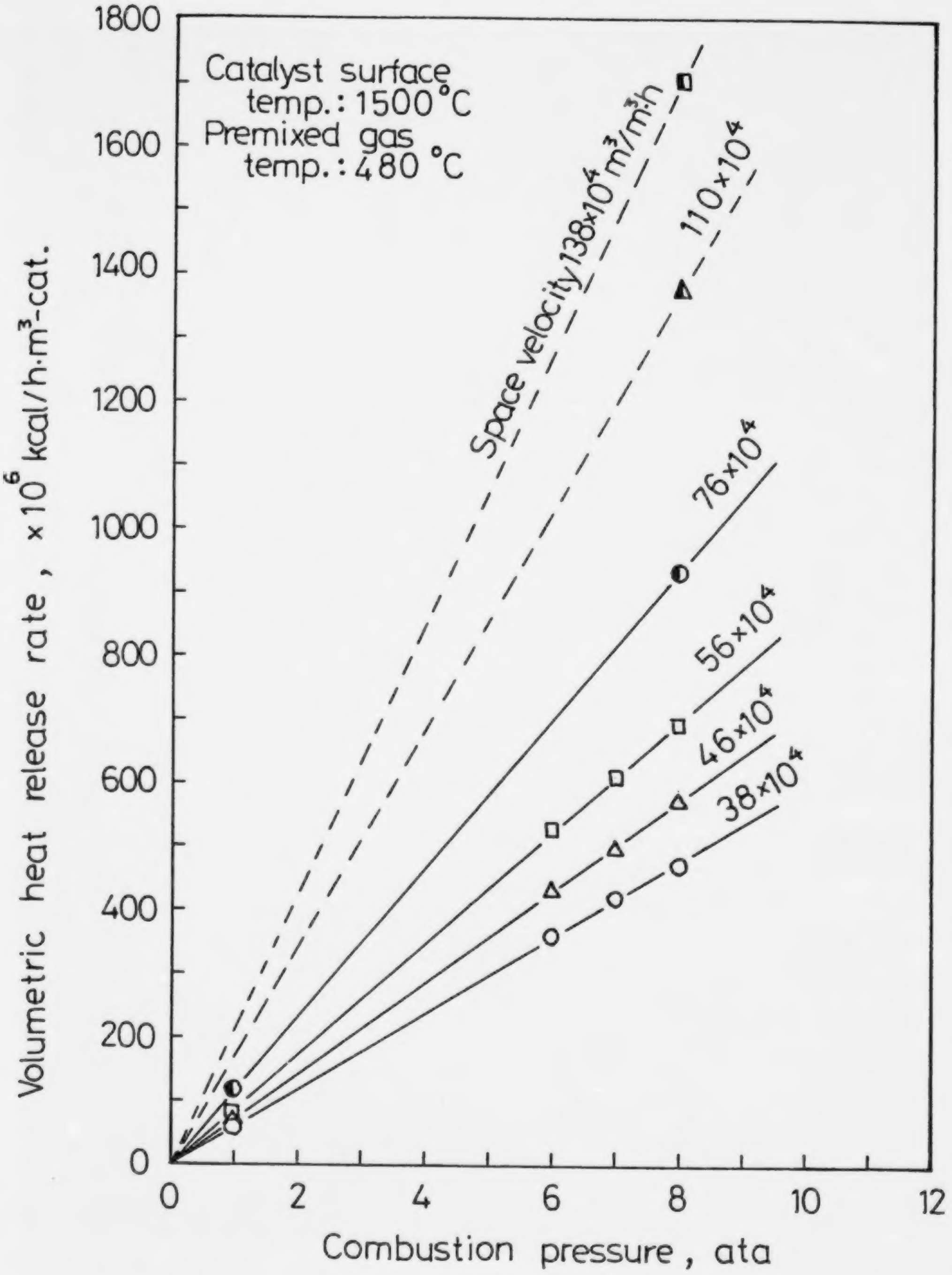

Figure 5. Relation between volumetric heat release rate and combustion pressure.

TABLE I. CRIEPI SCHEDULE FOR LOW NO_x EMISSION CATALYTIC COMBUSTOR PROGRAM

	Calendar Year			
	1979	1980	1981	1982
Development and selection of catalysts	▨	▨	▨	
Operating conditions and flue gas composition	▨	▨	▨	
Development of model catalytic combustor for gas turbine.			▨	▨

TABLE II. SPECIFICATION OF APPARATUS

	Atmospheric pressure type	Pressurized atmosphere type
Catalytic reactor		
Inside diameter (mm$^\phi$)	94	30 (55)
Maximum catalyst size (mm$^\phi$x mm L)	90 × 150	25×150 (50 × 150)
Combustion pressure (max. ata)	1	8
Air flow rate (max. Nm^3/h)	120	120
Fuel consumption (max. Nm^3/h)	2	4

DEVELOPMENT OF A CATALYTIC/RADIATIVE
WATERTUBE BOILER

by

M. A. Friedman, W. V. Krill, and J. P. Kesselring
Acurex Corporation, Energy & Environmental Division
485 Clyde Avenue
Mountain View, Calfiornia 94042

ABSTRACT

The development of a catalytic/radiative watertube boiler is continuing toward the prototype demonstration phase. Several small scale systems (2.64 x 10^8 J/hr) were designed and tested to establish the combustor radiant section geometry. An intermediate scaleup to a prototype small industrial sized boiler (1.055 x 10^9 J/hr) with steam generation was subsequently conducted. The results of these concept tests are reported.

Early tests with a staggered watertube/catalyst arrangement (separate watertubes and catalyst tubes) resulted in extremely low NO_x emissions (less than 2 ppmv) and a combustion efficiency of 37 percent. By eliminating cold exposed watertube surfaces with a concentric watertube/catalyst arrangement, the combustion efficiency was improved to 93 percent. However, increases in combustor operating temperature caused fracturing of the ceramic catalyst tube supports. This problem was resolved by using high strength, high thermal conductivity silicon carbide tubes. Several combustor section tube geometries were tested for high combustion efficiency and low thermal NO_x emissions. A close packed tube arrangement resulted in thermal NO_x emissions less than 20 ppmv at 110 percent theoretical air and 2.64 x 10^8 J/hr (250,000 Btu/hr) heat release rate. Combustion efficiencies greater than 99.9 percent were achieved with a 50 percent energy removal efficiency in the radiant section watertubes.

An intermediate scaleup to 1.055 x 10^9 J/hr (10^6 Btu/hr) was performed using a similar close packed concentric watertube/catalyst tube arrangement. The system incorporates an all-welded watertube and steam drum design for generation of low pressure steam in a naturally circulating cycle. A downstream adiabatic combustor with secondary air injection allows for staged combustion with distillate fuels. Initial testing with natural gas at 8.44 x 10^8 J/hr (800,000 Btu/hr) indicated a high combustion efficiency (greater than 99.9 percent) and thermal NO_x emissions of 30 ppmv at near stoichiometric conditions. Values of 10 ppmv or less are expected at 115 percent theoretical air.

A 3.69 x 10^9 J/hr (3.5 x 10^6 Btu/hr) scaleup to a small industrial sized watertube boiler is planned following completion of tests with the current design. Such a design would be packaged for operation on gaseous and distillate fuels at high combustion and energy removal efficiencies.

INTRODUCTION

Of an estimated 250,000 boilers installed in the United States each year, the majority are standard size watertube configurations with capacities of less than 113,400 kg of steam per hour (250,000 lbm/hr). The current emphasis in watertube boiler design is toward greater fuel flexibility, higher efficiency and reliability, and more stringent pollutant control. These objectives have been addressed primarily by increases in unit capacity, steam pressure and temperature, and refinements in heat transfer surface design, combustion control, safeguard equipment, and fabrication techniques. Control of particulates, oxides of sulfur, and oxides of nitrogen have been only a secondary consideration in design.

As pollution standards for stationary combustion sources become more stringent, particularly for oxides of nitrogen (NO_x), new combustion modification techniques will be required for the watertube boiler. Under Environmental Protection Agency Contract 68-02-2116, Acurex has investigated and developed catalytic combustion technology for application to stationary sources (Reference 1). Specifically, a radiative catalyst/watertube system and a catalytic two-stage combustor have been demonstrated with potential for watertube boiler applications. The current program has extended the development of small subscale systems to an intermediate-sized industrial boiler prototype with steam generation. These developments are discussed below.

SYSTEM CONCEPT

A 1.055×10^9 J/hr (10^6 Btu/hr) catalytic watertube boiler has been developed as a prototype to small industrial-sized boilers. Combustion occurs on the exterior surface of catalyzed cylinders in crossflow to a premixed reactant stream. Heat is radiated inward to concentric watertubes across a small air gap. Steam is generated in a naturally circulating water/steam cycle employing an all-welded watertube and steam drum configuration.

A representation of the overall system concept is shown in Figure 1. A stoichiometric fuel/air mixture is fed to the radiative section which contains a close-packed array of concentric catalyst elements and watertubes. The mixture is partially combusted by the catalyst which is kept at a low surface temperature by radiation heat loss to the watertubes. In the case of staged combustion with distillate fuels, the combustion products and remaining unburned fuel and air are passed to a downstream catalytic adiabatic combustor to complete the combustion reactions. A final convective section extracts energy from the fully combusted gases. Both catalyst sections operate well below the maximum use temperature of the catalyst substrate materials -- the radiative section by radiative cooling and the adiabatic section by dilution of the fuel/air mixture with exhaust products from the radiative section.

PREVIOUS DEVELOPMENTS

Early testing was conducted using a staggered tube arrangement (separate ceramic/catalyst tubes and watertubes) with results reported in Reference 2. The radiative section was run with natural gas at varying stoichiometry (40 to 220 percent theoretical air) and heat release rates between 1.09×10^8 and 3.44×10^8 J/hr (100,000 and 325,000 Btu/hr). Low levels of thermal NO_x (2 ppm) and conversion of fuel nitrogen to NO_x (20 percent at 55 to 60 percent theoretical air) were achieved. To improve the peak combustion efficiency of 37 percent and allow for operation on distillate fuels, a radiative combustor was designed with a closer tube packing arrangement and concentric ceramic catalyst tubes and watertubes. The resulting increase in combustor operating temperature improved combustion efficiency to 93 percent but promoted fracturing of the ceramic tubes. This problem was circumvented by using high strength, high thermal conductivity silicon carbide tubes. Two combustor geometries, a graded and nongraded concentric tube arrangement shown in Figures 2 and 3, were tested with chromium oxide on the silicon carbide catalyst supports. The graded tube spacing produces some level of aft end flameholding and raises downstream tube surface temperatures to a level required for lightoff. Both radiant combustor sections were tested with natural gas at a nominal 2.64 x 10^8 J/hr (250,000 Btu/hr) heat release rate.

Thermal NO_x data generated from these tests are compared in Figure 4. Excessive flameholding off the front cylinder rows in the graded design produced high levels of thermal NO_x (30 to 55 ppmv from 115 to 100 percent theoretical air, respectively). The flameholding became more severe with increased throughput and preheat temperature resulting in tube surface temperatures in excess of 1922K (3000°F). At these temperatures, however, the silicon carbide tubes displayed excellent structural integrity. The nongraded tube geometry decreased upstream flameholding and reduced values of thermal NO_x by a factor of two between 80 and 130 percent theoretical air. At 110 percent theoretical air and 2.64 x 10^8 J/hr (250,000 Btu/hr) heat release rate, values of thermal NO_x averaged less than 20 ppmv.

To ensure high combustion efficiency with a limited catalyst surface area, some degree of gas phase fuel burnout at controlled temperatures is desirable. However, high temperature gas phase combustion in regions with uncooled surfaces contributes to thermal NO_x production. Some gas phase combustion was visually observed in the open regions between the catalyst tubes and the inside surface of the refractory walls, and between the refractory liner and the outer steel casing that probably contributed significantly to the scatter in thermal NO_x data for the nongraded geometry. NO_x data at 477K (400°F) preheat are also shown in Figure 4. The higher preheat value intensifies the combustion along the walls resulting in increased values of thermal NO_x and degradation of the combustor refractory. Successful operation with diesel fuel at 2.64 x 10^8 and 3.69 x 10^8 J/hr (250,000 and 350,000 Btu/hr) was achieved before fracturing of the brick refractory forced termination of the tests.

The high values of thermal NO_x between 80 and 100 percent theoretical air in Figure 4 resulted from flameholding near the section inlet region. This is evident from a comparison of temperature profiles for lean and rich combustion in Figures 5 and 6. At 105 to 120 percent theoretical air at ambient (80°F) inlet temperatures (Figure 5), front row cylinder temperatures were between 366K and 394K (200°F and 250°F). Velocities between tubes were

19.8 m/sec to 22.9 m/sec (65 ft/sec to 75 ft/sec). The second row raises the temperature from 977K to 1255K (1300°F to 1800°F), varying with adiabatic flame temperature and velocity (at constant fuel input). The temperature rises to 1477K (2200°F) on the center rows and drops to 1366K (2000°F) on the sixth row as the remaining fuel is consumed. Under rich conditions (Figure 6), as inlet velocities are lowered (at constant fuel input) to approximately 16.8 m/sec (~55 ft/sec), the front row tubes light off, and the surrounding gas phase combustion intensifies. This is illustrated in Figure 6, showing front row temperatures of 1005K to 1561K (1350°F to 2350°F). By operating with front row velocities greater than 21.3 m/sec (70 ft/sec), this can be eliminated.

Throughput testing was performed to identify operating limits for the nongraded configuration. Figure 7 compares temperature profiles taken adjacent to the SiC tubes for 2.64×10^8, 3.69×10^8, and 4.45×10^8 J/hr (250,000, 350,000, and 432,000 Btu/hr) heat release rates at 100 percent theoretical air. As surface velocity increases with increasing throughput, tube temperatures in the front rows decrease, and downstream tube and exhaust temperatures increase. At greater than 110 percent theoretical air for 4.45×10^8 J/hr (422,000 Btu/hr) heat release rate, breakthrough begins to occur. Corresponding velocities between the tubes on the first and second rows are 35.1 m/sec and 25.9 m/sec (115 ft/sec and 85 ft/sec) representing an upper limit for this boiler geometry.

The reduction in surface temperature with increased throughput corresponds to a similar decline in watertube energy removal efficiency, shown in Figure 8. Here, the energy removed by the watertubes is compared with previous data for the graded concentric and nonconcentric designs. The high energy removal efficiency of the concentric graded design is the result of high tube surface temperatures (greater than 1923K) caused by in-bed gas phase reactions that were not evident with the nongraded design. The decline in watertube energy removal efficiency with increased throughput results in a greater energy loss to the exhaust. The optimum energy removal efficiency for this design is near 2.64×10^8 J/hr (250,000 Btu/hr) heat release rate where tube surface temperatures are uniform over the test section length.

Lean combustion efficiency for the nongraded combustor design averaged greater than 99.9 percent. This high value is influenced by gas phase combustion along the walls. Values of CO and UHC averaged between 20 and 100 ppmv. Reduction of these values are achievable with modifications to the boiler geometry or by addition of a monolithic reactor downstream for secondary fuel burnout. A 92 percent combustion efficiency at 30 percent theoretical air establishes an operating point for design of a two-stage watertube boiler.

The results above with the nongraded design established a twofold improvement in thermal NO_x reduction over the previous graded tube design. Throughput testing established nearly a 2:1 turndown rate for the nongraded tube design without the requirement of inlet preheat. Additional thermal NO_x reduction is possible by eliminating flameholding at the inlet and gas burning along the refractory walls. The former can be eliminated by operating at higher throughputs. Gas burning along the walls can be eliminated by decreasing the surface area/volume ratio, and moving catalyst tubes closer to the refractory walls.

CATALYTIC COMBUSTOR WITH STEAM GENERATION

The criteria selected for intermediate scaleup to 1.055×10^9 J/hr (10^6 Btu/hr) heat release rate were those related to watertube boilers in the small industrial sizes -- relatively low pressure boilers without superheat. The majority of these units are steam producers (rather than hot water) and operate wholly by natural circulation.

The preferred, first generation design of the catalytic furnace section would be a simulation of current boiler design configuration, having steam and mud drums with single pass steam risers and downcomers. The tube assembly would be an all-welded construction, requiring the catalyst ceramic tubes to clamshell around the watertubes and be supported at each end. The furnace must also be of rectangular cross section and not contain any of the watertube bends (incompatible with the ceramic catalyst tubes). An evaluation of the design showed a requirement for complex construction, uncertainties in durability of refractory linings and catalyst tube supports, and severe difficulties in installation of the catalyst half-cylinders. In addition, these design difficulties did not appear to lessen with increasing scale. As a result, an alternate concept was sought that would allow simpler catalyst installation and greater component durability.

These constraints can best be satisfied with a concentric watertube configuration. In this design, the downcomer tubes are situated inside the steam riser tubes, both of which are surrounded by a catalyzed SiC tube in the combustor section as shown in Figure 9. This configuration offers two advantages over the straight-through tube system with steam and mud drums. First, it allows the combustor walls and watertube bank to be constructed and disassembled as components. Second, it is possible to slip solid SiC tubes over the watertubes during assembly. This allows for ease in removal and installation of the SiC tubes during periods of recatalyzation.

Cross sections of the 1.055 x 10^9 J/hr catalytic/radiative watertube boiler design are shown in Figures 10 and 11. The system employs a close-packed array of 31 concentric silicon carbide tubes and watertubes shown in Figure 10. A premixed air and fuel stream enters the combustor section at velocities exceeding the flamespeed and expands gradually into the radiant section. High, uniform velocities within the combustor section establish mass transfer coefficients consistent with previous throughput testing. Gas phase combustion along the refractory walls is prevented by placement of silicon carbide catalyst tubes partially within the combustor walls. Cast refractory construction minimizes the surface area/volume ratio and combustor surface heat loss. An opposed jet igniter located upstream of the combustor section raises the catalyst tube surface temperature to 977K (1300°F) required for lightoff. A downstream adiabatic combustor with secondary air injection allows for staged combustion with distillate fuels.

Figure 11 displays a cross section of the combustor, watertubes, and steam drum. The concentric watertube design allows for absorption of radiant heat from the SiC tubes on the annulus (riser), producing a water-steam mixture of lower density than water in the center tube (downcomer). This difference in density provides the force available for natural circulation.

Subcooled water (due to the cooler makeup water) exits the steam drum in the downcomer and returns as a mixture of saturated water and steam in the riser. An internal steam drum liner promotes separation of the steam and water for venting of steam from the top of the vessel and also prevents entrainment of steam to the downcomer. The steam drum employs level control with room temperature makeup water added at the top of the tank.

Initial testing of the radiant combustor section on natural gas at 8.44×10^8 J/hr (800,000 Btu/hr) showed promising results despite the limited nature of the data. The catalyst tube bank appeared very uniform and stable. Natural circulation of water and steam through the concentric watertubes was excellent, with approximately 30 to 40 percent of the incoming energy used to raise steam. Thermal NO_x emissions were improved over the subscale system, peaking at 30 ppmv at near-stoichiometric conditions. Values of 10 ppm or less are expected at approximately 15 percent excess air. Both energy conversion to steam and emissions should improve nearer the 1.055×10^9 J/hr (1,000,000 Btu/hr) design condition.

Problems were encountered with the section insulating refractory which exhibited both erosion and thermal fracturing problems in critical areas of the combustor and subsequently terminated testing. This problem is currently being addressed by using a denser castable refractory with a higher alumina content and better erosion characteristics.

FUTURE DEVELOPMENT

A 3.69×10^9 J/hr (3.5×10^6 Btu/hr) scaleup to a small industrial sized watertube boiler is planned following completion of tests with the current design. Such a system would be operable on both gaseous and distillate fuels and would use a similar close-packed tube arrangement with silicon carbide catalyst tubes in the radiant section. A downstream convective section would insure a high energy removal efficiency. As the design is scaled to this higher heat release rate, the steam drum can be made more circular and designed for higher operating pressures.

REFERENCES

1. Kesselring, J. P., et al., "Design Criteria for Stationary Source Catalytic Systems," Acurex Final Report 78-278, March 1978.

2. Krill, W. V. and Kesselring, J. P., "The Development of Catalytic Combustors for Stationary Source Applications," Proccedings: Third Workshop on Catalytic Combustion, EPA-600/7-79-038, February 1979: pp. 239-268.

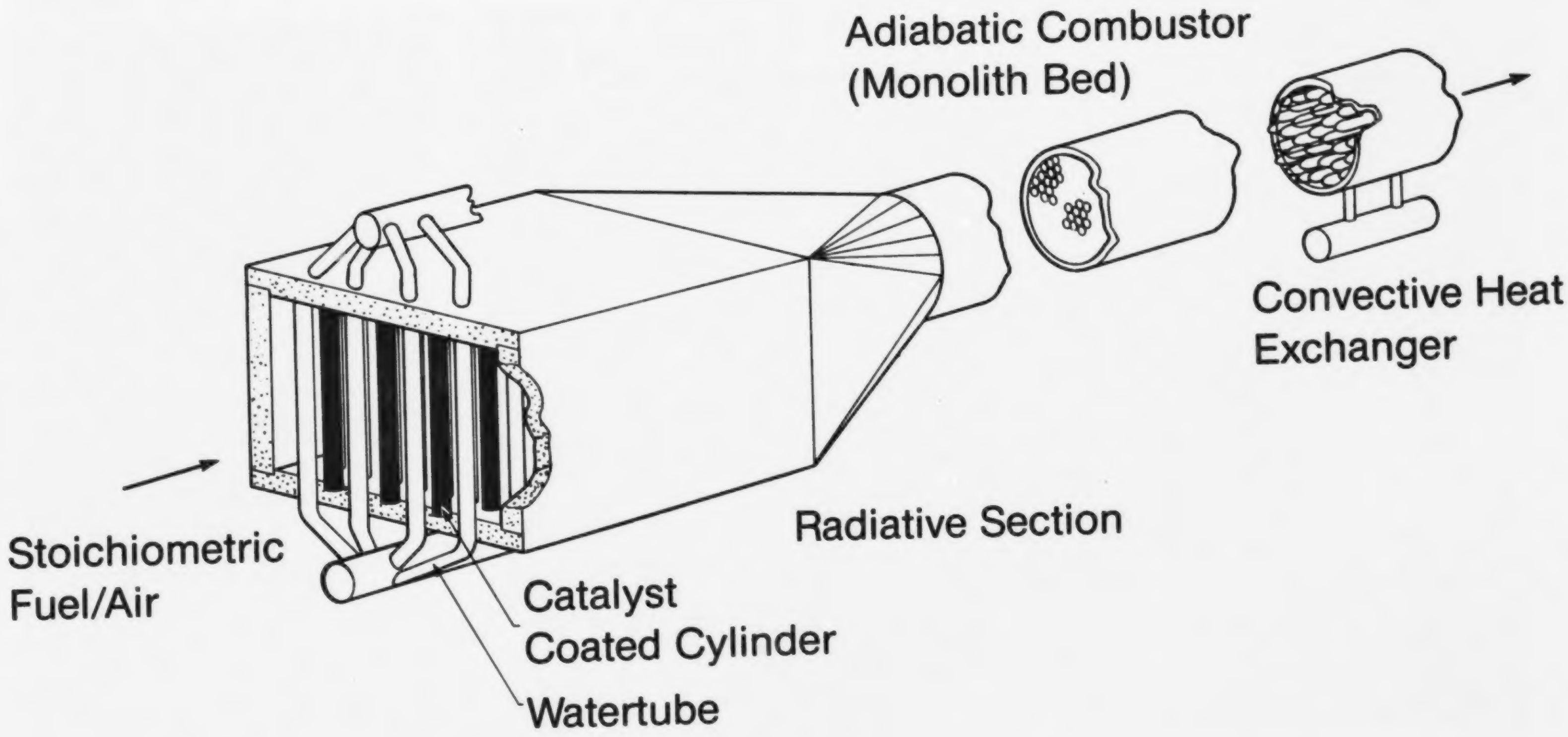
Adiabatic Combustor
(Monolith Bed)
Convective Heat
Exchanger
Stoichiometric
Fuel/Air
Radiative Section
Catalyst
Coated Cylinder
Watertube

Figure 1. Radiative catalyst watertube system.

EE/S-528c

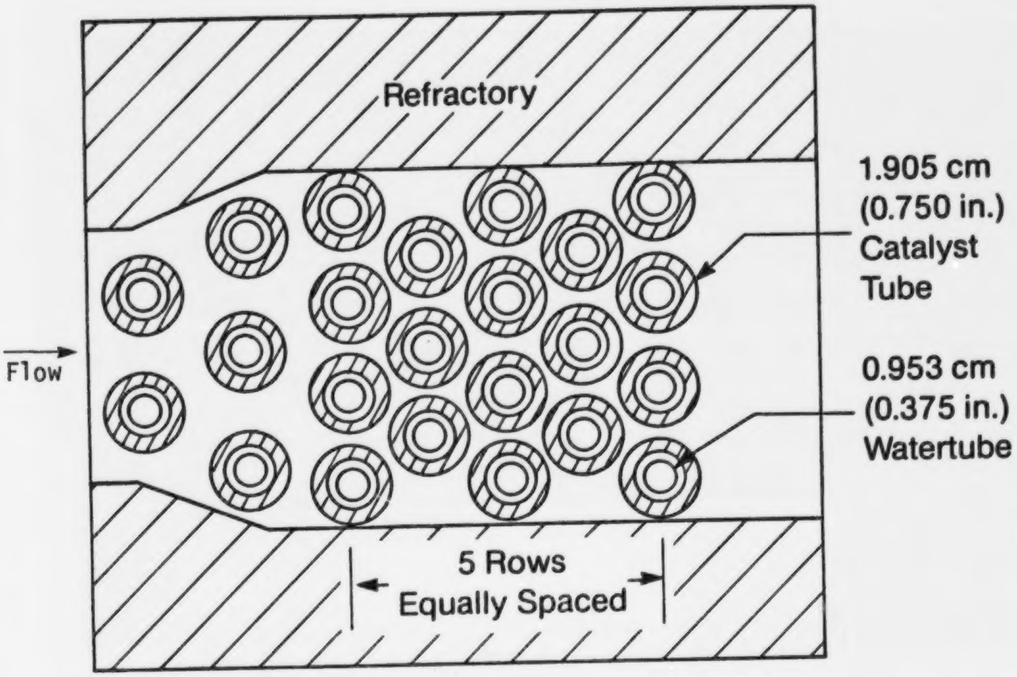
Refractory
1.905 cm
(0.750 in.)
Catalyst
Tube
Flow
0.953 cm
(0.375 in.)
Watertube
5 Rows
Equally Spaced

Figure 2. Radiative section geometry -- graded tube spacing.

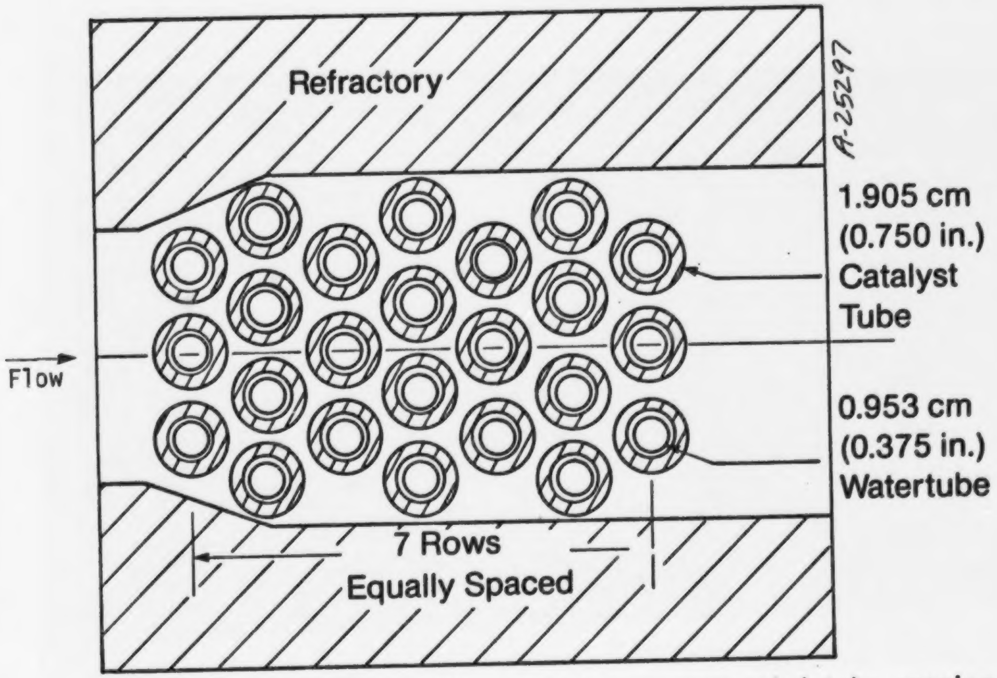
Refractory
A-25297
1.905 cm
(0.750 in.)
Catalyst
Tube
Flow
0.953 cm
(0.375 in.)
Watertube
7 Rows
Equally Spaced

Figure 3. Radiative section geometry -- nongraded tube spacing.

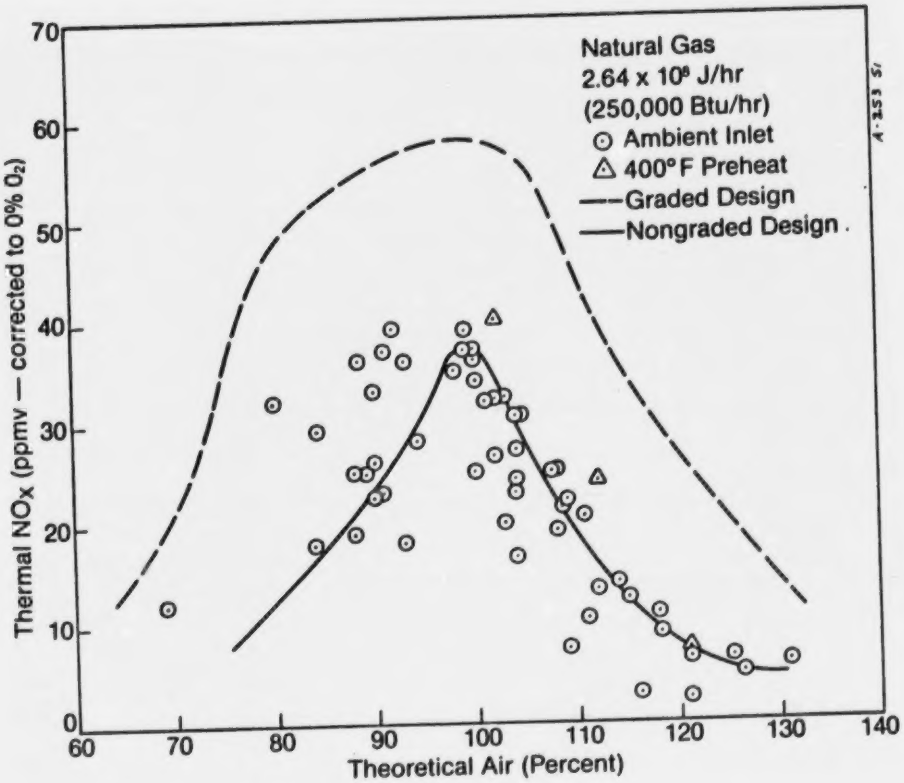

Figure 4. Watertube system thermal NO_x comparison.

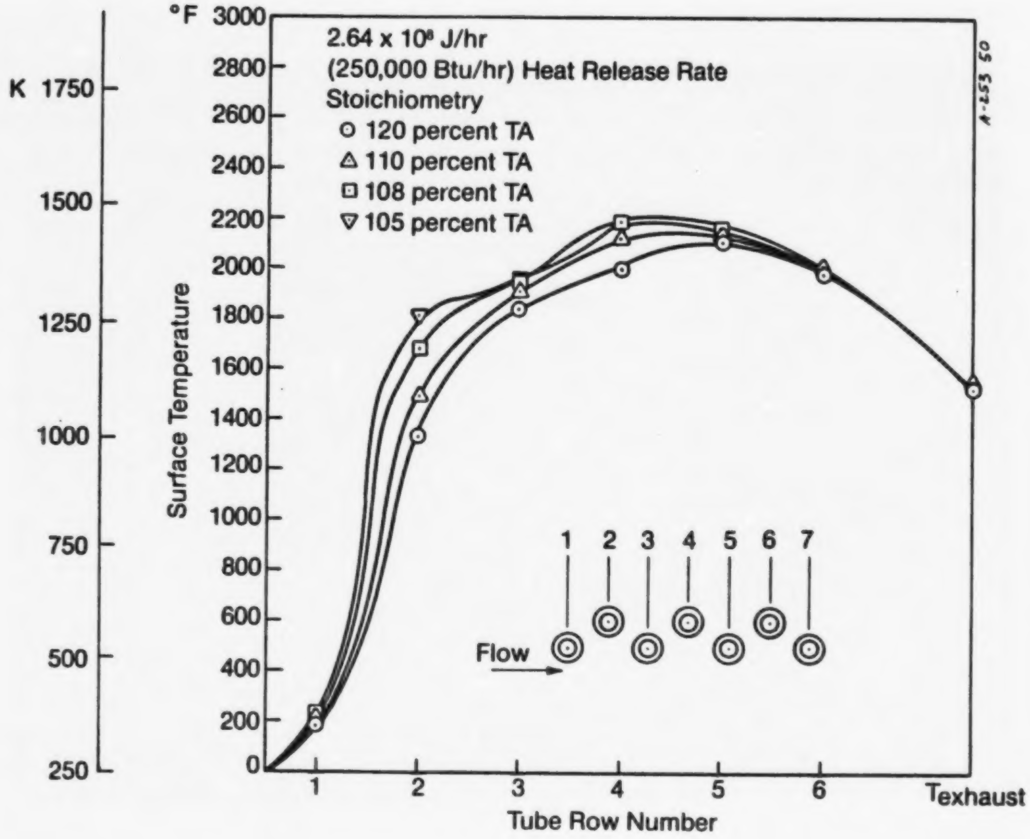

Figure 5. Tube temperature profile for lean combustion at 2.64 x 10^8 J/hr (250,000 Btu/hr).

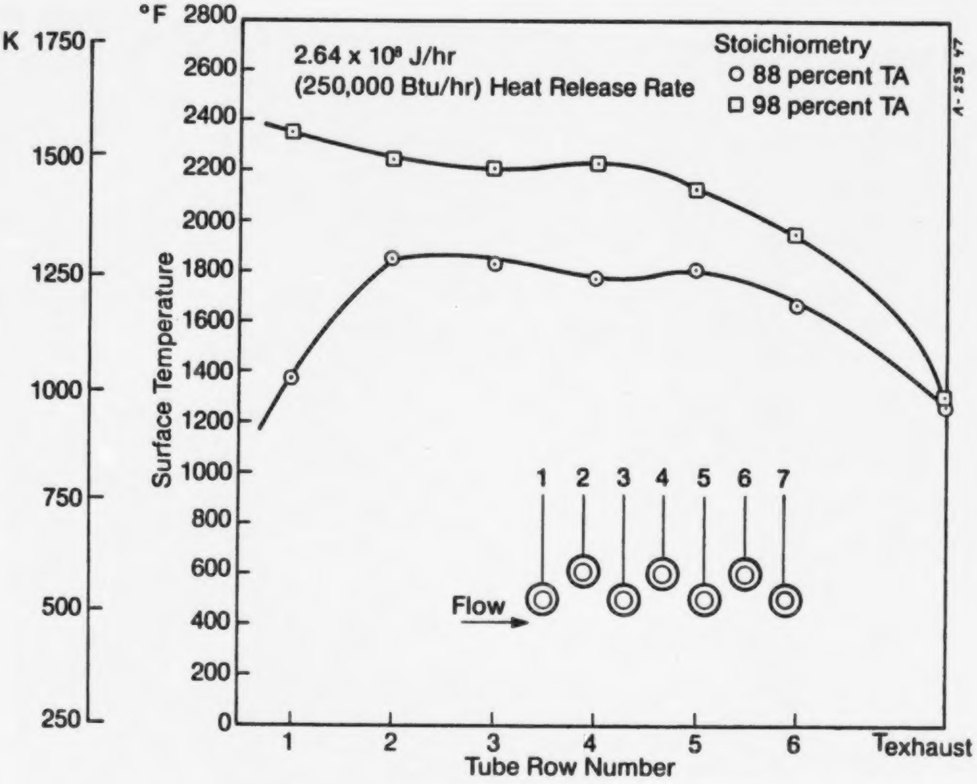

Figure 6. Tube temperature profile for rich combustion at 2.64 x 10^8 J/hr (250,000 Btu/hr).

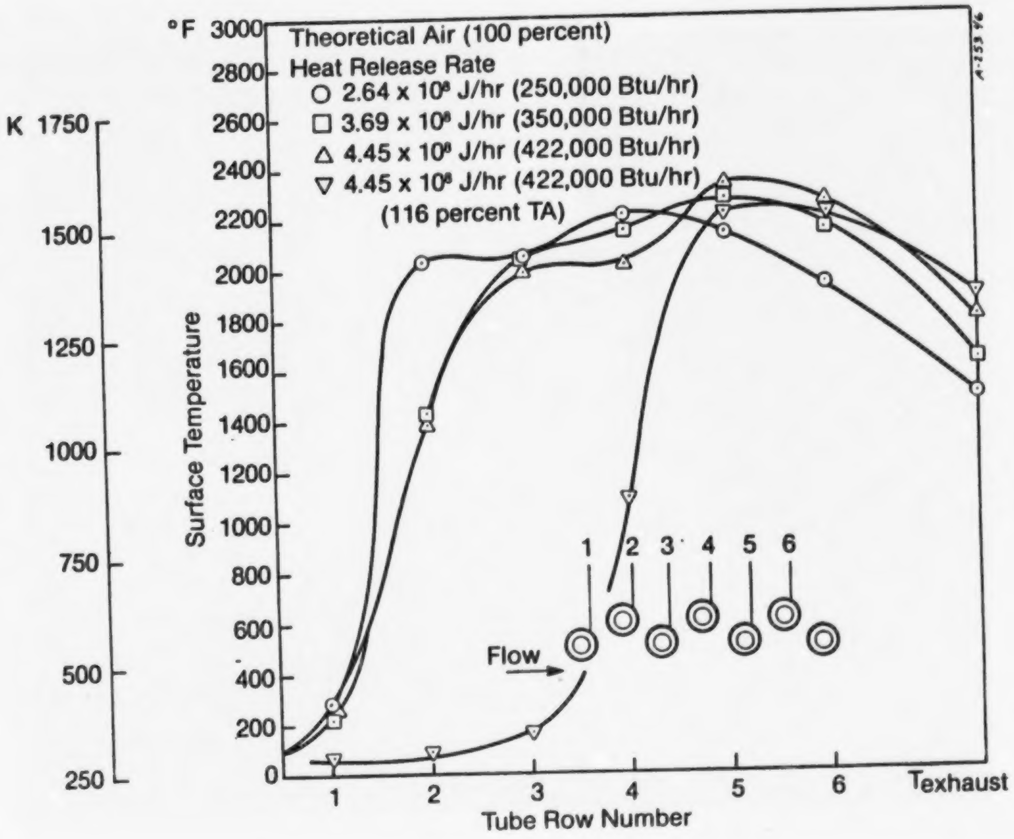

Figure 7. Tube surface temperature profile for throughput testing.

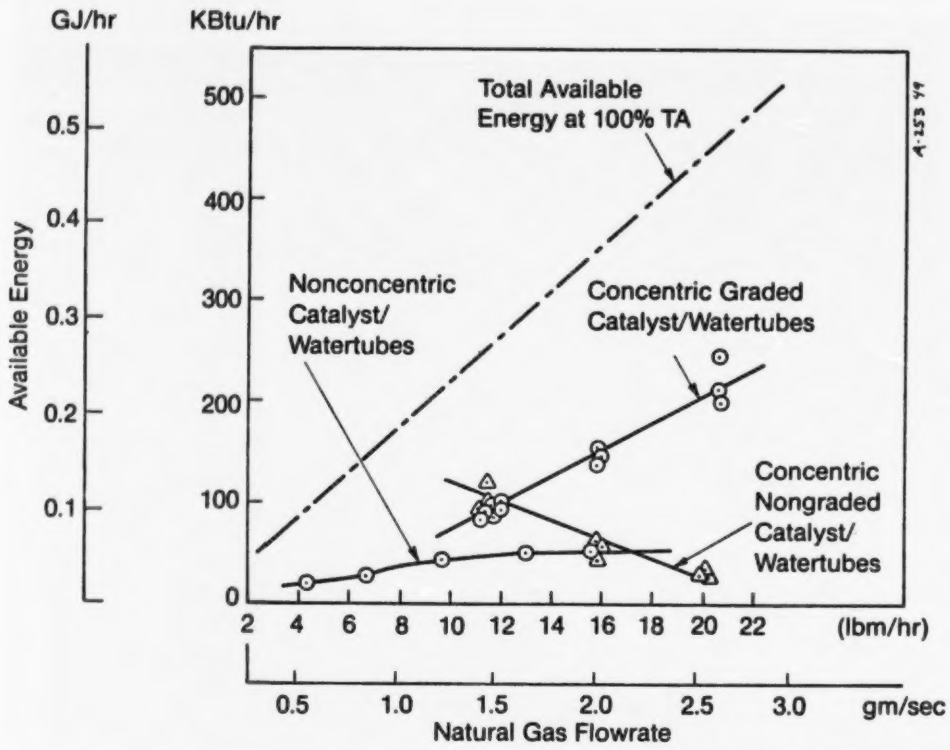

Figure 8. Radiative section energy transfer to watertubes.

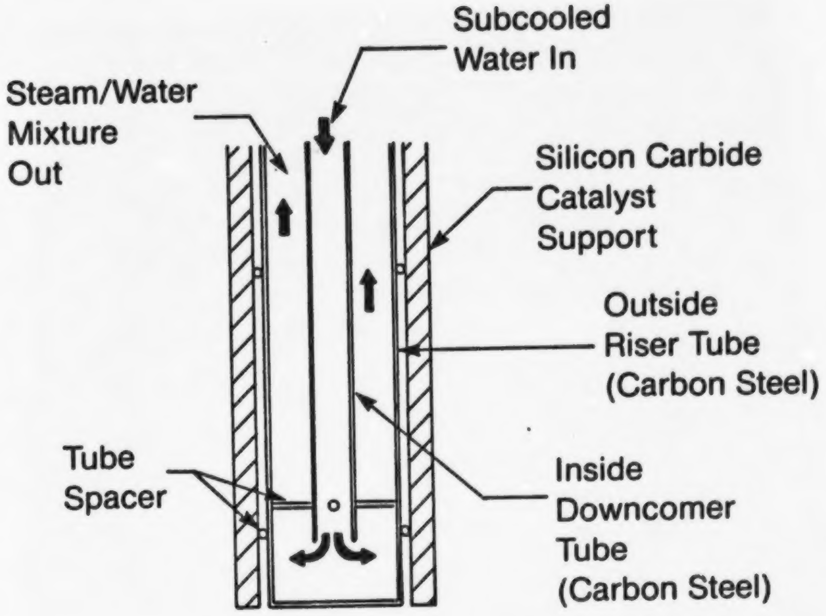

Subcooled Water In
Steam/Water Mixture Out
Silicon Carbide Catalyst Support
Outside Riser Tube (Carbon Steel)
Tube Spacer
Inside Downcomer Tube (Carbon Steel)

EE/S-534c

Figure 9. Schematic of single tube water/steam circulation.

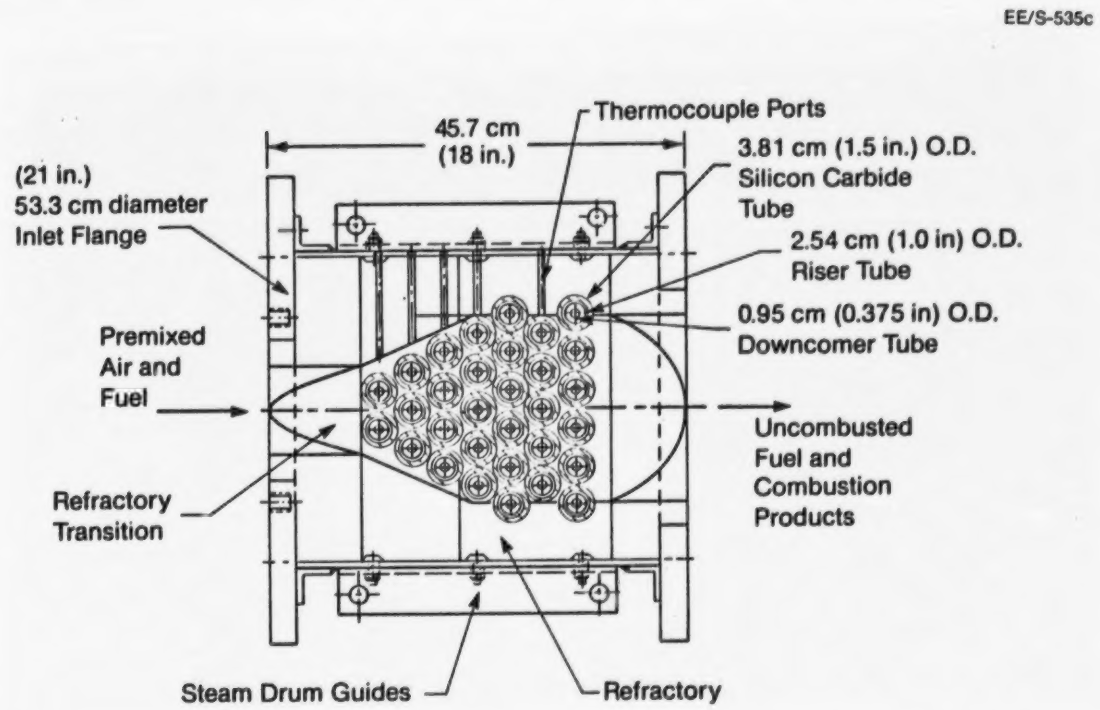
EE/S-535c
45.7 cm
(18 in.)
Thermocouple Ports
(21 in.)
53.3 cm diameter
Inlet Flange
3.81 cm (1.5 in.) O.D.
Silicon Carbide
Tube
2.54 cm (1.0 in) O.D.
Riser Tube
0.95 cm (0.375 in) O.D.
Downcomer Tube
Premixed
Air and
Fuel
Uncombusted
Fuel and
Combustion
Products
Refractory
Transition
Steam Drum Guides
Refractory

Figure 10. 1.055 x 10^9 J/hr radiative combustor tube geometry.

EE/S-536c

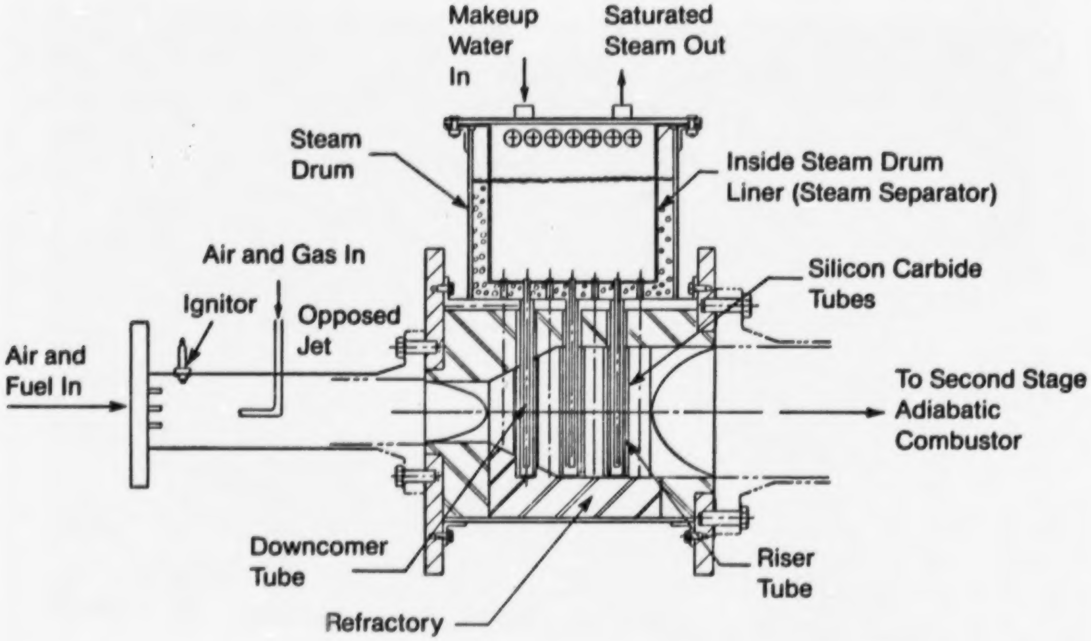
Makeup Water In
Saturated Steam Out
Steam Drum
Inside Steam Drum Liner (Steam Separator)
Air and Gas In
Silicon Carbide Tubes
Ignitor
Opposed Jet
Air and Fuel In
To Second Stage Adiabatic Combustor
Downcomer Tube
Riser Tube
Refractory

Figure 11. Cross section of 1.055×10^9 J/hr catalytic combustor and steam generator.

DEVELOPMENT OF A LOW NO_x COMBUSTOR FOR GAS-FIRED FIRETUBE BOILERS

E. B. Merrick, W. V. Krill, J. P. Kesselring, and M. A. Friedman
Acurex Corporation, Energy & Environmental Division
485 Clyde Avenue
Mountain View, California 94042

ABSTRACT

Development of a low-NO_x fiber matrix burner for gas-fired firetube boilers is in the demonstration phase. Preliminary data from fiber burner tests in a York-Shipley 25 hp firetube boiler show a 90 percent reduction in NO_x from the conventional burner. The burner is a matrix of ceramic fibers vacuum-formed to a capped cylindrical screen. During operation, premixed natural gas and air pass through the fiber matrix and are ignited, burning only on the outer surface. The surface radiates energy flamelessly to the firetube wall, controlling the combustion temperature to levels well below the NO_x formation temperature. The burner fits into the first pass of the firetube boiler with approximately the same volume as the conventional flame. Earlier subscale test results and these preliminary full-scale boiler results indicate that NO_x emissions from firetube boilers can be substantially reduced when retrofit with a fiber matrix burner.

INTRODUCTION

There are approximately 125,000 commercial gas-fired firetube boilers in the 180 to 880 KW (0.6 to 3 million Btu/hr) firing range currently in the United States. An additional 3000 new units are sold annually. These boilers produce about 150 ppmv NO_x each at 15 percent excess air, making gas-fired firetube boilers the 26th largest NO_x source in the U.S. at one percent of the total NO_x inventory. In addition, firetube boilers are usually located in population centers where their effect on air quality is even larger than the inventory percentage would indicate. In the interest of improving air quality, the Environmental Protection Agency has funded a program to develop low-NO_x burners for firetube boilers for retrofit into existing boiler designs.

PROGRAM APPROACH

The program approach was to select a burner concept that met the needs of the firetube boiler users, test the feasibility of the concept, identify a suitable burner material, test the burner concept in a subscale facility, and finally, demonstrate the concept as a retrofit burner in a commercial size firetube boiler.

CONCEPT SELECTION

During the first year of the program, three low-NO_x burner concepts were considered for firetube boilers:

1. Fiber matrix burner
2. Staged catalytic burner
3. Single stage catalyst with flue gas recirculation

The fiber matrix burner was selected for further development because it requires few changes to the conventional boiler system. In comparison, staging introduces undesirable hardware complexities, and flue gas recirculation requires additional blowers that increase cost. The fiber matrix burner is a single stage concept that can operate near stoichiometric with low NO_x and without flue gas recirculation, does not require preheat to operate with natural gas, and can potentially burn liquid fuels (with combustion air preheat). The last characteristic is important in the current marketplace, where dual-fueled boilers are most competitive. In this program, the fiber burner has been developed primarily for gas firing. Figure 1 shows the fiber burner concept in which the cylindrical burner fits inside the firetube (first pass) of the firetube boiler.

The fiber matrix burner is a layer of ceramic fibers vacuum-formed onto a screen of the desired shape. The close-packed fibers form a porous matrix. During operation, premixed gas and air pass through the fiber matrix and are ignited, burning only on the outer surface. The surface glows flamelessly and uniformly. The fibers radiate to the firetube wall, controlling the combustion temperature to between 1200 and 1366 K (1700 to 2000°F) which correspondingly reduces thermal NO_x formation. The burner nominally operates at a heat release rate per unit area of burner surface of 900 MJ/h4-m^2 (80,000 Btu/hr-ft^2). The burner is sized based on this operating condition, resulting in a cylindrical burner similar in volume to the conventional flame in a firetube boiler.

Although fiber burners operate best at surface velocities below the mixture flame speed, the inherent qualities of the burner help prevent flashback. Both the low conductivity of the fibers and the cooling flow of reactants insulate the inside of the burner from the combustion zone, thereby stabilizing combustion on the burner surface and preventing flashback.

INITIAL TESTS

Initial tests were conducted in laboratory facilities at Acurex to assess the feasibility of the fiber matrix burner. The materials used for feasibility testing were a fiber blanket material and vacuum-formed fiber cylinders of several manufacturers. The results verified that fiber matrix burners have potential for low NO_x. At nominal operating conditions of 900 MJ/hr-m^2 (80,000 Btu/hr-ft^2) heat release rate per unit of burner surface area and 10 percent excess air, the NO_x emissions were less than 25 ppm. The burner also showed potential for high combustion efficiency, stable operation at low excess air levels, and high radiation heat transfer. About one-third to one-half of the energy input was transferred to the load radiatively.

These initial tests also defined the operating range for fiber matrix burners, showed that flashback can be a problem, and identified the need for improved fiber matrix materials.

The burners operated stably from a heat release rate per unit surface area of 740 to 1700 MJ/hr-m^2 (65,000 to 150,000 Btu/hr-ft^2), corresponding to a turn-down ratio of 2.3 to 1. At each heat release rate, the burners were tested over the range of 0 to 80 percent excess air. Nominal operating conditions were defined as 900 MJ-hr-m^2 (80,000 Btu/hr-ft^2) and 10 percent excess air, based on minimum emissions and optimum burner temperature.

During the vacuum-formed cylinder tests, flashback failures occurred, causing an internal flame which damaged the burner and internal hardware. The flashback was not a function of reactant velocity, since each failure occurred at different operating conditions, but appeared to be due to nonuniformities in the wall thickness and erosion of the fiber matrix. Nonuniformities can cause hot spots which can lead to flashback. The erosion causes openings in the matrix which become enlarged by the flow over time. Eventually, blue flames appear at the openings and flashback occurs.

Since the major cause for flashback was poor quality fiber matrix material, a key finding of the initial tests was the need for an improved fiber matrix. In addition, the blanket material proved to be undesirable due to nonuniform construction and the difficulty in forming a leak-proof seam. Identifying better quality materials was the next step in the development of the fiber burner prior to subscale testing.

Desired characteristics of the fiber burner are flashback resistance, flame shaping, seamless construction, and uniform thickness. Vacuum-forming the fiber matrix provides the flame shaping and seamless, uniform construction. Flashback resistance also requires uniform construction to prevent hot spots, plus high quality fibers to avoid matrix erosion, and high emissivity to keep the burner surface cooler.

Two fabricators were found to have experience with vacuum-forming and radiant fiber burners. Burners from each source were purchased to be tested in the subscale facility. These burners were well constructed and uniform in appearance, and each had a high emissivity ingredient in the matrix material.

SUBSCALE TESTS

The subscale tests were conducted to further assess the fiber matrix burner as a potential firetube boiler retrofit burner. The tests were also to provide data on the flashback resistance and operating characteristics of burners previously identifed.

The test facility modeled a typical firetube boiler combustion chamber. The internal diameter was 0.20 m (8 in). The burners were approximately 0.15 m (6 in) in diameter, leaving an annulus of 0.025 (1 in) between burner and chamber wall. One burner, Burner A, was 1.06 m (42 in) long, with a 740 MJ/hr (700,000 Btu/hr) maximum heat input. Burner B was shorter than A due to fabrication constraints. Burner B was 0.61 m (24 in) long, with a 420 MJ/hr (400,000 Btu/hr) maximum heat input.

The burners were tested on natural gas at heat release rates per unit of burner surface area of 740 to 1420 MJ/hr-m^2 (65,000 to 125,000 Btu/hr-ft^2) and at 0 to 60 percent excess air. Both burners showed excellent results with low emissions, stable operation and no flashback over the entire test matrix. Test results for the two burners at nominal operating conditions of 900 MJ/hr-m^2 (80,000 Btu/hr-ft^2) and 10 percent excess air are shown in Table 1.

TABLE 1. SUBSCALE TEST RESULTS

	Heat Release MJ/hr (Btu/hr)	Emissions (ppmv)			Burner Temperature ^oK (^oF)	Pressure Drop Pa (in. w.g.)
		NO_x	CO	UHC		
Burner A	530 (500,000)	11	4	<1	1410 (2080)	996 (4)
Burner B	265 (250,000)	18	19	3	1240 (1780)	62 (0.25)

Note that the emissions for both burners are low, but the surface temperature and pressure drop through the matrix are very different for the two burners. The lower temperature of Burner B indicates higher radiant heat transfer, therefore potentially higher efficiency or capacity. The lower pressure drop of Burner B also enhances the efficiency by requiring lower horsepower.

Burner A underwent a cyclical 100-hour life test to investigate emissions and operating characteristics over an extended period. The test was conducted on natural gas at the nominal operating conditions of 900 $MJ/hr\text{-}m^2$ (80,000 $Btu/hr\text{-}ft^2$) and 10 percent excess air. Figure 2 shows the NO_x emissions which remained at about 12 ppm throughout the test. In addition, no degradation in CO, UHC, burner temperature, or combustion stability occurred.

The subscale tests confirmed that the fiber matrix has good potential as a low-NO_x burner for firetube boilers. In addition, two burner materials were shown to operate with low NO_x and without flashback. The next step in the burner development was to domonstrate a fiber burner in a commercial firetube boiler.

FIRETUBE BOILER DEMONSTRATION

The purpose of the demonstration is to show that the fiber burner operates as successfully in full-scale as in subscale. Comparing the full-scale boiler to the subscale test facility, the boiler is larger by nearly two in physical dimensions and in heat input, the firetube has cold water walls where the test facility had hot refractory walls, and the boiler has a two-pass convective section. In addition, the boiler is a closed system which can provide system efficiency data.

The approach in the demonstration phase was to:

1. Procure and install a commercial firetube boiler.
2. Test the as-received boiler for baseline data on natural gas.
3. Test the boiler Fiber Burner A on natural gas.
4. Test the boiler with Fiber Burner B on natural gas.

The boiler selected for this program was a York-Shipley 25 hp firetube boiler. The boiler has three passes, produces steam at low pressure, operates on either gas or light oil, and has an energy output of 890 MJ/hr (840,000 Btu/hr).

Baseline Testing

The as-received boiler was tested on natural gas over a range of stoichiometries at four load conditions. Excess air ranged from 0 to 80 percent. The four loads were 50, 65, 80, and 100 percent of full load.

At typical operating conditions of 100 percent load and 30 percent excess air, the NO_x emissions were 70 ppmv, CO was 30 ppmv and UHC was negligible. Boiler efficiency, calculated by the ASME Heat Loss Method was 81 percent. Figure 3 shows the NO_x emissions for 80 and 100 percent load with the highest NO_x of about 70 ppm occurring at full load. NO_x drops off slightly at lower loads and high excess air levels, corresponding to a decreasing temperature. The NO_x emissions for this boiler are roughly one-third the levels shown in the literature. However, these low levels are typical for boilers of this small size.

Fiber Burner Testing

Preliminary testing has been conducted on Fiber Burner A only thus far. The data will be discussed as a comparison to baseline data. Adapting the fiber burner to the existing system required retrofit design and hardware As shown in Figure 1, the fiber burner fits into the firetube (first pass) of the boiler. Figure 4 shows the fiber burner assembly. Minimal changes to the existing system were required. With the high pressure drop through Fiber Burner A of 1000 to 1250 Pa (4 to 5 inches w.g.), a larger blower was needed, while the existing blower will be used for Burner B. Port holes in the front burner flange were required for thermocouples and the igniter probe. The front burner flange with refractory ring was also replaced. The new flange allowed the refractory to be cast with instrumentation port holes, leaving the original flange intact for possible future baseline testing on oil. Figure 5 shows Fiber Burner A ready to be installed into the firetube boiler.

In operation, combustion air is premixed with the gas injected into four ports upstream of the burner. The reactants enter the burner, pass through the fiber matrix and are ignited with a standing pilot. Internally, a center body reduces the cross sectional flow area to minimize the combustion mixture volume while maintaining a high velocity for flashback prevention. A perforated metal cylinder supports the fiber matrix burner.

Testing was conducted on Fiber Burner A at 50, 65, 85, and 100 percent load. NO_x emissions for 85 and 100 percent load at 12 to 53 percent excess air are shown in Figure 3. NO_x for the fiber burner was from 80 to 90 percent less than for the conventional burner. Table 2 shows the results of both Burner A and the conventional burner at 100 percent load and 30 percent excess air. At these conditions, the fiber burner reduced NO_x by 87 percent and improved efficiency by 1 percentage point.

The temperature at the firetube exit, just before entering the second pass of the boiler, is substantially lower for the fiber burner. The decreased temperature indicates that more radiation heat transfer is occurring with the fiber burner compared with the conventional burner. Thus, fiber burners offer potential for increased capacity in the same size boiler.

TABLE 2. FIRETUBE BOILER TEST DATA

	Emissions (ppmv at 0% O_2)	Efficiency (%)	Firetube Exit Temperature K (°F)
Fiber Burner A	9	82	1220 (1706)
Conventional Burner	69	81	1330 (1905)

The preliminary data appears very promising and further testing with Fiber Burner A will provide more conclusive evidence that fiber burners have potential as low-NO_x burners for firetube boilers. Burner B is expected to show similar reductions in NO_x emissions as testing continues.

CONCLUSIONS

Low-NO_x fiber burners have been carried from concept into demonstration in a gas-fired firetube boiler. During the program, two successful fiber matrix materials were identified and the fiber burner operating range was defined. Preliminary demonstration data shows that fiber burners reduce NO_x by up to 90 percent from the baseline NO_x of the as-received boiler. The radiative nature of the burner may also be responsible for a slight increase in boiler efficiency.

Continued tests are planned on both Fiber Burners A and B. The burner demonstrating the best performance characteristics will then be selected for a cyclical life test of several hundred hours. The final demonstration will verify the low-NO_x, high efficiency operation of the fiber matrix burner with sufficient durability for boiler application.

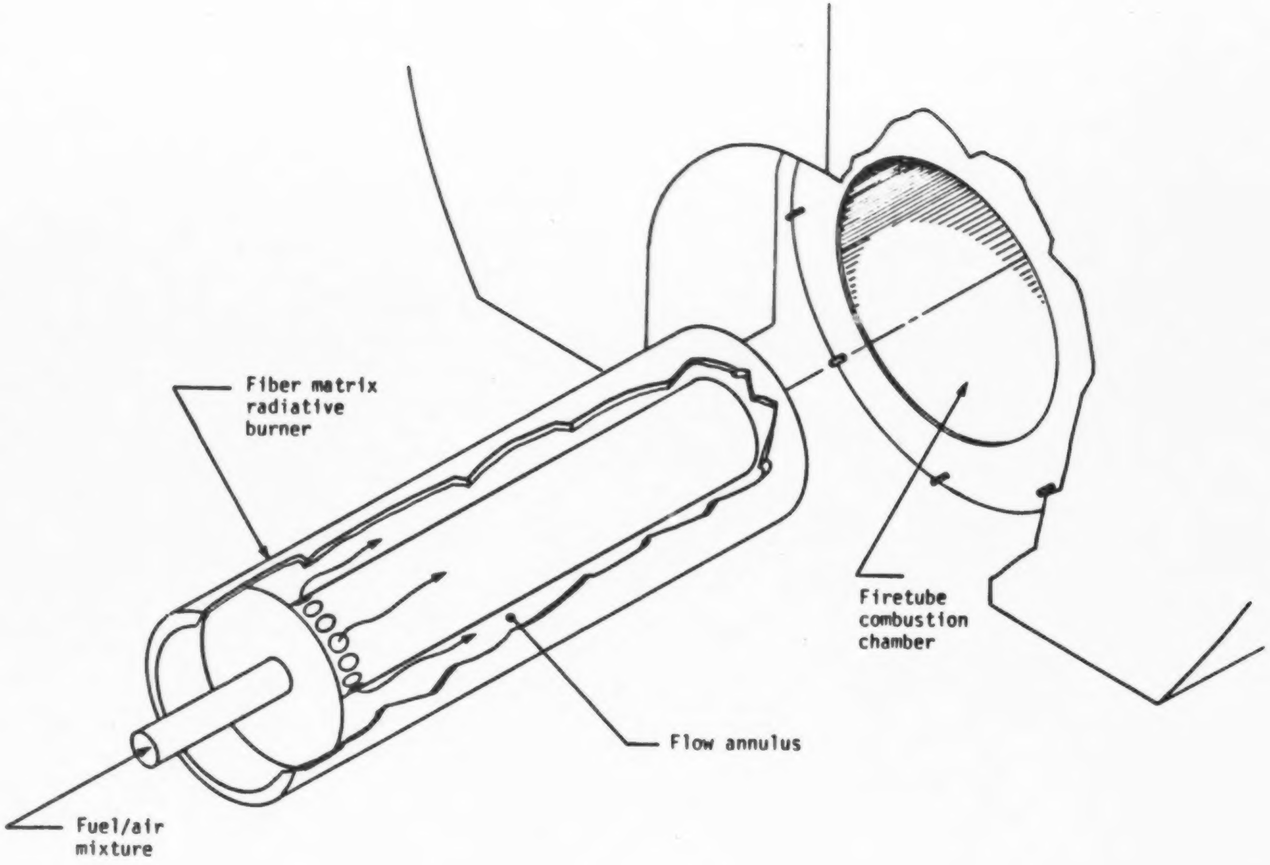
Fiber matrix
radiative
burner
Firetube
combustion
chamber
Flow annulus
Fuel/air
mixture

Figure 1. Firetube fiber matrix burner concept.

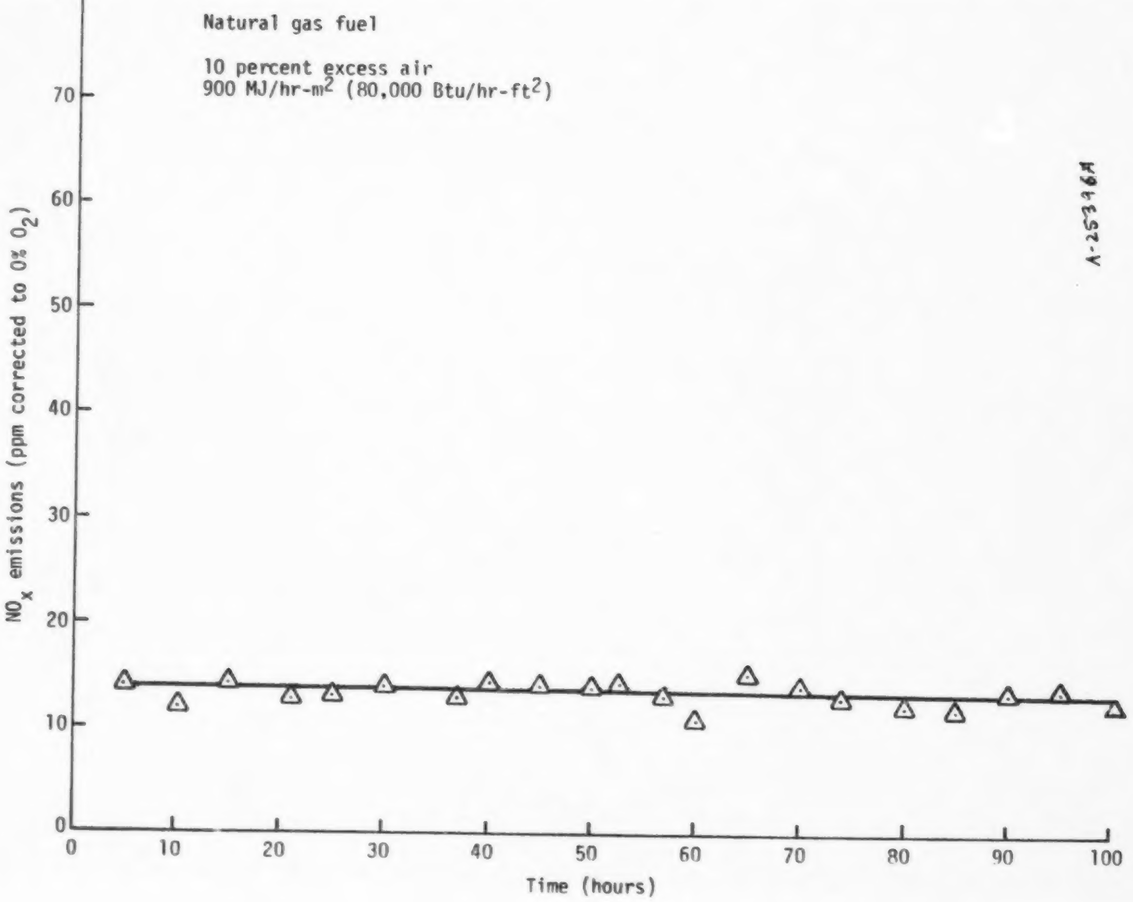

Figure 2. Burner A life test NO_x emissions.

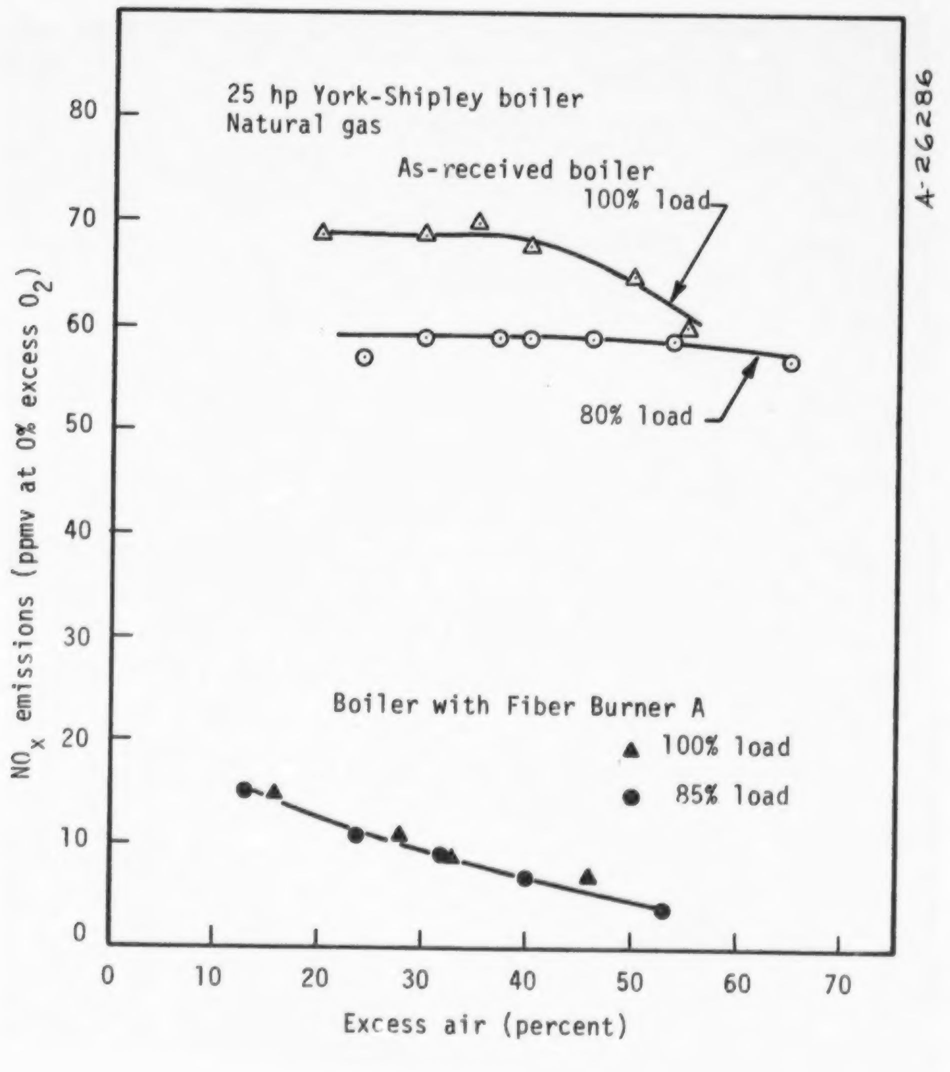

Figure 3. Firetube boiler NO$_x$ emissions.

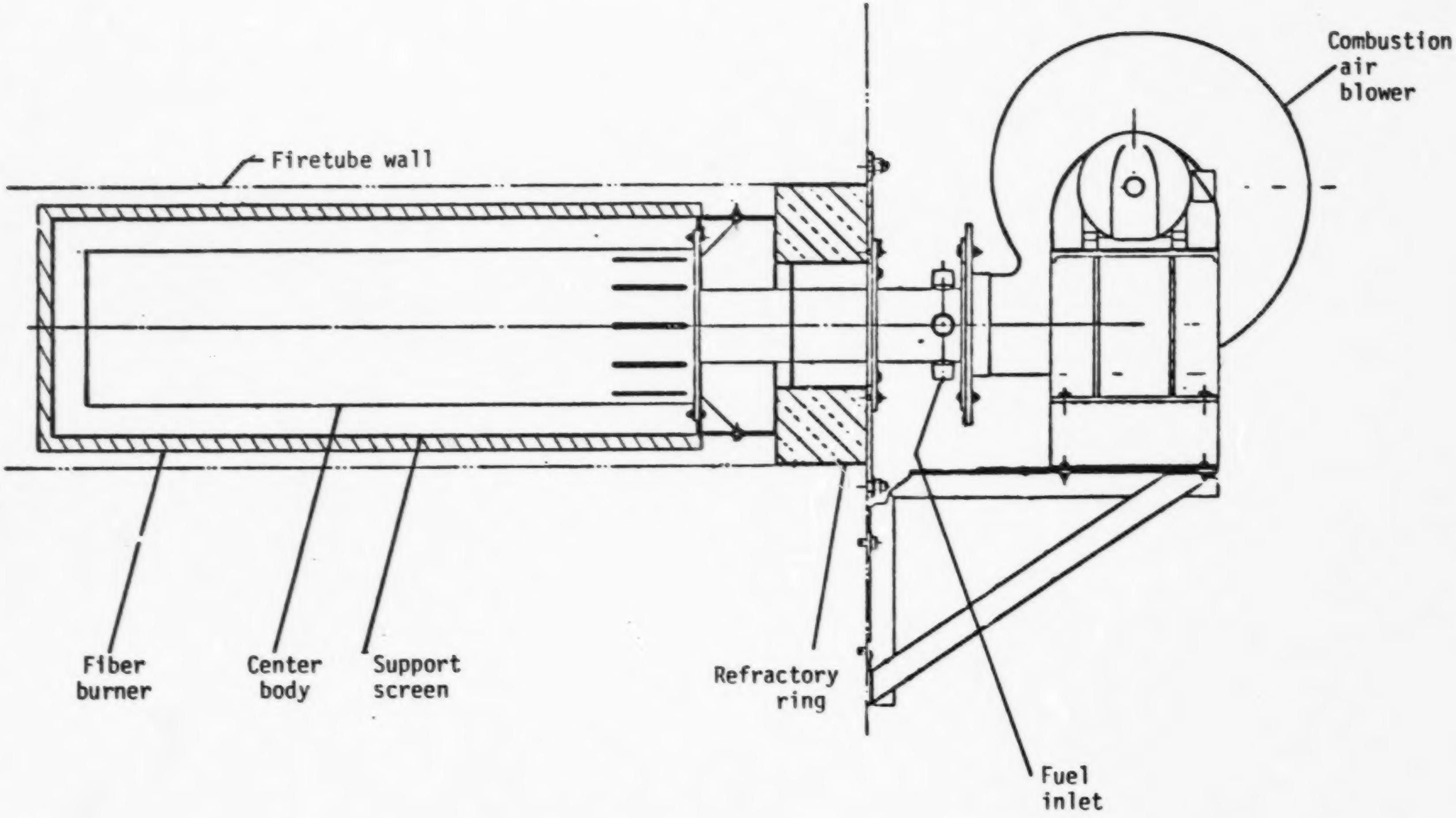
Combustion
air
blower
Firetube wall
Fiber
burner
Center
body
Support
screen
Refractory
ring
Fuel
inlet

Figure 4. Fiber burner assembly.

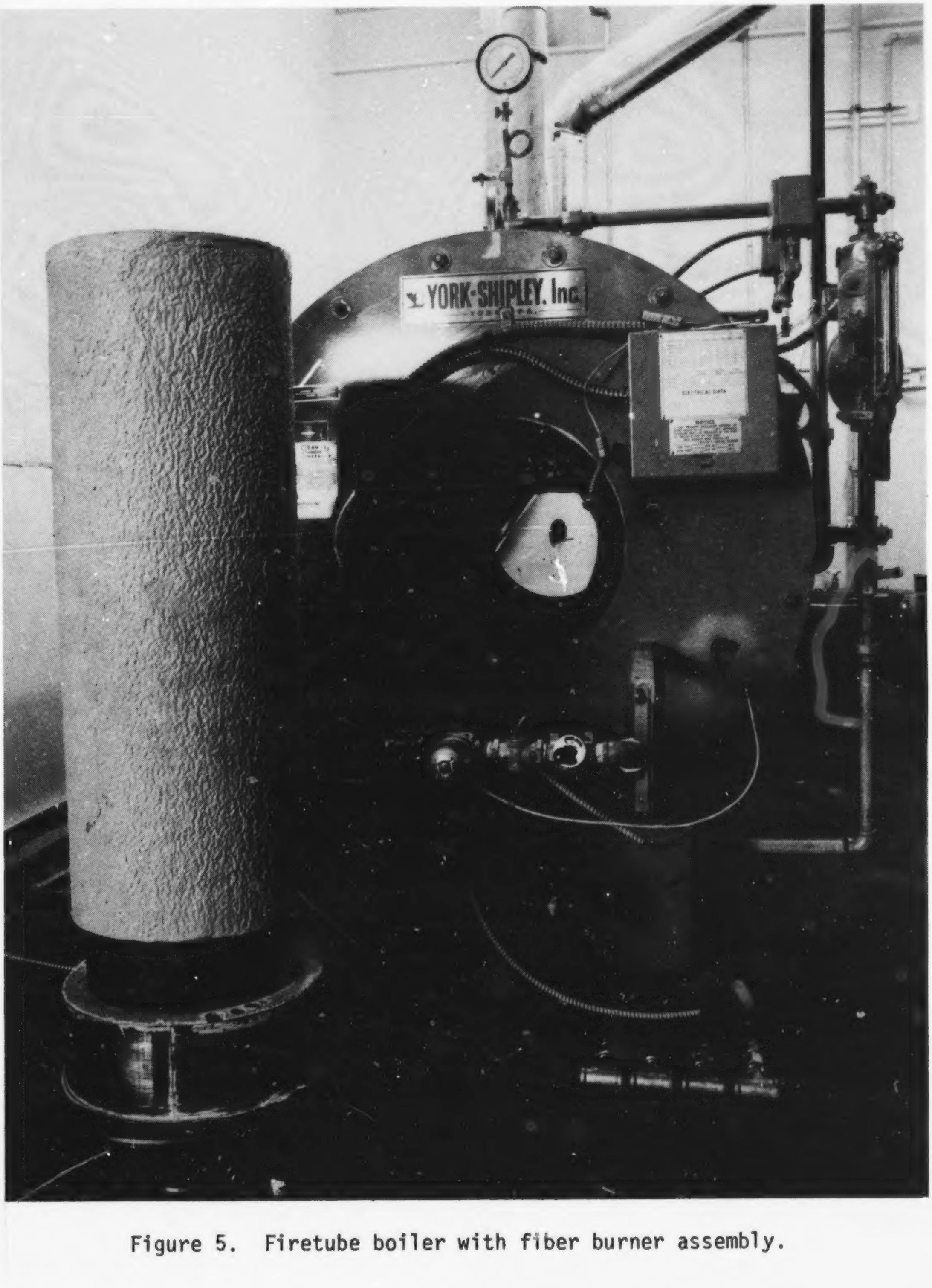
YORK-SHIPLEY, Inc.

Figure 5. Firetube boiler with fiber burner assembly.

FULL-SCALE, FULL-PRESSURE TESTS OF CATALYTIC BURNERS FOR COMBUSTION TURBINES

by:

P.W. Pillsbury, P.E. Scheihing, J.L. Toof
Westinghouse Electric Corporation
Combustion Turbine Systems Division
Concordville, Pennsylvania 19331

K.R. Burns
Engelhard Corporation
Engelhard Industries Division
Iselin, New Jersey 08830

PREPARED FOR PRESENTATION AT THE EPA 5TH WORKSHOP ON CATALYTIC COMBUSTION, SAN ANTONIO, TEXAS, SEPTEMBER 15-16, 1981.

ABSTRACT

Full-scale, full-pressure tests of catalytic burners designed for application in stationary combustion turbines have been conducted in test rigs at the Concordville, Pennsylvania laboratories of the Combustion Turbine Systems Division of the Westinghouse Electric Corporation during 1980 and 1981. The 14-inch diameter catalytic elements employed were designed and prepared by the Engelhard Industries Division of Engelhard Corporation, technical partner in this program. It may be said that concept feasiblility was demonstrated in steady state operation.

Extremely low NOx emissions were noted with No. 2 oil as fuel. Additional development tests are required to improve fuel-air distribution approaching the catalyst it was also apparent. Other work remaining includes demonstration of start-up and transient operation, improving performance, and durability verification. Related catalytic combustor design and development work is being performed by Westinghouse and Engelhard under Electric Power Research Institute Contract RP1657.

ACKNOWLEDGMENTS

The authors wish to acknowledge the contributions of many who participated in this program, especially;

At Westinghouse

- C. E. Hussey
- F. K. Gabriel
- S. M. DeCorso
- J. M. G. Emory
- J. H. Marlow
- T. A. Piaia
- V. G. Best
- G. R. Kaufman
- R. A. Kuhl
- W. V. Roache
- G. M. Sauermelch

At Engelhard

- I. T. Osgerby
- R. V. Carrubba
- H. C. Lee
- R. M. Heck
- B. A. Olson

INTRODUCTION

BACKGROUND

Full-scale, full-pressure tests of catalytic burners designed for application in stationary combustion turbines have been conducted in test rigs at the Concordville, Pennsylvania laboratories of the Combustion Turbine Systems Division of the Westinghouse Electric Corporation during 1980 and 1981. The 35.5 cm (14 inch) diameter catalytic elements employed were designed and prepared by the Engelhard Industries Division of the Engelhard Corporation, technical partner in the program.

Since 1973, Westinghouse and Engelhard have been conducting joint experiments with small catalytic combustors with the objective of developing an ultra-low NO_x emission burner system. Initial tests were at pressures of 3 to 5 atm. (Reference 1), but later tests included results obtained at 10 to 13 atm. (the usual full load burner pressure for large, stationary combustion turbines). These were discussed briefly at the Fourth EPA Workshop on Catalytic Combustion in May, 1980 (Reference 2). Fuel for these tests over the years has been primarily No. 2 distillate oil (the principal liquid fuel used in stationary combustion turbines), although coal gas has also been successfully tested. In the tests reported here, No. 2 oil was the sole fuel.

By 1979, promising small-scale tests encouraged Westinghouse and Engelhard to begin design and fabrication of full-scale catalytic combustors of the type reported in this paper. The principal objective was to identify problem areas unique to complete, full-scale combustors, since earlier test units were smaller and generally lacked the devices necessary to make them self-starting.

Since the objectives of this Westinghouse/Engelhard sponsored test series are limited to problem-definition and feasibility establishment, they are more modest than those of the related Electric Power Research Institute/Westinghouse/

Engelhard program also underway, as described at the Fourth EPA Workshop (Reference 3). In the EPRI program, extensive analytical design was performed to sift many possible configurations, and then to detail a prime concept. This latter embodies all major features needed for practical, reliable operation in current, or near-future stationary turbines.

DESIGN OF APPARATUS

Combustor Requirements That Result From Engine Characteristics

The experimental combustors of this program were designed for application in Westinghouse W501D type stationary turbines. They are prototype hardware, and differ from engine-ready units in that they employ a temporary arrangement for the secondary fuel injector piping and also do not incorporate the downstream combustor mounting arrangement needed for an engine. On the other hand, they are of a size and shape that would allow them to fit within the combustor section of the present W501D. A cross section of this engine appears in Figure 1, with the combustor section conventionally equipped, highlighted at the center. This unit is used exclusively for electrical generation, and is in the 90 MW class. It requires 16 combustors, which, as the figure indicates, are located in a large cylindrical casing surrounding the compressor exit. The volume of this casing is sufficiently generous to allow for the extra piping and slightly larger dimensions of catalytic combustors.

Combustor Requirements That Result From Catalyst Characteristics

The catalytic element, to meet pressure drop constraints, is not designed to function in the combustor when starting the machine, or operating it at idle or part-load conditions. Furthermore, the normal compression heating of the combustion air in the W501D does not bring it to a high enough temperature to meet the inlet needs of the catalyst for 99.9 percent efficient operation even at rated load. Therefore, in the Westinghouse/Engelhard design, Figure 2, a primary zone preburner upstream of the catalyst provides combustion during start-up of the machine. The preburner fuel is then cut back to a low level after start-up, but the preburner remains lit and slightly increases the air temperature going to the catalyst during steady state operation. In Table I, the conditions imposed upon the catalytic element by the combustion requirements of the W501D are highlighted.

Table I

COMBUSTOR OPERATING CONDITIONS IN THE W501D

	Compressor Discharge Conditions	Catalyst Approach Conditions	Catalyst Exit Conditions
(a) At Ignition:			
Temperature, K (°F)	311 (100)	1006 (1351)	1006 (1351)
Pressure, atm	1.177	1.171	1.123
Velocity, m/s (ft/sec)	--	21.5 (70.6)	--
(b) At Rated Load:			
Temperature, K (°F)	638 (689)	700 (800)	1474 (2193)
Pressure, atm	12.741	12.456	12.060
Velocity, m/s (ft/sec)	--	23.7 (77.7)	--

As indicated in Table I, that there is no temperature rise at all through the catalyst at the start-up condition. Instead, the entire 1006K (1351°F) required at the combustor outlet is provided by the primary zone preburner. At Rated Load, however, Take I shows a 744K (1393°F) rise in the catalytic element. The small preburner flame incrementally heats the compressor discharge air from 638K (689°F) to a 700K (800°F) mixture approaching the catalyst. This inlet temperature is necessary to assure that the catalyst will efficiently react the fuel/air mixture over the entire life of the catalyst.

The Experimental Combustor Design Description

The combustor design used for these tests is shown schematically (Figure 2) as it would appear in the engine. The first three rows of holes in the combustor nearest the primary fuel nozzle delineate the extent of the primary zone preburner. Also shown in this zone is the ignitor, which lights the conventional primary zone flame in the usual manner. Immediately downstream of the preburner, a ring of eight nozzles spray secondary fuel radially into the combustor, during catalytic combustor operation. This secondary fuel does not ignite, as described below in the paragraph on preparation of the secondary fuel/air mixture, but mixes with the hot preburner exhaust, and additional combustion air, vaporizes, and passes to the catalytic element where it is reacted via CATATHERMAL (tradename of Engelhard Corporation) combustion. The hot, catalyst exhaust products then accelerate in the funnel-shaped transition duct, and drive the turbine.

The Experimental Combustor as Fabricated for the Test

The first of the experimental combustors appears in Figure 3, as fabricated for the test. The primary fuel nozzle, not shown in this view, would be at the top of the combustor, as it stands vertically (Figure 3). The catalytic element is at the bottom, contained within the largest diameter section. The secondary fuel nozzles appear, mounted on the midsection of the combustor. Since they are continuous air atomizing types, both require fuel and high-pressure air supply tubing, which is shown being installed (Figure 3).

Preparation of the Secondary Fuel-Air Mixture for the Catalytic Element

The eight secondary fuel nozzles are located outside the combustor, to remove them from the hot combustion products of the preburner. This arrangement is shown in the close-up photo in Figure 4. These continuous air atomizing nozzles are designed to generate a cloud or fog of very fine fuel droplets. The droplets are carried into the large, bell-mounted combustion holes shown by their own momentum, and by that of the combustion air flowing into these large holes. (The combustion air is driven by normal burner pressure drop.) Once inside the combustor, the fuel fog turns and flows towards the catalyst, simultaneously mixing with the hot excess air and combustion products from the preburner, and vaporizing. Autoignition is avoided by keeping the preburner exit temperature low, avoiding rich regions, and limiting the residence time between secondary fuel injection and approach to the catalyst. A close-up of one nozzle is shown in Figure 5. It is a Delavan Swirl-Air, Cat. #35200-1, rated at 1 gallon per minute, and having a 50-degree spray angle. It was chosen due to its ability to produce 30 micron droplets, when adequate atomizing air is supplied.

The Catalytic Element as Fabricated for Test

Testing under this program was conducted with an Engelhard CATCOM* (tradename of Engelhard Corporation) catalyst,designated as DXE-442. The 35.5 cm (14 inch) diameter catalyst structure is of a monolithic configuration with two 5.1 cm (2 inch) long segments forming a total length of 10.2 cm (4 inches). The high temperature monolith substrate consists of a zircon composite ceramic material having approximately 40 channels per square cm (250 channels per square inch) of inlet area. This ceramic structure is coated with a catalyst of palladium dispersed and supported on high surface area alumina.

This catalyst has successfully undergone extensive testing, including durability testing to 1,000 hours under a NASA-sponsored program (Reference 4), and is properly suited for the testing requirements of this full scale, full pressure test program.

Catalytic Element Configuration Design --

The major objective associated with the design of the catalyst element configuration is to minimize the pressure loss across the catalyst while assuring essentially complete combustion under specified operating conditions.

Optimum configuration designs vary significantly according to operating condition requirements (especially flow velocities, pressure, and inlet/outlet temperature conditions) and must be designed accordingly for each application.

The catalytic element configuration for this program was designed through the use of Engelhard's CATATHERMAL (tradename of Engelhard Corporation) Combustion Configuration Design Program which models this combustion process on an analytical/empirical basis and affords the design of an optimum catalyst configuration for an application and also predicts the performance over the entire range of operating conditions.

The predicted pressure drop over the catalytic element for this design ranges from about 4.6 percent at base load to 5 percent at peak load of equivalent engine operation.

It is important to note that in the design of this catalytic configuration it was assumed that all combustion (99+ percent efficiency) takes place within the catalytic element. The potential beneficial effect of thermal reactions downstream of the catalyst (afterburn) have not been incorporated into this design. As has been presented by D.N. Anderson (Reference 5) the effect of afterburn can be significant. As additional understanding is gained with regard to properly utilizing the potential benefit of afterburn, it may be possible to modify the catalytic configuration with an associated improvement of pressure drop performance.

CATATHERMAL combustion is probably enhanced with the use of the flame preburner. It has been demonstrated (Reference 6) that a small concentration of unburned products from preburner operation can accelerate the CATATHERMAL combustion process because these fuel species are more reactive in the catalyst than is the primary fuel, #2 fuel oil. This consideration suggests that, depending upon preburner operating characteristics, it may be possible to further improve pressure drop performance through catalytic configuration design modification.

Catalyst Assembly Structural Design --

The structural characteristics of the catalyst assembly, which consists of the catalyst mounted in a metal housing, is an important factor with regard to adequate design of large scale catalytic combustor applications. The assembly must be capable of withstanding severe mechanical and thermal operating requirements.

The catalyst element is exposed to the large pressure drop conditions during engine operation, especially during preburner operation when the engine is being started. During this period the catalyst element is exposed to approximately 15 psi (8 percent) pressure drop which translates to the equivalent of 2300 pounds axial force uniformly applied to the catalyst. The most important considerations are the integrity of the catalyst to withstand bending and axial retention stresses. Vibration loading from engine operation imposes additional stresses on the catalyst assembly.

The ceramic catalytic element undergoes thermal expansion and contraction during operation and must be properly mounted to assure adequate retention during these thermal cycles. Additionally, the catalytic element will operate at temperature levels up to 1700K (2600°F) which far exceed the limits of the metallic holder; therefore, provisions must be made to insulate and cool the metal container.

The mounting design of the catalyst element to the metallic holder is a key factor in the capability of the CATCOM combustor to meet these structural operating requirements.

The specific catalyst mounting design used for this program is illustrated in Figure 6. The catalyst is contained under a compressive radial load by the metal mounting shell and the ceramic fiber mounting material. In addition to providing adequate thermal insulation, the ceramic fiber mounting material accommodates the difference between the thermal expansion properties of the catalyst and mounting shell to assure that the catalyst has adequate radial compressive loads under all operating temperatures. The axial retention rings are assisted by the compressed ceramic mounting material in retaining the catalyst under axial loads. Similar mounting designs have been presented for combustion systems using a catalyst (Reference 7) as well as for other high temperature applications of catalysts.

Prior to combustion tests, the catalyst assembly was successfully tested at room temperature with simulated axial loads at levels exceeding operating requirements.

CATATHERMAL Combustion Performance Analysis --

Analysis and interpretation of the program combustion test results requires an understanding of the basic process of CATATHERMAL combustion. As Reference 1 described in detail, this process consists of both heterogeneous catalytic and homogeneous thermal combustion reactions occurring in the catalytic combustor element. Heterogeneous catalytic reactions occur on the surface of the catalyst channel walls; whereas the homogeneous thermal reactions occur at elevated temperatures throughout the bulk gas stream within the catalyst channels.

Because the heterogeneous catalytic reactions occur at the surface of the catalyst walls it is necessary to transport, via mass transfer, reactant molecules from the bulk gas stream to the catalyst surface. With the specific combustor configuration designed for this program, only 65 percent of the reactant molecules can react catalytically because of mass transfer limitation. Design of catalyst which would produce 99 percent combustion efficiency via heterogeneous catalysis is generally not feasible for most combustion turbines from the standpoints of excessive catalyst size requirements and associated prohibitive pressure drop performance.

Homogeneous thermal reactions occur at a much higher rate than heterogeneous catalytic reactions because the reaction rate is not mass transfer limited; however, homogeneous thermal reactions do not occur until high temperature levels are achieved. For this combustor application, which uses #2 fuel oil, homogeneous thermal reactions commence at about 1090K (1500°F), depending more specifically upon operating conditions. In order to achieve essentially complete combustion within the catalyst, a significant amount of thermal reaction must occur such that the catalyst outlet temperature is above approximately 1260K (1800°F).

The predicted combustion performance for this program design can be roughly summarized as follows:

Outlet Temperature	Combustion Efficiency
<1090K (<1500°F)	65 %
1090K-1260K (1500-1800°F)	65-99%
>1260K (>1800°F)	>99%

As each catalyst channel is an individual combustion chamber the above applies to each catalyst channel, as well. Therefore, the overall performance of the catalyst requires a fairly uniform inlet temperature and fuel/air ratio profile such that the outlet temperature from individual catalyst channels range from at least 1260K (1800°F) to no more than 1700K (2600°F), the upper operating temperature unit of the catalyst.

METHOD OF TEST

Catalyst Instrumentation

Prior to test, the catalytic element was instrumented with approximately 30 thermocouples. Some were located on the inlet face of the catalyst, some on the exit, and two half-way along, axially. Figure 7 is a close view of the inlet face of the catalyst before test with thermocouples attached. Initially, platinum/platinum-rhodium thermocouples were used for the exit, and chromel/alumel for the inlet. Subsequently, it has been found possible to attain adequate instrumentation life with chromel/alumel at all locations. Thermocouple wire of 0.040 inch diameter is used, and the junctions are located 0.25 inches in from the catalytic element face (either upstream or downstream), in holes drilled in the catalyst substrate. Junctions are secured in the holes with high temperature cement. All thermocouple leads are located on the upstream face as shown in Figure 8. Downstream thermocouple leads pass from the periphery of the catalytic element to the desired junction location on the upstream face of the catalyst. Then they go to the downstream face through holes drilled in the catalytic element, parallel to its axis. In initial testing, the majority of the thermocouples were located on the upstream face to detect flashback. In subsequent testing this precaution has been found unnecessary, and the majority of the thermocouples are now located on the downstream face to measure exit temperature pattern. Figure 9 shows the thermocouple leads being threaded through the combustor body as it was being lowered on to the catalytic element prior to test. Also bundled together with the thermocouple leads were two slender tubes, used to sense catalyst upstream and downstream static pressure. Upstream of the catalytic element all leads passed to the exterior of the combustor, where they were gathered into armored flexible conduits. These conduits, together with others carrying leads from the combustor surface thermocouples, and carrying fuel or atomizing air, were all led to a heavy pressure closure cover located at the primary nozzle end of the combustor. Cover and conduits appear in Figure 10, which shows the completed catalyst/combustor assembly being carried by overhead crane to the test cell.

Test Rig

The test rig uses baffles to direct the airflow around the combustor in the same reverse flow pattern as in the combustor section of the engine. This is shown in the schematic of the test rig, Figure 11. An actual photo of the test rig appears in Figure 12. The rig is designed to handle in excess of the 12.7 atm pressure and 1480K (2200°F) exit temperature required for catalytic combustor operation. Furthermore, it is connected to an air supply facility capable of supplying unvitiated combustion air exceeding the 700K (800°F) and 20 kgm/sec (44 lb/sec) needed for evaluating these full scale combustors.

Test Procedure

With the catalytic combustor fully instrumented, and attached to the cover plate, the entire assembly was installed in the test rig as shown in Figure 13. All instrumentation leads pass through the cover, to allow rapid combustor changes.

For primary zone (preburner) testing, all fuel was directed to the primary nozzle only. Tests were made for ignition at a simulated cranking condition, for lean blowout at a condition representing the mode where the primary functions as a preburner, and for emissions and performance, in the mode where the preburner is supplying all turbine energy (idle to mid-load). Typical test conditions for these modes are shown in Table II.

Table II

TYPICAL TEST CONDITIONS

A. Primary Zone: Light-Off Tests

Inlet Pressure:	128 KPa	(18.6 psia)
Inlet Temperature:	335 K	(144°F)
Catalyst Approach Velocity:	12.5 m/s	(41 fps)
Fuel/Air Ratio:	0.0090	--

B. Primary Zone: Lean Blowout Tests

Inlet Pressure:	1100 KPa	(160 psia)
Inlet Temperature:	622 K	(660°F)
Catalyst Approach Velocity:	27 m/s	(90 fps)
Fuel/Air Ratio:	0.0020 to 0.0006	

C. Primary Zone: Performance Tests

Inlet Pressure:	1100 KPa	(160 psia)
Inlet Temperature:	622 K	(660°F)
Catalyst Approach Velocity:	27 m/s	(90 fps)
Fuel/Air Ratio:	0.002 to 0.014	

D. Secondary (Catalytic) Zone Tests

Inlet Pressure:	1100 KPa	(160 psia)
Inlet Temperature:	728 K	(850°F)
Catalyst Approach Velocity:	23 m/s	(75 fps)
Fuel/Air Ratio:	0.012 to 0.016	

For secondary, or catalytic mode combustion testing the preburner was not operated. Warm air was supplied by the facilities air heaters. Thus secondary, or catalytic zone tests were run completely free of any interaction with the primary burner. Eventually, it is planned to run tests in which the preburner is kept ignited at a low level, while the catalytic zone is tested. Such tests will not be undertaken until the primary and secondary zones have been developed adequately, by themselves.

In secondary zone testing, the test rig was brought up to the desired full pressure, temperature and catalyst approach velocity conditions with purge air flowing through the secondary fuel nozzles to keep them cool. When conditions appeared stable, secondary fuel was brought on gradually. Even though the test rig was at a high pressure, and at approximately 700K (800°F) temperature, no sudden pulse resulted. Instead, catalytic reaction began immediately, and was noted on the catalyst exit thermocouples. Fuel flow was gradually brought to the desired value to simulate full power operation, while pressure and airflow were continually reset to compensate for increasing pressure drop through the catalyst due to temperature rise. Catalyst inlet thermocouples were used to detect preignition of fuel-air mixture upstream of the catalyst.

RESULTS

The Preburner (or Primary Zone)

Primary zone operation resulted in such good values for ignitability and lean blowout that emphasis was shifted to secondary (catalytic) zone development. The primary zone had been designed to maximize stability, by using a small size, continuous-air-atomizing nozzle, and two air swirlers to give a very strong recirculation zone. As a result, light-off occurred at a lower fuel flow than standard conventional combustors, and lean blowout was also superior. This meant that the primary zone would be able to function well in its proposed roles as a preheater for the catalyst air, and also as a starting burner. At this point development emphasis shifted to the secondary (or catalytic) zone, and the facilities air heaters were substituted for the primary zone as a source of warm air for the catalyst. This was done to segregate primary zone effects during secondary zone testing.

A photo of the combustor as it appeared following both primary and secondary testing is shown in Figure 14. The combustor wall areas appear to have overheated from high fuel/air ratio primary zone operation. Certain temporary test hardware embodied in this combustor blocked wall film cooling locally. Furthermore, it appears that a finalized design would require an additional cooling louver between the Row 2 and Row 3 combustor holes, a relatively easy change.

The Catalytic Zone - General Observations

In its initial configuration, the secondary fuel/air preparation zone showed a tendency to deliver a centerline-peaked fuel/air profile to the catalytic element. Therefore, it has been determined that early development work will emphasize improving the secondary fuel/air presentation system. In spite of the center-peaked fuel/air distribution, it was possible to run for several hours, recording various types of data. Neither autoignition nor flashback presented a problem. There was no tendency to flamehold anywhere along the flaring combustor wall downstream of the fuel injectors. Fuel leakage in the experimental secondary fuel delivery hardware caused unexpected hot spots in some test runs, and is being remedied by design and fabrication improvements.

A photo of the catalytic element following the same primary and secondary zone testing series is shown in Figure 15. At the time of the photo, this element had been subjected to approximately 7 hours of high pressure high temperature secondary fuel operation, and 4 hours of primary zone firing. Temperature patterns recorded by thermocouples indicated the need to develop an improved secondary fuel/air distribution.

Emissions Results

Although fuel/air distribution is still under development, preliminary emissions measurements were also made to establish a benchmark (Figure 16). It should be remembered in interpreting the emissions results of Figure 16 that they were obtained with a center-peaked fuel/air profile approaching the catalyst. Examining first the emissions of oxides of nitrogen (NO_x) the extremely promising characteristic of this burner shows in a level of only 1 to 2 ppm NO_x in the catalytic mode (exhaust temperatures above 1144K/1600°F). In the preburner mode, shown on the same graph, NO_x increases sharply up to 70 ppm, as fuel to the primary increases. The increase with temperature follows the curve typical for all conventional diffusion-flame burners. Between outlet temperatures of 1117K (1550°F) and 1228K (1750°F), fuel is shifted completely from preburner to catalytic secondary, and NO_x emissions fall from 65 ppm to 1 or 2 ppm.

Emissions of carbon monoxide, CO, and unburned hydrocarbons, UHC, are also shown in Figure 16. In the preburner mode, these emissions are very low, indicating high combustion efficiency there. In the catalytic mode, CO and

UHC are high, due to the uneven fuel/air distribution approaching the catalyst. In the fuel rich central area the catalyst worked well, but around the periphery, the fuel mixture was too lean to obtain an outlet temperature of 1260K (1800°F) as required for efficient CATATHERMAL combustion and unburned or partially burned products were present in the exhaust. The high CO and UHC emissions will be reduced by fuel/air distribution system development.

Temperature Pattern Results

The effect of the fuel rich core is most clearly seen in exit temperature pattern. Figure 17 shows the exit temperature pattern at a predicted average catalyst outlet temperature of 1182K (1668°F). In the center, the outlet temperature is close to the safe upper limit of catalyst operation, 1700K (2600°F). Further increases in fuel/air ratio were not attempted. With such a distribution, the desired turbine inlet temperature of 1367K (2000°F) could not be attained. In continuing experimental efforts at Westinghouse, progress is being made to give a good catalyst inlet fuel profile, while retaining the durability advantages of nozzle location outside the combustor.

CONCLUSION

Full-scale, full-pressure tests at Westinghouse have shown that a catalytic combustor with fuel injection from the sides can operate on No. 2 distillate fuel under engine conditions. Ultra low emissions of NO_x have been demonstrated, as was expected, when operating in the purely catalytic mode. Further development is required and is currently in progress on secondary fuel/air distribution. Data being obtained as this report is written shows a greatly improved profile. Before engine application of these combustors, development work in engine control, primary/secondary interaction, and catalytic element durability is also needed. Analytical design for a catalytic combustor to be adapted to the requirements of a W501D combustion turbine was performed by Westinghouse and Engelhard under Electric Power Research Institute Contract RP1657 and will be reported at the 27th International ASME Gas Turbine Conference, March 1982.

REFERENCES

1. DeCorso, S.M., Mumford, S.E., Carrubba, R.V., and Heck, R.M., "Catalysts for Gas Turbine Combustors - Experimental Test Results," Am. Soc. of Mech. Engrs. Paper No. 76-GT-4, March 21, 1976.
2. Carl, D.E., Krepinevich, M.C., and Osgerby, I.T., "High Pressure Test Results," EPA Proceedings, Fourth Workshop on Catalytic Combustion, Cincinnati, Ohio, May, 1980.
3. Angello, L.C., "EPRI Stationary Gas Turbine Catalytic Combustor Development Program," EPA Proceedings, Fourth Workshop on Catalytic Combustion, Cincinnati, Ohio, May, 1980.
4. Osgerby, I.T., Olson, B.A., Lee, H.C., "CATCOM Catalyst 5 Atmosphere 1000 Hours Aging Study using #2 Fuel Oil," Proceedings Fourth Workshop on Catalytic Combustion (Cincinnati, Ohio, May 1980).
5. Anderson, David N., "The Effect of Catalyst Length and Downstream Reaction Distance of Catalytic Combustor Performance," EPA Proceedings Fourth Workshop on Catalytic Combustion (Cincinnati, Ohio, May 1980).
6. Osgerby, I.T., et al, "Effects of Vitiation on Axial Catalyst Bed Temperature Profiles," ASME Paper 81-GT-141, December, 1980.
7. Lew, H.G., et al, "Experimentally Determined Catalytic Reactor Behavior and Analysis for Gas Turbine Combustors," ASME Paper 79-GT-150, March 1979.

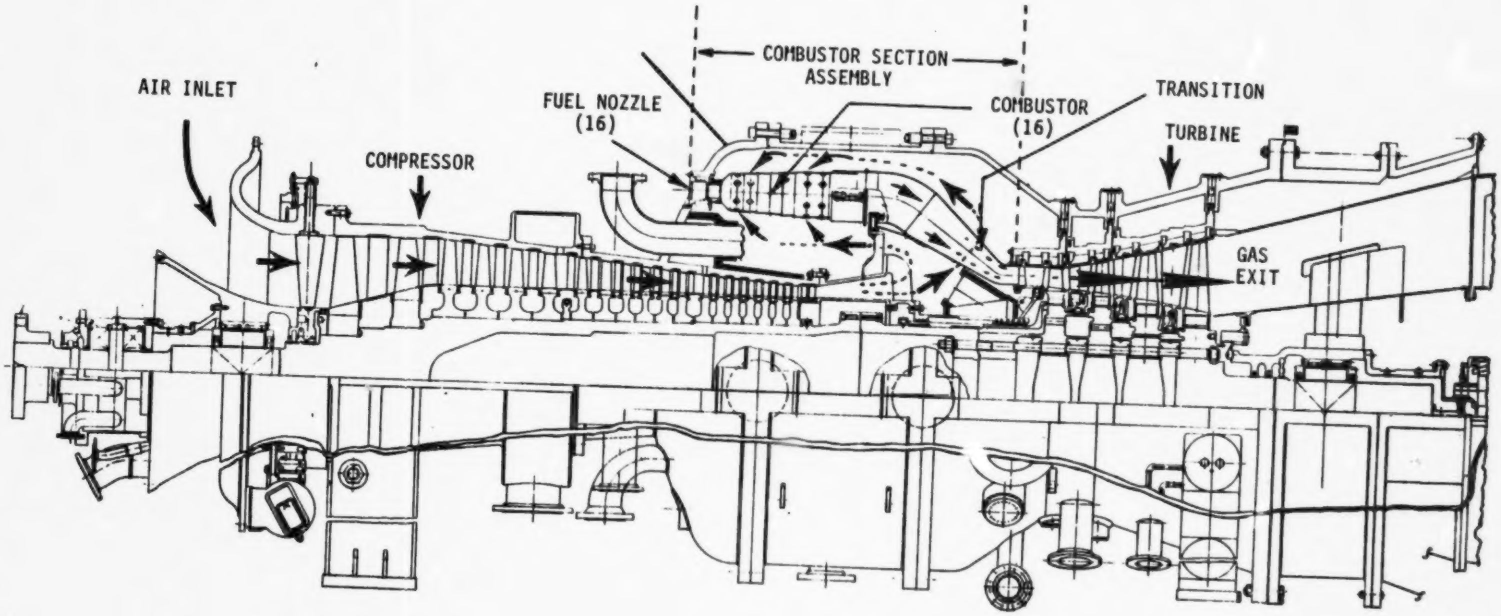
AIR INLET
COMPRESSOR
FUEL NOZZLE (16)
COMBUSTOR SECTION ASSEMBLY
COMBUSTOR (16)
TRANSITION
TURBINE
GAS EXIT

Figure 1. W501D Combustion Turbine

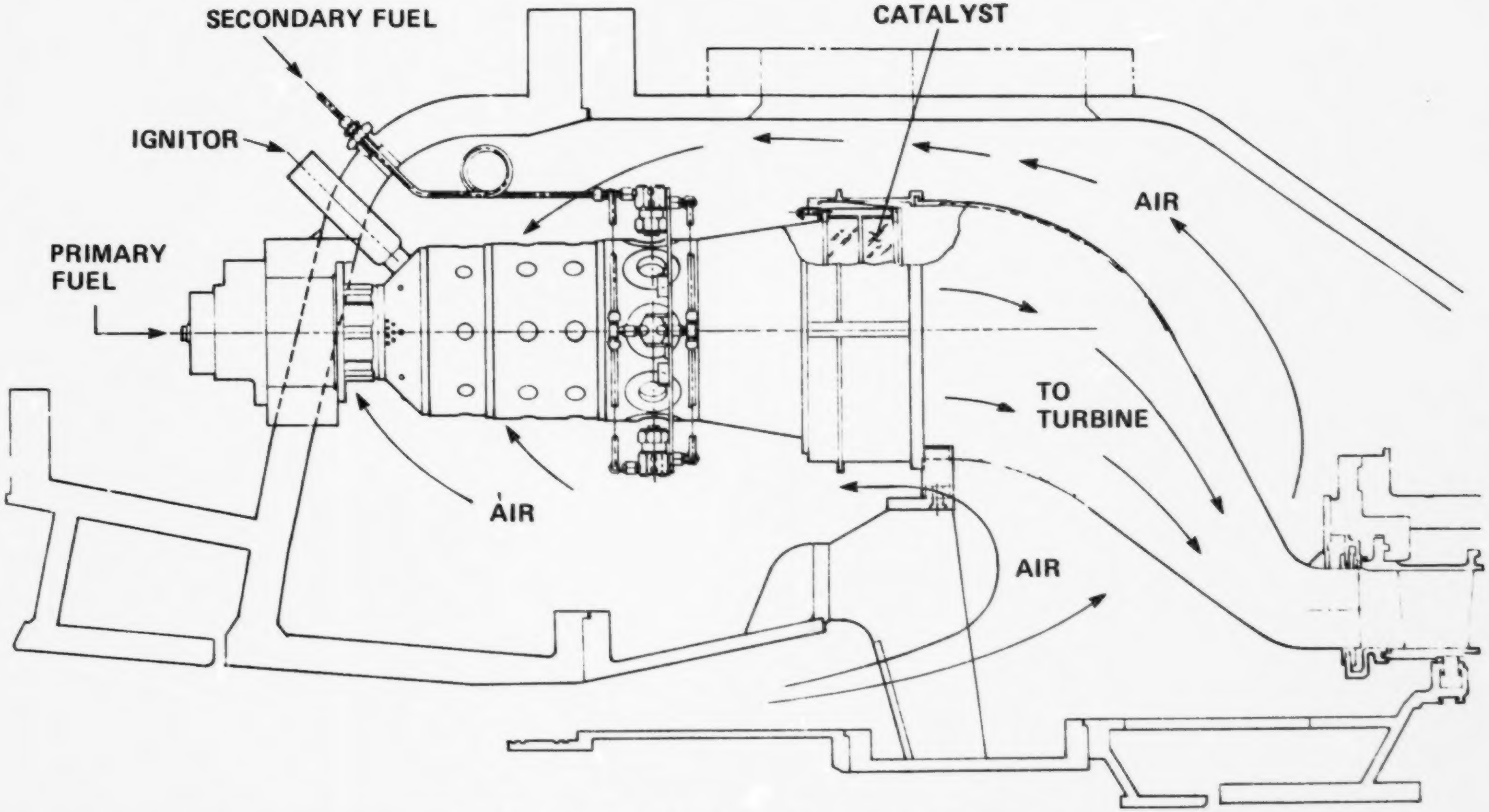
SECONDARY FUEL
CATALYST
IGNITOR
PRIMARY FUEL
AIR
TO TURBINE
AIR
AIR

SCHEMATIC OF THE WESTINGHOUSE/ENGELHARD CATALYTIC COMBUSTOR CONCEPT AS IT WOULD APPEAR IN AN ENGINE

Figure 2. Schematic of the Westinghouse/Engelhard Catalytic Combustor

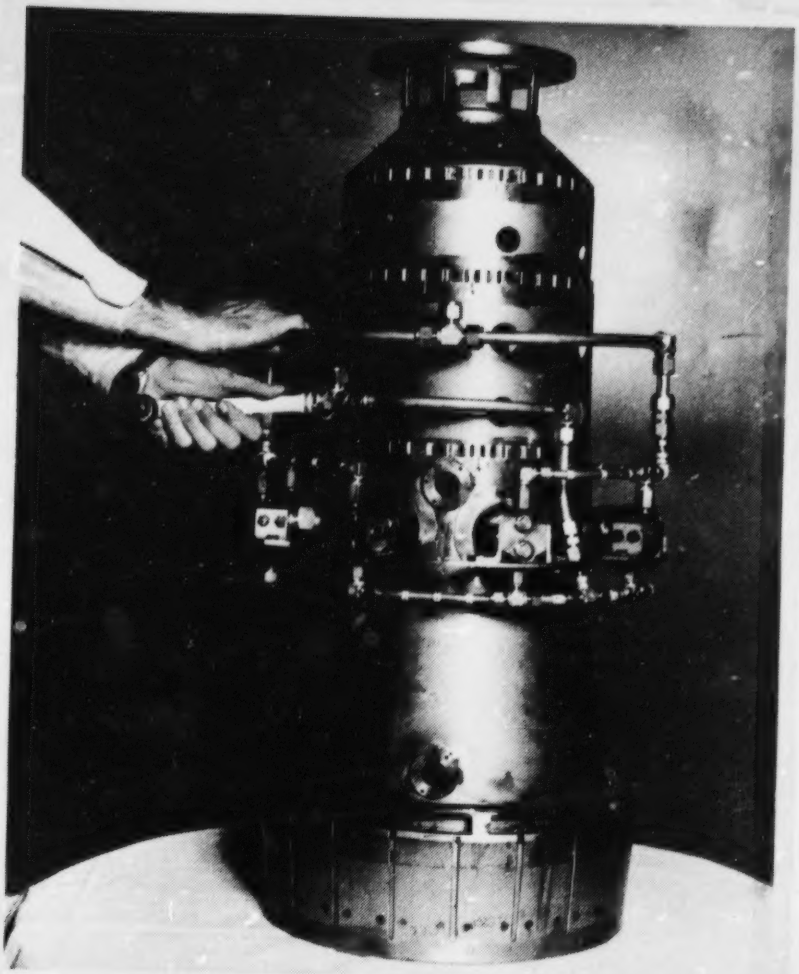

Figure 3. Photo of the Westinghouse/Engelhard Catalytic Combustor Concept as it would Appear in an Engine

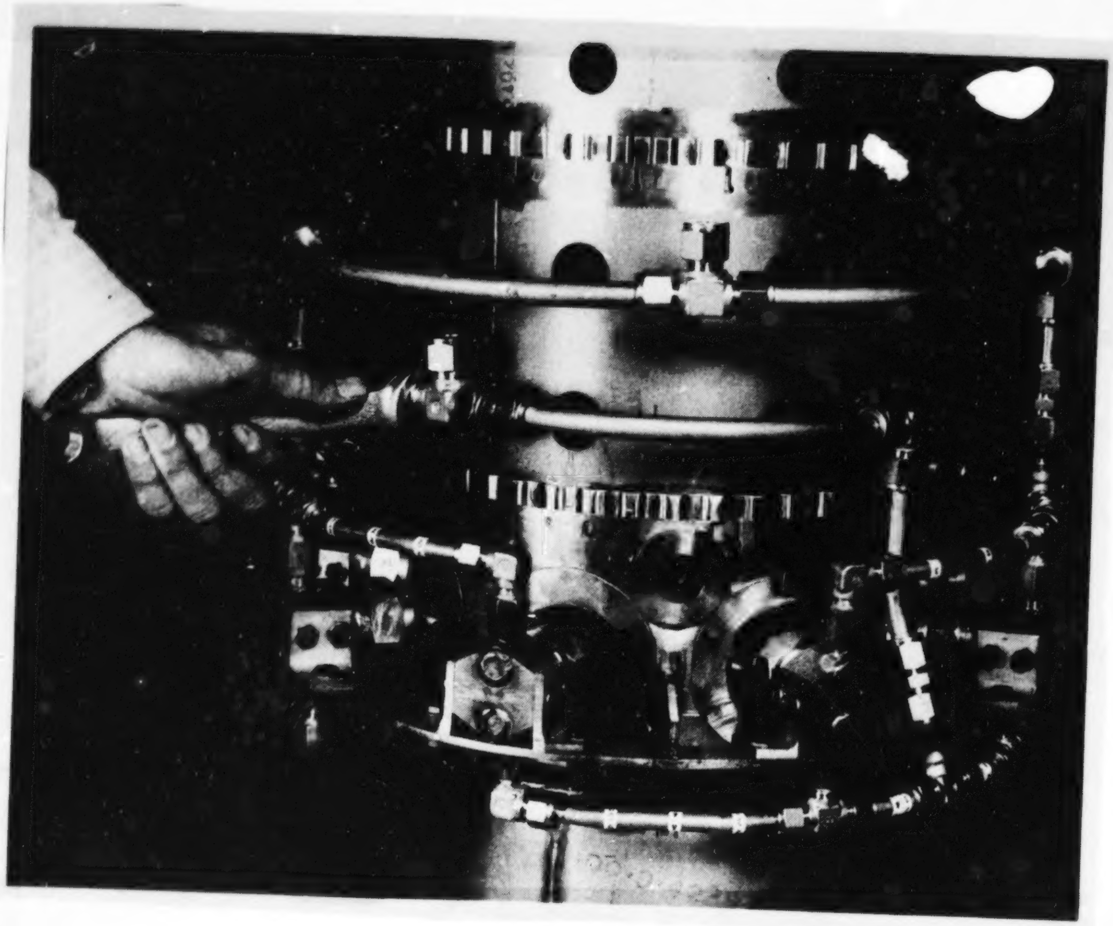

Figure 4. Photo of the Secondary Fuel Injection Section of the Experimental Catalytic Combustor Showing Fuel and Atomizing Air Tubing

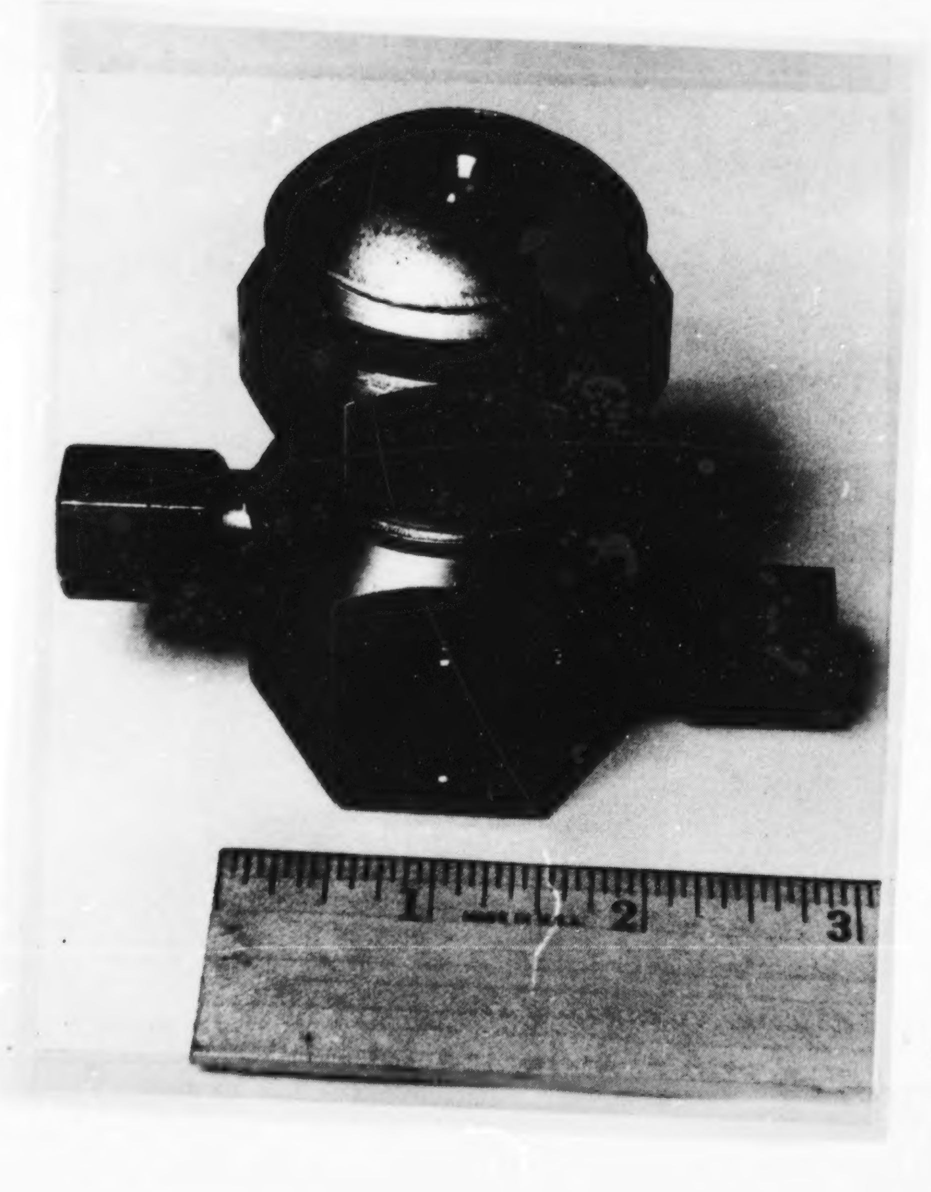

Figure 5. Photo of One of the Eight Continuous Air Atomizing Fuel Nozzles Used for the Secondary Zone

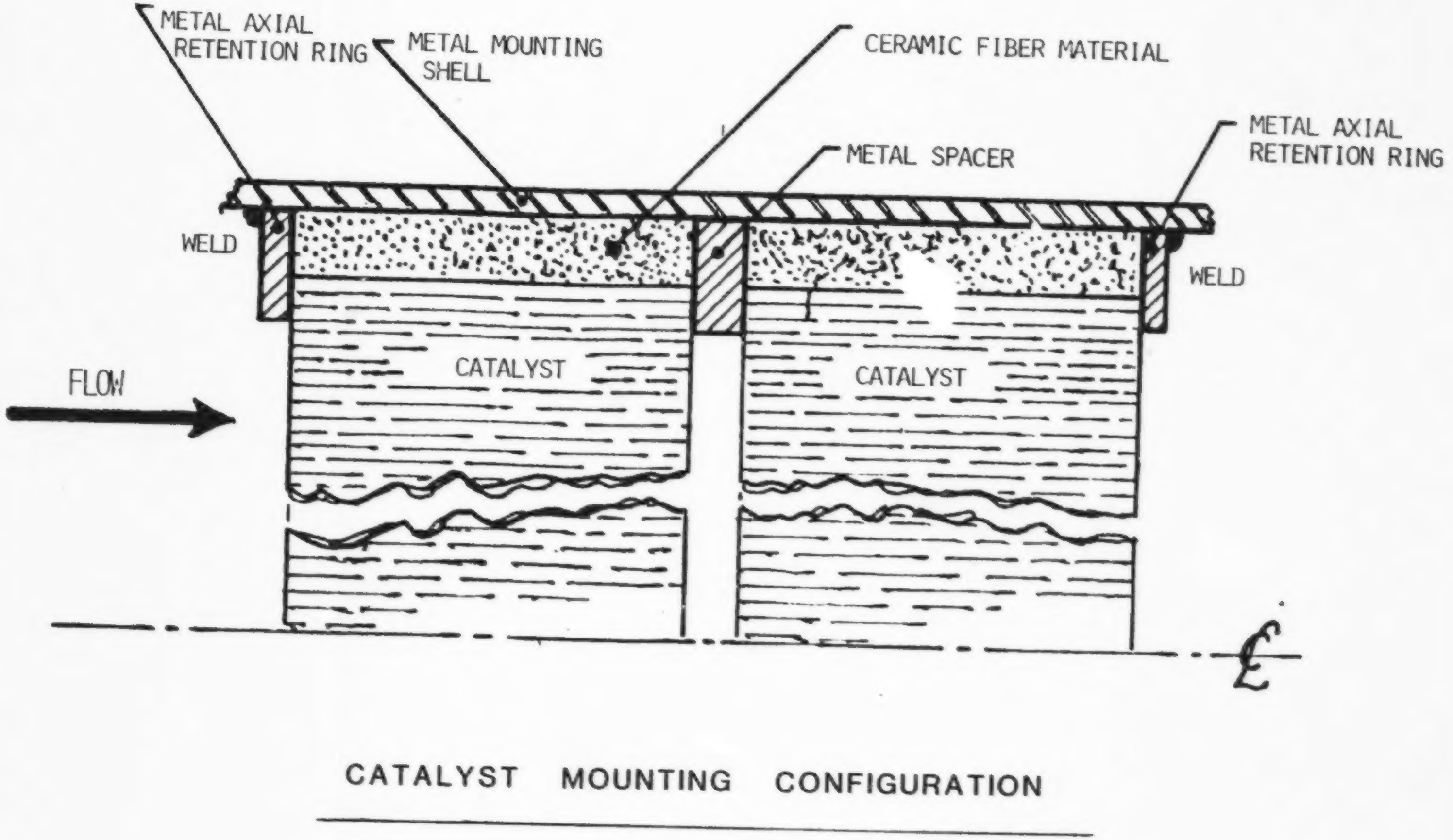
METAL AXIAL RETENTION RING
METAL MOUNTING SHELL
CERAMIC FIBER MATERIAL
METAL SPACER
METAL AXIAL RETENTION RING
WELD
WELD
FLOW
CATALYST
CATALYST
℄
CATALYST MOUNTING CONFIGURATION

Figure 6. Catalyst Mounting Configuration

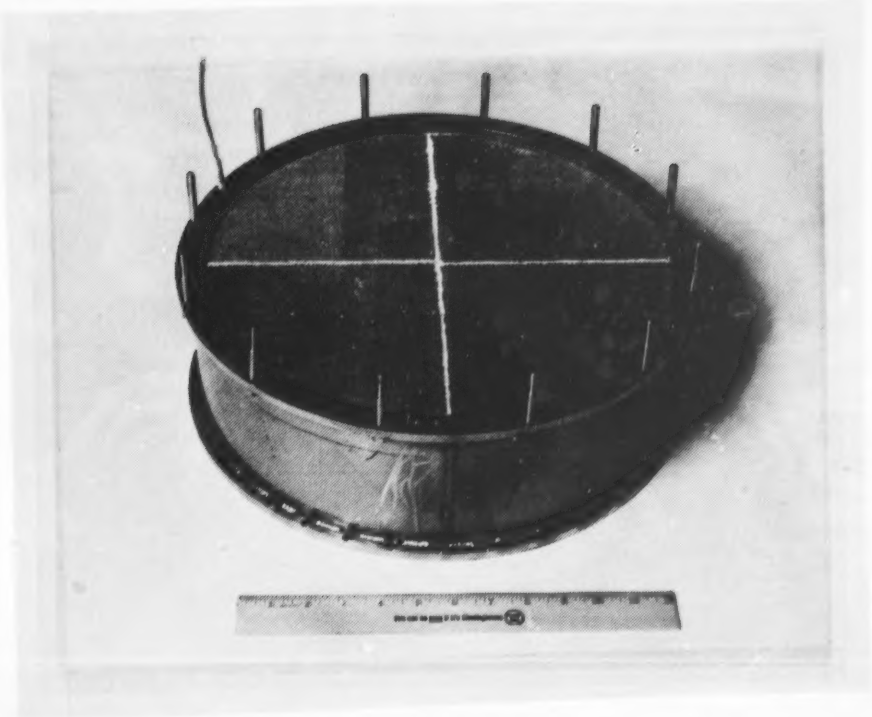

Figure 7. Photo of One of the Engelhard DXE-442 Catalytic Elements Used in this Test Series

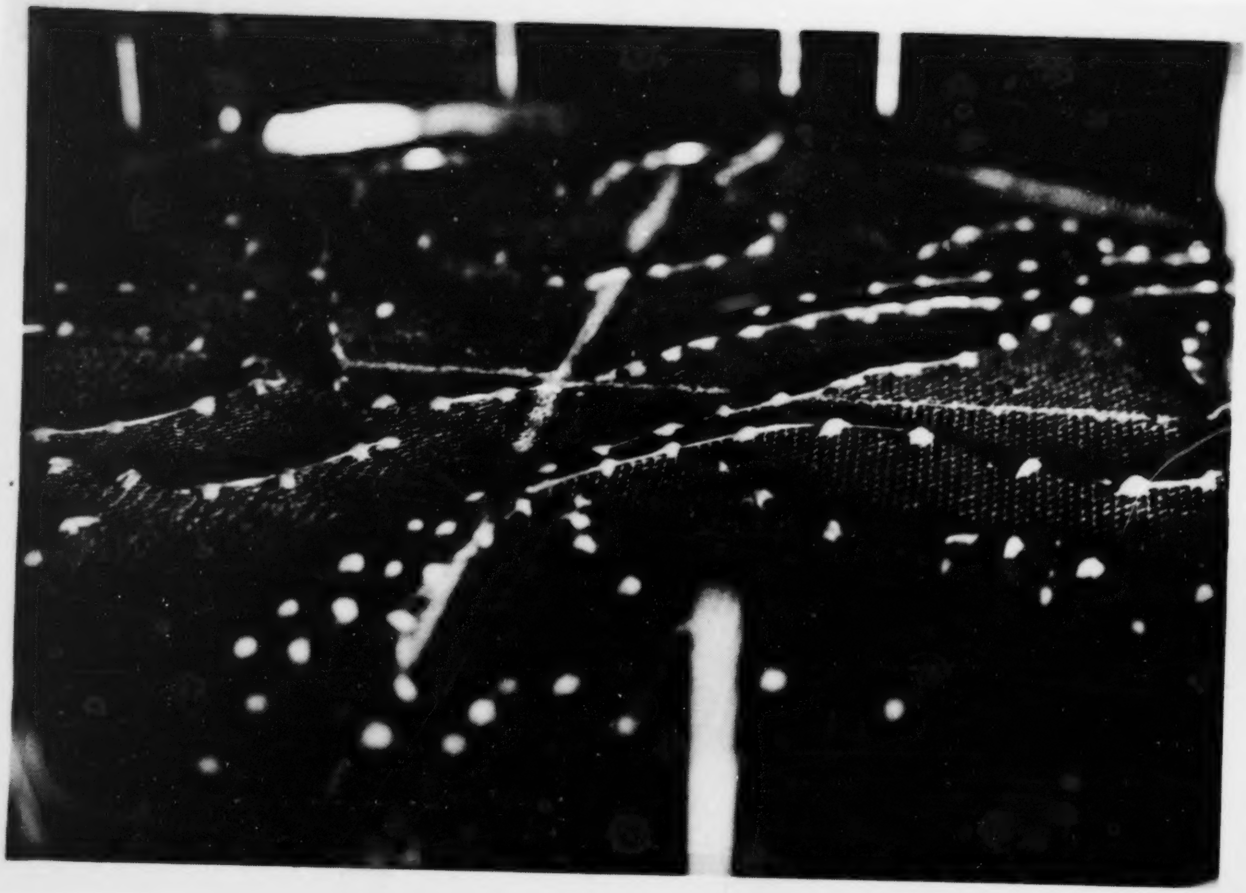

Figure 8. Close-up of Upstream Face of Catalystic Element, as Instrumented with Thermocouples Prior to Test

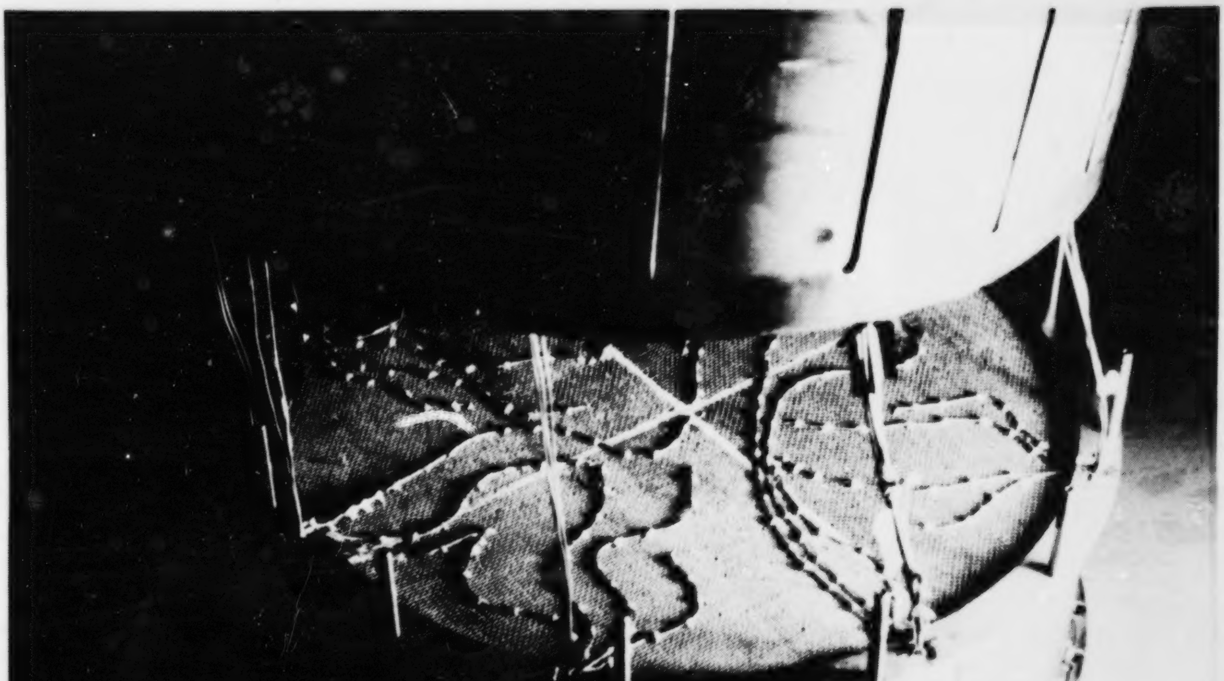

Figure 9. Photo Showing Test Combustor Being Lowered on to Instrumented Catalytic Element, Prior to Test

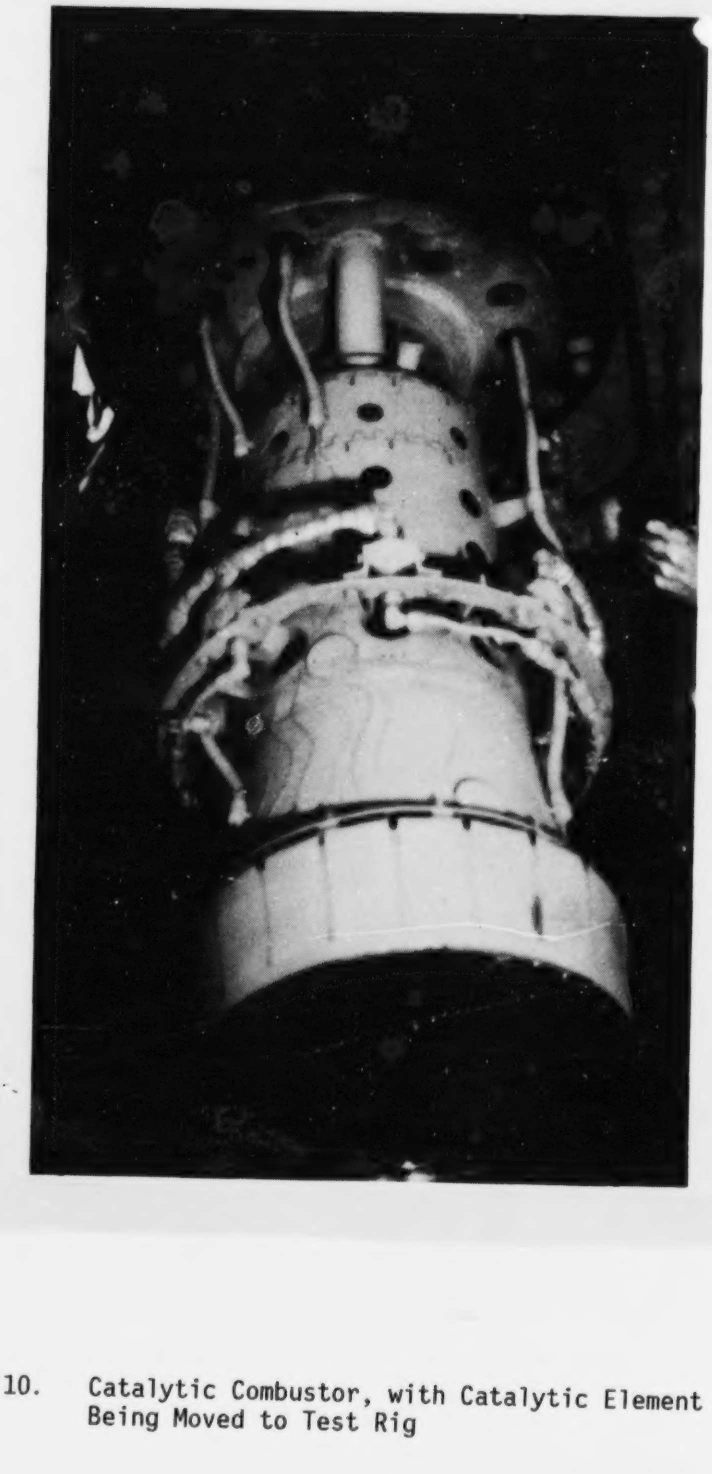

Figure 10. Catalytic Combustor, with Catalytic Element Installed, Being Moved to Test Rig

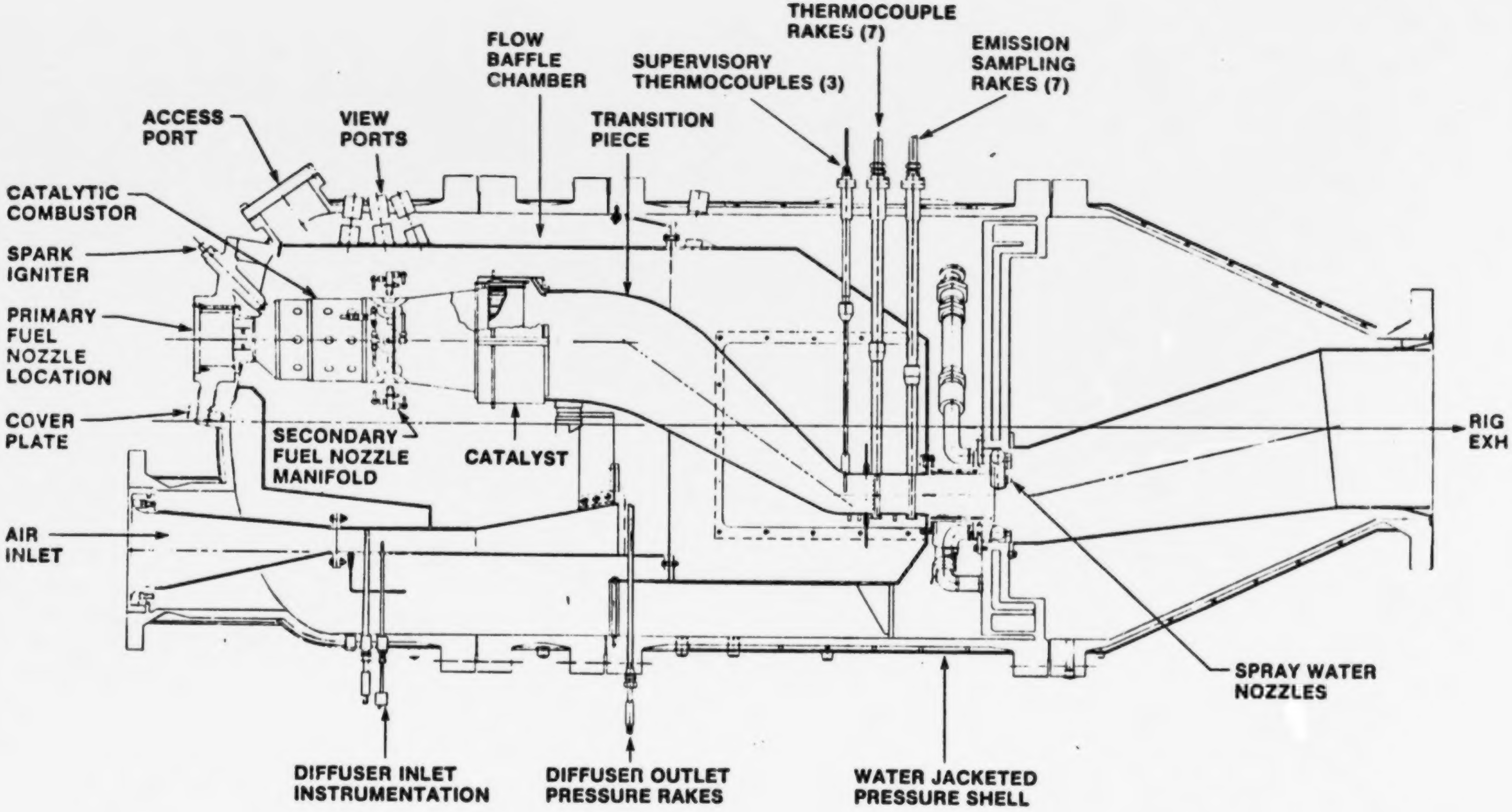
W501D COMBUSTOR DEVELOPMENT RIG
WITH CATALYTIC COMBUSTOR INSTALLED

THERMOCOUPLE RAKES (7)
FLOW BAFFLE CHAMBER
SUPERVISORY THERMOCOUPLES (3)
EMISSION SAMPLING RAKES (7)
ACCESS PORT
VIEW PORTS
TRANSITION PIECE
CATALYTIC COMBUSTOR
SPARK IGNITER
PRIMARY FUEL NOZZLE LOCATION
COVER PLATE
SECONDARY FUEL NOZZLE MANIFOLD
CATALYST
RIG EXH
AIR INLET
SPRAY WATER NOZZLES
DIFFUSER INLET INSTRUMENTATION
DIFFUSER OUTLET PRESSURE RAKES
WATER JACKETED PRESSURE SHELL

Figure 11. W501D Combustor Development Rig

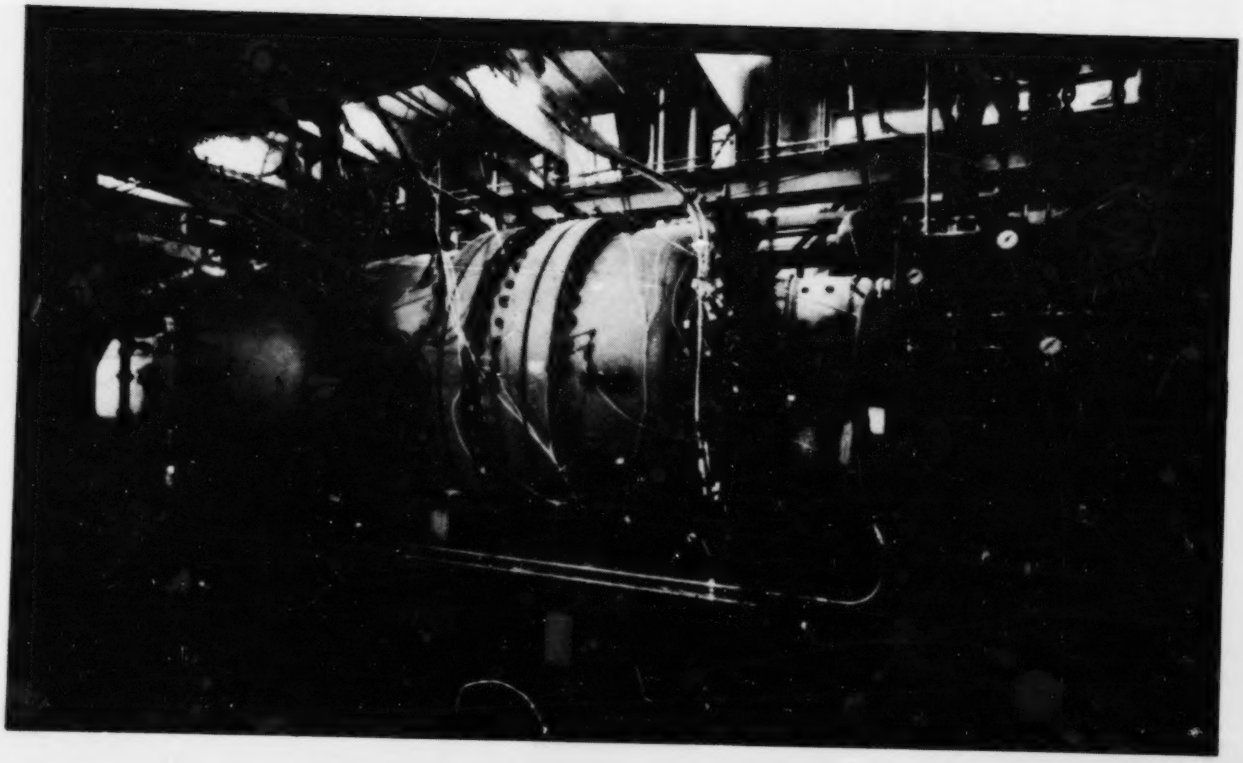

Figure 12. Photo: Full-scale Combustor Test Rig at Concordville Development Center

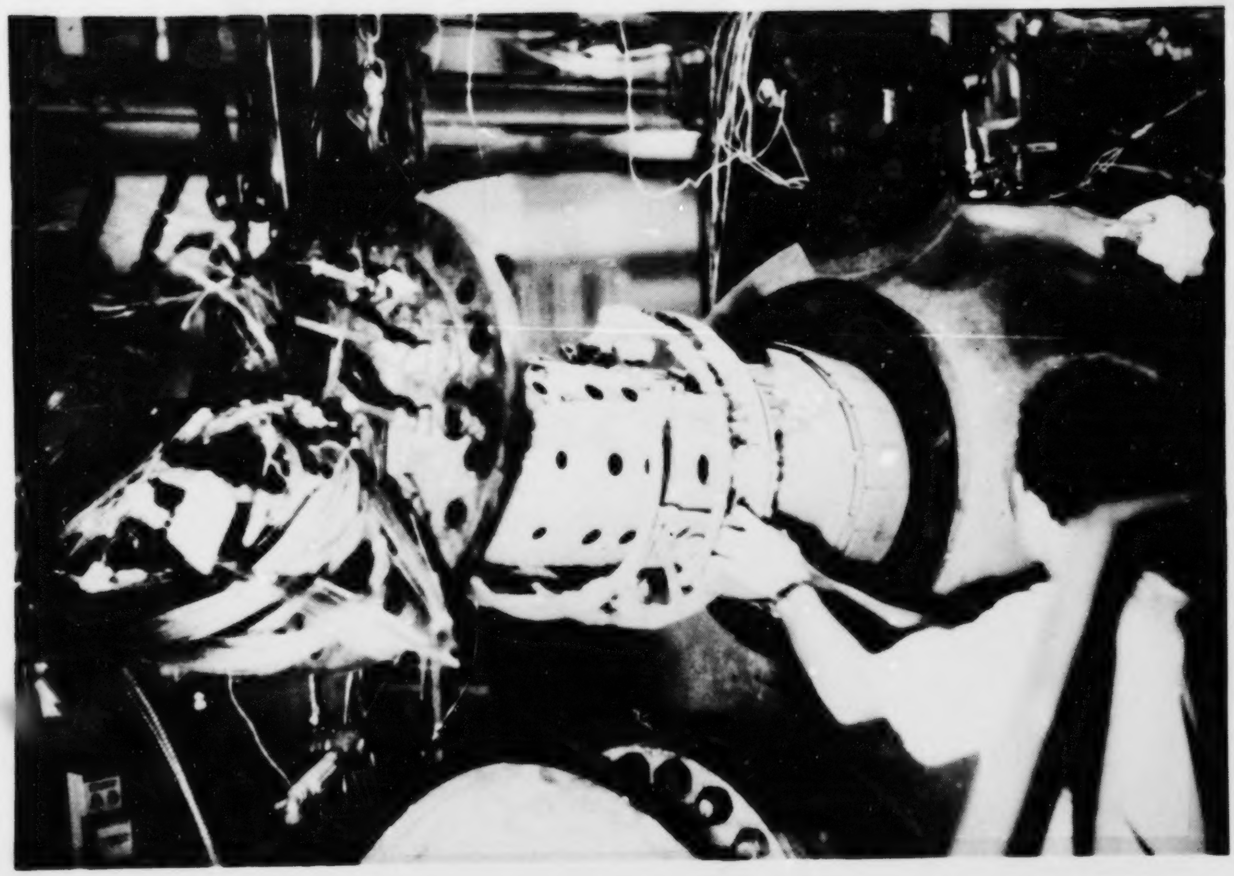

Figure 13. Guiding the Fully Instrumented Catalytic Combustor into the Test Rig

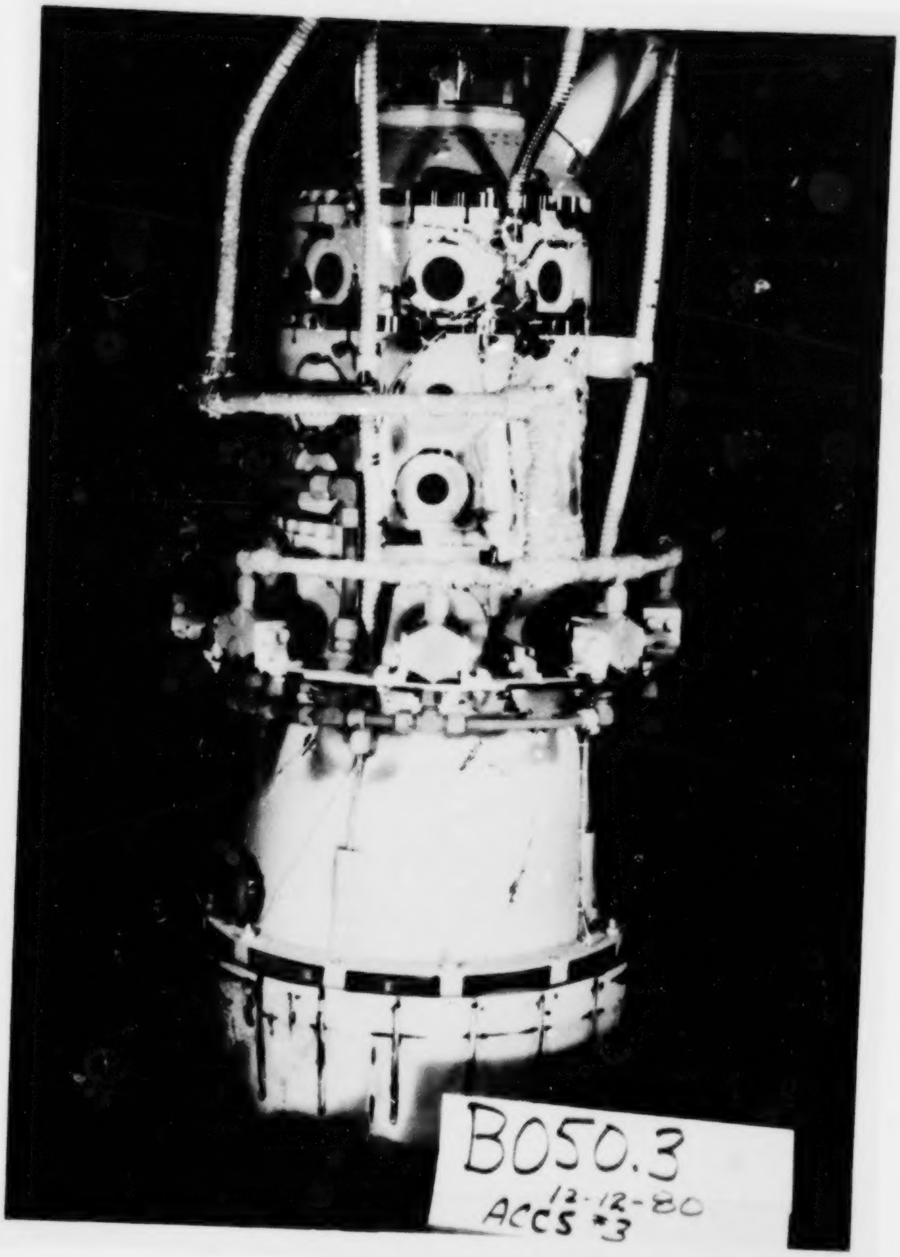
B050.3
12-12-80
ACCS *3

Figure 14. Photo of Catalytic Combustor, Following Combustion Tests of Both Primary and Secondary Zones

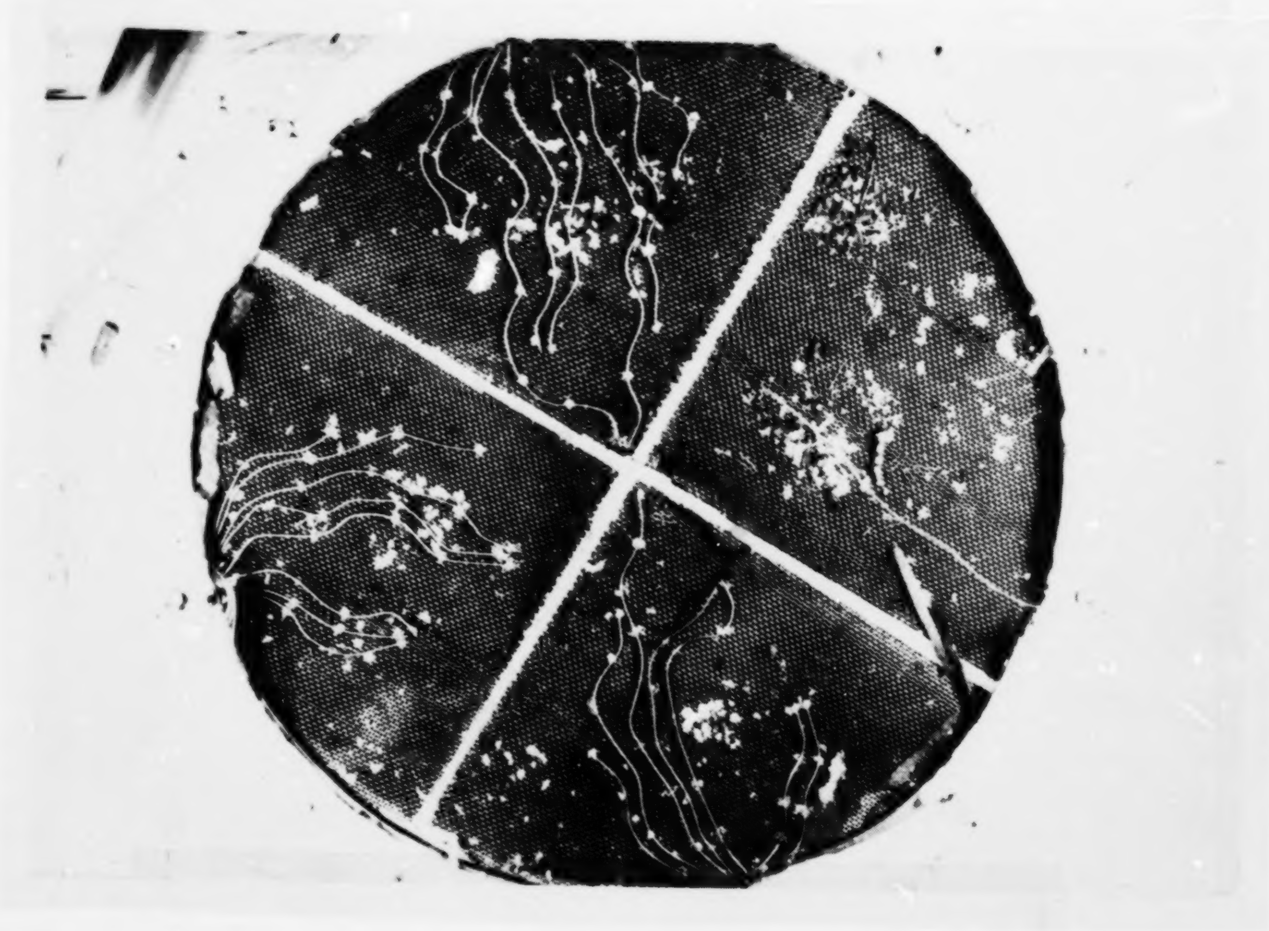

Figure 15. Upstream Face of Catalytic Element Following Combustion Testing in Both Primary-only and Secondary-only Modes

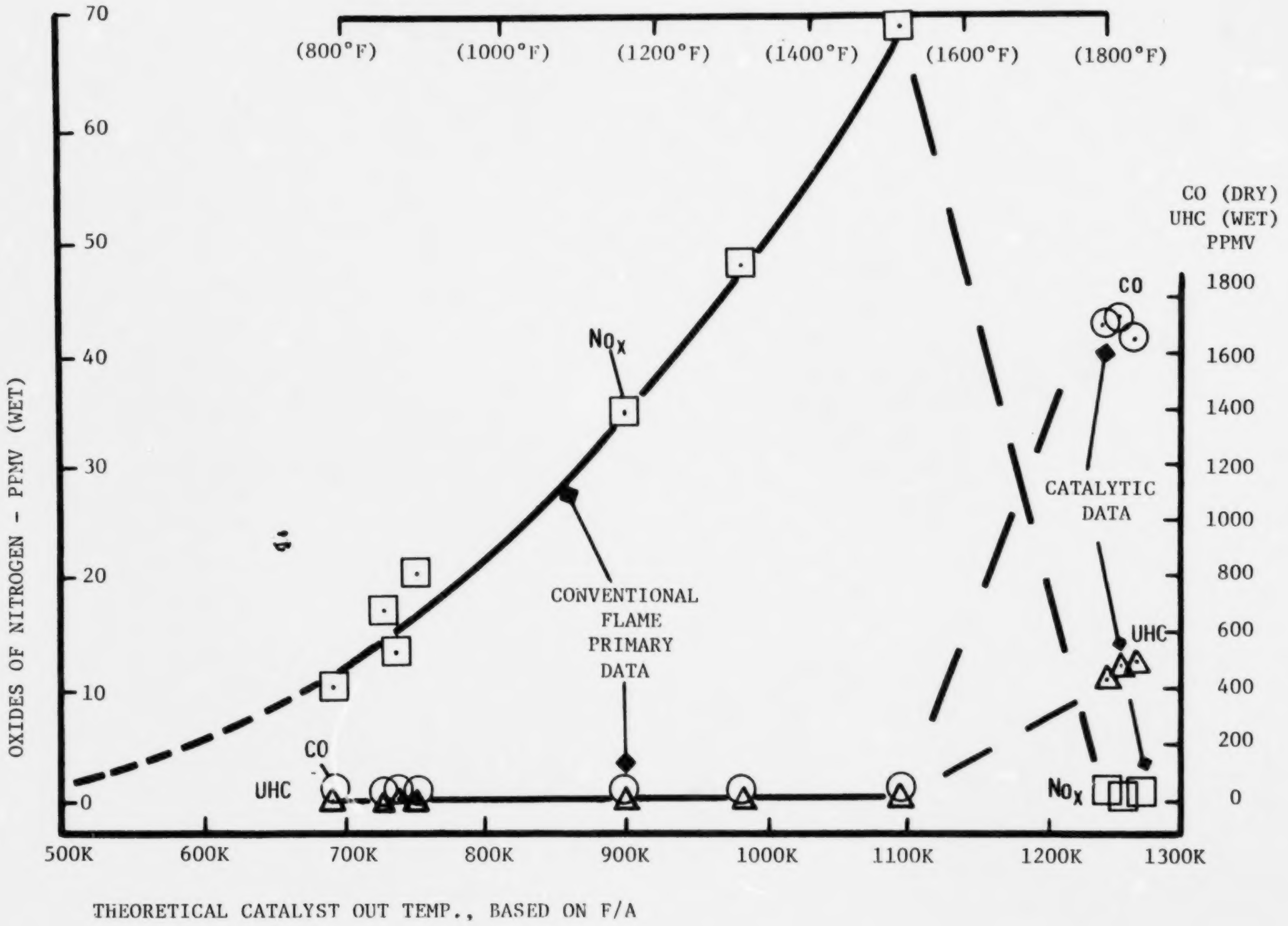

Figure 16. Preliminary Emissions Results

TEST No: B50. 2 RUN No: 2

T2C= 860. DEG F Tcatin= 847. DEG F

P2C= 101.2 PSIG Tcatout= 1668. DEG F

Vcat= 71.7 FT/S ΔP/Pcat= 3.26 %

CATALYST DIAMETER = 14.0 INCHES

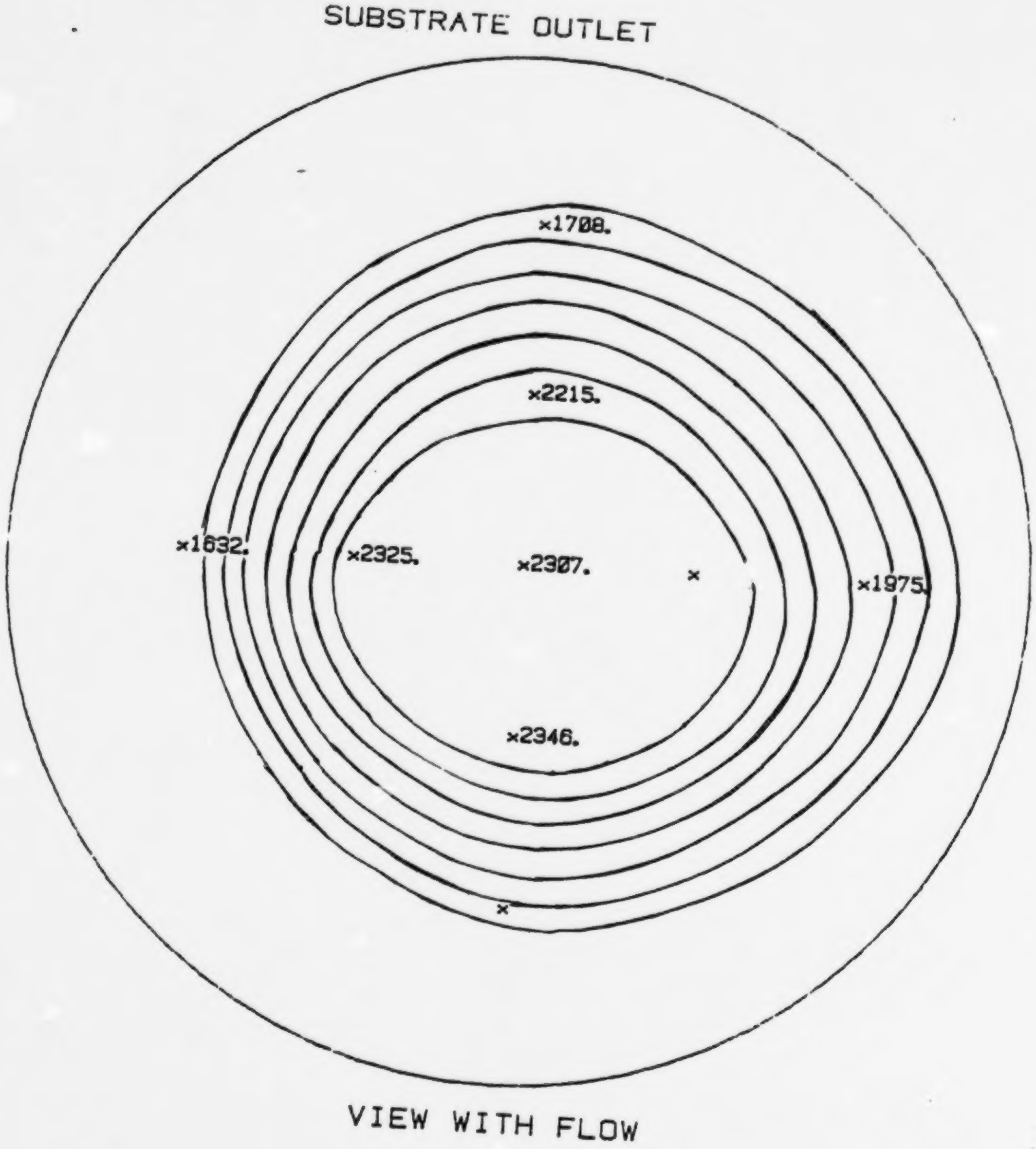

Figure 17. Catalyst Exit Face Isotherms

CATATHERMAL* COMBUSTION OF DIESEL EXHAUST TO PRODUCE AN INERT GAS

BY:
M. Durilla
K. R. Burns
ENGELHARD INDUSTRIES DIVISION
ENGELHARD CORPORATION
Iselin, New Jersey 08830

---

* Trade name of Engelhard Corporation

ABSTRACT

Under contract to Sandia National Laboratories, the generation of an inert gas from the exhaust gas of a 113 hp diesel engine has been demonstrated by Engelhard. This was accomplished by CATATHERMAL combustion of fuel oil with diesel exhaust gas to essentially eliminate oxygen and nitrogen oxides in the exhaust and as a result produce an inert gas consisting primarily of nitrogen, carbon dioxide, water and carbon monoxide. This method of generating an inert gas can be useful to overall operating process economics in locations where there is the need for operating diesel engines to do work. Areas of application include tertiary oil recovery from depleted oil wells, blanketing operations in petroleum tanker reservoirs, and the providing of noncorrosive drilling environments for geothermal drilling operations.

Diesel engine exhaust gas concentration of greater than 1,000 Vppm NO_x and 7 to 10% oxygen were reduced to less than 2 and 10 Vppm, respectively. Durability of the 8.75 inch diameter CATCOM* catalyst was demonstrated up to 200 hours of operation with numerous system start-ups and combustion temperatures of 2300°F. Optimum system operation was at or just slightly rich of stoichiometry.

---

* Trade name of Engelhard Corporation

SECTION 1

INTRODUCTION

Inert gases of various compositions serve a wide variety of industrial applications and expansion to additional uses would be possible if the costs of producing inert gases could be reduced as compared with current technologies, especially when the application involves the production of large volumes of inert gas. Three examples of such applications include "blanketing" of petroleum tanker cargo reservoirs to prevent explosions, injection into oil wells to assist with recovery of additional petroleum, and injection into geothermal wells during drilling as a noncorrosive drilling environment.

The method of producing an inert gas depends heavily upon the requirements of a particular application which includes the required quality of the inert gas, available fuel and energy sources, production volumes of inert gas, portability needs, and other economic and technical considerations. A few examples of current methods for producing inert gas are as follows:

- Cryogenic separation of nitrogen from atmospheric air yields a high quality inert gas consisting almost entirely of nitrogen. In addition to being quite costly, this method generally must involve production of large inert gas volumes which exceed certain application requirements. In virtually all cases, these production systems are not portable.
- Flame combustion of fuel and atmospheric air to produce an inert gas consisting primarily of nitrogen, carbon dioxide, and water with lower levels of oxygen, carbon monoxide, unburned hydrocarbons, oxides of nitrogen, and other contaminants. After treatment of the burner effluent including water precipitation, scrubbing, filtering, and catalytic treatment can refine the exhaust gas to a higher quality inert gas as required.

- Exhaust gas from a rich or near stoichiometric burning spark ignited engine with, in most cases, catalytic treatment to produce an inert gas consisting of nitrogen, carbon dioxide, and water. This method is of particular value because useful work can be obtained from the engine during the production of inert gas. In fact, in virtually all applications, the production of the inert gas is a by-product from the operation of the engine for another purpose. These applications are generally limited to the availability of gasoline or natural gas. Such equipment is usually portable.

With the latter production method, control of oxygen and nitrogen oxides (NO_x) is of particular concern because these constituents can be especially corrosive in certain cases; particularly when the application involves high operating pressures. In such cases these two gases can cause unacceptable corrosion to the system compressor and other equipment unless these are adequately controlled catalytically. Although among the least expensive methods for generating inert gas, this technology is limited in many respects because it cannot be used with diesel engines which operate very lean of stoichiometry. Lean operation involves a large percentage of oxygen in the exhaust gas which in itself is not acceptable and, furthermore, it precludes the catalytic reduction of NO_x.

Technology that could allow the generation of an inert gas from diesel engine exhaust and diesel fuel could be of significant value in situations where diesel engines are used and the use of an inert gas would afford operating advantages. Such situations are associated with certain geothermal and oil well drilling operations. In both cases the use of an inert gas can minimize equipment corrosion and in the case of oil drilling can minimize the potential occurrence of drilling fires or explosions. Because drilling wells is a temporary operation, the need for equipment portability is manditory.

Under sponsorship by Sandia National Laboratories (Contract Number 13-5071), Engelhard Industries has demonstrated the feasibility of generating an essentially inert gas via CATATHERMAL combustion of diesel fuel with diesel engine exhaust gas (References 1 and 2). This program was specifically oriented towards demonstrating this technology for application to drilling certain geothermal wells where corrosion costs are significant. Reference 3 explains CATATHERMAL combustion in detail.

The results obtained in this program substantiate the capability of this technology to generate an inert gas on a large scale basis and provide the necessary data base upon which a field demonstration system can be designed.

SECTION 2

EXPERIMENTAL FACILITIES

The test facility consisted primarily of a diesel engine, a CATCOM* inert gas generator, equipment controls, and appropriate analytical instruments as the schematic flow diagram illustrates in Figure 1. Figure 2 presents a photograph of the CATCOM inert gas generator unit and Figure 3 provides piping and instrumentation details.

The diesel engine utilized for this program was an Allis Chalmers DES-60 turbocharged unit rated at 113 hp. An electrical generator driven by the engine and electrical load bank were used as a means for operating the engine over an output range of 0-60 KW as required by desired operating conditions. Within this range the oxygen content in the diesel exhaust ranged from 7 weight % at full load to approximately 18 weight % at idle. The hot diesel exhaust was directly connected to the CATCOM inert gas generator unit.

The CATCOM inert gas generator unit consisted primarily of a fuel injection and mixing chamber, which affords proper mixing of the diesel exhaust gas and diesel fuel, and a proprietary Engelhard precious metal catalyst which promotes CATATHERMAL combustion of the reactant mixture to consume the remaining oxygen in the diesel exhaust and simultaneously catalytically reduce the NO_x generated by the diesel engine. The catalyst had a diameter of 8.75 inches and overall length of 9 inches.

In addition, the test apparatus was also equipped with an orifice in the flow stream to monitor exhaust gas flow rates, an engine exhaust by-pass line around the CATCOM reactor to regulate exhaust flow to the reactor unit, and numerous thermocouples for monitoring system temperatures.

Instrumentation capability was provided for monitoring HC, CO_2, CO, NO_x, and O_2 concentrations at various locations of system flow. Instrumentation sensitivities were capable of being altered to accurately measure these gaseous constituents both before and after the catalytic reactor.

---

*CATCOM is a trade name of Engelhard Corporation.

SECTION 3

EXPERIMENTAL PROGRAM

The experimental program consisted of parametric tests and catalyst durability evaluation. The parametric tests consisted of varying key operating parameters to determine system performance and sensitivity to operating conditions. Engine load was varied to change the catalyst inlet temperature, inlet oxygen concentration and exhaust gas flow rates. Further control of system flow rates was achieved via the use of an engine exhaust bypass line previously described. In addition to these conditions, the equivalence ratio* was scanned at each operating condition from fuel lean to fuel rich operation.

A 200 hour catalyst durability test was conducted subsequent to the parametric evaluations. The 200 hours durability was accumulated in approximately 6 hour start-up and shutdown intervals to simulate probable field operating conditions. The first 100 hours of durability was with an engine load of 60 KW while the second 100 hours was with a 48 KW load.

---

*Equivalence ratio = $\frac{\text{(Fuel/air) actual}}{\text{(Fuel/air) stoichiometric}}$

SECTION 4

DISCUSSION OF TEST RESULTS

CHARACTERIZATION OF DIESEL ENGINE EXHAUST

Prior to catalyst performance evaluation tests the basic exhaust gas emission characteristics of the Allis Chalmers DES-60 diesel engine were evaluated and are shown in Table I. Diesel engines do not have a throttled air flow and their output is regulated by the rate at which fuel is injected into the engine. For this reason the air/fuel ratio of diesel engines vary from extremely lean operation at idle to moderately lean at full load. This is quite unlike spark ignited engines which have throttled control of air intake and have, on a relative basis, a fairly constant air/fuel ratio, near to stoichiometry over most engine operating conditions.

As is evident in Table I, at idle the fuel/air ratio is extremely lean with measured oxygen concentrations approaching 18%. The diluent effects of the large amount of excess air are evident in the low CO_2 concentrations which were below 3%. As the load was increased the fuel/air progressively moves towards stoichiometric operation with associated lowering of excess oxygen levels and increasing levels of CO_2 and NO_x as the diluent air is decreased. Exhaust gas temperatures increase with engine load, as would be expected.

OXYGEN MONITORING REQUIREMENTS

Because of the necessity associated with monitoring extremely low oxygen concentrations after the catalyst, special efforts were made to assure accurate test procedures. In addition to detailed attention in making the system essentially leak-proof to ambient atmospheric oxygen, the oxygen analyzer's zero baseline was calibrated with a special oxygen-free calibration gas prior to each sample measurement. This calibration gas was generated by reacting a nitrogen (99.9%) and hydrogen (99.95%) mixture over an Engelhard Deoxo® catalyst, in which case any residual oxygen would combine with the hydrogen to form water which was subsequently removed via a dessicant drier. Resolution of the oxygen measurement analyzer was limited to 10 Vppm.

CATCOM INERT GAS GENERATION CHARACTERISTICS

CATCOM inert gas generation operation was studied at three engine loads; 60 KW (100% load), 48 KW (80% load) and 36 KW (60% load). At each load setting the exhaust gas flow rate was adjusted to three different flow rates and the equivalence ratio was scanned as presented in Figures 4 through 7. Operation over the range and load conditions demonstrated essentially equivalent performance as a function of stoichiometry indicating broad operating flexibility of the catalyst. Performance is discussed in further details as follows:

Effects of Stoichometry

As is illustrated in Figures 4 through 6, the influence of stoichiometry, identified in terms of equivalence ratio, directly affects the concentrations of O_2, CO_2, NO_x, and CO. As would be expected, CO_2 is at a maximum concentration when the equivalence ratio is near 1.0. The concentrations are decreased on either side of stoichiometric by the dilutions effects of excess air on the lean side and excess fuel (oxygen limitation) on the rich side. O_2 concentrations decrease rapidly as system operation approaches stoichiometry from lean operation and reach the detection limit of 10 Vppm (minimum resolution of O_2 measurement capability) for all conditions at and rich of stoichiometry.

NO_x concentrations are not altered by the catalyst under lean operation but are reduced as operation approaches stoichiometry. NO_x reduction is dramatically influenced as operation moves from slightly lean to slightly rich operation with concentrations going from 1000 to 1 Vppm. Even richer operation yields NO_x emissions in the order of 0.1 Vppm. This phenomena is created by the catalytic reduction of NO_x with CO to form CO_2 and N_2. As the reaction is dependent upon the absence of O_2 and the presence of CO, catalytic reduction of NO_x does not occur efficiently when operation is lean of stoichiometry. Under lean operation the CO preferentially reacts with O_2 rather than NO_x. Thus, slightly rich operation is required for adequate control of NO_x emissions. Further detail concerning this reaction is presented in References 4 and 5. NO_x emissions are summarized on Figure 7 and evidence the insensitivity to operation at various load conditions (catalyst space velocity).

CO concentrations, on the other hand, are very low under lean conditions and increase rapidly from stoichiometric to rich operation. The CO is generated by the incomplete combustion of the HC fuel which results from inefficient concentrations of O_2. Although not harmful (maybe beneficial in terms of corrosion resistance) excessive CO concentrations are not desirable because of associated fuel consumption penalties. Optimum system performance in terms of minimizing both NO_x and CO is predicated on operating at near stoichiometric conditions through the use of adequate system control devices.

Effects of Engine Load

In order to separate the interrelationship of engine load with exhaust flow rates and oxygen concentration, both of which vary with engine load, flow rates to the catalyst were varied systematically at each engine load condition by by-passing a portion of the exhaust flow before the catalyst.

Effect of Oxygen Concentration

As was indicated in Table I, the O_2 concentration in the exhaust gas varies from 7.50% at 60 KW load to 11.19% at 36 KW load. A major function of the CATCOM inert gas generator is to essentially eliminate O_2. As the O_2 is consumed by the fuel injected into the reactor, more fuel was required as the O_2 level increased with decreasing engine load conditions. The O_2 was effectively removed under all load conditions rich of stoichiometry as shown in Figure 9.

Effect of Flow Rates (Space Velocity)

Exhaust flow rates were varied from approximately 4,000 to 9,000 SCFH without an influence on emission characteristics (see Figures 4-6). Variation of flow rates at different engine loads (and O_2 concentrations) additionally did not indicate an influence on emission performance. These results suggest that the flow rates are within the capabilities of the catalyst and that a further increase of flow rates may be possible.

Catalyst Operating Temperatures

The operating temperatures of the catalyst are a function primarily of the inlet temperature and O_2 concentration in the diesel exhaust gas. As the O_2 concentration increases with decreasing engine loads, more fuel is used to consume that O_2 and, therefore, the catalyst operating temperature increases.

A maximum catalyst operating temperature of 2,300°F correlated with an exhaust O_2 concentration of approximately 10-11% (or 60% engine load) under the specific test conditions of this test program. That is to say that operation at engine loads less than 60% would not be indicated as such operation would cause excessive catalyst temperature conditions. The CATCOM system was a single stage system. A dual stage system could overcome this limitation.

Catalyst inlet temperatures ranged from 490° to 660°F at various operating conditions without altering catalyst performance characteristics. As the catalyst could be located much closer to the engine with a field operating unit, the anticipated exhaust gas temperature would conservatively equal or exceed these catalyst inlet temperature conditions for engine loads of greater than 60%, as indicated in Table I.

The high combustion temperatures had the beneficial effect of incinerating visible soot emissions from the diesel engine exhaust. The system piping downstream of the catalyst was essentially devoid of soot whereas the upstream section had significant deposits of soot, as is normal for diesel engine exhaust systems. Additional efforts are indicated to accurately quantify this phenomena.

COMPARISON OF MEASURED vs. THEORETICAL EQUILIBRIUM CONCENTRATIONS

An Engelhard computer program (Reference 6) was used to calculate theoretical equilibrium concentrations of species present in the generated inert gas. Comparisons of these equilibrium concentrations vs. actual measured concentrations are shown in Figures 8 (NO_x), 9 (O_2) and 10 (CO). Correlation of the theoretical vs. actual O_2 concentration levels is excellent and is only limited by the lower detection limit of the O_2 analyzer (10 Vppm). Both NO_x and CO correlate well under lean operation (within CO detection capability); however, measured values exceed theoretical values under rich operation. This is probably attributable to minor variations of the equivalence ratio at the inlet of the catalyst created by imperfect mixing of the fuel with the exhaust gas. Such variations were quite minor as the outlet temperature of the catalyst was quite uniform.

Nevertheless, these results suggest that further improvement of the fuel mixing system would afford reduction of CO and NO_x emissions at given equivalence ratios at or slightly rich of stoichiometry.

DURABILITY TEST

A 200 hour durability test was successfully completed showing the maintenance of constant levels of NO_x and O_2 emissions over the test period being less than 2 Vppm and 10 Vppm (limit of detection), respectively, as presented in Figure 11. The first 100 hours of durability was conducted at 60 KW engine load and the second 100 hours was at a 48 KW load. The catalyst performance was stable throughout the durability evaluation and the test was terminated in accordance with contract requirements. Much longer life would be expected.

SECTION 5

CONCLUSIONS

An experimental program was successfully conducted using an Engelhard CATCOM inert gas generator system to produce an inert gas by combusting diesel fuel and diesel engine exhaust gas in the presence of a catalyst. Primary results obtained in this program were:

1. Diesel engine exhaust concentrations of NO_x (>1,000 Vppm) and O_2 ($\sim$7-10%) can be dramatically reduced (NO_x <2 Vppm and $O_2 \leq 10$ Vppm) with a special Engelhard CATCOM catalyst under slightly fuel rich operation.

2. 200 hours of catalyst durability has been successfully demonstrated.

3. Engine exhaust concentration and exhaust gas flow rates had little, if any, influence on emission characteristics within program test conditions.

4. In order to minimize CO emissions while controlling NO_x to very low levels it is necessary to operate the system just slightly rich of stoichiometry. Further fuel mixing system improvements should result with further reduction of CO emissions.

5. The single stage CATCOM reactor cannot be operated with diesel engine loads producing O_2 exhaust concentrations in excess of approximately 10-11% due to temperature limitations of the catalyst.

ACKNOWLEDGMENTS

The authors wish to express appreciation for the invaluable assistance contributed to this program by Dr. R. V. Carrubba and Mr. P. E. Reed of Engelhard and as well as by Mr. E. R. Norster, a consultant.

Figure 1

Schematic Flowsheet of Test Rig

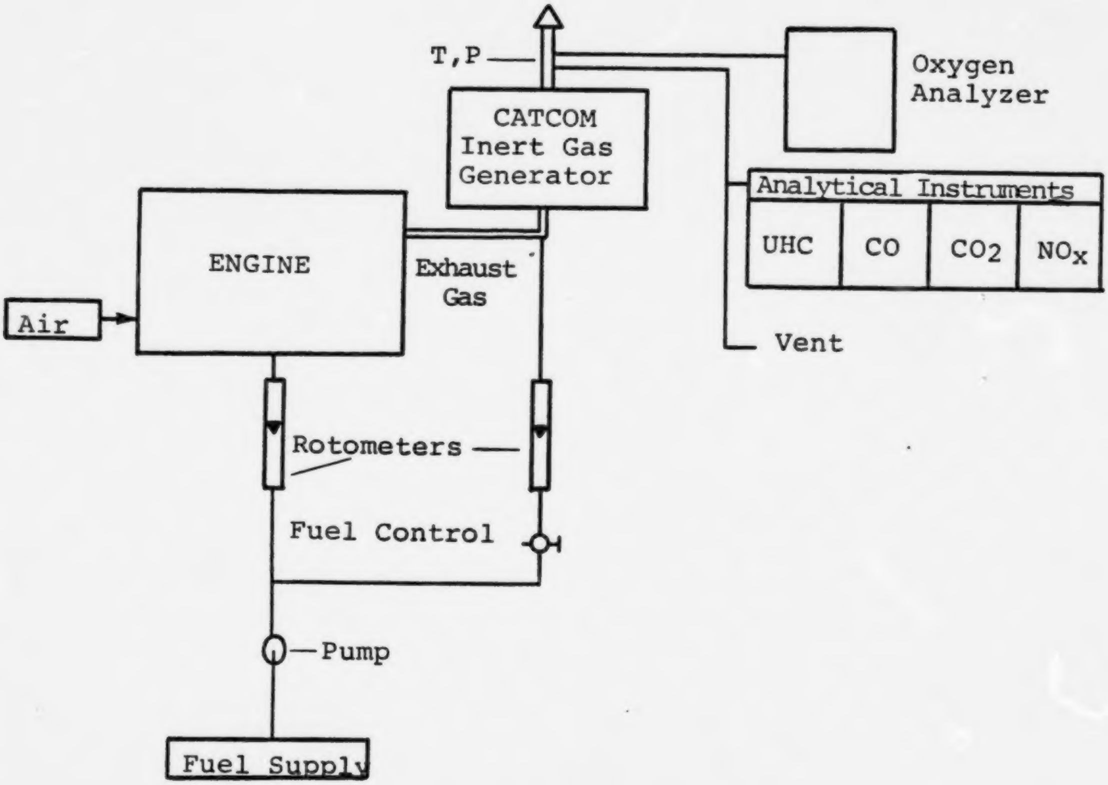

T,P
CATCOM Inert Gas Generator
Oxygen Analyzer
Analytical Instruments
UHC
CO
CO_2
NO_x
ENGINE
Exhaust Gas
Air
Vent
Rotometers
Fuel Control
Pump
Fuel Supply

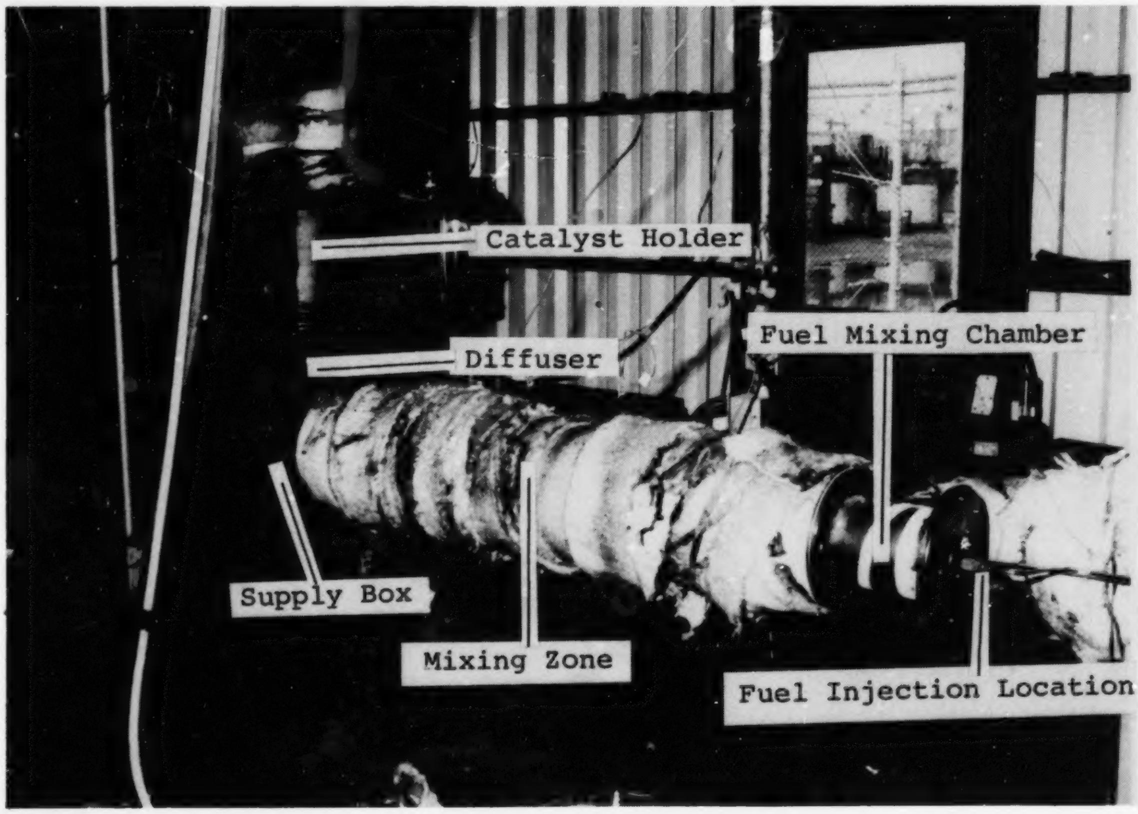
Catalyst Holder
Fuel Mixing Chamber
Diffuser
Supply Box
Mixing Zone
Fuel Injection Location

Figure 2 CATCOM Inert Gas Generator Unit

Figure 3

CATCOM Inert Gas Generator Unit and Instrumentation

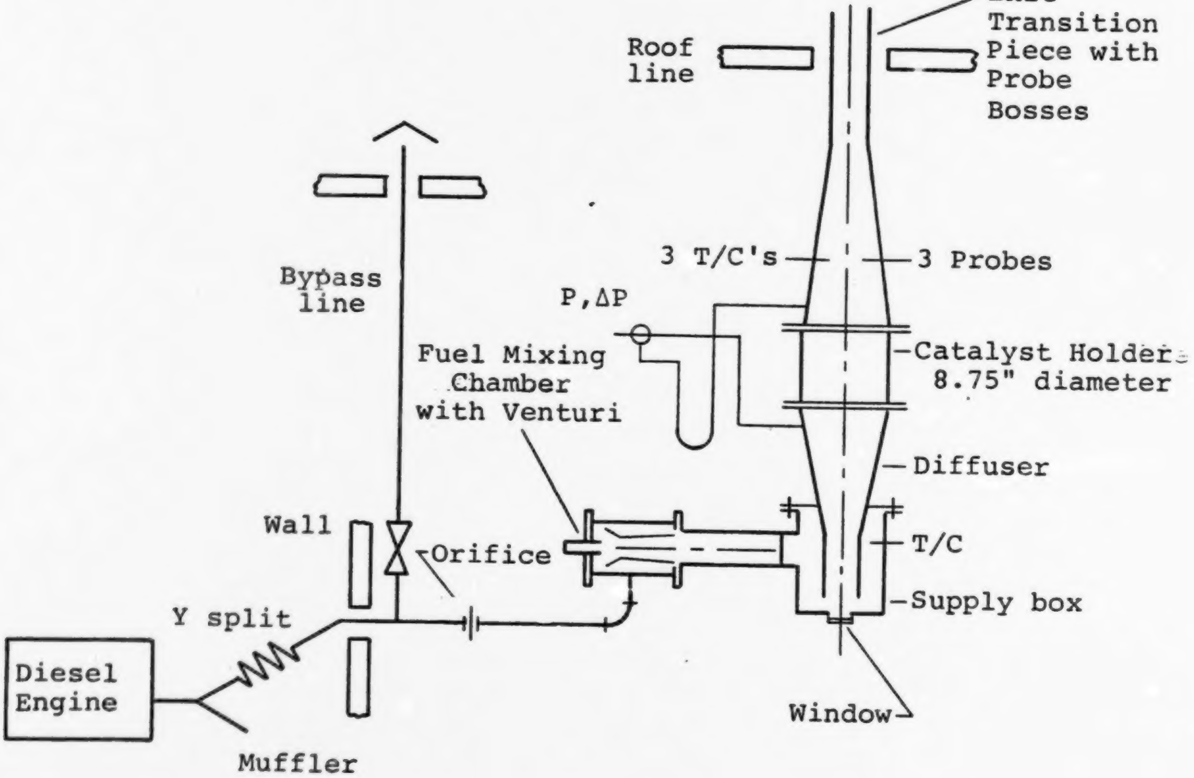
Exit
Transition
Piece with
Probe
Bosses
Roof
line
3 T/C's
3 Probes
Bypass
line
P,ΔP
Fuel Mixing
Chamber
with Venturi
Catalyst Holder
8.75" diameter
Diffuser
Wall
Orifice
T/C
Supply box
Y split
Diesel
Engine
Window
Muffler

Figure 4

Parametric Tests - 60 KW Engine Load -

Emisions vs. Equivalence Ratio

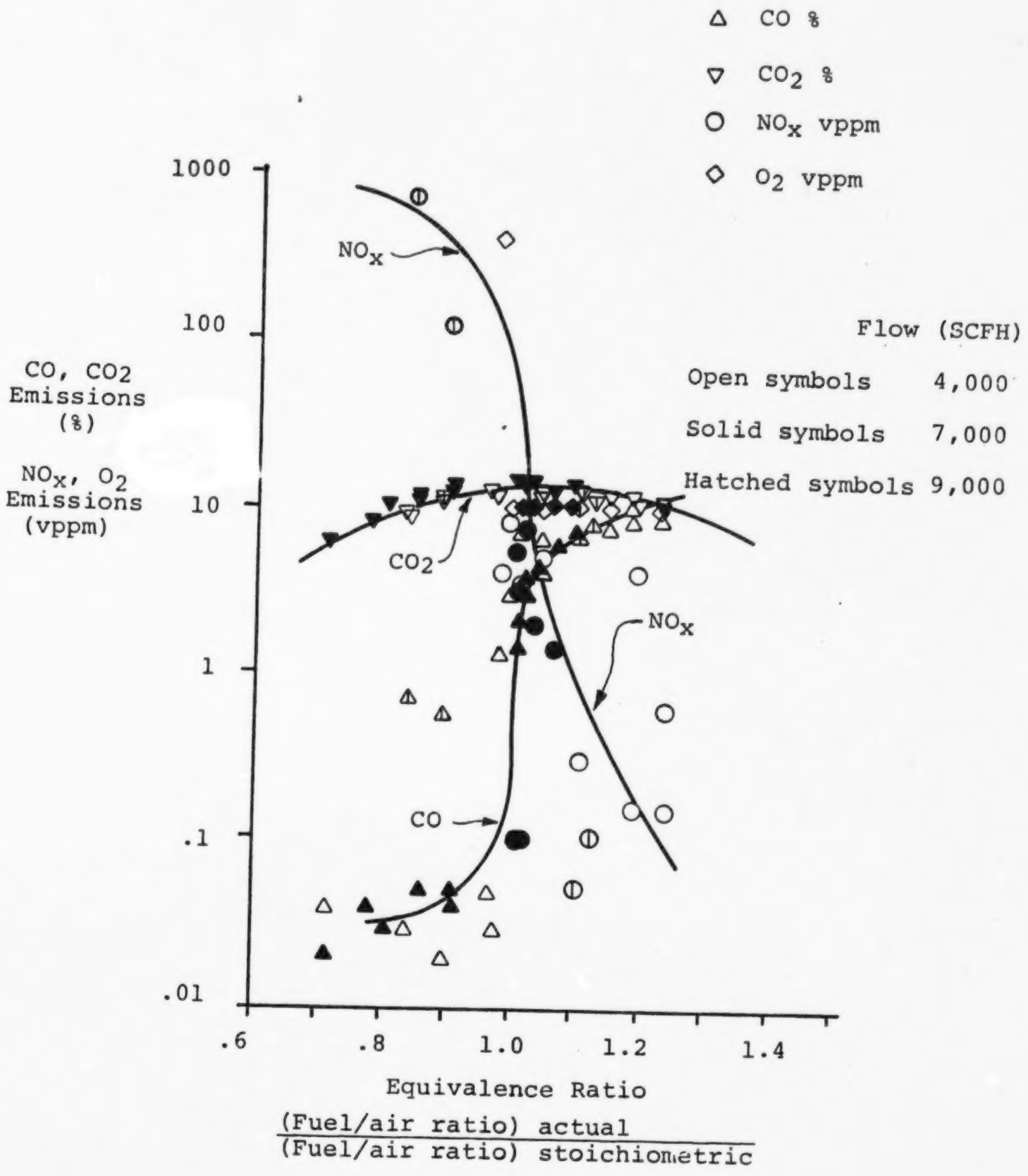

Figure 5

Parametric Tests - 48 KW Engine Load -

Emissions vs. Equivalence Ratio

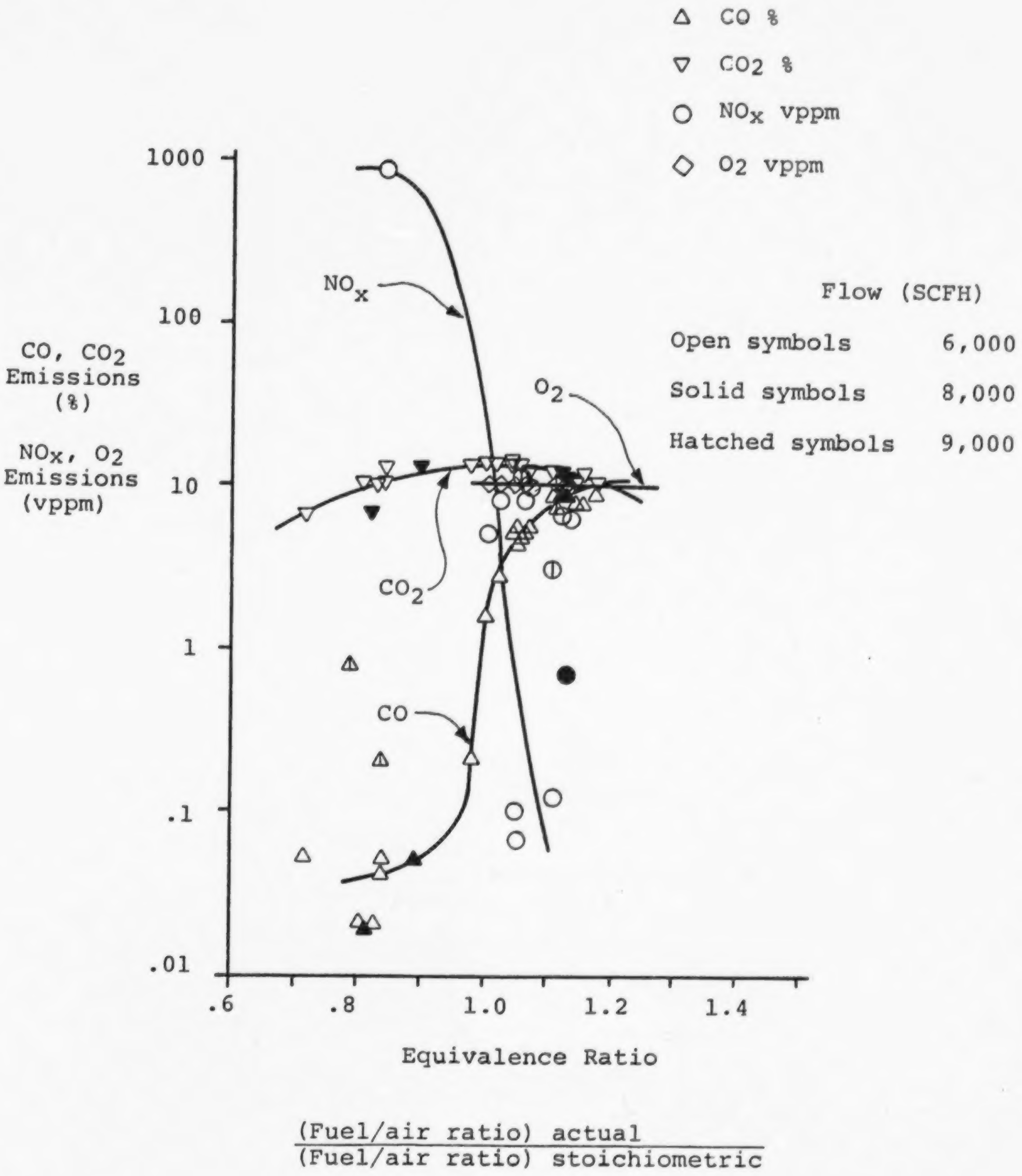

Figure 6

Parametric Tests - 36 KW Engine Load -

Emissions vs. Equivalence Ratio

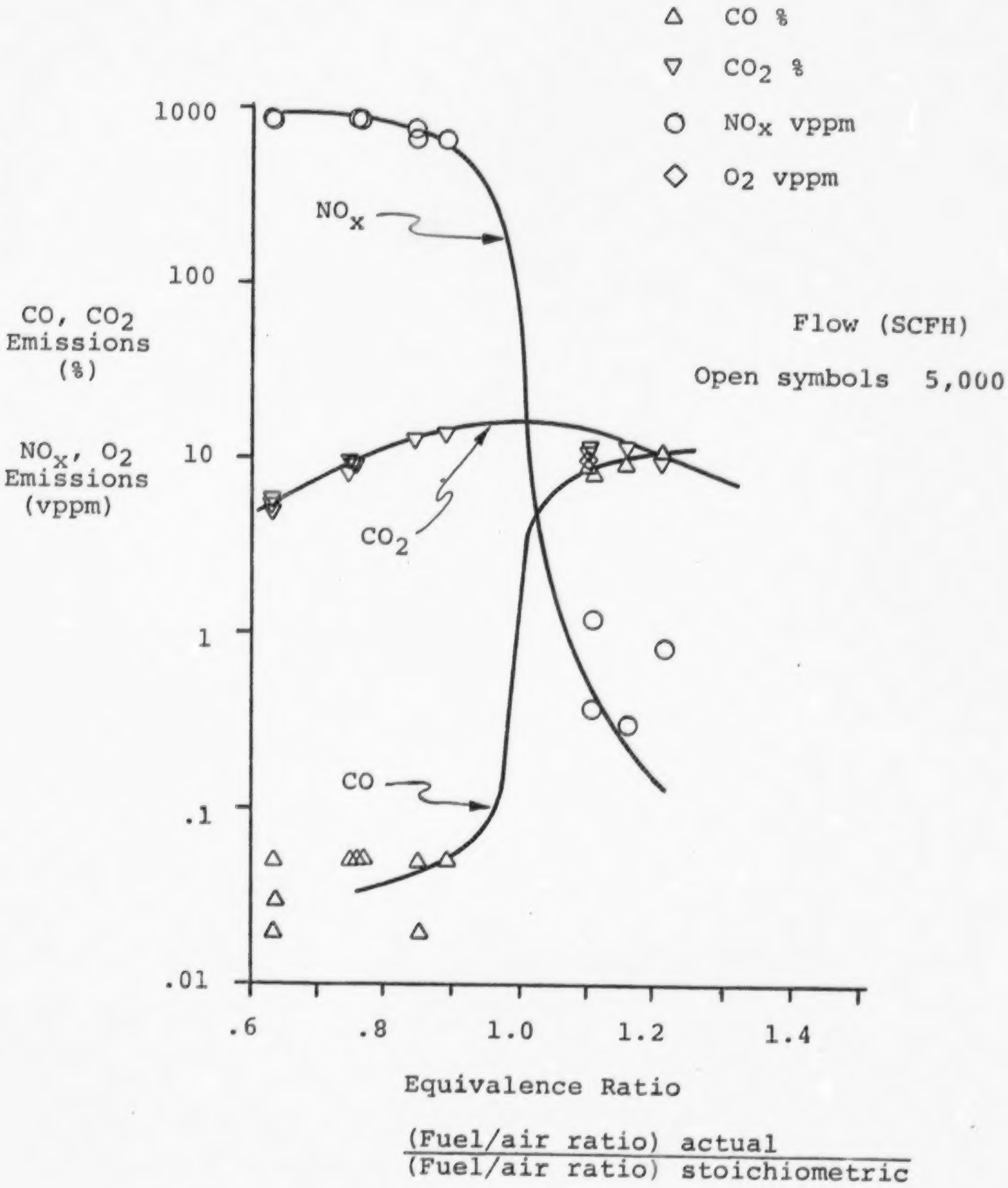

Figure 7

Parametric Tests

NO_x Emissions vs. Equivalence Ratio

Effect of Engine Load

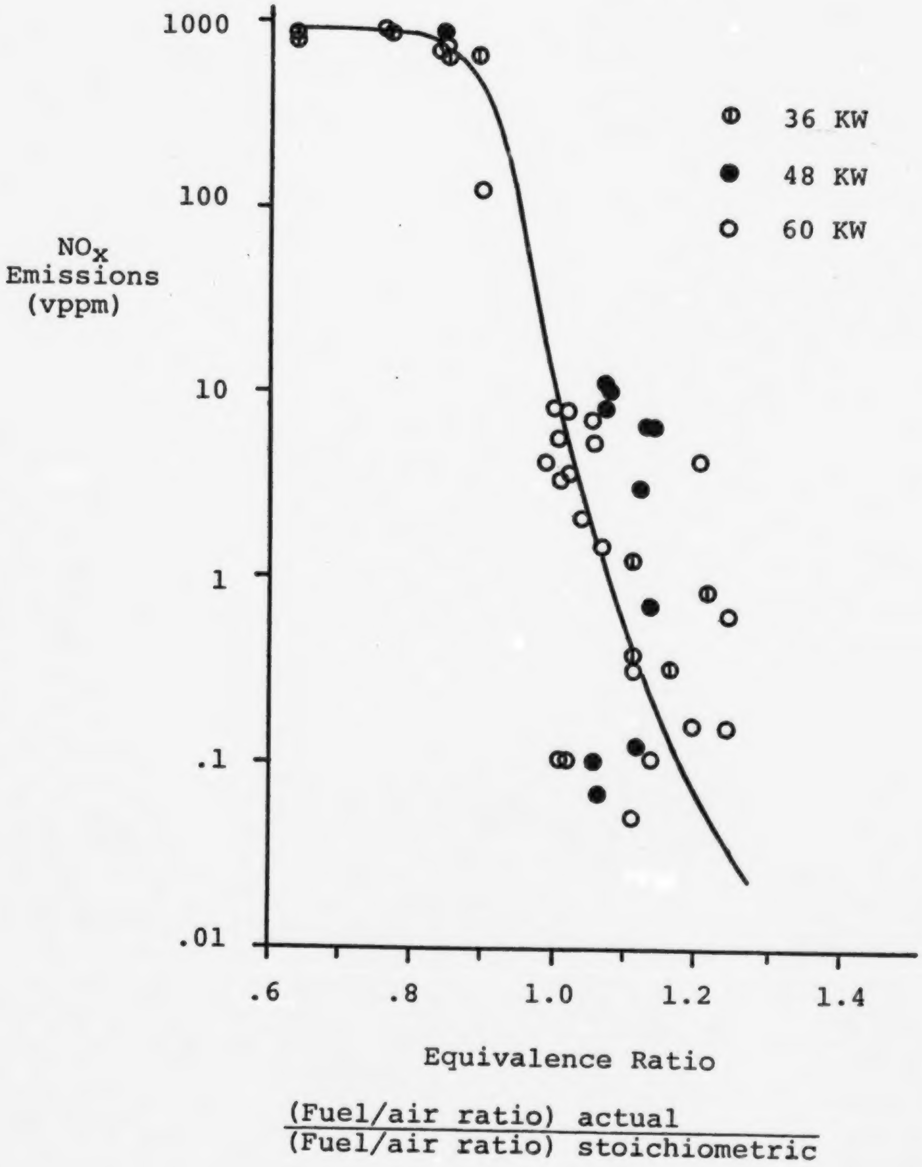

Figure 8

Reactor Exhaust NO_x:

Equilibrium vs. Measured Effect of Equivalence Ratio

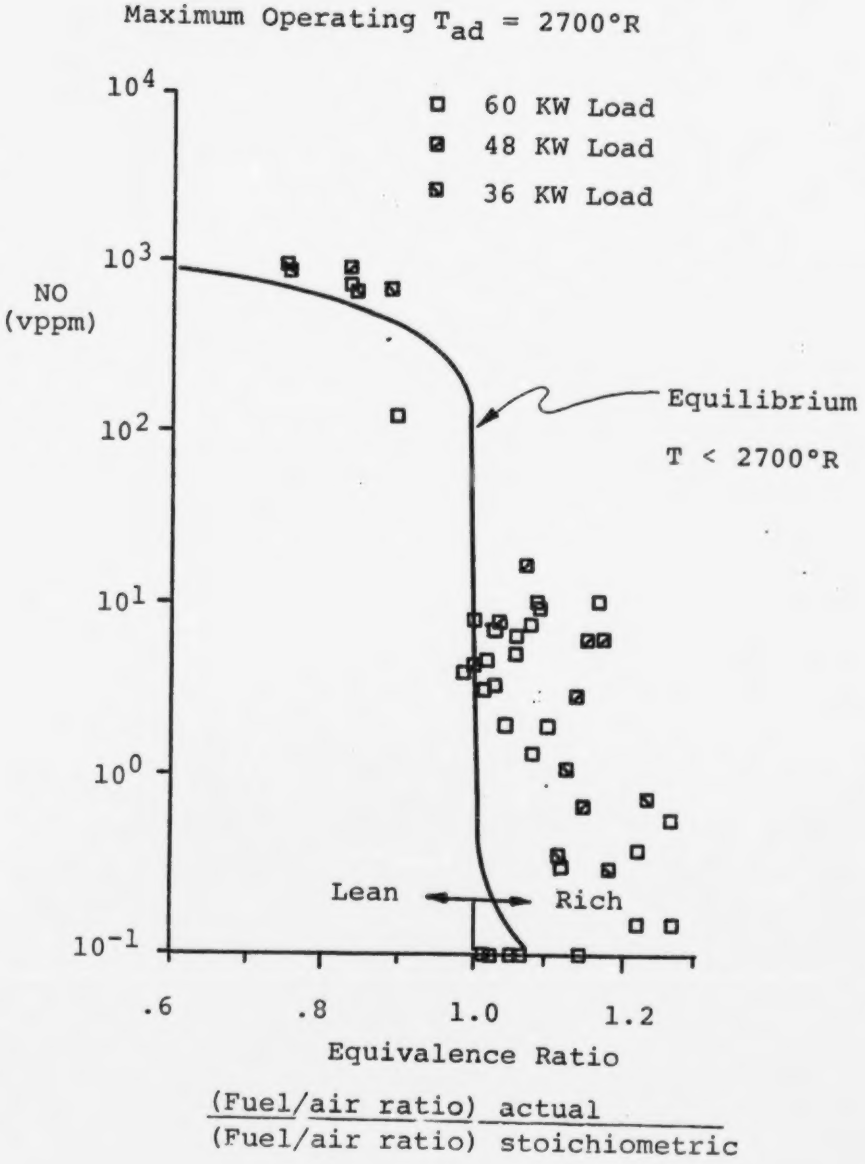

Figure 9

Reactor Exhaust O_2

Equilibrium vs. Measured Effect of Equivalence Ratio

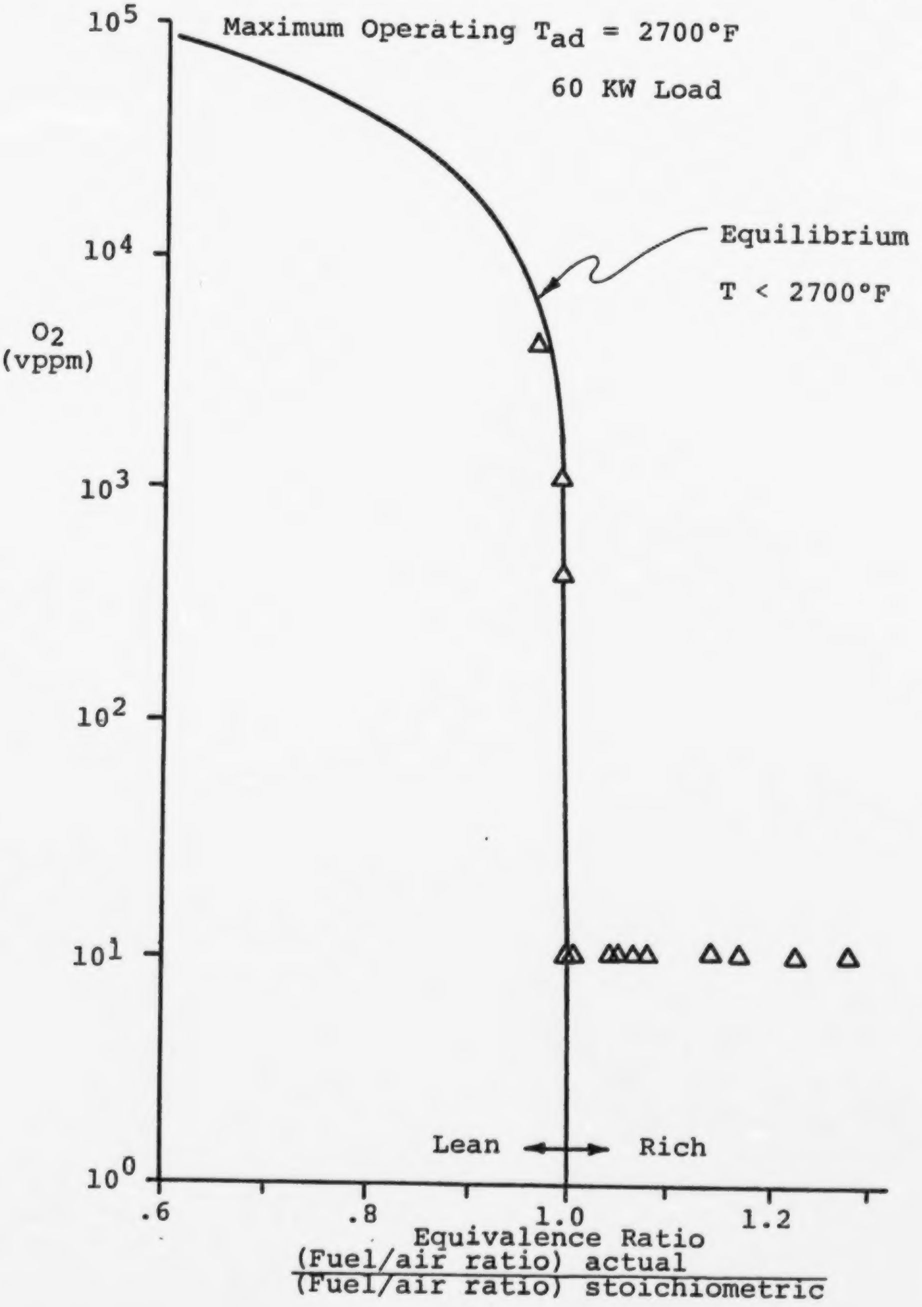

Figure 10

Reactor Exhaust CO:

Equilibrium vs. Measured Effect of Equivalence Ratio

60 KW Load

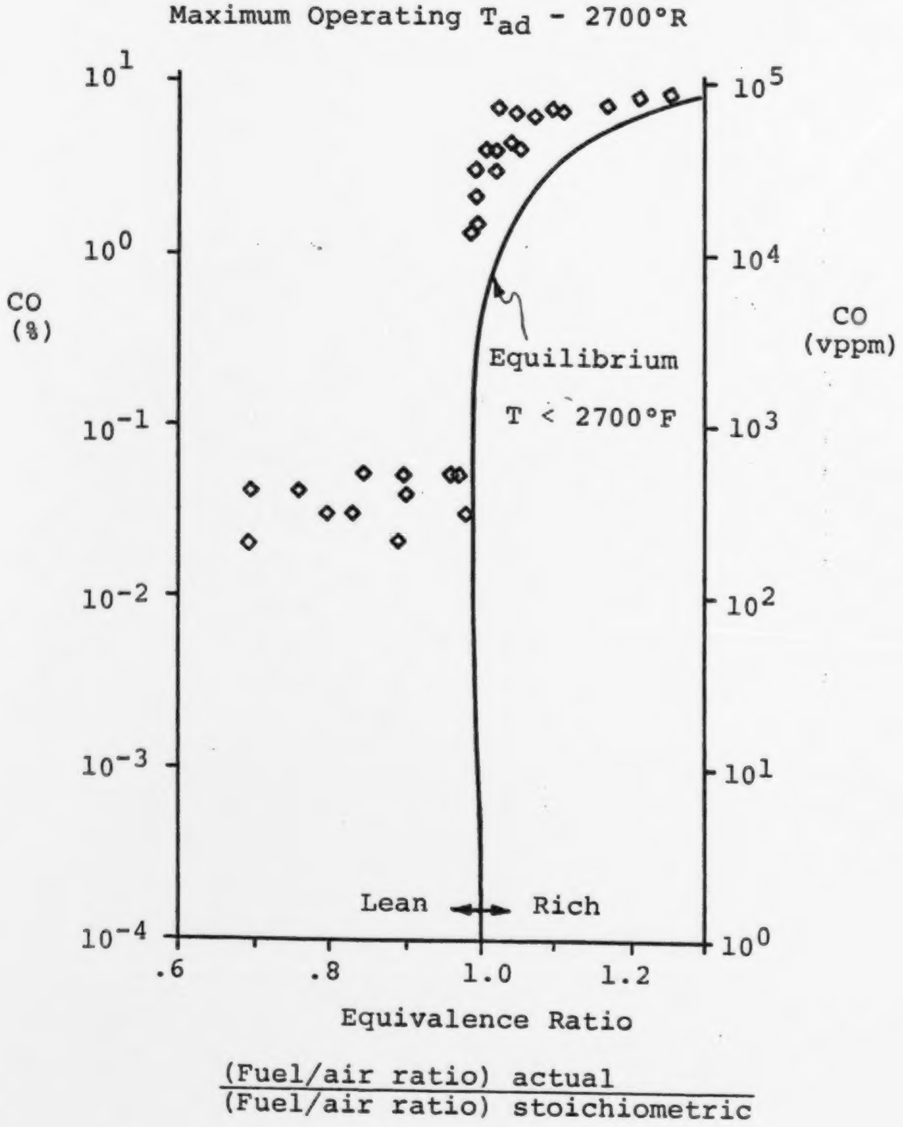

$$\frac{\text{(Fuel/air ratio) actual}}{\text{(Fuel/air ratio) stoichiometric}}$$

Figure 11

Durability Test Results

NO_x Emissions vs. Time

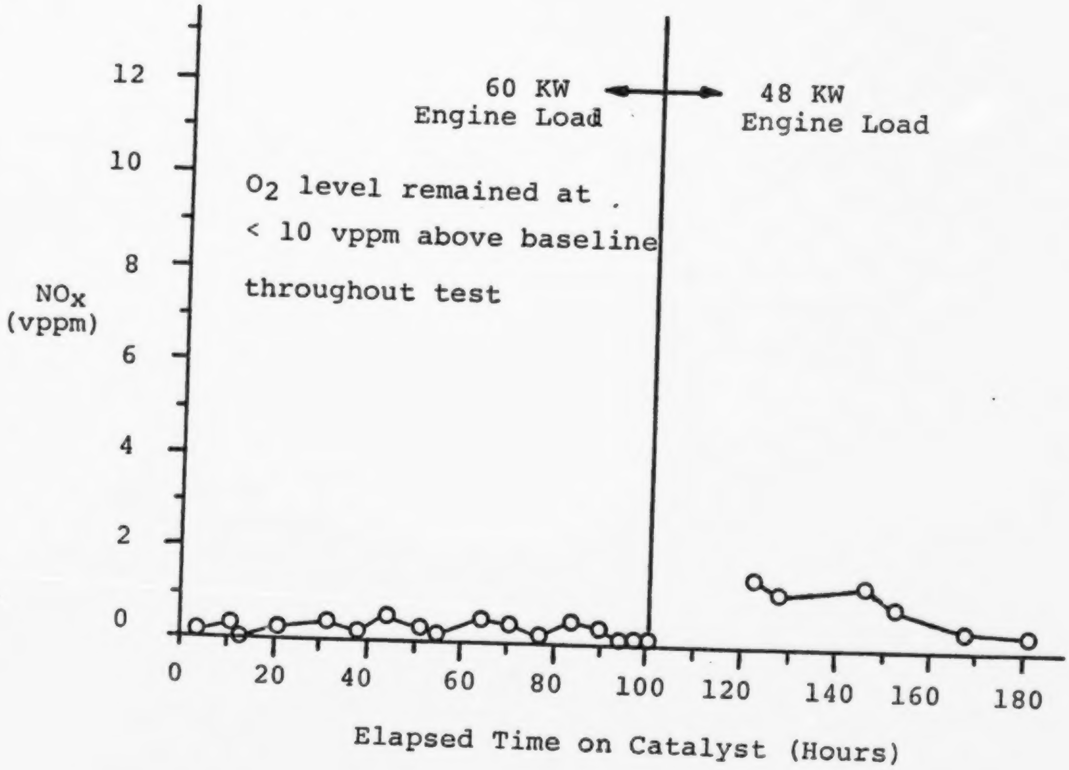

TABLE I

Allis Chalmers DES-60 Diesel Exhaust Characterization

Load (KW)	% Load	Manifold Exhaust Temperature (°F)	CO_2 (%)	CO (%)	O_2 (%)	NO_x (ppm)
0	0	360	2.3	0.05	17.66	500
12	20	450	3.2	0.05	16.14	650
24	40	570	4.5	0.05	12.33	>1000
36	60	650	5.6	0.05	11.19	>1000
48	80	700	6.2	0.05	9.59	>1000
60	100	740	6.6	0.05	7.50	>1000